INDIAN JOURNAL OF PHYSICS

VOL XIV

AND

PROCEEDINGS

OF THE

Indian Association for the Cultivation of Science, Vol. XXIII

(Published in Collaboration with the Indian Physical Society)

(With Fifteen Plates)

PRINTED AT THE CALCUTTA UNIVERSITY PRESS, 48, HAZRA ROAD, CALCUTTA,
BY BHUPENDRALAL BANERJEE AND PUBLISHED BY THE SECRETARY,
INDIAN ASSOCIATION FOR THE CULTIVATION OF SCIENCE,
210, Bowbazar Street, Calcutta.
1940

Price Rs. 12 or £1-2-6

CONTENTS OF VOL. XIV

PART I

PAGE

1. Splitting of Spectral Lines at Scattering by Liquids—By Sachindra Mohan Mitra ... ...
2. Imput Impedance of High-Frequency Parallel Wire Transmission Lines Immersed in an Absorbing Medium—By S. S. Banerjee ... 13
3. Degeneracy in Non-Relativistic Bose-Einstein Statistics—By D. V. Gogate and D. S. Kothari 21
4. Secondary K-Absorption Edges of Cobalt Salts in Solid and Liquid Solutions—By B. B. Roy, S. R. Das and N. Bagchi 37
5. On Sources of Stellar Energy—A Criticism of the Bethe-Gamow Theory —By Ram Nivas Rai 55
6. On the Width of the K-Absorption Edge of Cobalt—By N. Bagchi ... 61
7. The Spiral Arms of a Configuration of rotating Compressible mass having uniform density and surrounding an incompressible Spheroid of homogeneous mass—By A. C. Banerji 67
8. Second Maximum of Rossi Curve—By A. K. Dutta 79

PART II

9. The Secondary K-Absorption Spectra of Sulphur—By N. Bagchi ... 85
10. A note on the Origin of the D-layer—By S. Deb 89
11. Production of Ultra-high Frequency Radio Waves by Electric Oscillations—By S. S. Banerjee and A. S. Rao 93
12. Early Morning Variation of Ionisation and the True Height of region F of Ionosphere—By S. P. Ghose 101
13. A Relation between Velocity of Sound in Liquids and Molecular Volume—By M. Rama Rao 109
14. The Theory of Compton-Effect—By K. C. Kar 117
15. Rotational Raman Scattering in Liquid Oxygen—By Bishnupada Saha 123
16. Magnetic Susceptibilities of Solutions of Sodium and Potassium Nitrates —By S. P. Ranganadham and M. Qureshi 129
17. Mutual Influence of Water and Heavy Water—By I. Ramkrishna Rao and Y. Paramasiva Rao 135
18. Electrolytic Dissociation in Sulphuric Acid as Studied by Raman Effect —By N. Rajeswara Rao 143
19. Studies on some Indian Vegetable Oils, Part V.—Temperature Effect on Gas Absorption and other Physical Properties—By Chandrasekhar Ghosh 153
20. A Simple Laboratory Method of Producing Continuous Ultra-violet Light—By Haribansh Narayan Yadav 169

Part III

PAGE

21. Geometrical Note on Van Der Waal's Equation—By Haridas Bagchi ... 173
22. A New Technique for determining Ultra sonic Velocities in Liquids—By R. L. Narasimhaiya and C. S. Doraiswami 187
23. Measurement of Cosmic Rays at Agra and Kodaikanal—By A. K. Das and M. Salaruddin 191
24. Raman Spectra of Sugar—By A L. Sundara Rao 207
25. On the Dielectric Constant of an Electronic Medium at Medium Frequency—By S. R. Khastgir and C. Chowdhury 213
26. Determination of the Structure of m-dinitrobenzene by Patterson Fourier Summation—By K. Banerjee and M. Ganguly 231
27. A note on the Refractive Index of Shellac—By G. N. Bhattacharya ... 237
28 High-frequency Measurements of the Amplification Factor and Internal Resistance of a Thermionic Valve—By M. Kameswar Rao ... 247

Part IV

29 On the Origin of Solar System—By P. L. Bhatnagar 253
30 On the Intensity Variations of the Down-coming Wireless Waves from the Ionosphere—By S. R. Khastgir and Anil Kumar Ray ... 283
31. On wide band-pass effect in crystals associated with negative impedance elements and development of wide-band low-loss crystal band-pass filters—By S. P. Chakravarty and N. L. Dutt 295
32. An Apparent Influence of the Earth on Solar Prominences—By A. K. Das and B. G. Narayan 311
33. Variation of Field-strength in the Vicinity of an Ultra-short-wave Horizontal Transmitting Aerial—By S S. Banerjee and Paramanand 325

Part V

34. Association of Acetic Acid in non-Aqueous Solvents—By P. Koteswaram 333
35. Molecular Association in Acetone and Methyl-ethyl-ketone—By P. Koteswaram 341
36. Molecular Association as studied by Raman Effect—by P. Koteswaram 353
37. Frequency Changes in Raman Spectrum of Sulphuric Acid—By N. Rajeswara Rao 359
38. Effect of Temperature on the Raman Spectrum of Glycerin—By A. L. Sundara Rao 365
39 Motion of Gases in the Sun's Atmosphere—Part I. On the Mechanism of Formation of Solar Dark-markings—By A. K. Das ... 369

PAGE

40. A Note on the Energy and Wave-length Maxima in Fermi-Dirac and Bose-Einstein Distributions—By A. G. Chowdri and B. N. Singh 387
41. A Precision Direct-reading Spectrophotometer—By A. L. Narayan and C. K. Anathasubrahmanyam 393
42. Evaporation from Earthen Jugs—By H. L. Gupta, A. C. Jain and N. N. Khanna 401
43. The Effect of an Electric Field of Strength $-1/2\alpha F^2$ on the Polarizability Constant of the Normal Hydrogen Atom—By William H. Robinson 405
44 A Note on a New Method of Determination of 'J'—By A. G. Chowdri and D. S. Kothari 409

PART VI

45. Specific Heat of Lac—By G. N. Bhattacharya 415
46. The First-spark Spectrum of Tellurium—By K. R. Rao and M. G. Sastry 423
47 Interferometric Measurements of certain Lines in the Spectrum of Bromine—By M. G. Sastry 429
48. Study of Thermal Neutrons in the Atmosphere—By S. D. Chatterjee ... 435
49 Adsorption of Moisture from the Moist Air by the Soils—By L. D. Mahajan 441
50. Penetration of Thin Ionospheric Layers—By A. C. Deb 451
51. Joule-Thomson and Joule Effects for Bose-Einstein and Fermi-Dirac Gas—By B. N. Singh 459
52. Dynamics of the Pianoforte String and the Hammer, Part IV (Study of Duration of Impact)—By M. Ghosh 475
53. Dynamics of the Pianoforte String and the Hammer, Part V (Some Special Theories)—M. Ghosh 489
54. Book Review 499

AUTHOR INDEX

		Page
Ananthasubrahmanyam, C. K.	See Narayan, A. L.	
Bagchi, N. ...	On the Width of K-absorption Edge of Cobalt	61
	The Secondary K-absorption Spectra of Sulphur	85
	See Roy, B. B.	
Bagchi, Haridas	A Geometrical Note on van der Waal's Equation	173
Banerjee, S. S.	Input Impedance of High-Frequency Parallel Wire Transmission Lines Immersed in an Absorbing Medium ...	13
Banerjee, S. S., and ... Paramanand	Variation of Field-strength in the Vicinity of an Ultra-short Wave Horizontal Transmitting Aerial	325
Banerjee, S. S., and Rao A. S.	Production of Ultra-high-frequency Radio Waves by Electronic Oscillations ...	93
Banerjee, A. C.	The Spiral Arms of a Configuration of rotating Compressible mass having uniform density and surrounding an incompressible Spheroid of homogeneous mass ...	67
Banerjee, K., and Ganguly, M.	Determination of the Structure of m-dinitrobenzene by Patterson Fourier Summation	231
Bhatnagar, P. L.	On the Origin of Solar System ...	253
Bhattacharya, G. N.	A Note on the Refractive Index of Shellac	237
	Specific Heat of Lac	415
Chakravarty, S. P. and Dutt, N. L.	On Wide Band-pass Effect in Crystals associated with negative Impedance elements and developments of wide-band low-loss crystal band-pass filters ...	295
Chatterjee, S. D.	Study of Thermal Neutrons in the Atmosphere	435
Choudhury, C.	See Khastgir, S. R.	
Chowdri, A. G., and	A Note on the Energy and Wavelength	

		Page
Singh, B. N.	Maximum in Fermi-Dirac and Bose-Einstein Distributions	387
Chowdri, A. G., and Kothari, D. S.	A Note on a new Method of Determination of "J"	409
Das, A. K., and Salaruddin, M.	Measurement of Cosmic Ray at Agra and Kodaikanal	191
Das, A. K.	Motion of Gases in the Sun's Atmosphere, Part I—On the Mechanism of Formation of Solar Dark-markings	369
Das, A. K., and Narayan, B. G.	An Apparent Influence of the Earth on Solar Prominences	311
Das, S. R. ...	See Ray, B. B.	
Deb, S. ...	A Note on the Origin of the D-layer ...	89
Deb, A. C. ...	Penetration of Thin Ionospheric Layers ...	151
Doraiswami, C. S. ...	See Narashimhaiya, R. L.	
Dutta, A. K. ...	Second Maximum of Rossi Curve ...	79
Dutt, N. L. ...	See Chakravarty, S. P.	
Ganguly, M. ...	See Banerjee, K.	
Ghose, S P. ...	Early Morning Variation of Ionisation and the true height of region F of Ionosphere	101
Ghosh, Chandrasekhar ...	Studies on Some Indian Vegetable Oils, Part V.—Temperature Effect on Gas Absorption and other Physical Properties	153
Ghosh, M. ...	Dynamics of Pianoforte String and the Hammer, Part IV—(Study of Duration of Impact)	475
Ghosh, M. ...	Dynamics of the Pianoforte String and the Hammer, Part V—(Some Special Theories)	489
Gogate, D. V., and Kothari, D. S.	Degeneracy in Non-Relativistic Bose-Einstein Statistics	21
Gupta, H. L., Jain, A. C., and Khanna, N. N.	Evaporation from Earthen Jugs ...	401
Jain, A. C. ..	See Gupta, H. L.	
Kar, K. C. ...	Theory of Compton Effect	117
Khanna, N. N. ...	See Gupta, H. L.	
Khastgir, S. R., and Choudhury, C.	On the Dielectric Constant of an Electronic Medium at Medium Radio Frequency	213

		PAGE
Khastgir, S. R., and Ray, Anil Kumar	On the Intensity Variation of the Down-coming Wireless Waves from the Ionosphere	283
Koteswaram, P. ...	Association of Acetic Acid in Non-Aqueous Solvents	333
	Molecular Association in Acetone and Methyl-ethyl-ketone	341
	Molecular Association as Studied by Raman Effect	353
Kothari, D. S. ..	See Chowdri, A. G.	
	See Gogate, D. V.	
Mahajan, L. D. ..	Adsorption of Moisture from the Moist Air by the Soils	441
Mitra, Sachindra Mohan	Splitting of Spectral Lines at Scattering by Liquids	
Narashimhaiya, R. L. and Doraiswami, C. S.	A new Technique for Determining Ultra-sonic Velocities in Liquids	187
Narayan, B G. ...	See Das, A. K.	
Narayan, A. L , and Ananthasubrahmanyam C. K.	A Precision Direct-reading Spectrophotometer	393
Paramanand ...	See Banerjee, S. S.	
Qureshi, M. ...	See Ranganadham, S. P.	
Rai, Ram Nivas ...	On Sources of Stellar Energy—A Criticism of Bethe-Gamow Theory ...	55
Ranganadham, S. P., and Qureshi, M.	Magnetic Susceptibilities of Sodium and Potassium Nitrates	129
Rao. A. S. ..	See Banerjee, S S.	
Rao, M. Rama ..	A Relation between Velocity of Sound in Liquids and Molecular Volume ...	109
Rao, I. Ramakrishna, and Rao, Y. Paramasiva	Mutual Influence of Water and Heavy Water	135
Rao, Y. Paramasiva .	See Rao, I. Ramakrishna.	
Rao, N. Rajeswara ..	Electrolytic Dissociation in Sulphuric Acid as Studies by Raman Effect ...	143
	Frequency Changes in Raman Spectra of Sulphuric Acid	359
Rao, A. L. Sundara ..	Raman Spectra of Sugar	207
	Effect of Temperature on Raman Spectra of Glycerin	365

		Page
Rao, M. Kameswar	High-frequency Measurements of the Amplification Factor and Internal Resistance of a Thermionic Valve ...	247
Rao, K. R., and Sastry, M. G.	The First spark Spectrum of Tellurium	423
Ray B. B., Das, S. R., and Bagchi, N.	Secondary K-absorption Edges of Cobalt Salts in Solid and Liquid Solutions ...	37
Ray, Anil Kumar ...	See Khastgir, S. R.	
Robinson, William H.	The Effect of an Electric Field of Strength $-\frac{1}{2}\alpha F^2$ on the Polorizability Constant of the Normal Hydrogen Atom ...	405
Salaruddin, M. .	See Das, A. K.	
Saha, Bishnupada ..	Rotational Raman Spectrum in Liquid Oxygen	123
Sastry, M. G. ..	Interferometric Measurements of certain Lines in the Spectrum of Bromine ...	429
	See Rao, K. R.	
Singh, B. N. ..	Joule-Thomson and Joule Effects for Bose-Einstein and Fermi-Dirac Gas ...	459
	See Chowdri, A. G.	
Yadav, Haribansh Narayan.	A Simple Laboratory Method of producing continuous Ultra-violet Light ...	169

SUBJECT INDEX

SUBJECT	AUTHOR	PAGE
Adsorption of Moisture from the Moist Air by the Soils.	L. D. Mahajan	441
Association of Acetic Acid in non-Aqueous Solvents.	P. Koteswaram	333
Association in Acetone and Methel-ethyl-ketone, Molecular.	P. Koteswaram	341
Compton-Effect, The Theory of	K. C. Kar	117
Cosmic Rays at Agra and Kodaikanal, Measurement of	A. K. Das and M. Salaruddin	191
Degeneracy in Non-Relativistic Bose-Einstein Statics.	D. V. Gogate and D. S. Kothari	21
D-layer, A Note on the origin of the	S. Deb.	89
Dielectric Constant of an Electronic Medium at Medium Radio-Frequency.	S. R. Khastgir and C. Choudhury	213
Evaporation from Earthen Jugs.	H. L. Gupta, A. C. Jain and N. N. Khanna	401
Fermi-Dirac and Bose-Einstein Distribution, A Note on the Energy and Wave-length Maximum in	A. G. Chowdri and B. N. Singh	387
Field-strength in the vicinity of an Ultra-short-wave Horizontal Transmitting Aerial.	S. S. Banerjee and Paramanand	325
First-spark Spectrum of Tellurium, The	K. R. Rao and M. G. Sastry	423
High-Frequency Parallel Wire Transmission Lines Immersed in an Absorbing Medium, Input Impedance of	S. S. Banerjee	13
High-Frequency Measurements of the Amplification Factor and Internal Resistance of a Thermionic Valve.	M. Kameswar Rao	247
Ionisation and the true height of region F of Ionosphere, Early Morning Variation of	S. P. Ghose	101
Indian Vegetable Oils, Studies on some, Part V-Temperature Effect of Gas Absorption and other Physical Properties.	Chandrasekhar Ghose	153

Subject	Author	Page
Interferometric Measurements of certain Lines in the Spectrum of Bromine.	K. R. Rao and M. G. Sastry.	423
Ionosphere, On the Intensity Variation of the Down-coming Wireless Waves from the	S. R. Khastgir and Anil Kumar Ray	283
Ionospheric Layers, Penetration of Thin.	A. C. Deb	451
'J', A Note on a New Method of Determination of	A. G, Chowdri and D. S. Kothari	409
Joule-Thomson and Joule Effects for Bose Einstein and Fermi-Dirac Gas	B. N. Singh	459
K-Absorption Edges of Cobalt Salts in Solid and Liquid Solutions, Secondary.	B. B. Ray, S. R. Das and N. Bagchi	37
K-Abosrption Edge of Cobalt, On the Width of	N. Bagchi	61
K-Absorption Spectra of Sulphur.	N. Bagchi	85
Magnetic Susceptibilities of Solutions of Sodium and Potassium Nitrates	S. P. Ranganadham and M. Qureshi	129
Mutual Influence of Water and Heavy Water	I. Ramakrisna Rao and Y. Paramasiva Rao	135
Pianoforte String and the Hammer, Dynamics of the, Part IV (Study of Duration of Impact).	M. Ghosh	475
Pianoforte String and the Hammer, Dynamics of the, Part V (Some Special Theories)	M. Ghosh	489
Polarizability Constant of Normal Hydrogen Atom, The Effect of an Electric Field of strength—$\frac{1}{2}\alpha F^2$	William, H. Rabinson	405
Raman Scattering in Liquid Oxygen, Rotational	Bishnupada Saha	123
Raman Effect, Electrolytic Dissociation of Sulphuric Acid as Studied by	N. Rajeswara Rao	143
Raman Spectra of Sugar	A. L. Sundara Rao	207
Raman Effect, Association as Studied by	P. Koteswaram	353
Raman Spectrum of Sulphuric Acid, Frequency Changes in	N. Rajeswara Rao	359
Raman Spectrum of Glycerin, Effect of Temperature on the	A. L. Sundara Rao	365
Refractive Index of Shellac, A Note on the,	G. N. Bhattacharya	237

Subject	Author	Page
Rossi Curve, Second Maximum of	A. K. Dutta	79
Scattering by Liquids, Splitting of Spectral Lines at	Sachindra Mohan Mitra	1
Solar System, on the Origin of	P. L. Bhatnagar	253
Solar Prominences, An Apparent Influence of the Earth on	A. K. Das and B. G. Narayan	311
Specific Heat of Lac	G. N. Bhattacharya	415
Spectrophotometer, A Precision Direct-reading	A. L. Narayan and C. K. Ananthasubrahmanyam	393
Spiral arms of a Configuration of rotating Compressible mass having uniform density and Surrounding an Incompressible Spheriod of Homogeneous mass, The	A. C. Banerjee	67
Stellar Energy, On Sources of,—A Criticism of Bethe-Gamow Theory	Ram Nivas Rai	55
Structure of m-dinitrobenzene by Patterson Fourier Summation, Determination of the	K. Banerjee and M. Ganguly	231
Sun's Atmosphere, Motion of Gases in, Part I. On the Mechanism of Formation of Solar Dark-markings.	A. K. Das	369
Thermal Neutrons in the Atmosphere, Study of	S. D. Chatterjee	435
Ultra-high-frequency Radio waves by Electronic Oscillations, Production of	S. S. Banerjee and A. S. Rao.	93
Ultra-sonic Velocities in Liquids, A new Technique for determining	R. L. Narashimhaiya and C. S. Doraiswami	187
Ultra-violet Light, A simple Laboratory Method of producing continuous.	Haribansh Narayan Yadav	169
van der Waal's Equation, A Geometrical Note on	Haridas Bagchi	173
Velocity of Sound in Liquids and Molecular Volume, A Relation between	M. Rama Rao	109
Wide band-pass effect in crystals associated with negative Impedance elements and development of wide-band low-loss crystal band-pass filters, On.	S. P. Chakravarti and N. L. Dutt	295

SPLITTING OF SPECTRAL LINES AT SCATTERING BY LIQUIDS *

By SACHINDRA MOHAN MITRA

Physics Laboratory, Dacca University

(Received for publication, December 3, 1939)

ABSTRACT. The fine structure of the Rayleigh line due to the molecular scattering in liquids has been investigated with a F P etalon and the two fine structure components are identified, the higher component reported by Gross being absent. The question of the reality of the red shift of the Rayleigh line observed by Cabannes and his co-workers with a F. P. etalon has also been examined and it has been shown that there is no such red shift.

The observed values of the shifts of the displaced components from the central ones were always found to be greater than the values calculated from the Brilouin's equation.

The dependence of the frequency shifts of the splitted components from the central main-lines, on the following has also been investigated :-

(a) The frequency of the incident light.

(b) Angle of the scattering.

The influence of temperature on the splitted components has also been examined and it is found that the splitted components become fainter and broader, gradually merging with the central undisplaced components as the temperature of the liquid is raised The intensity of the central components also is gradually increased. On the other hand, opposite effects were observed on lowering the temperature of the liquid.

The state of polarisation of the three components was also examined. The results indicate that all of them are completely polarised

INTRODUCTION

It is now well known that the molecules of a gas are capable of three types of movements, namely, translational, rotational and vibrational movements. When a beam of monochromatic light passes through a gaseous medium and is scattered by it, each of the aforesaid movements are capable of giving rise to changes of frequency in the scattered radiation, *viz.*, a Doppler effect due to the translatory motion of the molecules of the gases and Raman effect due to their rotations and vibrations respectively. The Doppler effect, generally, shows its presence in the form of a simple Maxwellian broadening of the lines in the scattered spectrum; the broadening would be a function of the angle of observation, being zero in the direction of the incident light and maximum in the reverse direction.

* Part of a thesis approved for the D.Sc. degree, Dacca University, 1938.

But when we pass from the case of a gaseous medium to that of a liquid, various complications arise from the fact that the positions and the velocities of the molecules are no longer distributed "at random" and as such it is not possible to regard the molecules as being completely independent scattering centres. The nature of the Doppler effect expected in such a medium would naturally be complex. An insight into the nature of the Doppler effect in liquids was furnished by the theory of the light scattering originally put forward by Einstein.[1] In his theory the molecular structure of the scattering medium is ignored and fluctuation of density are regarded as arising in it from the presence of sound waves of various wavelengths associated with the thermal energy of the medium. These sound waves produce stratifications in the optical density of the medium and give rise to a selective scattering in directions determined by the wavelength of the incident light and of the reflecting sound wave.

Later Brillouin [2] pointed out that on this view, the light reflected by the trains of sound waves should exhibit a Doppler effect which would take the simple form of a doubling of the lines in the incident spectrum, the frequency of the splitted components being given by the relation

$$\nu=\nu_0 \pm 2\nu_0 \frac{v}{c} \sin \theta/2 \qquad \ldots \qquad (1)$$

where v and c are the velocity of the sound and of light in the medium, θ the angle of scattering, ν_0 the frequency of the incident light.

A similar relation was also deduced by Mandelstam[3] from a somewhat different consideration. The possibility of a change in light frequency according to the equation of Brillouin was also pointed out by Rocard & Bogros.[4]

During the last few years a large number of workers reported the results of their investigations on the subject of the fine structure of the Rayleigh radiation in liquids, but their results are highly contradictory as will be evident from the following. Cabannes,[5] while investigating the nature of the Rayleigh scattering in liquids and gases with a Fabry-Parot etalon, claimed to have observed a shift of the Rayleigh lines at scattering towards the greater wavelength, generally designated as "Cabannes red shift." Very similar results were also obtained by Vacher [6] with a F. P. etalon. Later Gross,[7] working with a Lummer Plate, found the splitting of the incident spectral line at scattering by the liquids, *i.e.*, a line in the position of the incident radiation accompanied by a series of components symmetrically situated on either side of the central line. The frequencies of these components were found to satisfy the relation

$$\nu=\nu_0 \pm 2n\nu_0 \frac{v}{c} \sin \theta/2 \qquad (2)$$

where $n = 1, 2, 3 \cdots\cdots\cdots$, and ν_0 the frequency of the incident radiation. But Rafalowski,[8] working with Lummer Plate, was unable to observe either the "Gross splitting" or the "Cabannes red shifts." Mayer and Ramm [9] and later Ramm,[10] working with an etalon grating, claimed to observe the first Gross components on either side of the central undisplaced line but could not detect the other components as reported by Gross. In view of the unsatisfactory state of the subject we undertook a systematic study of the subject using a Fabry-Parot etalon. The choice of this instrument was guided by the fact that those who used the same were unable to observe the Gross splitting but instead some found the Cabannes red shift—a fact which is rather very perplexing. In our investigation,[11] in all the cases of the liquids we have found the splitting as reported by Gross, the first components corresponding to $n = \pm 1$ in (2) being alone present. We were unable to find either the higher components or the red shift. Simultaneously with our investigation Rao[12] and Khvostikov[13] all independently claimed to have been able to observe the Gross splitting with a Fabry-Parot etalon.

The present paper gives a detailed report of our investigation under the following heads :—

A. How far the value of the shifts $\nu - \nu_0$ as observed agree with the value calculated from the Brillouin's equation.

B Dependence of $\Delta\nu = \nu - \nu_0$ on the angle of scattering.

C. Dependence of $\Delta\nu$ on the wave-length of the incident light.

D. Influence of temperature.

E. The nature of the polarisation of the splitted components as well as of the central undisplaced components.

EXPERIMENTAL ARRANGEMENTS

The experimental arrangement, at first adopted in our experiment, is practically the same as that employed by Cabannes and his co-workers. The arrangement is shown in figure 1 which will speak itself. Light from a cooled mercury arc is condensed with a lens through the window w, on to the centre of two horn-shaped cross-tubes containing the liquid under investigation. The radiation scattered at right angles condensed on to the slit of a spectrograph by lenses after has passed through the Fabry-Parot etalon. In the cases of the observations at angles 135° and 45° cross-tubes of the forms given in figurss 2 and 3 were employed. For the observations at 180°, we have followed the experimental arrangements of Mayer and Ramm.[9, 10]

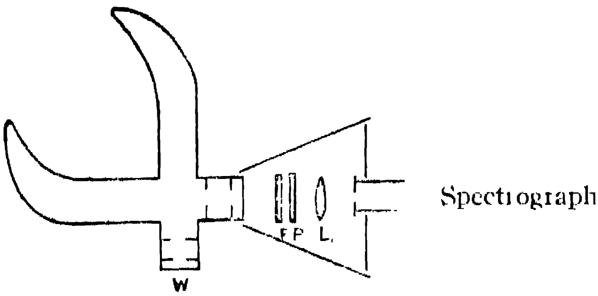

FIGURE 1.

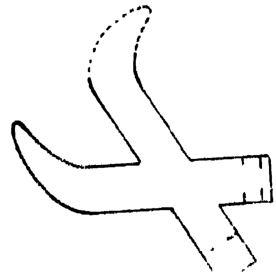

FIGURE 2.

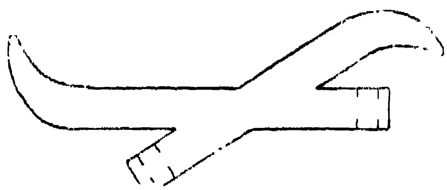

FIGURE 3.

In some cases we also employed the following arrangement. The repeatedly vaccum distilled liquid was contained in a horizontal Wood tube. A parallel beam of light from a horizontal mercury arc lamp was made to illuminate the side of the Wood-tube along its axis by means of a big lens. The interference rings system was focussed on to the slit of the spectrograph. In order to remove the possibility of stray light getting into the F. P. etalon a cone-shaped cap was placed on the observation side as shown in the figure. The Wood tube was surrounded by another tube and cold water at the laboratory temperature was continually circulated through the annular space by means of a small circulating pump in order to maintain the temperature of the liquid constant. We have employed the spectrograph in conjunction with the F. P. etalon because of its great advantage that the interference patterns of a number of lines could be photographed at a time on the same plate.

In the case of the polarisation measurements a large square-ended nicol is placed between the observation side of the cross-tube (Fig. 1) or the Wood tube and the F.P. etalon—the fringes being focussed on the slit of the spectrograph by another lens. Two separate spectra were recorded in each case, one with the nicol having its vibration axis vertical and another with the vibration axis horizontal.

The interference patterns of the three lines λ4358, 4078 and 4047A were examined and the displacements of the new-splitted components measured without any confusion arising from the presence of the hyperfine structures components.

HOW FAR THE VALUES OF THE SHIFT $\Delta\nu$ AGREE WITH THAT CALCULATED WITH HELP OF THE BRILLOUIN'S EQUATION ?

We have studied the scattered radiations with the F.P. etalon in the case of a large number of liquids—benzene, toluene, carbon tetrachloride, carbon disulphide, methyl alcohol, cyclohexane, cyclohexanol, etc., with a view to finding out how far the value of the shifts $\Delta\nu$ agree with those calculated from the Brillouin's formula. For if a complete agreement between the calculated and the observed value of the shifts $\Delta\nu$ be obtained, then this splitting of the spectral lines at scattering by liquids gives us an optical method for the determination of the velocity of sound in liquids.

In all the cases of the liquids—as already mentioned—we have found the splitting as reported by Gross, *the first component corresponding to $n = \pm 1$ being alone present.* The higher components observed by Gross were totally absent. *The Cabannes red shifts were also never observed.* The values of the shifts are given in the following table 1. The values of $\Delta\nu$ calculated from the Brillouin's equation

$$\Delta\nu = 2\nu_o \frac{v}{c} \sin \theta/2$$

are also included in the tables

TABLE I

Angle of Observation = $\pi/2$

Wavelength of the incident light = 4358 A

Liquids		$\Delta\nu$ in cm.$^{-1}$		
		Observed.	Calculated.	Difference.
Benzene	...	·237	·206	·031
Toluene	...	·235	·214	·021
Carbon tetrachloride	...	·177	·154	·023
Carbon disulphide	...	·239	·211	·028
Methyl alcohol	...	·194	·170	·024
Chlorobenzene		·237	·214	·023
Cyclohexane	...	·213	·192	·021
Cyclohexanol	...	·289	·265	·024

The values of $\Delta\nu$ as observed are always found to be greater than that calculated from the formula, the difference being shown in column 4. In these calculations the experimental values for the velocity of sound obtained chiefly by Kundt tube method were employed. The velocity of sound calculated from the coefficient of compressibility and density of the liquids also do not give values of $\Delta\nu$ which are in agreement with the observed values of $\Delta\nu$.

TABLE II

Angle of Observation $= \pi$
Wavelength of the incident light $= 4357$A

Liquid		$\Delta\nu$ in cm.$^{-1}$ Observed.	Calculated.	Differences
Benzene	..	·332	·295	·037
Carbon tetrachloride	...	·248	·211	·027

Such a difference between the observed and the calculated values has also been observed by Gross* and Mayer and Ramm with a Lummer Plate. But Rao working with F.P. etalon reported fair agreement within the errors of measurements. Their values are given below together with ours in table 3.

TABLE III

Benzene
Angle of scattering $= \pi$
Wavelength of the incident light $= 4358$A

Authors.		$\Delta\nu$ in cm.$^{-1}$ Calculated.	Observed.	Difference.
Mayer and Ramm	...	·295	·326	·031
Rao	...	,,	·306	·011
Mitra	...	,,	·332	·037

It is evident from the above table that our values agree with those of Mayer and Ramm rather than with Rao's.

* Gross in his earliest communication reported complete agreement between the calculated and observed values, but later on he observed a difference.

In all the cases of the liquids, there was a continuous background superimposed on the interference patterns. The intensity of this continuous background was most intense in the case of carbon disulphide and cyclohexanol and very feeble in the case of carbon tetrachloride. This intense continuous background radiation made the distinct reproduction of the spectrograms impossible.

The width of the displaced and unshifted components as well as their intensities were not the same for the different liquids. The width is less in carbon disulphide, carbon tetrachloride, toluene, which gave shifted components very distinct. Methyl alcohol, cyclohexanol and cyclohexane gave rather diffused components whereas the width in the case of benzene was midway between the aforesaid two classes. Here it is to be noted that we have been able to observe splitting in the case of viscous liquid, cyclohexanol, which is very significant in the face of the result obtained by the Raman and Rao [11] and by Raman and Venkataswaran.[15]

The intensities of the displaced components in the case of carbon tetrachloride were most intense.

According to the Brillouin theory, the central unmodified lines (corresponding to $n=0$ in equation 2) should not be present in the liquids. But they were observed in our investigations with all the liquids. The intensity of this central undisplaced component was most intense in the case of carbon tetrachloride, showing that its presence is not to be primarily ascribable to the optical anisotropy of the liquid.

DEPENDENCE OF THE SHIFT $\Delta\nu$ ON THE WAVELENGTH OF THE INCIDENT LIGHT

Brillouin theory points out that the frequency shifts should depend on the frequency of the incident light. Here we experimentally attempted to observe whether the shifts do depend on the incident frequency.

The following tables give the results of our investigation. It might be noted here in passing that our values of $\Delta\nu$ in the case of CCl_4 agree with those of Rao,[10] who has recently redetermined them using improved technique.

TABLE IV

Angle of scattering $=\pi$

Liquid.	Wavelength.	Observed.	Calculated.	Difference
Benzene	4358	·332	·295	·037
	4078	·348	·315	·033
	4047	·251	·318	·033
Carbont etrachloride	4358	·248	·321	·027
	4078	·258	236	·022
	4047	·264	238	·026

We have also calculated the differences of the shifts $\Delta\nu$ for $\lambda 4047$ and $\lambda 4358$ for benzene and carbon tetrachloride, the following gives the result.

TABLE V

Difference between the shifts $\Delta\nu$ for $\lambda 4047$ and 4358A

Angle of scattering $=\pi$

Liquid.	$\Delta\nu$ in $cm.^{-1}$ Observed.	$\Delta\nu$ in $cm.^{-1}$ Calculated.
Benzene	·019	·023
Carbon tetrachloride	·016	·017

Measurements were also made at 90° angle of scattering; the following gives the results of our measurements.

TABLE VI

Angle of scattering $=\pi/2$

Liquids.	Wavelength.	$\Delta\nu$ in $cm.^{-1}$ Observed.
Benzene ...	4358	·237
	4078	·249
	4047	·241
Carbon tetrachloride ..	4358	·177
	4078	·190
	4047	·194
Carbon disulphide ...	4358	·239
	4078	·259
	4047	·264
Cyclohexane ...	4358	·213
	4078	·224
	4047	·231

The foregoing results conclusively show experimentally that the frequency shifts of the splitted Gross components depend on the frequency of the incident light. Here also we find that the calculated and observed values do not agree whatever be the incident wavelength, and the difference between the calculated and observed values is nearly the same for all the wavelengths of the incident light.

VARIATION OF THE SHIFTS $\Delta\nu$ ON THE ANGLE OF SCATTERING

In our present investigation we have also examined the scattered radiation at the different angles of scattering in order to study the variation of the shifts with the angles of scattering. We may here point out that the Brillouin's equation points out that $\Delta\nu$ varies with the angle of scattering.

The following table gives the values of the shifts for the four angles of scattering. We do here also find a great dependence of the amount of the shifts of the Gross components on the angle of the scattering, as would be expected from the Brillouin's equation.

TABLE VII

Wavelength of the incident light=4358A

Liquids.	$\Delta\nu$ in cm.$^{-1}$		Observed.		$\dfrac{\Delta\nu_{180^\circ}}{\Delta\nu_{90^\circ}}$	
	180°	135°	90°	45°	Observed.	Calculated
Benzene	·332	·289	·237	·149	1·42	1·42
Carbon disulphide	·328	·292	·239	150	1 38	1·42
Carbon tetrachloride	·248	—	·177	—	1·40	1·42
Chlorobenzene	·335	·268	·237	—	1·41	1·42
Toluene	·316	·270	·235	—	1·35	1·42
Methyl alcohol	·274	—	·194	—	1·41	1·42
Cyclohexane	·302	—	·213	—	1·41	1·42
Cyclohexanol	·407	·318	·289	—	1·41	1·42

According to the formula the ratio of the amounts of the shifts at 180° and 90° is equal to the ratio of the sine of 90° and 45°, *i.e.*, $\dfrac{\Delta\nu_{180^\circ}}{\Delta\nu_{90^\circ}}=\dfrac{\sin 90^\circ}{\sin 45^\circ}=1{\cdot}42$; this fairly agrees with the values calculated from the observed shifts, as is shown in the aforesaid table.

INFLUENCE OF TEMPERATURE

We have also examined in our present investigation the influence of temperature on the Doppler components. Besides the data collected by Rao and Raman[17] and Rao [18] very little work seems to have been done in this direction. Moreover their results are more or less of qualitative nature. In view of the expectation that the results obtained in the study of the influence of temperature might lead to interesting points we carried out an investigation on the influence of temperature on the Gross components in benzene, carbon tetrachloride, toluene.

In the case of the present measurements, the experimental arrangements are as follows. The liquid under observation was contained in the wood tube, which was contained in a bath, the temperature of which can be varied at ease.

For the measurements at the higher temerature the liquid (water) in the bath was heated electrically by a small nichrome spiral immersed in it. By regulating the current through the nichrome wire, the temperature of the bath may be made constant to any desired point. In case of the low temperature measurements, the bath contained iced water. An accurate thermometer in the wood tube served to measure the temperature Our results are summarised below

The spectrum of the light scattered by the aforesaid liquid at the ordinary temperature (28°-30° C) shows the Doppler components more or less distinctly on either side of the central unshifted line when examined through the F P. etalon in all the cases of the liquids examined. But as the temperature is gradually raised the following changes take place.—

(*a*) The amount of the shifts $\Delta\nu$ decreases gradually.

(*b*) The Doppler components become fainter and broader, ultimately merging with the central component.

(*c*) The intensity of the central components gradually increases.

On the other hand, when the temperature is gradually lowered the following opposite changes were observed :—

(*a*) The amount of the shifts increases gradually.

(*b*) The Doppler component, on either side of the central line, become more sharp and intense.

(*c*) The intensity of the central camponent gradually decreases.

ON THE POLARISATION OF THE DOPPLER COMPONENTS

In our present investigation we have measured the state of polarisation of the splitted as well as of the undisplaced component in the case of the liquids cyclohexane, cyclohexanol, methyl alcohol.

Previously, Gross [19] also investigated the nature of the polarisation of the displaced and undisplaced components in the case of carbon tetrachloride and benzene. He found that while the two Brillouin components were completely polarised, as is to be expected theoretically, the central undisplaced component was also completely polarised. His conclusion was later confirmed by Rao.[20]

In our investigations in all the liquids examined we observed that all the three components are completely polarised, as was reported by the aforesaid workers.

In conclusion the author thanks Prof. S. N. Bose and Mr. S. K. Mukherjee for their kind interest in the work.

REFERENCES

1 Einstein, *Ann. der. Phys.*, **33**, 1275 (1910).
2 Brillouin, *Ann. der. Phys.*, **17**, 88 (1922).
3 Mandelstam, *Jour. Russ. Phys. Chem. Ges.*, **58**, 831 (1926).
4 Rocard & Bogros, *Jour de Phys. et le Rad.* **10**, 72 (1929).
5 Cabannes, *Trans. Faradey Soc.*, **25**, 813 (1929).
6 Vacher, *Compt. Rend.*, **191**, 1121 (1930).
7 Gross, *Zeit. fur Phys.*, **63**, 685 (1930); *Nature*, **126**, 209, (400); **129** 603 (1930), 722 (1932).
8 Rafalowski, *Nature*, **128**, 495 (1931).
9 Mayer & Ramm, *Phys. Zeit.*, **33**, 270 (1932).
10 Ramm, *Phys. Zeit.*, **35**, 111 (1934).
11 Mitra & Mehta, *Ann. der. Phys.*, **22**, 311 (1935).
12 Rao, *Proc. Ind. Acad. Sci*, **1**, 261, 478 (1934-35)
13 Khvostikov, *Phys. Zeit. der Sov. Union*, **6**, 343 (1934).
14 Raman & Rao, *Nature*, **139**, 585 (1937); **141**, 242 (1938).
15 Raman & Venkataswaran, *Nature*, **142**, 791 (1938)
16 Rao, *Nature*, **139**, 885 (1937); *Proc. Ind. Acad. Sci.*, **7**, 163 (1938)
17 Rao & Raman, *Nature*, **135**, 761 (1935).
18 Rao, *Proc. Ind. Acad. Sci.*, **1**, 765 (1935).
19 Gross, *l.c.*
20 Rao, *Proc. Ind. Acad. Sci.*, **2**, 236 (1935), 3, 607 (1936).

INPUT IMPEDANCE OF HIGH-FREQUENCY PARALLEL WIRE TRANSMISSION LINES IMMERSED IN AN ABSORBING MEDIUM *

By S. S. BANERJEE, D.Sc.,

Benares Hindu University

(Received for publication, December 21, 1939)

ABSTRACT. The input impedance of high frequency parallel wire transmission lines, quarter wavelength long, has been mathematically calculated when the lines are immersed in an absorbing medium. The calculated values have been verified by actually determining the impedance of such lines immersed in dry soil. The impedance has been determined for lines short-circuited at their far ends and also when these ends are open. The method of performing the experiments has been described. The measurements have been made within the frequencies of 31 megacycles / sec to 114 megacycles / sec. The results obtained have been compared with those when there is no absorbing medium between the two parallel wires. It has been observed that within the range of the frequencies employed for observations, the input impedance of such system of quarter-wave lines remains nearly equal to the surge impedance of the lines at higher frequencies, when the attenuation is fairly high, for both open as well as close terminated lines. It tends to increase as the frequency is lowered and the attenuation constant is below 3×10^{-2}, in the case of the lines with short-circuited termination. For the open-ended lines however, the impedance decreases as the frequency is reduced.

INTRODUCTION

Parallel-wire high frequency transmission lines have gained a very wide application within the last decade in connection with communications by means of ultra-short radio waves. In most of the cases, such lines have been used for the purpose of transferring energy from one part of the apparatus to the other or as an impedance matching transformer. Recently, however, such transmission lines have been employed by the present author and his collaborators (1,2,3) for the determination of various electrical constants of an absorbing medium like soil and ionized gas at ultra-high frequencies. In whatever form the transmission lines may be used, the knowledge of input impedance of such a system is essential for proper functioning of the lines. The impedance of such lines for different lengths, when placed in air, has been worked out by various authors (4,5) but attention has not been directed to its effective value when the lines are immersed in an absorbing medium. In the present paper the input impedance of parallel-wire high-frequency transmission lines, quarter-wavelength long, with

* Communicated by the Indian Physical Society.

open as well as short-circuited terminations, has been worked out mathematically and the values thus obtained have been verified experimentally. The results have been compared with those when there is no absorbing medium between the wires The medium used was well-sieved dry soil as employed in the previous experiments (1) for the determination of electrical constants of soil. The observations were made with the frequencies between 31 megacycles per second to 114 megacycles per second.

THEORY

The input impedance of a system of parallel wire transmission lines is given by,

$$Z_i = \left[\frac{Z_a \cosh l\,(A+jB) + Z_o \sinh l\,(A+jB)}{Z_o \cosh l\,(A+jB) + Z_a \sinh l\,(A+jB)}\right] \qquad (1)$$

where,
A = Attenuation constant,
B = Wavelength constant,
Z_o = Surge impedance of the lines,
Z_a = Impedance at the far end of the lines,
l = Geometrical length of the lines.

Let us now consider the condition when there is enough absorption due to the presence of soil or any such medium between the two wires, so that the attenuation may not be neglected. By expanding the terms in equation (1) and after further simplification, we get,

$$Z_i = Z_o \left[\frac{Z_a\{\cosh lA \cos lB + j \sinh lA \sin lB\} + Z_o\{\sinh lA \cos lB + j \cosh lA \sin lB\}}{Z_o\{\cosh lA \cos lB + j \sinh lA \sin lB\} + Z_a\{\sinh lA \cos lB + j \cosh lA \sin lB\}}\right] \qquad \ldots \quad (2)$$

For the sake of convenience, lines quarter-wavelength long have been used for the measurements and therefore, the impedances for such lengths only have beed discussed below.

For lines quarter wavelength long, we have $lB = \pi/2$ and substituting this value of lB in equation (2), the input impedance of the lines will be given by,

$$Z_i = Z_o \frac{Z_a \sinh lA + Z_o \cosh lA}{Z_o \sinh lA + Z_a \cosh lA} \qquad (3)$$

The input impedance of the lines for two terminal conditions have been considered. First, when the line is short-circuited at its far end and the second when it is terminated with open ends.

Case (1). Quarter-wave long transmission lines with short-circuited termination.

When the line is short-circuited at its far end, the terminal impedance $Z_a = 0$. and substituting this value of Z_a in equation (3), the input impedance of

the line will be given by,

$$Z_i = Z_0 \coth (A\lambda/4) \qquad \ldots \quad (4)$$

Some interesting points may be noted in equation (4). When attenuation is large, which is true for most of the practical cases at higher frequencies, we have the input impedance nearly equal to the surge impedance of the line. But when there is no absorbing medium between the parallel wires, we have the input impedance, $Z_i = \infty$, obtained from the well-known relation $Z_i = Z_0^2/Z_a$. Thus we may conclude that whenever there is an absorbing medium between the line wires, the input impedance of the line, quarter-wavelength long and short-circuited at the far end, ceases to be very high and for most of the practical purposes it is equal to the surge impedance of the line. This has been experimentally verified as shown in the later section.

Case (2). Quarter-wave long transmission lines with open-circuited termination.

In this case the terminal impedance of the lines, $Z_a = \infty$. Substituting this value of Z_a in equation (3), the input impedance of the line will be given by,

$$Z_i = Z_0 \tanh (A\lambda/4) \qquad \ldots \quad (5)$$

It will be observed from equation (5) that for greater attenuation, the impedance of such line becomes equal to the surge impedance of the line. When there is no absorbing medium between the line wires, the input impedance of such line vanishes. The values of the input impedance calculated from equation (5) were verified experimentally as shown later.

It will be further noted from equation (3) that when the quarter-wave line immersed in soil is terminated at its far end with a resistance equivalent to the surge impedance, Z_0, of the line, the input impedance remains equal to the surge impedance under all conditions. This is similar to the case of the line without being immersed in an absorbing medium.

EXPERIMENTAL ARRANGEMENTS AND OBSERVATIONS

The soil after being properly sieved was kept in an open, rectangular, long wooden box of dimensions, 250 cm. × 11 cm. × 10 cm. with two smaller sides made of ebonite. Two bare copper wires, no. 14 s.w.g., were fixed on one of the small ebonite sides with binding screws and the wires were made tight and to run parallel along the length of the box. They were terminated on the other small ebonite side and were attached to two adjustable hooks for proper tension. The wires were placed 5 cm. apart from each other. When the measurements were taken with lines closed at its far end, the line wires were short-circuited with a metal bridge M (Fig. 1) at that end. The line wires LL were completely covered with soil pressed by its own weight. The wires could be connected by means of a double-pole double-throw switch S to a small variable micro-condenser C, an inductance loop loosely coupled with a valve-generator G and a radio-frequency

thermo-galvanometer T. The valve-generator could emit out waves of lengths 2 metres to 10 metres as required by the experiment.

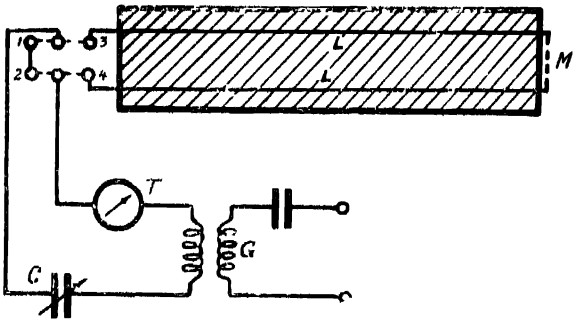

FIGURE 1

The switch S is thrown on the terminals 1, 2 (Fig. 1) and the circuit is tuned for resonance at the particular frequency generated by the valve oscillator with the help of the variable condenser C. The switch is then thrown on 3, 4 and again the resonance capacity is observed in the micro-condenser. The resonance conditions are observed by the maximum response in the thermo-galvanometer. If C_1 and C_2 be the two values of the capacities at resonance, the line impedance is computed from $\omega C_1 \quad \omega C_2$, where ω is the angular frequency of the waves.

As the values of the capacities C_1 and C_2 were both small, being only some fraction of the micro-condenser itself, the exact magnitudes of these were determined by a separate Lecher wire system with the same frequencies at which the observations were taken for finding out the resonance capacities. The micro-condenser was connected to one end of a pair of Lecher wires and positions of current antinodes were observed by a thermo-galvanometer. The capacity was calculated as shown below, from the difference between the length measured from the end containing the condenser to the first antinode and the length between two consecutive antinodes. If the difference in the length is denoted by δl, the unknown capacity C_x can be calculated from the relation,

$$C_x = \frac{lC}{\pi} \tan \frac{\pi \delta l}{l}$$

where l = distance between two consecutive antinodes,

C = capacitance of the Lecher wires.

A calibration graph was drawn from different values of the micro-condenser C from which any value of C_x could be determined knowing the corresponding value of δl. The attenuation constant of the soil was measured at different frequencies by the method applied by us (1) in the previous experiments on electrical constants of soil.

Table I below gives the attenuation constants determined at the wavelengths used in the experimental investigation.

Surge impedance of the line = 470 ohms

TABLE I

Frequency in megacycles/sec.	Attenuation constant.
113·64	$9{\cdot}68 \times 10^{-2}$
93·75	6·41 ,,
81·08	5·38 ,,
69·42	4·21 ,,
63·16	3·15 ,,
57·91	2·12 ,,
49·83	1·01 ,,
40·00	$6{\cdot}20 \times 10^{-3}$
32·61	4·10 ,,

Table II below gives the input impedance of the transmission lines immersed in soil, quarter-wavelength long and short circuited at the far end. Table III gives the same for transmission lines terminated with open ends. Second column of these tables shows the calculated values and the third column indicates the observed ones.

TABLE II

Frequency in megacycles/sec.	Input impedance in ohms calculated from $Z_s = Z_0 \coth\,(A\lambda/4)$	Input impedance in ohms observed experimentally.
113·64	470·0	461·4
93·75	470·0	466·7
81·08	470·0	455·4
69·42	470·1	452·8
63·16	470·7	479·6
57·91	473·3	479·6
49·83	518·2	532·2
40·00	572·5	596·8
32·61	639·5	632·0

TABLE III.

Frequency in megacycles/sec.	Input impedance in ohms calculated from $Z_i = Z_0 \tanh(A\lambda/4)$.	Input impedance in ohms observed experimentally.
113·64	470·0	463·6
93·75	470·0	474·3
81·08	470·0	462·8
69·42	469·9	459·4
63·16	469·3	455·8
57·91	466·1	455·0
49·83	426·3	410·3
40·00	385·9	404·6
32·61	345·4	312·3

Comparing the values of attenuation constant from Table I with those of the impedance of the lines given in Tables II and III for the same frequencies, it will be observed that for higher frequencies, when the attenuation is considerable, the impedance of the quarter-wave long transmission lines with open as well as closed terminations, remains equal to the surge impedance of the lines. As the frequency is lowered till the attenuation constant goes below 3×10^{-2}, the impedance of the lines with closed termination gradually increases and that of the line with open termination decreases.

The variations of input impedance of quarter-wave long transmission lines for short-circuited and open-circuited terminations, when they are immersed in soil, have been shown graphically in Figs. 2 and 3 respectively. The continuous

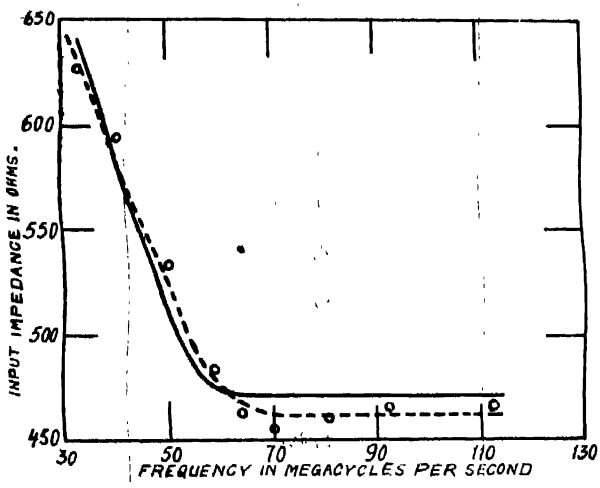

FIGURE 2

lines have been drawn from the calculated values and dotted ones from the experimentally observed results.

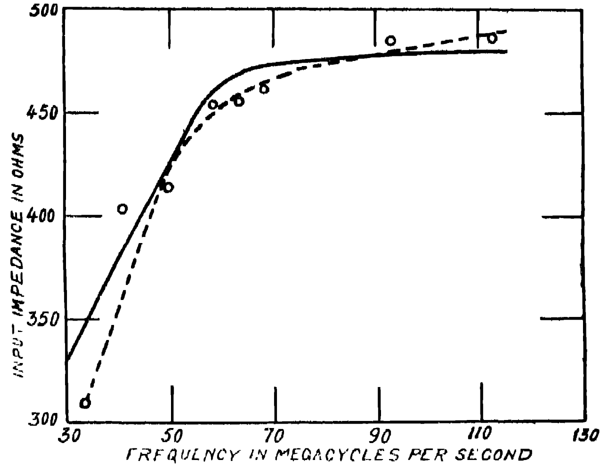

FIGURE 3

SUMMARY AND CONCLUSIONS

The input impedance of parallel-wire high-frequency transmission lines quarter-wavelength long has been mathematically calculated and verified by experiments. Lines have been used with their far ends open and also when they are short-circuited. Results obtained have been compared with those when the lines are not immersed in an absorbing medium. The frequencies used for the purpose of measurement of the impedance were between 31 megacycles/sec. to 114 megacycles/sec. It has been observed that within this range of frequencies the input impedance of quarter-wave long transmission lines with open as well as closed terminations remains nearly the same as the surge impedance of the lines at higher frequencies, when the attenuation is considerable. At lower frequencies, however, when the attenuation constant decreases below 3×10^{-2}, the impedance of the lines with far ends short-circuited, increases as the frequency is lowered. For lines with open termination, the impedance decreases as the frequency is reduced.

The author desires to express his thanks to Dr. B. Dasannacharya, Head of the Department of Physics, for giving all possible facilities during the course of the above investigations.

WIRELESS SECTION,
PHYSICS LABORATORY,
BENARES HINDU UNIVERSITY.

REFERENCES

[1] Banerjee, S. S. and Joshi, R. D., *Phil. Mag.*, **25**, 1025 (1938).
[2] Banerjee, S. S. and Singh, B. N., *Nature*, **141**, 511 (1938).
[3] Singh, B. N., *Phil. Mag.*, **26**, 244 (1938).
[4] Roder, H., *Proc. Inst. Rad. Eng.*, **21**, 290 (1933).
[5] Walmsley, T., *Phil. Mag.*, **22**, 1054 (1936).

DEGENERACY IN NON-RELATIVISTIC BOSE-EINSTEIN STATISTICS

By D. V. GOGATE

AND

D. S. KOTHARI

(University of Delhi)

(*Received for publication, Jan. 9, 1940*)

ABSTRACT. Simple and direct proofs (substantially following Kennard and Condon) are given of the three distribution laws, *viz.*, Maxwell-Boltzmann, Fermi-Dirac and Bose-Einstein distribution. The properties of Bose-Einstein degenerate gas are discussed and compared with those of Fermi-Dirac degeneracy.

The thermal anomaly exhibited by helium at 2·19° Abs.—generally known as the λ-point*—has been the subject of many investigations during recent years. At this temperature helium shows a discontinuity in its specific heat, indicating a characteristic type of phase transition.† It has been found that its viscosity decreases suddenly at the λ-point, and the entropy difference between the liquid and the solid phase tends towards zero with decreasing temperature, showing that the liquid phase goes into a peculiar state below the λ-point. Recently Allen and Jones [1] have discovered that a transfer of momentum accompanies heat flow (the so-called fountain effect) in He II while Daunt and Mendelssohn's investigations [2] show that a large part of the heat must be carried by some form of material transport.

These unusual characteristics of liquid helium II have led F. London [3] to propose a new theory based on a peculiar condensation phenomenon of an ideal Bose-Einstein gas mentioned by Einstein [4] some years ago in his well-known papers on the degeneracy of an ideal gas. This interesting discovery of Einstein, however, was seriously questioned and adversely criticised by Uhlenbeck [5] and remained buried in Einstein's papers for many years. The credit of resuscitating it goes to F. London [6] who not only proved the correctness of Einstein's view but has also applied it in formulating a theory of condensation mechanism which has established, for the first time, the connection of Bose-Einstein degene-

* The λ-point temperature decreases with increase of pressure (about 1/50°C per atmosphere). When the pressure is increased to about 25 atmospheres, liquid He II passes into the solid state.

† See Ehrenfest, *Text-book of Thermodynamics*, 1937, pp. 128-133.

racy with the problem of liquid helium. Uhlenbeck [7] also has now withdrawn his former objection to Einstein's suggestion.

According to F. London He II may be regarded as a degenerate Bose-Einstein gas, *i.e.*, as a system in which one fraction of the substance is distributed over the excited states in a way determined by the temperature while the rest is condensed in the lowest energy level. If N_0 denotes the number of atoms condensed in the lowest energy state and $(N-N_0)$ the number of energetic particles, *i.e.*, the particles distributed over the excited states, then

$$\frac{N_0}{N}=\left[1-(T/T_0)^{\frac{3}{2}}\right]$$

where T_0 indicates the "temperature of degeneracy." The phenomenon of Bose-Einstein degeneracy has received only a desultory attention so far, partly because it appeared to be devoid of any practical significance, all real gases being condensed before the temperature T_0 and also because the magnitude of the various physical effects, *e.g.*, Joule-Thomson effect, Effusion, Thermal transpiration, etc., exhibited by an ideal Bose-Einstein gas is extremely small. However, the very smallness of an effect adds to it, at times, a special importance and interest. It will therefore be not altogether useless—and particularly because of the recent attempts at the application of degenerate Bose-Einstein statistics to the problem of He II—to discuss the phenomenon of Bose-Einstein degeneracy in detail, contrasting it with Fermi-Dirac degeneracy and (classical) non-degeneracy. The present paper is mainly intended to serve as a necessary background for subsequent papers dealing with physical properties of degenerate Bose-Einstein gas. We accordingly begin with a simple proof (substantially following Kennard [9] and Condon [8])* of the three distribution laws, *viz.*, Maxwell-Boltzmann, Bose-Einstein and Fermi-Dirac distribution. The second section is devoted to the derivation of expressions for the number and energy of particles of an ideal Bose-Einstein gas in the state of degeneracy as well as non-degeneracy. The continuity of the energy curve from the non-degenerate to the degenerate region, the discontinuity of the specific heat at $T=T_0$ and the dependence of pressure on concentration are discussed in the third section and expressions for entropy (non-degenerate and degenerate) are also derived in the end.

1. THE DISTRIBUTION LAWS*

We know that the wave function of any free particle enclosed in a cube of volume $V=L^3$ is

$$\psi=C\sin\frac{l\pi x}{L}\sin\frac{m\pi y}{L}\sin\frac{n\pi z}{L} \quad \ldots \quad (1)$$

* The proof is here extended to include Bose-Einstein statistics. Kennard has dealt with the classical statistics, and Condon has included the Fermi-Dirac statistics also.

characterised by the energy value

$$E_{l,m,n} = \frac{h^2}{8mL^2}(l^2+m^2+n^2). \quad \dots \quad (2)$$

The normalisation constant C is easily found to be

$$C = 2\left(\frac{2}{V}\right)^{\frac{1}{2}}. \quad \dots \quad (3)$$

Let us now consider an assembly of ν similar non-interacting particles in the cube. The state of the assembly will be characterised by 3ν quantum numbers (l_1, m_1, n_1), (l_2, m_2, n_2), (l_3, m_3, n_3) ......, etc., one bracket for each of the ν particles. The energy of the assembly will be

$$W_k = \frac{h^2}{8m\,L^2}\sum_{r=1}^{r=\nu}(l_r^2+m_r^2+n_r^2). \quad \dots \quad (4)$$

The number of independent wave functions of energy less than or equal to W, *i.e.*, $W_k \leqq W$, will be $\frac{1}{2^{3\nu}}$ times the volume of a 3ν-dimensional sphere of radius $\left(\frac{8m\,L^2W}{h^2}\right)^{\frac{1}{2}}$. This is easily seen if we note that to each state there corresponds a unit volume in a space of 3ν dimensions (with co-ordinates l_1, m_1, n_1; l_2, m_2, n_2; etc.). The factor $\frac{1}{2^{3\nu}}$ arises, for we are concerned with only the positive values of l_r, m_r, n_r. Thus the number of states (independent wave functions) * of energy $\leqq$ W is

$$C_\nu(W) = \frac{1}{\Gamma\left(\frac{3\nu}{2}+1\right)}\left(\frac{2\pi mL^2W}{h^2}\right)^{\frac{3\nu}{2}}. \quad \dots \quad (5)$$

The number of wave functions lying between W and $W+dW$ will therefore be

$$C_\nu'(W)dW = \frac{\left(\frac{2\pi mL^2W}{h^2}\right)^{\frac{3\nu}{2}}}{\Gamma\left(\frac{3\nu}{2}+1\right)}\cdot\frac{3\nu}{2}\,\frac{dW}{W}. \quad \dots \quad (6)$$

* This is the total number of wave functions neglecting symmetry restrictions that characterise Fermi and Bose Statistics.

We have now to introduce the concept of temperature and this can be done in two ways: (*i*) by an appeal to the second law of thermodynamics in one form or the other, (*ii*) by using the property of a classical perfect gas, that the average energy per particle, for it, is $\frac{3}{2}kT$. We shall follow here the second alternative and consider the system (or the assembly) whose law of energy distribution has to be investigated in thermal contact with a perfect gas thermometer.

In the case of a perfect gas we can rewrite (6) in a form suited to subsequent applications. In this case $W=\frac{3}{2}\nu kT$, and for w very small compared to W, we have from (6)

$$\frac{C_\nu'(W-w)}{C_\nu'(W)}=\left(1-\frac{w}{W}\right)^{\frac{3\nu}{2}-1}=e^{-\frac{w}{kT}} \qquad \dots \quad (6a)$$

Suppose a system A has energy levels w_0, w_1, w_2, ...and the corresponding weight factors* g_0, g_1, g_2, ... Let us find the probability $P(a)$, that this system A has energy w_a. Let the total energy of the composite assembly, the system A in thermal contact with the perfect gas thermometer, be W to $W+dW$. The energy associated with the system A is w_a and with the perfect gas thermometer (containing ν particles), $W-w_a$ to $(W-w_a)+dW$. The number of wave functions such that A is in the state of energy w_a and the ν particles are in the state of energy $(W-w_a)$ to $(W-w_a)+dW$ will be

$$=g_a.C_\nu'(W-w_a)dW \qquad \dots \quad (7)$$

and therefore the probability $P(a)$ will be

$$P(a)=\frac{g_a.C_\nu'(W-w_a)dW}{\sum_s g_s.C_\nu'(W-w_s)dW} \qquad \dots \quad (8)$$

where $\sum_s$ denotes the sum over all the states of A. Let the probability of A being in the state of lowest energy w_0 be P(o);

then,
$$P(o)=\frac{g_0.C_\nu'(W-w_0)dW}{\sum_s g_s.C_\nu'(W-w_s)dW} \qquad \dots \quad (9)$$

* The weight factor of a state denotes the number of distinct wave functions corresponding to that state.

and using (6*a*) we have
$$\frac{P(a)}{P(o)}=\frac{g_a}{g_o}\cdot\frac{e^{-\frac{w_a}{kT}}}{e^{-\frac{w_o}{kT}}} \qquad \ldots \quad (10)^*$$

or
$$P(a)=c.g_a e^{-\frac{w_a}{kT}} \qquad \ldots \quad (11)$$
where c is a constant.

If the system A is a free particle, then from (6) applied to one particle, we have the number of states lying in the kinetic energy range ϵ, $\epsilon+d\epsilon$,
$$a(\epsilon).d\epsilon=g_a=\left(\frac{2\pi m L^2}{h^2}\right)^{\frac{3}{2}}\cdot\frac{1}{\Gamma(\frac{3}{2})}.w_a^{\frac{1}{2}}dw_a \qquad \ldots \quad (12)$$
and therefore (omitting the subscripts),
$$P(w)=bw^{\frac{1}{2}}dw.e^{-\frac{w}{kT}} \qquad \ldots \quad (13)$$
where b is a constant.

This is Maxwell's distribution law. The constant b can be easily determined by the normalisation condition that
$$\int_o^\infty P(w)dw=b\int_o^\infty w^{\frac{1}{2}}\,dw.e^{-\frac{w}{kT}} \qquad \ldots \quad (14)$$
or
$$b=\frac{2}{\sqrt{\pi}}(kT)^{-\frac{3}{2}} \qquad \ldots \quad (15)$$

We shall now derive the distribution law for Fermi-Dirac and Bose-Einstein Statistics. We suppose the system A, referred to in the above discussion, to consist of an assembly of N similar (indistinguishable) particles—this assembly being in thermal contact with the perfect gas thermometer. Let ϵ_r $(r=1,\ 2,\ \ldots)$ denote the eigen-values of the energy of a particle in the assembly A, and N_r the number of particles in the energy state ϵ_r. Then
$$N=\Sigma N_r\ ;\ w_a=\Sigma\epsilon_r N_r \qquad \ldots \quad (16)$$
where w_a is the total energy of the assembly A.

Let us think of a particular particle-energy-state ϵ_s and let $\underset{(N_s)}{\Sigma}F$ represent the sum (for any function F) taken over all those states of the assembly for which, in the energy-level ϵ_s, there are N_s particles (no more and no less), *i.e.*, the sum extends over all possible values of w_a consistent with this one restriction that there be N_s particles in the level ϵ_s.

* It will be noticed that the exponential factors arise because the system is in contact with classical perfect gas thermometer and shares energy with it.

Writing * and

$$\left.\begin{aligned} F &= e^{-w_a/kT} \\ w_a &= w_a' + N_s\epsilon_s \end{aligned}\right\} \qquad \ldots \quad (17)$$

we have

$$\sum_{(N_s)} e^{-\frac{w_a}{kT}} = e^{-\frac{N_s\epsilon_s}{kT}} \sum_{(N_s)} e^{-\frac{w_a'}{kT}}. \qquad \ldots \quad (18)$$

$\sum\limits_{(N_s)} e^{-\frac{w_a'}{kT}}$ is the sum for an $(N-N_s)$-particle assembly from which the state ϵ_s is excluded (*i.e.*, this sum is independent of ϵ_s).

Let

$$\sum_{(N_s)} e^{-\frac{w_a'}{kT}} \Big/ \sum_{(N_s-1)} e^{-\frac{w_a'}{kT}} = A, \qquad \ldots \quad (19)$$

then A being the ratio of the sums for $(N-N_s)$-particle and $[(N-N_s)+1]$-particle assemblies (the state ϵ_s being excluded for both) will be independent of N_s as N is very large compared to N_s.†

Let us first find the distribution law for the case of Fermi-Dirac statistics. In this case no two particles can be in the same quantum state, and therefore the allowed values of N_s are only 0 and 1. For some of the states of the assembly, there will be a particle in the level ϵ_s, $(N_s=1)$ and for the rest, the level ϵ_s will be unoccupied, $(N_s=0)$. We have to find the average value of N_s for all possible states of the assembly.

Noting, from (11), that the probability factor associated with each state of the assembly is proportional to $e^{-\frac{w_a}{kT}}$, the expression for the average value of N_s will be, using (17) and (19),

$$\bar{N}_s = \frac{\sum\limits_{(0)} 0 \times e^{-\frac{w_a}{kT}} + \sum\limits_{(1)} 1 \times e^{-\frac{w_a}{kT}}}{\sum\limits_{(0)} e^{-\frac{w_a}{kT}} + \sum\limits_{(1)} e^{-\frac{w_a}{kT}}} = \frac{1}{\frac{1}{A}\cdot e^{\frac{\epsilon_s}{kT}} + 1} \qquad \ldots \quad (20)$$

* $\Sigma e^{-\frac{w_a}{kT}}$ is known as the partition function.

† Strictly, there are states for which N_s will be comparable to N, but these states, because of the exponential factor $e^{-\frac{N_s\epsilon_s}{kT}}$, will be ineffective in our calculations. [See equation (22).]

or the number $N(\epsilon)d\epsilon$ of the particles lying in the energy range ϵ to $\epsilon+d\epsilon$ is

$$N(\epsilon)d\epsilon = \bar{N}_\epsilon \, a(\epsilon)d\epsilon = \frac{a(\epsilon)d\epsilon}{\frac{1}{A}e^{\frac{\epsilon}{kT}}+1} \qquad \ldots \quad (21)$$

where $a(\epsilon)$ is given by (12).

We now consider the case of Bose-Einstein Statistics. In this case there is no restriction on the number of particles in the same quantum state, *i.e.* no restriction on the value of N_s. The average value will therefore be given by

$$\bar{N}_s = \frac{\sum\limits_{(0)} 0\times e^{-\frac{w_a}{kT}} + \sum\limits_{(1)} 1\times e^{-\frac{w_a}{kT}} + \sum\limits_{(2)} 2\times e^{-\frac{w_a}{kT}} + \ldots\ldots}{\sum\limits_{(0)} e^{-\frac{w_a}{kT}} + \sum\limits_{(1)} e^{-\frac{w_a}{kT}} + \sum\limits_{(2)} e^{-\frac{w_a}{kT}} + \ldots\ldots} \qquad \ldots \quad (22)$$

which on using (17) and (19) reduces to

$$\bar{N}_s = \frac{Ae^{-\frac{\epsilon_s}{kT}}\left[1+2Ae^{-\frac{\epsilon_s}{kT}}+3A^2e^{-\frac{2\epsilon_s}{kT}}+\ldots\right]}{\left[1+Ae^{-\frac{\epsilon_s}{kT}}+A^2e^{-\frac{2\epsilon_s}{kT}}+\ldots\ldots\right]}$$

$$= \frac{Ae^{-\frac{\epsilon_s}{kT}}\left(1-Ae^{-\frac{\epsilon_s}{kT}}\right)^{-2}}{\left(1-Ae^{-\frac{\epsilon_s}{kT}}\right)^{-1}}$$

$$= \frac{1}{\frac{1}{A}e^{\frac{\epsilon_s}{kT}}-1}. \qquad \ldots \quad (23)$$

The number $N(\epsilon)d\epsilon$ of particles lying in the energy range ϵ, $\epsilon+d\epsilon$, is

$$N(\epsilon)d\epsilon = \bar{N}_\epsilon \, a(\epsilon)d\epsilon = \frac{a(\epsilon)d\epsilon}{\frac{1}{A}e^{\frac{\epsilon_s}{kT}}-1} \qquad \ldots \quad (24)$$

where $a(\epsilon)$ is given by (12).

To obtain the distribution law for a classical assembly in this way, we have to note that for a classical assembly all states are accessible, whereas for a Bose-assembly the "symmetry requirement" imposes a severe restriction on

the number of the accessible states.—*This restriction from the view-point of the phase-cells means that in classical statistics the particles are distinguishable from each other while in quantum statistics they are indistinguishable.* Therefore, the number of states for a $(N-N_s)$-particle assembly (classical) will be proportional to $N!/N_s!N-N_s!$, the number of ways of selecting $(N-N_s)$ particles out of the total number N, and thus instead of (19) we have

$$\sum_{(N_s)} e^{-\frac{w_a}{kT}} \Big/ \sum_{(N_s-1)} e^{-\frac{w_a}{kT}} = e^{-\frac{\epsilon_s}{kT}} \frac{A}{N_s}$$

or

$$\sum_{(N_s)} e^{-\frac{w_r}{kT}} \Big/ \sum_{(0)} e^{-\frac{w_r}{kT}} = e^{-\frac{N_s\epsilon_s}{kT}} \frac{A^{N_s}}{N_s!} .$$

and

$$\frac{\sum\limits_{(N_s)}}{\sum\limits_{(1)}} = e^{-\frac{(N_s-1)}{kT}} \frac{A^{(N_s-1)}}{N_s!} .$$

Thus, for a classical assembly (22) simply reduces to

$$\bar{N}_s = \frac{\sum\limits_{(1)}}{\sum\limits_{(0)}} = Ae^{-\frac{\epsilon_s}{kT}} ,$$

which is the classical distribution law.

2. We shall now proceed to derive the thermodynamical properties of a Bose-Einstein assembly consisting of N similar non-interacting particles occupying a volume V. The distribution law, on substituting in (24) for $a(\epsilon)d\epsilon$ from (12) becomes

$$N(\epsilon)d\epsilon = \frac{2\pi(2m)^{\frac{3}{2}}V}{h^3} \frac{\epsilon^{\frac{1}{2}}d\epsilon}{1/Ae^{\epsilon/kT}-1} \quad \dots \quad (25)$$

and

$$N = \int_0^\infty N(\epsilon)d\epsilon. \quad \dots \quad (26)$$

Defining a dimensionless number A_0 (usually called the degeneracy-discriminant) by the relation

$$A_0 = \frac{N}{V}\left(\frac{h^2}{2\pi mkT}\right)^{\frac{3}{2}} \quad \dots \quad (27)$$

we have from (25) and (26), $A_0 = F(A)$,

where

$$F(A)=\frac{2}{\sqrt{\pi}}\int_0^\infty \frac{u^{\frac{1}{2}}du}{1/Ae^u-1}=\sum_{n=1}^{\infty}\frac{A^n}{n^{\frac{3}{2}}} \text{ for } A<1 \text{ and } u=\epsilon/kT \quad \ldots \quad (28)$$

Now A cannot be greater than unity, otherwise the expression (25) for $N(\epsilon)$ would be negative, for some values of ϵ, which is inadmissible. The maximum (admissible) value of $F(A)$ is $F(1)$ which is given by

$$F(1)=\zeta\left(\frac{3}{2}\right)=1+\frac{1}{2^{\frac{3}{2}}}+\frac{1}{3^{\frac{3}{2}}}+\frac{1}{4^{\frac{3}{2}}}+\ldots=2\text{·}612 \quad \ldots \quad (29)$$

where $$\zeta(t)=\frac{1}{(t-1)!}\int_0^\infty \frac{x^{t-1}dx}{e^x-1}$$

denotes the Riemann zeta-function.*

Therefore, no solution A(T) of equation (28) can be found for which $A_0>$ 2·612 *i.e.*, for which

$$N>\frac{V}{h^3}(2\pi mkT)^{\frac{3}{2}}2\text{·}612$$

or $$T<T_0$$

where $$T_0=\left(\frac{n}{2\text{·}612}\right)^{\frac{2}{3}}\frac{h^2}{2\pi mk}=\left(\frac{A_0}{2\text{·}612}\right)^{\frac{2}{3}}T, \quad \ldots \quad (30)$$

n being the number of particles per unit volume. If m denotes the mass of the He-atom, N the Avogadro-number and V a molecular volume of 27·6 cm^3 for liquid He II, then

$$T_0=3\text{·}13°K.$$

The total energy E is given by

$$E=N\epsilon=\frac{2\pi(2m)^{\frac{3}{2}}V}{h^3}\int_0^\infty\frac{\epsilon^{\frac{3}{2}}d\epsilon}{1/A\cdot e^{\epsilon/kT}-1}$$

$$=\frac{kTV}{h^3}\cdot\frac{2}{\sqrt{\pi}}(2\pi mkT)^{\frac{3}{2}}\int_0^\infty\frac{u^{\frac{3}{2}}du}{1/A\cdot e^u-1} \quad \ldots \quad (31a)$$

$$=\frac{kTV}{h^3}\frac{2}{\sqrt{\pi}}(2\pi mkT)^{\frac{3}{2}}\int_0^\infty u^{\frac{3}{2}}duAe^{-u}(1-Ae^{-u})^{-1}$$

or $$E=\frac{3}{2}\cdot\frac{kTV}{h^3}(2\pi mkT)^{\frac{3}{2}}A\left[1+\frac{A}{2^{\frac{5}{2}}}+\frac{A^2}{3^{\frac{5}{2}}}+\ldots\right]^{\dagger} \quad \ldots \quad (31b)$$

* For a table of values of the Riemann zeta-function, see the Appendix.

† This result is obtained by making use of the relation

$$\int_0^\infty u^n e^{-ru}du=\frac{1}{r^{n+1}}\Gamma(n+1)$$

Now from (28) we have

$$A_0 = A\left[1 + \frac{A}{2^{\frac{3}{2}}} + \frac{A^2}{3^{\frac{3}{2}}} + \frac{A^3}{4^{\frac{3}{2}}} + \dots\right] \qquad \dots \quad (32)$$

Let us write

$$A = A_0 + aA_0^2 + bA_0^3 + cA_0^4 + dA_0^5 + \dots \qquad \dots \quad (33a)$$

and
$$A_0 = A + qA^2 + rA^3 + sA^4 + tA^5 + \dots$$

Then substituting the first series in the second, we get

$$\begin{aligned} A_0 = A_0 &+ A_0^2(a+q) + A_0^3(b+2aq+r) \\ &+ A_0^4(c + a^2q + 2bq + 3ar + s) \\ &+ A_0^5(d + 2abq + 2cq + 3a^2r + 3br + 4as + t) + \dots \end{aligned}$$

Equating coefficients of equal powers of A_0 on both sides of the above equation, we have

$$\left. \begin{aligned} & a = -q,\ b = 2q^2 - r,\ c = -s + 5qr - 5q^3, \\ & d = 14q^4 - 21q^2r + 6qs + 3r^2 - t \end{aligned} \right\} \qquad \dots \quad (33b)$$

or for the particular case we are considering,

$$\left. \begin{aligned} a &= \left(-\frac{1}{2^{\frac{3}{2}}}\right) = -0{\cdot}353553 \\ b &= \left(\frac{1}{4} - \frac{1}{3^{\frac{3}{2}}}\right) = 0{\cdot}057550 \\ c &= \left(-\frac{1}{8} + \frac{5}{2^{\frac{3}{2}}\,3^{\frac{3}{2}}} - \frac{5}{2^{\frac{9}{2}}}\right) = -0{\cdot}005764 \end{aligned} \right\} \qquad \dots \quad (34)$$

Substituting for A in terms of A_0 in the energy equation (31*b*) we have

$$\begin{aligned} E = \frac{3}{2}RT\Bigg[1 &+ A_0\left(a + \frac{1}{2^{\frac{5}{2}}}\right) + A_0^2\left(b + \frac{2a}{2^{\frac{5}{2}}} + \frac{1}{3^{\frac{5}{2}}}\right) \\ &+ A_0^3\left(c + \frac{a^2+2b}{2^{\frac{5}{2}}} + \frac{3a}{3^{\frac{5}{2}}} + \frac{1}{4^{\frac{5}{2}}}\right) + \dots\dots\Bigg] \end{aligned}$$

which after substituting the values of *a*, *b*, *c* from (34) reduces to

$$E = \frac{3}{2}RT\left[1 - 0{\cdot}1768A_0 - 0{\cdot}0033A_0^2 - 0{\cdot}00011A_0^3 - \dots\right] \qquad \dots \quad (35)$$

or replacing A_0 by (T_0/T) with the help of (30), we obtain the non-degenerate Bose-Einstein expression for energy

$$E_1 = \frac{3}{2}RT\left[1 - 0{\cdot}462(T_0/T)^{\frac{3}{2}} - 0{\cdot}0225(T_0/T)^3 - 0{\cdot}00197(T_0/T)^{\frac{9}{2}} - \dots\right] \qquad \dots \quad (36)$$

and
$$C_{v+}=\left(\frac{dE}{dT}\right)_{+}=\frac{3}{2}\,R\left[1+0{\cdot}231\left(\frac{T_0}{T}\right)^{\frac{3}{2}}\right.$$
$$\left. +\,0{\cdot}045\left(\frac{T_0}{T}\right)^{3}+0{\cdot}0069\left(\frac{T_0}{T}\right)^{\frac{9}{2}}+\,\ldots\ldots\right] \quad \ldots \quad (37)$$

Equations (36) and (37) are the same as equations (7*b*) and (8*b*) appearing in F. London's paper (*Phy. Rev.* 1938, *54*, p. 950) except for a numerical error in the coefficients of $\left(\frac{T_0}{T}\right)^{\frac{9}{2}}$.

Let us now derive the degenerate expression for energy. In the degenerate case when $T \leqq T_0$, A becomes equal to unity * and (31*a*) reduces to

$$E_-=\frac{kTV}{h^3}\,\frac{2}{\sqrt{\pi}}\,(2\pi mkT)^{\frac{3}{2}}\int_0^\infty \frac{u^{\frac{3}{2}}du}{e^u-1} \quad \ldots \quad (38)$$

But from (30) $\qquad (2\pi mkT)^{\frac{3}{2}}=\dfrac{nh^3}{2{\cdot}612}\left(\dfrac{T}{T_0}\right)^{\frac{3}{2}}$

Hence we have

$$E_-=\frac{2}{2{\cdot}612}\,\frac{RT}{\sqrt{\pi}}\left(\frac{T}{T_0}\right)^{\frac{3}{2}}\int_0^\infty \frac{u^{\frac{3}{2}}du}{e^u-1} \quad \ldots \quad (39)$$

$$=\frac{3}{2}\,RT(T/T_0)^{\frac{3}{2}}\,\frac{\zeta(2{\cdot}5)}{\zeta(1{\cdot}5)}$$

$$=0{\cdot}514\cdot\frac{3}{2}\,RT.\,(T/T_0)^{\frac{3}{2}} \quad \ldots \quad (40)$$

and
$$C_{v-}=\left(\frac{dE}{dT}\right)_{-}=\frac{15}{4}.\,0{\cdot}514.R(T/T_0)^{\frac{3}{2}} \quad \ldots \quad (41)$$

It will be of interest to note the ratio of the energy and the specific heats for the degenerate Bose and Fermi Statistics. In the case of the Bose Statistics, exact expressions are obtained for the degenerate case, but for Fermi Statistics, exact expressions cannot be obtained and the various physical quantities are expressed as a power series in (1/log A). In comparing degenerate Bose and Fermi Statistics, we take, in the latter case, only the first term of the series. We then have

$$E_-(\text{Fermi})=\frac{3}{10}\,\frac{h^2}{m}\,N\left(\frac{3n}{4\pi}\right)^{\frac{2}{3}}$$
$$=\frac{3}{5}\left(\frac{3}{4\pi}\right)^{\frac{2}{3}}\pi\left[\zeta\left(\frac{3}{2}\right)\right]^{\frac{2}{3}}RT\left(\frac{T_0}{T}\right) \quad \ldots \quad (42)$$

* Unity is the maximum value A can take. It cannot exceed unity, otherwise N(ϵ) will become negative for some values of ϵ which is inadmissible.

and $$C_{v-}(\text{Fermi}) = \frac{\pi^2 mk}{h^2}\, RT\left(\frac{4\pi}{3n}\right)^{\frac{2}{3}}$$

$$= \frac{\pi}{2}\left(\frac{4\pi}{3}\right)^{\frac{2}{3}} \frac{R}{[\zeta(\frac{3}{2})]^{\frac{2}{3}}} \left(\frac{T}{T_0}\right) \qquad \text{(43)}$$

and therefore, $$\frac{E_-(\text{Bose})}{E_-(\text{Fermi})} = \left[\frac{5}{2}\left(\frac{4}{3\sqrt{\pi}}\right)^{\frac{2}{3}}\zeta\left(\frac{5}{2}\right)\right] \times \frac{1}{A_0^{\frac{5}{3}}}$$

$$= 2{\cdot}77\left(\frac{1}{A_0^{\frac{5}{3}}}\right) \qquad \ldots \text{(44)}$$

and $$\frac{C_{v-}(\text{Bose})}{C_{v-}(\text{Fermi})} = \zeta\left(\frac{5}{2}\right)\frac{15}{2\pi}\left(\frac{3}{4\pi}\right)^{\frac{2}{3}} \frac{1}{A_0^{\frac{1}{3}}} = \frac{1{\cdot}23}{A_0^{\frac{1}{3}}} \qquad \ldots \text{(45)}$$

3. If we plot E/RT against T/T_0 using the non-degenerate expression

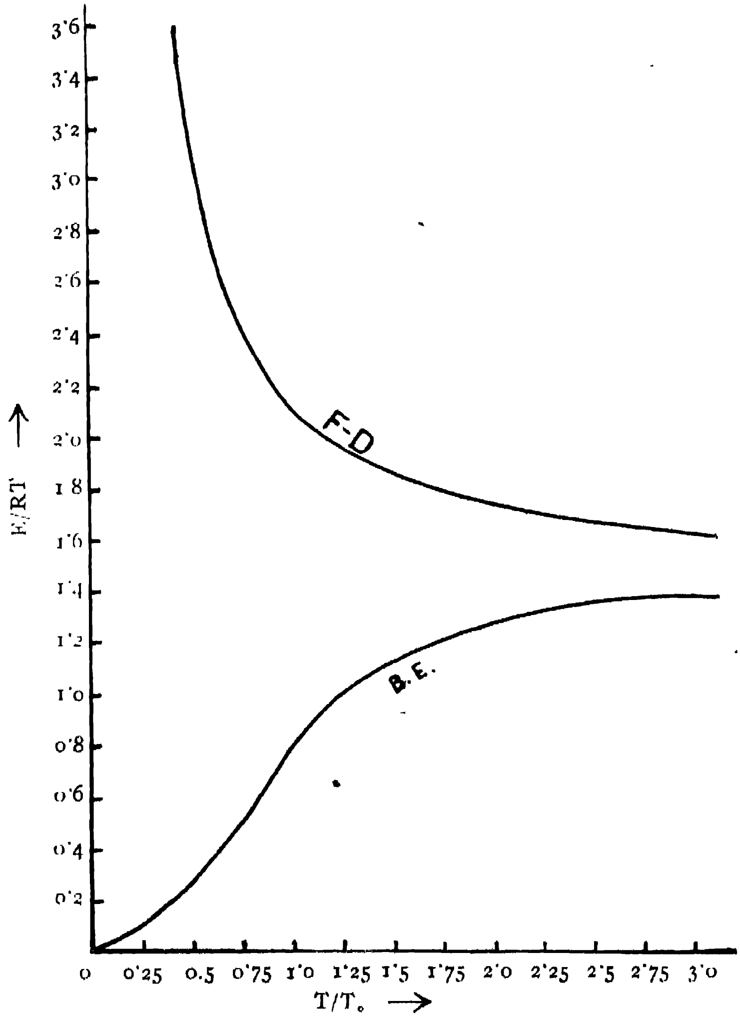

FIGURE 1

(36) for E_+ in the region in which $T > T_0$ and the degenerate expression (40) for E_- in the region of $T < T_0$, we obtain the lower curve in figure 1. The upper curve (given for the sake of comparison) is a plot of E/RT against T/T_0 for the Fermi-Dirac Statistics. This is obtained with the help of the data from Stoner's paper (*Phil. Mag.*, 1938, Vol. 25, p. 907). It can be easily seen that the two branches corresponding to E_+ and E_- in the lower curve are continuous at $T = T_0$ with a continuous tangent. This result can be theoretically verified by differentiating with respect to T, the expressions (36) and (40) and noting that $(dE/dT)_+$ becomes equal to $(dE/dT)_-$ when $T = T_0$.

The second derivative of E, however, is discontinuous and the run of the specific heat (C_v) curve has therefore a break at $T = T_0$. This is clearly shown in figure 2, where (C_v/R) is plotted against (T/T_0) following F. London. Differentiating the expressions for $(C_v)_+$ and $(C_v)_-$ and putting $T = T_0$ we get

$$\frac{d}{dT}(C_v)_+ = -0{\cdot}77\,\frac{R}{T_0} \tag{46}$$

and

$$\frac{d}{dT}(C_v)_- = 2{\cdot}89\,\frac{R}{T_0} \tag{47}$$

From the values of the two tangents given by (46) and (47), the angle of discontinuity between the two branches $(C_v)_+$ and $(C_v)_-$ at $T = T_0$ is easily found to be (about) 71°. For comparison, the specific heat curve for the

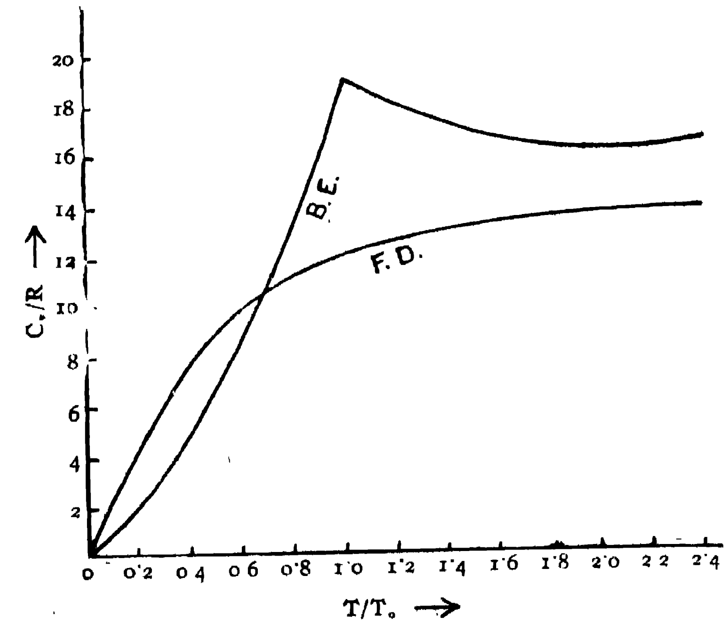

FIGURE 2

Fermi-Dirac Statistics is also plotted in figure 2 from the data in Stoner's paper referred to above.

From the relation $p=\frac{2}{3}\frac{E}{V}$ we get

$$p_+=\frac{RT}{V}\left[1-\frac{0{\cdot}462}{cVT^{\frac{3}{2}}}-\frac{0{\cdot}0225}{(cVT^{\frac{3}{2}})^2}-\frac{0{\cdot}00197}{(cVT^{\frac{3}{2}})^3}\cdots\right] \quad \ldots \quad (48)$$

and

$$p_-=0{\cdot}514cRT^{\frac{5}{2}} \quad \ldots \quad (49)$$

where

$$c=\frac{2{\cdot}612}{N}\left(\frac{2\pi mk}{h^2}\right)^{\frac{3}{2}}. \quad \ldots \quad (50)$$

To get the expressions for the free energy F, we make use of the Gibbs-Helmholtz relation

$$F=E+T\left(\frac{dF}{dT}\right)_V \quad \ldots \quad (51)$$

then

$$\frac{d}{dT}\left(\frac{F}{T}\right)=-\frac{E}{T^2}$$

and

$$F=-T\int_0^T\frac{E}{T^2}\,dT \quad \ldots \quad (52)$$

Substituting the values of E_+ and E_- from (36) and (40) in the above equation, we get

$$F_+=-\frac{3}{2}RT\left[ln\left(\frac{T}{T_0}\right)+0{\cdot}308\left(\frac{T_0}{T}\right)^{\frac{3}{2}}+0{\cdot}0075\left(\frac{T_0}{T}\right)^3+0{\cdot}00044\left(\frac{T_0}{T}\right)^{\frac{9}{2}}+\ldots\right] \quad \ldots \quad (53)$$

and

$$F_-=-\frac{\zeta(\frac{5}{2})}{\zeta(\frac{3}{2})}RT\left(\frac{T}{T_0}\right)^{\frac{3}{2}} \quad \ldots \quad (54)$$

as obtained by F. London.

The entropy S is given by the well-known relation

$$F=E-TS \quad \ldots \quad (55)$$

Hence

$$S_+=\left(\frac{E-F}{T}\right)_+=\frac{3}{2}R\left[1+ln\left(\frac{T}{T_0}\right)-0{\cdot}154\left(\frac{T_0}{T}\right)^{\frac{3}{2}}-0{\cdot}015\left(\frac{T_0}{T}\right)^3-0{\cdot}0016\left(\frac{T_0}{T}\right)^{\frac{9}{2}}-\ldots\right] \quad \ldots \quad (56)$$

and

$$S_-=\frac{5}{2}R\left(\frac{T}{T_0}\right)^{\frac{3}{2}}\frac{\zeta(2{\cdot}5)}{\zeta(1{\cdot}5)}=\frac{5}{2}0{\cdot}514RcT^{\frac{3}{2}}V \quad \ldots \quad (57)$$

The entropy for a degenerate Fermi gas is (to a first approximation) given by the expression

$$S_{-}\,(\text{Fermi}) = \frac{Rk\pi^2 Tm}{h^2}\left(\frac{4\pi}{3n}\right)^{\frac{2}{3}}$$

$$= \frac{\pi}{2}\left(\frac{4\pi}{3}\right)^{\frac{2}{3}} \frac{R}{[\zeta(\frac{3}{2})]^{\frac{2}{3}}} \left(\frac{T}{T_0}\right) \qquad \ldots \quad (58)$$

and hence $$\frac{S_{-}\,(\text{Bose})}{S_{-}\,(\text{Fermi})} = 5\left(\frac{3}{4\pi^{\frac{5}{2}}}\right)^{\frac{2}{3}} \frac{\zeta(\frac{5}{2})}{A_0^{\frac{1}{3}}} \qquad (59)$$

$$= 0{\cdot}821 \frac{1}{A_0^{\frac{1}{3}}}. \qquad \ldots \quad (60)$$

APPENDIX

Values of ζ-function for different values of x.

x	$\zeta(x)=\Sigma \frac{1}{n^x}$;
$\frac{3}{2}$	$2{\cdot}612$;
2	$1{\cdot}645 = \frac{\pi^2}{6}$;
$\frac{5}{2}$	$1{\cdot}341$;
3	$1{\cdot}202$;
$\frac{7}{2}$	$1{\cdot}127$;
4	$1{\cdot}0823 = \frac{\pi^2}{90}$;
$\frac{9}{2}$	$1{\cdot}0573$;
5	$1{\cdot}0369$.

REFERENCES

[1] J. F. Allen and H. Jones, *Nature*, **141**, 243 (1938) ; **143**, 227 (1939); J. F. Allen and E. Ganz, *Proc. Roy. Soc.*, **171**, 242 (1939) ; J. F. Allen and A. D. Misener, *Proc. Roy. Soc.*, **172**, 467 (1939) ; J. F. Allen and J. Reekie, *Proc. Camb. Phil. Soc.*, **35**, 114 (1939)

[2] J. G. Daunt and K. Mendelsshon, *Nature*, **141**, 911 (1938); *Nature*, **142**, 475 (1938); *Proc. Roy. Soc.*, **170**, 423 (1939).

[3] F. London, *Phy. Rev.*, **54**, 947 (1938).

[4] A. Einstein, *Ber. Berl. Akad.*, 261 (1924) ; 3 (1925).

[5] G E. Uhlenbeck, *Dissertation* (Leiden, 1927).

[6] F. London, *loc. cit.*

[7] G. E. Uhlenbeck and B. Kahn, *Physica*, **5**, 399 (1938).

[8] E. U. Condon, *Phys. Rev.*, **54**, 937 (1938).

[9] E. H. Kennard, *Kinetic Theory of Gases*, p. 390.

SECONDARY K-ABSORPTION EDGES OF COBALT SALTS IN SOLID AND LIQUID SOLUTIONS*

By B. B. RAY, S. R. DAS

AND

N. BAGCHI

(*Received for publication, Jan. 11, 1940*)

ABSTRACT. The paper deals with the experimental measurements on the primary and secondary K-absorption edges of cobalt metal, its oxides, and its compounds both in the forms of solids and solutions. It is found that

(*a*) Though the primary K-edge of cobalt shifts to the shorter wavelength side of the spectrum as one passes from the metallic form of the element to its compounds, the secondary structures of all the solid compounds of cobalt show a similarity with that of the metal itself.

(*b*) The similarity between the structures in cobalt metal and that in anhydrous cobaltous chloride is significant. Though both these substances form hexagonal crystals, the metallic cobalt is non-ionic while the other is of the ionic type.

(*c*) CoO and Co_2O_3 (cubic and hexagonal respectively) show the same type of structures.

(*d*) Near the K-absorption edge, the relative intensity of the structures (*i.e.*, contrast between the white and dark lines) are quite prominent, and it decreases gradually at first with increasing separation from the main edge, and afterwards increases again before it vanishes.

(*e*) On passing from the solid polar compounds to solutions up to 1N the similarity of the secondary structures in all cases is noteworthy. It is suggested that in solutions up to 1N, most of the molecules are not at all dissociated.

(*f*) In the case of dilute solutions of strengths of the order of N/10 and N/20, the structure near the primary is quite different from what has been observed with strong solutions (e). Here it is suggested that only a small percentage of the molecules are dissociated. The positions of the secondary structures show that they originate from undissociated molecules.

(*g*) The solution of $Co(NO_3)_2.\ 6H_2O$ in conc. HNO_3 shows the same structure as is exhibited by strong solution of the same substance in water (e).

INTRODUCTION

Experiments on the K-absorption edges of lower elements by Lindsay and Van Dyke[1] have clearly shown that after the K-absorption edge, there are fluc-

* Communicated by the Indian Physical Society.

tuations of the intensity (Maxima and Minima) in the general absorption spectra in the short wavelength region of the main K-edge. These white and dark lines (or bands) in addition to the main edge form the complete X-ray absorption spectra. Later works by Lindsay and Voorhees,[2] Lindsay and Keivit,[3] Lindh,[4] Hanawalt,[5] Coster [6] and his associates have definitely shown such structures in the K and L series of many elements in different compounds having different crystalline modifications. For the origin of these secondary edges Ray,[7] Coster,[8] Lindsay[9] and others put forward the theory of simultaneous transition of two electrons by a single encounter of an X-ray quantum. But this theory could not satisfactorily explain the dependence of absorption spectra (1) on chemical and physical state, (2) on the nature of crystals of the compound, and (3) on the effect of temperature on the position of the secondary edges.

Further it cannot explain the absence of secondary structure in the case of an isolated atom. The theoretical explanation of the origin of these structures (secondary) was first given by Kronig[10] who investigated the energy spectrum of an electron moving in the lattice of the crystal. He was able to show that under the influence of a crystalline field the electron cannot have all the values of energy but it possesses an energy spectrum consisting of allowed and forbidden energy zones. This spectrum extends to a large energy distance (of the order of several hundred electron volts) from the first optical level. For the zones low in the energy spectrum, the allowed zones are much sharper than the forbidden ones. But reverse is the case as we go upwards and finally there remains no forbidden energy zones.

During the process of X-ray absorption, the electrons ejected from the deeper energy levels (the X-ray limits) accommodate themselves in these allowed energy zones following certain selection principles. In the case of a 'simple atom and 'ions' we obtain only sharp fine structure lines in the absorption spectrum, whereas in the case of crystal and polyatomic molecules the secondary absorption spectrum extends to very high energy distances from the primary edge.

Kronig has shown that in the case of metals or the cubic crystals the energy values of the mean positions in the forbidden zones are given by

$$E_n = \frac{n^2 h^2}{8md^2}$$

where E_n = mean energy of the nth forbidden zone, n = an integer similar to quantum number, d = the side of the unit cell of a cubic crystal and h = Planck Constant.

Kronig[11] has further developed his theory for the existence of secondaries in the case of polyatomic gases. Hartree, Kronig and Patersen[12] calculated the numerical values of the position of the structures of the K-edges of Ge in $GeCl_4$ by considering the chlorine ions situated at the corners of a regular tetrahedron.

Though Kronig's theory of secondary structure has explained many of the experimental results concerning the X-ray absorption by the atoms in pure metal and in non-polar compounds, yet there are certain difficulties with which it is faced in the case of the ionogenic compounds. Coster and Klammer[13] have studied the secondary structures to the K-edges of potassium and chlorine in an ionic crystal KCl and have found that the structures of potassium and chlorine are totally different though according to Kronig's theory they would be similar. Similar observations were made by G. P. Brewington[14] which bear the evidence that although Kronig's theory holds good in the case of elements and their compounds involving non-polar bonds it fails in the case of the polar compounds.

Although the results, stated up till now, have thrown considerable light on X-ray absorption spectrum and the electron energy states in crystalline solids including metals and their compounds, no systematic investigation has been carried out for a detailed study in the case of ionic crystals and solutions. So far as the absorption spectra of a solute in a solvent are concerned, mention may be made of the attempts of Yost,[15] Meyer[16] and Hanawalt.[5] In a short note in *Philosophical Magazine*, Yost has shown that the primary K-edges of Manganous and Chromate ions in ionic crystals $MnCl_2$ and K_2CrO_4 are the same as they are obtained with solutions. Mayer also found no detectable difference in the position of the K-edge of bromine in $NaBrO_3$ in the solid states and in aqueous solutions. Hanawalt also obtained the structure to the K-edge of Br in solid $NaBrO_3$ and in its solution and found that there was no appreciable change except that one structure near the primary K-edge of Br in the solid substances was absent in the case of solutions. Stelling[17] obtained the primary K-edge of chlorine in NaCl in the form of solid and solution and found that the wavelength in solution is a little greater than that for solid NaCl. Owing to difficulties in obtaining an extended structure in case of substance in solution no further work is known to have been done in this line.

Though the preliminary works by Hanawalt[5] showed no appreciable change of the position of the primary K-edge of bromine in $NaBrO_3$ in solid and in solutions of different strengths, it was thought proper to study systematically the absorption spectra of an element in different chemical combinations both in the solid state and in a state of solution.

For a detailed study of the influence of polar crystals on the absorption spectrum and the influence of water molecules in the ionic solutions of different strengths on primary and secondary absorption spectra, we have chosen cobalt and its compounds because of the fact that

(*a*) The K-absorption edge of cobalt is not placed either in the very soft or in the very hard region.

(*b*) The dispersion in this region of the spectrograph is quite sufficient for our purpose.

(c) Cobalt gives two series of compounds and forms hydrated ionic salts, which in some cases may be obtained in the anhydrous form though with much difficulty.

ABSORPTION SCREENS AND CELLS FOR ABSORPTION SPECTRA AND THEIR PREPARATIONS

The preparation of absorption screens and cells for obtaining extended secondary structures associated with the main edge is of prime importance and causes great difficulty. The thickness and uniformity of the absorbing screen always play an important part in these investigations. There is some optimum range of thickness of the screen for which a good record can be obtained. It is found that if the thickness of the screen is below or above a certain range of thickness, all the structures associated with the main edge do not come in prominently. Up till now, theoretically no definite relation has been put forward for the screen thickness, although it is found experimentally that a thickness which reduces the intensity of the general radiation to half its original value gives satisfactory results (Johnson's formula is applied here to find the screen thickness).

(a) *Solids*

Several methods were tried for obtaining screen of a suitable thickness, but the following proved to be convenient.

In the case of absorption spectra for solids the following methods were adopted :

(a) The subtance is finely powdered in a mortar and the powder is then pressed in uniform thickness over a piece of zig-zag paper or ordinary filter paper. In the case of hydrated salts the substance is pressed on filter paper.

(b) For solid substances which are not soluble in water the following method is particularly suitable. The substance is finely powdered in a mortar and a drop of seccotine is then added to it. After mixing it uniformly, a little quantity of water is added and an emulsion is obtained. This emulsion is allowed to pour on a piece of ordinary paper resting on a plate which is levelled. On drying, a screen of uniform thickness is obtained.

(c) For the study of the absorption edges of anhydrous $CoCl_2$, a cell holder of special design was used. The cell holder consists of cylindrical syndanio tube in the interior of which another tube was fitted over three-fourths of the length of the former. The two ends can be fitted on the cap attached to the cone carrying the slit. Inside the inner tube there are three circular rings of syndanio plates having rectangular openings in them which are parallel to the length of the slit. There are two perforations in the body of the tube through which a current

of dry gaseous HCl can be passed. The cell is shown diagrammatically in the following figure.

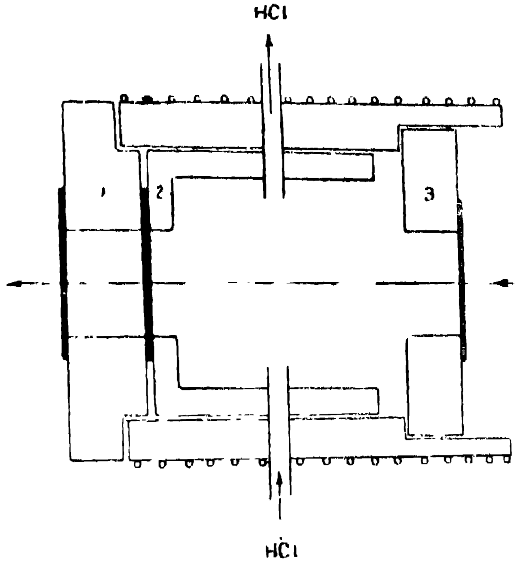

On the second ring an absorbing screen of $CoCl_2$, $6H_2O$, prepared by dipping a filter paper in a saturated solution of the substance, is pressed with secotine. The first ring is pressed on this ring, the outer end of which is covered with thin cellophane. On the third ring another piece of cellophane paper is mounted and between 2 and 3 a supply of dry gaseous HCl is made. On the outer syndanio tube is wound an electrical heater.

The two extreme circular rings were cemented with the outer syndanio tube by Plaster of Paris, so that the cell could be air-tight. The inlet and exit tubes of the cell for passing HCl gas could be sealed at the constrictions. The screen was heated at a temperature of 120°C in a constant supply of dry HCl gas and the temperature was recorded by a thermocouple.

(*b*) *Solutions*

In order to obtain absorption spectra of a substance in solution, one must use a cell which will not be attacked by the solution and at the same time will transmit the radiation. In the case of solution the proper thickness was attained by placing the solution between two thin films separated by a rubber sheet of requisite thickness. When the strength of the solution was altered, the thickness of the rubber sheet was also changed accordingly. The walls of the absorbing cell consisted of extremely thin celluloid on one side and aluminium foil ·007 mm. thick on the other in the case of solutions of cobalt nitrate and cobalt sulphate. But in the case of cobalt chloride solutions, the aluminium window must be dispensed with, as aluminium is found to be attacked by the solution. Thinner films of mica or

extremely thin pieces of celluloid were tried in some exposures but none of these methods led to the desired results. The use of cellophane as cell walls was also tried but in that case the uniformity of the thickness of the cell was lost. By coming in contact with the liquid, the cellophane bulges inward in some positions and outwards in others. With gold beater's skin as cell wall, there was no question of non-uniformity but the solution was found to be coloured blue. Thinner films for cell walls were prepared by dissolving celluloid in acetone and pouring the solution on a clear glass plate resting on a levelled platform. The preparation of thin films of uniform thickness by this method, is a very difficult task, and often it was found that as the films became thinner there was a greater chance of non-uniformity, which in many cases resulted in a leak in the films. Moreover, the films prepared in this way seemed to be porous, and air bubbles entered into the cell after some hours and the liquid leaked out This difficulty could not be avoided and the presence of solution in the cell was examined thrice a day and the cell freshly filled up whenever air bubbles were found inside the cell.

THE CELL HOLDER

The cell holder consisted of a rectangular brass plate, 4 cm. × 2·5 cm., in which a rectangular slot, 2 cm. × 0·7 cm., was cut out. Another plate was prepared having the dimensions, and with a rectangular opening having the same area, so that when one was placed on the other, they coincided The two brass plates can be screwed at the four corners. The lower plate was fitted with a cylindrical cap attached to the cone carrying the slit of the spectrograph. Absorbing screens could be placed between the two brass plates for exposure. The cell holder is indispensable in the case of solutions.

EXPERIMENTAL ARRANGEMENTS

A Siegbahn Vacuum spectrograph fitted with an electron tube was used. The slit through which the X-rays from the electron tube falls on the analysing calcite crystals is 0·1 mm. in breadth. The high vacuum of the electron tube is separated from the comparatively low vacuum in the spectrograph by thin aluminium foils. The heating filament is a spiral of tungsten wire fed by a low tension transformer. The crystal was oscillated at random through 2° $30'$ in a few cases by the hand but frequently by the following device.

A low-speed motor was connected to two wheels. In the bigger one was fitted a cam whose groove was cut in the form of a Casenis spiral. One end of a long brass rod was fixed to the crystal holder and the other to a pin which moved in the groove of the cam, the motion of the rod being controlled by a guide.

After the preliminary adjustment of the crystal and the plate holder, their zero positions were determined. For the reference lines in this connection the W L l, W L α_1 α_2 and Cu K α_1 α_2 emission lines were chosen. The Cu K α lines, which are highly absorbed by cobalt, were not very strong in the photograph

and did not cause any great inconvenience, though they fell in the secondary absorption region.

In the case of absorption spectroscopy, choice of photographic films and developers is of utmost importance. In our case best results were obtained with double-coated Agfa Sino Films with which a good contrast in the intensity of the absorption spectrum is obtained. Agfa Röntgen developers of constant strength were always used, and the plate was finally fixed in hypo solution.

Agfa Sino Films are very sensitive to temperature, and at temperatures above 20°C there is the possibility of the film being damaged by heat. The film was dried under a fan and in some cases dust particles settled on the film, which when analysed by the microphotometer show several kinks. In order to eliminate these spurious maxima and minima in the photometer curves, photometers were taken at different positions of the plate and in almost all cases by using more than one film.

The X-ray tube was run at 10 K.V. The time of exposure as well as the current in the X-ray tube was not the same in all the cases. Experiments showed that an exposure of 50 to 70 hours and a current of 20 to 35 milliamperes gave in general good results, with a screen of proper thickness. As is well known, the thickness of the screen plays a very important part in these investigations and it is difficult to obtain a good plate in which the contrast between the white and dark lines appears prominently. The screen was placed between the X-ray tube and the crystal. An interesting feature found in this investigation is that all compounds of cobalt do not give the extended structure with the same ease. In some cases they are obtained with greater difficulty than in others. As for example, we can cite the case of cobaltous oxide where some fifteen exposures were tried in vain in order to obtain a good record of extended structures, whereas in the case of the other oxide, cobaltic oxide, the edges are quite prominent.

A dispersion of 2·4 X.U. per mm. was obtained on the photometric record of the absorption spectrum. There are several absorption bands which show a 'fine structure,' that is, if these bands are noticed very carefully under suitable light and magnification, or are analysed by the microphotometer, the presence of bright and dark lines of faint intensity may be detected, which cannot be easily measured by a glass scale. The exact position of any edge in the secondary spectrum being impossible to locate, there may be a maximum error of 2·0 X.U. in the measurements of weak maxima and minima in the photometer curve. In the positions of the primary K-edge and the more prominent dark and white lines, the maximum error that can be expected may not exceed 1 X.U.

MEASUREMENTS AND DISCUSSIONS

In the measurements of the primary and secondary absorption edges, the dispersion in each photometric record was obtained from known emission lines

W $L\alpha_1$ (1473·4 X.U.). Cu K α_1 (1537·4 X.U.) and W $L\lambda$ (1675·0 X.U.) and position of these edges was determined with W $L\alpha_1$ line as the standard of reference.

As the exact position of the "Edge" is very difficult to determine, different observers chose different positions of the photometric curve for calculating the wavelength of the primary edge. Thus, some use the point of inflection, others use the middle portion of the jump in the curve as the exact position of the primary edge. But in our measurements, we have followed the procedure adopted generally by Lindh and Sandstorm,[18] *i.e.*, the primary edge was measured from the middle point of the straight portion of the primary absorption jump in the photometric curve. The points of inflection of the maxima and minima in the photometric curve were considered to determine the position of the "dark" and "white" bands.

It may be remarked here that our results on cobalt metal are in good agreement with the values given by Keivit and Lindsay who have also found some of the structures found by us for this element.

It may be remarked here that Swada[19] has followed an entirely novel procedure in the measurement of the absorption edges, and it seems that he has succeeded in measuring the beginning and the end of each of the dark bands in the secondary edges; his values are thus very difficult to compare with those of other investigators.

The absorption edges of the following substances are investigated.

(*a*) (*i*) Cobalt Metal (Hexagonal)
(*ii*) CoO (Blue Oxide, Cubic)
(*iii*) Co_2O_3 (Black Oxide, Hexagonal)
(*iv*) $CoSO_4$, $7H_2O$ (Crystal type unknown, though the CoSO is orthorhombic)
(*v*) Co $(NO_3)_2$, $6H_2O$ (Cobaltous Nitrate)
(*vi*) $CoCl_2$, $6H_2O$ (Structure unknown and $CoCl_2$ (Anhydrous)
(*vii*) Cobalt Nitrite.

All these compounds except cobalt metal are ionic.

(*b*) Solution in water—
(*i*) 1·7N, 1N, N/10, and N/20 Solns. of $CoSO_4$, $7H_2O$.
(*ii*) 1·5N, 1N, N/10, N/20 Solns. of $CoCl_2$, $6H_2O$.
(*iii*) 1·9N, ·64N, ·32N Solns. of Co $(NO_3)_2$, $6H_2O$

(*c*) Solutions in acids—
Saturated Solns. of Co $(NO_3)_2$, $6H_2O$ in strong HNO_3

TABLE II

$Co(NO_3)_2, 6H_2O$

[illegible]	[illegible]	[illegible]	[illegible]	[illegible]	[illegible]	[illegible]	[illegible]	a_6	k_6	a_7		a_8	k_8	a_9	k_9	a_{10}	k_{10}	a_{11}

TABLE IV

k_2	a_3	k_3	a_4	k_4	a_5	k_5	a_6	k_6	a_7		c_8	k_8	a_9	k_9	a_{10}	k_{10}	a_{11}	k_{11}
1590	1586	1582	1579	1575	1572	1568	1563	1557	1551			1523			1517	1513		1505
13	17	21	24	28	31	35	40	46	52			80			86	90		9[illegible]
573·13	574·57	676·06	577·12	578·59	579·69	581·17	583·02	585·27	587·74			598·34			600·71	602·33		605·5
4·65	6·09	7·58	8·64	10·11	11·21	12·67	14·54	16·79	19·06			29·86			32·33	33·85		37·[illegible]
63·08	82·58	102·8	114·5	137·1	152·0	172·0	197·2	227·7	258·4			405·0			437	459·0		502

Cu $K\alpha_1\ \alpha_2$ Region

1591	1586	1582	1576	1572	1569	1563	1560	1558	1553	1518	1512	1506	1502
12	17	21	17	31	34	40	43	45	50	85	91	97	101
572·76	574·57	576·06	578·22	570.69	580.8	583·02	584·15	584·89	586·74	600·31	602·69	605·09	606·7
4·28	6·99	7·58	9·74	11·21	12·32	14·54	15·67	16·41	18·26	31·83	34·21	36·61	38·22
58·04	82·58	102·8	131·0	152·0	167·0	197·2	212·5	222·5	247·7	432·6	463·8	496·5	518·3
1591	1585	1583	1577	1574	1571			1560	1556	1520	1514	1510	1507
12	18	20	26	29	32			43	47	83	89	93	96
572·76	574·93	575·66	577·92	578·95	580.06			584·15	585·5	599·52	601·9	603·49	604·69
4·28	6·45	7·18	9·4	10·47	12·58			15·67	17·0	31·04	33·4	35·01	36·21
58·04	87·0	97·25	128·0	141·9	159·2			212·5	230·5	421·0	452·0	474·6	491·0
1591	1585			1579	1573	1570	1564	1553	1550	1524	1516	1510	1504
16	22			28	34	37	43	54	57	83	91	97	103
572·76	574·93			577·12	579·32	580·43	582·65	586·74	587·92	597·95	601·1	603·49	605·90
5·69	7·86			10·05	12·25	13·36	15·58	16·67	20·85	30·86	34·03	36·42	38·83
77·16	106·6			136·6	166·0	181·2	211·2	266·8	282·8	418·6	461·5	494·0	526·5
1590	1585	1581	1579	1574	1571			1563	1556	1522	1512	1506	1503 ?
17	22	26	28	33	36			44	51	85	95	101	104
573·13	574·93	576·39	577·12	578·95	580·06			583·02	585·5	598·73	602·69	605·09	606·30
6·06	7·86	9·32	10·05	11·88	13.0			15·95	18·43	31·66	35·62	38·02	39·23
82·3	106·5	126·4	136·6	161·2	176·3			216·3	250·0	429·1	482·9	515·6	532.0

Table I shows the position of the primary and secondary edges of cobalt (Metal) and various cobalt compounds in the solid state including anhydrous cobalt chloride.

Table II the same in $Co(NO_3)_2$, $6H_2O$ in forms of solid, aqueous solutions of different strengths and in saturated solutions in concentrated nitric acid.

Table III the same in $CoSO_4$, $7H_2O$, in forms of solids and aqueous solutions, while, table IV in $CoCl_2$, $6H_2O$, in solid forms, in aqueous solutions and also in anhydrous state.

The figures (k, k_1, k_2, etc.) refer to white lines, the primary edge being denoted by k, while (α_1, α_2, α_3, etc.) denote black bands. The secondary structures extend beyond the Cu.K $\alpha_1\alpha_2$ lines (1537 and 1541 X.U.) in all cases. In the region between Cu.K $\alpha_1\alpha_2$ and WL $\alpha_1\alpha_2$ the structures are quite prominent

(A) SOLIDS

The table I shows clearly how the primary K-edges of cobalt shift to the shorter wavelength side of the spectrum as we pass from the metallic form of the element to its compounds. This shift of the primary K-edge is outside the limits of experimental error and is similar to the earlier observations made by Lindh and others on the shift of the K-absorption edges of an element in its pure form and its compounds.

Pauling[20] has put forward a qualitative explanation for the shift of the primary K-edges by considering the following factors in his calculations. The work required to remove an electron is influenced by the external screening exerted by the external ions in the vicinity of the parent ion. This energy of course will depend on the sign of the ions.

He also assumes the law of inverse squares between the ions and introduces the idea that the crystal itself will have an electron affinity which will aid in the process of photoionisation. With these ideas he has attempted to account for the shift of the primary K-edges in a very general way.

The similarity between the structure in cobalt metal and that in anhydrous cobaltous chloride is significant as well as interesting (Table I). Here the two substances form hexagonal crystals, the metallic cobalt being non-ionic while the others are of the ionic type. The positions of all the secondary bands are the same with the exception of that of the primary one. For cobalt ($a=2{\cdot}54$, $c=4{\cdot}10$) while for $CoCl_2$ ($a=6{\cdot}14$, $\alpha=33°26'$, $U=0{\cdot}25$). Perhaps the influence of the chlorine ions at a definite distance from the cobalt ion in the lattice of $CoCl_2$, and the peculiar shape of this crystal (Rhombohedral Hexagonal) affect the field near the cobalt ion in such a way that the values of the allowed and the forbidden zones for the K-electron do not change appreciably from those observed for cobalt metal.

Another interesting feature is that the structures and their positions do not

change in passing from CoO to Co_2O_3 which are respectively cubic and hexagonal in structure. Coster has pointed out (*Physica*, Vol. II, p. 604) that cubic close-packed and hexagonal crystal lattices give the same secondary X-ray absorption edge if we confine ourselves to the positions of the maxima and minima, relative to the main edge. As regards the form of the maxima and minima, some typical difference in the form of the secondary structures in the substances still persists. This he has shown in the case of the copper-zinc alloys known as α and ϵ brass; α brass has the same structures as Cu (face centered cubic) and ϵ brass is hexagonal just as pure zinc. After reducing the values of α and ϵ brass in terms of the close-packed cubic and hexagonal forms, he has verified the relations stated above. Coster's work is confined only to non-ionic crystals but in the case of CoO and Co_2O_3, the crystals are polar and they are not close-packed but the similarity found in our experiment in the positions of the secondary bands is very significant. As the colours of the two oxides are different it was easily seen that one was not converted into the other during exposure.

A peculiar feature of the secondary structures of all solid compounds of cobalt (Table I) lies in their similarity with those of the metal itself, although in some cases one or two structures are found to be absent. Near the absent edges, the deviation from the corresponding secondary is large. These differences may be caused by the missing band. It should be mentioned here that the microphotometric records, which could not bring out the absent edges as mentioned above, exhibited a flatness of the curve in the region where they would have appeared. This flatness may introduce the above-mentioned discrepancy in the values of the band positions in the neighbourhood of the absent bands. It is quite probable that in such cases the so-called absent bands are not really absent but owing to some unknown factors the contrast between the consecutive dark and white bands has been so much reduced that their separate existence could not be recorded with certainty by the photometer curves. The observed flatness of the curve and also the discrepancy about the band positions may be explained in this way.

The relative intensities of the black and white bands as revealed in the original plate and also in the photometric records, shows a peculiarity which is not yet understood properly. It has been found that near the K-absorption edge, structures and their relative intensities decrease gradually with the increasing separation from the main edge beyond which there is again a marked rise in relative intensity which persists even beyond the Cu K $\alpha_1\alpha_2$ lines (1537·4, 1541·2.) and in some cases it extends even to a distance of 480 volts from the main edge. It is generally found that the contrast between the white and dark bands lying just on the longer wavelength side of the Cu K α lines is generally feebler than that of those on the shorter wavelength side of those emission lines. This peculiarity is not only confined to the structures in solids but is present also in dilute solutions and may be regarded as a general effect. In very dilute solutions only, it has been observed that the first white band of the secondary (*i.e.*, the second white

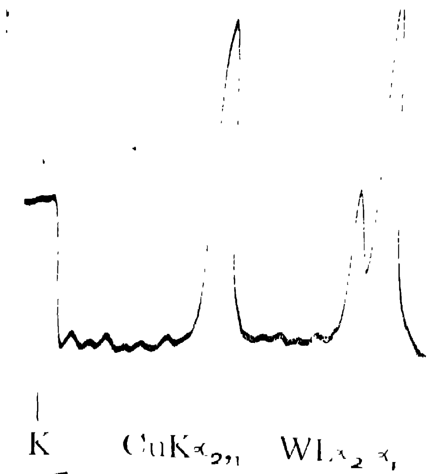

Fig. 1.

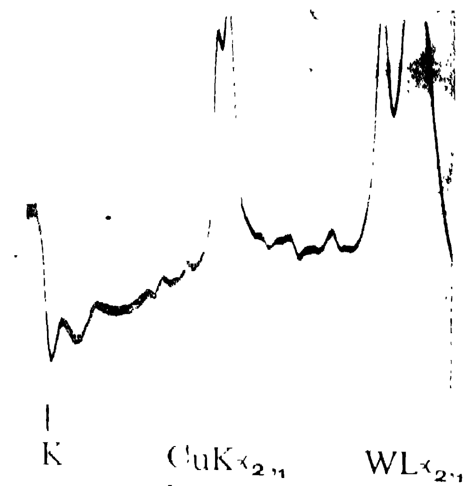

Fig 2.

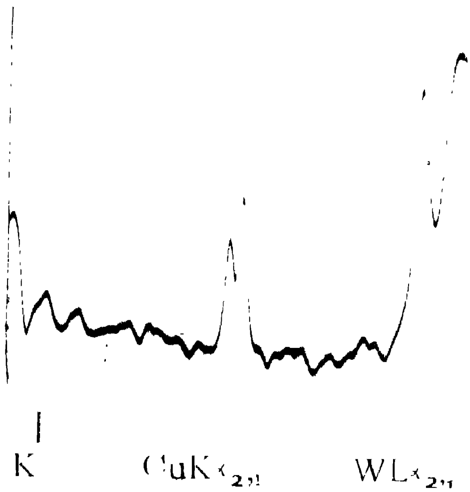

Fig. 3.

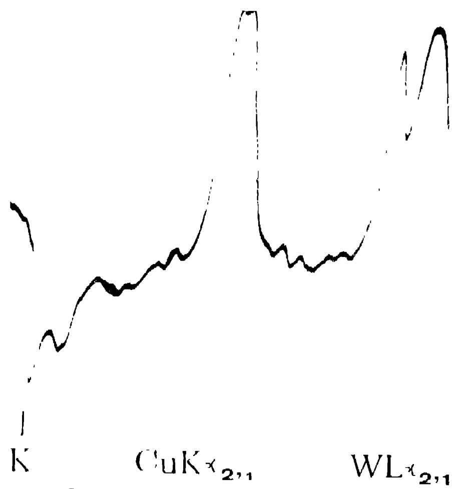

Fig. 4.

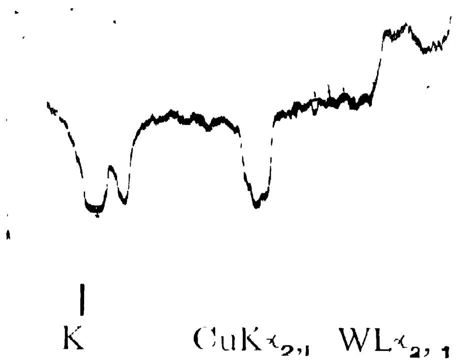

Fig. 5.

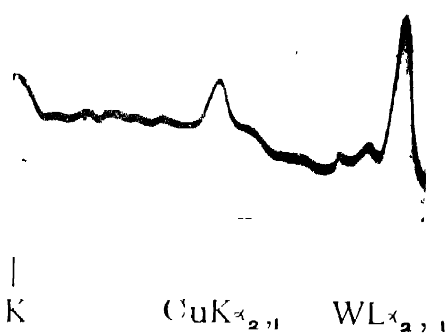

Fig. 6.

Description of figures

Fig. 1 Cobalt nitrite

Fig. 2 $CoCl_2$, 6 H_2O

Fig. 3 $CoCl_2$, 6 H_2O sol^n 1 N

Fig. 4 $Co(NO_3)_2$,6H_2O sol^n 0·3 N

Fig. 5 $CoSO_4$, 7 H_2O sol^n N/10

Fig, 6 Saturated sol^n of $Co(NO_3)_2$ 6H_2O in HNO_3

line in the plate) is as strong as, and sometimes even stronger than, the primary K-edge. This point raises some interesting questions about the nature of the absorbing medium and will be discussed in the last section. Hanawalt remarked that the secondary discontinuities near to the principal edge are always sharper than those further from the edge. The diffuseness of these further out, makes it impossible to state their positions accurately. In our observations, we have found that some of the bands, which are away from the main edge, are sharper than those near it.

STRONG SOLUTIONS (*i.e.*, Strength up to 1N)

On passing from the solid polar compounds to solutions up to 1N, the similarity of the structures in all cases is not only striking but interesting as well (Tables II, III, IV). This raises some speculations about the nature and binding of the 'Cobalt' ion in strong solutions, and we are now in a position to discuss them one by one.

(*a*) The substance when dissolved in water may form "ions" which are free in the sense that they are not influenced by one another, and are similar to "pure or isolated atom." If this view is accepted, two states of affairs are expected in the X-ray absorption spectra.

(1) The ion being doubly charged (Co^{++} ion), the primary K-edge will be shifted to the shorter wavelength side of the absorption spectra and will almost coincide with the primary K-edge of an element with an atomic number greater than it by two units (Cu-K-edge).

(2) The ions will resemble an isolated atom in which the K-electron can travel with all values of kinetic energy, *i.e.*, no secondary edges are expected. Fine structures, as defined before, may be found up to distance of about 20 volts only from the primary.

But it has been found experimentally that the K-edge of strong solution nearly coincides with that of Co-K-edge of the metal (difference about 4 volts) and the secondaries have not only the same wavelength as in the solid compound itself but also extend to a distance about 400 volts from the main edge. The facts clearly point out that the suggestion made in (*a*), *i.e.*, the hypothesis of free ion in the solution, is not satisfactory.

Prins,[21] from his diffraction experiments in Uranium nitrate and Thorium nitrate solutions of different strengths, has concluded that in solutions the ions of Uranium and Thorium are not absolutely free in the sense as mentioned above but they exert force on each other. He further suggests that, as with the increase in dilution the distance between the neighbouring atoms increases, the ions in the solutions form groups among themselves as conceived by the Cybotactic hypothesis of Stewart in long-chain organic liquids. Though the suggestion of Prins seems very reasonable, we have tried in vain to have diffraction pattern of strong solutions of Cobalt compounds with the Nickel radiation. Only the

haloes of water appeared in the photographic plate, which shows that the semi-lattice structure of cobalt ions in solutions in our case is absent though it may be present in the solutions of the compounds of heavier metals as mentioned by Prins.

(*a*) The trend of thought at the present moment is directed towards the idea that crystals of many simple salts are not dissociated completely in water or in any other solvent. If the positive and negative ions present in the crystals go to the solutions separately and all of them remain as separate positive and negative ions, there would be no neutral solute molecules present at all. But the experimental results of both the conductivity and osmotic pressure methods appear to indicate the presence of a large number of neutral molecules in solutions (even in the dilute solutions of the substances). Thus from the experiments on the osmotic pressure of $MgSO_4$ solution in water, one can see that even in the case of 1/500 molar solution there are at least 20% of the neutral molecules. Other substances also show the same phenomena (Gurney, *Ions in Solution*, Chapter XI).

It has been shown by Hanawalt [5] that secondary structures of a crystalline solid and the vapours* of the same compound have the same secondary structure though there are some differences in the structures near the main edge. As for example, $AsCl_3$ in the solid form shows an additional structure near the main edge which does occur in its vapour. From our experiments on the similarity of the secondary structures both for the solid compound and the solutions up to 1N, we may easily conclude that the structures in these strong solutions must have been due to the presence of a very large number of neutral molecules in the solution. If really there are dissociated molecules in the solutions, their percentage must be small.

WEAK SOLUTIONS (*i.e.*, Strength lower than 1N)

In the case of dilute solutions of the order of N/10 and N/20, we are presented with an entirely different picture of the absorption edges near the primary edge. It has been mentioned before that the second white band, *i.e.*, the first secondary, is as strong as, if not stronger than, the real primary edge and the latter is again shifted towards the longer wavelength side of the corresponding edge for solid compounds.

In the case of dilute solutions we know from the experiments on conductivity and osmotic pressure that a certain portion of the molecules is really dissociated into ions. But, as mentioned previously, these ions cannot remain in the "Free state." We may assume here that these ions are surrounded by water molecules, giving us a picture of the "Complex ionic group." In this case,

* It may be mentioned here that the temperature effect on the secondary structure of the molecules in the vapour state has been neglected.

the water dipoles influence the cobalt ions and thus set up a field of force which brings about allowed and forbidden zones as contemplated by Kronig. Thus, in dilute solutions, we have to consider the effects of undissociated cobalt salts in water and also of the "Complex ionic group" as mentioned before. As the secondary edges, excepting the first edge in dilute solutions, have the same structure as found in strong solutions, it is hereby concluded that even in dilute solutions a large percentage of molecules really remains undissociated.

As for change observed near the primary K-edge of the dilute solutions, we may offer the following explanations. The "Complex ionic group" as contemplated above has a field of force inside it, restricting the motion of the K-electrons only to a number of allowed zones. These big "ionic complexes" will therefore produce primary edges. We assume that the number of such complexes in the solutions examined by us is rather small compared to that of the undissociated molecules. We further assume that the whole absorption spectrum, due to the "Complex ionic group," is shifted towards the long wavelength side of the spectrum. Thus in the absorption spectra of dilute solutions, we have to consider the superpositions of two types of spectra :

(*i*) One due to the undissociated molecules in the solution, and

(*ii*) the other due to the "Complex ionic group" in the solution.

The edge due to the latter is shifted towards the long wavelength side relative to the former.

As the intensity of the former is much greater than that of the latter, it is to be expected that the intensity of the secondary spectrum due to the ionic complexes will be extremely poor and the secondary structures in dilute solutions will be practically produced entirely by the undissociated molecules. The experimental data support this contention. But near the primary edge we have to consider the superposition of the primary and the first secondary of the "Complex ionic group" with reference to the primary of the undissociated molecules.

As is well known, the intensities of the primary absorption are very much stronger than those of the secondary edges and we should naturally expect two strong primary white lines, of which one is due to the undissociated molecules and the other coming from the complex ionic groups. As suggested before, the wavelength of the K-edge of the latter is longer than that of the former. The difference in wavelength ($\delta\lambda$) between the edges is (2X U.) and is easily separated in our plate. Hence we should expect two strong white lines (of which the second one is perhaps the stronger, as the percentage of undissociated molecules has been assumed to be large) near the primary edge. The breadth of the dark line separating the two white lines, depends evidently on the shift of one system with respect to the other. In the case where the separation of the primary K-edges of the two systems is small, there would appear only one broad white band, the intensity within which will be of a fluctuating nature, In our experiments on

cobalt compounds, primary edges are resolved by the spectrograph and the nature of the absorption spectra as revealed on the photographic plates supports our contention about the superposition of the two systems of edges.

Further investigations on other metal compounds in the solid states and in solutions are necessary before any definite interpretation could be given as to the mode of existence of solute particles in solution. Experiments are being continued in this direction.

REFERENCES

[1] Lindsay and Van Dyke, *Phys. Rev.*, 2, **27**, **28** (1926).
[2] Lindsay and Voorhees, *Phil. Mag.*, **6** (1928) *Phys. Rev.*, (2) **31** (1928).
[3] Keivit and Lindsay, *Phys. Rev.*, **36** (1930).
[4] Lindh, *Zeit. f. Phys.*, **3** (1920).
[5] Hanawalt, *Journal of the Franklin Inst.*, **214** (1932)
[6] Coster and Veldkamp, *Zeit. f. Phys.*, **70** (1931).
[7] Ray, *Nature*, **122**, 771 (1928).
[8] Coster, *Zeit. f. Phys.*, **25**, 83 (1924).
[9] Lindsay, *Zeit. f. Phys.*, **71**, 5-6 (1931).
[10] and [11] Kronig, *Zeits. f. Phys.*, **70**, 5-6 (1931); *Zeits. f. Phys.*, **75**, 3-4 (1931), **76**, 7-8 (1932).
[12] Hartree, Kronig and Patersen, *Physica*, **1** (1934).
[13] Coster and Klammer, *Physica*, **1** (1934).
[14] Brewington, *Phys. Rev.*, **46** (1934).
[15] Yost, *Phil. Mag.*, **8**, 845 (1929).
[16] Mayer, *Wissenschaftliche veroffentlichungen aus dem Siemmens-Konzern*, **7**, 101 (1929).
[17] Stelling, *Zeils. f. Phys. Chem.*, **19**, Abt. B 6 (1932).
[18] Sandstrom, *Phil. Mag.*, **22** (1936).
[19] Swada, *Kyoto Coll. Sci. Mem.*, **14** (1931).
[20] Pauling, *Phys. Rev.*, **34** (1929).
[21] Prins, *Physia*, **2** (1935).

Some photometric records are shown in plate 1.

Fig. 1. Cobalt nitrite.
Fig. 2. $CoCl_2, 6H_2O$.
Fig. 3. $CoCl_2, 6H_2O$ Solution 1·0N.
Fig. 4. $Co(NO_3)_2, 6H_2O$ Solution 0·3N.
Fig. 5. $CoSO_4, 7H_2O$ Solution N/10.
Fig. 6 Saturated Solution of $Co(NO_3)_2, 6H_2O$ in nitric acid.

X-RAY LABORATORY,
UNIVERSITY COLLEGE OF SCIENCE,
2, UPPER CIRCULAR ROAD,
CALCUTTA.

ON SOURCES OF STELLAR ENERGY—A CRITICISM OF THE BETHE-GAMOW THEORY*

By RAM NIVAS RAI,

Lecturer, Allahabad University

(*Received for publication, January 17, 1940*)

ABSTRACT. A review of the existing theories of energy production in white dwarfs and other stars has been made and it has been shown that the existence of neutrons and high pressure due to the degenerate electron gas inside the white dwarfs may explain the low energy production in the white dwarfs.

In a series of papers Weizsäcker (1937), Bethe and Critchfield (1938), Bethe (1939), Gamow (1939), Gamow and Teller (1939) have applied recent researches in nuclear physics to the explanation of the production of energy in stars and to stellar evolution. By applying the formula of Atkinson and Houtermans (1929), as improved by Gamow and Teller (1938) for the probability of a nuclear reaction in a gas obeying the Maxwellian distribution of velocities, Bethe (1939) has shown that the energy production in the stars of the main sequence is due to carbon and nitrogen acting as catalysts, the net result being the formation of a helium nucleus and two positrons out of the four protons. Part of the surplus energy is radiated away in the form of two neutrinos when N^{13} and O^{15} disintegrate into C^{13} and a positron and into N^{15} and a positron respectively. In each cycle therefore we get 4.0×10^{-5} ergs of useful energy, part of which is radiated away in space and part is used in raising the temperature of the star.

As a result of this cycle of reactions, the star decreases a little in mass but grows brighter, hotter, and a little larger, till, according to Gamow (1939), the energy production due to the cycle is no longer able to maintain the temperature of the star and a contractive evolution sets in, which is very rapid if the matter inside the star continues to obey the laws of an ideal gas. Before long, however, degeneracy sets in which checks this rapid contraction and the star reaches the white dwarf stage.

For the evolution of the red giants, Gamow and Teller (1939) have shown that energy production by the carbon-nitrogen cycle and due to the direct combination of protons is negligible, and that in this case the production of energy is due to the reaction of protons with the lighter elements H^2, H^3, Li^6, Li^7, Be^9, Be^{10}

* Communicated to the Indian Physical Society by Prof. M. N. Saha.

and B^{11}. They have shown that definite bands exist in the radius-luminosity diagram which correspond to energy production by different elements. It is the object of this paper to point out some of the difficulties in the evolution of the red giants and the white dwarfs and an attempt has been made to explain them.

WHITE DWARFS

The behaviour of the white dwarfs is very peculiar and puzzling in as much as their production of energy is extremely low for their accepted values of temperature and density. As has been emphasized by Gamow (1939), we should have to assume very low temperatures ($\sim 10^6$ degrees) for the interior of white dwarfs in order to bring down the energy production due to the reaction $H^1 + H^1 \rightarrow H^2 + \beta^+$ to the observed values.* On the other hand, if we preclude the presence of hydrogen, the energy production by any other reaction will be negligible even for white dwarfs up to very high temperatures. Table I shows that the energy production by $C^{12} + He^4 = O^{16}$ reaction is very small even up to temperatures of the order of eighty million degrees and for a density of the order of 10^6. At lower temperatures the energy production is negligible. Calculations have been made from the formula given by Bethe (1939), p. 434, formula (16).

TABLE I

Temperature in million degrees	τ	$p/\rho x_1$	p for $\rho x_1 = 10^6$.	Energy in ergs gm^{-1} sec^{-1}.
20	119	3.6×10^{-21}	3.6×10^{-15}	4.2×10^{-20}
40	94.5	1.04×10^{-10}	1.04×10^{-4}	1.2×10^{-9}
60	82.5	1.23×10^{-5}	1.23×10	1.4×10^{-5}
80	75.0	1.93×10^{-2}	1.93×10^4	2.2×10^{-1}
100	69.6	3.55	3.55×10^6	4.1×10

But values of the mean molecular weight from different theories of internal structures of stars show that some of the white dwarfs still contain nuclei of atomic weight one. For example, according to Chandrasekhar (1939), Sirius B contains about 52% hydrogen and Van Mannen star No. 2, 66%. We cannot therefore assume a low temperature for the interior of the white dwarfs. Calculations of the temperature variation in the outer atmosphere, where ordinary gas laws are expected to hold, show that the temperature reaches a value of the order

* At low temperatures, the energy production by the carbon cycle is negligible in comparison with the energy production due to the above reaction. See Bethe (1939), Fig. 1, p. 452.

of 20×10^6 degrees before degeneracy sets in [see Kothari (1933) and Strömgren (1937)]. The temperature in the interior must, if anything, be higher than this value.

The only way out of this difficulty seems to be to suppose that in the interior of the white dwarfs either (a) there are certain processes which liberate a very small amount of energy, or (b) there are some endothermic reactions going on which partly counterbalance the energy production and thus cause the net production of energy to be appreciably reduced. In the last case we have to give up partly the non-equilibrium theory of energy production which is the basis of Bethe and Gamow's works.

THE NEUTRON HYPOTHESIS

Since irrespective of the presence of other nuclei, the hydrogen nuclei themselves cause the evolution of more energy in the white dwarfs than is actually observed, the supposition has been made that hydrogen nuclei are totally absent from the interior of white dwarfs and the reduction in the observed mean molecular weight of the white dwarfs is due to the presence of neutrons. The formation of neutrons at very high densities and not too high temperatures was first indicated by Sterne (1933). The pressure due to the degenerate electrons being much larger than that due to other nuclei, their disappearance will ultimately lead to a reduction of pressure. But such a process will not lead to the liberation of vast amount of energy due to gravitational contraction, as has been supposed by Baade and Zwicky* (1924), as the neutronic mass is greater than the combined mass of a proton and an electron.

We cannot, however, suppose that all nuclei inside the white dwarfs have been transformed into neutrons. The effective opacity co-efficient of white dwarfs requires that other nuclei should also be present in their interior.

Since Bethe (1939) has shown that during the earlier history of a star all elements lighter than carbon, except He^4, are converted *into* He^4 *and that the abundance of* C^{12} *and* O^{16} remains practically unchanged, inside the white dwarfs, we must have neutrons, He^4, C^{12} and O^{16} in addition to other heavy nuclei. In view of the fact that fission is produced by neutrons in heavier nuclei, we shall, however, exclude the discussion of heavier nuclei and confine our attention only to the above four.

We have already shown that up to temperatures of the order of 50 million degrees, which may be taken to be a probable value of temperature for the interior of the white dwarfs, there will be no mutual interpenetration and

* The total gravitational energy released if the Sun contracts to one-thousandth of the present radius will be of the order of 10^{51} ergs. This will be just sufficient to convert all atomic nuclei into neutrons.

occurrence of reaction possible between the heavier nuclei. We shall therefore only consider the action of neutrons on the other three nuclei.

He^4

Although we have got some experimental evidence on the scattering of neutrons by helium, we have no experimental evidence either of capture of, or disintegration by, neutrons in the case of helium. We have therefore to be guided solely by energy and probability considerations. The following show all the possible reactions between He^4 and neutrons :

$$He^4+n^1 \longrightarrow He^3+n^1+n^1 \qquad \ldots \quad (1)$$

$$He^4+n^1 \longrightarrow H^4+H^1 \qquad \ldots \quad (2)$$

$$He^4+n^1 \longrightarrow H^3+H^2 \qquad \ldots \quad (3)$$

$$He^4+n^1 \longrightarrow He^5+\gamma \qquad \ldots \quad (4)$$

Reactions of the type (1) and (2) are well known, but reactions of type (3) have not been observed. But in view of the fact that Chadwick and Goldhaber (1935) have observed the emission of H^3 by bombarding Li^6 and B^{10} by slow neutrons (the reaction according to them has a cross-section of 10^{-21} cm.^{2}) and Oliphant, Kempton and Rutherford (1935) have observed the emission of H^2 by bombarding Be^9 by protons, (3) may be possible with some of the lighter nuclei.

He^5 has been observed in certain disintegration experiments, but there is some doubt regarding its stability. Most probably it is just stable. (See a letter by Sirkar and Rai in 'Science and Culture', February, 1940.)

Of the above reactions the first three are endothermic and the energy of the bombarding neutron, from mass considerations, comes out to be so large for the reactions to be possible that there will be a negligible number of neutrons with those energies in the interior of the white dwarfs. After making even the most favourable assumptions for the probability of the reactions, it can be shown that they will be of little importance. We shall therefore consider only the reaction (4) in the case of He^4.

C^{12}

Unlike helium, a large number of reactions have actually been observed with carbon. These are summerised below :

$$C^{12}+n^1 \qquad Be^9+He^4 \qquad (5)$$

$$C^{12}+n^1 \qquad 3He^4+n^1 \qquad (6)$$

$$C^{12}+n^1 \qquad B^{12}+n^1 \qquad (7)$$

$$C^{12}+n^1 \qquad C^{11}+n^1+n^1 \qquad (8)$$

$$C^{12}+n^1 \qquad C^{13} \qquad (9)$$

With the exception of the last reaction, all other reactions listed above are endothermic requiring large energies (order of several Mev.) for their realisation. The reaction (9) listed above will therefore be the only reaction which will be of importance. Similar considerations with oxygen show that radiative capture will be the only process which needs to be considered.

Our knowledge of the cross-section for thermal neutrons in helium, carbon and oxygen is at present very scanty. Unless however low energy resonance levels are present in these elements, the cross-sections must be very small and must decrease as the energy of the neutron is increased. Carrol and Dunning (1938) have obtained a value $1{\cdot}51 \times 10^{-21}$ for the scattering cross-section of thermal neutrons in helium, and according to Straub and Stephens (1939), who have measured the ratio of cross-section of neutrons in helium and hydrogen, no appreciable increase in the ratio occurs till the neutrons reach an energy of 0·8 Mev. As this is too high for the thermal neutrons in the stellar interiors, we shall not consider the modification introduced in the value of the cross-section by the presence of resonance levels.

A similar estimate of the nuclear cross-section for thermal neutrons in the case of carbon and oxygen is not possible. According to Amaldi, Bocciarelli, Rasetti and Trabacchi (1939) and Goloborodko and Leipunski (1939), the cross-section for neutrons of energies 130 Kev. to 350 Kev. is of the order of 2×10^{-21} cm.^{2} both for carbon and oxygen.

We can therefore put $\sigma \simeq \dfrac{\pi h^2}{2mE}$.

Putting this value and integrating, we shall get the total number of collisions. This is to be multiplied by the ratio of the probabilities of γ-ray and particle emissions which is

$$\frac{\Gamma r}{h/mr^2} = \frac{\Gamma m r^3}{h^2}$$

where Γ is the γ-ray width in ergs and r the nuclear radius.

Table II gives the γ-ray width for the different reactions, calculated according to Bethe (1939) (eq. 10).

TABLE II

Original nucleus.	Product nucleus.	γ-ray energy in MMU.	γ-ray width in ergs.
He^4	He^5	~ 0.02	0.64×10^{-14}
C^{12}	C^{13}	5.69	4.50×10^{-12}
O^{16}	O^{17}	4.75	3.14×10^{-12}

The total number of captures per sec. per gram is finally given by

$$N = \int_0^{\infty} \frac{4xy\rho\,\sigma}{m_1 m_2 (kT)^{\frac{3}{2}}} \left(\frac{2\pi}{m}\right)^{\frac{1}{2}} \frac{\Gamma m \Gamma_1^2}{h^2}\, e^{-E/kT}\, E\, dE$$

$$= \frac{\pi xy\rho}{m_1 m_2}\left(\frac{2\pi}{m\,kT}\right)^{\frac{1}{2}} \Gamma_1^2$$

$$\simeq xy\,\frac{(A_1 + A_2)^{\frac{7}{2}}}{(A_1A_2)^{\frac{3}{2}}}\,\Gamma \times 6.58 \times 10^{44}$$

where A_1, A_2 = Atomic weights of the nuclei and the neutron

$$m = \text{reduced mass} = \frac{m_1 m_2}{m_1 + m_2}.$$

This shows that even for helium for which the probability of capture is the least, the number of captures gm.$^{-1}$ sec.$^{-1}$ will be of the order of 10^{24} This will lead to a very large amount of energy being produced in the white dwarfs.

It thus appears that the reverse processes will play a large part in these reactions. Taking for example C^{12} as a representative case, C^{13} will either be transformed into C^{14} or C^{12} by the neutron bombardment. The latter process will absorb energy. Also on account of the degeneracy of the electrons, the transformation of C^{14} into N^{14}, an electron and a neutrino will not be possible as this will lead to an increase of pressure due to the degenerate electron gas. These will therefore be ultimately broken up by neutrons and building of heavier nuclei will be a very very slow process. It may thus happen that ultimately very little production of energy takes place.

In conclusion the author has great pleasure in thanking Prof. M. N. Saha for his kind interest and valuable advice.

REFERENCES

Amaldi E., Bocciarelli D., Rasetti, and Trabacchi G. C., (1939), *Phys. Rev.* **56**, 881.
Atkinson R. d'E, and Houtermans F. G., (1929), *Zeits f. Phys.*, **54**, 656,
Baade F., Zwicky F., (1934), *Proc. Nat. Acad. Sci.* **20**, 263.
Bethe H. A., (1939), *Phys. Rev*, **55**, 434.
Bethe H. A., and Critchfield C L, (1938), *Phys Rev* **54**, 248
Carrol H., Dunning J. R., (1938), *Phys. Rev.*, **54**, 541.
Chadwick J., Goldhaber M., (1935) *Nature*, **136** 65.
Chandrasekhar S, (1939), *An Introduction to the Study of Stellar Structure*, 433.
Gamow, G., (1939), *Phys Rev.*, **55**, 718, 769. See also *Nature*, **144**, 575, 620.
Gamow G., and Teller E. (1938), *Phys. Rev.*, **53**, 608.
Gamow G, and Teller E. (1939), *Phys. Rev.*, **55**, 654, 791.
Goloborodko T., and Leipunski A. (1939), *Phys. Rev*, **56**, 681.
Kothari D, S. (1933), *Mon. Not.*, **93**, 61
Oliphant M. L. E, Kempton A. E., and Rutherford (Lord) (1935), *Proc Roy. Soc. A.* **150**, 241.
Sterne Th, *Mon. Not.*, (1933), **93**, 736.
Strömgren B. (1937), *Eng. Exact. Naturwiss*, **16**, 508.
Von Weizsäcker (1939), *Phys. Zeits.*, **38**, 176.

ON THE WIDTH OF THE K-ABSORPTION EDGE OF COBALT

By N. BAGCHI, M.Sc.

(*Received for publication, January 17, 1940*)

Plate II

ABSTRACT. The width of the K-absorption edge of cobalt metal and the compounds CoO; Co_2O_3; $Co(NO_3)_2, 6H_2O$; $CoSO_4, 7H_2O$; $CoCl_2$ (anhydrous); $CoCl_2, 6H_2O$ in the solid form and in aqueous solutions of $CoSO_4, 7H_2O$; $CoCl_2, 6H_2O$ and $Co(NO_3)_2, 6H_2O$ having different strengths together with a concentrated solution of cobalt nitrate in nitric acid has been studied. It has been observed that so far as the compounds of cobalt in the solid states are concerned the pure metallic element shows the largest width, whereas in solid metallic compounds and their aqueous solutions, the solid has the smallest width. The width of the edge in a concentrated solution of cobalt nitrate in nitric acid deserves particular attention as it is not only appreciably larger than the same obtained in the solid nitrate and in its aqueous solutions but also is largest obtained in this set of investigations.

It has also been found in the case of metallic element and blue oxide CoO that neither the inflection point which determines the wavelength of the edge nor the full width or the idealised width is affected by the screen thickness. The presence of structure edge K′ is also reported in the case of cobalt metal and its black oxide Co_2O_3.

INTRODUCTION

The measurements of the widths of the X-ray absorption edges have not yet received so much attention as the X-ray emission lines. In the later cases, widths are expressed in terms of the well-defined half-width of the emission lines as in the case of optical spectra. In the X-ray absorption spectra, however, two definitions are generally used to define the width of the edge. The first is defined by the full width and is measured by the distance of two points of maximum and minimum intensity in the photometric curve. The other definition first suggested by Ross [1] measures the distance between the intersection points of the tangent through the inflection point and the two horizontal lines passing through the points of maximum and minimum intensities. Really it is very difficult to ascertain the maximum point, *i.e.*, the long wavelength in the edge with any accuracy mainly because of the smooth decline of the curve. The determination of the wavelength of the edge is now generally made by measuring the middle point of the edge, *i.e.*, the inflection point or really the middle point of

Communicated by the Indian Physical Society

the straight portion of the edge in the photometric records, as all absorption edges are more or less asymmetrical.

Richtmeyer and Barnes [2] from theoretical considerations have pointed out that the screen thickness may have a profound influence not only on the shape but also on the position and the widths of the absorption edges.

Sandstrom [3] carried out a systematic investigations in the L-absorption edges of 30 Zn to 52 Te, and found that with the varying thickness of the absorber 34 Se there is no systematic variation of the wavelength of the edge. It was also found that the point of inflection, which corresponds with a fair degree of accuracy with the middle portion of the straight part of the photometric curve is unaffected by the screen thickness. Sandstrom has measured the full widths of the most of L_{II} and L_{III} edges and some L_I edges in the region 30 Zn to 52 Te, showing the variation of the width with atomic numbers.

Cioffari [4] has investigated the width of the edges of Bromine and Iodine in the element itself in solid, liquid and vapour phases and also in chemical combination by the double-crystal spectrometer. He reports that chemical combination seems to have very little effect on the width of the K-absorption edges. Most of the compounds of bromine and iodine showed nearly the same width as that of the pure element, no matter in what phase it was. The only exceptions were shown by IBr vapour which had a slightly narrower width and CH_3Br which had a larger value for the width.

The similarity of the structures of the K-edge of Cobalt, in cobalt metal, in its various compounds and also in aqueous solutions of different strengths of some of these compounds was reported before. [6] It was also stated there that with only dilute solutions of strengths of the order of N/10 and N/20, a quite different structure of the edges adjacent to the main one was found. In this connection it was thought proper to investigate the effect on the width of the edges under different combinations and also with aqueous solutions of different strengths.

EXPERIMENTS

A Siegbahn Vacuum spectrograph was used with a calcite crystal. The latter was rotated through 2°-30′ about the mean angle for the K-absorption edge of cobalt. The width of the slit was 0·1 mm. and was covered with thin aluminium foils of thickness .002 cm. to separate the high vacuum part of the X-ray tube from the spectrograph.

The dispersion in the plate was found to be 16.41 X. U. per mm. The photometric records magnified the lines to 6.78. All measurements of the widths of the edge were made with the photometric record.

A large number of plates was taken with absorption screen of varying thickness of cobalt metal and cobaltous oxide (CoO). Although actual measurements of screen thickness were not made, it was found that neither the point of inflec-

tion which determines the actual position of the absorption edge, nor the "full-width" or "idealised" widths showed any change with varying thickness.

In some absorption spectrum with cobaltous oxide (CoO) as the absorption screen was made very thick, the contrast between the black and white bands on the short-wavelength side of the main edge was so poor that only a continuous white band appeared in the photographic plate without any secondary structures.

Barnes [5] has found that the K-edges of the elements $_{25}Mn - _{29}Cu$ have a fine structure in the edge itself. In the element cobalt and in Co_2O_3 similar "structure edge" K′ whose wavelength is about 1 X.U. shorter than the primary edge has also been found in our experiments.

As it is extremely difficult to locate the actual position of maximum and minimum intensities preceding and following an absorption jump as well as the direction of the tangent at the point of inflection, an error as high as 20 per cent is quite likely in these measurements. The photometric records of cobalt metal (Fig. 1); Co_2O_3 (Fig. 2); Co-nitrite (Fig. 3); $CoCl_2, 6H_2O$ (Fig. 4); $Co(NO_3)_2, 6H_2O$ (Fig. 5); $Co(NO_3)_2, 6H_2O$ in .3N Sol. (Fig. 6); $Co(NO_3)_2, 6H_2O$ Sol. in HNO_3 (Fig. 7); and $CoCl_2, 6H_2O$ in 1.5N sol. (Fig. 8) are given here.

The following table gives the results on the measurements on the idealised widths.

TABLE I

Solid Substance	Strength.	Idealised Width of the K-edge of Cobalt in X.U.
Cobalt metal (Co)	...	4·1
Cobaltous oxide (CoO)	...	3·0
Cobaltic oxide (Co_2O_3)	...	2·0
Cobalt nitrite	...	2·2
Cobalt sulphate ($CoSO_4, 7H_2O$)	...	2·5
Cobalt Nitrate ($Co(NO_3)_2, 6H_2O$)	...	3·6
Cobaltous chloride ($CoCl_2, 6H_2O$)	...	3·6
Cobalt Chloride ($CoCl_2$) (anhydrous)	...	2·6
Solutions		
$Co(NO_3)_2, 6H_2O$	solid	3·6
$Co(NO_3)_2, 6H_2O$	1·9N	4·1
$Co(NO_3)_2\ 6H_2O$	·6N	4 6
$Co(NO_3)_2, 6H_2O$	3N	4·4
$Co(NO_3)_2, 6H_2O$	concentrated sol. in nitric acid	6·8

TABLE I (contd.)

Solution.	Strength.	Idealised width of the K-edge of cobalt in X.U.
$CoSO_4$ $7H_2O$	solid	2.5
$CoSO_4$, $7H_2O$	1.7N	3.6
$CoSO_4$, $7H_2O$	1N	4.8
$CoSO_4$, $7H_2O$	N/10	4.8
$CoSO_4$, $7H_2O$	N/20	4.8
$CoCl_2$	anhydrous	2.6
$CoCl_2$, $6H_2O$	hydrated solid	3.6
$CoCl_2$, $6H_2O$	1.5N	3.0
$CoCl_2$, $6H_2O$	1N	2.9
$CoCl_2$, $6H_2O$	N/10	2.9
$CoCl_2$. $6H_2O$	N/20	3.6

In this region, 4.1 X. U. is equivalent to an energy value of 20 Volts.

From the table I, it is apparent that of all the solid substances investigated, cobalt metal definitely shows the largest width. In Co_2O_3 we have the smallest width. An error in this measurement is quite large because of the presence of a peculiar position of the fine structure in the edge itself. Cobalt nitrat cannot be obtained in the pure form ; it is always a mixture of cobaltous and cobaltic nitrites as well as cobaltous nitrate.

From a survey of the results obtained in the cobaltous nitrate, $Co(NO_3)_2$, $6H_2O$, in states of solid and aqueous solutions, one can conclude that the solid shows the smallest width, which rises in the case of solution ; as a matter of fact from 1N to .3N solutions, the width is fairly constant. Concentrated solution of $Co(NO_3)_2$, $6H_2O$ in strong HNO_3 shows the largest width. (Fig. 7.)

In $CoSO_4$, $7H_2O$ we have an analogous result; the width is definitely smaller in the solid state than in solutions. From 1N to N/20, it is fairly steady with an intermediate value for 1.7N solution.

From the table I, it will be seen that $CoCl_2$ (anhydrous) has the smallest width and $CoCl_2$, $6H_2O$ (solid) and aqueous solutions of different strengths show the same width within experimental error.

It may be mentioned here that the anhydrous salts of $Co(NO_3)_2$ and $CoSO_4$ could not be easily prepared and so in the solid state, $Co(NO_3)_2$,$6H_2O$ and $CoSO_4$, $7H_2O$ only were examined. The widths of the K-edges of these salts in solid

PHOTOMETRIC RECORDS OF SOME ABSORPTION EDGES

MAGNIFICATION 6·78 x

Fig. 1

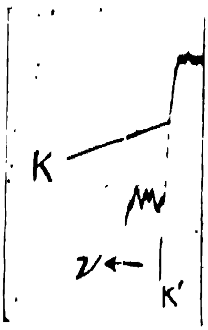

Co-metal

Fig. 2

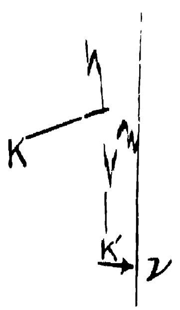

Co_2O_3

Fig. 3

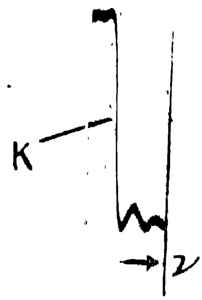

Co-nitrite

Fig. 4

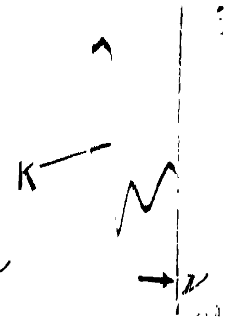

$CoCl_2 6H_2O$

Fig 5

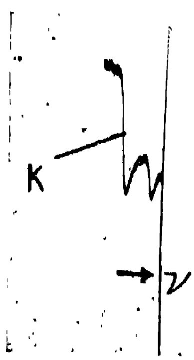

$Co(NO_3)_2, 6H_2O$

Fig 6

$Co(NO_3)_2,6H_2O$ Soln. ·3N

Fig 7

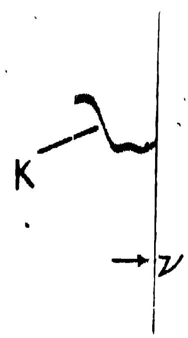

$Co(NO_3)_2,6H_2O$, Soln. in HNO_3,

Fig 8

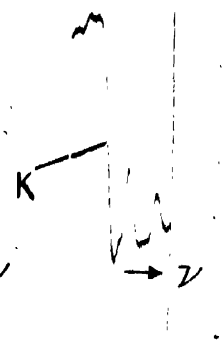

$CoCl_2,6H_2O$ Soln. 1·5 N

The K edge and some secondaries are shown.

K′ - the fine structure with the edge K

states were definitely smaller than those obtained in aqueous solutions. It is quite likely that the anhydrous salts of $CoSO_4$ and $Co(NO_3)_2$ might possess smaller widths than the hydrated ones ; but unlike $CoSO_4, 7H_2O$, and $Co(NO_3)_2, 6H_2O$, K-edges have approximately the same width in $CoCl_2, 6H_2O$, as in its aqueous solutions.

It may be concluded that so far as the compounds of cobalt in the solid states are concerned the pure metallic element shows the largest width whereas in the solid metallic compounds and their aqueous solutions the solid has the smallest width.

In conclusion the author expresses his sincere thanks to Prof. B. B. Ray for the interest he has taken during the progress of the work.

University College of Science,
Khaira Laboratory of Physics,
92, Upper Circular Road,
Calcutta.

REFERENCES

[1] Ross, *Phys. Rev.*, **44** (1933).
[2] Richtmeyer and Barnes, *Phys. Rev.*, **45** (1934).
[3] Sandstrom, *Phil. Mag.*, **22** (1936).
[4] Cioffari, *Phys. Rev.*, **51** (1937).
[5] Barnes, *Phys. Rev.*, **44** (1933).
[6] Ray, Das and Bagchi., *Ind. Jour. Phys.*, Vol. 14.

"THE SPRIAL ARMS OF A CONFIGURATION OF ROTATING COMPRESSIBLE MASS HAVING UNIFORM DENSITY AND SURROUNDING AN INCOMPRESSIBLE SPHEROID OF HOMOGENEOUS MASS"*

By PROF. A. C. BANERJI

(*Received for publication, Jan. 29, 1940*)

ABSTRACT. The author has investigated the condition necessary for the formation of spiral arms in the equatorial plane of a rotating gaseous configuration of uniform density which surrounds a spheroidal homogeneous mass of incompressible material. The size of the central mass is assumed to be small compared to that of the outer boundary of the gaseous structure It is evident that the density of the gaseous structure can only be uniform if the angular velocity ω is variable and satisfies a certain relation. The author has also determined the relation that would exist between the distance ϖ from the axis of rotation and the angular velocity ω.

Particular cases of our Galactic System and the Andromeda Nebula have also been considered. For spiral formation, it is found that the diameter of the inner central core should be less than 270 parsecs for the Galactic System and less than 560 parsecs for the Andromeda Nebula.

Banerji, Bhatnagar and Nizamuddin have worked out in a recent paper[1] the case of a rotating spheroidal central mass of small but finite dimensions and uniform density, surrounded by a spheroidal structure of rotating compressible gas of variable density. They have also investigated the condition necessary for the formation of spiral arms. Lindblad[2] has also considered the case of a condensed point-nucleus which is surrounded by a spheroidal galaxy of stars of uniform density from which arms emanate. Now recent investigations by Plaskett[3] and Pearce about our galactic system show that "the whole galactic system is immersed in a gaseous substratum consisting of atoms of various elements . . . the separate atoms while obeying *ordinary gas laws* participate in a rotational movement around a distant central mass in galactic longitude 325°." So for a mathematical investigation it seems proper to assume that the central core is surrounded by a gaseous mass instead of a galaxy of stars, as assumed by Lindblad Moreover Eddington's[4] theoretical researches as well as Plaskett[5] and Pearce's observational investigations show that interstellar space (within the confines of the galaxy) is not empty but is filled with a very highly rarified gas of "substantially *uniform* density." Smart[6] also remarks "the observed feature of galactic rotation may be ascribed to a highly concentrated central mass together with a *uniform* spheroidal

* Communicated by the Indian Physical Society.

distribution of matter." For mathematical analysis the author has assumed a configuration in which there is a central rotating spheroidal core of homogeneous and incompressible material whose density is ρ_0 and which is of small but finite dimensions. This core is again surrounded by a rotating gaseous configuration of *mean* density ρ_1, which differs slightly from the actual density at any point of the gaseous mass. In fact, it will be shown later on that a rotating gaseous configuration cannot have uniform density, but if it be a very much flattened spheroid, then the variation of density may be quite small provided a suitable law for the variation of angular velocity is assumed. It may be pointed out here that the bounding surface of a rotating gaseous mass is a pseudo-spheroid.[7] If the angular velocity everywhere is small, the pseudo-spheroid differs slightly from the spheroid. So without any serious error we can assume that this bounding surface is a spheroid.

We shall take 'a' to be the equatorial radius of the outer boundary of the spheroidal gaseous configuration of *mean* density ρ_1, and $k_0 a$ to be the equatorial radius of the spheroidal boundary of the central mass of density ρ_0. It is assumed that both these spheroids are similar in form. k_0 is taken to be small although it is of finite magnitude. It need hardly be mentioned that ρ_0 is greater than ρ_1.

Now we have to investigate the path of a particle or a small amount of matter, which may have been ejected from the equatorial plane of the galactic configuration due to a slight perturbation. The total intensity of attraction at an external point in the equatorial plane may be assumed to be made up of *two* parts, *viz.*, one part is due to the attraction of the larger spheroid of equatorial radius 'a' and density ρ_1, and the other is due to the smaller spheroid of equatorial radius $k_0 a$ and density $(\rho_0 - \rho_1)$.

If f be the total attraction, e the eccentricity of each spheroid, we have[8]

$$f = 2\pi\left(1-e^2\right)^{\frac{1}{2}}\rho_1\left[\frac{2}{3}\cdot\frac{a^3}{r^2}+\frac{1}{5}\cdot\frac{a^5}{r^4}e^2+\ldots\ldots\right.$$

$$\left.+\frac{1.3\ldots(2n-1)}{2.4\ldots\ldots 2n}\cdot\frac{2}{2n+3}\cdot\frac{a^{2n+3}e^{2n}}{r^{2n+2}}\right]$$

$$+2\pi\left(1-e^2\right)^{\frac{1}{2}}\left(\rho_0-\rho_1\right)\left[\frac{2}{3}\cdot\frac{k_0^3a^3}{r^2}+\frac{1}{5}\cdot\frac{k_0^5a^5}{r^4}\cdot e^2+\ldots\right.$$

$$\left.+\frac{1.3\ldots\ldots(2n-1)}{2.4\ldots\ldots 2n}\cdot\frac{2}{2n+3}\cdot\frac{k_0^{2n+3}a^{2n+3}e^{2n}}{r^{2n+2}}\right], \quad \ldots \quad (1)$$

where terms containing powers of e higher than $2n$ have been neglected.

Hence,

$$f = 2\pi\,(1-e^2)^{\frac{1}{2}}\left[\frac{2}{3}\cdot\frac{a^3}{r^2}\left\{k_0^3\rho_0+\rho_1\left(1-k_0^3\right)\right\}+\frac{1}{5}\,\frac{a^5}{r^4}e^2\right.$$

$$\times\left\{k_0^5\rho_0+\rho_1\left(1-k_0^5\right)\right\}+\ldots\ldots+\frac{1.3\ldots(2n-1)}{2.4\ldots2n}\cdot\frac{2}{2n+3}\cdot\frac{a^{2n+3}\,e^{2n}}{r^{2n+2}}$$

$$\left.\times\left\{k_0^{2n+3}\rho_0+\rho_1\,(1-k_0^{2n+3})\right\}\right] \qquad \ldots \quad (2)$$

$$=\frac{A_0}{r^2}+\frac{A_1}{r^4}+\ldots+\frac{A_n}{r^{2n+2}},$$

where $A_0 = 2\pi\,a^3\,(1-e^2)^{\frac{1}{2}}\,\rho_0\,\frac{2}{3}\cdot\left\{k_0^3+\frac{\rho_1}{\rho_0}\,(1-k_0^3)\right\}=2\pi a^3\,(1-e^2)^{\frac{1}{2}}\,\rho_0\alpha_0$

$$A_1 = 2\pi a^5\,(1-e^2)^{\frac{1}{2}}\,\rho_0\,\frac{1}{5}\cdot\left\{k_0^5+\frac{\rho_1}{\rho_0}\,(1-k_0^5)\right\}=2\pi a^5\,(1-e^2)^{\frac{1}{2}}\,\rho_0\alpha_1$$

... ...

$$A_n = 2\pi a^{2n+3}\,(1-e_2)^{\frac{1}{2}}\,\rho_0\,\frac{1.3\ldots(2n-1)}{2.4\ldots2n}\cdot\frac{2}{2n+3}$$

$$\times\left\{k_0{}^{2n+3}+\frac{\rho_1}{\rho_0}\,(1-k_0^{2n+3})\right\}$$

$$=2\pi a^{2n+3}\,(1-e^2)^{\frac{1}{2}}\,\rho_0\alpha_n,$$

where $\alpha_0=\frac{2}{3}\cdot\left[k_0^3+\frac{\rho_1}{\rho_0}\,(1-k_0^3)\right]$

$$\alpha_1=\frac{1}{5}\cdot\left[k_0^5+\frac{\rho_1}{\rho_0}\,(1-k_0^5)\right]$$

... ...

$$\alpha_n=\frac{1.3\ldots(2n-1)}{2.4\ldots2n}\cdot\frac{2}{2n+3}\cdot\left[k_0^{2n+3}+\frac{\rho_1}{\rho_0}\,(1-k_0^{2n+3})\right]$$

The equation of the orbit of an external particle which has just been ejected in the equatorial plane is

$$\frac{d^2u}{d\theta^2}+u=\frac{f}{h^2u^2}=\frac{1}{h^2}\left[A_0+A_1u^2+A_2u^4+\ldots+A_nu^{2n}\right], \quad \ldots \quad (3)$$

where $u=1/r$.

If there be a slight perturbation, h will remain unchanged, and we can take $h=a^2\omega_1$, ω_1 being the angular velocity at any point on the equatorial circular boundary of the gaseous configuration. Remembering that when $u=u_0=1/a$, the orbit is circular and $\frac{du}{d\theta}=0$, we have

$$\frac{du}{d\theta}=\pm\sqrt{\frac{2}{h^2}\left(A_0u+\frac{A_1}{3}u^3+\ldots+\frac{A_n}{2n+1}u^{2n+1}\right)-u^2+u_0^2 -\frac{2}{h^2}\left(A_0u_0+\frac{A_1}{3}u_0^3+\ldots+\frac{A_nu_0^{2n+1}}{2n+1}\right)}\,.$$

we get

$$\frac{dr}{d\theta}=\pm r^2\sqrt{\frac{2}{h^2}2\pi a^3\rho_0\left[\frac{\alpha_0}{r}+\frac{\alpha_1}{3}\frac{a^2e^2}{r^3}+\ldots+\frac{\alpha_na^{2n}e^{2n}}{(2n+1)r^{2n+1}}\right](1-e^2)^{\frac{1}{2}}-\frac{1}{r^2}+\frac{1}{a^2} -\frac{2}{h^2}2\pi a^3\rho_0\left[\frac{\alpha_0}{a}+\frac{\alpha_1}{3}\frac{e^2}{a}+\ldots+\frac{\alpha_ne^{2n}}{(2n+1)a}\right](1-e^2)^{\frac{1}{2}}} \quad \ldots \quad (4)$$

For a spiral form $\frac{dr}{d\theta}$ must be real, finite, and continuous, and of the same sign as r changes with θ. Hence in order that the spiral form may be possible, the expression under the root sign must be positive for all values of $r > a$. Substituting $a^2\omega_1$ for h for all values of $r > a$, we must have

$$\frac{1}{a^2}-\frac{1}{r^2}>\frac{2}{a^4\omega_1^2}2\pi\cdot a^3\rho_0\left[\alpha_0\left(\frac{1}{a}-\frac{1}{r}\right)+\frac{\alpha_1e^2}{3}\left(\frac{1}{a}-\frac{a^2}{r^3}\right) +\ldots+\frac{\alpha_ne^{2n}}{2n+1}\left(\frac{1}{a}-\frac{a^{2n}}{r^{2n+1}}\right)\right](1-e^2)^{\frac{1}{2}}\,. \quad \ldots \quad (5)$$

On slight reduction we get the condition

$$\frac{r+a}{r} > \frac{4\pi\rho_0}{\omega_1^2}\left[a_0 + \frac{a_1 e^2}{3}\left(1+\frac{a}{r}+\frac{a^2}{r^2}\right)+\ldots+\frac{a_n e^{2n}}{2n+1}\left(1+\frac{a}{r}+\ldots+\frac{a^{2n}}{r^{2n}}\right)\right]$$

$$\times(1-e^2)^{\frac{1}{2}} \quad \ldots \quad (6)$$

As $r > a$, the conditions for spiral formation is *all* the *more* satisfied if

$$\frac{r+a}{r} > 1 > \frac{4\pi\rho_0}{\omega_1^2}\left[a_0 + a_1 e^2 + \ldots + a_n e^{2n}\right](1-e^2)^{\frac{1}{2}} \quad \ldots \quad (7)$$

i.e., if

$$\frac{\omega_1^2}{2\pi\rho_0} > 2(1-e^2)^{\frac{1}{2}}\left[a_0 + a_1 e^2 + a_2 e^4 + \ldots + a_n e^{2n}\right] \quad \ldots \quad (8)$$

i.e., if k_0 is small and we neglect k_0^3 and higher powers of k_0 the above condition reduces to

$$\frac{\omega_1^2}{2\pi\rho_0} > 2(1-e^2)^{\frac{1}{2}}\left[\frac{2}{3}\left(1-\frac{\rho_1}{\rho_0}\right)k_0^3 + \frac{\rho_1}{\rho_0}\left\{\frac{2}{3}+\frac{1}{5}e^2+\ldots+\frac{1.3\cdots(2n-1)}{2.4\cdots 2n}\right.\right.$$

$$\left.\left.\times\frac{2}{2n+3}e^{2n}\right\}\right]. \quad \ldots \quad (9)$$

If this condition is satisfied then the two values of $\frac{dr}{d\theta}$ which are equal in magnitude but opposite in sign show that two similar spiral arms may emanate from two diametrically opposite points in the equatorial plane.

Now we shall discuss the conditions under which the density of the gaseous configuration may be assumed to be more or less constant.

Now we have the three equations of relative equilibrium

$$\frac{\partial p}{\partial x} = \rho\frac{\partial V}{\partial x} + \rho\,\omega^2 x$$

$$\frac{\partial p}{\partial y} = \rho\frac{\partial V}{\partial y} + \rho\omega^2 y$$

$$\frac{\partial p}{\partial z}=\rho\frac{\partial V}{\partial z},$$

where p is the pressure and V the gravitional potential at any point of the gaseous mass.

We get $$\frac{dp}{\rho}=dV+\frac{\omega^2}{2}.\ d(x^2+y^2)$$

or $$kd\log\rho=dV+\frac{\omega^2}{2}.\ d(x^2+y^2).$$

If ρ is constant then $$dV+\frac{\omega^2}{2}\ d(x^2+y^2)=0$$

$$\therefore\quad V+\int\frac{\omega^2}{2}\ d(x^2+y^2)=\text{const.}\qquad\text{(10)}$$

or $$2V+\int\omega^2\, d\,\widehat{\omega}^2=\text{const.},$$

where $$\widehat{\omega}^2=x^2+y^2.$$

Put $$\omega^2=F'(\widehat{\omega}^2)=\frac{dF}{d\widehat{\omega}^2}$$

$$\therefore\quad 2V+F(\widehat{\omega})^2=\text{const.}\qquad\text{(11)}$$

Now we can take for any point P in the gaseous configuration outside the central core $$V=V_o+V_i,$$

where V_o is the potential at P due to the larger homogeneous spheroid of density ρ_1 and V_i is the potential at P due to a central core of density $(\rho_o-\rho_1)$.

Now [10]

$$V_o=\frac{a^2}{2}\rho_1\left\{\frac{D}{a^2}-A\frac{\widehat{\omega}^2}{a^2}-\frac{Cz^2}{a^2}\right\},\qquad\text{(12)}$$

where A, C, D are given by

$$D=\frac{4\pi a^2}{e}\sqrt{1-e^2}\quad\tan^{-1}\frac{e}{\sqrt{1-e^2}}\;;$$

$$C=\frac{4\pi}{e^3}\left[e-\sqrt{1-e^2}\tan^{-1}\frac{e}{\sqrt{1-e^2}}\right];$$

$$A=\frac{2\pi}{e^3}\left[e(e^2-1)+\sqrt{1-e^2}\quad\tan^{-1}\frac{e}{\sqrt{1-e^2}}\right].$$

V_i clearly satisfies the Laplace's equation $\nabla^2 V_i=0$ at P which is external to the central core.

We can write this equation as

$$\frac{\partial^2 V_i}{\partial z^2}+\frac{\partial^2 V_i}{\partial \widehat{\omega}^2}+\frac{1}{\widehat{\omega}}\frac{\partial V_i}{\partial \widehat{\omega}}+\frac{1}{\widehat{\omega}^2}\frac{\partial^2 V_i}{\partial \phi^2}=0 \qquad \dots \quad (13)$$

where ϕ is the azimuthal angle. A particular solution is

$$V_i=e^{\pm\lambda\frac{z}{a}}\,\chi(\widehat{\omega}),\qquad \text{where } \lambda \text{ is constant,}$$

provided

$$\chi''(\widehat{\omega})+\frac{1}{\widehat{\omega}}\chi'(\widehat{\omega})+\frac{\lambda^2}{a^2}\chi(\widehat{\omega})=0. \qquad \dots \quad (14)$$

The solution which is finite for $\widehat{\omega}=0$, must be in the form of an ascending series, and it can be written as

$$C\,J_0\left(\frac{\lambda}{a}\widehat{\omega}\right),$$

where

$$J_0(\zeta)=1-\frac{\zeta^2}{2^2}+\frac{\zeta^4}{2^2.4^2}-\;\dots \qquad \dots \quad (15)$$

as $V_i \longrightarrow 0$ when $z\longrightarrow\infty$ ..., we should have for the particular solution

$$V_i=e^{-\lambda\frac{z}{a}}\,J_0\left(\frac{\widehat{\omega}\lambda}{a}\right). \qquad \dots \quad (16)$$

In the case of the central core of density $(\rho_o - \rho_1)$, V_i must be of the form

$$V_i = a_1 e^{-\lambda_1 \frac{z}{a}} J_o\left(\frac{\widehat{\omega}\lambda_1}{a}\right) + a_2 e^{-\lambda_2 \frac{z}{a}} J_o\left(\frac{\widehat{\omega}\lambda_2}{a}\right) + \ldots, \qquad \ldots \quad (17)$$

where a_1, a_2,.........and λ_1, λ_2, have determinate values.

Therefore we have $2a_1 e^{-\lambda_1 \frac{z}{a}} J_o\left(\frac{\widehat{\omega}\lambda_1}{a}\right) + 2a_2 e^{-\lambda_2 \frac{z}{a}} J_o\left(\frac{\widehat{\omega}\lambda_2}{a}\right) + \ldots$

$$+ a^2\rho_1\left\{\frac{D}{a^2} - A\frac{\widehat{\omega}^2}{a^2} - C\frac{z^2}{a^2}\right\} + F(\widehat{\omega}^2) = \text{const.} \qquad \ldots \quad (18)$$

If the gaseous configuration is a very much flattened spheroid then $\frac{z}{a}$ becomes very small, and also A and D have negligible values, we therefore write the above equation approximately as

$$2a_1 J_o\left(\frac{\widehat{\omega}\lambda_1}{a}\right) + 2a_2 J_o\left(\frac{\widehat{\omega}\lambda_2}{a}\right) + \ldots\ldots\ldots \ldots + F(\widehat{\omega}^2) = \text{const.}$$

Now, $\omega^2 = F'(\widehat{\omega}^2)$

$$= -2a_1 \frac{dJ_o\left(\frac{\widehat{\omega}\lambda_1}{a}\right)}{d\widehat{\omega}^2} - 2a_2 \frac{dJ_o\left(\frac{\widehat{\omega}\lambda_2}{a}\right)}{d\widehat{\omega}^2}. \qquad \ldots \quad (19)$$

If λ_1, λ_2, etc., are small, then for comparatively small values of $\widehat{\omega}$ we can write

$$\omega^2 = B_1 - B_2\left(\frac{\widehat{\omega}}{a}\right)^2. \qquad \ldots \quad (20)$$

It may be mentioned now that photographs [11] of different lengths of exposure suggest very forcibly that inner layers of a nebula are rotating more rapidly than the outer layers. It is therefore necessary that both B_1 and B_2 should be positive and that B_1 should be greater than B_2. We shall now calculate the upper limit for k_o in the case of our galaxy and of Andromeda nebula.

. *Our Galactic System* :—

Equatorial diameter $=30{,}000$ parsecs
Polar Diameter $=6000$ parsecs
Period of rotation $=2{\cdot}3\times10^8$ years.

Then
$$1-e^2=\frac{1}{25} \quad \text{and} \quad e^2=\frac{24}{25}.$$

It is easily seen that in this case the series

$$\frac{2}{3}+\frac{1}{5}e^2+\ldots\ldots+\frac{1\cdot3\ldots(2n-1)}{2\cdot4\ldots\ldots\ldots\ldots2n}\cdot\frac{2}{2n+3}\quad e^{2n}$$

in equation (9) is less than $2{\cdot}5$.

Moreover it is reasonable to suppose that ρ_1 is small as compared with ρ_0. We thus find that (9) is all the more statisfied if

$$\frac{\omega_1{}^2}{2\pi\rho_0}>\frac{4}{15}k_0^3+\frac{\rho_1}{\rho_0}. \qquad \ldots \quad (21)$$

In the case of our galaxy it becomes

$$\frac{1{\cdot}2\times10^{-31}}{\rho_0}>\frac{4}{15}k_0^3+\frac{\rho_1}{\rho_0}$$

or
$$\frac{1{\cdot}2\times10^{-31}-\rho_1}{\rho_0}>\frac{4}{15}k_0^3.$$

It shows that the maximum value that ρ_1 can have is of order 10^{-31} c.g.s unit, as k_0 cannot have a negative value.

We may also note that if ρ_0 becomes greater, k_0 becomes smaller.

As a particular case we shall take

$$\rho_0=10^{-25} \text{ c.g.s. unit.}$$
$$\rho_1=10^{-31} \text{ c.g.s. unit.}$$

We find that

$$k_0^3<\frac{15}{4}\times\frac{1}{5}\times10^{-6}$$

$$\therefore\ k_0^3<\frac{9}{1000}$$

The diameter of inner core must be less than 270 parsecs for the spiral formation.

For Andromeda Nebula:—

Equatorial diametor of the outer spheroid = 20,000 parsecs
Polar diameter = 1000 parsecs
Period of rotation = 16,000,000 years.

$$1-e^2=\frac{1}{400} \text{ and so } e^2=\frac{399}{400}.$$

It is easily seen that in this case the series

$$\frac{2}{3}+\frac{1}{5}e^2+\dots\dots\dots+\frac{1\cdot 3\dots\dots\dots(2n-1)}{2\cdot 4\dots\dots\dots 2n}\cdot\frac{2}{2n+3}\cdot e^{2n}$$

in equation (9) is less than 10.

Taking ρ_1 to be small as compared with ρ_0 we find, in this case, that (9) is all the more satisfied if

$$\frac{\omega_1^2}{2\pi\rho_0}>\frac{k_0^3}{15}+\frac{\rho_1}{\rho_0}.$$

In the case of Andromeda Nebula it becomes

$$\frac{2\cdot 5\times 10^{-29}}{\rho_0}>\frac{k_0^3}{15}+\frac{\rho_1}{\rho_0}$$

or
$$\frac{2\cdot 5\times 10^{-29}-\rho_1}{\rho_0}>\frac{k_0^3}{15}.$$

The maximum value which ρ_1 can have is of order 10^{-29} c.g.s. unit as k_0 can not have a negative value.

As in the other case, we find that if ρ_0 becomes greater, k_0 becomes smaller.

As a particular case we shall take

$$\rho_0=10^{-23} \text{ c.g.s. unit}$$
$$\rho_1=10^{-29} \text{ c.g.s. unit.}$$

We find that
$$k_0^3<15\times 1\cdot 5\times 10^{-6}$$

$$\therefore \quad k_0<\frac{7}{250}.$$

The diameter of the inner core must be less than 560 parsecs for the spiral formation.

REFERENCES

1 Banerji, Bhatnagar, and Nizamuddin—*Phil. Mag.*, **28**, p. 118 (1939).

2 Lindblad : *Stockholms Observatoriums Annales*, Band 12, No. 4 (1936)

3 Plaskett: "*Dominion Astrophysical Observatory*" Vol. 5, No. 3, p 174 (1933).

4 Eddington: "*Bakerian Lecture*"—*Proc. Roy. Soc. A.*, **111**, p. 424 (1926).

5 Plaskett: "*Dominion Astrophysical Observatory*" Vol. 5, No 3, p. 221 (1933).

6 Smart. "*Stellar Dynamics*," p. 392 (1938).

7 Jeans. "*Astronomy and Cosmogony*," p. 249, (1929).

8 Banerji, Bhatnagar, and Nizamuddin - *Phil. Mag.*, **28**, 122 (1939)

9 Banerji, Bhatnagar, and Nizamuddin—*Phil. Mag*, **27**, 173 (1939).

10 Routh: "*A Treatise on Analytical Statics*," **2**, 110 (1908).

11 Jeans: "*Astronomy and Cosmogony*," pp 351-55 (1939)

SECOND MAXIMUM OF THE ROSSI CURVE*

By A. K. DUTTA, D.Sc.

(*Received for publication, December 21, 1939*)

ABSTRACT. The Second Maximum of the Rossi Curve, as observed by Schmeiser and Bothe with triple coincidence counting system, had not been observed by Nielsen, Morgan and Morgan with a fourfold counting system. They, therefore, consider that the second maximum is caused in some way by the background count. It has been shown in the present work that, due to the geometrical configuration of the threefold and fourfold counting systems, the countings in the fourfold systems would be very much suppressed, specially those coming at a large angle with the vertical. Further, with a fourfold coincidence, the first maximum should fall more gradually than with a threefold counting system. These may cause a suppression and a masking of the second maximum, so that it has not been clearly observed with a fourfold coincidence arrangement.

The existence of a second maximum in the Rossi Curve was a point of dispute for some time, until Schmeiser and Bothe[1] had shown by their experiment that the second maximum appears with marked intensity for small angle showers, with a scatterer thickness of 17 cms. lead. According to their experiment, the second maximum does not appear in the case of large angle showers. Schmeiser and Bothe recorded the showers with four counters, the upper two counters being connected together. They, therefore, registered triple coincidence showers, the upper two counters together behaving as a single counter. Recently, Nielsen, Morgan, and Morgan[2] have experimented with fourfold coincidence system and have studied the large angle and the small angle showers. They find no definite indication of a second maximum for either the large angle or the small angle showers. If they connect the upper two counters, so as to make their experimental arrangement identical with that of Schmeiser and Bothe, they get a hump at 200 grs. per sq. cm. This corresponds to the same thickness of lead scatterer as obtained by Schmeiser and Bothe for their second maximum. Nielsen, Morgan, and Morgan consider that, since there is no second maximum with fourfold coincidence, no such effect is caused by showers from the scatterer, but that the second maximum with threefold coincidence is an effect of the background radiation.

Before proceeding to discuss the experiments of Nielsen, Morgan, and Morgan critically, we shall first point out certain experimental evidences which show that there are showers recorded that indicate an increase in number, as the thickness of the material traversed increases.

* Communicated by the Indian Physical Society.

Street and his school of workers[3] have photographed cosmic ray showers in Wilson chamber and have analysed them into three different classes. Firstly, there are soft showers caused by multiplication process in small thickness of the material. Secondly, there are two classes of showers recorded in Wilson chamber with 15 cms. of lead acting as a scatterer. In one class the number of shower particles is limited to a small number and one of them is definitely a hard particle. In the other case there is a large number of shower particles, many of them being hard. From Street's analysis it follows that these two classes are positively different from one another. We would refer to the second group of hard shower (obtained with 15 cms. of lead scatterer) as an explosion shower. According to Street, the occurrence of the explosion is 1 in 2,000 for a lead thickness of 1·3 cms. of lead, whereas the percentage rises to about 10 per cent of the showers that pass through 15 cms. of lead. This shows that showers that pass through 15 cms. of lead has to be analysed into two groups. The large group comprising mostly of two ray showers, one of them at least being hard, and a smaller group comprising of a larger number of particles developed, generally, after traversal of large thickness of matter.

The growth of a hard shower with increasing thickness of matter is evident also from an experiment by Maass.[4] The experimental arrangement is as shown in Fig. 1, where the Blocks B have the same thickness as the scatterer S. Counting the coincidences with and without the Blocks B, with different thickness of S, he has obtained the following results :—

Thickness of absorber in cms. of Fe.	Coincidence per unit of time.	
	Without B.	With B.
10	1·705	1·74
20	1·50*	1·64

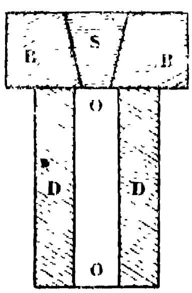

FIGURE 1

* Taken from hi graph.

From the geometrical condition, the increase due to Blocks B must be due to showers generated in B and it is apparent from the data that the increase is only about 2% of the vertical counts with 10 cms. of Fe and 10% with 20 cms. of Fe. This shows again a growth of hard shower with thickness of matter. This has been verified also without the side screens D.

Thus from the above considerations we reach the conclusion that with increasing thickness of material there is a growth of a particular type of hard shower and this should give rise to a second maximum, recorded with coincidence counters. We will now proceed to examine the geometry of the threefold and fourfold coincidences critically, and try to find out if the absence of a hump in the fourfold coincidence experiment could be attributed to the geometrical arrangement.

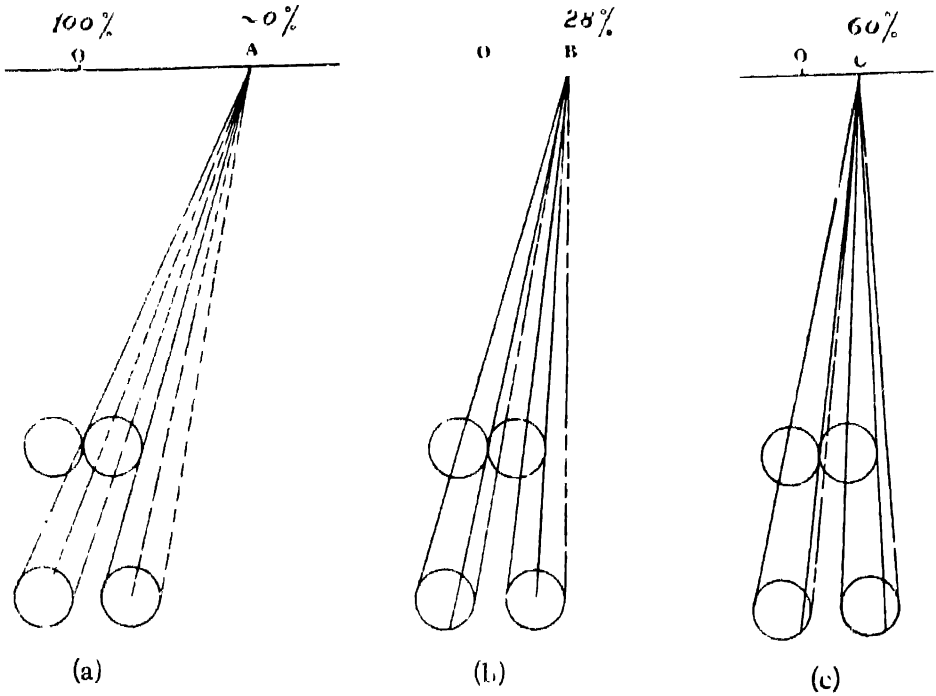

FIGURE 2

Nielsen, Morgan, and Morgan have shown the arrangement of their counting system drawn to scale and these have been redrawn in Fig. 2. The size of the scatterer is limited to such an extent that from the remotest region just a pair of rays passes tangentially through the fourfold coincidence system. The rays are marked ' F ' in fig. 2 (a). But for the triple coincidence, any pair of a whole bunch of rays passes through the system. These are shown by dashed lines. In the figures 2 (b) and 2 (c) we have drawn again the angles through which rays for a fourfold coincidence and a threefold coincidence should diverge from the points B and C respectively, where B is a point midway between the centre and

the extreme end and C is a point vertically over the limit of the upper counters. The addition due to threefold coincidences is shown by dashed lines. The percentage of fourfold coincidence to triple coincidence from the points O, C, B and A are respectively 100%, 60%, 28%, and ∽ 0%. Considering the average contribution from the portions of the scatterer lying between O to A, A to B, and B to C to the fourfold and threefold coincidences respectively, we find the mean ratio of the probability of their occurrences a little over $\frac{1}{3}$. The showers that give rise to the second maximum must, therefore, diminish by about $\frac{1}{3}$ in the fourfold system. This would bring down the magnitude of the hump to the order of the statistical error. In Nielsen, Morgan, and Morgan's work, even with fourfold coincidence, there is an indication of a small rise at about the same material thickness as in the triple coincidence system.

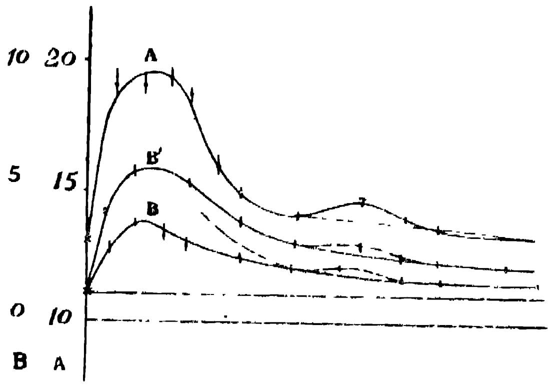

FIGURE 3

A—Triplet coincidence
B—Fourfold coincidence
C—Fourfold concidence with larger scatterer.

The same proportional reduction of intensity should also hold for the first maximum and this is evident from Nielsen, Morgan, and Morgan's work. Further, in the first maximum, the shower from the remote region of the scatterer would be more easily absorbed as they come slantingly through the medium. Since the major contribution of shower from the remote region is detected by the triple system, it follows that the triple coincidence counting would show a steeper rate of absorption at the first maximum than the fourfold coincidence. As a consequence, the hump and the second maximum has a chance of being overlooked due to the slow gradient of the fourfold coincidence curved beyond the first maximum compared to that of the threefold coincidence curve. These points would be clear from a study of Fig. 3, where Nielsen, Morgan, and Morgan's graphs have all been redrawn on the same scale.

It should be pointed out, however, that the diminished intensity in the fourfold coincidence is independent of the analysis of the different types of showers

giving rise to the Rossi curve. It is determined only by the geometric limitation of the fourfold coincidence in comparison with the threefold coincidence. The analysis here put forward, is in view of evidences from different experiments.

My thanks are due to Prof. D. M. Bose for helpful discussion.

REFERENCES.

[1] Schmeiser and Bothe—*Ann. der. physik.* **32**, 161 (1938).

[2] Nielsen, Morgan, and Morgan—*Phy. Rev.*, **55**, 995 (1939).

[3] Street—*Jour. Frank. Inst.*, **227**, 765 (1939).

[4] Maass—*Ann. der. physik* , **27**, 507 (1936).

THE SECONDARY K-ABSORPTION SPECTRA OF SULPHUR*

By N. BAGCHI, M.Sc.

(*Received for publication, February 13, 1940*)

Plate III

Abstract. The X-ray K-absorption spectrum of Sulphur shows pronounced structure extending up to an energy distance of 87 volts from the main edge. The spectrum obtained shows definitely two definite absorbing regions, and the intensity of some bands at large energy distance from the primary are higher than those adjacent to the main edge. The intensities of the dark and white bands do not follow any regular sequence.

INTRODUCTION

The X-ray absorption spectrum of sulphur was studied by Lindh[1] who observed the influence of chemical bindings on the positions of the primary K edges alone. But he did not investigate the nature of the extended secondary structures of the spectrum. He further noticed that the positions of the primary edge in monoclinic and rhombic varieties of sulphur were almost the same within the limits of experimental error whereas in the case of compounds the position depended on the valency of sulphur. The aim of the present investigation was to study the secondary structure of the absorption spectrum obtained with the various allotropic modifications of sulphur. Das[2] has recently found a new allotrope of sulphur (S_ω), of which the structure is not yet fully known. It was suspected that the mode of interatomic linkage inside a molecule of sulphur in the S_ω lattice is different from that present in orthorhombic crystals (S_α). In the latter type of crystalline sulphur, each molecule of sulphur contains eight atoms in a puckered ring. Now, we know that in the case of molecules possessing a large number of atoms, the secondary absorption spectrum does not depend much on the state of aggregation of these molecules. For, in these cases the intermolecular binding is so very strong in comparison with that between the molecules that the position of the energy levels (or allowed and forbidden energy zones) remain almost unaffected by the alterations of the mode of aggregation of the molecules. Thus one may expect that the sulphur molecules in S_α and S_ω really possess different stoichiometric structures, and this difference must also manifest itself in the secondary absorption spectra of these allotropes. With this idea, we took up the work which though still incomplete is being continued

* Communicated by the Indian Physical

EXPERIMENT

As the soft X-rays lying in the region of the K-absorption spectrum of sulphur are very much absorbed by air, the effective path of the radiation in air was reduced by evacuating the spectrograph with the help of a Cenco Megavac Pump, and the tube was operated at 5 K. V. with a current varying from 25 to 50 milliamperes for different exposures which varied from 60 to 100 hours. The crystal used was Calcite and was oscillated through 2° 30′ by means of a specially devised arrangement. The slit through which the X-rays enter the Seigbahn spectrograph from the electron tube was 0·1 mm in breadth and was covered by very thin gold-beaters skin coloured red with magenta solution In this particular investigation the choice of the photographic films presented a great difficulty which was, however, overcome by trial. Several films and plates were tried but the intensity of the absorption bands even after an exposure of 90 to 100 hours with a current as high as 30 milliamp was not sufficient to produce a good contrast between the white and dark bands. Best results are obtained with doubly-coated Agfa Sino Films and Agfa Röntgen developer. The range through which the crystal is to be oscillated for obtaining all the absorption edges associated to the K-edge of sulphur (5008 X.U.) was first tested with the oscillation arrangement by photographing $MoL\beta_1$ (5041 X.U.) and $MoL\beta_2$ (4910 X.U.) on the same film. The reference lines, however, were taken to be 3 $NiK\alpha_1\alpha_2$ (4974 X.U.) and 2 $TiK\beta_1$ (5018 X.U.) emission lines.

PREPARATION OF ABSORBING SCREEN

The preparation of the absorbing screen caused the greatest trouble. The critical absorption wavelength of sulphur lies in the neighbourhood of 5 A.U. and the screen could not be prepared on ordinary paper or filter paper due to the high absorption by paper in this region of soft X-rays.. The substance was finely powdered in a mortar and uniformly spread by rubbing the powder between two ground glass plates when the sulphur stuck to one plate. On removing the upper plate, a dilute solution of celluloid in acetome was poured over it. When the thin film of celluloid was pulled off on drying, a uniform layer of sulphur stuck to the surface of the thin film of celluloid.

Other methods were also tried for the absorption screen of sulphur. In one method, the sulphur was finely powdered in a mortar and to the powder a little quantity of celluloid acetate solution was added. After preparation of an emulsion, the substance was allowed to pour on a clean glass plate levelled on a platform. On drying the film of celluloid, coated uniformly with sulphur, was obtained. But this method did not prove efficient as the one previously described

Another method of the preparation of the absorbing screen of sulphur is dentical to the one first mentioned, the only difference being that instead of

TABLE I

Absorption Spectrum of Sulphur

The wavelengths are given in X.U.

	K	a_1	K_1	a_2	K_2	a_3	K_3	a_4	K_4	a_5	K_5	a_6	K_6	a_7	K_7	a_8	K_8	a_9
λ	5008.2	4998	4991	4981	4970	4960	4951	4949	4935	4924	4916	4895	4885	4875	4869	4858	4849	4840
			W		S		W	W				W			W	S	S	S
$\Delta\lambda$	0	10.2	17.2	27.4	38.2	48.2	57.2	59.2	73.2	84.2	92.2	113.2	123.2	133.2	139.2	158.2	159.2	168.2
ν/R	181.87	182.33	182.582	182.95	183.36	183.72	183.97	184.13	184.69	185.07	185.37	186.17	186.54	186.97	187.12	187.55	187.89	188.28
$\sqrt{\nu/R}$	13.486	13.503	13.512	13.526	13.541	13.553	13.564	13.57	13.59	13.604	13.615	13.64	13.658	13.674	13.679	13.695	13.686	13.77
$\Delta\nu/R$	0	.46	.70	1.08	1.49	1.85	2.10	2.26	2.82	3.20	3.50	4.20	4.67	5.12	5.25	5.68	6.02	6.42
ΔV	0	6.2	9.6	15	20	25	29	31	38.23	43	48.0	57	63	67	71	77	82	87

depositing them on the surface of thin films prepared by dissolving celluloid in acetone, the deposition was performed on a thin film prepared by dissolving collodion in a mixture of equal parts of alcohol and ether.

RESULTS

After several careful attempts with the orthorhombic variety (S_α) of sulphur, we were successful in obtaining one or two good absorption photographs which showed secondary structures extending over a large energy range on the short wavelength side of the primary. One of them is reproduced here (Fig. 1) where a large number of secondary edges is clearly visible. The wavelength and the usual values of λ, $\Delta\lambda$, ν/R, $\Delta\nu/R$, $\sqrt{\nu/R}$ and ΔV are given in the Table (1). The K, K_1, K_2 refer to the white lines and α_1, α_2, α_3, etc., denote the black bands, the primary edge being denoted by K.

No successful plate has yet been obtained with S_ω. In this case another additional difficulty is to be overcome. This is due to the unstable nature of S_ω. If the substance is seriously disturbed by heat or any mechanical operation as powdering, it transforms rapidly to insoluble S_α. So a special technique has to be devised for the preparation of the absorbing screen of S_ω.

Over and above the usual structures, another peculiarity is noticed in the photographic plate. It is found that over a certain range lying in the neighbourhood of the main edge, the general absorption is well marked, but at a certain point the intensity of absorption suddenly falls so that the whole range of absorption shows two distinct regions. The fluctuation of intensity and the general diffuseness of the band do not follow any regular sequence. The strong and weak absorption edges (both black and white) are marked by S and W in the Table. From measurements, the structures extend up to 87 volts from the primary edge. It may be mentioned here that this is for the first time that such an extended structure has been observed in the case of a lower element like sulphur. The positions of the bands were measured with a glass scale with 3 Ni$K\alpha_1$ and 2 Ti$K\beta_1$ as reference lines.

In conclusion, the author wishes to express his gratitude to Prof. B. B. Ray for his valuable suggestion and able guidance and his thanks to Mr. S. R. Das for occasional friendly helps.

KHAIRA LABORATORY OF PHYSICS,
92, UPPER CIRCULAR ROAD,
CALCUTTA.

REFERENCES

[1] Lindh - Spectroscopie der Röntgenstrahlen, M. Siegbahn.
Das—The Structure and Stability of S_ω (not yet published).

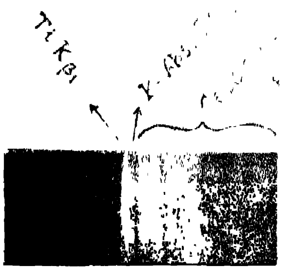

Fig.

A NOTE ON THE ORIGIN OF THE D-LAYER

By S. DEB, D.Sc.

(*Received for publication, December 22, 1939*)

ABSTRACT The origin of D-layer of the upper atmospheres is here considered to be due to the settling of dust-like metallic particles of meteoric origin on the inversion level at 55-60 kilometres. The inversion of temperature with its consequent over-stability is considered to be due to the heating of the atmosphere by high-speed meteors that come to earth continuously from space. With this idea a number of optical and electrical phenomena found associated with this layer is tried to be accounted for. Lastly it is also found that the potentiality of this layer for radio fade-outs discovered by Dellinger can be well explained by such a hypothesis.

The mechanism of formation of the three important stratification of the upper atmospheres, the E- and the F-ionisation layers and of the low-lying ozone layer, except for the details, is by now, more or less, correctly understood mainly from the contributions of Lenard,[1] Pennekoek,[2] Chapman,[3] Saha[4] and Mitra.[5] Lately another layer intermediate between the low ozone layer and the well-known E-layer has been discovered.[6] This layer is generally known as D-layer. The height at which it is found to exist is between 55 and 60 km. The existence of such a layer of stratification at such low heights is difficult to account for on any theory, but it appears to be confirmed by the discovery of the phenomenon of radio fade-outs that are observed to occur on the sun-lit parts of the earth's atmosphere practically simultaneous with the appearance of intensely luminous patches on the face of the sun.[7] It is found that the layer of temporary "ionospheric winds" responsible for the above fade-outs exists also at a height below that of E-layer at about 55-60 km, practically same as that of the D layer.[8]

The cause of such a layer of stratification at about that height is as yet uncertain. And in the absence of any definite theory about its origin it is vaguely assumed[9] that it is caused as a reaction to the process of continuous formation and dissociation of ozone molecules which is going on in the upper atmosphere. Recently Prof. S. K. Mitra and Dr. J. N. Bhar and Mr. S. P. Ghosh have dealt with the problem of the formation of this layer.[10] They are of opinion that the D-layer is formed by the photo-ionisation of O_2 at its first ionisation potential. But the main difficulty with this layer is that its existence is not a contiruous one. Moreover, there should exist in it a potentiality to develop itself suddenly to the particular state that is responsible for the phenomenon of radio fade-outs.

The ozone hypothesis about the cause of this D-layer is untenable for various reasons, the most significant of which is the fact that perhaps the entire ozone of the upper atmospheres is confined between 15 and 40 kilometres as recently established by Götz, Dobson and Meetham and others,[11] with a maximum concentration at about 23 kilometres.[12] And along with this, if one takes into account that the total vertical amount of ozone is hardly 2 mm. in thickness (N.T.P) at the equator and 2·5 mm. in high latitudes (northern),[13] one fails to understand how this can effect the formation of a layer that can so strongly influence the passage of radio waves.

A very significant fact about the stratifications in the upper atmospheres is that they are also the positions where the law of normal vertical temperature distributon is disobeyed. Just at the lower base of the ozone layer the normal vertical temperature distribution comes to a standstill for some height and, after that, instead of a fall there is actually a rise with height. Similarly in the case of E- and F-layers they are also the seats of raising of temperature of atmospheres at those levels. The temperature of the E-layer is taken to be about 300°K and of the F_2-layer sometimes as high a figure as 1000°C is ascribed.[14] Had the ordinary law of vertical distribution of temperature been satisfied, the temperatures of these layers would have been much different.

If one looks at these stratifications from this direction one can immediately see that they can very well be interpreted as cases of temperature inversions. As is well-known in Dynamical Meteorology, all temperature inversions cause layers of atmospheres to deviate to greater stability and can, in this way, act against the forces of gravity in stopping heavier particles to have their natural fall. But the stability of these layers (ozone, E and F), as now interpreted, is not primarily due to the forces of inversion.

In the case of D-layer, on the other hand, it can be said to possess properties of temperature inversion. At about 65 km. height the temperature of the atmosphere is found to be as high as 380° Absolute, from the investigations of Lindemann and Dobson[15] and those of Öpik[16] on meteors and that of Pekeris[17] on atmospheric oscillations. Just beyond the ozone layers at about 40 km. there is a tendency of the atmosphere to cool down. The layer of atmosphere in between the two limits of 50 km. and 60 km. is subjected to the forces of inversion and thus assumes a state of permanency that in its turn becomes strong enough to resist the forces of mixing which exist both above and below.

The cause of the heating of the atmosphere between 60 and 80 km. do not introduce any difficulty. This part of the upper atmosphere is continually subjected to the bombardment of innumerable meteoric particles from space. The kinetic energy of these meteors is partly used to disrupt the particles into their constituent molecules and is partly absorbed by the atmosphere through which they happen to pass. From the average number of meteors entering the Earth's

atmosphere per sec., from an estimate of their average mass and the constituent and also remembering that the average velocity of these meteoric particles is something like 20 kilometres per second, the rate at which the energy is absorbed by the layer can be estimated. Assuming that the atmosphere is essentially composed of N_2 and O_2 molecules in their normal proportions even at this height the rate of heating can be calculated. After allowing for the loss by radiation to both upper and lower layers the temperature at which the layer attains an equilibrium temperature can be estimated. This is found to be about 450° Absolute at about 65 kilometres height, in turn creating a level of temperature inversion at a height of about 55 kilometres.

The heavy meteoric particles now reduced to metallic dust try to settle down and come to the surface of the earth, but the inversion at 55 kilometre level stops them to fall further. They temporarily settle themselves at this level, and continue on accumulating till they overcome the forces of inversion, when there occurs a collapse of this metallic layer. After a collapse again another accumulation continues on. This may be the reason why the D-layer is only detected strongly at times and practically undetectable at others.

This layer being made up of particles chiefly of iron and silicon and perhaps also of sodium produces various effects upon a number of terrestrial phenomena. It is not possible to deal with them adequately in a note like this. A full discussion will appear in the main paper. Yet one or two points may be mentioned here. The spectrum of the night sky shows a fluorescence of continuous background superposed on which lie the bands of nitrogen molecule and metastable oxygen atoms. Elvey and Roach[18] have proved that this fluorescent background lies at a height of 50-65 kilometres. The layer being a metallic one can very well account for a continuous emission.

Recently the lines of atomic sodium are detected in the night-sky spectrum by Cabannes and his co-workers.[19] They place this sodium in the upper atmospheres at a height of 130 km., whereas Bernard[20] suggests that the sodium D light is emitted from a thin layer at about 60 km. Assuming that the layer of inversion is also a seat of heavy particles to accumulate, it can be asserted that the level of sodium should begin somewhere at this height. This receives a support from the observation that at sunset when the sun's rays rise past this level, the D-light intensity falls within a minute or two to about 1 per cent. of its former value.[21]

The theories of terrestrial magnetism demand a conducting layer at a certain height in the upper atmospheres. This layer of metallic particles, perhaps chiefly of iron, satisfies very well the demand. I have as yet not considered the subject in any detail. But I hope to discuss the effect of a mantle of iron particles round the earth on terrestrial magnetism in a separate contribution.

I have already referred to the phenomenon of solar eruptions and its associated effect of radio fade-outs, which is caused in this D-layer round the sub-solar point. It has been found that all the solar eruptions cannot impart the particular characteristics to this layer responsible for the fade-out effects. Considering all the points I am very much tempted to suggest that if iron line can be detected in emission during such an eruption and if a spectro-heliogram can be taken of the sun with this line, there may be found a one-to-one correspondence between the two phenomena.

In conclusion I wish to express my thanks to Prof. M. N. Saha, F.R.S., for a complete discussion on the subject and also to Prof. S. K. Mitra, D.Sc., for a number of helpful suggestions.

INDIAN ASSOCIATION FOR THE CULTIVATION OF SCIENCE,
210, BOWBAZAR STREET, CALCUTTA.

REFERENCES

[1] P Lenard, *Sitzungsberichte d Heidelberger, Akad*, **12**, 75, 1911.
[2] A. Pannekoek, *Proc. Roy. Soc. Amsterdam*, **29**, 1165, 1926.
[3] S. Chapman, *Proc. Roy. Soc. A.*, **132**, 353, 1931.
[4] M. N. Saha, *Proc. Roy. Soc. A.*, **160**, 155, 1937.
[5] S K Mitra, *Nature*, **142**, 914, 1938.
[6] E. V. Appleton, *Proc. Roy. Soc A.*, **126**, 558, 1930 ; Mitra and Syam, *Nature*, **135**, 953, 1935.
[7] J. H. Dellinger, *Phys. Rev.*, **48**, 705, 1935.
[8] A. G. McNish, *Terr. Mag*, **42**, 109, 1937.
[9] F. A. Lindemann, *Quat. Jour. Roy. Met. Soc.*, **65**, 333, 1939.
[10] Mitra, Bhar and Ghosh, *Ind. Jour. Phys.*, **12**, 455. 1938.
[11] Götz, Meetham and Dobson, *Proc. Roy Soc. A.*, **145**, 416, 1934 ; F.W.P. Götz, *Ergebn. Kosmischen Physik*, III, 253, 1938 ; V. H. Regener, *Zeits f. Physik*, **109**, 642, 1938.
[12] Coblentz and Stair, *Nat. Bur. Std. Journ. Research*, **22**, 573, 1939.
[13] Meetham aud Dobson, *Proc. Roy. Soc. A.*, **148**, 598, 1935
[14] Martyn and Pulley, *Proc Roy. Soc. A.*, **154**, 455, 1936.
[15] Lindemann and Dobson, *Proc. Roy Soc. A.*, **102**, 411, 1922.
[16] E. Opik, *Acta. Comm. Univ. Tartuensis (Dorpatensis) A*, XXVI$_3$, 1933.
[17] Pekeris, *Proc. Roy. Soc. A.*, **158**, 650, 1937.
[18] Elvey and Roach, *Astro. Journ.*, **85**, 213, 1937.
[19] Cabannes Dufay and Gauzit, *Astro. Journ.*, **88**, 164, 1938 : also R. Bernard *Zeits. f Physik*, **110**, 291. 1938.
[20] R. Bernard, *Nature*, **141**, 788, 1938.
[21] S. Chapman, *Astro. Journ.*, **90**, 309, 1939.

PRODUCTION OF ULTRA-HIGH FREQUENCY RADIO WAVES BY ELECTRONIC OSCILLATIONS*

By S. S. BANERJEE, D.Sc.,

AND

A. S. RAO, M.Sc.

Benares Hindu University

(*Received for publication, February 7, 1940*)

ABSTRACT Detailed investigation has been made of the mode of production of ultra-high frequency radio waves by electronic oscillations in a triode valve. The effect of emission current and grid potential on the lengths and intensity of the generated waves has been critically examined and a new relation between them has been derived, *viz.*, $\lambda E_g^{\frac{1}{2}} I_e^{\frac{1}{4}} =$ constant, where λ is the wavelength generated, E_g is the grid potential, and I_e is the emission current. This relation has been experimentally verified by means of Barkhausen and Kurz oscillator with modification of Gill and Morrell. It is concluded that the emission current plays an important part in predicting the lengths of the generated waves. It has been observed that, for the same grid potential, the intensity of the generated waves increased with the increase of emission current. The lengths of such waves, however, decreased when the emission current was increased. The waves generated in the present investigations were of Gill and Morrell type as has been shown by the method of Cockburn from the variation of anode current with grid potential. It has also been shown that for such oscillations the lengths of the generated waves were altered with the variation of length of external circuit associated with the valve.

INTRODUCTION

With the advent of television and aircraft communications attention has been greatly centred in the study of generation of continuous radio waves of ultra-high frequencies. It has now become customary to call the radio waves below 10 metres as 'ultra short waves' and those below 1 metre as 'micro waves.'

The only satisfactory method till now known for powerful production of these ultra-high frequency waves is based on the use of electronic oscillations in a triode and in magnetron valves. In 1919, Whiddington [1] generated radio waves of about 500 metres by the electronic oscillations in a soft triode with high positive grid. Near about the same time Barkhausen and Kurz[2] succeeded in producing radio waves of about 1 metre length by using hard triode valves with

* Communicated by the Indian Physical Society.

high positive grid compared to the anode and put forward the theory of the same. According to their theory the wavelength produced should depend only on the dimensions of the electrodes and the working conditions of the tube.

Since the time of Barkhausen and Kurz various investigators [3-11] have tried to verify the laws established by them, and in many instances results have been obtained which do not completely agree with the original theory of Barkhausen and Kurz. Gill and Morrell,[3] for instance, reported in 1922 that the external circuit connected with the valve plays an important part in prediction of the wavelength produced. The results of Gill and Morrell were confirmed by other workers in this field. It is, however, now admitted that there are two types of oscillations produced inside a vacuum tube. One is the Barkhausen and Kurz oscillation which is independent of the external circuit and the other is the Gill and Morrell type which is dependent on the external circuit. Cockburn [11] has, however, shown that there is no fundamental difference between these two types of oscillations and he has pointed out that the Gill and Morrell oscillations occur when the external circuit associated with the valve happens to be in resonance with Barkhausen and Kurz oscillations.

In the present investigations the study has been made of the mode of production of ultra-high frequency waves by electronic oscillations in a triode valve with high positive potential being applied to the grid. A preliminary note [12] on this work has already been published recently. The relations existing between the grid potential applied, emission current and the wavelengths produced have been critically examined and it has been observed that the consideration of emission current is not less important than the grid potential in establishing such relation. Thus a new equation indicating the connection between the wavelengths produced and both the grid potential and emission current has been derived from the equations of Barkhausen and Kurz [2] and Tank.[5] This equation has been found to agree very closely with the observed results for a considerable range of grid potentials. It was also observed that the intensity of the generated waves was increased as the emission current was increased for the same grid potential. The wavelengths, however, decreased with the increase of the emission current, as has also been observed by other investigators mentioned in the following section. In the present investigation all the observations were taken in the region of Gill and Morrell as the wavelengths were found to vary with the external circuit. This has also been substantiated by the curves showing the variation of anode current with increasing grid potential.

THEORY

For plane electrodes, Barkhausen and Kurz worked out a formula showing the relation between the wavelength produced, distances between the filament and anode, and filament and grid and the potentials applied to the anode and grid compared to the filament. Subsequently Scheibe [4] gave more rigorous

formula for cylindrical electrodes. Tank,[5] Gill [13] and various other workers pointed out later on that the relations given by Barkhausen and Kurz and Scheibe were not adequate to establish the wavelength generated, as they found that the wave-length decreased when the emission current was increased. Gill worked out a theoretical formula which included the emission current also. Potapenko,[14] however, investigated experimentally the formula of Gill in details. The results of Potapenko showed considerable discrepancies between calculated and observed values. Very recentiy Gill [15] has produced ultra-short waves of length 1 to 3 metres by split anode valve and has suggested the explanation of the reduction of wavelength with increase in emission for a fixed grid voltage. Tonks[7] gave a physical explanation of the possibility of decrease of the wavelength produced as the emission current is increased, a brief description of which will be given below for reference.

When the emission currents are small, the electrons which leave the filament are accelerated by the positive grid till they pass through it and are acted by retarding field when they enter the grid-anode space. Since the anode is originally at the same potential as the filament, the retarding electrons will have zero velocity when they reach the anode and may be collected on it or reflected. In this case the space charge in the grid-anode space depends on the total electron current and accordingly the potential distribution between the grid and anode is the same as in the case when the plate itself becomes the emitter of electrons. But as the emission from the filament is increased the space-charge in the grid-anode space also increases and makes the field zero even at a space nearer to the grid than the plate itself. Consequently the electrons turn back from the plane without reaching the plate. This plane of zero potential, which is called ' virtual cathode,' will move away from the anode towards the grid as the emission current is increased. This will decrease the transit time of the electrons in grid-anode space and consequently the wavelength will be decreased.

The various relations with the wavelengths produced, grid potential applied and the emission current as mentioned previously, have beeen critically studied by us and it has been observed that the consideration of the emission current is as important as the grid potential in predicting the lengths of the waves produced by electronic oscillations. A new relation connecting the wavelength produced and both the grid potential and emission current has been derived by the combination of the equations of Barkhausen and Kurz and Tank.

The relation of Barkhausen and Kurz for the wavelength genarated in a triode valve with cylindrical grid and anode is given by

$$\lambda = \frac{10^3}{E_g^{\frac{1}{2}}} \left[\frac{d_a E_g - d_g E_a}{E_g - E_a} \right]$$

where E_g and E_a are grid and anode potentials in volts, d_g and d_a are the dia-

meters of the grid and anode in cms. respectively and λ is the wavelength generated in cms.

For a simplified case as employed in the present investigations, when the anode is maintained at the same potential as the negative end of the filament, we get

$$\lambda^2 E_g = \text{constant} \qquad \ldots \quad (1)$$

The relation of Tank for the wavelength generated and the emission current is given by

$$\lambda^3 I_e = \text{constant} \qquad \ldots \quad (2)$$

From equations (1) and (2) we get

$$\lambda E_g^{\frac{1}{2}} I_e^{\frac{1}{3}} = \text{constant}. \qquad \ldots \quad (3)$$

The above equation has been experimentally verified as described in latersection.

EXPERIMENTAL ARRANGEMENT AND OBSERVATIONS

The apparatus used for the present investigations was almost similar to that used by Barkhausen and Kurz after the modification of Gill and Morrell. A pair of Lecher wires LL (Fig. 1), each 130 cm. long and spaced 5·5 cm. apart, was connected to the grid and anode of a triode valve. The anode and grid were concentric cylinders encircling the straight filament at the common central axis. The desired effective length of the external circuit was obtained by altering the position of a sliding bridge consisting of a fixed condenser C of 0·002 micro-farad capacity. A high variable positive potential was applied to the grid through a filter F, which was connected to 440-volts D C. mains. The anode was connected to the negative end of the filament through a sensitive calibrated galvanometer CG. The grid and anode potential leads were connected to the two ends of the bridge condenser C as shown in the figure. The filament current was measured with an ammeter A in Fig. 1. A milli-ammeter MA in the grid circuit and the galvanometer CG in the anode circuit together measured the total emission current. After the filament was heated to the desired temperature, the potential applied to the grid was measured by means of an electrostatic voltmeter to avoid any leakage of current through the instrument

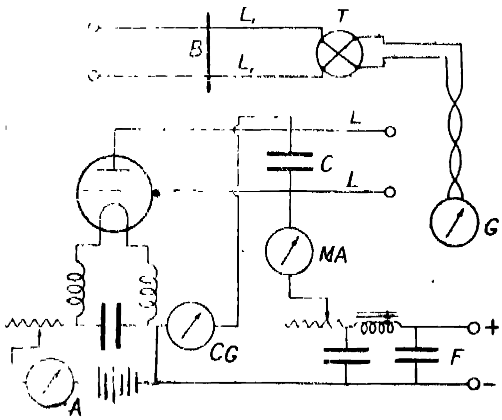

Fig 1.

The lengths of the ultra-high frequency waves generated were measured by an auxiliary Lecher wire system L_1L_1, loosely coupled to the oscillator. Two ends of the auxiliary Lecher wires were joined to the heater terminals of the vacuo thermo junction T which was connected to a sensitive galvanometer G. A metal sliding-bridge B was moved on the auxiliary Lecher wire system in order to get the position of maximum current in the glavanometer from which the wavelength could be determined. Equation (3) of the last section was verified with various lengths of the external circuit. The wavelengths produced have been noted with different grid potentials and different emission currents obtained by changing the filament heating current. Total emission current was obtained from the sum of grid and anode currents Two typical sets of observations verifying equation (3) are given below in Tables I and II for two fixed lengths of the external circuit. The second column of these tables show the values of total emission current. For observations in Table I the bridging condenser was placed at 50 cms. away from the grid terminal and for those in Table II it was placed 100 cms. away

TABLE I

Grid potential (E_g) in volts.	Emission current (I_e) in milli-amperes.	Wavelength generated (λ) in cms.	$\lambda E_g^{\frac{1}{2}} I_e^{\frac{1}{3}}$.
80	50	171	573·3
80	68	156	569·5
80	76	152	560·2
100	52	152	582·2
100	70	144	593·4
100	98	128	589·6
120	52	144	588·0
120	115	100	586·1
120	160	94	576·5
140	65	120	570·9
140	110	106	587·2
160	80	106	577·9

TABLE II

Grid potential (E_g) in volts.	Emission current (I_e) in milli-amperes.	Wavelength generated (λ) in cms.	$\lambda E_g^{\frac{1}{2}} I_e^{\frac{1}{4}}$.
80	60	194	679·4
80	68	186	679·0
80	70	184	677·0
100	68	168	687·7
100	95	150	684·4
100	95	144	675·4
120	72	148	671·6
120	120	126	681·0
120	145	118	679·2
140	80	132	673·2
140	140	110	675·0

It will be noted from the above tables that the values in the last column are nearly constant. The numerical value of this constant, however, changes by a small amount with the variation of the external circuit associated with the valve. This is due to the change in wavelength produced by altering the length of the external circuit as the observations were taken in the region of Gill and Morreil. It will be further observed from each of the above tables that, for the same value of the grid potential, the length of the emitted wave was reduced as the emission current was increased. The intensity of the oscillations, however, increased with the increase of the emission current.

Table III shows below how the wavelength varies with the gradual change of length of the associated external circuit.

Grid Potential = 80 Volts.
Emission Current = 55 Milli-amperes.

TABLE III

Length of the external circuit in cms.	Wavelength generated (λ) in cms.
0	144·0
25	148·6
50	150·4
75	156·0
100	158·8
125	162·6

That the waves generated for the experimental observations were of the Gill and Morrell type was further tested by the method of Cockburn by drawing the curves showing the variation of anode current with grid potential. The portions of such curves within which the anode current remains constant, indicate the

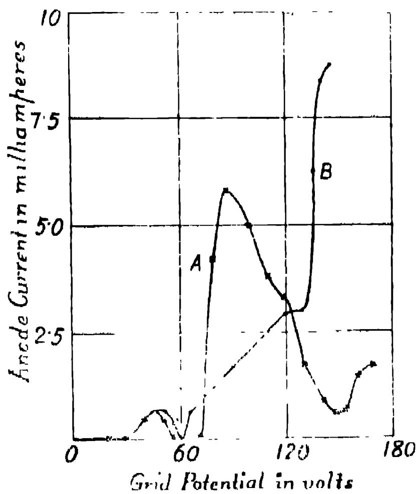

Fig. 2

region of grid potentials for the production of Barkhausen and Kurz oscillations. The other parts of the curve in which the anode current is constantly varying, correspond to Gill and Morrell oscillations. The variations of anode current with grid potential have been shown in Fig. 2. Curves A and B have been drawn for two values of filament-heating currents used in the above experiments. It will be observed from these curves that, within the limits of grid potentials (80 to 140 volts) used in the above experiments, there is no part of the curves for which the anode current remained constant for a considerable range of grid potential.

SUMMARY AND CONCLUSION

A detailed study of the generation of ultra-high frequency radio waves by electronic oscillations in a triode valve has been made in the present investigation. The effect of the emission current on the lengths and intensity of the waves generated has been critically examined and a relation concerning the emission current, grid potential and the wavelength generated has been derived. This has been experimentally verified and typical observations have been recorded. It has been concluded that the consideration of emission current is of considerable importance in predicting the wavelengths generated by these oscillations. It has been found that the lengths of the generated waves decreased as the emission current was increased at the same value of grid voltage. The intensity of the waves, however, increased under the same condition. The oscillations generated

in the present investigations belonged to Gill and Morrell type. This has been shown by the method of Cockburn by drawing curves indicating the variation of of anode current with grid potentials. It has been further shown that, for such oscillations, the lengths of waves generated altered with the change of length of the external circuit associated with the valve.

The authors desire to express their thanks to Dr. B. Dasannacharya, Head of the Department of Physics, for giving all facilities during the course of the above investigations.

WIRELESS SECTION,
PHYSICS LABORATORY,
BENARES HINDU UNIVERSITY.

REFERENCES

1 Whiddington, R., *Radio Review*, **1**, 53 (1919).
2 Barkhausen, H. and Kurz, K., *Phys. Zeits.*, **21**, 1 (1920).
3 Gill, E. W. B. and Morrell, J. H., *Phil. Mag.* **44**, 161 (1922) and **49**, 379 (1925).
4 Sheibe, A., *Ann. der. Phys.*, **73**, 54 (1924).
5 Tank, F., *Arch. Sc. Phys. et Natur.*, **6**, 320 (1924).
6 Sahanek, J. *Phys. Zeits.*, **26**, 368 (1925).
7 Tonks, L., *Phys. Rev.*, **30**, 501 (1927).
8 Hollman, H. E., *Proc. Inst. Rad. Eng.*, **17**, 229 (1929).
9 Benham, W. E. *Phil. Mag.*, **5**, 641 (1928) and **11**, 457 (1931).
10 Leyshon, W. A., *Proc. Phys. Soc.*, **47**, 277 (1935) and **48**, 469 (1936).
11 Cockburn, R., *Proc. Phys. Soc.*, **49**, 38, (1937).
12 Banerjee, S. S. and Rao, A. S., *Science and Culture*, **5**, 64 (1939).
13 Gill, E. W. B., *Phil. Mag.*, **12**, 843 (1931).
14 Potapenko, G., *Phil. Mag.*, **14**, 1126 (1932).
15 Gill, E. W. B., *Phil. Mag.*, **28**, 203 (1939).

EARLY MORNING VARIATION OF IONIZATION AND THE TRUE HEIGHT OF REGION F OF THE IONOSPHERE*

By S. P GHOSH

(Received for publication, February 23, 1940)

ABSTRACT Results of observations carried out at Calcutta (22°33' N) for a period of one year (1937-38) on the early morning variation of F-ionization are described. It is found that the average F-ionization, which decreases during the earlier part of the night, begins to increase after attaining a minimum. The hour, at which the increase begins, varies with the season. It occurs earliest in mid-winter and shifts towards the early morning hour with the approach of summer In mid-summer, there is no pre-sunrise increase of ionization This interesting result is explained as due to cooling of the layer as a whole It is obvious that the effect of contraction due to cooling is observable only if there be sufficient hours of darkness. The shifting of the hour of pre-sunrise increase towards the early morning hours and the absence of same in summer are thus easily explained. Further, it is found that the early morning minimum occurs *after sunrise at Region F* in all seasons.

In order to find out the hour of sunrise at Region F, its true height has been calculated from the observed (P' - *f*) curves Generally, the true height has been found to be about 80 km less than the observed equivalent height

Curves depicting the variation of the hour of sunrise with height, taking into account the effect of atmospheric refraction, have been drawn.

I. INTRODUCTION

It is well known that the upper ionized Region F of the ionosphere is split up during daytime into two regions—F_1 (lower) and F_2 (upper). With the progress of night, F_1 gradually merges into F_2 and only one ionized upper region remains The Region F_1 in common with Region E_1 shows regular diurnal and seasonal variations of ionization. The Region F_2, however, does not do so. In fact, in many respects the variation of F_2-ionization with respect to the zenithal distance of the sun may be said to be erratic, and till now has received no satisfactory explanation. It is therefore necessary to make observations on the variation of F_2-ionization in relation to the incidence of solar radiation under as varied conditions as possible. An interesting and informative study is to find out how the F_2-ionization changes when the first rays of the rising sun strike it obliquely from below the horizon. Such a study has been made for the case of Region E_1 and an interesting fact has been discovered. It has been found [1] that the E_1-ionization begins to increase *not* when the early morning solar rays strike

* Communicated by the Indian Physical Society.

Region E_1 by grazing the surface of the earth *but* when they do so by grazing the top (at a height of about 35 km.) of the ozonosphere. It is important and interesting to enquire if some similar phenomena occur in the case of Region F_2.

Study of the correlation between the incidence of the rising sun's rays on Region F and the consequent change of ionization, if any, involves two subsidiary studies. It is necessary firstly to prepare a chart showing the hours of sunrise in different seasons at various heights above the earth's surface and secondly to determine the true height as opposed to the virtual height for every observation on Region F. The method of doing these and the results obtained are described in sections IV and V. In what follows we discuss the observed results on the assumption that these two data are known.

II. METHOD OF OBSERVATION

The variation of F-ionization was studied by measuring the critical frequency at intervals of about 10 minutes. Since it was not possible to vary continuously the frequency of the exploring waves, the whole range of frequencies used was divided into steps 0·2 to 0·3 megacycle. The penetration frequency was determined by the usual method Each measurement took about 4 minutes.

During the months of July to December, 1937, weekly observations were taken from about one hour before sunrise (at Region F) to about ground sunrise. For reasons given later, it was decided in January, 1938, to extend the period of observation from 2300 hours to ground sunrise on the next day.

III. RESULTS AND DISCUSSION

In Figs. 1 to 8 the penetration frequencies have been plotted against time. The day-to-day variation of penetration frequency is irregular. The average variation for the month is therefore given and is shown by the thick continuous line. The hours of ground sunrise and the sunrise at the mean height of the F-layer are marked on the abscissa.

Inspite of the erratic nature of the variation of ionization, certain regular characteristic features of the average change of ionization during the early morning hours could be recognised. These are discussed below.

(a) *Pre-sunrise Increase of Ionization*

Inspection of Figs. 1 to 3, 5 and 6 shows that there is in general an increase of ionization in the hours of darkness before the rising of the sun in the F-layer. It is also observed that the hour at which the ionization begins to increase recedes from the hour of sunrise (at F-layer) with the approach of the winter solstice.

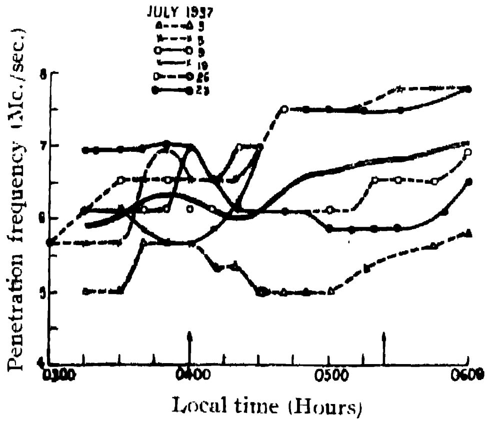

FIGURE 1

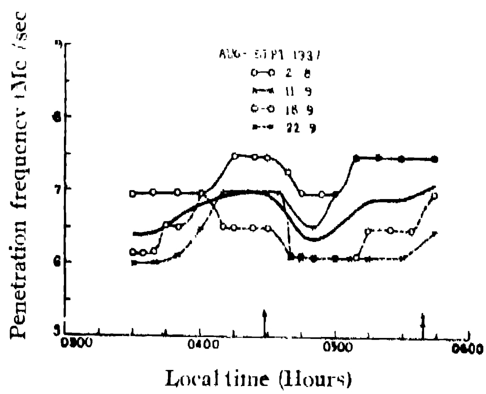

FIGURE 2

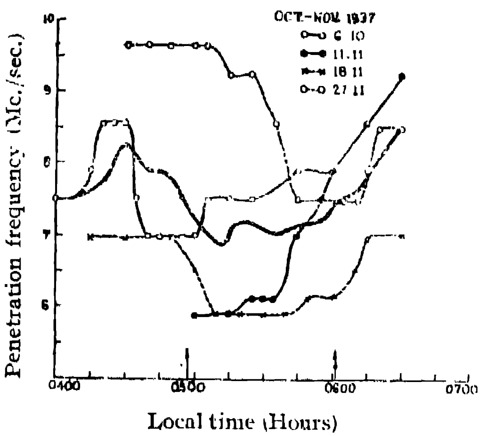

FIGURE 3

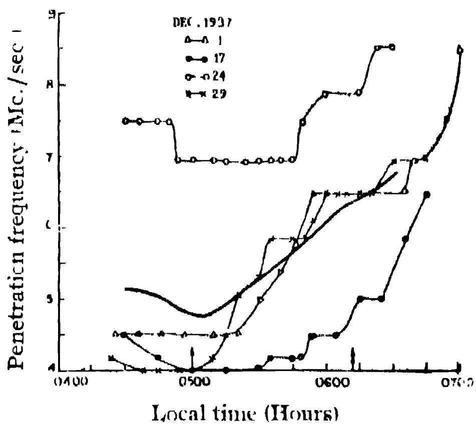

FIGURE 4

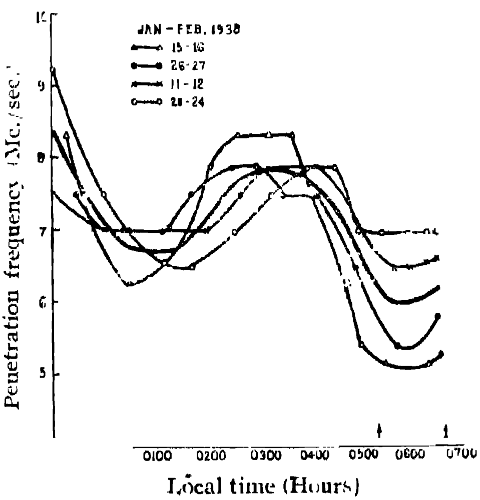

FIGURE 5

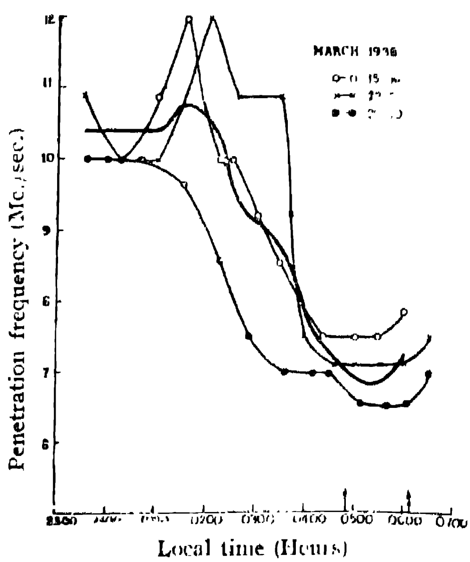

FIGURE 6

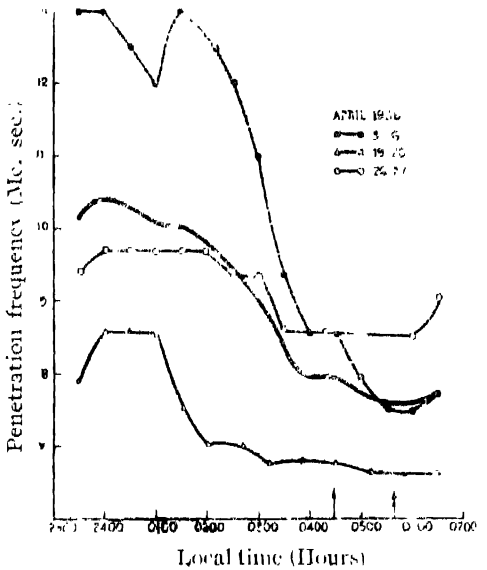

FIGURE 7

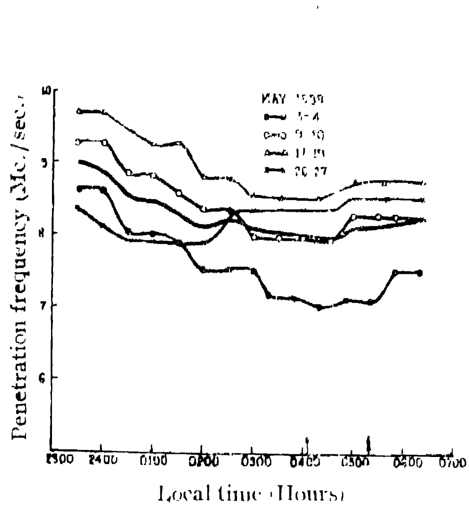

FIGURE 8

We note, for instance, that in the month of July, 1937, the hour of increase is 0320, that is, 40 minutes before the sunrise, whereas in January, 1938, the hour of increase is 0200, that is, 3 hrs. 20 mins. before the sunrise at F-layer.

Note.—The hour of increase of ionization could not be recorded in the month of December, 1937, as observations were not started early enough in the morning. The fact that we were unable to record the pre-sunrise increase of ionization by beginning our observations at the hour hitherto employed (about one hour before the sunrise in F-layer) led us to commence our observations in the following months at 2300 h.

The pre-sunrise increase of ionization has been observed by several workers amongst whom mention might be made of Gilliland,[2] Appleton and Naismith,[3] and Martyn and Pulley.[4] The last-named authors interpret this curious increase as due to the cooling of the layer as a whole and remark that this effect of cooling would be observable only in winter when sufficient hours of darkness are available. This hypothesis offers a simple explanation of the shifting of the hour of pre sunrise increase of ionization towards the earlier part of the night in winter. Since the sunset occurs earlier, the effect of contraction by cooling also occurs earlier. It should be noted further that with the approach of summer solstice, *i.e.*, in the months of April and May, 1938, no pre-sunrise increase is observed. This also can be explained if we remember that in these months the hours of darkness are small and hence before the contraction due to cooling is fully effective the sun's rays strike the layer and begin to warm it.

(*b*) *Correlation with Sunrise*

As mentioned before, the ionization after increasing in the small hours of the morning begins to show a decrease. This phenomenon is very general and

has been noticed by many investigators. One may explain this decrease as due to expansion by warming by the incidence of solar radiation as opposed to contraction by cooling during the dark hours. If this hypothesis is correct, then the hour of decrease must correspond to the hour of sunrise in the F-layer. Our observations indicate that some correspondence exists between the two only during the months of July to November (Figs. 1 to 3). But the evidence seems to be too weak to warrant any general conclusion.

One interesting point may be noted here. The ionization attains a minimum value after the sunrise at F-layer. This hour of minimum ionization is found to be farthest removed from the hour of sunrise in summer. With the approach of winter solstice, this hour tends to coincide with the hour of sunrise at F-layer. Thus the height of sunrise corresponding to the hour of early morning minimum of ionization is greater in winter than in summer. This has also been observed by Appleton and Naismith [3] in England and by Mathur [3] at Allahabad. This shifting of the hour of early morning minimum of ionization may be explained as follows:

In the early morning, after sunrise at Region F, the F-ionization density depends primarily upon two factors—(*i*) the rate of detachment of electrons from negative ions of atomic oxygen and (*ii*) the rate of heating and consequent decrease in density of the layer by the incidence of solar radiation. From the data it thus appears that the effect of heating at first predominates over that due to detachment of electrons. This effect persists for a longer time in summer than in winter.

IV TRUE HEIGHT OF REGION F

For the purpose of determining true height from the observed virtual height, a method suggested by Murray and Hoag [5] has been adopted. A full description of the method is to be found in their paper. For calculation by this method it is not necessary to assume any particular type of ionization gradient of the layers. The method is, however, laborious, as, for each point of the curve showing the variation of true height with wave-frequency, it is necessary to carry out a long set of calculations. Recently, an elegant and more convenient method of calculation has been indicated by Booker and Seaton.[6] This method, however, assumes a parabolic gradient of ionization and yields reliable results only if the actual gradient conforms to this type of gradient.

In Figures 9 to 12 the results of a calculation of the true height from the observed $(P'-f)$ curves for the Regions E and F are shown. The continuous line curves A′ and A are the $(P'—f)$ curves for the Regions E and F respectively and the broken-line curve B gives the true height to which a radio wave of a particular frequency rises before suffering reflection. It will be seen from the figures that, on an average, the true height is less than the virtual height by about 100 km.

The difference between the two increases as the critical frequency is approached. It is to be noted also that the average difference varies from day to day. In Figs. 10 and 11, the average differences are about 80 km. on 6th October, 1937, and about 150 km. on 1st December, 1937, respectively.

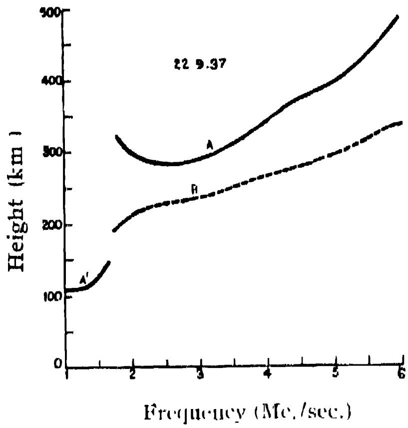

FIGURE 9

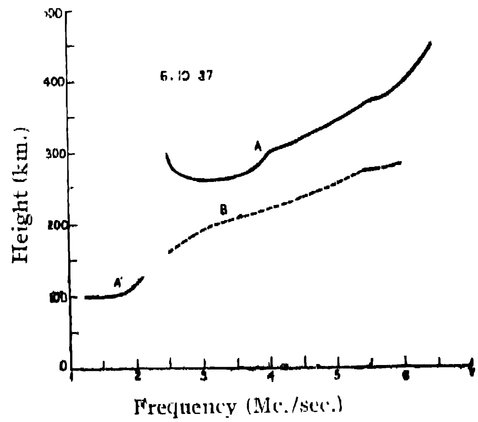

FIGURE 10

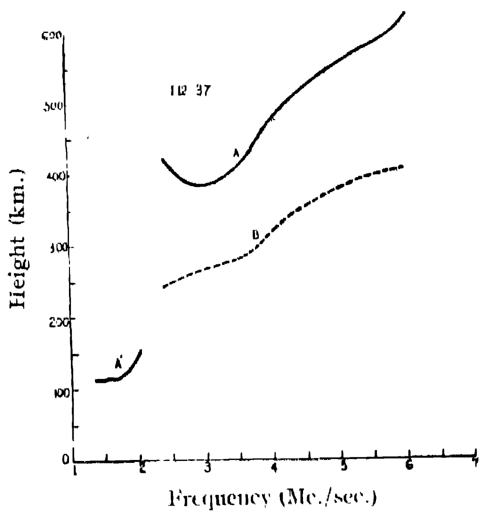

FIGURE 11

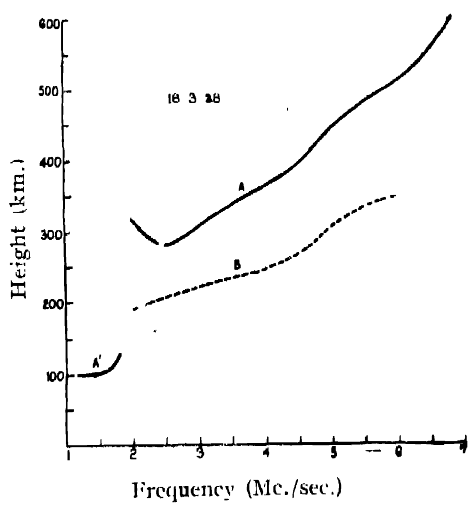

FIGURE 12

V. HOURS OF SUNRISE AT DIFFERENT LEVELS OF THE ATMOSPHERE

The hours of sunrise in different seasons at various heights above the earth's surface have been calculated by using the well-known astronomical relation between the zenith distance of the sun, latitude of the place of observation and the hour angle of the sun for sunrise at any particular height. The effect of refrac-

tion which accelerates the time of sunrise has been taken into account. In Figs. 13 and 14 curves delineating the variation of the hour of sunrise for the latitude of Calcutta (22° 33′ N) with height are given. Since it is not practicable to give the curves for all days on which observations have been made, these are drawn here for a complete year at intervals of about a fortnight so that they may be used by the ionospheric investigators in this country.

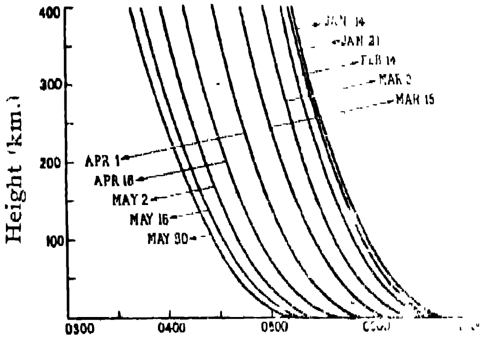

FIGURE 13

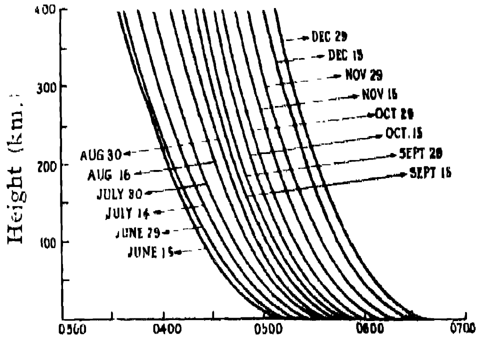

FIGURE 14

ACKNOWLEDGMENTS

The investigations described in this communication were undertaken at the suggestion of Prof. S. K. Mitra and I take this opportunity of recording my sincere thanks to Prof. Mitra for his advice and guidance in conducting the investigations.

I have much pleasure in thanking Mr. A. K. Banerjee, M.Sc., for the help he gave me in taking the observations during the latter part of the programme.

WIRELESS LABORATORY,
UNIVERSITY COLLEGE OF SCIENCE,
92, UPPER CIRCULAR ROAD,
CALCUTTA.

REFERENCES

[1] Ghosh, *M.Sc. Thesis* (1938), Calcutta University; Mitra, *Science and Culture*, **3**, 496 (1938).

[2] Gilliland, *Jour. Res. Nat. Bur. Standards*, **14**, 283 (1935); R. P. 769.

[3] Appleton and Naismith, *Proc. Roy. Soc. A*, **160**, 685 (1935); Mathur, *Proc. Nat. Acad Sciences, India*, **7**, 222 (1937).

[4] Martyn and Pulley, *Proc. Roy. Soc. A.*, **154**, 455 (1936).

[5] Murray and Hoag, *Phys. Rev.*, **51**, 333 (1937); *Ibid*, **51**, 779 (1937)

[6] Booker and Seaton, *Internat. Association Terr. Mag and Elect.*, Washington Assembly Sept., 1939.

A RELATION BETWEEN VELOCITY OF SOUND IN LIQUIDS AND MOLECULAR VOLUME

By M. RAMA RAO, M.Sc.
Department of Physics, University of Mysore, Bangalore

(Received for publication, March 15, 1940)

ABSTRACT. The relation $v^{\frac{1}{3}} . V = R$ between the velocity of sound in liquids (v) and molecular volume (V) holds good in a large number of liquids. Combining this with the expression for the energy of a vibrating molecule and Debye's expression for the frequency of a vibrating molecule, it is shown that the energy of a vibrating molecule, is proportional to its frequency of vibration. An expression for the variation of the velocity of sound with temperature is given and a fair estimate of the critical temperature is shown to be possible therefrom.

In recent years a numbei of investigators [1] have determined the velocity of sound in liquids particularly for the ultrasonic range of frequencies. Data for the velocity of sound in some liquids at different temperatures are also available.[2] All other liquids except water show a considerable increase in compressibility

Table I

Liquid.	Temperature °C.	Temperature Co-efficient of acoustic velocity × 10^3.	Temperature coefficient of volume expansion × 10^3.	Ratio.
Benzene	15	−3·71	1·19	−3·12
	35	−3·68	1·24	−2·98
	45	−3·82	1·27	−3·00
Ether	15	−4·55	1·56	−2·92
Carbon tetra-chloride	15	−3·61	1·21	−2·99
	45	−3·55	1·26	−2·82
Heptane	25	−3·64	1·24	−2·93
	45	−3·89	1·29	−3·01
Octane	25	−3·52	1·12	−3·01
	45	−3·65	1·19	−3·05
Chlorobenzene	20	−2·79	0·89	−3·12
Aniline	25	−2·41	0·84	−2·87

with temperature, resulting in a decreased velocity of sound. Physical properties of a liquid like compressibility, density, etc., are intimately connected with the cohesive factor in van der Waal's equation being largely dependent on the internal forces between the molecules. According to Wheeler [3] it is possible to calculate the values of a number of properties of a liquid from a knowledge of the molecular volume at a given temperature and of the gaseous molecular attractive force constant and force coefficient, or alternatively of the parachor. Any simple relation between the velocity of sound and molecular volume of a liquid should therefore be interesting and fundamental.

A study of the measurements of the velocity of sound in liquids at various temperatures shows that the ratio of the temperature coefficient of acoustic velocity to the coefficient of volume expansion is constant for a number of liquids. Table I gives the values of the temperature coefficient of acoustic velocity, the coefficient of volume expansion, and their ratio for a number of liquids.

The mean value of the ratio is -3 ± 0.12

Thus

$$\frac{\frac{1}{v} \cdot \frac{dv}{dt}}{\frac{1}{V} \cdot \frac{dV}{dt}} = -3 \qquad \ldots (1)$$

where v = velocity of sound in the liquid at temperature $t°C$.

V = volume of the liquid at the same temperature.

From the above result (1) empirically obtained, it follows

$$v^{\frac{1}{3}}.V = R \qquad \ldots (2)$$

where R is a constant independent of the temperature of the liquid.[4] Table II gives the velocity of sound and density of the liquid at various temperatures. The variation of acoustic velocity with frequency (if any) is neglected and the liquids are assumed to have no acoustic dispersion. R, the product of the molecular volume V and $v^{\frac{1}{3}}$, is seen to be fairly constant over the entire temperature range for which values are available.

TABLE II

Liquid	Temperature °C	Velocity of sound m /sec.	Density.	R.
Benzene	10	1375	0·8896	975·7
	20	1324	0·8790	975
	30	1278	0·8684	975·4
	40	1231	0·8576	975·4
	50	1184	0·8467	975·2

TABLE II (*contd.*)

Liquid.	Temperature °C.	Velocity of Sound m./sec.	Density.	R.
Toluene	0	1414	0·8848	1168
	10	1370·5	0·8752	1168
	20	1327·5	0·8657	1169
	30	1284·5	0·8563	1169
	40	1242	0·8470	1168
	50	1199	0·8378	1168
Carbon tetra-chloride	0	1008	1·6327	944·3
	10	970	1·6134	944·1
	20	935	1·5939	943·4
	30	904	1·5748	944·3
	40	873·5	1·5557	945·0
	50	843	1·5361	945·8
Aniline	0	1742	1·0389	1077
	10	1700	1·0303	1078
	20	1659	1·0216	1077
	30	1619	1·0130	1078
	40	1579·5	1·0044	1079
	50	1540	0·9957	1079
Chlorobenzene	0	1362·5	1·1279	1106
	10	1322·5	1·1180	1105
	20	1284·5	1·1060	1106
	30	1248	1·0980	1104
	40	1212	1·0844	1106
	50	1178	1·0730	1108
Heptane	0	1235	0·7005	1533
	10	1196	0·6920	1536
	20	1154	0·6826	1538
	30	1112	0·6751	1536
	40	1070	0·6665	1536
	50	1028	0·6579	1536

TABLE II (*contd.*)

Liquid.	Temperature °C	Velocity of Sound m./sec.	Density.	R.
Octane	0	1277	0·7185	1724
	10	1235	0·7103	1724
	20	1192	0·7021	1723
	30	1150	0·6940	1722
	40	1108	0·6859	1721
	50	1060	0·6770	1719
Ether	0	1095	0·7362	1037
	10	1054	0·7248	1040
	20	1006	0·7135	1040
	30	949	0·7019	1037
Acetone	0	1273	0·8125	774·1
	10	1231	0·8014	776·4
	20	1190	0·7905	778·2
	30	1146	0·7788	780
	40	1102	0·7672	781·6
	50	1057	0·7554	782·9
Bromoform	10	953	2·886	862
	20	928	2·858	863·2
	30	907	2·830	864·8
	40	886	2·802	866·4
	50	865	2·774	868·4
Methyl alcohol	0	1187	0·8100	418·6
	10	1154	0·8007	419·5
	20	1121	0·7913	420·4
	30	1088	0·7818	421·3
	40	1056	0·7723	422·3
	50	1023·5	0·7627	423·1

TABLE II (*contd.*)

Liquid.	Temperature °C.	Velocity of Sound m./sec	Density.	R
Glycerine	10	1941·5	1·2671	906·5
	20	1923	1·2613	908
	30	1905	1·2553	909·3
	40	1886·5	1·2491	910·7
	50	1868·5	1·2427	912·2
Nitrotoluene	63	1373	1·116	1365
	67	1363	1·114	1365
	74	1335	1·105	1367
	95	1277	1·86	1370
	98	1267	1·083	1370
	123	1191	1·061	1370
	126	1176	1·058	1368
p-Dichloro-benzol.	72	1082	1·230	1227
	84	1050	1·219	1226
	94	983	1·208	1211
	150	837	1·142	1213

Since the molecular volume of a liquid is proportional to the cube of the inter-molecular distance it follows from the result $v^{\frac{1}{3}}.V = R$ that the velocity of sound in a liquid varies inversely as the ninth power of the distance between the molecules. According to Wheeler [5] the energy of a vibrating molecule is inversely proportional to the 10th power of the mutual distance between two molecular centres.

Hence $$E \propto \frac{1}{\;{}^{10}} \qquad \ldots \quad (3)$$

From the empirical result we have obtained, it follows that

$$v \propto \frac{1}{\sigma^{9}}\,. \qquad \ldots \quad (4)$$

Combining (3) and (4) it follows that

$$E \,/\, \frac{v}{} = \text{constant, independent of temperature.} \qquad (5)$$

According to Debye, the frequency of a vibrating molecule in a liquid is given by

$$\left(\frac{3N}{4\pi V}\right)^{\frac{1}{3}} \cdot v$$

where N = avogadro number,

V = molecular volume,

v = velocity of sound in the liquid.

Since $\frac{V}{N}$ is proportional to σ^3

we have $$\nu = c\,\frac{v}{\sigma} \qquad \ldots \quad (6)$$

where c = constant.

Combining (5) and (6) we have

$$\frac{E}{\nu} = \text{constant.} \qquad (7)$$

This result shows that the energy of a vibrating molecule is proportional to its frequency.

VARIATION OF THE VELOCITY OF SOUND WITH TEMPERATURE

The equation, $v^{\frac{1}{3}}.V$ = constant, shows that the change in the velocity of sound with temperature is determined by the dependence of the density of the liquid on temperature. The variation of density[6] with temperature from the freezing point to the critical point is represented for non-associated liquids by the equation

$$D - d = D_o\left(1 - \frac{\theta}{\theta_c}\right)^{\frac{3}{10}}$$

where D = density of the liquid at $\theta°$ Abs.,

d = density of the vapour at $\theta°$ Abs.

The equation also holds good for associated liquids over the lower part of the temperature range and in some cases nearly to the critical point. The zero volume $\frac{1}{D_o}$ is nearly proportionai to the critical volume for most of the liquids. Further, the critical temperature predicted from density observations are in good agreement with the observed values.

In the lower temperature range the density of the vapour is small and may be neglected in comparison with D and so we have

$$D = D_o \left(1 - \frac{\theta}{\theta_c} \right)^{\frac{3}{10}}.$$

Combining this with

$$\frac{v^{\frac{1}{3}} . M}{D} = \text{constant},$$

we have

$$v = v_o \left(1 - \frac{\theta}{\theta_c} \right)^{\frac{3}{10}}.$$

This equation gives the variation of the velocity of sound with temperature. The critical temperatures deduced from sound velocity measurements are collected in Table III and are compared with the observed values. The agreement is satisfactory.

TABLE III

Liquid.	θ_c Cal.	θ_c Expt.
Benzene	546	561·5
Carbon tetrachloride	551	556·1
Chlorobenzene	607	632
Diethyl ether	477	467
Toluene	572	594
Octane	549	569
Heptane	543	540
Nitrotoluene	734	754
p-Dichlorobenzene	660	675

While considering the temperature variations of physical properties of a liquid, we have found it necessary to define a new characteristic temperature Θ given by $\frac{\theta_c - \theta}{\theta_c - \theta_f}$ where θ_c and θ_f refer respectively to the critical temperature and the melting point of the liquid. It has been shown that, expressed in terms of this characteristic temperature, many of the physical properties of the liquid vary with temperature according to a simple law[7]

$$Z = Z_f \, \Theta^n,$$

where Z_f = value of the physical entity, at the melting point θ_f
n = a positive or negative fraction.

In terms of this reduced temperature the variation of velocity of sound with emperature in particular is given by

$$v = v_f \,\Theta^{0.9} \quad .$$

In conclusion it gives me great pleasure to thank Mr. L. Sibaiya for his guidance during this investigation and Professor A. Venkat Rao Telang for his encouragement.

REFERENCES

[1] Freyer, Hubbard, Andrews, *J. Amer. Chem. Soc.*, **51**, 759 (1929); Parthsarathy, *Ind. Acad. Sci*, **2A**, 497 (1935); *Ind. Acad. Sci.*, **4A**, 59 (1936), *Ind. Acad. Sci.*, **3A**, 285, 297, 482 and 519; Schaafs, *Zeits. f. physik*, **105**, 658 (1937) and Swanson, *J. Chem. Phys.*, **2**, 689 (1934).

[2] Freyer Hubbard, Andrews, *J. Amer. Chem Soc*, **51**, 759 (1929); Schaafs, *Zeits. f. physik*, **106**, 658 (1937).

[3] Wheeler, *Trans. Nat. Inst. Sc. of India*, **1**, 333 (1938).

[4] M. Rama Rao, *Curr. Sci.*, **8**, 510, (1939).

[5] Wheeler *Trans. Nat. Inst. Sc. of India*, **1**, 333 (1938).

[6] Sugden, *J. Chem. Soc.*, 1780-86 (1927); *J. Chem. Soc.*, 1055 (1929).

[7] L. Sibaiya and M. Rama Rao. *Curr. Sci.*, **8**, 359 (1938).

THE THEORY OF COMPTON EFFECT

By K. C. KAR

(*Received for publication, March 18 1940*)

ABSTRACT. The wavestatistical theory of interaction between radiation and matter previously developed is extended by taking into account the energy and momentum of recoil of the scattering electron The well-known Einstein-Dirac formula for the intensity of Compton scattering is derived

While discussing recently certain problems[1] on the interaction between radiation and matter from the standpoint of wavestatistics, I have derived, among others, Thomson's classical formula for the scattering of radiation by an electron. In so doing I have neglected the change of frequency that is produced by the recoil of the scattering electron. The object of the present paper is to show that the intensity of Compton scattering may be easily derived by the above method if the change of frequency mentioned above is taken into account.

Now the fundamental assumption made in the previous paper is that as soon as the incident radiation $h\nu_s$ approaches the scattering electron up to a critical distance r_{0s}, both the q- and p- components of the phase space for the region surrounding the electron ($r \leqq r_{0s}$) temporarily acquires negative viscosity relative to the region outside ($r \geqq r_{0s}$). As a result of that, $h\nu_s$ enters the inner region thereby considerably increasing its phase density. Consequently the region immediately develops positive viscosity relative to that outside and the radiation is scattered away in different directions. This is in short the mechanism of scattering as imagined in wavestatistics. It may, however, be noted that the critical distances of approach and scattering may not in general be the same.

As already shown the wave equations are

$$\Delta\chi_1 + \frac{8\pi^2 m}{h^2}\left(E + \frac{b^2 h^2}{4\pi^2 E}\right)\chi_1 = 0, \quad \text{inside} \qquad \dots \quad (1)$$

$$\Delta\chi_1 + \frac{8\pi^2 m}{h^2}(E + \bar{U}_2)\chi_1 \qquad = 0, \quad \text{outside} \qquad \dots \quad (2)$$

and similarly for χ_2-wave. In the above b denotes the viscosity and $\bar{U}_2$ the average interaction potential between radiation and the free electron. It is evident that $\bar{U}_2 = 0$ for the region inside, while $\bar{U}_2 \neq 0$ for the region outside. This may be taken as the condition which helps the growth of viscosity in a given

phase space. It is shown before that the interaction potential for s-type radiation is given by

$$U_2^s = \frac{8\pi e^2}{\Omega m} \cdot \overline{\alpha_s^2 Q_s^2 \sin^2\gamma_s} \qquad \ldots \quad (3)$$

where m is the mass of the electron, Ω the volume, α_s unit vector in the direction of the electric field of the electromagnetic wave, Q_s the coordinate of radiation and γ_s the phase. As eqs. (1) and (2) must be identical at the boundary we have for s-type radiation

$$b_1^s = b_2^s = \frac{2\pi}{h}\sqrt{h\nu_s \cdot \overline{U_2^s}} \qquad \ldots \quad (4)$$

where b_1^s and b_2^s are of the nature of the viscosity coefficients of the q- and p-spaces respectively.

It is shown before that the wavestatistical average

$$\bar{Q}_s = e^{-2\pi i\nu_s t}\left(\frac{hn_s}{8\pi^2\nu_s}\right)^{\frac{1}{2}} \qquad \ldots \quad (5)$$

and as we have approximately $\overline{Q_s^2} = (\bar{Q}_s)^2$ the interaction potential in (3) becomes

$$\overline{U_2^s} = \frac{he^2}{\pi\Omega m} \cdot \frac{n_s}{\nu_s} \cdot \overline{\alpha_s^2 \sin^2\gamma_s} \cdot e^{-4\pi i\nu_s t} \qquad \ldots \quad (6)$$

Let ν_s be the frequency of the primary radiation. Its number densities before and after scattering are evidently $\frac{n_s}{\Omega}$ and $\frac{n_s - 1}{\Omega}$ respectively. Consequently the number densities of the scattered radiation of frequency ν_σ before and after scattering would be 0 and $\frac{1}{\Omega}$ respectively. Hence we have for the scattered radiation corresponding to (6)

$$\overline{U_2^\sigma} = \frac{he^2}{\pi\Omega m} \cdot \frac{1}{\nu_\sigma} \cdot \overline{\alpha_\sigma^2 \sin^2\gamma_\sigma}\, e^{4\pi i\nu_\sigma t} \qquad \ldots \quad (7)$$

On substituting in (4) the value of U_2^s from (6) we get for the damping coefficients of s-type radiation

$$b_1^s = b_2^s = 2\pi\left\{\frac{n_s e^2}{\pi\Omega m} \cdot \overline{\alpha_s^2 \sin^2\gamma_s}\right\}^{\frac{1}{2}} e^{-2\pi i\nu_s t} \qquad \ldots \quad (8)$$

Similarly we have for the scattered radiation

$$b_1^\sigma = b_2^\sigma = 2\pi\left\{\frac{e^2}{\pi\Omega m} \cdot \overline{\alpha_\sigma^2 \sin^2\gamma_\sigma}\right\}^{\frac{1}{2}} e^{2\pi i\nu_\sigma t}. \qquad \ldots \quad (9)$$

On putting $b_1^s = \dot{a}_1^s$ we get from (8) after integration with respect to t

$$a_1^s = 2\pi \left\{ \frac{n_s e^2}{\pi \Omega m} \cdot \overline{\alpha_s^2} \ \overline{\sin^2 \gamma_s} \right\}^{\frac{1}{2}} \cdot \frac{e^{-2\pi i \nu_s t}}{-2\pi i \nu_s} \qquad \dots (10)$$

Hence we get for the rate of scattering in the q-space

$$b_1^{s\sigma} = a_1^s b_1^\sigma = \frac{2e^2}{\Omega m} \left\{ \overline{\alpha_s^2 \alpha_\sigma^2 \sin^2 \gamma_s \sin^2 \gamma_\sigma} \right\}^{\frac{1}{2}} n_s^{\frac{1}{2}} \cdot \frac{e^{-2\pi i (\nu_s - \nu_\sigma) t}}{-i\nu_s} \qquad \dots (11)$$

It should be noted that the above represents the rate of scattering by *one* electron. So to get the rate of scattering by a volume-element $d\tau$, where the *instantaneous* number density of the scattering electron is given by

$$D d\tau = \chi_{1,m}^* \chi_{2,n}^* \cdot e^{\frac{2\pi i E_m t}{h}} \cdot e^{-\frac{4\pi i E_m (\text{kin.})}{h} t} d\tau, \qquad \dots (12)$$

one has to take the product of (11) and (12). Now, putting $E_n - E_m = h\nu'$ we find from (12)

$$D d\tau = e^{-2\pi i \nu' t} \cdot \chi_{1,m}^* \chi_{2,n}^* \cdot e^{\frac{2\pi i E_n}{h} t} e^{-\frac{4\pi i E_n (\text{kin.})}{h} t} d\tau \qquad \dots (12{\cdot}1)$$

It is well-known in wavestatistics[1] that because the phase waves are stationary, the last two exponential time factors may be dropped while integrating over the phase space.

Thus the rate of scattering per electron when there is change of momentum of the scattering electron, is given by

$$b_1^{s\sigma} = \frac{2e^2}{\Omega m} \left\{ \overline{\alpha_s^2 \alpha_\sigma^2 \sin^2 \gamma_s \sin^2 \gamma_\sigma} \right\}^{\frac{1}{2}} \cdot n_s^{\frac{1}{2}} \frac{e^{-2\pi i (\nu_s + \nu' - \nu_\sigma) t}}{-i\nu_s} \times \int \chi_{1,m}^* \chi_{2,n}^* \, d\tau . \qquad \dots (13)$$

It is evident that the integral in (13) representing the scattering electron is unity. It would be, however, noted that the above integral for a free electron does not vanish because the electron before and after scattering moves in different directions. We have then from (13)

$$b_1^{s\sigma} = \frac{2e^2}{\Omega m} \left\{ \overline{\alpha_s^2 \alpha_\sigma^2 \sin^2 \gamma_s \sin^2 \gamma_\sigma} \right\}^{\frac{1}{2}} \cdot n_s^{\frac{1}{2}} \cdot \frac{e^{-2\pi i (\nu_s + \nu' - \nu_\sigma) t}}{-i\nu_s} . \qquad \dots (13{\cdot}1)$$

Now as $b_1^{s\sigma} = \dot{a}_1^{s\sigma}$ we have on integrating (13·1) with respect to time and remembering that $a_1^{s\sigma} = 0$ at $t = 0$,

$$a_1^{s\sigma} = \frac{e^2}{\pi \Omega m} \left\{ \overline{\alpha_s^2 \alpha_\sigma^2 \sin^2 \gamma_s \sin^2 \gamma_\sigma} \right\}^{\frac{1}{2}} \cdot n_s^{\frac{1}{2}} \cdot \frac{1 - e^{-2\pi i (\nu_s + \nu' - \nu_\sigma) t}}{\nu_s (\nu_s + \nu' - \nu_\sigma)} . \qquad \dots (14)$$

Similarly

$$a_2^{s\sigma} = \frac{e^2}{\pi\Omega m}\left\{\overline{a_s^2 a_\sigma^2 \sin^2\gamma_s \sin^2\gamma_\sigma}\right\}^{\frac{1}{2}} \cdot n_s^{\frac{1}{2}} \cdot \frac{1-\epsilon^{2\pi i(\nu_s+\nu'-\nu_\sigma)t}}{\nu_s(\nu_s+\nu'-\nu_\sigma)} \qquad \ldots \quad (15)$$

Now the total number of quanta scattered in any component is

$$N^s = \sum_\sigma a_1^{s\sigma} a_2^{s\sigma}. \qquad \ldots \quad (16)$$

In order to replace the summation by integration one has to multiply (16) by $\frac{2\pi\Omega\nu_\sigma^2 d\nu_\sigma \sin\theta d\theta}{c^3}$ giving the number of $h\nu_\sigma$ -quanta of one kind of spin in the volume Ω, moving at an angle θ with the direction of the incident radiation. Moreover, since γ_σ and γ_s are the values of the phases at the boundaries, we may take

$$\frac{\sin\gamma_\sigma}{\sin\gamma_s} = \frac{\sin\left(\frac{2\pi\nu_\sigma}{c} r_{0\sigma} + \delta\right)}{\sin\left(\frac{2\pi\nu_s}{c} r_{0s} + \delta\right)} = \frac{\sin\frac{2\pi\nu_\sigma}{c}\left(r_{0\sigma} + a_\sigma\right)}{\sin\frac{2\pi\nu_s}{c}\left(r_{0s} + a_s\right)} \qquad \ldots \quad (17)$$

where $r_{0\sigma}$, r_{0s} are the boundaries for σ- and s-type radiations.

Let us assume that for the q-space

$$\nu_\sigma r_{0\sigma} = \nu_s r_{0s} \qquad \ldots \quad (17\cdot1)$$

which means that the harder ray is more penetrating. So from (17) we get

$$\sin\gamma_\sigma / \sin\gamma_s = 1. \qquad \ldots \quad (17\cdot11)$$

The above assumption cannot be valid in the p-space. It is assumed that in this space

$$r_{0\sigma} + a_\sigma = r_{0s} + a_s \qquad \ldots \quad (17\cdot2)$$

and so $r_{0\sigma}$ is, as it should be, nearly equal to r_{0s}. Consequently from (17) we get approximately

$$\sin\gamma_\sigma / \sin\gamma_s = \frac{\nu_\sigma}{\nu_s}. \qquad \ldots \quad (17\cdot21)$$

Again we have

$$\overline{\sin^2\gamma_s} = \tfrac{1}{2}. \qquad \ldots \quad (18)$$

Hence, on substituting the values given in (17·11) and (17·21), on remembering (18) and replacing the summation by integration, we get from (14), (15) and (16)

$$N_s = \frac{2e^4}{\pi\Omega m^2 c^3} \cdot \frac{n_s}{\nu_s^3} \int_0^\pi \sin\theta d\theta \int_0^\infty \overline{a_s^2 a_\sigma^2} \cdot \frac{\sin^2\pi(\nu_s + \nu' - \nu_\sigma)t}{(\nu_s + \nu' - \nu_\sigma)^2}\, \nu_\sigma^3 d\nu_\sigma \,. \qquad (19)$$

If the incident beam moving along x-axis is unpolarised, then for scattered radiation at an angle θ we have[2]

$$\overline{a_s^2 a_\sigma^2} = \tfrac{1}{2}(1 + \cos^2\theta) \,. \qquad \ldots \quad (20)$$

Now in Compton scattering, the loss of energy of the free electron, *viz.*, $E_n - E_m = h\nu'$, depends on the direction of its recoil, *i.e.*, from the conservation of momentum, on the angle of scattering of the radiation. Thus we may put

$$\nu_\theta = \nu_s + \nu' \qquad \ldots \quad (21)$$

where ν_θ is the frequency of scattered radiation at angle θ and from conservation of energy and momentum it may be easily shown that

$$\nu_\theta = \frac{\nu_s}{1 + \alpha(1 - \cos\theta)}\,;\ \alpha = \frac{h\nu_s}{m_0 c^2} \,. \qquad \ldots \quad (21'1)$$

Hence (19) takes the form

$$N_s = \frac{e^4}{\pi\Omega m^2 c^3} \cdot \frac{n_s}{\nu_s^3} \int_0^\pi (1 + \cos^2\theta)\sin\theta d\theta \int_0^\infty \frac{\sin^2\pi(\nu_\theta - \nu_\sigma)t}{(\nu_\theta - \nu_\sigma)^2}\, \nu_\sigma^3 d\nu_\sigma \qquad \ldots \quad (22)$$

Because the value of the expression, within the sign of integration with respect to ν_σ, is concentrated near $\nu_\sigma = \nu_\theta$, one may take ν_σ^3 out of the integral as ν_θ^3. The integral that is left can be readily transformed to the standard form

$$\int_{-\infty}^{+\infty} \frac{\sin^2 kx}{x^2}\, dx = \pi k \,.$$

Hence we have from (22)

$$N_s = \frac{\pi e^4}{\Omega m^2 c^3} \cdot \frac{n_s}{\nu_s^3}\, t \int_0^\pi \nu_\theta^3 (1 + \cos^2\theta)\sin\theta d\theta \,. \qquad \ldots \quad (23)$$

Let I_θ denote the intensity of Compton scattering at angle θ at a distance r from the scattering electron and $I_0 = \frac{n_s}{\Omega}$ the intensity of incident radiation.

We have from (23)

$$I_\theta = I_0 \cdot \frac{e^4}{2r^2 m^2 c^4} (1+\cos^2\theta) \cdot \frac{\nu_\theta^3}{\nu_s^3} \qquad \ldots \quad (24)$$

which is the formula for the intensity of Compton scattering, as given by Einstein, Dirac and others.

If we neglect the energy of the recoil of the scattering electron, $\nu' = 0$ and so from (21) $\nu_\theta = \nu_s$. Hence from (23) after integrating with respect to θ

$$I = \frac{8\pi}{3} \cdot \frac{e^4}{m^2 c^4} \cdot I_0 \qquad (25)$$

which is the well-known Thomson formula of classical scattering.

PHYSICAL LABORATORY,
PRESIDENCY COLLEGE,
CALCUTTA.

REFERENCES

K. C. Kar, *Phil. Mag.* (February, 1940).

[2] A. H. Compton, *X-rays and Electrons*, p. 60.

ROTATIONAL RAMAN SCATTERING IN LIQUID OXYGEN

By BISHNUPADA SAHA, M.Sc.

(Received for publication, April 2, 1940)

Plate IV

ABSTRACT. The rotational wing due to liquid oxygen has been studied using a special technique to remove suspended particles from the liquid and a spectrograph capable of resolving the rotational lines of O_2 in the region of 4046 A.U. It has been found that rotational scattering does not consist of sharp lines but it consists of a continuous wing in which the position of maximum intensity is the same as in the case of the gas and also the extent of the wing agrees with that of the rotational Raman spectrum observed in case of gaseous O_2. The significance of the results is discussed.

INTRODUCTION

The distribution of intensity in the continuous spectrum which appears in the neighbourhood of the Rayleigh line in the spectrum of light scattered by many liquids has been studied by various observers.[1] It has been reported by most of these observers that the observed distribution of intensity does not agree with that expected according to the theory of scattering due to free rotation of the molecules. As is well known, if the rotational lines be too close to each other to be resolved by ordinary spectrographs, a continuous rotational wing is expected to appear in the neighbourhood of the Rayleigh line, the intensity in the wing being zero up to a short distance from the centre of the Rayleigh and after rising to a maximum value at a certain distance from the Rayleigh line depending on the moment of inertia of the molecule, falling off gradually and becoming zero at another distance. The observed rotational Raman scattering in the case of liquid hydrogen consists of discrete lines similar to those observed in the case of the gas, but in the case of many other liquids with simple molecules (1) the position of maximum intensity is not clearly separated from the Rayleigh line and (2) the wing extends to a larger distance than expected from the above theory.

Various explanations have been offered to explain this discrepancy. Gross and Vuks[2] attribute the origin of the "wing" in the neighbourhood of the Rayleigh line to lattice oscillations in quasi-crystalline groups of molecules which according to them persist in the liquid state. They observed some new lines in the neighbourhood of the Rayleigh lines in the case of some organic crystals which in the molten state produce intense wing close to the Rayleigh line. They think

that the lines observed in the solid state spread out to form the wing in the liquid state. It has been shown by Sirkar[3] and Sirkar *et al*[4] that the wing cannot have iss origin in the lattice oscillations and there is no quantitative correspondence between the intensity of the new lines observed in the case of any substance in the solid state and that of the wing due to the same substance in the liquid state. Sirkar and Gupta[5] have also pointed out that the observed facts lead to the conclusion that the major portion of the wing is due to rotation of the molecules in the liquid state; but, superposed on it, there is another portion having some other origin.

Bhagavantam[6] put forward the hypothesis that the portion of the wing far away from the Rayleigh line may be due to hindered rotation of the molecules, or, in the other words, to the angular oscillation of the molecules about the position of equilibrium in quasi-crystalline groups Rousset[7] has pointed out that the intensity of the scattered light due to such oscillations varies with the amplitude of oscillation and is negligible for the amplitudes postulated by Bhagavantam

Rousset[8] has put forward different hypotheses to explain the discrepancies mentioned above. According to him the wing extending from the centre of the Rayleigh line consists of two parts, *e.g.*, (1) one part lying within 20 cm^{-1} from the Rayleigh line originating from fluctuation of molecular field, this part being called by him "the Cabannes Daure Effect" and (2) the other part due to rotation of molecules with restricted space quantisation. The restriction in this space quantisation postulated by him is as follows: when the molecule is free to rotate in all directions, the number of molecules in the quantum state J is $(2J+1)e^{-BJ(J+1)}$, where $B = \frac{h^2}{8\pi^2 I k T}$ This number is maximum when $(2J+1)^2 = \frac{\;}{B}$ In the liquid state cybotactic groups are formed and the axis of molecules in such a group can rotate only in one plane and therefore the space quantisation is absent, and the number of molecules in the state J is $e^{-BJ(J+1)}$. This number is maximum when $J = -\frac{1}{2}$ or approximately the position of maximum intensity coincides with the first rotational line. It can be tested by studying the rotational Raman scattering in liquids having simple molecules whether such a restriction in space quantisation actually occurs. In the case of liquid hydrogen, McLennan and McLeod[9] observed two lines with relative intensities the same as observed by Bhagavantam[10] in the case of the gas. But no definite conclusion can be drawn from this fact because the two lines due to the transition $0 \rightarrow 2$ and $1 \rightarrow 3$ are due to para- and ortho-molecules respectively and the relative numbers of these two types of molecules change with time. The next simple diatomic molecule giving intense scattered light is O_2 and the rotational scattering due to gaseous oxygen at various pressures has been investigated thoroughly by Bhagavantam[11] and Trumpy.[12] It has been observed by Trumpy that even at a pressure of 60 atmospheres discrete rotational lines appear in the spectrum of

PLATE IV

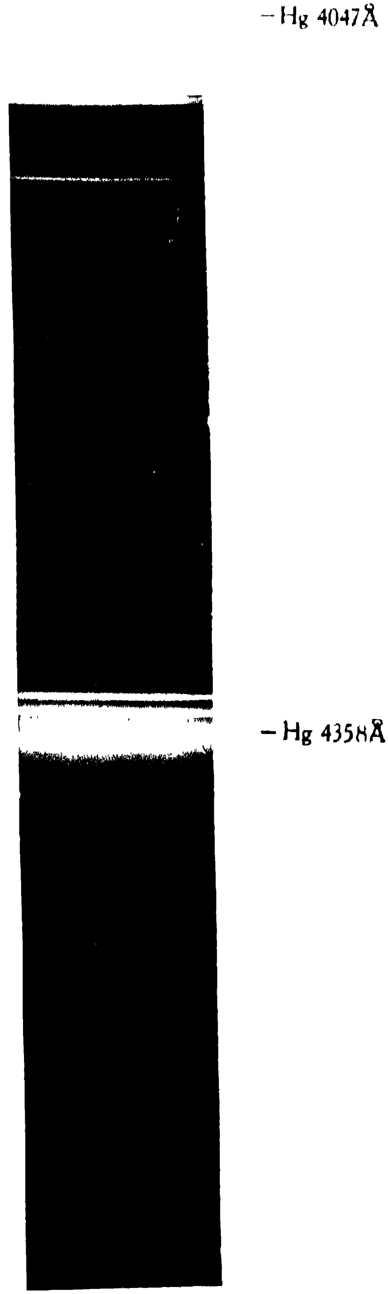

Figure 1

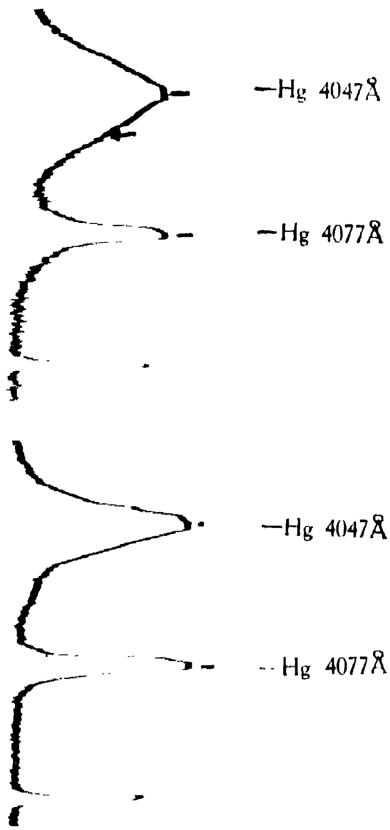

(a)

(b)

Figure 2

scattered light and the observed relative intensity of the lines agree with those calculated according to the theory of scattering due to free rotation of the molecules. The lines at 60 atmospheres, however, are much broader than those at 5 atmospheres.

It would be interesting, therefore, to investigate whether similar lines are observed in the case of liquid oxygen. The Raman spectrum of liquid oxygen has, therefore, been studied with suitable technique in order to investigate the distribution of intensity in the rotational wing and the results ars discussed in the present paper.

EXPERIMENTAL

The main difficulty in recording the rotational wing due to liquid oxygen is due to the fact that the commercial liquid oxygen when exposed to atmosphere becomes turbid owing to the condensation of moisture and the formation of small particles of ice in the liquid. These ice particles scatter light very strongly and hence the Rayleigh line becomes over-exposed and spread out so as to mask the rotational wing. In the present investigation an arrangement was made to prevent the formation of ice particles in the liquid oxygen used The liquid oxygen supplied by the local manufacturers was contained in a vertical unsilvered Dewar vessel of Pyrex glass ; but, before introduction into the vessel, the liquid underwent three stages of filtration, the first stage being through a bed of solid carbon dioxide and the other two through filter papers only. The first filter bed was present at the mouth of the Dewar vessel throughout the exposure and thus prevented subsequent absorption of moisture by the liquid air below. The liquid was illuminated by light from two mercury arcs focussed by two large glass condensers of short focal length. Also a metallic curved reflector at the back of each lamp was used to improve the illumination. A Fuess glass spectrograph with a dispersion of about 11·5 A.U. in the region 4046 A.U. was used. The Stokes side of the Hg-line 4046 A.U. obtained with this spectrograph is free from coma for moderate intensities but when the exposure is long enough to record the 4145 A.U. line of Hg, the line 4046 A.U. spreads up to about 30 cm^{-1} from the centre of the line. The spectrograph can, however, resolve clearly about 11 cm^{-1} in this region, and, as the distance between two successive rotational lines of O_2 is 11·5 cm^{-1}, this spectrograph can resolve these rotational lines excited by 4046 A. U and is almost as efficient as that used by Trumpy in his investigation on the rotational Raman spectrum of O_2. Both Ilford Special Rapid and Golden Iso-zenith plates were used and two good spectrograms, one on each of the above plates were obtained. In each case a continuous exposure of 15 hours was given and liquid oxygen was added every half an hour. The room was darkened sufficiently to prevent any stray daylight from entering into the spectrograph by scattering and reflection. The spectrum of Hg-light was also photo

graphed in such a way that its density of the lines was almost the same as that in the spectrogram due to the scattered light obtained on the same plate.

RESULTS AND DISCUSSIONS

The spectrogram of the scattered light as well as the microphotometric records of the scattered and incident Hg-line 4046 A. U. obtained with a Moll's self-registering microphotometer are produced in plate IV. It can be easily observed that no discrete rotational lines have appeared, but only a continuous wing has been obtained. The wing extends up to about 140 cm^{-1} from the Rayleigh line on the Stokes side and this agrees with the extent of the rotational Raman spectrum due to the gas recorded by Trumpy. Also the position of the maximum intensity in the wing is at a distance of about 50 cm^{-1} from the centre of the Rayleigh line and agrees with that of the most intense rotational lines observed by Trumpy. Of course, in the microphotometric record this maximum intensity is not represented by any pronounced peak owing to the presence of a coma close to the Rayleigh line but a narrow gap has been observed in the spectrogram between the edge of the coma and the intense portion of the wing. This gap is visible with an ordinary magnifying lens but the microphotometric record taken even with a fine thermopile slit shows only an inflection (indicated in fig. 2(*a*) plate IV by the arrow).

The above result leads to the conclusion that in the case of the simple diatomic molecule like O_2 in the liquid state the rotational lines become much broader than those in the case of molecules in the gaseous state, even at a pressure of about 60 atmospheres. This is probably due to the effect of intermolecular field in the liquid state. At higher pressures in the gaseous state this intermolecular field begins to show its influence on the width of the line. The widening at 60 atmospheres is not very large and it can be correlated to the fact that the intermolecular field at the pressure in the gaseous state compared to that in the liquid state is small. The intermolecular field in the gaseous state may be identified with the van der Waals' force, $\frac{a}{V^2}$ and that in the liquid state may be indentified with the internal pressure $\left.\frac{\partial u}{\partial V}\right)_T$, *i.e.*, the force per sq. cm. with which the molecules are drawn inwards. Tentatively we may compare the van der Waals' force, $\frac{a}{V^2}$ for gaseous oxygen at 60 atmospheres and the internal presssure $\left(\frac{\partial u}{\partial V}\right)_T$ of liquid oxygen at its boiling point. Unfortunately the data in the desired region of temperature and pressure are not available. However it may be useful to calculate $\frac{a}{V^2}$ and $\left(\frac{\partial u}{\partial V}\right)_T$ near about the desired region.

It can be shown that $\frac{a}{V^2} = (a_p T_o - 1) p_o$ where a_p is the mean pressure coefficient between 0° and 100°C, and p_o = pressure in atmosphere and $T_o = 273.2$. The value of a_p for gaseous oxygen at 100 atmosphere is available. The value of a_p at 60 atmospheres will, however, be much smaller. Using this larger value for $a_p = .00492$, the van der Waals' force, $\frac{a}{V^2}$ beomes about 20 atmospheres. The correct value is certainly much less, because a_p is much less at 60 atmospheres.

It can be shown from thermodynamical considerations that the internal pressure

$$\left(\frac{\partial u}{\partial V}\right) = TE a_v - p,$$

where E = modulus of bulk elasticity,
and a_v = coefficient of volume expansion.

In the case of liquid O_2 the values of a_v and compressibility $\beta\left(=\frac{1}{E}\right)$ at 20.2°K are available. Assuming these values of a_v and β to be valid at the boiling point of the liquid oxygen, $\left(\frac{\partial u}{\partial V}\right)$ is about 60 atmospheres. This value of internal pressure is quite large as compared with the value of $\frac{a}{V^2}$ for gaseous O_2 at 60 atmospheres. Although this value of internal pressure is quite small in comparison with that calculated in case of other substances in the liquid state, it is many times larger than the value of $\frac{a}{V^2}$, calculated at 60 atmospheres. Hence it seems that the observed broadening of the rotational lines in case of liquid state may be correlated with the internal pressure.

The space quantisation, however, is not restricted in this case by the formation of cybotactic groups in the liquid, because in that case the position of maximum intensity would coincide with the first rational line and would be at a distance of 14.4 cm^{-1} from the centre of the Rayleigh line. As already mentioned, the observed distance of the position of maximum intensity is at about 50 cm^{-1} from the centre of the Rayleigh line.

The vibrational Raman line of O_2 at $\Delta\nu$ equal to 1550 has been recorded with large density and no other faint vibrational Raman line has been observed in the spectogram. This fact shows that percentage of any complex molecule such as O_4, if such molecules are present in the liquid, is very small. Hence this rotational wing is not affected by the presence, if any, of such molecules in the liquid. The scattering due to fluctuation of intermolecular field is not very intense in this case, because, as can be seen from the comparison of the microphotometric records of the scattered and the incident lines, the top portion of the

curve due to scattered line is not much broader than that due to incident line, but the curves show the presence of feeble Cabannes Daure effect. The principal effect of the intermolecular field is therefore to make each individual rotational line broader. In the case of molecules with larger moment of inertia, the position of maximum intensity is much nearer to the centre of the Rayleigh line, *e.g.*, in case of benzene the position of maximum is at 26 cm^{-1} from the centre of the Rayleigh line. If the individual lines become much broader in the liquid state, the maximum becomes flattened. It is evident, therefore, that if the Cabannes Daure Effect is superimposed on the rotational wing in the case of the liquid state, the probability of observing a position of pronounced maximum intensity in the wing diminishes very much.

ACKNOWLEDGMENTS

The author is indebted to Prof. M. N. Saha, F.R.S., for his kind interest in the investigation and helpful discussions and the author's best thanks are due to Dr. S. C. Sirkar for suggesting the problem and helpful discussions during the progress of the work.

REFERENCES

[1] Weiler, *Z. f. Phys.*, **68**, 782 (1930), Ranganatham, *Ind. J. Phys.* **7**, 353 (1932); Bhagavantam, *Ind. J. Phys.*, **3**, 107 (1933); Bhagavantam and Rao, *Ind. J. Phys.*, **8**, 437 (1934); Rao, *et al*, *Proc. Ind. Acad. Sc.*, **1**, 273 (1934).

[2] Gross, and Vuks, *Nature*, **136**, 100, **431**, 998 (1935)

[3] Sirkar, *Ind. J. Phys.*, **10**, 75 (1936).

[4] Sirkar and Mookerjee, *Ind. J. Phys.*, **10**, 375 (1936); Sirkar and Gupta, *Ind. J. Phys.*, **12**, 35 (1938).

Sirkar and Gupta, *loc. cit*

[6] Bhagavantam, *Proc. Ind. Acad. Sc.*, **2**, 63 (1935).

[7] Rousset, *Jour. de Phys.*, **6**, 507 (1935).

[8] Rousset, *loc. cit.*

[9] McLennan and McLeod, *Nature*, **123**, 116 (1929).

[10] Bhagavantam, *Ind. J. Phys.* **7**, 107 (1932)

[11] Bhagavantam, *Ind. J. Phys.*, **6**, 319 (1931).

[12] Trumpy, *Z. f. Phys.* **84**, 282 (1933).

MAGNETIC SUSCEPTIBILITIES OF SOLUTIONS OF SODIUM AND POTASSIUM NITRATES

By S. P. RANGANADHAM

AND

M. QURESHI

(Received for publication, March 26, 1940)

ABSTRACT. Dia-magnetic susceptibilities of solutions of sodium and potassium nitrate have been determined over a wide range of concentration (1 to 20%), employing a modified form of Quinke's method with a photographic recording arrangement. The susceptibility—concentration graph is, in each case, a straight line cutting the susceptibility axis at a point corresponding to the susceptibility of pure water (-0.72×10^{-6}), the maximum departure from linearity being not more than 1 %. The gram-ionic susceptibility of NO_3^- calculated from these measurements, using the theoretically calculated values for Na^+ and K^+, is different in each case, being less for the potassium salt. In view of the fact that there is a lack of agreement between the values for Na^+ and K^+ arrived at by different workers and the theoretical values calculated by different methods, no definite conclusion can be drawn with regard to the specific influence of the positive ion It is, however, clear that the experimental values are, on the whole, much less than the theoretical value for NO_3^-, which is an indication of ionic deformation.

INTRODUCTION

In a previous paper, [1] a study was made of the dia-magnetic susceptibilities of nitric acid solutions at different concentrations. It was found that the susceptibility-concentration curve departed appreciably from a linear relation and that deviations occurred at concentrations corresponding to some known hydrates. The present communication deals with the investigation of the dia-magnetic susceptibilities of sodium and potassium nitrate solutions. The choice of the salts was dictated by two considerations. In the first instance, these salts have not been thoroughly investigated for their magnetic susceptibilities in solutions. Secondly, as we had already studied the susceptibility of nitric acid, the investigation of other nitrates was expected to yield some information with regard to the influence of kation on the susceptibility of the NO_3 ion.

EXPERIMENTAL

The experimental arrangement was essentially the same as that used in our work on nitric acid. Two narrow glass tubes of equal and uniform bore, each

connected by a glass tubing to a wider tube so as to form a sort of U-tube, were placed vertically and side by side between the parallel pole-pieces of an electro-magnet. One of the U-tubes contained the standard liquid, benzene, selected for its non-sticking property and the other, the solution, whose susceptibility was to be determined. The value for benzene was found to be -0.704×10^{-6} in comparison with that of water (-0.720×10^{-6}). The displacement of the liquid levels in the tubes was recorded photographically by throwing an oblique beam of light from a powerful incandescent lamp placed in front of the U-tubes When the tubes are illuminated horizontally, full images of the tubes with their contents, are obtainable on the camera screen ; but when the light source is gradually displaced below the horizontal line, a position is ultimately reached when every-thing, except the two menisci, disappear completely from the field of view.

This arrangement is of great advantage inasmuch as it enables one to obtain simultaneous and almost instantaneous records of changes in the levels of the two liquids and thus to avoid all possible errors due to irreproducibility of the magnetic field and different heating effects, which are difficult to avoid where only one liquid is under observation at a time.

The tubes were thoroughly cleaned before each experiment, the solutions showing no sign of sticking. In the course of experiments, readings were also taken with the same liquid in both the tubes and corrections applied for the very slight differences in the displacement of liquids in the two tubes.

The electromagnet used was a large-size Pye's Electromagnet, capable of giving a field of about 25,000 gauss with a current of 10 amps. at 110 volts. The magnet was excited for a few seconds only for each exposure. The salts were Kahlbaum's pure reagents, purified by further re-crystallisation and carefully dried. They were found free from para-magnetic impurities.

RESULTS

The relative displacements of the menisci of the two liquids, as recorded on the photographic plate, were measured with the help of the Hilger Micrometer. In doing this, care was taken to focus the cross-wires at the centres of the minisci in each case. The ratio of the displacements gave the ratios of the susceptibilities after a correction had been applied for the para-magnetic effect of the air-vapour mixture above the liquid column. The results are given in the tables below. The susceptibility value given for each concentration is the average of results obtained from three different records.

TABLE I

Magnetic Susceptibilities of Sodium Nitrate Solutions

Gm. $NaNO_3$ in 100 gms. of solution	$-\chi \times 10^6$	Gm. $NaNO_3$ in 100 gms. of solution	$-\chi \times 10^6$
14·78	0·653	5·40	0·692
12·75	0·660	5·0	0·698
11·99	0·66[illegible]	4·5	0·700
10·9	0·671	4·0	0·702
10·0	0·675	3·5	0·702
9·5	0·677	2·5	0·706
9·0	0·678	2·0	0·705
8·5	0·680	1·5	0·70[illegible]
8·0	0·685	1·0	0·712
7·5	0·68[illegible]	0·50	0·720
7·0	0·682	0·0	0·720
6·5	0·688		

TABLE II

Magnetic Susceptibilities of Potassium Nitrate Solutions

Gm. KNO_3 in 100 gms of solution	$-\chi \times 10^6$	Gm. KNO_3 in 100 gms. of solution	$-\chi \times 10^6$
21·6	0·625	10·0	0·674
20·0	0·634	9·0	0·680
18·9	0·635	8·0	0·691
18·0	0·637	7·0	0·692
17·0	0·649	6·0	0·695
16·0	0·651	5·0	0·698
14·82	0·657	4·0	0·697
14·0	0·657	3·0	0·702
13·0	0·666	2·0	0·709
12·0	0·668	1·0	0·718
11·0	0·671	0·0	0·720

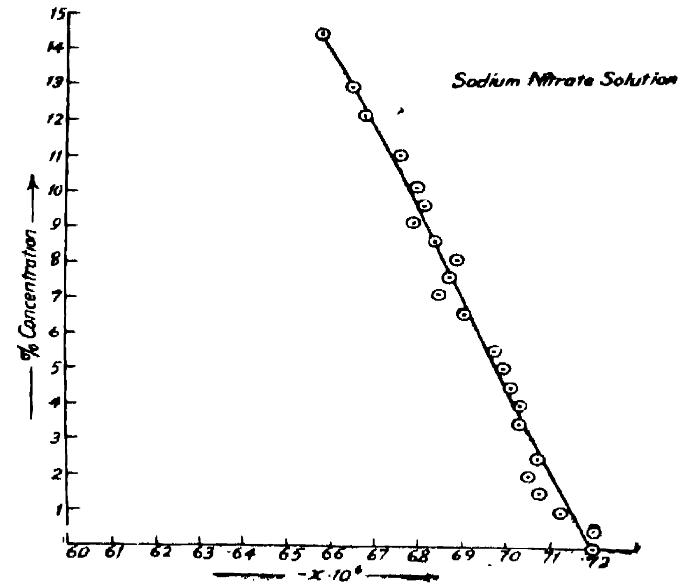
Sodium Nitrate Solution
% Concentration
15
14
13
12
11
10
9
8
7
6
5
4
3
2
1
60
61
62
63
64
65
66
67
68
69
70
71
72
$-\chi \cdot 10^6$

Fig 1.

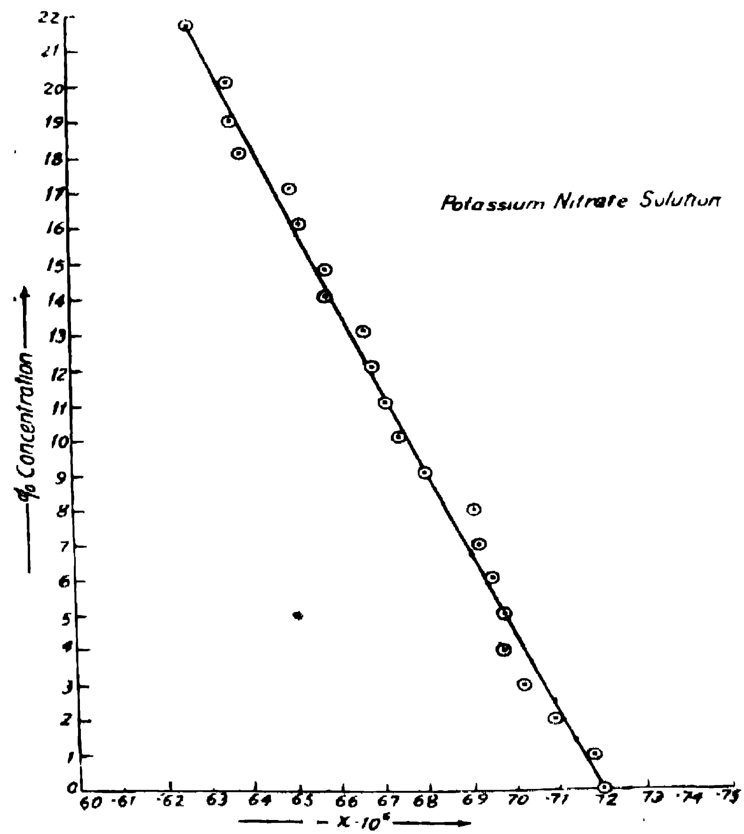
Potassium Nitrate Solution
% Concentration
22
21
20
19
18
17
16
15
14
13
12
11
10
9
8
7
6
5
4
3
2
1
0
60
61
62
63
64
65
66
67
68
69
70
71
72
73
74
75
$-\chi \cdot 10^6$

Fig. 2.

CONCLUSIONS

The changes of susceptibility with concentration in the case of both the solutions can be representated graphically by a straight line (Figs. 1 and 2), the maximum deviation from linearity being not more than 1% in each case. The equations for the two graphs are as follows :—

For sodium nitrate solution $Z = 0{\cdot}72 - 0{\cdot}0014 \times C$,

,, potassium nitrate solution $Z = 0{\cdot}72 - 0{\cdot}0041 \times C$,

where Z and C represent the susceptibility and concentration, respectively. From these equations, the gram-susceptibilities of sodium and potassium nitrate come out to be -0.28×10^{-6} and -0.31×10^{-6} respectively. These values, multiplied by the molecular weights of the salts, yield the following values for the gram-molecular susceptibilities of the two salts in the dissolved state :

Sodium nitrate	$-23{\cdot}86 \times 10^{-6}$
Patassium nitrate	$-31{\cdot}62 \times 10^{-6}$

Brindley and Hoare [2] have recently determined, with a great deal of precision, the gram-molecular susceptibilities of alkyl halides in the solid state, which are fairly additive. The ionic susceptibilities derived from this set of values show a fairly good agreement with the values, calculated theoretically by Angus for the free ions, except in the case of Na^+, for which the experimental value is $-6{\cdot}1 \times 10^{-6}$, whereas the theoretical value is $-3{\cdot}7 \times 10^{-6}$. The experimental value for K^+ ($-14{\cdot}6 \times 10^{-6}$) is greater than the theoretical value ($-13{\cdot}1 \times 10^{-6}$). Taking these theoretical values as approximately true for Na^+ and K^+ in solution, the values for the gram-ionic susceptibility of NO_3^- calculated from the gram-molecular susceptibilities of the two salts are shown in the following table. The value for the susceptibility of NO_3^- arrived at from our previous measurements with HNO_3 and the theoretical values are also given.

Gram-ionic susceptibility of NO_3^- $(-\chi \times 10^6)$

Experimental value			Theoretical value	
From measurement with HNO_3 in solution	From measurements with $NaNO_3$ in solution.	From measurements with KNO_3 in solution.	Angus [3]	Pauling [4]
20·8	20·1	18·5	34	38

It appears that the value for NO_3^- is different in the three combinations, being least in the case of the potassium salt. But in view of the fact that there is no general agreement between the values for the ionic susceptibilities of sodium and potassium arrived at by different workers and the theoretical values calculated by different methods, no definite conclusion can be drawn from the above results with regard to the influence of the positive ion. It is, however, clear that the experimental values are, on the whole, less than the theoretical value for NO_3, which is an indication of ionic deformation.

REFERENCES

[1] *Zeit f. Phys. Chem.* (B), **33**, 290, 1936.
[2] *Proc. Roy. Soc. (Lond).* (A), **152**, 342, 1935
[3] *Magneto-chemie* by Dr. Wilhelm Klemm, p 151
[4] *Proc. Roy. Soc. (Lond).* (A), **114**, 181, 1926

MUTUAL INFLUENCE OF WATER AND HEAVY WATER*

BY I. RAMAKRISHNA RAO

AND

Y. PARAMASIVA RAO
Andhra University, Waltair.

(*Received for publication, April 18, 1940*)

Plate V

ABSTRACT. The Raman bands of H_2O and D_2O for the pure liquids and their mixture containing equal proportions are described. The changes in the frequencies and the distribution of intensity of these bands are explained, partly, on the basis of the depolymerisation of these liquids in the mixture, and partly on the hypothesis of the formation of the HDO molecules.

INTRODUCTION

The Raman spectrum of heavy water was first studied by R. W. Wood,[1] who reported a broad and diffuse band with a maximum of intensity at 2517 cm.$^{-1}$. Later, Ananthakrisnan[2] found that this band consisted of three components with Raman frequencies of 2363, 2515 and 2662 cm.$^{-1}$. He reported additional bands, feeble in intensity, at 1110 and 1250 cm.$^{-1}$. Bauer and Magat[3] observed three more low frequency bands at 170, 350 and 500 cm.$^{-1}$, besides the one at 1207. They could, however, find only two components at 2389 and 2509 cm^{-1} in the principal band, but could not confirm the 1110 band of Ananthakrishnan. Rank, Larson and Bordner[4] working with vapour containing 34% proportion of water recorded a fairly sharp line at 2666 cm.$^{-1}$, which they attributed to the pure D_2O molecule. One of us with Koteswaram[5] studied the temperature variation in the structure and intensity distribution of the band for heavy water and explained the changes as due to splitting up of associated molecules with increase of temperature. The low frequency bands at 170, 350, 500, 1110 and 1250 cm.$^{-1}$, reported by other workers, were not noticed in these investigations. On account of the similarity in the Raman spectra and other properties of D_2O and H_2O, the authors have undertaken the study of the Raman bands in mixtures of the two liquids, as a preliminary to the more extensive investigation on the effect of dissolved electrolytes and non-electrolytes upon the Raman band of D_2O.

* Communicated by the Indian Physical Society.

Mixtures of water and heavy water were studied only by R. W. Wood.[1] He worked with two samples containing 18 and 80% of heavy water. The intensity maximum at 2517 in the 80% mixture shifted to 2623 in the 18% sample. The 18% mixture was estimated to have a composition of 0·034 D_2O, ·30 DOH and 0·66 H_2O, the corresponding proportions for the 80% mixture being 0·64 D_2O, 0·32 DOH and 0·04 H_2O. In the former, the number of DOH molecules is nine times that of D_2O, while in the latter it is only half. So he concluded that the band with its maximum of intensity at 2623 obtained with the 18% sample is mostly due to DOH molecules, while the band with its maximum at 2517 has its origin in D_2O as it is obtained with the 80% sample which has a larger proportion of D_2O molecules. Wood never studied the Raman band for pure D_2O and hence could not compare his observations for the mixture with this. For example, he had not observed the two components of the principal band of D_2O reported by other workers. Thus his investigations were not complete. The authors have studied the Raman spectrum of a 50-50 mixture of heavy and ordinary waters and compared the results thus obtained with the Raman spectra of 99·4% D_2O and pure H_2O

EXPERIMENTAL

The apparatus used is similar to that already described by one of us[7] and consists of a Wood's tube made of quartz, provided with a metal cooling jacket and supported on a suitable stand. A mercury arc 15 cm. in length was placed close to the tube. A steady current of water flowing through the metal jacket prevents the liquid in the tube from getting heated by the radiation of the mercury lamp. The water flow also serves as a sensitive temperature control for the contents of the tube. During the experiments the temperature did not vary by more than $\pm 1°$ C. After proper collimation, the scattered radiation was focussed on to the slit of the spectrograph.

With water and heavy water an exposure of four hours was enough to get the corresponding Raman band with sufficient intensity. For the Raman spectrum of the mixture, however, the time of exposure was doubled to compensate for the diminution of the number of molecules of each component to half. The mixture containing equal volumes of H_2O and D_2O, contains equal numbers of these molecules, as the ratios of molecular weight to density for H_2O and D_2O are almost identical.

The three spectra were photographed on the same plate, together with a series of density marks given by varying slit widths. It was ensured that the Raman spectra with the pure liquids and the mixture were taken under identical conditions with respect to the position of Wood's tube relative to the arc, the temperature of the liquid contained in it and the running voltage and current of the arc, so that the changes, that are observed in the intensity of the bands from

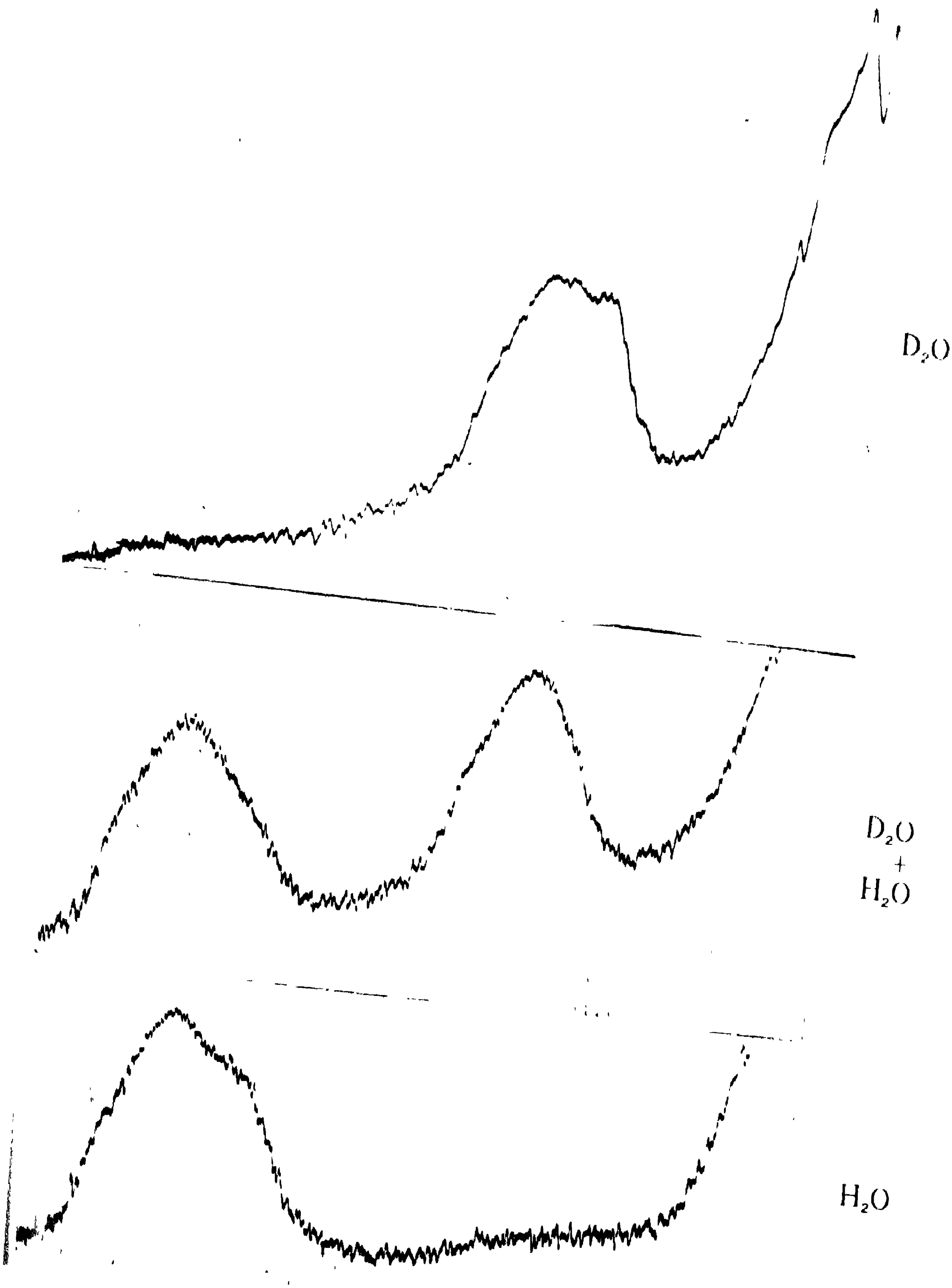

Microphotometric curves of H_2O and D_2O bands for the pure liquids and their mixture.

the pure state to the mixture, are due to the mutual influence of the liquids and not due to any variations in the external conditions either of illumination, or of temperature. The densities of the bands were determined from a microphotometric curve and the intensities of the bands calculated in the usual manner. The Raman frequencey at any point on the microphotometric curve is determined by extrapolating from a dispersion curve drawn with the mercury lines as the standards.

RESULTS

The bands excited by 4047Å of the mercury arc are studied. The microphotometric curves for the D_2O and H_2O bands in the pure state and in the mixture are reproduced in Plate V The heavy water band shows two distinct maxima, and one inflexion at a longer frequency. The maximum at the lower frequency is less intense. These are the three components of the principal band reported by Ananthakrishnan.[2] The shape of the D_2O band is very much altered in the mixture, the maximum with the smaller Raman frequency, so prominent in pure D_2O, being completely absent, and replaced by an inflexion. Wood [1] could not study this interesting change from the pure liquid to the mixture, as he did not work with pure D_2O.

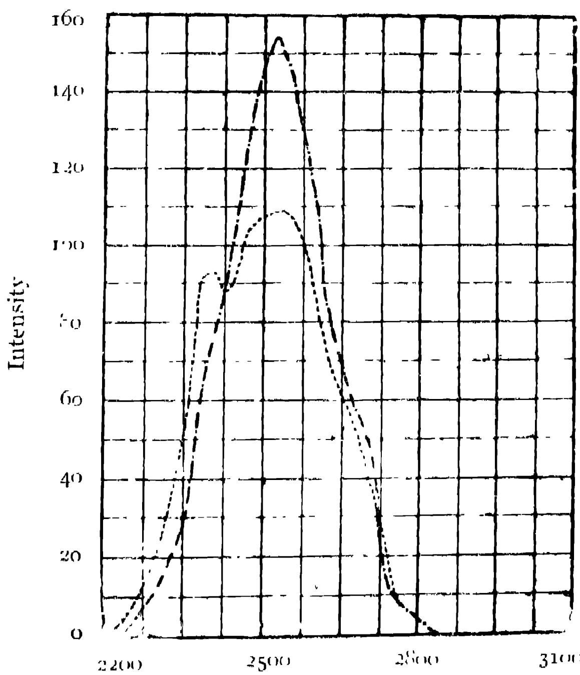

Intensity Distribution in the Raman Band of heavy water in the pure state (- - -)
and in the mixture with H_2O (-- -·-).

FIG. 1

In pure water, there is no maximum at shorter frequency. But the inflexion is distinct enough to indicate that there is superposition of a second band over the central band of water. There is no trace of this component in the mixture. But, in both heavy and ordinary waters, the shape of the band on the side farther away from the Rayleigh line is not altered perceptibly. The mutual influence of H_2O and D_2O, in this respect, seems to resemble the effect of dissolved acetone upon the water band as observed by C. S. Rao [6]. He remarks therein that dissolved non-electrolytes do not sharpen the band on the lower frequency side.

Figure 1 gives the intensity curves for the D_2O band in pure heavy water and in the mixture. Besides the absence of the maximum of smaller frequency, there is a large increase in the intensity of the second maximum in the mixture. The band is sharpened and its extent diminished. Also, the position of the maximum has shifted slightly towards smaller frequency.

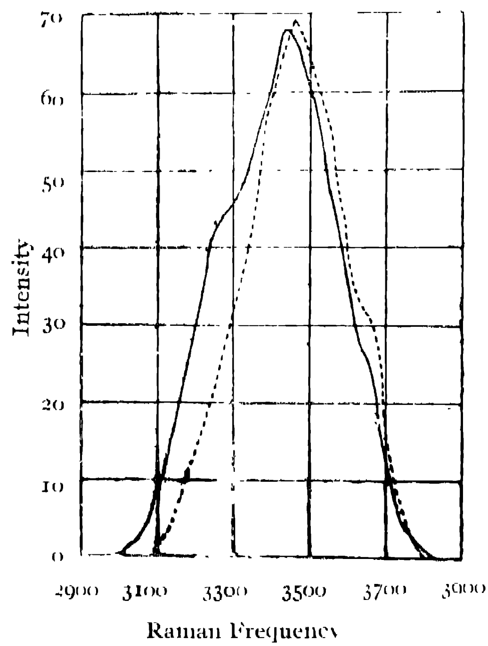

Intensity Distribution in the Raman Band of H_2O in the pure state (———) and in the mixture with D_2O (- - - - -).

FIG. 2

Figure 2 gives the intensity curves of the H_2O band in pure water and in the mixture. As in the case of D_2O, the band is sharper in the mixture than for the pure state, and is less in extent. The position of the maximum has shifted slightly towards longer frequency. The intensity of the maximum has slightly increased but it is not comparable to the increase in the intensity of the D_2O band in the mixture.

Table 1 gives the important characteristics of the H_2O band in the mixture and in the pure liquid.

TABLE I

Frequencies and Intensities of the H_2O Band

		Extent	Central Maximum	First Component	Second Component
Pure H_2O	Raman frequency	2971 – 3817 (840 cm.$^{-1}$)	3443	3229	3632
	Intensity	...	68	39	27·5
H_2O in the mixture	Raman frequency	3080 – 3808 (728 cm.$^{-1}$)	3461	3226	3640
	Intensity		69	18	32

The corresponding table for D_2O is given below.

TABLE II

Frequencies and Intensities of the Raman Band of D_2O

		Extent	Central maximum	First Component	Second Component
Pure D_2O	Raman frequency	2194 – 2844 (650 cm.$^{-1}$)	2538	2400 (second maximum)	2698
	Intensity	..	109	93	40
D_2O in the mixture	Raman frequency	2244—2810 (566 cm.$^{-1}$)	2523	2394	2685
	Intensity	...	154	71	54

The intensity of the maximum of the D_2O band has increased by 50% in the mixture, while that of the water band has remained practically the same. This is a highly interesting aspect of the problem the significance of which will be discussed in the next section. The position of the maximum in D_2O is not shifted to longer frequency, but slightly in the opposite direction. To allow for any errors of location of the maxima, the authors have studied two sets of photographs and have consistently found that the shift is not to a greater frequency but the other way and of the order of 15 cm.$^{-1}$.

To sum up, in both cases the bands are sharpened and the components of smaller frequency suppressed. The difference in their behaviour, however,

lies in the increase of intensity in the case of D_2O from the pure state to the mixture.

DISCUSSION

The principal bands of D_2O and H_2O have each three components. One of us,[7] working with water at various temperatures, found that, with increase of temperature, the component of smaller frequency gradually becomes less intense, the central one remains almost the same, the third component showing a slight increase in intensity. The three components were attributed to H_2O, $(H_2O)_2$ and $(H_2O)_3$. The triple molecules are less stable and are depolymerised with increasing temperature. C. S. Rao, studying the influence of dissolved electrolytes and non-electrolytes upon water, found that the proportion of trihydrols was very much less in solutions than in pure water. Increase of temperature or presence of any foriegn matter seems to split up these higher polymers. The phenomenon, in so far as temperature effect is concerned, is found to be similar in heavy water.

Wood[1] reports that he could not find any structure for the water band. His inability to note the lower frequency components of D_2O band, which is conspicuous in our picture with pure D_2O, is probably due to the fact that he worked with mixtures only, and even a small percentage of H_2O suppresses this component. But his failure to get the structure of the water band is perplexing especially in view of the fact that he must have worked at much lower temperatures than ours, where the lower frequency band of water ought to be more intense. This may probably be due to want of sufficient time of exposure in his case, and a microphotometric study of the band by him would have revealed the other components. Pure water shows that it is not a single symmetrical band but is the result of the superposition of at least two bands.

The general changes in the structure of the bands of both H_2O and D_2O are capable of being explained on the basis of the changes in the equilibrium between their polymers, which both these compounds are supposed to consist of. These changes are similar to those brought about by change of state or of temperature. The diminution of the intensity of the H_2O band on the lower frequency side in the mixture indicates the depolymerisation of the $(H_2O)_3$ molecules, to which this portion of the band is supposed to correspond. This change in the structure of the H_2O band lends support to the view that the $(H_2O)_3$ molecules are less stable than the other polymers as postulated by one of us.[7]

A similar explanation serves for the changes in the structure of the D_2O band. The maximum at 2400 cm.$^{-1}$ corresponds to the trihydrols of heavy water and these are less stable in the presence of the water in the mixture. So the component due to them is diminished in intensity.

If this were the only change, the large increase in intensity of the D_2O band in the mixture cannot be reconciled with the absence of any corresponding change in water unless it is assumed that $(D_2O)_3$ is less stable than $(H_2O)_3$, a postulate not warranted from results of temperature influence. For water also, there must be an increase on account of the breaking up of $(H_2O)_3$ into lower polymers, unless the equilibrium is such as to keep the number of $(H_2O)_2$ molecules unchanged, the higher polymers dissociating directly to single molecules. But the intensity of the higher frequency component in water does not show any appreciable increase to support such a conclusion.

The other possibility is the formation of HDO. The frequencies of this compound as calculated by Van Vleck and Cross [8] are 1400, 2720 and 3750 cm.$^{-1}$, the experimental value reported by Rank, Larson and Bardener [4] for the vapour being 2718 cm.$^{-1}$. The latter found no trace of any lines corresponding to 3750 cm.$^{-1}$ and 1400 cm.$^{-1}$ for HDO Though it is surprising to note the absence of OH oscillation in HDO while the corresponding O—D oscillation is conspicuous, the above results seem to be confirmed by our work also. While there is a considerable increase in the intensity of the D_2O band from the pure state to the mixture, the corresponding H_2O band increases only slightly in intensity.

As required by the law of mass action, the proportion of HDO molecules formed in a 50 : 50 mixture of H_2O and D_2O studied by us should be 48·6%, while H_2O and D_2O are each 25·7%, if the equilibrium constant is assumed to be 3·28 as given by Urey and Rittenberg.[9] The abnormal increase in the intensity of the D_2O band must be due to the superposition of the HDO band over it, while in the case of the H_2O band the slight increase in intensity is due only to the splitting up of higher polymers of water into the lower which thus increases the number of the double molecules giving rise to the maximum at the centre of the H_2O band, there being no contribution to this increase by the O—H oscillation of the HDO molecules as no band due to this oscillation was detected by Rank, Larson and Bordner for the vapour and is therefore probably absent for the liquid state as well.

The D_2O band should show a decrease in intensity due to conversion of some molecules into HDO on combination with H_2O. But the change in the equilibrium between its polymers may increase the number of the D_2O molecules giving rise to the maximum of the band for the mixtures upon which is superposed the band due to HDO molecules. Thus while there are two factors, *viz.*, increase in double molecules of D_2O and superposition of the HDO band, which increase the intensity of the band in the case of D_2O, after counterbalancing the diminution in the number of the D_2O molecules on account of the conversion into HDO molecules, there is only one factor which tends to increase the intensity of the water band, *viz.*, the increased number of $(H_2O)_2$ molecules due to depolymerisation of $(H_2O)_3$ molecules which are just

more than counterbalancing their diminution due to conversion into HDO molecules.

There is still the question of the Raman frequency of HDO band. Wood[1] gives it a frequency of 2623, shifted towards longer frequency by 100 cm.$^{-1}$ from the central maximum of D_2O. The calculated value of this band is 2720 and the frequency observed by Rank and co-workers is 2718. Wood observes that when the proportion of HDO molecules to D_2O is 9:1, the shift is to 2623 from 2515. In the mixture studied by us the ratio is 2:1 and not only do we not record any shift towards longer frequency, but there is a decisive shift in the opposite direction. It is likely that the HDO frequency in the liquid state is much closer to the central component of D_2O, than found by R. W. Wood.[1]

We expect that the further study contemplated by us will settle the doubts about the Raman frequency of HDO in the liquid state and throw greater light on the equilibrium between H_2O and D_2O. The absence of the O-H oscillation in HDO is a very interesting observation.

REFERENCES

1 R. W. Wood, *Phys. Rev.*, **45**, 392 (1934)
2 R. Ananthakrishnan, *Pro. Ind. Acad. Sciences* **2A**, 201 (1935).
3 Bauer and Magat, C. R, **201**, 667 (1935).
4 Rank, Larson, and Bordner, *Jour. Chem. Phys.*, **2**, 184 (1934).
5 I. Ramakrishna Rao and P. Koteswaram, *Ind. Jour. Phys.* **12**, 63 (1938)
6 C. S. Rao, *Phil. Mag.*, **20**, 587 (1935).
7 I. Ramakrishna Rao, *Proc. Roy. Soc.*, A, **145**, 489 (1934)
8 Van Vleck and Cross, *Jour. Chem. Phys.*, **1**, 357 (1933)
9 Urey and Rittenberg, *Jour. Chem. Phys.*, **1**, 137 (1933)

ELECTROLYTIC DISSOCIATION IN SULPHURIC ACID AS STUDIED BY RAMAN EFFECT*

By N. RAJESWARA RAO, M.Sc.
Andhra University, Waltair

(*Received for publication, April 18, 1940*)

ABSTRACT. The Raman spectrum of sulphuric acid and its salts at different concentrations is studied, and the changes, with dilution, in the intensity of the lines observed in the spectra are made use of to study the electrolytic dissociation of the acid. An observation made by I. R. Rao and C. S. Rao, that the alkali salts are completely dissociated even in concentrated solutions, is made use of to calculate the absolute degree of dissociation of the acid. On calculating the number of dissociated and undissociated molecules in solutions of the acid and $KHSO_4$, it is observed that (1) the rate of dissociation of the acid is less in dilute solutions than in moderately concentrated solutions, (2) in equimolecular solutions of sulphuric acid and acid sulphate the dissociation of HSO_4 molecules is larger in acid sulphate than in the acid. The above results are explained as due to the fact that in the solutions of the acid there is a larger abundance of H ions, than in the acid salt which therefore favour the formation of more HSO_4 ions, in the acid.

INTRODUCTION

The Raman spectra of sulphuric acid has been studied by a large number of workers including Nisi,[1] Woodward and Horner,[2] Ramakrishna Rao,[3] Bell and Jeppson,[4] Angus and Leckie[5] and Koteswaram.[6] The changes observed in the Raman spectrum of the acid on dilution are taken to be due to successive dissociation of the acid into HSO_4' and SO_4'' ions, on lines similar to the explanation given by Ramakrishna Rao[7] in the case of nitric acid. But, nobody made a quantitative estimation of the degree of dissociation of this acid, as the spectrum was superposed by an intense continuum which masked the Raman lines to a large extent and made the determination of the intensities of the lines quite uncertain. The present work is undertaken with the purpose of making a quantitative study of the dissociation of the acid and its salts in aqueous solutions.

Woodward and Horner[2] observed that the continuous spectrum of the acid increases on diluting it to a certain extent and on further dilution it diminishes in intensity. They explained that this increase is due to the formation of

* Communicated by the Indian Physical Society.

complex molecules which excite a continuous Raman spectrum. Medard[8] observed that the continuous spectrum could be diminished to a large extent by heating the acid with a few crystals of $KMnO_4$. Koteswaram[6] observed that this could be achieved by employing any oxidising agent, $K_2Cr_2O_7$ or nitric acid, or by mere heating to about 200°C. The acid employed in the present work was treated with about 10 c.c. of pure nitric acid for about 200 c.c. of the pure acid and heated to about 200°C for about half an hour. With this sample, the author found absolutely no evidence for the increase in the continuous spectrum in the intermediate dilutions, reported by Woodward and Horner.[2]

EXPERIMENTAL

Solutions of the acid at various concentrations, and of $KHSO_4$ and $(NH_4)_2SO_4$ are prepared, using the same sample of conductivity water for all the solutions. $KHSO_4$ is purified by repeated crystallisation, and $(NH_4)_2SO_4$ is prepared by taking the pure sample of sulphuric acid and passing NH_3 gas into it. The gas is made to pass through a tube packed with cotton in order to eliminate dust. Solutions of $KHSO_4$, $(NH_4)_2SO_4$ and H_2SO_4 of the same molal concentrations are taken.

The arrangement for photographing the Raman spectra is essentially the same as that used by Ramakrishna Rao,[7] with some modification. It consists of a brass jacket which is rectangular in shape and has two cylinders of length 3 cm. and diameter just larger than that of the Wood's tube. The Wood's tube is passed through the cylinders and made water-tight by rubber washers. The box is open at the top, and the cooling water entering it by a narrow tube at the bottom passes over the Wood's tube and flows out by a wide outlet tube soldered at a corner throughout the height of the jacket. The mercury arc is placed right above the Wood's tube and in the space between the arc and the tube, there is sufficient layer of water to cool the Wood's tube from the heat radiated by the arc. The scattered light, after passing through a metallic tube which is blackened inside to avoid reflections on the walls of the tube, is focussed by means of an achromatic lens on to the slit of a spectrograph which has a high dispersion and good light-gathering power.

For the determination of relative intensities of the Raman lines, the spectra are taken with the different concentrations of the acid under identical conditions, in respect of the distance between the mercury arc and Wood's tube, the temperature of the liquid, the running voltage and current and the disposition of the arrangement for focussing the scattered light with respect to the slit of the spectrograph. The time of exposure for each of the solutions was exactly 5 hours. Thus, the changes in the intensity of the Raman lines from one concentration to another are due only to changes in the concentration of the acid and to changes in the nature of the molecular species arising

out of dilution, but not due to any external factors. The intensities of the lines are determined in the usual manner by taking a number of density marks with a Zeiss step-filter, on the same plate on which the Raman spectra are taken.

The process is repeated for the series of spectra obtained with solutions of $KHSO_4$, $(NH_4)_2SO_4$ and H_2SO_4 all having 3 gram-molecules per 1000 c.c. of solution. As the solution of $KHSO_4$ gives a large continuum, a solution of $NaNO_2$ is used as a filter to cut off radiations beyond 4358 towards ultraviolet. For this purpose the Wood's tube with a jacket containing the filter is used. Everytime the solution is changed the filter is also replaced afresh as it may undergo photochemical decomposition during the exposure, which is of 8 hours' duration for these three solutions.

RAMAN LINES IN SULPHURIC ACID AND THEIR ORIGIN

A characteristic feature of this acid is that all its Raman lines are broad, diffuse and bright. Hence, it is very difficult to locate the maxima of the bands exactly by micrometric measurement. That is the reason why the values of the frequecies given by various authors are found to differ. In such cases a microphotometric curve will be very useful in locating the positions of the maxima and the limits of the bands.

The assignment of the lines in the spectum of sulphuric acid was made on the basis of the changes that they undergo on dilution Ramakrishna Rao[3] found that the 1043-line increases in intensity on dilution and hence attributed it to HSO_4' formed on dilution as it is also found with considerable intensity in solutions of $KHSO_4$. The 980-line which appears in higher dilutions and also in solutions of sulphates is attributed to SO_4''. The lines 1171 and 1365, which could not be attributed to any radical containing SO_4'' ion, but which were found to be analogous to similar lines with SO_2 solution were attributed to molecules of the type $SO_2(OH)_2$. The 910 line which decreases in intensity on dilution is due to undissociated H_2SO_4 molecules. The bands 416 and 562 are of composite nature having a number of maxima and their variation in intensity with dilutions is irregular. So it is concluded that they are excited by all the three types of radicals, *viz.*, H_2SO_4, HSO_4' and SO_4''.

THE INTENSITIES OF THE RAMAN LINES

There are only three lines in the spectrum of sulphuric acid with Raman frequencies 910, 980, and 1043, for which the determination of the intensity is possible. These are as pointed out in the previous section excited by H_2SO_4, SO_4'' and HSO_4' respectively. The other lines are either too feeble, or are superposed by lines excited by the different types of molecules. So it is

considered that no useful purpose is served by determining their intensities.

Now, since the width of the lines 910 and 1043 is varying with dilution of the acid, the intensity of the maximum does not represent the intensity of the line. Curves are therefore drawn taking the intensity of the band at each point as ordinate and wave-number at the point as abscissa. The area of the curve is taken as a true measure of the intensity of the band.

Though Raman and Venkateswaran [9] announced recently that they have reason to believe that the Raman scattering is, to some extent at least, coherent, and that they are conducting some experiments which are expected to throw more light on the subject, it is generally accepted that the Raman scattering is incoherent. The intensity of the light scattered by a medium is therefore proportional to the number of molecules contained in it. Then the intensities of the lines excited by H_2SO_4, HSO_4' and SO_4'' in solutions of various concentrations will be respectively proportional to the number of these molecules in the different concentrations. In the case of solutions of nitric acid, Ramakrishna Rao [7] suggested that if 'n_c' is the number of NO_3' ions at concentration 'c' and 'n_0' that at infinite dilution c_0 then α, the degree of dissociation is given by

$$\alpha = \frac{n_c}{c} \Big/ \frac{n_0}{c_0}$$

and since n is proportional to the intensity I,

$$\alpha = \frac{I_c}{c} \Big/ \frac{I_0}{c_0}$$

But, with dilute solutions, very long exposures are required to obtain lines of measurable intensity. Therefore, by this method, it is possible to calculate only the degree of dissociation relative to one of the concentrations.

In a later publication, Ramakrishna Rao and C. S. Rao, [10] after studying a large number of strong electrolytes in aqueous solutions, arrived at the following results:

1. The salts of alkali elements dissociate completely at all concentrations.

2. The acid salts of the alkali elements dissociate completely as far as the alkali radical is concerned and the acid radical dissociates progressively.

3. Halogen acids, *viz.*, HCl, HBr, HI, dissociate completely at all concentrations.

4. Oxy-acids dissociate progressively on dilution.

The first two results can be made use of to calculate the absolute degree of dissociation of sulphuric acid. Instead of taking an infinitely dilute solution to

calculate $\frac{I_o}{c_o}$, the solution of a salt having the same acid radical can be taken and the intensity of the line excited by the acid radical determined. If c' is the concentration of this solution, then $\frac{I_o}{c_o} = \frac{I_{c'}}{c'}$, since in both the cases, there is complete dissociation.

In fact, the intensity of radiation excited by each ion can be calculated, by determining the intensity of the line excited by the ion and dividing this by the total number of ions. This is specially useful, in calculating the degree of dissociation in a solution of a polybasic acid, for example, sulphuric acid taken up in the present work. By measuring the intensity of the SO_4'' line in the spectrum of the solution of $(NH_4)_2SO_4$, the intensity of radiation excited by 1N SO_4'' ions, where N represents the Avagadro number, is determined. Then, the intensities of the lines due to HSO_4' and SO_4'' in the solution of $KHSO_4$ are measured, and, by dividing the intensity of the SO_4'' line in this spectrum by the intensity of radiation excited by 1N SO_4'' ions calculated above, the number of SO_4 ions in the $KHSO_4$ solution is calculated. By subtracting this number from the total

TABLE I

Concentration of the solution in gm. moles per 1000 c.c.	Intensity of 910-line.	Equivalent intensity of 910-line	No. of H_2SO_4 molecules in gm. moles. 1	2	Intensity of 1043-line.	Equivalent intensity.	No. of HSO_4'-ions	Intensity of 980-line.	Equivalent intensity.	No. of SO_4''-ions	Percentage degree of dissociation of H_2SO_4 molecules.
16·9	2330	2330	15·7	15·7	860	860	1·2		—	—	7·1
14·9	1700	1935	13·0	14·0	1800	2046	2·9	—	—	—	17·2
12·8	1150	1518	10·2	10·5	3120	4120	6·5	—	—	—	38·2
10·8	765	954	6·3	6·7	1350	6839	9·8	11·8	18·5	0·4	60·3
8·7	—	—	—	4·2	4412	8375	11·9	15·2	29·5	0·6	74·1
6·8	—	—	—	3·2	3678	10570	13·1	13·0	32·6	0·7	85·3
3·0	—	—	—	1·1	1800	9223	15·0	6·5	36·6	0·8	93·3
$(NH_4)_2SO_4$ 3 gm. moles.	—	—	—	-	—	—	—	140·5	790·9	16·9	100
$KHSO_4$ 3 gm. moles.	—	—	—	—	1890	10647	15·7	8·7	49·0	1·2	100

number of $KHSO_4$ molecules, the number of HSO_4' ions present is determined. Knowing the intensity of the line excited by HSO_4' ions in this solution and the number of undissociated HSO_4' ions as calculated above, the intensity of radiation excited by 1N HSO_4' ions is calculated Now, knowing the intensities of the radiations excited by each of HSO_4' and SO_4'' ions and knowing the intensities of the lines in solutions of sulphuric acid excited by these ions, the number of HSO_4' and SO_4'' molecules in these solutions are determined. Dividing these numbers by the total number of molecules, the degrees of dissociation are calculated.

INTENSITIES AND DEGREE OF DISSOCIATION OF H_2SO_4 MOLECULES INTO HSO_4' AND SO_4'' IONS

In the above table, the first column gives the concentration in gram-molecules of the acid in 1000 c.c. of the solution. In the second column the intensities of the lines of Raman frequency 910, corresponding to each concentration, are given. If there were no dissociation of the acid, the intensity of this line must be proportional to the concentration, as the times of exposure are equal. Thus, if with different concentrations the times of exposure were inversely proportional to the concentration, the intensities ought to be equal. To arrive at an idea as to how far there is dissociation of the acid, intensity of this line, as it ought to be if the times of exposures were inversely proportional to concentration, are calculated and given in column 3. From the values of the intensity in column 3, the number of undissociated H_2SO_4 in gram-moles per 1000 c.c. of the solution, is calculated by the method indicated in the previous paragraph, and given in the first sub-column of column 4. For concentrations less than 10·75 gm.-molecules, the intensity of this line is too feeble to permit of quantitative determination. In the next sub-column is given the number of H_2SO_4 molecules obtained by subtracting the number of HSO'_4 and SO''_4 ions from the total number of molecules. The closeness with which the values in these two columns agree indicate the validity of these calculations, and the validity of the conclusions drawn by I. R. Rao and C. S. Rao[10] regarding the dissociation in the salt solutions. The next three columns give the corresponding values for HSO_4' ions, and the next three for SO_4'' ions. The 11th column gives the proportion of the dissociated H_2SO_4 molecules to the undissociated which is the ratio of the sum of HSO_4' and SO_4'' ions to the total number of molecules.

DISCUSSION OF RESULTS

The following main points are to be clearly noticed in calculating the numbers of the H_2SO_4, HSO_4' and SO_4'' radicals in solutions of the acid, $KHSO_4$ and $(NH_4)_2 SO_4$.

1. As the concentration of the solution is decreased, the number of H_2SO_4 molecules becomes smaller and the number of HSO_4 molecules increases. This merely indicates that the H_2SO_4 molecules are dissociated into HSO_4' ions in dilute solutions.

2. The rate of fall of H_2SO_4 molecules or the rate of increase of the HSO_4' ions is large in moderately concentrated solutions, but in dilute solutions the rate is less as is evidenced by the Figs. I and II, where the curves are steep at moderate concentrations and as the dilution is increasing they get flattened.

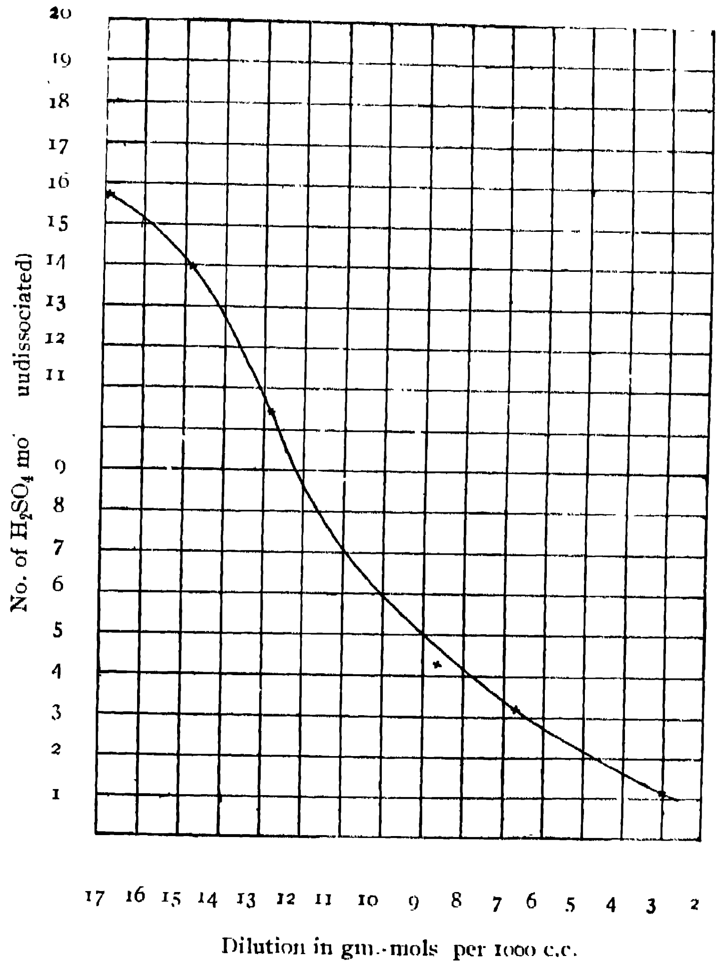

FIGURE I

The decrease in the rate of formation of HSO_4' ions in dilute solutions might be explained as due to their further dissociation into SO_4'' ions. But the decrease in the rate of fall of the number of H_2SO_4 molecules indicates that the

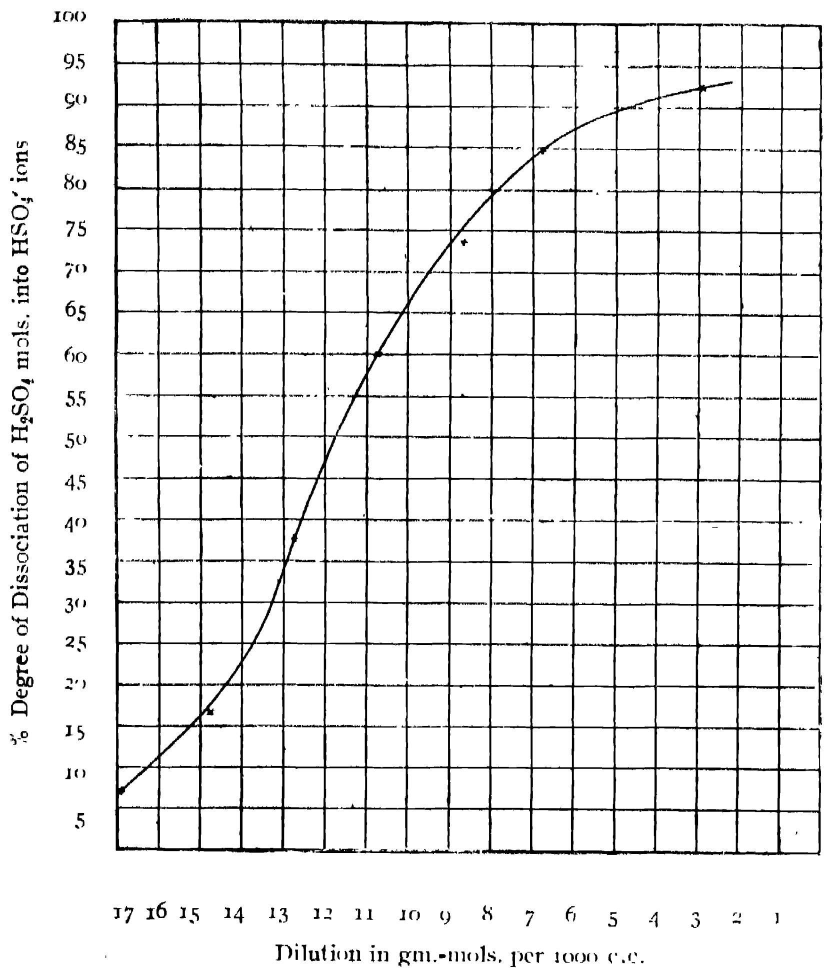

FIGURE 2

rate of dissociation is less in these solutions. This is further supported by the fact that the number of SO_4'' ions is very small even in dilute solutions, which means that the dissociation of HSO_4' into SO_4'' ions is very small.

This can be easily seen from the consideration that the equations

$$H_2SO_4 \longrightarrow HSO_4' + H^+ \qquad \dots \quad (1)$$

and

$$HSO'_4 \longrightarrow SO_4'' + H^+ \qquad \dots \quad (2)$$

are reversible. As the dilution is increased, the number of H^+ ions increases and hence the reverse action is more favoured. That is why, even at the concencentration of 3 gram-moles per 1000 c.c., there is a considerable number of H_2SO_4 molecules.

3. But in the case of the solution of $KHSO_4$, the dissociation of HSO_4' into H^+ and SO_4'' is larger than in an equivalent solution of the acid. This

is because the number of H^+ ions is less in this solution than in that of the acid, where H^+ ions are produced by both the reactions, whereas in the solution of the acid salt the reaction represented by (1) is absent.

4. The number of SO_4'' ions in the solution of $(NH_4)_2SO_4$, which assumed to dissociate completely is much larger than in the equimolecular solution of H_2SO_4 or $KHSO_4$, as is expected, in view of the above considerations.

5. The above results state that the molecules in solutions of the acid or of the acid salt are not completely dissociated even in solutions of the order worked with in the present investigation. This means that the postulate of Debye and Hückel that in dilute solutions all strong electrolytes completely dissociate is not applicable to these dilutions. They do not contemplate any sub-classes in strong electrolytes, acids, salts, alkalis or acid salts. In very dilute solutions where there is complete dissociation, such classification is not necessary, but, for concentrations dealt with here, such classification is necessary as pointed out by I. R. Rao and C. S. Rao.

The author finds great pleasure in thanking Dr. I. Ramakrishna Rao under whose direction the present work is undertaken.

REFERENCES

1 Nisi, *Jap. J. Phys.*, **8**, 119 (1932).

2 Woodward and Horner, *Proc. Roy. Soc.*, A, **144**, 129 (1934).

3 Rao, I. R., *Ind. Journ. Phys.*, **8**, 123 (1933).

4 Bell and Jeppson, *J. Chem. Phys.*, **2**, 711 (1934)

5 Angus and Leckie, *Proc. Roy. Soc.*, **149**, 327 (1935).

6 Koteswaram, P., *Ind. Journ. Phys.*, **12**, 299 (1938).

7 Rao, I. R., *Proc. Roy. Soc.*, (*Amsterdam*), **33**, 632 (1930).

8 Medard, *Compt. Ren*, **197**, 582 (1933)

9 Raman, C. V. and Venkateswaran, C. S., *Nature*, Dec. (1938).

10 I. R Rao and C. S. Rao, *Nature*, April (1936).

STUDIES ON SOME INDIAN VEGETABLE OILS. PART V. TEMPERATURE EFFECT ON GAS ABSORPTION AND OTHER PHYSICAL PROPERTIES

By CHANDRASEKHAR GHOSH

(Received for publication, April 24, 1924)

ABSTRACT. The absorption of air, hydrogen, nitrogen and carbon dioxide by castor oil at different temperatures within the range 20°C–90°C has been measured by the manometric method and the Bunsen absorption coefficients determined It has been observed that for all the gases there is a certain temperature at which the Bunsen coefficient attains a maximum value, and a mechanism of association between the gas and liquid molecules is suggested to explain the phenomena.

The values of viscosity at different temperatures within the same range have been measured in absolute units by the capillary method suggested by Gemant. The values obtained have been found not to satisfy the logarithmic relation of Andrade, and the logarithms of viscosity have been fitted into an equation of the form $\log\eta = \log A - \alpha t + \beta t^2 - \gamma t^3 + \delta t^4$ and the difference between observed and calculated values determined.

The variation of refractive index with temperature within the range 0°C–70°C has been determined and the variation is found to be a linear one.

INTRODUCTION

The present investigation deals with the variation with temperature of the coefficients of absorption of air, H_2, N_2 and CO_2 by castor oil and of other physical properties, such as viscosity, density, refractive index, dielectric constant, etc., within the working range of temperature, *viz.*, 20°C—90°C.

In the International Critical Tables [1] one finds considerable amount of literature on the absorption of gases by inorganic and organic liquids. The only data on the absorption of gases by mineral oils are those of A. Gemant [2] and F. M. Clark,[3] but very little work has been done on the gas absorption and other physical properties of vegetable oils at different temperatures. The only work on the same line on vegetable oils is that of G. N. Bhattacharyya,[1] who measured the absorption of air by some Indian vegetable oils at room temperatures only. Gemant in his measurement of gas absorption by mineral oils found that the absorbed amount of air per unit volume of mineral oil remained practically constant at 20°C and 80°C. He, however, gives no account of the absorption at intermediate temperatures. Clark, on the other hand, has shown that there is a definite increase in the absorption coefficient (of about 10%), within the above range of temperature ; but in his graph representing the variation of

absorption with temperature, one notices that there is a tendency towards a decrease in the absorption for higher temperatures.

In connection with drying and insulating oils the investigations on their coefficient of gas absorption have an important bearing. F. M. Clark [5] has shown that the dielectric strength of oils is dependent on the nature and amounts of dissolved gases. He also suggests that most theories of breakdown of solid dielectric impregnated with oil are not satisfactory because of the neglect of this gas-absorption factor. Quite recently Race,[6] while discussing the tests on oil-impregnated paper, draws attention to the different causes of electric breakdown of impregnated paper insulation as preceded by gaseous ionisation. He states that in a nominally gas-free liquid-filled system the dielectric strength should increase with the degree of degasification. Copelmann and Gyemant [7] supposes an electrode layer of high stress due to space charge acting on a layer of adsorbed gas, thus creating gas pockets or filaments leading to gaseous ionisation and breakdown and one would expect that in the case of liquids with a tendency of high absorbing power for gases the dielectric strength will suffer.

Hill[8] has considered the phenomena of heterogeneous equilibrium between gas and liquid according to the Distribution Law and the Phase Rule, and has discussed Henry's Law and its modifications due to association and dissociation. But the effect of temperature on the absorption of gases has not been discussed.

The use of vegetable oils as solvents of paints and as lubricants are generally known, but sufficient data as regards their other physical properties are not available, though a fair amount of data is available in the case of mineral oils. Hence, in order to investigate the applicability of vegetable oils for the purposes in which mineral oils are used, it is of interest to have a thorough study of all the above-mentioned properties. In almost all these applications the oils have to work within a certain range of temperature, and hence a study of the effect of variation of temperature within this range on these properties is of importance. It is, also, worthwhile to have an idea of the mechanism of absorption of gases and the variation of the coefficients of absorption in oils within the same range of temperature.

An account of the investigations so far carried out on vegetable oils has already been given by G. N. Bhattacharyya[9] of this laboratory. The same author published the results of the variation of viscosity of several vegetable oils with temperature and his results are in Redwood units and Fahrenheit degrees. It is thought worthwhile to measure the viscosity in absolute units to enable one to have an idea of the mechanism of viscous forces acting in the case of vegetable oils.

THE MECHANISM OF ABSORPTION OF GASES BY LIQUIDS

In order to form a mental picture of the mechanism of gas absorption in liquids, one can imagine the molecules of gas, enclosed in a chamber containing

a liquid to enter into the liquid surface during their random motions by virtue of their kinetic energy. Having entered the liquid, these molecules move from one position to another, and in their motion any of the following incidents may take place : they may come in close proximity of a liquid molecule, as a result of which the two may form a combination, executing motions as a whole ; or they may come into collision with each other or with combinations of the first kind and thereby knock off the gas molecules with sufficient energy to drive them out of the liquid altogether ; or, thirdly, they may in their motion come out of the liquid without encountering any other molecule.

One can, therefore, assume that on an average a number of gas molecules are in association, so to say, with the liquid molecules, which are supposed to be in a state of oscillation about a slowly displaced position of equilibrium ; the total number of such molecules depending on the pressure of the gas, the nature of the liquid and gas molecules and the prevailing temperature. So that at any instant there are a number of liquid and gas molecules associating together to form a juxtaposed type of molecule.

One can imagine that a number n_1 of the free gas molecules is entering into the liquid at any instant, while a number n_2 is coming out of the liquid. At a certain stage, for a particular temperature, n_1 becomes equal to n_2 and an equilibrium is reached, and the number of molecules confined within the liquid in the above associated state measures the coefficient of absorption.

The association or mutual cohesion between the two molecules can take place due to anyone of the several types of forces, such as, van der Waal attractive forces (otherwise known as dynamic polarisation), electrostatic forces due to permanent dipoles, ionic forces, polarisation forces. Of these, the energy due to van der Waal forces have been found to vary inversely as the sixth power of the distance between the molecules, whereas the forces between dipoles vary inversely as the cube of the distance. It may be either or both of the first two types, but since the second type, *viz.*, the force between dipoles is stronger and the type of liquids under consideration are known to have a chain-like structure, it is reasonable to suppose that the latter type of force preponderates in the phenomenon of gas absorption.

One can thus picture such an associated molecule having a certain mutual potential energy E, executing oscillations about a slowly displaced position of equilibrium. The thermal agitation due to variation of temperature as also the change in intermolecular forces in the gas due to variation of pressure will, therefore, interfere with this phenomenon of association. The magnitude of the absorption is thus dependent on the value of this mutual potential energy E, while the variation of the coefficient of absorption with temperature will be governed by the fraction of the total number of molecules possessing this energy E. At a definite pressure the probability of association of the gas and the liquid molecules will be maximum at a certain temperature. For lower or higher tem-

peratures there would be fewer molecules in the associated state. There is thus an equilibrium condition at a definite temperature between the molecules of the gas and the liquid-gas associated groups similar to that which occurs between different phases of a substance which can pass from one phase to the other.

In deriving the expression for Wien's law for black-body radiation Lorentz[10] has pointed out that the equilibrium between rays of different frequencies as affected by temperature is analogous to the equilibrium condition which obtains between different phases of a substance which can pass from one phase to the other.

In the case of Wien's law the energy of radiation is a function of frequency and temperature and an exponential relationship between these factors are operative. Extending the analogy to the present case, one would expect that the energy of association is governed by an exponential relation between temperature and pressure and the corresponding oscillatory energies of gas and liquid molecules.

Thus for a pressure P and temperature T the energy

$$E = C_1 T^{-a} e^{-\frac{C_2}{TP}}.$$

The values of the constants C_1, C_2, a, would depend on the oscillation frequencies of gas and liquid molecules, the nature of permanent dipole moments and induced moments of the molecules and the Boltzmann constant. These factors are difficult to reckon due to the uncertainty of our knowledge of the actual magnitudes of the forces and the actual expression for the interactive forces in operation.

VISCOSITY AND ITS VARIATION WITH TEMPERATURE

The mechanism of the viscosity of liquids has been the object of investigation since Newton who conceived the existence of a shearing stress at any point of a liquid moving in parallel layers. Since Newton, the same question has been discussed by various investigators from different physical aspects, which has been described by G. N. Bhattacharya[9] in his paper on the Viscosity of Vegetable Oils.

Andrade[11] has treated the theory of viscosity from the point of view of the communication of momentum from layer to layer taking place at the extreme libration of molecules in each layer oscillating about a very slowly displaced position of equilibrium. He considered the variation of viscosity with temperature as due to the effect of change of temperature on this interchange of momentum. He considered the change of potential energy of the system, due to change in temperature, in the light of Boltzmann's distribution law, and arrived at the relation

$$\eta_t = Ae^{C/T}$$

where A and C are constants.

He next considered the effect of temperature on the volume of the liquid, and on the distance between the molecules, since the distance between the molecules increases as $v^{1/3}$ and the number of molecules per unit area diminishes as $v^{2/3}$ where v is the specific volume of the liquid, the decrease in viscosity due to this effect alone is as $v^{-1/3}$. He further assumes that the potential energy involved in the condition of communication will be a function of the volume, $f(v)$, so that, taking all these effects into consideration, the relation changes to

$$\eta_t = Ae^{cf(v)/T} \cdot v^{-1/3}.$$

Since the average potential energy of a molecule is to a first approximation given by a/v in van der Waal's equation, it is supposed that the part of the potential energy considered in the case of viscosity varies in a similar way, and hence the relation can be taken as

$$\eta_T = Ae^{c/vT} \cdot v^{-\frac{1}{3}}$$

or

$$\eta_T \cdot v^{\frac{1}{3}} = Ae^{c/vT}$$

or

$$\log_e \eta_T = \log_e A + \frac{c}{vT} - \tfrac{1}{3}\log_e v.$$

Whereas Andrade starts on the basis of a static equilibrium between the forces exerted by the various molecules on each other, van der Waals (Jr.)[12] has treated the theory of viscosity in the same light of transportation of momentum due to collision, but has based his theory on the consideration of heat motion from the start.

He obtained the relation

$$\eta = \frac{2\sqrt{2\pi}}{15} n^2 d^4 ma. \quad e^{\frac{-E/RT}{-b/v}}$$

where d is the diameter of a molecule ; $a\sqrt{3/2}$ is the quadratic mean velocity of the molecule ; b is the quantity occurring in the equation of state which is connected with the total volume of the molecules contained in volume v ; and E is the difference between the mean potential energy of the molecules in the liquid, and the potential energy at the moment of collision (calculated per mole).

This relation can be transformed into the form in which Andrade expressed the relation for viscosity by considering every molecule in a liquid as being surrounded by a set of " first neighbours," and thus is practically enclosed in a sort of cavity of irregular form, not much greater than the molecule itself.

From the above relation it will be seen that the change of viscosity with temperature is influenced mostly by the factor $(1-b/v)$, and by a which is $\sim\sqrt{T}$, n the number of molecules per unit volume and the exponential factor.

Frenkel [13] worked out an expression on the basis of approximate equality of the specific heat of the same substance in the liquid state at low temperature and in the solid state. Batschinski,[14] Macleod,[15] and Lederer[16] found similar expressions all on the assumption that η is primarily a function of the specific volume.

All the different theories have been fully discussed by the Committee for the study of viscosity of the Academy of Sciences at Amsterdam,[17] and it would seem that the relation between viscosity and specific volume of a liquid is of primary importance and that the particular dependence of the viscosity upon temperature should for a large part be explained as a secondary effect, to be derived from the relation between specific volume and temperature. Though the experimental results are in agreement in a number of cases with the different expressions stated above it is found that in considerable number of liquids, specially the oils, the theoretical expressions are not in conformity with the experimental results.

In this connection it might be of interest to note that in the final expression deduced by Andrade, *viz.*, $\eta v^{\frac{1}{3}} = Ae^{\frac{c}{vT}}$ the effect of temperature on the potential energy has not been taken into account. An attempt has been made therefore to consider the effect of temperature on the van der Waal's constant a/v. One can express the relation as

$$\log \eta = \log A - \alpha t + \beta t^2 - \gamma t^3 + \delta t^4 - \ldots\ldots\ldots\ldots$$

This has been done by fitting the logarithmic curve by the method of least squares.

EXPERIMENTAL

For the measurement of co-efficient of absorption of gases, the same manometric method as described by G. N. Bhattacharyya[4] was utilised. To obtain measurements at different temperatures, the flask containing the oil was kept completely enclosed in a thermostatic arrangement. A box, the inner wall of which was provided with resistance wires for heating purposes, was suitably lagged for maintenance of uniform temperature inside it, and by means of variable resistances used in series with the heating coils the temperature inside the box could be regulated very nicely. Hydrogen was obtained by electrolysis from water, and was dried by passing through a series of calcium chloride towers before being passed into the flask. Nitrogen gas was obtained by the action of

a solution of ammonia and ammonium carbonate on copper turnings by the method described by C. V. Brunt.[16] The gas, before collection, was passed through wash towers containing solutions of sulphuric acid, pyrogallic acid and caustic potash for the removal of impurities, such as ammonia, oxygen and carbon dioxide. Before being passed into the flask it was again passed through a second set of wash bottles containing the same solutions and then through calcium chloride towers. Carbon dioxide gas was purchased in cylinder and was stored in aspirator jars for controlling the pressure of the gas passed into the flask. The gas was passed through towers containing pumice stone soaked with sulphuric acid for the removal of moisture. The Bunsen absorption coefficient was determined in the same way as done by Bhattacharyya. The results obtained are given in Tables II-V.

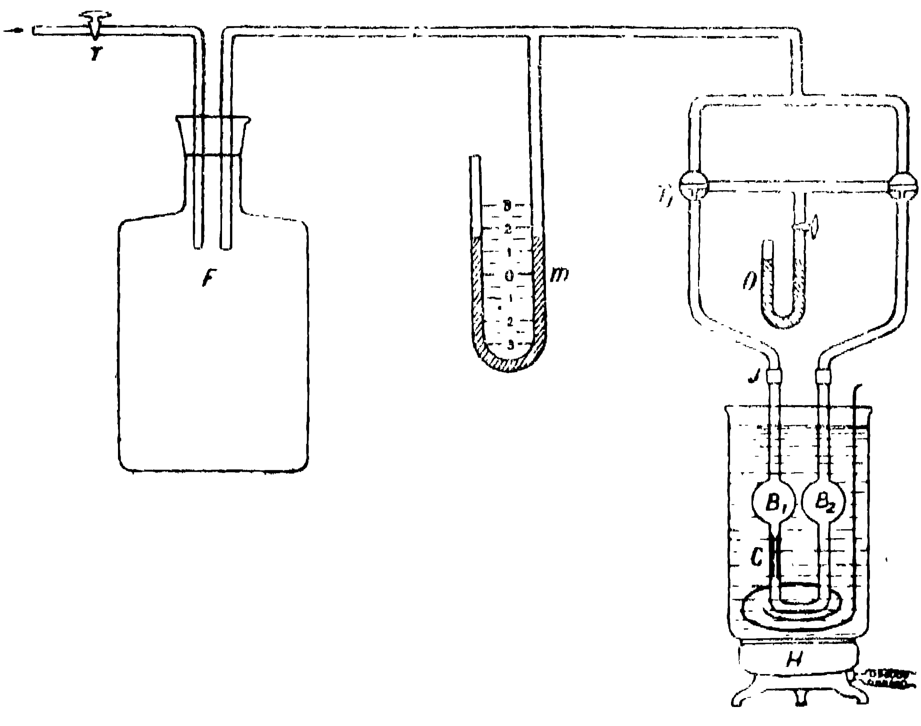

FIGURE 1

The apparatus used for the determination of viscosity in absolute units was as shown in Fig. 1 and was designed in the laboratory after Gemant.[2] As shown in the figure, the apparatus consists of a big flask F which acts as a reservoir of air at a pressure indicated by the mercury manometer *m*, and because of its large capacity the pressure of air remains almost constant during the time taken by the liquid to flow through the capillary tube. The flask is connected to the measuring apparatus through the three-way stop-cocks T_1 and T_2. The measuring apparatus is a U-tube with two bulbs B_1 and B_2 near the top of the

two limbs, the bulb B_2 being slightly bigger than B_1. A portion C in the limb containing B_1 is a capillary tube of length about 10 cms. The two limbs of the U-tube are joined to the three-way stop-cocks T_1 and T_2 by means of rubber tubing at JJ. Two marks at the top and bottom of the bulb B_1 indicates the volume of liquid which flows out of B_1, through the capillary tube C into B_2 Between T_1 and T_2 is connected an oil manometer O,which indicates any small difference in level in the two limbs of the U-tubes. The temperature of measurement could be maintained constant by immersion of the U-tube in a water bath heated electrically.

The length and diameter of the capillary portion C was measured by taking several measurements of the weights of mercury required to fill in different lengths of the capillary and the total weight required to fill up the whole length. The volume of the bulb B_1 between the marks was also determined in a similar way.

The method of procedure consists in thoroughly cleaning and drying the U-tube and then filling it up with a quantity of the oil sufficient to fill up the bulb B_2. Next keeping T_1 in the position where the limb B_1 is open to the atmosphere, the limb B_2 is connected to the reservoir F, in which the air has previously been compressed to a pressure of about 20 cms. of mercury, by means of the stop-cock T_2, and thereby the oil is transferred from the limb B_2 to the limb B_1, the flow being stopped by rotating T_2 into its position for connection of limb B_2 with the atmosphere, when the level of oil in limb B_1 has reached about 2 cm. above the mark. With T_2 in the position mentioned, the level of oil in limb B_1 slowly begins to fail ; when the level has reached the mark above bulb B_1, the stop-cock T_1 is turned so that communication is made between limb B_1 and the reservoir F. Simultaneously with the opening of stop-cock T_1 to the reservoir F, the stop-watch is started and the pressure in the manometer m is noted. Finally, as the liquid column reaches the mark below bulb B_1, the stop-watch is stopped and the pressure in the manometer again noted. The mean of the two readings of the manometer is taken as the effective pressure on the liquid during the period it flows out of B_1. For each temperature several readings are taken with different mean effective pressures to obtain consistent results

According to Poiseulle the relation between the viscosity of a liquid and its flow through capillary tubes at a constant temperature is given as

$$\eta = \frac{P\pi R^4 T}{8LV}.$$

Adding the correction factor when the kinetic energy of the out-flowing liquid is taken into consideration, the relation becomes

$$\eta = \frac{P\pi R^4 T}{8(L+nR)V} - \frac{m\delta V}{8\pi(L+nR)T}$$

where η = the viscosity of the liquid,

P = the effective pressure,

R = radius of capillary,

V = volume of out-flowing liquid in time T,

L = length of the capillary tube of radius R,

n = a certain constant depending on the characteristics of the ends of the tube,

δ = the density of the liquid at the temperature of measurement,

m = a constant.

The value of $n = 1.64$ and $m = 1$. In the case of vegetable oils δ is generally $= 1$. By making L considerably large, and since V/T for oils is naturally small, the second term can be neglected. For the apparatuas in use, since the values V, R and L are constants, by using a liquid of known viscosity, the apparatus can be calibrated such that for any liquid the viscosity as measured by the apparatus will be obtained from the relation

$$\eta = K.P.T,$$

where K = is the constant of the apparatus obtained by measurement with a liquid of known viscosity,

P = is the mean pressure acting on the liquid expressed in cms. of mercury column,

and T = is the time taken for out-flow expressed in seconds.

This is the relationship used in the present investigation.

The result obtained in the case of castor oil are given in Table VI, and curves of viscosity against T and $\log \eta$ against $1/T$ are shown in figures 8 and 9 respectively.

The densities and refractive indices of the oil under investigation were measured at the different temperatures and are given in Table I. The refractive indices were determined with an Abbe direct-reading refractometer provided with an arrangement for controlling the temperature. The densities were measured with a pyknometer and a sensitive chemical balance.

DISCUSSION

It is known that the absorption of gases by an oil takes place very slowly when it is kept at rest, and even when shaken the maximum absorption takes place after a period of time. In the present investigation, for each reading the shaking was continued till the maximum absorption was obtained, as indicated by the rise in mercury column in the manometer, the time taken being about 20 to 30 minutes, this period decreasing at higher temperatures.

The Bunsen absorption coefficient at different temperatures between the range 20°C—90°C were obtained by the method already described, and the results have been plotted in Figs. 2—5. The expansion of oil due to temperature rise has been taken into consideration and the absolute values of absorption coefficient calculated. From the curves it will be seen that in the case of all the gases

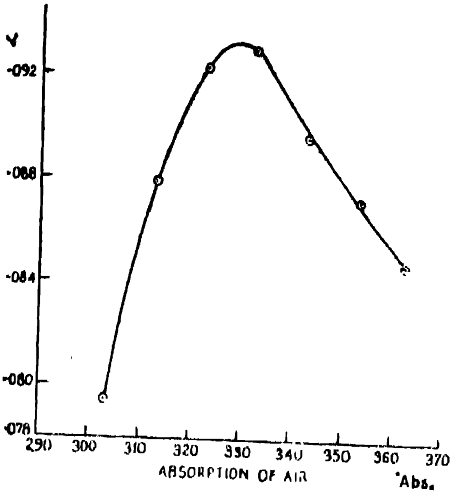

FIGURE 2

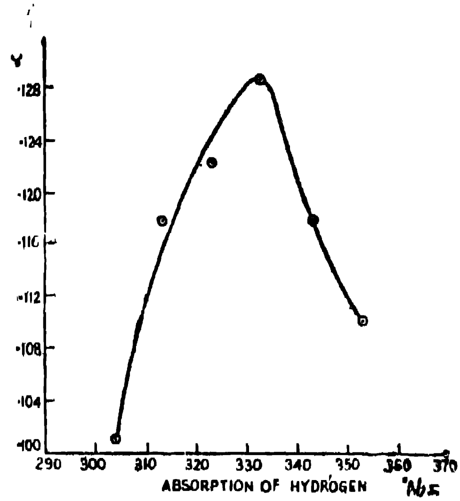

FIGURE 3

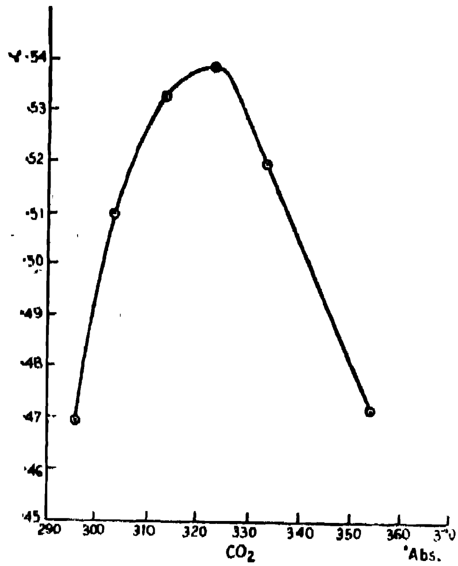

ABSORPTION OF CO_2

FIGURE 4

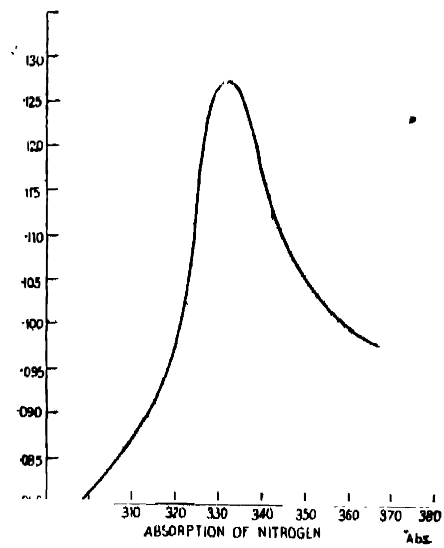

FIGURE 5

considered the absorption coefficient at first increases with temperature and after reaching a maximum value decreases with temperature. It will be seen that the nature of variation of absorption coefficient with temperature is almost similar for all the gases, the maximum absorption taking place at a temperature near about 60°C. The values obtained in the case of air and nitrogen are of the same order, perhaps because of the high percentage of nitrogen present in air. The values obtained in the case of CO_2 is much greater in comparison with those in the case of air, hydrogen and nitrogen. This is of particular interest on account of the fact that the structure of CO_2 (O=C=O) is almost similar to the chain-

like structure of the molecules of oil, and it is not known whether this higher absorption is due to a larger force of attraction between these two types of molecules.

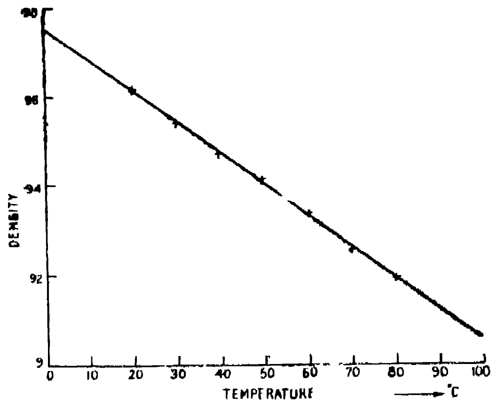

FIGURE 6

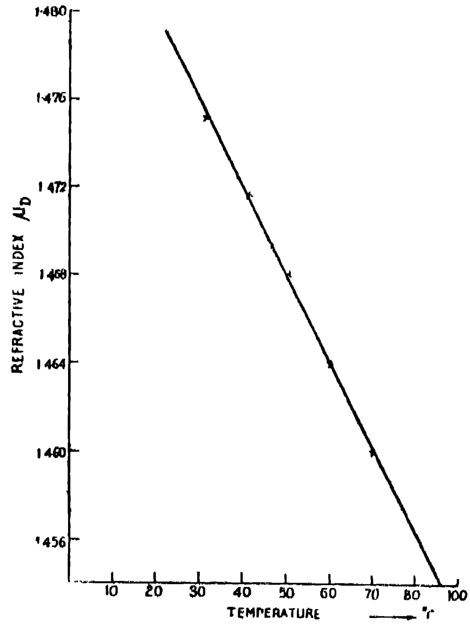

FIGURE 7

The variation of density and refractive index with temperature are shown in Figs. 6 and 7 respectively, and it will be seen that the variations are linear.

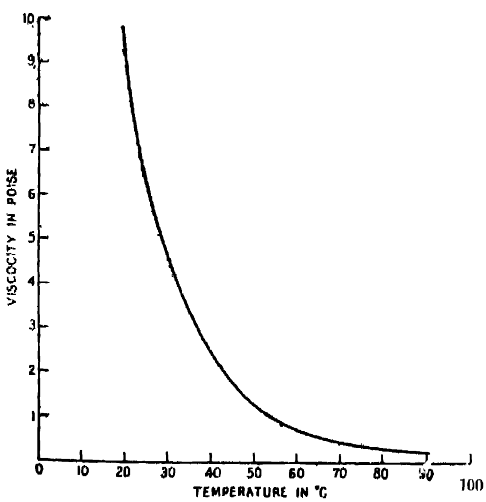

FIGURE 8

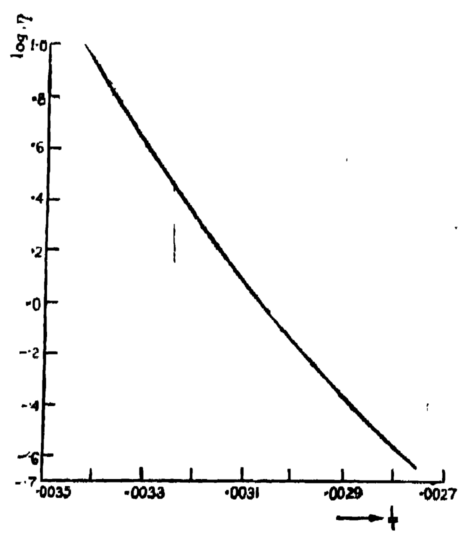

FIGURE 9

The variation of viscosity with temperature within the same range is shown in Fig. 8 and it will be seen that the viscosity decreases considerably with

increasing temperatures. The curve showing the change of logarithms of viscosity with $1/T$ is given in Fig. 9 and it will be observed that the curve is non-linear which shows that the variation of viscosity is due to some factor in addition to temperature. The logarithms of viscosity have been fitted by the method of least squares and the values of constants α, β, γ, δ, and log A have been worked out.

TABLE I

Data for Density and Refractive Index

(See Figs. 6, 7)

Temp. °C	Density	Refr. Index
20	.96122	1.4788
30	95396	1.4750
40	94704	1.4716
50	.94152	1.4680
60	.93380	1.4640
70	.92564	1.4600
80	.91973	..
90	91374	..

TABLE II

Data for Absorption of Air

Vol. per cm. of the tube = 0.16484 c.c. Vol. of oil = 49.45 c.c.

(See Fig. 2)

Temp. of oil in °C	Rise of mercury column in cm.	Vol. of gas absorbed in c.c.	Absorption Coeff. α	Density of oil	α corrected for vol. expansion of oil
20	—	—	—	.96122	—
30	27.0	4.451	.0811	.95396	.0794
40	31.1	5.128	.0904	.94704	.0879
50	33.9	5.589	.0955	.94152	.0923
60	35.5	5.862	.0970	.93380	.0930
70	35.5	5.862	.0942	.92564	.0895
80	35.8	5.902	.0923	.91973	0871
90	35.8	5.902	.0987	.91937	.0847

TABLE III

Data for Absorption of Hydrogen

Vol. of oil=49.4 c.c.

(See Fig. 3)

Temp. of oil in °C	Rise of mercury column in cm.	Vol. of gas absorbed in c c.	Absorption Coeff. α	Density of oil	α corrected for vol. expansion of oil
20	—	—	—	—	—
30	34 3	5.654	103	9533	.100
40	41·5	6.841	·120	·94704	·117
50	44·9	7·401	126	·94152	.122
60	49 0	8·078	·134	·93380	.128
70	46 8	7 714	·124	·92564	.118
80	45·3	7·467	116	·91973	·110
90	—	—	—	—	—

TABLE IV

Data for Absorption of Carbon-dioxide

Vol. of oil=11.1 c.c.

(See Fig. 4)

Temp. of oil in °C	Rise of mercury column in cm.	Vol. of gas absorbed in c.c.	Absorption coeff. α	Density of oil	α corrected for Vol. expansion of oil
23	34.8	5·737	·476	·95904	·469
30	38.9	6.412	·520	95396	·509
40	42·3	6.970	·548	·94704	·532
50	44·4	7 319	·557	·94152	·538
60	44·5	7·336	540	·93380	519
70	45·0	7·401	·530	·92564	·504
80	43·5	7·171	·499	·919973	·471
90	—	—	—	—	—

TABLE V

Data for absorption of Nitrogen

Vol. of oil = 37.30 c.c.

(See Fig. 5)

Temp. of oil in °C.	Rise of mercury column in cm.	Vol. of gas absorbed in c.c.	Absorption coeff. α	Density of oil	α corrected for vol. expansion of oil
26.5	19.875	3.2751	0.084	0.9562	0.080
30	19.950	5.5382	0.087	0.9539	0.083
40	23.100	3.8067	0.093	0.9470	0.088
50	27.700	4.5650	0.108	0.9415	0.102
60	36.025	5.9345	0.137	0.9338	0.128
70	32.150	5.2987	0.118	0.9256	0.109
80	32.133	5.2956	0.114	0.9197	0.105
90	31.475	5.1375	0.108	0.9137	0.099

TABLE VI

Viscosity Data

(See Figs. 8, 9)

Temp. in °Abs.	η in poise.	$\log_{10}\eta$ (obs.)	$\frac{1}{T}\times 10^2$	$\log_{10}\eta$ (calc.)	obs. − cal.
293	9.82	.9921	·3413	9904	·0017
303	4.53	.6561	·3301	·6527	- .0034
313	2.31	·3636	·3192	·3600	.0036
323	1.28	.1072	·3096	.1073	·0001
333	0.769	−.1141	3003	.1110	.0031
343	0.506	− 2958	.2915	·3006	.0048
353	0.344	−.4634	·2831	·4678	.0044
363	0.240	−.6198	·2755	.6190	.0008

$$\log_{10}\eta = \cdot 9904 - \cdot 3619\times 10^{-1}.\, t + \cdot 249\times 10^{-3}.\, t^2 - \cdot 776\times 10^{-6}.\, t^3 - \cdot 139\times 10^{-8}.\, t^4.$$

The measurements of absorption of different gases in the case of other oils are in progress and the results so far obtained agree with the observations made in this paper. Measurements on the conductivity of vegetable oils have also been taken up. These will be reported in a separate communication.

ACKNOWLEDG...

The author acknowledges his grateful thanks to Prof. P. N. Ghosh ... encouragement and continued interest during the progress of the work.

REFERENCES

[1] International Critical Tables, Vol. **3** (1928).

[2] Gemant A., *Trans. Faraday Soc.* **32**, Part 4, April (1936); Liquid Dielectrics (1933).

[3] Clark, F. M., *Jour. Franklin Inst.* **215**, 39, 1 (1933).

[4] Bhattacharyya, G. N., *Ind. Jour. Phys.*, **11**, 65 (1937).

[5] Clark, F. M., *Trans. Am. Inst. Elec. Eng.*, **54**, 50 (1935).

[6] Race, H. H., ,, ,, ,, ,, ,, **55**, 590 (1936).

[7] Whitehead, J. B., ,, ,, ,, ,, **56**, 1346 (1937).

[8] Taylor, *Physical Chemistry*, Vol. **1**, Chap , 9 (1924).

[9] Bhattacharyya, G. N., *Ind. Jour. Phys.*, **10**, 209, (1936); **10**, 281 (1936); **10**, 403 (1936).

[10] Lorentz, H. A , *Lectures on Theoretical Physics*, Vol. II (1927).

[11] Andrade, E. N. da C., *Phil. Mag.*, **17**, 407 & 698, (1934).

[12] J. van der Waals (Jr), *Proc. Acad. Amsterdam*, **21**, 743 (1918-19).

[13] Frenkel, J., *Zeits. f. Phys.*, **35**, 6626 (1926) ; *Trans. Farad. Soc* , **33**, 58 (1937).

[14] Batschinski., *Zeits. f. Physik Chemie*, **84**, 643 (1913).

[15] Macleod, D. B., *Trans. Farad. Soc.*, **19**, 6 (1923) ; **21**, 151 (1925).

[16] Lederer, *Kolloid Beihefte*, **34**, 370 (1932).

[17] Second Report on Viscosity and Plasticity. Prepared by the Committee for the Study of Viscosity of the Academy of Sciences, Amsterdam (1938).

[18] Brunt, C. V., *Am. Chem. Soc. Jour.*, **36**, 1448 (1914).

APPLIED PHYSICS LABORATORY,
UNIVERSITY COLLEGE OF SCIENCE,
CALCUTTA.

A SIMPLE LABORATORY METHOD OF PRODUCING CONTINUOUS ULTRA-VIOLET LIGHT

By HARIBANSH NARAYAN YADAV, M.Sc. (Pat.)
Patna University Research Scholar

(*Received for publication, April 16, 1940*)

Plate VI

ABSTRACT. A convenient method of producing hydrogen continuum from visible to 2200 Å has been described. A diagram of the arrangement and a photograph of the continuum have also been given.

INTRODUCTION

These days one can buy a ready-made source of Hydrogen Continuum from Messrs. Adam Hilger & Co which gives a fairly extended continuous ultra-violet background. It will not be, however, out of place if a very cheap and simple method of obtaining almost the same result is described here. There are so many designs tried by different workers [1] but they are comparatively difficult and in some cases practically impossible to build in an ordinary laboratory workshop. The design tried here is due to Leifson[2] with only a slight modification. The apparatus can be assembled even in an ordinary laboratory. Also the working has been so simplified that the discharge gives nothing but continuous background whenever it glows. One need not be particular about pressure of hydrogen in the tube. In the hope that it may be of any help to the workers in this line a description of the apparatus with its working is given here.

DESCRIPTION

The apparatus is shown below in a schematic diagram. Hydrogen was generated by means of electrolysis of 20% solution of NaOH contained in the U-tube T, the electrodes employed being of Nickel. An electric current of 2 to 2·5 amperes from a D. C. main of 110 volts was used for electrolysis. In order to keep the U-tube cool it was put in a water bath W_1. The oxygen escaped by bubbling through mercury in the tube M and the hydrogen passed over platinised asbestos in the tube A heated to 100° C by an electric current through a coil of nichrome wire wound round the tube. The platinised asbestos acted as a catalytic agent in removing any trace of oxygen, which might come with hydrogen, in the form

of water which collected in the bulb B kept cool in the water bath W_2. Hydrogen bubbled through a bottle containing $Ba(OH)_2$ solution which absorbed any trace of CO_2. Finally the hydrogen was dried by passing through concentrated H_2SO_4 This method of preparing pure hydrogen is due to Bodenstein and Dux.[3] The discharge tube consists of pyrex-glass tubing one centimetre in diameter and attached to a flask of obout 700 c.c. capacity. Aluminium electrodes (obtained from Tube Light Engineering Company) have been sealed, about 25 cm. apart, to the tube as shown in the diagram. To keep the electrodes cool they are immersed in seperate water baths W_1 and W_4. Q is a quartz window attached to the tube with hard sealing-wax. H is a mercury manometer.

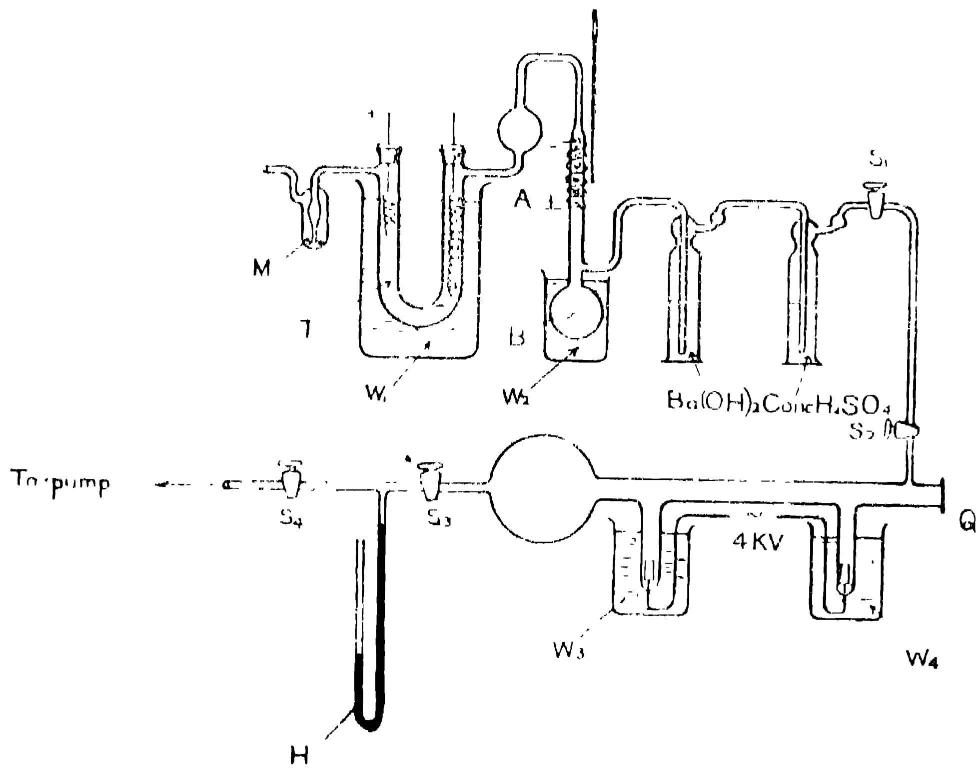

The discharge tube was evacuated by means of an oil-air pump. Hydrogen was allowed to enter it by manipulating the stopcocks S_1 and S_2. Before starting the discharge the tube was thoroughly washed by repeating a number of times the process of evacuating the tube and refilling it with hydrogen. The potential applied to the electrodes of the discharge tube was 4 kv. from a transformer supplied by Messrs. Adam Hilger & Co. When hydrogen was not allowed to pass the discharge was due to the occluded gases coming out of the electrodes and the tube ; whereas, when the hydrogen was passing and the pump was running continuously the glow was entirely due to hydrogen, the occluded gases being


(a) (b) (c)
5218·2
5153·2
5105·5
3274
3248
2618·3
2199·6

carried away in the sweep. If the flow of hydrogen exceeded a certain rate the glow automatically ceased. Thus whenever there was a glow with maximum rate of flow of hydrogen the desired continuous light was obtained. One must be careful not to expose the plate when hydrogen is not flowing. In that case banded spectrum due to occluded gases is obtained.

There is, however, one disadvantage of this arrangement. The rate of generation of hydrogen is too slow. The quantity of hydrogen which collects in about 5 minutes flows away in about half a minute. Thus for every flow one has to wait for 5 minutes. Consequently for a total exposure of 15 minutes one has to expose 30 times at an interval of 5 minutes between consecutive exposures.

The photograph was taken with a small quartz-spectrograph. In the photograph (see plate VI), (*a*) is the continuous spectrum, (*b*) is the copper arc comparison and (*c*) is a spectrum with which we are not concerned here. The continuity extends from the visible to the shortest wavelength transmitted by the quartz window used

REFERENCES

1 Lawrence and Edlefson, *Review of Sc. Inst.*, **1**, 45 (1930); Hopfield, *Astrophys. Jour.*, **72**, 137 (1930); Kistiakowsky, *Rev. Sc. Inst.*, **2**, 549 (1931); Urey, Murphy and Duncan, *Rev. Sc. Inst.*, **3**, 495 (1932); Rathenau, *Zeit. fur Phys.*, **32**, 87 (1933); Collins and Price, *Rev. Sc. Inst.*, **5**, 423 (1935).

2 Leifson, *Astrophys. Jour.*, **63**, 73 (1926).

3 Bodenstein and Dux, *Zeit. f. Phys. Chemie.*, **85**, 297 (1913).

GEOMETRICAL NOTE ON VAN DER WAAL'S EQUATION*

By HARIDAS BAGCHI

Lecturer, Calcutta University

(*Received for publication, April 22, 1930*)

ABSTRACT. The object of the present paper is to study mathematically the (graphical) representation of van der Waal's equation in the (Euclidean) space of three dimensions. The investigations, conducted in this paper, centre round the geometry of the resulting graph (Ω), and takes account of the *Cremona* (or *birational*) transformations which convert Ω into a plane. Put in a nut-shell, the main results obtained are as follow :—

(*i*) that Ω is a unicursal quartic scroll and has a triple line at infinity;

(*ii*) that the line of striction of Ω is a unicursal quartic curve;

(*iii*) that the Hessian of Ω is a degenerate surface of the eighth degree, consisting of eight coincident planes;

(*iv*) that *every* polar quadric of Ω is a hyperbolic paraboloid;

(*v*) that the locus of a point, whose polar quadric is a pair of parallel planes, is virtually a plane;

(*vi*) that the '*critical point*' *P* (of Ω),—defined in the first instance as the point whose (Cartesian) co-ordinates are respectively the *critical pressure, critical volume* and *critical temperature*—is geometrically designable as the uniquely determinate point, having one of its inflexional tangents parallel to the axis of volume;

(*vii*) that the mean curvature of Ω vanishes at *P*; and,

(*viii*) that Ω has no curve of *zero* Gaussian curvature, although it has a curve of *zero* mean curvature.

INTRODUCTION

In the present paper I have discussed the geometrical representation of van der Waal's classical equation :

$$\left(p+\frac{a}{v^2}\right)(v-b)=\mathrm{RT}$$

in the (parabolic) space of three dimensions. No attempt has been made to enter into the merits of the underlying physical hypothesis. Rather the subject has been developed from a purely mathematical standpoint, and its interest lies mainly in the geometrical characterisation of the graph in question (Ω).

As a matter of convenience the subject has been sub-divided into four sections. Section I takes account of the line of striction of the quartic Ω, and

* Communicated by the Indian Physical Society.

an associated group of *birational* (or *Cremona*) transformations—very often contracted as *C.T.*'s. Section II deals with the Hessian and the system of polar quadrics (degenerate and non-degenerate) of the surface Ω. Section III treats principally of certain cardinal properties of the '*critical point*,' defined initially as the point (on Ω), whose Cartesian co-ordinates are respectively equal to the *critical pressure*, *critical volume* and *critical temperature*. Lastly Sec. IV disposes of certain organic curves of Ω, *e.g.*, curves of constant mean curvature or of constant specific curvature. In certain places the contraction *w.r.t.* has been used for the phrase '*with respect to.*'

SECTION I

(Definition and birational transformation of the V-surface)

1. According to van der Waal, the pressure p, volume v and absolute temperature T of a given mass of gas conform to the well-known relation :

$$\left(p+\frac{a}{v^2}\right)(v-b)=\mathrm{R}T, \qquad \dots \quad (1)$$

where a, b, R are constants.

If we now take any three concurrent and orthogonal lines OX, OY, OZ as axes of co-ordinates, and take OX as the axis of pressure, OY as the axis of volume and OZ as the axis of (absolute) temperature, the three-dimensional graph of the equation (1) is evidently a surface of the fourth degree, whose Cartesian equation is

$$\left(x+\frac{a}{y^2}\right)(y-b)=\mathrm{R}z. \qquad \dots \quad (2)$$

This quartic surface (Ω) will be frequently designated as the V-surface. It may be remarked in passing that, when a, b are put $=0$ (as a first approximation), Ω degenerates into a paraboloid, of which the two systems of generating lines are parallel respectively to the planes $x=0$ and $y=0$. This trivial case will be ignored throughout this paper, so that the constants a, b (however insignificant) will be supposed to have *non-zero* values.

2. Elementary reasoning readily reveals the *ruled character* of the surface Ω, the *general* equations of the set of generating lines being

$$\left.\begin{aligned} y &= \lambda, \\ \text{and} \qquad x+\frac{a}{\lambda^2} &= \frac{\mathrm{R}}{\lambda-b}\, z, \end{aligned}\right\} \qquad \dots \quad (1)$$

where λ is a variable parameter.

To find the line of striction on Ω, we observe in the first place that, the generators being all parallel to the plane $y=0$, the shortest distance between any two consecutive members is parallel to the y-axis. If, then, (x', y', z') be the

point, where an arbitrary generator, as defined by (1), is met by the shortest distance from the consecutive generator, *viz.*,

$$\left.\begin{aligned} y &= \lambda + d\lambda, \\ x + \frac{a}{(\lambda+d\lambda)^2} &= \frac{R}{\lambda + d\lambda - b} \cdot z, \end{aligned}\right\} \qquad \dots (2)$$

the line $(x=x',\ z=z')$ must intersect the line (2). The condition for this to be possible is plainly

$$x' + \frac{a}{(\lambda+d\lambda)^2} = \frac{R}{\lambda+d\lambda-b} \cdot z'. \qquad \dots (3)$$

Besides, we have

$$y'=\lambda \qquad \text{and} \qquad x' + \frac{a}{\lambda^2} = \frac{R}{\lambda - b} z'. \qquad \dots (4)$$

Solving (3) and (4) for x', y', z' and omitting the dashes, we learn that the line of striction of Ω is a unicursal quartic curve, definable by the parametric equations :

$$x = \frac{a(\lambda - 2b)}{\lambda^3}, \qquad y = \lambda, \qquad z = \frac{2a}{R} \cdot \frac{(\lambda-b)^2}{\lambda^3}.$$

3. We shall now establish a remarkable property of the surface Ω, *viz.*, that it admits of conversion into a plane by means of a *Cremona transformation* (*C.T.*).

To that end we observe firstly that the *C. T.*, definable by either of the two *equivalent* triads of equations :

$$\left.\begin{aligned} &(i) \qquad \xi = x + \frac{a}{y^2}, \qquad \eta = y - b, \quad \zeta = Rz, \\ &(ii) \qquad x = \xi - \frac{a}{(\eta+b)^2}, \quad y = \eta + b, \quad z = \frac{\zeta}{R}, \end{aligned}\right\} \qquad \dots (I)$$

changes the surface Ω into the paraboloid

$$\xi\eta = \zeta .$$

Secondly this paraboloid can be turned into a plane (*viz.*, $X=Y$) by the *C. T.*, definable by either of the two equivalent sets of equations :

$$\left.\begin{aligned} &(iii) \qquad X = \frac{\zeta}{\xi}, \qquad Y = \eta, \quad Z = A\xi + B\eta + C\zeta ; \\ &(iv) \qquad \xi = \frac{Z - BY}{A + CX}, \quad \eta = Y, \quad \zeta = \frac{X(Z-BY)}{A+CX}. \end{aligned}\right\} \qquad \dots (II)$$

It follows conclusively that the *C. T.*, compounded of the two *C. T.*'s (I) and (II), converts the original surface Ω into a plane. The presence of the

arbitrary constants A, B, C as well as the (obvious) *arbitrariness* in the selection of the two components $C.T.$'s bring home to one's mind that the surface Ω can be carried over into a plane by means of an infinitude of $C. T.$'s. Bearing in mind that transformability into a plane by aid of a $C. T.$ is a *characteristic* property of a unicursal surface, we infer that Ω is a unicursal surface. This can be substantiated more simply as follows.

Introduce a *rational*—but not necessarily integral—function of μ, say $\phi(\mu)$, and equate z to $\phi(\mu)$ in the equations (1) of Art. 2. Clearly, then, the surface Ω admits of the following *rational* parametric representation, *viz.*,

$$\left.\begin{aligned} x&=\frac{R\phi(\mu)}{\lambda-b}-\frac{a}{\lambda^2},\\ y&=\lambda,\\ z&=\phi(\mu),\end{aligned}\right\}(\lambda,\ \mu \text{ being parameters}).$$

So once again the unicursal property of Ω is manifest. A third proof of the same result will be considered in the next article.

4. We shall now re-write the equation of Ω in the form :

$$(xy^2+a)\ (y-b)-Ry^2z=0, \qquad \dots \quad (1)$$

and use the symbols L and M to denote respectively the two right lines, along which the plane at infinity is cut by the two planes :

$$x=0 \quad \text{and} \quad y=0.$$

Since xy^3 represents the only term of the *fourth* order in (1), we gather that the section of Ω by the plane at infinity is a (plane) quartic curve, consisting of the line M (counted thrice) and the line L (counted once). A cursory glance at the equations (1) of Art. 2 suggests that M is a *common transversal* (or director) of the ∞^1 of generators of the surface.

It is easy to see that M is a *triple line* of the surface Ω. For an *arbitrary* plane through M being taken in the form :

$$y=\lambda,$$

its complete curve of intersection with Ω plainly consists of the line M (counted thrice), and the line

$$y=\lambda,\quad x+\frac{a}{\lambda^2}=\frac{Rz}{\lambda-b}. \qquad \dots \quad (2)$$

The inevitable conclusion is that M is a triple line, and that the line (2) lies wholly on Ω for all values of λ. This last result is already a proved fact (*cf.* Art. 2).

The surface Ω, endowed, as it is, with a triple line, must needs be *unicursal* and so each of its plane sections is a unicursal quartic. It must not be overlooked

that this result is quite in consonance with the more general proposition which states that, if any algebraic surface of degree n possesses a multiple curve of degree $n-1$, this curve must be a right line and at the same time the surface must be unicursal.

SECTION II

(Systems of polar quadrics and the Hessian of Ω)

5. Let us now specify the position of an arbitrary point P by means of *homogeneous co-ordinates* (x, y, z, w), referred to the tetrahedron formed by the three (Cartesian) co-ordinate planes (yz), (zx), (xy) and the plane at infinity. Evidently, then, the first three homogeneous co-ordinates are the same as its Cartesian co-ordinates, whereas the fourth co-ordinate w may be put equal to unity. So the homogeneous equation of the surface Ω, as given by (1) of Art. 4, may be written in the symbolic form :

$$\phi(x, y, z, w)=0, \qquad \ldots \quad (1)$$

where
$$\phi\equiv(xy^2+aw^3)(y-bw)-Ry^2zw.$$

Partial differentiations give

$$\left.\begin{aligned}
&\frac{\partial\phi}{\partial x}=y^3-by^2w\ ;\quad \frac{\partial\phi}{\partial y}=3xy^2-2bxyw-2Ryzw+aw^3\ ;\\
&\frac{\partial\phi}{\partial z}=-Ry^2w\ ;\quad \frac{\partial\phi}{\partial w}=-bxy^2-Ry^2z+3ayw^2-4abw^3\ ;\\
&\frac{\partial^2\phi}{\partial x^2}=0\ ;\quad \frac{\partial^2\phi}{\partial x\partial y}=3y^2-2byw\ ;\quad \frac{\partial^2\phi}{\partial x\partial z}=0;\quad \frac{\partial^2\phi}{\partial x\partial w}=-by^2\ ;\\
&\frac{\partial^2\phi}{\partial y^2}=6xy-2bxw-2Rzw\ ;\quad \frac{\partial^2\phi}{\partial y\partial z}=-2Ryw\ ;\\
&\frac{\partial^2\phi}{\partial y\partial w}=-2\,bxy-2\,Ryz+3aw^2\ ;\quad \frac{\partial^2\phi}{\partial z^2}=0\ ;\\
&\frac{\partial^2\phi}{\partial z\partial w}=-Ry^2\ ;\quad \frac{\partial^2\phi}{\partial w^2}=6ayw-12abw^2.
\end{aligned}\right\}\quad \ldots \quad (1)$$

Palpably, then, the Hessian of Ω, which is geometrically definable as the

locus of points whose polar quadrics are cones, and is analytically definable by the equation :

$$\begin{vmatrix} \frac{\partial^2\phi}{\partial x^2}, & \frac{\partial^2\phi}{\partial x\partial y}, & \frac{\partial^2\phi}{\partial x\partial z}, & \frac{\partial^2\phi}{\partial x\partial w} \\ \frac{\partial^2\phi}{\partial y\partial x}, & \frac{\partial^2\phi}{\partial y^2}, & \frac{\partial^2\phi}{\partial y\partial z}, & \frac{\partial^2\phi}{\partial y\partial w} \\ \frac{\partial^2\phi}{\partial z\partial x}, & \frac{\partial^2\phi}{\partial z\partial y}, & \frac{\partial^2\phi}{\partial z^2}, & \frac{\partial^2\phi}{\partial z\partial w} \\ \frac{\partial^2\phi}{\partial w\partial x}, & \frac{\partial^2\phi}{\partial w\partial y}, & \frac{\partial^2\phi}{\partial w\partial z}, & \frac{\partial^2\phi}{\partial w^2} \end{vmatrix} = 0,$$

takes the form :

$$\begin{vmatrix} 0, & \frac{\partial^2\phi}{\partial x\partial y}, & 0, & \frac{\partial^2\phi}{\partial x\partial w} \\ \frac{\partial^2\phi}{\partial y\partial x}, & \frac{\partial^2\phi}{\partial y^2}, & \frac{\partial^2\phi}{\partial y\partial z}, & \frac{\partial^2\phi}{\partial y\partial w} \\ 0, & \frac{\partial^2\phi}{\partial z\partial y}, & 0, & \frac{\partial^2\phi}{\partial z\partial w} \\ \frac{\partial^2\phi}{\partial w\partial x}, & \frac{\partial^2\phi}{\partial w\partial y}, & \frac{\partial^2\phi}{\partial w\partial z}, & \frac{\partial^2\phi}{\partial w^2} \end{vmatrix} = 0.$$

When expanded in terms of the first row and reduced, this equation can be easily put in the form :

$$\Delta^2 = 0,$$

where $$\Delta \equiv \begin{vmatrix} \frac{\partial^2\phi}{\partial y\partial x}, & \frac{\partial^2\phi}{\partial y\partial z} \\ \frac{\partial^2\phi}{\partial w\partial x}, & \frac{\partial^2\phi}{\partial w\partial z} \end{vmatrix}.$$

Since $\Delta = -3Ry^4$ by (I), it follows that the Hessian of the V-surface is a *degenerate* surface of the eighth degree and consists simply of the plane $y=0$, counted *eight* times.

6. We know that the polar quadric of a point P (x, y, z) with respect to a surface, given by the Cartesian equation

$$F(x, y, z) = 0,$$

is a paraboloid, if, and only if, the determinant D, defined by

$$D \equiv \begin{vmatrix} \dfrac{\partial^2 F}{\partial x^2}, & \dfrac{\partial^2 F}{\partial x \partial y}, & \dfrac{\partial^2 F}{\partial x \partial z} \\ \dfrac{\partial^2 F}{\partial y \partial x}, & \dfrac{\partial^2 F}{\partial y^2}, & \dfrac{\partial^2 F}{\partial y \partial z} \\ \dfrac{\partial^2 F}{\partial z \partial x}, & \dfrac{\partial^2 F}{\partial z \partial y}, & \dfrac{\partial^2 F}{\partial z^2} \end{vmatrix}$$

vanishes at P. So in the general case (when $D \neq 0$ identically) the equation $D = 0$ represents the surface-locus of a point, whose polar quadric is a paraboloid. In the *exceptional* case when $D = 0$ *identically, every* polar quadric is a paraboloid.

When we apply the above lemma to the surface Ω, we set

$$F(x, y, z) = \phi(x, y, z, 1)$$

and note the three relations of I (Art. 5), *viz.*,

$$\frac{\partial^2 \phi}{\partial x^2} = 0, \quad \frac{\partial^2 \phi}{\partial z^2} = 0 \text{ and } \frac{\partial^2 \phi}{\partial x \partial z} = 0.$$

Manifestly then $D = 0$ independently of x, y, z. We cannot therefore escape the conclusion that *the polar quadric of every point with respect to the V-surface is a paraboloid.* This result is susceptible of independent verification as follows.

The Cartesian equation of the polar quadric of a point P (x', y', z') (with respect to Ω) is

$$\left(x \frac{\partial}{\partial x'} + y \frac{\partial}{\partial y'} + z \frac{\partial}{\partial z'} + w \frac{\partial}{\partial w'}\right)^2 \cdot \phi(x', y', z', w') = 0,$$

where w, w' are to be put $= 1$ after differentiations. When the left side is expanded and the relations (I) of Art. 5 are utilised, the equation can be easily thrown into the symbolic form :

$$y(\lambda x + \mu y + \nu z) + lx + my + nz + p = 0, \qquad \dots \quad (1)$$

$$\text{where} \quad \left.\begin{aligned} &\lambda \equiv y'(3y' - 2b) \; ; \quad \mu \equiv 3x'y' - bx' - Rz' \; ; \\ &\nu \equiv -2Ry' \; ; \quad l = -by'^2 \; ; \\ &m \equiv -2Ry'z' - 2bx'y' + 3a \; ; \quad n = -Ry'^2 ; \\ &p \equiv 3a(y' - 2b). \end{aligned}\right\} \qquad \dots \quad (2)$$

Inasmuch as the quadratic terms are the product of the two linear factors :

$$y \text{ and } \lambda x + \mu y + \nu z,$$

we conclude that, wherever the point P may lie, its polar quadric with respect to the surface Ω is a paraboloid, one system of whose generating lines are parallel to the *fixed* plane $y = 0$.

The geometrical explanation is not far to seek. For a multiple curve (of multiplicity p), known to lie on a surface Π must be a multiple curve (of multiplicity $p-q$) on the qth polar surface of every point ($w.r.t.$ Π), provided that $q < p$. Applying this lemma to the surface Ω, and recollecting (Art. 4) that M is a triple line on Ω, we infer that the polar quadric of an *arbitrary* point ($w.r.t.$ Ω) must have M for a multiple curve of multiplicity $1 (\equiv 3-2)$. In other words, every polar quadric (of Ω) must have M for an ordinary generator and must $\therefore$ cut the plane at ∞ along two right lines, one of which is M. That is to say, an arbitrary polar quadric of Ω has a *degenerate 'conic at infinity'*, and is accordingly a paraboloid. This corroborates the previous result.

7. Let us now look for the locus of points, whose polar quadrics $w.r.t.$ Ω are cylinders. Since a cylinder is the only type of quadric, which is at once a paraboloid and a cone, we promptly perceive that the necessary and sufficient condition for the (paraboloidal) polar quadric of a point P (x', y', z') to be a cylinder is that P should lie on the Hessian $(y^8 = 0)$. Thus any point, whose polar quadric is a cylinder, may be taken as $(x', 0, z')$, (where x', z' are *arbitrary*), and the actual equation of the associated (cylindrical) polar quadric is by (1) of Art. 6 seen to be

$$\mu y^2 + my + p = 0,$$

where $\mu = -bx' - Rz'$, $m = 3a$ and $p = -6ab$. Obviously the cylinder is of the degenerate type and consists merely of two parallel planes.

We may summarise our conclusions in the following manner :—

Whereas all possible polar quadrics—numbering, of course, ∞^3—are paraboloids, only a ∞^2 of them are cylinders, and consist simply of pairs of parallel planes. Furthermore the ∞^2 of points, whose polar quadrics are cylindrical, are all situated on the Hessian.

8. Before we close this chapter we shall touch briefly on the system of polar cubics of the surface Ω.

In accordance with the geometrical lemma (quoted in the previous article), it follows that the triple line of Ω, *viz.*, the line M, is a double line on *every* polar cubic. Remembering that a cubic surface, endowed with a double line, is either a cubic scroll or else a cubic cone, we gather that every polar cubic of Ω is a ruled surface. That any such polar cubic is a scroll (and *not* a cone) is obvious from the fact that its double line M is situated wholly in the plane at infinity. Alternative reasoning also points to the same conclusion.

For the homogeneous equation to the polar cubic of (x', y', z', w') is

$$x' \frac{\partial \phi}{\partial x} + y' \frac{\partial \phi}{\partial y} + z' \frac{\partial \phi}{\partial z} + w' \frac{\partial \phi}{\partial w} = 0.$$

Putting $w, w' = 1$ and using (I) of Art. 5, we easily derive its Cartesian equation in the form :

$$x'(y^3 - by^2) + y'(3xy^2 - 2bxy - 2Ryz + a) - Rz'y^2$$
$$- bxy^2 - Ry^2z + 3ay - 4ab = 0$$

Manifestly, then, this is a scroll, the series of generators being given by

$$y = \mu \text{ and } x(3y'\mu^2 - b\mu^2 - 2by'\mu) - Rz(2\mu y' + \mu^2)$$
$$+ x'(\mu^3 - b\mu^2) + ay' - R\mu^2 z' + 3a\mu - 4ab = 0,$$

where μ is a parameter. This confirms the previous result.

SECTION III

(Location of the critical point of Ω)

9. The aggregate of tangents to any given surface Π evidently forms a *line-complex*, which includes within its fold the *inflexional congruence* Σ, made up of the ∞^2 of inflexional tangents (to Π). Clearly the *order* of this congruence Σ is = the no. of lines that pass through an arbitrarily *assigned* point P and is therefore equal to no. of lines that are parallel to an arbitrarily *assigned* line L. For special positions of the point P or of the line L, this number may suffer a diminution and so may fall short of the *order*.

The avowed object of the present section is to find a point P (α, β, γ), lying on the surface Ω and having one of the two inflexional tangents (thereat) parallel to the y-axis. So one of the two inflexional tangents to Ω at P must be the line (N)

$$x = \alpha, \; z = \gamma. \quad \ldots \quad (1)$$

Making the substitutions (1) in the equation of Ω, *viz.*,

$$(xy^2 + a)(y - b) - Ry^2 z = 0, \quad \ldots \quad (2)$$

we readily perceive that the resulting equation in y, *viz.*,

$$(\alpha y^2 + a)(y - b) - R\gamma y^2 = 0$$

must be identical with

$$(y - \beta)^3 = 0.$$

Accordingly the requisite conditions—at once necessary and sufficient—are

$$3\beta = \frac{b\alpha + R\gamma}{\alpha}, \quad 3\beta^2 = \frac{a}{\alpha}, \quad \beta^3 = \frac{ab}{\alpha}.$$

These lead to

$$\alpha = \frac{a}{27b^2}, \; \beta = 3b, \; \gamma = \frac{8}{27} \cdot \frac{a}{Rb}. \quad \ldots \quad (\mathrm{I})$$

It can be easily seen that the values of α, β, γ, as given by (I), are respectively the *critical pressure*, *critical volume* and *critical temperature* (of the given

mass of gas). If we now introduce the nomenclature *critical point* to represent that particular point (on Ω), whose Cartesian coordinates (taken in order) are the critical press., critical vol., and critical temp., we are entitled to present our conclusions in the following manner :—

The critical point is geometrically designable as the uniquely determinate point (on Ω), one of whose inflexional tangents is parallel to the axis of volume.

10. In order to find the second inflexional tangent (N') at $P(\alpha, \beta, \gamma)$, we may take its equations in the form :

$$\frac{x-\alpha}{l} = \frac{y-\beta}{m} = \frac{z-\gamma}{n} \ (= r), \tag{1}$$

where $l : m : n$ are quantities to be determined. Putting

$$x, y, z = \alpha + lr, \ \beta + mr, \ \gamma + nr,$$

in the equation of Ω, *viz.* (2) of Art. 9, we find that the four points of intersection of (1) with Ω depend on the following biquadratic in r :—

$$Ar^4 + Br^3 + Cr^2 + Dr = 0, \tag{2}$$

where
$$\left.\begin{aligned} A &= lm^3 \ ; \quad B = 3lm^2\beta + m^3\alpha - m^2(bl + Rn) \ ; \\ C &= 3lm\beta^2 + 3m^2\alpha\beta - m^2(b\alpha + R\gamma) - 2m\beta(bl + Rn) \ ; \\ D &= l\beta^3 + 3m\alpha\beta^2 - \beta^2(bl + Rn) - 2m\beta(b\alpha + R\gamma) + am. \end{aligned}\right\} \tag{3}$$

Plainly the conditions (necessary as well as sufficient) for (1) to be an inflexional tangent are

$$C = 0 \text{ and } D = 0.$$

When the values of α, β, γ as given by (I) of Art. 9 are made use of, the two relations last written can be thrown into the forms :

$$\left.\begin{aligned} m(7bl - 2Rn) &= 0, \\ \text{and} \qquad 2bl - Rn &= 0. \end{aligned}\right\}$$

So the two sets of values of $l : m : n$ are

$$\left.\begin{aligned} &0 : 1 : 0 \ ; \qquad (4) \\ \text{and} \qquad &R : 0 : 2b. \qquad (5) \end{aligned}\right\}$$

For obvious reasons the first solution refers to the inflexional tangent N considered in Art 9 As a matter of course, the second solution must then refer to the other inflexional tangent N', whose equations may be written as

$$\frac{x-\alpha}{R} = \frac{y-\beta}{0} = \frac{z-\gamma}{2b}.$$

A comparison of (4) and (5) reveals the mutual perpendicularity of the two inflexional tangents N and N' at the critical point P. The irresistible

conclusion is that *the indicatrix of the V-surface Ω at this point is an equilateral hyperbola and that the mean curvature (of the surface) vanishes thereat.*

The tangent plane to the surface Ω at P, containing, as it does, the two inflexional tangents N, N', must then have for its Cartesian equation

$$2b(x-\alpha)-R(z-\gamma) = 0,$$

i.e., $$18b^2x-9Rbz+2a = 0. \quad \ldots \quad (6)$$

This certainly admits of independent verification.

11. When we look for the polar quadric of P *w. r. t.* the surface Ω, we have to take recourse to (1) of Art 6 and to write

$$x' = \alpha = \frac{a}{27b^2}; \quad y' = \beta = 3b; \quad z' = \gamma = \frac{8}{27}\cdot\frac{a}{Rb} \quad \text{(Art. 9)}$$

in (2) of Art. 6. So the polar quadric (Γ) of P may be exhibited in the form:

$$y(\lambda x+\mu y+\nu z)+lx+my+nz+p = 0, \quad \ldots \quad (1)$$

where $$\left.\begin{aligned} \lambda &= 21b^2; \quad \mu = 0; \quad \nu = -6Rb; \quad l = -9b^3; \\ m &= a; \quad n = -9Rb^2; \quad p = 3ab. \end{aligned}\right\}$$

The equation (1) of Γ being re-written in the form:

$$3by(7bx-2Rz)-9b^3x+ay-9Rb^2z+3ab = 0,$$

it is not difficult to see that Γ contains the whole length of each of the two inflexional tangents (N, N') at P. Having regard to the obvious fact that Γ touches the tangent plane to Ω at P as given by (6) of the preceding article, we may re-state the set of results in the following garb :—

The polar quadric Γ of the critical point P with respect to the surface Ω is a hyperbolic paraboloid, touching Ω at P. Further, the two inflexional tangents of Ω, that pass through P, are none other than the two generators of Γ, that pass through the very same point. That is to say, Γ and Ω possess the *same* tangent plane and the *same* pair of inflexional tangents at the point P.

SECTION IV

Certain organic curves on the V-surface

12. For the surface Ω:

$$\left(x+\frac{a}{y^2}\right)(y-b) = Rz,$$

the partial differential coefficients

$$\frac{\partial z}{\partial x}, \quad \frac{\partial z}{\partial y}, \quad \frac{\partial^2 z}{\partial x^2}, \quad \frac{\partial^2 z}{\partial x\partial y}, \quad \frac{\partial^2 z}{\partial y^2},$$

(symbolised respectively as p, q, r, s, t) are given by

$$\left.\begin{aligned} Rp &= y-b, \quad Rq = x - \frac{a}{y^3}(y-2b), \\ Rr &= 0,\ Rs = 1, \text{ and } Rt = \frac{2a}{y^4}(y-3b). \end{aligned}\right\}$$

So the mean curvature H and the specific (or Gaussian) curvature K at a point on Ω are easily found to be

$$\left.\begin{aligned} H &= \frac{(1+p^2)t - 2pqs + (1+q^2)r}{(1+p^2+q^2)^{\frac{3}{2}}} \\ &= \frac{\frac{2a}{y^4}(y-3b)\{(y-b)^2+R^2\} - 2(y-b)\left\{x - \frac{a}{y^3}(y-2b)\right\}}{\left[R^2+(y-b)^2+\left\{x-\frac{a}{y^3}(y-2b)\right\}^2\right]^{\frac{3}{2}}}, \\ \text{and} \quad K &= \frac{rt-s^2}{(1+p^2+q^2)^2} = -\frac{R^2}{\left[R^2+(y-b)^2+\left\{x-\frac{a}{y^3}(y-2b)\right\}^2\right]^2}. \end{aligned}\right\} \quad \ldots\text{(I)}$$

Since K is negative (except when $y = 0$), it appears that the surface Ω is *anticlastic* throughout the finite portion of space.

13. Evidently the curves of *constant* mean curvature (on Ω) are to be found by equating to a constant the value of H, as given by (I) of the foregoing article. In particular, the curve of *zero* mean curvature ($H = 0$) is the intersection of Ω with the sextic surface :

$$a(y-3b)\{(y-b)^2+R^2\} - y(y-b)\{xy^3 - a(y-2b)\} = 0.$$

It is a pleasant exercise to verify that this equation is satisfied by the co-ordinates (α, β, γ) of the critical point P (Art. 9). The immediate inference is that the curve of no mean curvature goes through P. This is however, a foregone conclusion, seeing that the locus of points of zero mean curvature (on *any* surface) is essentially the same as the locus of points whose inflexional tangents are orthogonal, or as the locus of points whose indicatrices are rectangular hyperbolas (Art. 10).

The specific curvature at the point P being given by

$$K = -\frac{R^2}{(R^2+4b^2)^2},$$

the two principal radii of curvature at the same point must be

$$\pm\frac{R^2+4b^2}{R}.$$

In like manner a curve of constant *non-zero* Gaussian curvature (say, $-c^2$) is the intersection of Ω with the surface :

$$(y-b)^2+\left\{x-\frac{a}{y^3}(y-2b)^2\right\}=\pm\frac{R}{c}-R^2.$$

Manifestly the parabolic curve—or what is the same thing, the curve of *zero* specific curvature—is *non-existent* on the surface Ω.

REFERENCES

1. Salmon's *Geometry of Three Dimensions*.
2. Basset's *Treatise on Surfaces*.
3. Hudson's *Cremona Transformations*.
4. Bagchi's *Geometrical Analysis*.

(symbolised respectively as p, q, r, s, t) are given by

$$\left.\begin{aligned} Rp &= y-b, \quad Rq = x - \frac{a}{y^3}(y-2b), \\ Rr &= 0, \; Rs = 1, \text{ and } Rt = \frac{2a}{y^4}(y-3b). \end{aligned}\right\}$$

So the mean curvature H and the specific (or Gaussian) curvature K at a point on Ω are easily found to be

$$\left.\begin{aligned} H &= \frac{(1+p^2)t - 2pqs + (1+q^2)r}{(1+p^2+q^2)^{\frac{3}{2}}} \\ &= \frac{\frac{2a}{y^4}(y-3b)\{(y-b)^2+R^2\} - 2(y-b)\left\{x - \frac{a}{y^3}(y-2b)\right\}}{\left[R^2+(y-b)^2+\left\{x-\frac{a}{y^3}(y-2b)\right\}^2\right]^{\frac{3}{2}}}, \\ \text{and} \quad K &= \frac{rt-s^2}{(1+p^2+q^2)^2} = -\frac{R^2}{\left[R^2+(y-b)^2+\left\{x-\frac{a}{y^3}(y-2b)\right\}^2\right]^2}. \end{aligned}\right\} \quad \ldots\text{(I)}$$

Since K is negative (except when $y = 0$), it appears that the surface Ω is *anticlastic* throughout the finite portion of space.

13. Evidently the curves of *constant* mean curvature (on Ω) are to be found by equating to a constant the value of H, as given by (I) of the foregoing article. In particular, the curve of *zero* mean curvature ($H = 0$) is the intersection of Ω with the sextic surface :

$$a(y-3b)\{(y-b)^2+R^2\} - y(y-b)\{xy^3 - a(y-2b)\} = 0.$$

It is a pleasant exercise to verify that this equation is satisfied by the co-ordinates (α, β, γ) of the critical point P (Art. 9). The immediate inference is that the curve of no mean curvature goes through P. This is however, a foregone conclusion, seeing that the locus of points of zero mean curvature (on *any* surface) is essentially the same as the locus of points whose inflexional tangents are orthogonal, or as the locus of points whose indicatrices are rectangular hyperbolas (Art. 10).

The specific curvature at the point P being given by

$$K = -\frac{R^2}{(R^2+4b^2)^2},$$

the two principal radii of curvature at the same point must be

$$\pm \frac{R^2+4b^2}{R}$$

In like manner a curve of constant *non-zero* Gaussian curvature (say, $-c^2$) is the intersection of Ω with the surface :

$$(y-b)^2+\left\{x-\frac{a}{\sqrt{3}}(y-2b)^2\right\}^2=\pm\frac{R}{c}-R^2.$$

Manifestly the parabolic curve—or what is the same thing, the curve of *zero* specific curvature—is *non-existent* on the surface Ω.

REFERENCES

1 Salmon's *Geometry of Three Dimensions*.

2 Basset's *Treatise on Surfaces*.

3 Hudson's *Cremona Transformations*.

4 Bagchi's *Geometrical Analysis*.

A NEW TECHNIQUE FOR DETERMINING ULTRA-SONIC VELOCITIES IN LIQUIDS

By R. L. NARASIMHAIYA

AND

C. S. DORAISWAMI

Department of Physics, University of Mysore, Bangalore

(*Received for publication, April 14, 1940*)

Plate VII

ABSTRACT. A method is developed for determining the ultra-sonic velocity in liquids by obtaining simultaneously the diffraction pattern over the entire region of the visible spectrum using white light and a spectrograph. A superposed iron-arc enables the diffracted angles to be computed for a number of standard wave-lengths. The calculation of the angle involves the determination of the focal length of the camera lens for various wavelengths with its attendant errors; but this difficulty has been overcome by obtaining on the same photographic plate the diffracted pattern from a grating, the number of lines per centimetre of which is known. Knowing in addition the ultra-sonic frequency and the ratio of the displacements due to diffraction by the grating and by the liquid—a ratio constant at all wavelengths—the velocity of sound in the liquid is calculated.

Various investigators have determined the velocity of propagation of ultra-sonic waves in liquids using the diffraction of monochromatic light by a liquid in which ultra-sonic waves are generated. In all these investigations the diffraction angles are either directly measured or deduced by photographing the diffraction pattern ; in the latter case the focal length of the camera lens for the particular radiation employed should be known precisely. When the experiment is to be repeated for different optical wave-lengths, the choice of suitable filters and fresh determination of focal length become necessary. Two slightly different methods are here developed by means of which ultra-sonic velocities can be determined more precisely by obtaining a diffraction pattern for a number of wave-lengths simultaneously. The first method is to use an incandescent lamp L along with a spectrograph having two slits at right angles ; the light is focussed on to this crossed slit S (*vide* Fig. 1), and the parallel beam from the collimator passes through an optically good parallel-sided vessel V containing the liquid with the oscillating quartz-crystal on top partly immersed in the liquid. The quartz-crystal is set in vibration by connecting it across the split-stator variable condenser of the tank circuit of an oscillator employing two RCA 830 B

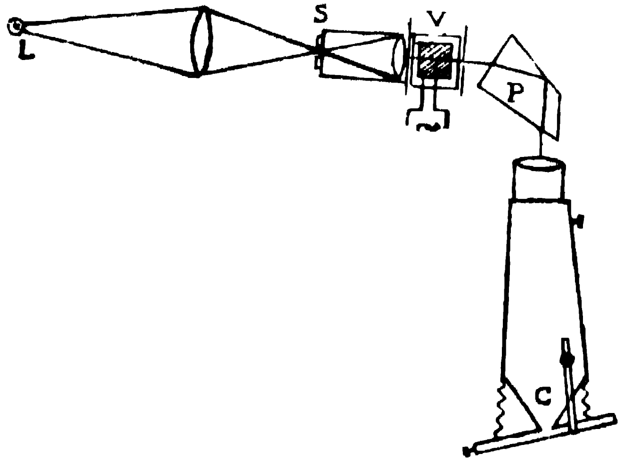

FIGURE 1

valves in push-pull. The frequency of the oscillations is measured by an absorption wave-meter built round a Muirhead Standard variable air-condenser calibrated against a precision wave-meter. The light both direct and diffracted by the liquid passes through the prism P and the spectrum is then focussed on to the photographic plate in the camera C attached to the spectrograph. After the necessary exposure, which is of the order of 1 minute in duration, the crossed slit above the ordinary slit is removed and the iron-arc is exposed for a few seconds. Fig 2 A (see plate VII gives the result obtained by this method in toluene ; while the optical dispersion is along the length of the figure as indicated by the iron-arc spectrum, the diffraction due to the acoustic waves takes place at right angles and shows at a glance the dependence of the angle of diffraction on the wave-length of light used. A measurement of the first and higher order diffraction angles is possible at various standard wave-lengths on a cross-slide micrometer. Fig. 2 B gives the diffraction spectrum obtained with conductivity water.

A second method which while avoiding the double exposure indicated above has all the advantages of the first method is to use the iron-arc itself in place of the incandescent lamp. Fig. 2 C shows a spectrum of this type obtained with carbon tetrachloride. It must, however, be mentioned that, in consequence of the intensity variations along the length of the spectrum in this method, the diffraction angles as measured by the previous method are comparatively more accurate.

The computation of the velocity of sound from the above photographs requires a knowledge of the focal length of the camera lens at various wave-lengths. A direct determination of these focal lengths, though not difficult, involves errors of the order of 1 per cent ; it is therefore necessary to eliminate this uncertainty in precision measurements of velocity. The method adopted finally is to obtain the diffraction pattern arising from a transmission grating

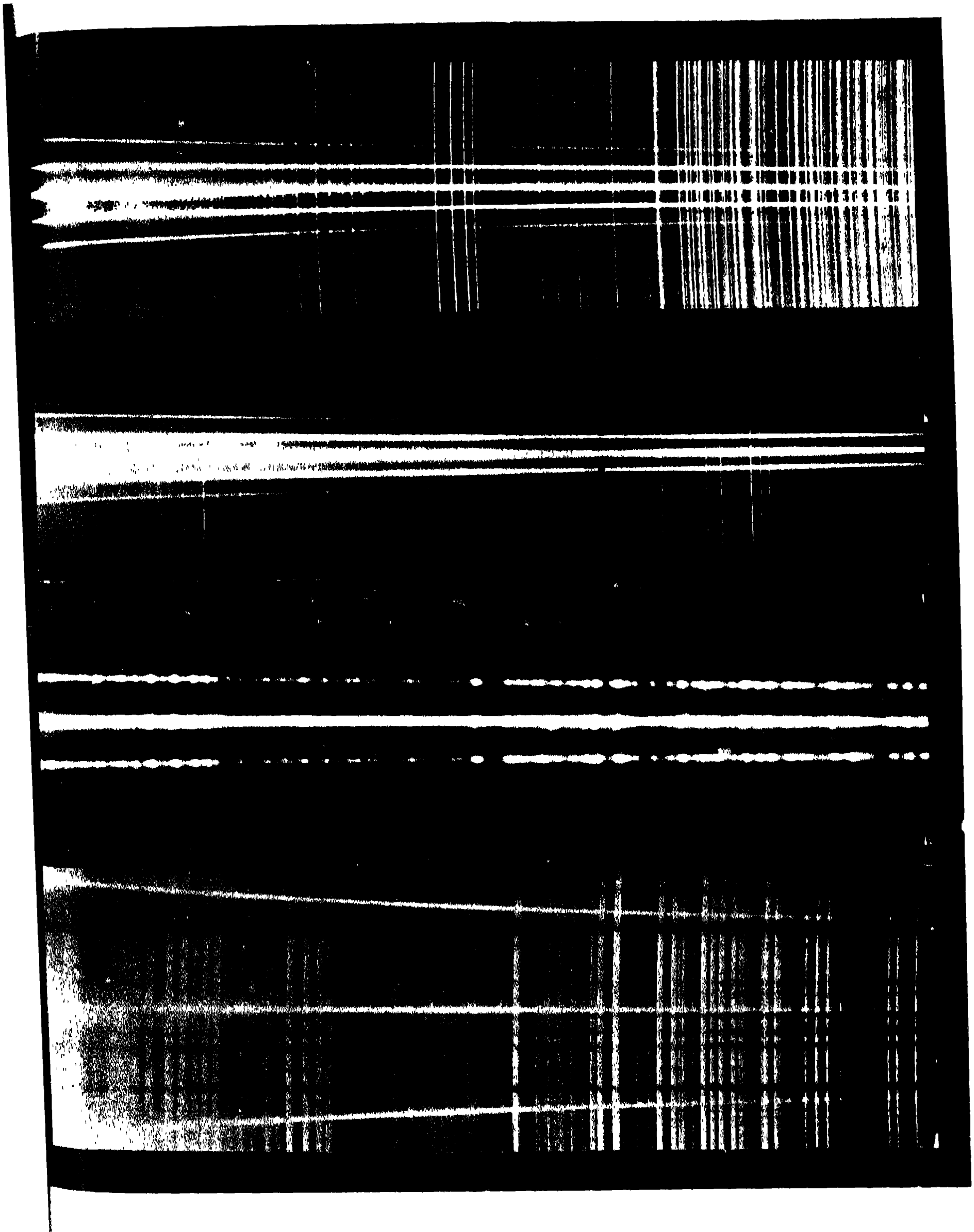
(A)
(B)
(C)
(D)

Fig.

Diffraction patterns of continuous spectra produced by ultra-sonic waves in

(A) toluene, and (B) conductivity water.

(C) Diffraction pattern of iron arc spectrum by ultra-sonic waves in carbon tetrachloride.

(D) Diffraction pattern of continuous spectrum by a grating. Iron arc lines are superposed on (A), (B) and (D).

of 231·5 lines per centimetre without altering the setting of the spectrograph. The vessel containing the liquid and the quartz oscillator is removed and the grating is placed after the collimator with its lines horizontal. Using white light and a point slit (obtained by use of the crossed slit), a diffraction pattern very similar to that of the liquid is obtained; the iron-arc spectrum is superposed on it (*vide* Fig. 2 D) If f_λ represents the focal length of the camera lens for a wave-length λ, in the case of the liquid for the first order

$$\sin\Theta = \frac{\lambda}{\Lambda} = \frac{d_l}{f_\lambda} \qquad \ldots \quad (1)$$

where Λ is the wave-length of sound in the liquid and d_l the linear shift of the first-order diffraction on the photograph at λ. At the same wave-length the shift d_g in the case of the first-order diffraction in the grating spectrum is given by

$$\frac{d_g}{f_\lambda} = N\lambda \qquad \ldots \quad (2)$$

where N is the number of lines per centimetre on the grating. It follows from (1) and (2) that

$$\Lambda = \frac{1}{N} \cdot \frac{d_g}{d_l},$$

and if the ultra-sonic frequency is F Hz, the velocity of sound in the liquid

$$v = F\Lambda = \frac{F}{N} \cdot \frac{d_g}{d_l}.$$

Using toluene and an ultra-sonic frequency of $5{\cdot}080 \times 10^6$ Hz, the velocity of sound in toluene has been obtained as 1314 ± 2 metres per second at 20·4 °C.

This method is being used for the determination of ultra-sonic velocities in solutions and liquid mixtures.

We thank Mr. L. Sibaiya for kindly suggesting the experiment and for guiding us during the course of this investigation.

MEASUREMENT OF COSMIC RAYS AT AGRA AND KODAIKANAL

By

A. K. DAS

AND

M. SALARUDDIN

(*Received for publication, April 8, 1940*)

Plates VIII & IX

ABSTRACT. Cosmic-ray intensities have been measured at Agra and Kodaikanal by means of a Kolhörster apparatus with a shield of iron 5"·5 thick. The intensities have been reduced to standard pressures, for Agra and Kodaikanal separately, by means of the regression coefficients calculated from the intensity and pressure data. The mean intensity values obtained after correcting for barometer effect are for Agra $1{\cdot}545 \pm 0{\cdot}007$ and for Kodaikanal $2{\cdot}333 \pm 0{\cdot}010$ pairs of ions $cm.^{-3}$ $sec.^{-1}$

From these values, after allowing for latitude effect the absorption coefficient of cosmic rays has been calculated. The absorption coefficient obtained, *viz.*, 0·202 per metre of water agrees well with the values obtained by Millikan and Cameron.

By means of this coefficient of absorption the absolute intensities of cosmic rays without shield have been deduced. These values of 2·907 and 1·925 pairs of ions per cm^3 sec^1 for Kodaikanal and Agra respectively compare well with Compton's intensity values for the same latitudes. The intensity data for Agra and Kodaikanal are then analysed according to mean and sidereal times. The curves for the mean solar time for the two stations agree with each other and with the corresponding curves of other investigators but no similarity has been found between the sidereal time curves of the two stations.

Mean daily cosmic-ray intensities have been correlated with solar activity represented by sunspot numbers and flocculi figures but no relationship has been found to exist between them.

In recent times the geographical distribution of cosmic-ray intensities has formed one of the important aspects of the study of cosmic radiation. The world surveys of cosmic radiation organized by A. H. Compton and by R. A. Millikan have shown the utility of such studies particularly with regard to the discovery of the nature of the particles which constitute this radiation. In spite of these expensive surveys it has not been possible, we believe, to collect data from as many representative countries as would have been desirable and it is likely to be helpful for a general study to secure observational data from such latitudes as do not seem to have been well represented in the world surveys. India seems to be one of the countries from which very little data on cosmic ray intensity are

available. The only references that we have been able to find about this type of work in India are the measurements by J. M. Benade in August, 1932, at Lahore under the scheme of co-ordination initiated by Compton [1] and the balloon observations made at Madras in October, 1936, by H. V. Neher [2], a collaborator of Millikan. The measurements considered in the present paper, though not numerous, have therefore appeared to us to be worth publishing. It is, however, intended that the measurements should be continued for a few years in order to obtain a sufficiently long series of data capable of yielding definitive values of the intensity of cosmic radiation in India.

EXPERIMENTAL ARRANGEMENTS

The measurements discussed in this paper were made at Agra (Lat. 27° 8′ Long. 78° 1′) and at Kodaikanal (Lat. 10° 14′ Long. 77° 28′). Although the choice of these two stations was dictated by reasons other than the requirements of this investigation, these stations happen to represent typical localities well suited for this kind of work. They differ appreciably in latitude and considerably in altitude, Agra being practically a sea-level station about 554 feet above mean sea level and Kodaikanal a hill station about 7700 feet above mean sea level. The apparatus used for these observations was a Kolhörster electroscope of the latest type belonging to the India Meteorological Department. It had proved to be perfectly satisfactory for the measurements of cosmic radiation made by one of us (A.K.D.) during two sea voyages between India and Europe and at Cambridge.[3] As it has frequently been contended by workers on cosmic rays that intensity measurements are affected by instrumental bias, it seems desirable to give a brief description of our apparatus although the principle of this instrument is well known from Kolhörster's descriptions. The complete apparatus shown in Plate VIII consists of a cylindrical ionisation chamber 'A' made of sheet iron 2·5 mm thick and fitted with a brass lid of 3·5 mm. thickness. The chamber is sealed air-tight and filled with air (at nearly atmospheric pressure) specially dried and freed from radio-active substances. The air-tightness of the ionisation chamber can be checked by means of a thermometer 'T' and a precision aneroid barometer 'P' attached to the instrument. The electrometer is sealed inside the ionisation chamber and its deflections can be read with the help of a microscope fitted to the lid. It consists of a pair of exactly similar loops of quartz fibre mounted on a frame with a nickel-steel-quartz temperature compensation, the frame being fixed upon the objective of the viewing microscope. The electrometer being well insulated from the walls of the ionisation chamber, the loss of charge through leakage is extremely small. Through the microscope the quartz loops can be seen only edgewise so that they appear as two straight dark filaments against the microscope scale divisions. The filaments and the scale divisions are illuminated by means of a small

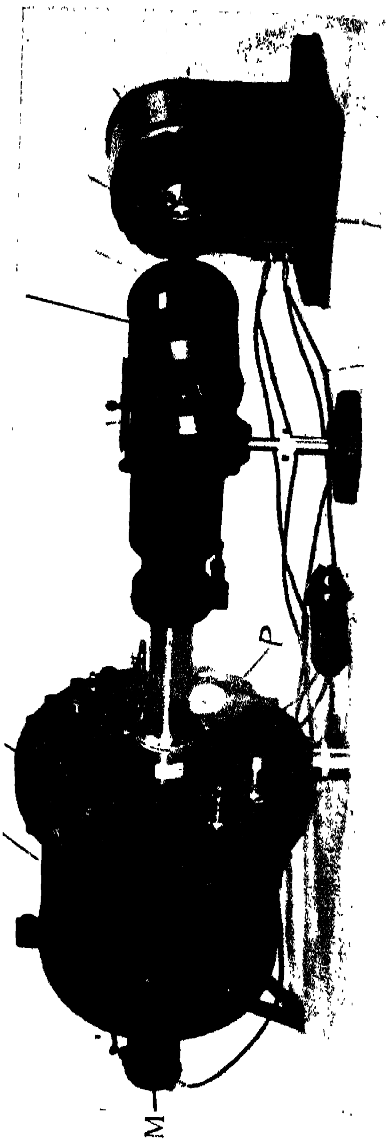

PLATE VIII

KODAIKANAL CHART No. 8 (Feb. 17–18)

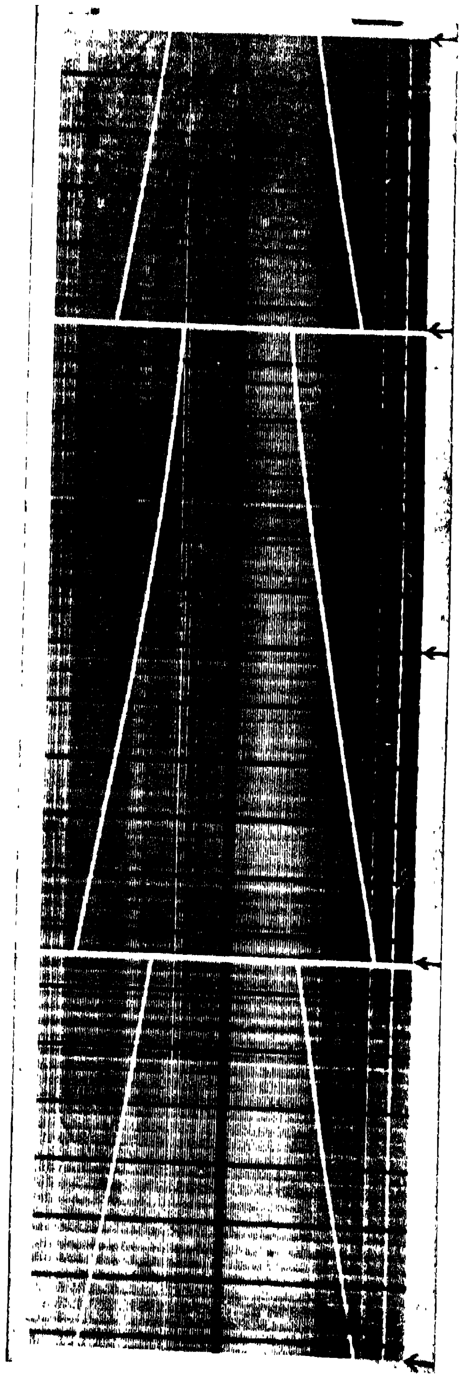

SAMPLE RECORD FROM KOLHÖRSTER'S APPARATUS

PLATE IX

electric lamp fitted inside a metal tube 'M' and screwed on to the window at the back of the ionisation chamber. The instrument can be used for visually reading the deflections of the electroscope ; it is, however, provided with a camera 'C' (with a rotating drum for photographic paper) which can be fixed on the eye piece end of the microscope for obtaining a continuous photographic record of the separation of the electroscope filaments. For the present observations, the latter method was exclusively employed.

The walls of the ionisation chamber are thick enough to prevent any α or β rays from entering it ; but in order to eliminate the possible effect of even the most penetrating γ rays of known radio-active origin, the apparatus was enclosed in an iron shield of 5·5 inches thickness all round The shield was built up as a rectangular box from several iron plates for convenience of manipulation. For charging the electrometer at intervals, it was necessary to make one wall of the shield easily removable and consequently it was found essential to keep down its weight as much as possible. Accordingly, the shield was made just large enough to enclose the ionisation chamber only, so that the end of the microscope tube carrying the camera projected out of the shield through a hole in the movable wall. The movable wall itself had to be made of two halves mounted in such a way that they could be slid along iron grooves with ball runners. This arrangement necessarily involved a certain amount of leakage of γ rays into the ionisation chamber, but we do not think that it could have been large enough to affect materially the measurements of the cosmic rays.

The experimental material utilised in this work consists of complete records for 23 days in June-July, 1936, at Agra and for 13 days in February, 1938, at Kodaikanal. At Agra the whole apparatus was installed in a canvas tent well away from buildings and at Kodaikanal the apparatus was housed in a wooden hut previously used for housing magnetic instruments. The electrometer was charged each time to about 300 volts and was allowed to discharge itself till the voltage dropped to 100 volts. Below 100 volts the ionisation current no longer corresponded to saturation, so that the electrometer had to be charged up again. This necessitated charging the electrometer twice a day at Agra and three times daily at Kodaikanal where the loss of charge through ionisation was faster. Charging of the electrometer was done with the help of a magnetic probe and a charging terminal fixed on the lid of the ionisation chamber but insulated from it by means of an amber insulator. The battery used for charging was a Zamboni pile the positive pole of which was connected to the charging terminal of the electrometer, the other pole being earthed. The probe which is inside the ionisation chamber was then brought into contact with the inner end of the charging terminal by turning it over with the help of a horse-shoe magnet attached to the outside of the lid. The charging now finished, the probe was again turned back to its initial position so as to keep the electrometer disconnect-

ed from the charging terminal. The separation of the electrometer filaments when charged could be observed through a window in the camera by means of a reflex arrangement. The time of the opening or the closing of the shutter was noted whenever this was done for charging the electrometer or for changing the photographic paper. A sample record obtained from the instrument is shown in Plate IX. This is a copy of the Kodaikanal record of February 17-18, 1938 on a reduced scale. There are three pairs of electrometer traces on the chart. Each pair begins with full charge when there is the greatest seperation between the filament traces and then gradually the traces come nearer together as the charge decreases. The very fine and close lines running along the sheet are the traces of the microscope scale divisions. The rather thick lines across the sheet are the hour marks which are registered by means of a device in the clock work which short-circuits the lamp once every hour. The sheets were measured by means of a low-power travelling microscope. The procedure was to count the number of scale divisions between the electrometer traces at every hour mark and at every point corresponding to the time of the opening and closing of the exposing shutter. The times corresponding to the hour marks were deduced from the times of the opening and closing of the shutter after making due allowances for the rate of the clock. The linear distances between the electrometer traces, *i.e.*, the number of scale divisions counted, were then converted to volts by means of a calibration curve prepared by one of us (A.K.D.) with the help of a fine precision potentiometer at the Electrical Engineering Laboratory of the University of Cambridge.

Since all other sources of ionisation have been eliminated by the use of the iron shield, the loss of charge of the electrometer must be due to cosmic rays alone. Accordingly the rate of ion formation is a measure of the intensity of the cosmic radiation. In order to obtain the rate of ionisation, all the readings of the electrometer in volts were tabulated against the corresponding times so that the values of volt difference (dv) and of time difference (dT) were directly obtained from the tables. The rate of ionisation, *i.e.*, the number of ion-pairs per cm.^{3} per second, was then calculated according to the usual formula for this kind of instrument.

$$J = \frac{C}{300 \times 60 \times e \times L} \cdot \frac{dv}{dT} = 8{\cdot}193 . \frac{dv}{dT},$$

where J = number of ion-pairs/cm.^{3}/sec., C = capacity of the electrometer = 0·268 cm.

L = internal volume of the ionisation chamber reduced to 0°C and 760 mm. pressure = 3801·06 cm.^{3}, e = electronic charge = $4{\cdot}78 \times 10^{-10}$ e.s.u. and $\frac{dv}{dT}$ = decrease of voltage per minute.

The residual ionisation of the apparatus, as determined and given by the makers, Günther and Tegetmeyer of Braunschweig, is 1·145 ion-pairs per cm.[3] per second. By subtracting this value of the residual ionisation from the total ionisation represented by J, the ionisation due to external causes or the intensity of cosmic rays 'I' was obtained.

BAROMETER EFFECT

The intensity of cosmic radiation measured at the surface of the earth must be expected to be influenced by meteorological conditions and consequently it is essential to reduce all observations made at different times to standard meteorological conditions in order that they may be comparable. The atmospheric factor which affects cosmic-ray intensity most is the barometric pressure, the effect of temperature, humidity and other elements being comparatively small. This fact observed by most investigators, was brought out very clearly by the method of multiple correlation used by A. Corlin [4] who obtained the following correlation coefficients for pressure (RIB) temperature (RIT) and humidity (RIH) for the three periods for which he analysed his data.

Period	I	II	III
RIB	−0·585 ± 0·030	−0·369 ± 0·040	−0·450 ± 0·054
RIT	−0·157 ± 0·045	−0·023 ± 0·047	+0·059 ± 0·068
RIH	+0·125 ± 0·045	−0·138 ± 0·047	+0·016 ± 0·068

It is clear from the above table that only pressure has a real influence on the intensity of cosmic rays, the other factors having a very small and uncertain influence. We have therefore applied only correction for the pressure effect in the present work.

The barometer effect was deduced by arranging the intensities according to different values of pressure, working out their means and then applying the method of regression coefficients. The pressures at the mean times of observation were obtained from the charts of self-recording microbarographs of the Agra and Kodaikanal observatories. During the periods of observation here considered the barometric pressure varied between 28·85″ and 29·09″ at Agra and between 22·69″ and 22·90″ at Kodaikanal. In order to reduce the intensity values for each station to some standard pressure, the following procedure was adopted. All the intensity values were tabulated separately for Agra and Kodaikanal according to different values of pressure at intervals of 0·01″. The mean values of intensity 'I' for different values of pressure P were deduced and the regression coefficients

R between these values were then calculated from the following formula

$$R = \frac{s.\{I(P-p)\}}{s.\{(P-p)^2\}}$$

where p is the mean of all P values.

The regression coefficients derived from Agra and Kodaikanal data are -0.078 I and -0.040 I per inch of mercury respectively. With these coefficients the values of I for Agra and Kodaikanal were reduced to the standard pressures of 29.0″ and 22.8″ respectively. We denote these intensity values reduced to standard pressure by I_0.

ABSORPTION COEFFICIENT OF COSMIC RAYS

The mean value of the intensity of cosmic rays at any place depends primarily upon the altitude and the latitude of the station. If for the mean values of I_0 obtained for Agra and Kodaikanal allowance is made for the effect of latitude, then the remaining difference between the intensity values would be mostly due to the effect of altitude and from this the absorption coefficient of cosmic rays can be calculated. The fact that cosmic-ray intensity varies with the geomagnetic latitude* is now well established. The results obtained by Clay, Compton, Hoerlin, Neher and others show that cosmic-ray intensity is nearly constant from about latitude 50° to the pole both in the northern and southern hemispheres, but decreases steadily towards the equator, the decrease amounting to about 14 per cent. at sea level and much higher at higher altitudes. The geographical latitudes of Agra and Kodaikanal are 27° 8′ N and 10° 14′ N and their geomagnetic latitudes are 17° 21′ N and 0° 37′ N respectively. The geomagnetic latitudes were calculated from the formula

$$\sin\lambda = \sin\psi\cos\theta\cos\phi + \cos\psi\sin\theta,$$

where λ is the geomagnetic latitude, ψ the colatitude of the north pole of uniform magnetisation, θ the geographical latitude of the place and $\phi + 69°\ 8'$ is the west longitude of the place.

From Compton's [1] intensity geomagnetic latitude curve for sea level (which includes the data of Clay, Millikan and others), the percentage decrease in intensity from latitude 17° to the equator is about 1 and the same from the curve for 2000 metres (about 6600 ft.) altitude is 2.5. The altitude of Agra and Kodaikanal being 554 feet and 7688 feet respectively, the intensity at Kodaikanal has to be increased by 2 per cent. to reduce it to Agra latitude. Then this corrected intensity can be compared with the intensity at Agra and the altitude effect can be deduced.

* By geomagnetic latitude is meant the latitude relative to the pole of uniform magnetisation of the earth which is at 78° 32′ N and 69° 8′ W and is different from the magnetic latitude which is defined by the formula $\tan\mu = \frac{1}{2}\tan\delta$, where μ is the magnetic latitude and δ is the dip of the magnetic needle.

The mean cosmic-ray intensities measured at Agra and at Kodaikanal are $1{\cdot}545 \pm {\cdot}007$ and $2{\cdot}333 \pm {\cdot}010$ ion-pairs cm.$^{-3}$ sec.$^{-1}$ respectively. The intensity at Kodaikanal reduced to Agra latitude would then be $2{\cdot}380$ ion-pairs cm.$^{-3}$ sec.$^{-1}$ We can take it that the intensity of $2{\cdot}380$ ion-pairs cm.$^{-3}$ sec.$^{-1}$ becomes reduced to $1{\cdot}545$ ion-pairs cm.$^{-3}$ sec.$^{-1}$ through absorption by an air column of depth corresponding to $6{\cdot}2''$ of mercury, this being the difference between the mean barometric pressures of Agra and Kodaikanal. Assuming that the cosmic rays are absorbed exponentially, their absorption coefficient can then be calculated by means of the simple formula

$$I_1 = I_2\, e^{-\mu d} \text{ or } \mu = \left(\frac{2{\cdot}3026}{d} \right) (\log I_1 - \log I_2),$$

where μ is the absorption coefficient, I_1 and I_2 are the intensities of rays when they enter and when they leave the absorbing layer respectively, and d is the depth of the layer. Using appropriate values for Agra and Kodaikanal in the above formula we obtain

$$\frac{2{\cdot}306}{6{\cdot}2 \times 13{\cdot}6 \times 2{\cdot}54} (\log 2{\cdot}380 - \log 1{\cdot}545)$$

$$= 0{\cdot}00202 \text{ cm.}^{-2} \text{ gm.}^{-1}$$

$$= 0{\cdot}202 \text{ per metre of water.}$$

This value of absorption coefficient agrees with the values obtained by Millikan and Cameron [5] in their experiments in the high altitude lakes of America.

ABSOLUTE INTENSITIES OF COSMIC RAYS

The mean cosmic-ray intensity values of $2{\cdot}333$ and $1{\cdot}545$ ion-pairs/cm.^{3}/sec. obtained at Kodaikanal and Agra respectively are those measured inside an iron shield of $5{\cdot}5$ inches thickness. The absolute intensities I_K and I_A (*i.e.*, the intensities without the shield) can be calculated for the two stations from the coefficient of absorption already determined and from the density of iron. We again use the exponential formula $\mu = \frac{2{\cdot}3026}{d}$ $(\log I_1 - \log I_2)$. Substituting the values of μ, d and I_2 for Kodaikanal we have

$${\cdot}00202 = \frac{2{\cdot}3026}{5{\cdot}5 \times 2{\cdot}54 \times 7{\cdot}8} \cdot (\log I_K - \log 2{\cdot}333)$$

or $$I_K = 2{\cdot}907 \text{ ion-pairs cm.}^{-3} \text{ sec.}^{-1}$$

Similarly for Agra we have

$$I_A = 1{\cdot}925 \text{ ion-pairs cm.}^{-3} \text{ sec.}^{-1}$$

The intensities corresponding to the altitudes of Agra and Kodaikanal from Compton's intensity-barometer curve for latitudes $0° - 20°$ are $2{\cdot}8$ and $1{\cdot}7$ respec-

tively. These values lie between those obtained from the present measurements with and without shield. But if we take into account the fact that Compton's values are for a shield of 2·5 cm. of bronze and 5·0 cm. of lead (which roughly corresponds to about half the thickness of the shield used in our experiments), then there is close agreement between these values and those arrived at in the present paper.

DIURNAL VARIATION OF COSMIC-RAY INTENSITIES WITH SIDEREAL AND MEAN TIMES

During 1926-29 a number of investigators were engaged in finding out whether the intensity of cosmic rays varied with sidereal time. In 1926 W. Kolhörster and G. v. Salis from their observations in Mönchgipfel in Switzerland found variations up to 15 per cent. following a daily period according to sidereal time with maximum at 6^h and 16^h and minimum at about 10^h. Later Büttner, Steinmaurer and Steinke from their observations at different places confirmed the results of Kolhörster and v. Salis. The results obtained by different investigators were plotted by A. Corlin [6] and are reproduced here in Figure 1. As will be seen, all these curves agree with one another excepting those of Lindholm at Muottas Muraigl. Corlin [7] also got the same results as Kolhörster and others by analysing his data at Abisko.

But later observations by a number of other investigators did not confirm these results. Among the later observations may be mentioned those of R. Steinmaurer at Sonnblick (1929-30), of Lindholm at Stockholm (1930-31) and of Compton and others at Mt. Evans (1931). Though these investigators did not find any unquestionable variations in intensity according to sidereal time, yet when their data were analysed and plotted against mean solar time, they found very good agreement in all the curves with maximum at noon or in the afternoon. These curves are also reproduced here in Figure 2 from Corlin. [8]

The intensity data for Agra and Kodaikanal were analysed according to sidereal and mean solar times to see how far they agreed with the results of other investigators. To get the mean hourly intensity values according to sidereal time, all the mean times of observation were converted to sidereal times. Intensity-sidereal time curves were then drawn for every day From these curves the intensity values at every sidereal hour were read off and their means for each hour were calculated for Agra and Kodaikanal separately. Similarly mean hourly intensity values were calculated according to mean solar time (in this case Indian Standard Time). These values were plotted separately for Agra and Kodaikanal and are shown here in Figure 3.

It will be seen from Figure 3 that the mean time curves for Agra and Kodaikanal agree with each other and also with those of other investigators shown in Figure 2. Both these curves show a maximum intensity in the afternoon (Agra

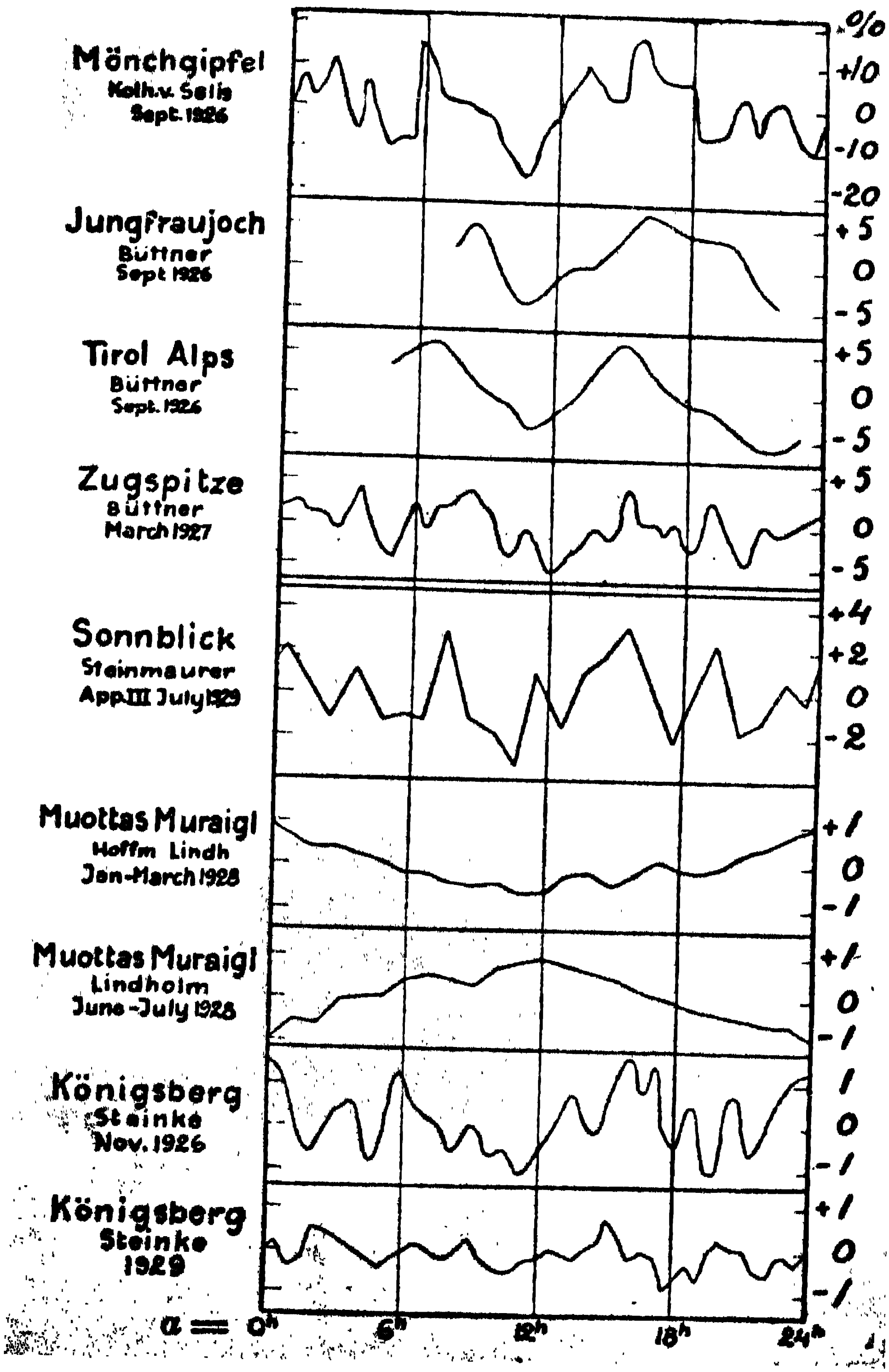

The sidereal time period as observed in 1926 29

FIGURE 1

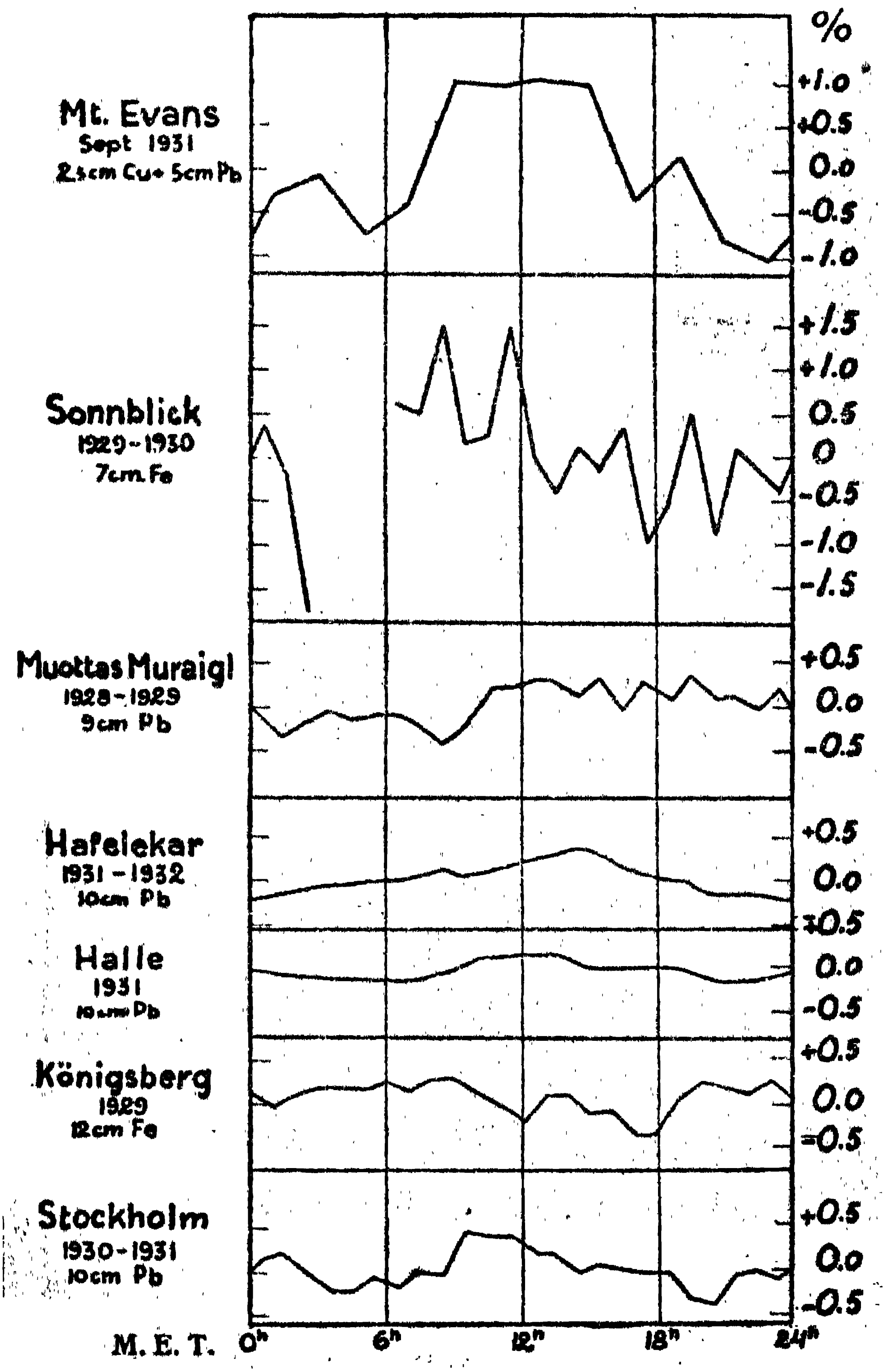

The mean time period as observed with closed shield in 1929-32.

FIGURE 2

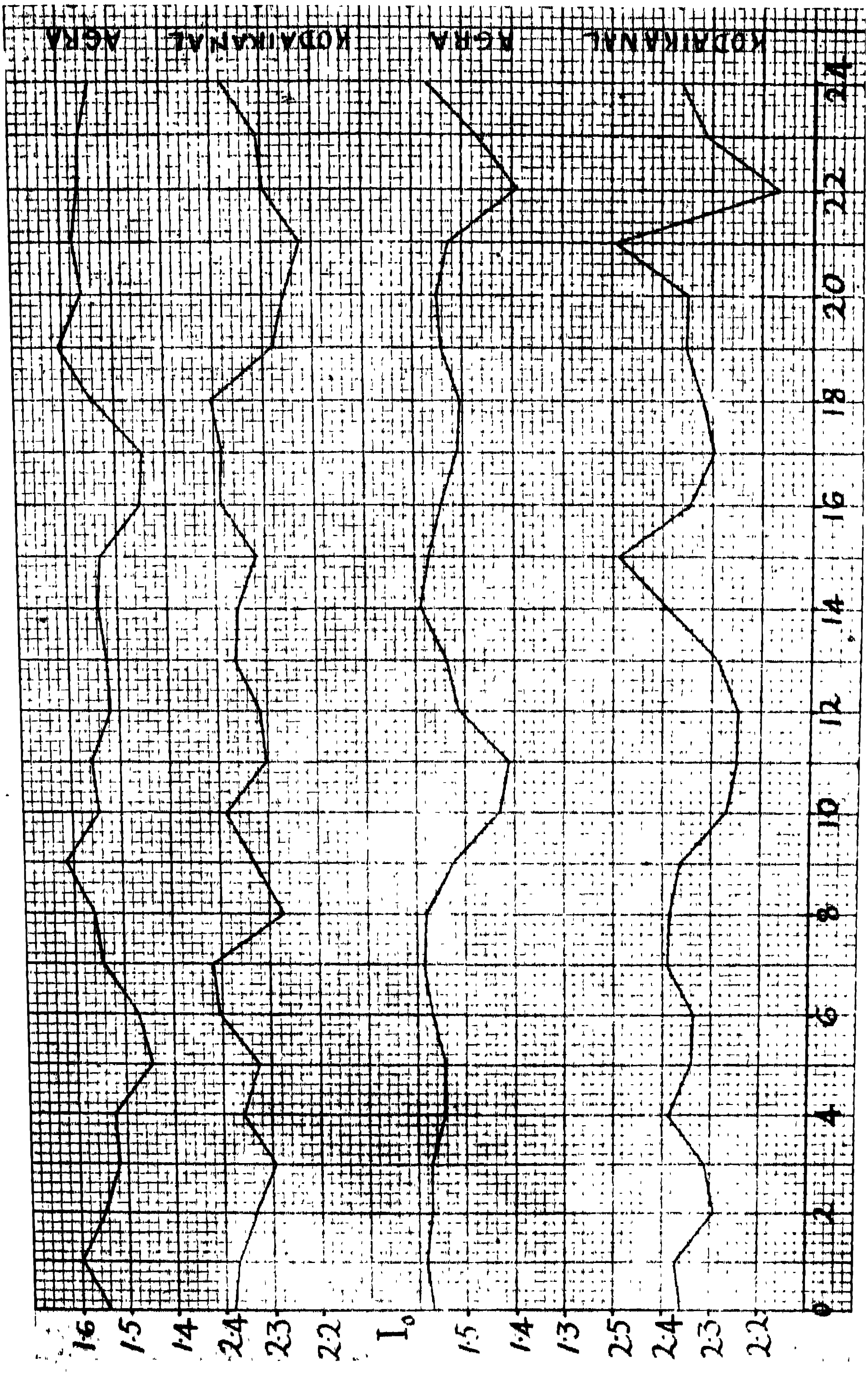

Sidereal-Time Curves Mean Time Curves

Hours

FIGURE 5

at 14^h and Kodaikanal at 15^h) and minimum intensities at 11^h and 22^h. But the sidereal-time curves for these two stations do not show any conformity either with each other or with corresponding curves of other investigators shown in Figure 1. On the other hand, a close examination of these two curves shows that they are more or less opposite in phase, *i.e.*, the minimum in the curve of one station corresponding to the maximum of the other. This can be explained by the fact that the Kodaikanal data refer to the month of February and that of Agra to the months of June-July. Between the corresponding sidereal times of February and July there is a difference of about 12 hours according to mean time, and as these curves agree according to mean time, they are opposite in phase according to sidereal time. Therefore, it can be said that the Agra and Kodaikanal data do not confirm the results of Kolhörster and others but confirm those of later investigators who find variations according to mean solar time.

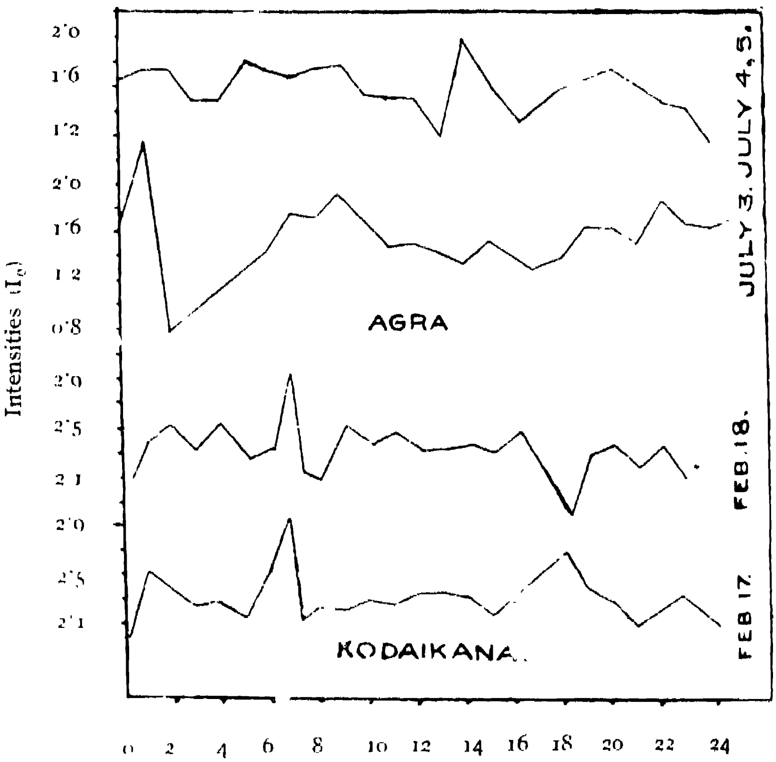

FIGURE 4

But it should be noted that the data of Agra and Kodaikanal are very meagre to draw any definite conclusions. For such kind of work, data ranging over very long periods are required so as to minimise the effect of abnormal changes (the so-called "variations of the second kind") often shown by cosmic-ray intensity from hour to hour. These variations of the second kind can be seen from the curves given in Figure 4 where the intensities for two days each for Agra and Kodaikanal are plotted against sidereal time. But in the mean curves shown

TABLE I

Solar activity and cosmic-ray intensity (Agra)

Date	Daily mean sunspot numbers	K Flocculi figure	H. Bright Flocculi figure	H. Dark Flocculi figure	Sum of the 3 Flocculi figures	Mean daily cosmic-ray intensity
18-6-36	60	2.8	2.8	2.3	7.9	1.344
19-6-36	101	3.0	2.9	2.5	8.4	1.326
20-6-36	88	3.0	3.0	2.2	8.2	1.214
21-6-36	119	3.1	2.8	1.8	7.7	1.566
22-6-86	100	2.9	3.0	2.2	8.1	1.475
23-6-36	76	3.0	2.7	2.0	7.7	1.544
24-6-36	71	3.1	2.8	2.4	8.3	1.585
25-6-36	89	3.2	3.0	2.5	8.7	1.622
26-6-36	112	3.1	3.5	2.2	8.8	1.512
27-6-36	103	3.2	3.5	2.8	9.5	1.621
29-6-36	68	2.8	2.7	2.8	8.3	1.383
30-6-36	79	2.8	2.8	3.2	8.8	1.590
1-7-36	79	2.9	3.0	3.0	8.9	1.550
2-7-36	74	3.0	3.0	3.0	9.0	1.585
3-7-36	44	2.9	2.0	2.8	7.7	1.596
4-7-36	50	2.9	2.7	3.0	8.6	1.616
5-7-36	52	2.8	2.8	2.2	7.8	1.670
7-7-36	30	2.5	2.0	2.1	6.6	1.537
8-7-36	47	2.4	2.0	2.0	6.4	1.561
9-7-36	43	2.6	2.1	1.8	6.5	1.571
10-7-36	47	2.8	1.5	1.5	5.8	1.572
11-7-36	49	2.1	2.0	2.0	6.1	1.574
13-7-36	67	2.9	2.2	1.0	6.1	1.502
14-7-36	76	2.9	2.5	1.0	6.4	1.692
15-7-36	67	3.1	2.7	1.0	6.8	1.[illegible]58
16-7-36	69	3.1	2.8	1.0	6.9	1.370
17-7-36	57	2.9	2.8	1.0	6.7	1.576
18-7-36	53	3.1	3.0	1.0	7.1	1.566

TABLE 2

Solar activity and cosmic-ray intensity (Kodaikanal)

Date	Daily mean sunspot figure	K Flocculi figure	H_α Bright Flocculi figure	H_α Dark Flocculi figure	Sum of the 3 Flocculi figure	Mean daily cosmic-ray intensity
9-2-38	101	3.1	2.8	2.8	8.7	2.211
10-2-38	133	3.4	4.0	3.5	10.9	2.303
11-2-38	137	3.8	3.3	3.6	10.0	2.376
12-2-38	161	3.8	4.2	4.5	12.5	2.230
13-2-38	160	3.8	4.3	3.7	11.8	2.352
14-2-38		4.2	5.0	5.0	14.2	2.303
15-2-38		4.1	5.0	3.0	12.1	2.346
16-2-38		4.4	5.0	2.0	11.4	2.331
17-2-38	171	4.1	4.8	2.5	11.4	2.353
18-2-38	171	4.1	5.0	2.3	11.4	2.355
19-2-38	145	3.9	4.1	2.6	10.6	2.342
20-2-38	98	3.8	4.0	2.2	10.0	2.286
21-2-38	100	3.2	3.5	2.0	9.6	2.379

in Figure 3 these variations are much less pronounced and if longer periods are taken the curves may be expected to become very much smoother.

COSMIC RAYS AND SOLAR ACTIVITY

Whether the sun at all contributes to the intensity of cosmic rays does not seem to have been conclusively established. Some observers have, however, claimed to have detected a small solar contribution as the result of their analysis of a long series of measurements. Another way of detecting solar influence on cosmic-ray intensity is to correlate the mean daily intensity with solar activity. Accordingly the mean daily cosmic-ray intensities for Agra and Kodaikanal were calculated from the values of I_0 and the sunspot numbers and flocculi figures were taken from the quarterly bulletins for character figures of solar phenomena published under the auspices of the International Astronomical Union. In the bulletins the flocculi figures are given separately for calcium flocculi, $H\alpha$ bright markings and $H\alpha$ dark markings, each for the whole disc and for the inner circle (half the radius of disc) of the sun. The sum of the three 'whole disc' figures was taken

for the purpose of correlation. All these results are collected in Tables 1 and 2 for Agra and Kodaikanal respectively. These figures were plotted as dot diagrams in order to see whether any relationship exists either between the intensity and flocculi figures but no relationship of any kind was detected. The data considered are, however, very meagre for drawing any definite conclusions.

The senior author takes this opportunity of thanking Dr. C. W. B. Normand, C.I.E., Director-General of Observatories, for purchasing the Kolhörster apparatus at his request. He is indebted also to Rai Bahadur G. Chatterjee, Superintending Meteorologist, Agra, who had the iron shield constructed at the Agra Observatory besides providing him with all facilities for the part of the work done at Agra and Dr. N. K. Sur, Meteorologist, for the valuable assistance he gave him in the reduction of the cosmic-ray records at Agra. Our thanks are also due to Dr. A. L. Narayan, Director of the Kodaikanal Observatory, for his interest in the part of the work done at Kodaikanal.

REFERENCES

[1] A. H. Compton, *Phys. Rev.*, **43**, 387 (1933).
[2] I. S. Bowen, R. A. Millikan and H. V. Neher, *Phys. Rev.*, **52**, 80 (1937).
[3] A. K. Das, *Nature*, **136**, 29 (1933).
[4] A. Corlin, *Annals Lund Obs.*, No. 4, P. A. 56 (1934).
[5] R. A. Millikan and G. H. Cameron, *Nature*, **121**, 19 (1928) and *Phys. Rev.*, **37**, 235 (1931).
[6] A. Corlin, *Annals Lund Obs.*, No. 4, P. A. 15 (1934).
[7] *Ibid.*, P. A. 110.
[8] *Ibid.*, P. A. 19.

RAMAN SPECTRUM OF SUGAR

BY A. L. SUNDARA RAO, M.Sc.
Andhra University, Waltair

(Received for publication, April 27, 1940)

Plate X

ABSTRACT. By an improved method, sugar was purified and the Raman spectrum of its solution taken. This revealed 16 Raman lines and the usual water band. The frequencies of the lines are 377*, 464*, 549*, 599*, 649, 753*, 856, 943, 1088, 1135, 1272, 1333*, 1370*, 1408*, 1472, 2865 and the water band extending from 3298—3681. The frequencies marked with asterisks have been observed for the first time. A general assignment of frequencies as due to the C—C, C—O, C—H, δ (C—H) oscillations has been made. These lines are compared with those obtained with glucose and crystalline sucrose.

INTRODUCTION

In view of the interest in the constitution of sugars from an organic or biochemical standpoint, a study of the Raman effect of this class of substances is of special importance. But it is suprising to note that very little work has been done in this direction. This is most probably due to the fact that heavy molecules of this type give rise to a strong continuous background which is found, in many cases of Raman spectra, to completely mask the lines characteristic of the molecule. The classical example of this type is glycerine—$(OH)H_2C.CH(OH)CH_2(OH)$. The continuous background in the Raman spectrum of this substance is so prominent that even with the liquid distilled in vacuum it could not be entirely eliminated. (It may incidentally be mentioned here that the author has obtained, using an improved method of distillation, an extremly good Raman spectrum for Glycerine and the results are being published.) This substance is comparatively simple when compared to heavier molecules containing a larger number of carbon atoms. Various workers have attributed this phenomenon to various causes, but with all the work done so far, the weight of evidence is that the continuum arises from an impurity and is not due to a genuine Raman scattering.

Whiting and Martin[1] were able to partly eliminate the continuous spectrum by making the solution of sucrose dust-free by precipitating with Al $(OH)_3$. They were able to record after 144 hrs. of exposure, four faint Raman lines, with frequencies 1090, 1480, 2870 and 3420 cm.$^{-1}$, the last being the water band or a superposition of this over the O-H band arising out of the O-H in sugar.

Polara[2] working with sugar solutions reported a large number of lines; the Raman frequencies of which are 625, 668, 689, 858, 945, 1037, 1134, 1224, 1339, 1425, 1488, 1683, 2016, 2055, 2113, 2164, 2404, 2718, 2813.

Kutzner[3] tried with a number of saccharides and obtained frequencies given below.

Glucose	454, 513, 1143
Galactose	1138
Fructose	1179
Maltose	1135, 1140
Saccharose	1130-1188 (broad band)

A comparison of the results obtained by Polara with those of Whiting and Martin on the one hand, and Kutzner on the other, will indicate the large discrepancies between the frequencies of the lines obtained by them. With a view to investigate the cause of these discrepancies, a study of the Raman spectrum of sugar was undertaken, the results of which are given below.

EXPERIMENTAL

While studying the Raman effect, it is important to ensure that exciting light was not decomposing the substance under investigation. N. A. Yajnik and co-workers[4] have shown that solutions of sucrose, when exposed to ultraviolet light, undergo hydrolysis even in the complete absence of acid. Hence, the solutions studied in these investigations were always tested with Fehling's solution for the abscence of reducing sugars, both before and after the exposure to the mercury arc light used as the exciting radiation. The light from the arc was condensed by a 9″ glass condenser on to the Wood's tube containing the sucrose solution. After several trials with various light filters, a combination of two filters consisting of sodium nitrite and the solution of the proper strength of Iodine in carbon tetrachloride was chosen and placed between the condenser and the scattering medium. This served to eliminate the 4047-line of the arc and beyond on the shorter wavelength region and also the continuous spectrum between 4358 Å and 4916 Å, present in the light from the mercury arc. Care was taken to run the mercury arc at a low voltage—which considerably helps to reduce the continuum. Thus the exciting source is 4358 Å which is undoubtedly the best mercury line for this work, as decomposition of sugar is avoided and the Raman lines appear between the lines 4358 Å to 4916 Å, a region free from mercury lines.

The scattered light was focussed on to the slit of the spectrograph by means of an achromatic lens. A two-prism spectrograph of high light-gathering power (which was kindly designed and constructed by the Instruments Manufacturing Section attached to the Applied Physics department) was used

to record the Raman spectrum on Ilford Isochrom plates. A comparison spectrum of copper was given on the same plate using a Hartmann's diaphram and the wavelengths determined by measuring with a Hilger comparator.

METHOD OF PURIFICATION OF SUGAR SOLUTION

A 60% solution of sucrose was prepared with redistilled water and was found to be contaminated with appreciable amounts of suspended impurities and was straw yellow in colour. Various methods of purification suggested by previous workers were tried with little success. Purification by repeated crystallisations did not appreciably improve the nature of the spectrum. Hence, a modified method of purification was adopted in this investigation. The sucrose solution was treated with the decolourising carbon-Norit A. The quantity of carbon used was about 2% of the solids in the melt and the 'wet filling' method was adopted for clear filtration. The first liquor which flowed from the filter was generally cloudy, but after fifteen or twenty minutes of running to refiltration, this cleared up. The solution was further rendered clear by centrifuging in a Sharple's super centrifuge at 5,500 r.p.m., the outflow from the centrifuge being directly collected in the Wood's tube.

RESULTS

In Plate X, figure 1 shows the Raman spectrum of sugar solution before purification with an exposure of 2 hours. Even with such a short exposure the continuous background was so strong that it was not possible to observe any Raman lines. Noting that the continuous spectrum was too strong to permit of observation of any Raman lines, attempts were made to eliminate it by purification of the solution by the method described above and by the use of suitable light filters.

Figure 2 shows the enlarged Raman spectrum of the purified solution with an exposure of 15 hours using $NaNO_2$ solution and Noviol glass as filters.

Figure 3 shows the Raman spectrum of the same solution using $NaNO_2$ and Iodine in carbon tetrachloride filters. The time of exposure in this case was 30 hours.

It is evident that in figure 3, the continuous background is least in intensity showing that this combination of filters is most efficient. The Raman lines are prominent enough to permit of the measurement of their wavelengths with a Hilger Comparator. For such of the lines which are broad and diffuse, the location of the maximum with the Comparator not being possible, a microphotometric record of the entire Raman spectrum was taken. From this record, it was easy to find both the position of such lines and their quality in respect of width and diffuseness.

The following table gives the Raman frequencies of sucrose taken as a mean of measurements made with two independant plates. The figures in parentheses indicate the relative visual estimates of the intensities.

TABLE I

Raman Frequencies of Sugar		Raman Frequencies of Glucose		
Solution I	Crystal II	Kutzner (1932) III	Wiemann (1936) IV	Author V
377* (3)	-	—	—	—
464* (3)	423	454	435 ± 25	423 (3)
549* (4) br	549	513	519 ± 11	549 (3)
599* (4) br	—	--	—	—
649	649	—	—	624 (1)
753*	723	—	—	—
856 (5)	846	—	853 ± 10	856
—	—	—	911 ± 14	919
943 (3)	—	—	—	—
—	992	—	—	—
—	—	—	1020 ± 10	—
1088 (10) br	1088	—	1067 ± 12	1064 (7) br
1135 (10) br	1135	1143	1145 ± 9	1159 (10) br
1272	—	—	1200 1262 ± 8	1270
—	1300	—	—	—
1333* 1370* 1408* } Broad diffuse band.	—	—	1373 ± 19	1370
1472 (7) sh	1463	—	1464 ± 7	1463
2865 (7) br	—	—	—	2804 (5) br
3298 3457 3681	—	—	—	3260

For purposes of comparison, the Raman spectrum of Glucose was also investigated. The Glucose employed was Merck's which was further purified by the method adopted for solutions of sucrose. The lines obtained with Glucose were, however, much more feeble than those for sucrose as is evident from Figure 4. Table I, column V, gives the frequencies of Glucose compared with those reported previously by other investigators.

CRYSTALLINE SUCROSE

Sugar was investigated in the solid state also. The crystal powder was contained in a triangular cell, similar to the one used by Krishnamurty [5]. Owing to the inherent difficulty in the technique involved, none of the liquid filters which are generally employed could be used and the filter made use of was the Zeiss C glass expected to transmit only the 4358-line of the mercury arc, so that the excited Raman lines originate out of this line only. A copper trough of small thickness was devised for placing between the mercury arc and the cell containing sugar crystals. Cooling water was kept in constant circulation in the trough to prevent heating and the consequent charring of the crystals. A fairly good spectrum could be obtained with 20 hours' exposure but the Raman lines were masked by the overlapping continuous spectrum and they were so faint as to be barely discernable on the enlarged print which is therefore not reproduced in the plate. Table I, column II gives the frequencies obtained for sugar in the solid state.

DISCUSSION

A reference to Table I would show that many new frequencies (noted with asterisk) have been observed in the present investigation and many points of detail, missed by previous workers, have also been recorded.

The Raman lines in solutions of sucrose may be classified as arising from the C−C, the C−O, the C−H and the δ (C−H) frequencies. Those in the region 800−950, *i.e.*, 943, 856, 753 (?), may be taken as aliphatic C−C frequencies corresponding to similar lines obtained with all aliphatics containing at least two carbon atoms. The C−O frequencies come in the region 1000−1150. In sugar the corresponding frequencies for this band are 1088, 1135. The broad and strong line at 2865 is the valence C−H frequency and the line 1472 is the δ(C−H) frequency. The lines 1333, 1370, seem to be the (C−H) deformation frequencies. But as pointed out by Koteswaram [6] the presence of a strong line at 1392 for formic acid makes this assignment uncertain. The band 3298−3681 with its intensity maximum at 3457 is well known to be due to water.

A comparison of the frequencies obtained for sugar with those for glycerine shows the close resemblance between the two and some of the other frequencies observed in sugar agree well with frequencies found in alcohols.

The following Raman frequencies of sugar bear close resemblance to those of glycerine

464, 549, 649, 856, 943, 1472

and those below compare well with the frequencies found in alcohols

1088, 1135, 1333.

The frequency 1134 is found in the Raman spectrum of butyl and isobutyl alcohols.

Besides these, the low frequencies recorded occur in many of the aliphatic compounds and are usually attributed to the external frequencies between the different groups in these molecules.

Polara (*loc. cit.*) reported a line at 1683, which is attributed to the C=O oscillation, but the author could find no trace of any line in this region with either sucrose or glucose. This is to be expected as there is no C=O in either of the molecules as will be evident from the structural formulæ of these compounds given below :

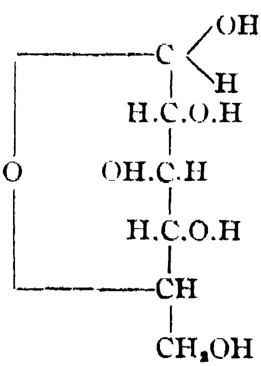

Glucose

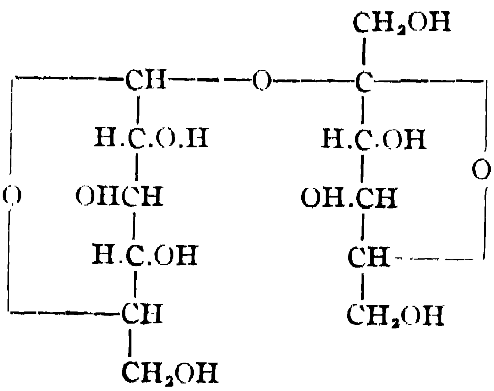

Sucrose

Most of the frequencies obtained by Polara between 2016 and 2718 were not noticed by the author and are highly improbable.

In conclusion, the author desires to express his grateful thanks to Dr. I. Ramakrishna Rao for his helpful guidance throughout the progress of this investigation.

REFERENCES

[1] Whiting and Martin, *Roy. Soc., Canada*, **26**, 96 (1931).
[2] Polara, *Accad. Lincei. Atti.*, **14**, 293 (1931).
[3] Kutzner, *Naturwiss.*, **20**, 331 (1932).
[4] Yajnik and others, *Z. Anorg. Chem.*, **126**, 24 (1935).
[5] Krishnamurty, *Ind. J. Phys.*, 5, 1 (1930).
[6] Koteswaram, *Zeit. f. Phys.*, **110**, 118 (1938).

Fig. 1

Fig. 2

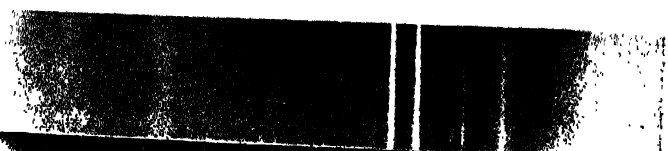

Fig. 4

Fig. 3

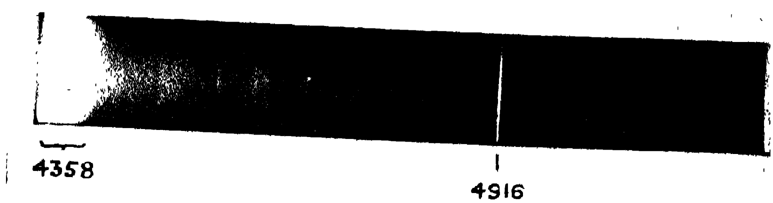

ON THE DIELECTRIC CONSTANT OF AN ELECTRONIC MEDIUM AT MEDIUM RADIO-FREQUENCY*

By S. R. KHASTGIR, D.Sc. (Edin.), Mem.I.R.E.

AND

C. CHOUDHURY, M.Sc.
Dacca University

(Received for publication, May 8, 1940)

ABSTRACT. The results of an investigation on the variation of the dielectric constant of an electronic medium in the anode=screen-grid space of a Philips A 442 valve under various conditions for medium radio-frequencies are given in this paper. The measurements of the effective dielectric constant were made by following the no-beat technique of a double heterodyne method The effect of the conductivity of the medium was allowed for in estimating the effective dielectric constant of such a medium.

The experimental results were found consistent with Lorentz's formula for the dielectric constant of a frictionless electronic medium after introducing a multiplying factor to obtain the effect of the time of stay of the electrons in the inter-electrode space. The multiplying factor was found independent of the wavelength of the measuring field and was found to depend only on the transit time.

The *parabolic* variation in the value of the dielectric constant of the electronic medium with the variation in the *magnitude* of the measuring field as reported by Prasad and Verma was not, however, observed in the experiments performed to test any such variation. In some cases a steady variation was found and this has been explained.

INTRODUCTION

Usually the electronic medium under investigation is a high-vacuum space in a thermionic valve filled with electrons from a heated filament under the influence of an electric field. Since the time of stay of the electrons in the inter-electrode space is only a small fraction of the period which corresponds to the radio-frequency of the alternating field, the contribution of the electrons towards the change of the dielectric constant should therefore be correspondingly small. Benner[1] considered this effect of the finite time of transit of the electrons and deduced a correction factor to the well-known Eccles-Larmor expression for the dielectric constant of a purely electronic medium. Recently Hollmann and Thoma[2] criticised Benner's equations. From their theory of the inversion of electrons and using Maxwell's equations they deduced a formula for dielectric constant of electronic medium, which was different from Benner's. Their main result about the dielectric constant was that as the product of frequency and

* Communicated by the Indian Physical Society

transit-time increases from zero, the dielectric constant followed a damped cyclic curve about unity. The dielectric constant of an electronic medium could therefore be less than, equal to, or greater than unity, the value depending on the product of the frequency and the transit-time.

Coming to the experimental determinations of the dielectric constant of space containing electrons, the results of Bergmann and Düring[3] who were the earliest workers on the subject showed that the dielectric constant of the electronic medium in their investigation was less than unity and steadily diminished with increasing electron concentration. Following Bergmann and Düring's experiments Sil[4] observed a decrease, an increase and also no change of dielectric constant at ultra-high frequency. These experimental results were explained as due to the non-uniform distribution of the electrons in the medium and also due to the effect of the time of stay of the electrons as determined from Benner's formula. Some experiments[5, 6] on the subject with ultra-high-frequency measuring field were also performed in this laboratory. The following were established :

(1) With a definite ultra-high frequency, the effective dielectric constant of the electronic medium in a screen-grid valve was found less than unity and decreased on the whole nearly proportionately with the increase of the anode current.

(2) When the wevelength was changed keeping the anode and screen-grid voltages and the filament current constant, the effective dielectric constant of the medium decreased steadily with the increase of the wavelength. There was, however, an anomaly beyond a certain wavelength when a gradual increase in the value of the dielectric constant was observed. As the wavelength was further increased, the dielectric constant assumed values greater than unity and after attaining a maximum value at a particular wavelength decreased again with further increase of wavelength. It was also observed that the wavelength at which the dielectric constant of the electronic medium attained a maximum value was distinctly larger for the smaller electron concentration.

These results were explained by supposing that the inductance of the short external connection and the inter-electrode capacity of the valve constituted an oscillatory circuit so that the anomaly appeared in the region of the resonance frequency of such an oscillatory circuit. The condition for this resonance according to Hund[7] is the same as that for the plasma electronic resonance of Tonks and Langmuir. This explained also the observed shift of the peak value of the dielectric constant towards the longer wavelength when electron concentration was reduced. It is, however, significant that neither Benner's nor Hollmann and Thoma's formula was found to agree with these experimental results. Attributing, however, a natural frequency to the electrons corresponding to the resononce of the previously mentioned oscillatory circuit in the valve and

introducing a multiplying factor to obtain the effect of the time of stay of the electrons in the inter-electrode space of the valve, the Lorentz expression for the dielectric constant for a frictionless medium was found consistent with these ultra-high frequency measurements.

SCOPE OF THE PRESENT INVESTIGATION

The object of the present investigation was to extend the measurements of dielectric constant of electronic medium to much lower frequencies. Prasad and Verma[8] had previously published some experimental results with medium radio-frequencies between 3.7×10^6 and $.58 \times 10^6$ cycles per sec. (wavelength 51 m. to 512 m.). Following the double-beat method they found the dielectric constant of an electronic medium inside a screen-grid valve always less than unity within the range of the concentrations and the wavelengths employed in their investigations. They showed that (1) the dielectric constant decreased with increasing concentration and that (2) it also decreased with increasing wave-lengths. Their measurements of dielectric constant and the theoretical deductions from these measurements were, however, vitiated by the fact that in determining the dielectric constant of the electronic medium the effect of the conductivity of the medium was not considered at all.

The usual experimental procedure is to measure the capacity between the two electrodes inside a valve with and without electrons filling the inter-electrode space. When the space is filled with electrons there are generally two effects: (1) a change in the dielectric constant of the medium and (2) a conductivity effect. For both of these effects it is expected to obtain a change in the capacity of the oscillating system in the measurement circuit. If the dielectric constant is less than unity, the change in the capacity is a decrease, whereas the effect of the conductivity due to the electrosn, short-circuiting, so to say, the two electrodes in their transit from the filament to the anode of the experimental valve is *always* an increase in the effective capacity necessary to restore the resonance condition of the oscillating system. This latter effect is sometimes appreciable and can be directly tested by putting a high resistance across the two electrodes. Accurate measurements of the effective dielectric constant of the electronic medium for medium radio-frequencies were therfore felt necessary by considering the effect of the conductivity of the medium and investigations were accordingly undertaken. The experiments were arranged in three main parts:

I. Variation of the effective dielectric constant of the electronic medium in the inter-electrode space of a screen-grid valve with the thermionic current through the valve for a definite frequency of the alternating field.

II. Variation of the effective dielectric constant of the similar electronic medium with the frequency of the alternating field for a definite electron concentration.

III. Dependence of the effective dielectric constant of the electronic medium inside a screen-grid valve on the time of stay of electrons in the inter-electrode space.

EXPERIMENTAL ARRANGEMENTS AND PROCEDURE

The experimental condenser consisted of the screen-grid and the anode of a Philips A 442 valve. This condenser of capacity C_V was in parallel with the tuning condenser of capacity C of the oscillatory circuit of a suitable Hartley oscillator. The change in the capacity of C_V when the inter-electrode space was filled with electrons was balanced by changing the capacity of an accurately calibrated small variable vernier air condenser C_A in parallel with C_V and C, so that the total capacity (C_V+C+C_A) remained constant. The high-frequency signal from the oscillator was received by an oscillator-detector valve-circuit which was exactly similar to the oscillator circuit. When the detector circuit was nearly in tune with the oscillator, the familiar heterodyne whistle was heard in the telephones placed in the anode circuit of the receiver. The audio-frequency voltage developed across the telephone was then amplified by a three-valve amplifier of the conventional type and fed into a loudspeaker which gave a loud musical note. On introducing into the same loudspeaker an audio-frequency current from an audio-oscillator capable of producing an intense note of fixed frequency, beats were heard by suitably adjusting the heterodyne frequency. A variable resistence was placed in series with the secondary coil of the audio-oscillator to match the intensity of the heterodyne whistle with that of the audio-frequency note. Adjustments of the variable vernier condenser C_A in the oscillator to produce *no* beats were then made successively *first* when the inter-electrode space was devoid of electrons and *next* when the same space was filled with electrons. In other words, the change in the capacity of C_A was noted with the filament of the experimental valve off and on after having given suitable high voltages to the anode and the screen-grid. To this was added a correction to allow for the effect of the conductivity of the medium. From a knowledge of this corrected change of capacity and the inter-electrode capacity of the valve, the effective dielectric constant of the medium was calculated. The procedure adopted to obtain the conductivity correction will be described in a subsequent section.

The diagram of the entire arrangement is shown in fig. 1. The anode of the experimental valve was given a suitable high voltage from a separate dry battery ; the screen-grid was also given *practically* the same voltage from the same battery through the inductance coil of the Hartley oscillator. The filament of

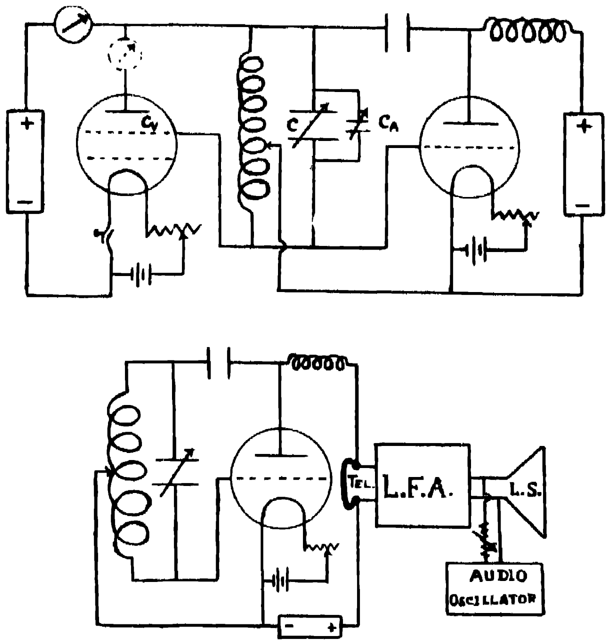

FIGURE 1

the experimental valve was fed by a low tension battery and the filament current was suitably controlled by a rheostat. The variation of the thermionic current through the valve was made by varying the filament current only, the anode and the screen-grid voltages having been kept fixed. The constancy of these voltages ensured the constancy of the time of stay of the electrons in the inter-electrode space, so that the variation of the dielectric constant of the electronic medium with varying thermionic currents (keeping the frequency constant) and the similar variation (for a constant thermionic current) with varying frequencies of the measuring field were studied for a definite value of the transit-time of the electrons.

CORRECTION FOR THE CONDUCTIVITY OF THE ELECTRONIC MEDIUM

In correcting for the conductivity effect the following procedure was adopted.

Let us first consider the set of experiments where the change in the anode= screen-grid capacity of the experimental valve was observed for each different thermionic current through the valve for a definite frequency of the measuring field. Immediately after this set of experiments, the H. F. series-resistance of the electronic medium was measured by the distuning method for each different thermionic current through the valve, the anode and the screen-grid voltages remaining exactly the same as in the preceding experiment. For these

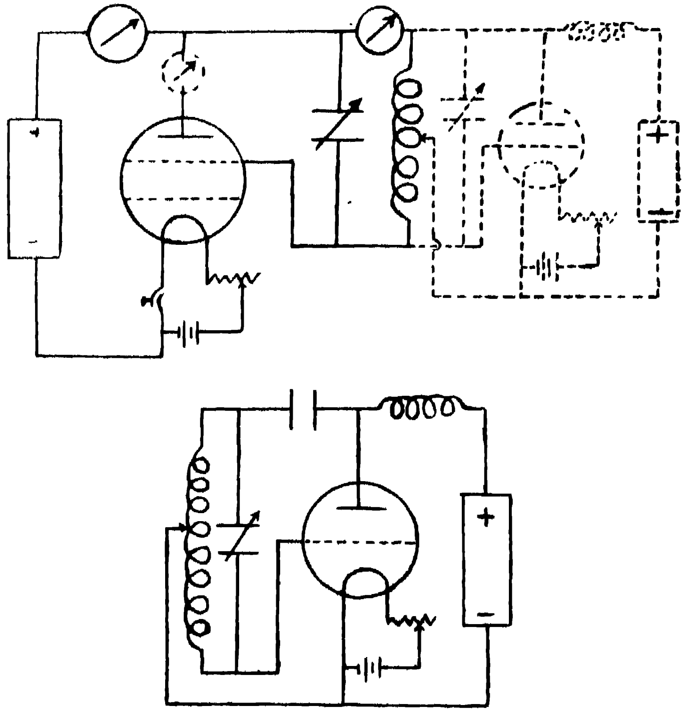

FIGURE 2

measurements the valve of the Hartley oscillator was not worked and only the tuning condenser C of the oscillatory circuit (or the small variable balancing condenser C_A whichever was suitable) and the anode = screen-grid capacity C_V each in parallel with the inductance were used with a radio-frequency thermal galvanometer in the circuit as shown in fig. 2. The detector-oscillator unit was used as a mere oscillator to induce currents into the neighbouring oscillatory circuit. A pair of resonance curves were constructed showing current against the capacity-value, first where the filament was off and next when the filament was on. Pairs of such resonance curves for different thermionic currents through the experimental valve were constructed. From each pair of such resonance curves, the H. F. series-resistance r of the electronic medium was determined by the usual formula. The corresponding shunt resistance R was then calculated for each different thermionic current through the valve by the standard formula

$$R=\frac{1}{\omega^2 C^2 r},$$

where ω is the angular frequency of the field and C the capacity in farads, across which the shunt resistance R is supposed to work. A graph was then plotted showing $1/R$ against the thermionic current. Next in a separate experiment the anode and the screen-grid electrodes of the experimental valve were shunted by different non-inductive metal film high resistances (of negligible self-capacity) and the corresponding increase in the effective capacity of the oscillating system (with no

electrons inside the inter-electrode capacity) due to leakage for each different shunt resistance to restore resonance condition of system was accurately measured by following again the no-beat technique of the double-heterodyne method already described in the previous section. Another graph was then constructed from the observed data showing the increase in the capacity against the reciprocal of the actual shunt-resistance employed. With the help of these two graphs it was possible to obtain the increase in the value of the effective capacity of the oscillating system due to the conductivity of the medium in the inter-electrode capacity. To take an example, let us find the conductivity correction for a definite thermionic current. From the $1/R$ = current graph it is possible to obtain the value of $1/R$ which corresponds to the desired value of the current. The other graph (showing the increase in the capacity of the oscillating system for each actual resistance shunted across the inter-electrode capacity) enables us to obtain the increase in the capacity corresponding to this value of $1/R$ which, as we have already seen from the previous graph, corresponds to the desired value of the thermionic current.

The conductivity correction $(\Delta C)_\sigma$, obtained in this way, was then added to the observed decrease of the anode = screen-grid capacity ΔC for the respective value of the thermionic current through the valve. The change in the capacity due to the dielectric constant change for this value of the current was then given by

$$(\Delta C)_\epsilon = \Delta C + (\Delta C)_\sigma .$$

The dielectric constant was thus calculated from

$$\epsilon = 1 - \frac{(\Delta C)_\epsilon}{C_v} .$$

In the set of experiments where the frequency of the measuring field was varied by keeping the thermionic current constant and the change in the anode = screen-grid capacity observed with the filament of the valve off and on, the procedure for the conductivity-correction was as follows. Working with the circuit diagram shown in fig. 2, pairs of resonance curves were constructed with the same constant thermionic current on and off for various wavelengths within the range of our observations. From each pair of such resonance curves the H. F. resistance r of the medium (with a definite electron concentration) was determined. Thus the corresponding equivalent shunt resistance R as calculated from the series-resistance was obtained for each wavelength λ. A graph was then plotted showing $1/R$ against λ. Next, the anode = screen-grid electrodes were shunted as described before by different non-inductive hgih resistances of negligible self-capacity and the increase in the effective capacity of the oscillating system to restore resonance was determined for each such shunt resistance for the required range of wavelengths by following the no-beat technique of the double-heterodyne method in the way described before. Different graphs were thus obtained showing the increase of effective capacity

against the reciprocal of the actual shunt resistance for different wavelengths. The conductivity corrections $(\Delta C)_\sigma$ corresponding to the various equivalent shunt resistances for respective wavelengths (as known from the previous $1/R=\lambda$ graph) were then determined from these graphs. Each of these corrections was then added to the observed value of ΔC. The dielectric constant of the medium for each different wavelength was thus calculated from the ratio of this total change of capacity to the electron-free inter-electrode capacity

EXPERIMENTAL RESULTS

Variation of the effective dielectric constant of the electronic medium for different thermionic currents for a fixed frequency of the measuring field :

In table I are given the results of a typical set of measurements of the dielectric constant for varying thermionic currents employing a measuring field of 309.9 kc. frequency ($\lambda=750$ m.) These are graphically shown in fig. 3 Two other typical sets of similar measurements for frequencies, 608.5 kc. and

TABLE I

Frequency : 309.9 kc./sec. ($\lambda=750$ m.), Anode = screen-grid capacity = $8\mu\mu f$

Thermionic current	ΔC $\mu\mu f$	Correction $(\Delta C)_\sigma$ $\mu\mu f$	$(\Delta C)_\epsilon$ $\mu\mu f$	ϵ	$\delta=1-\epsilon$	$\frac{\delta}{1-a\delta}$ Lorentz term $a=\frac{1}{3}$
.25 m.a × k	·3	.04	·34	.96	·04	.041
5 ,, ,,	.63	.10	·73	.92	08	.082
·75 ,, ,,	1.1	.16	1.26	.84	.16	17
1.00 ,, ,,	1.4	.22	1 62	·79	.21	·23
1.25 ,, ,,	2.1	28	2.38	·70	30	33
1.5 ,, ,,	2.6	·36	2.96	.63	·37	·42
1.75 ,, ,,	3·2	.48	3.68	·54	46	·54
2.0 ,, ,,	3 7	.64	1·34	·46	·54	.66
2.25 ,, ,,	4 3	·74	5 04	·37	.63	.80
2 5 ,, ,,	5.0	.81	5.81	.28	·72	·94

811 kc. ($\lambda=493$ m. and $\lambda=370$ m.), are illustrated in fig. 4. In both the figures the values of dielectric constant ϵ of the electronic medium are plotted against

various values of the anode current. In fig. 3 are also shown the values of $\delta\,(=1-\epsilon)$ and of $\frac{\delta}{1-a\delta}$ against the different values of the anode current for

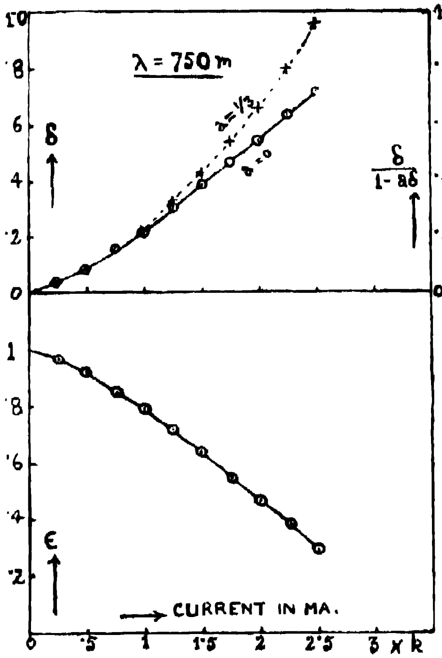

FIGURE 3

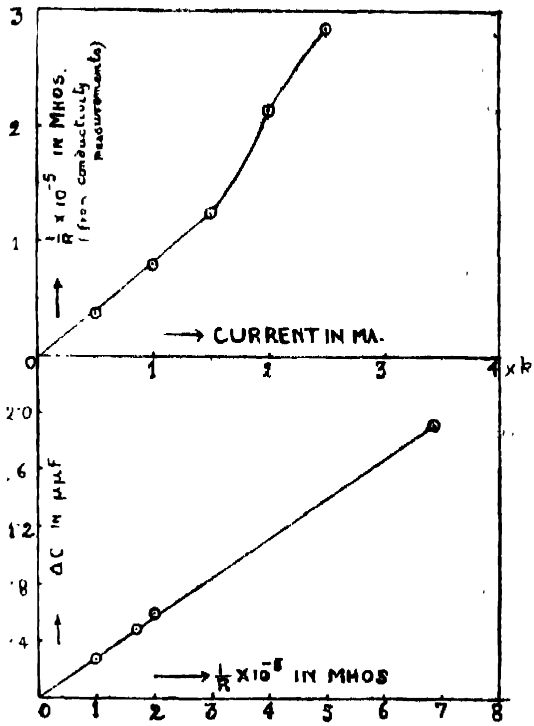

FIGURE 3(*a*)

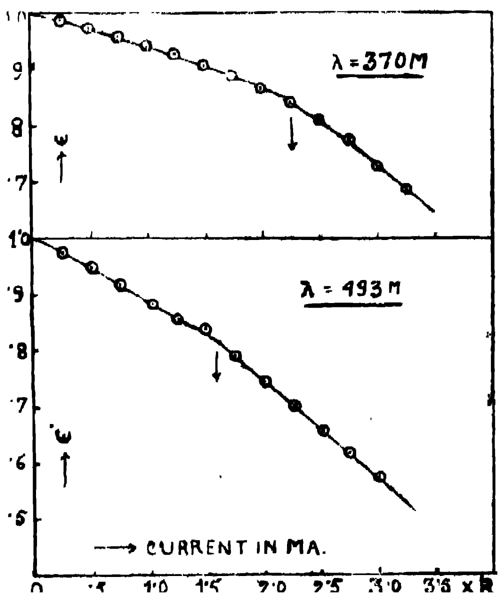

FIGURE 4

$\lambda=750$ m. (freq: 399.9 kc.) of the measuring field ('a' being the Lorentz term). The calibration graphs from which the conductivity corrections were made for this set are shown in fig. 3(a).

It can be seen from fig. 3 that for $\lambda=750$ metres, a linear relation holds between the dielectric constant of the electronic medium and the thermionic current, except for very small values of the latter. The linear relation also seems to hold for the other two wavelengths except for a sudden discontinuity in each case at a certain value of the thermionic current. The discontinuity in each diagram of fig. 4 is indicated by an arrow mark.

DEDUCTIONS FROM THE ABOVE EXPERIMENTS

Accepting Lorentz's expression for the dielectric constant of a frictionless electronic medium and introducing a multiplying factor μ to obtain the effect of the finite time of stay of the electrons in the inter-electrode space, we have

$$\epsilon=n^2-\frac{c^2k^2}{\omega^2}=1-\frac{4\pi N\mu e^2}{m\omega^2+a(4\pi N\mu e} \qquad (1)$$

where ϵ = dielectric constant, μ = a multiplying factor,

k = absorption index, n = refractive index,

ω = angular frequency of the measuring field, c = velocity of light,

N = elctron concentration, a = Lorentz term,

e = charge on an electron, m = mass of an electron.

Putting $\delta=1-\epsilon$ we obtain

$$\frac{\delta}{1-a\delta}=\frac{4\pi e^2(N\mu)}{m\omega^2} \qquad \ldots \quad (2)$$

When $a=0$
$$\delta=\frac{4\pi e^2}{m\omega^2}(N\mu).$$

If the anode and the screen-grid voltages are kept fixed throughout a set of measurements it is evident that the velocity of the electrons would remain constant so that the electron concentration could be normally taken as proportional to the thermionic current* through the anode=screen-grid space. Again, since the time of stay of the electrons in the inter-electrode space and the frequency are usually kept fixed in one set of observations, the multiplying factor could be regarded as constant so that for the Lorentz formula to hold, $\frac{\delta}{1-a\delta}$ should vary directly as the thermionic current. In fig. 3, both δ and $\frac{\delta}{1-a\delta}$

are plotted against the thermionic current for one set of observations (freq. 399.9 kc./sec., λ =750 m.). The variation of ϵ is also shown in the same diagram. It will be seen from fig. 3 that δ or ϵ was found to vary proportionately with the thermionic current except when the latter was very small. The law of direct proportionality, however, fails when the values of $\frac{\delta}{1-a\delta}$ are plotted for the different values of the thermionic current. The conclusion that can be drawn under the circumstances is that either the Lorentz term $a=0$ or alternatively for some unknown reason the electron density increased with the increase of the thermionic current at a rate more than the proportionate rate of increase The latter could perhaps be expected if the secondary electrons were emitted at the anode and the screen-grid surfaces.

Variation of the effective dielectric constant of the electronic medium with the wavelength (or frequency) of the measuring field for a definite electron concentration of the medium

The experimental data for the evaluation of the dielectric constant of the electronic medium are collected in table II. The observed shift ΔC, the con ductivity correction $(\Delta C)_\sigma$ and the corrected shift $(\Delta C)_\epsilon$ due to the dielectric constant change alone are all entered in separate columns.

TABLE II

Thermionic current = 1.5 m.a. × k. Inter-electrode capacity = $8\mu\mu f$.

Wavelength (Metres)	λ^2 Sq.cm.	ΔC $\mu\mu f$	Conductivity Correction $(\Delta C)_\sigma$ $\mu\mu f$	$(\Delta C)_\epsilon$	ϵ	δ	$\frac{\delta}{1-a\delta}$ $a=\frac{1}{3}$
350	1.225 × 10^9	.35	.30	.05	.92	.08	.082
400	1.600 ,,	.40	50	.90	.89	.11	.114
450	2.025 ,,	.55	.65	1.20	.85	.15	.16
500	2.05 ,,	.65	.78	1.43	.82	.18	.19
550	3.025 ,,	.80	.83	1.63	.80	.203	.22
600	3.60 ,,	1.2	.83	2.03	.75	.253	.28
650	4.225 ,,	1.6	.78	2.38	.70	.30	.33
700	4.9 ,,	2.1	.6	2.70	.66	.34	.38
750	5.69 ,,	2.75	.34	3.09	.61	.39	.45

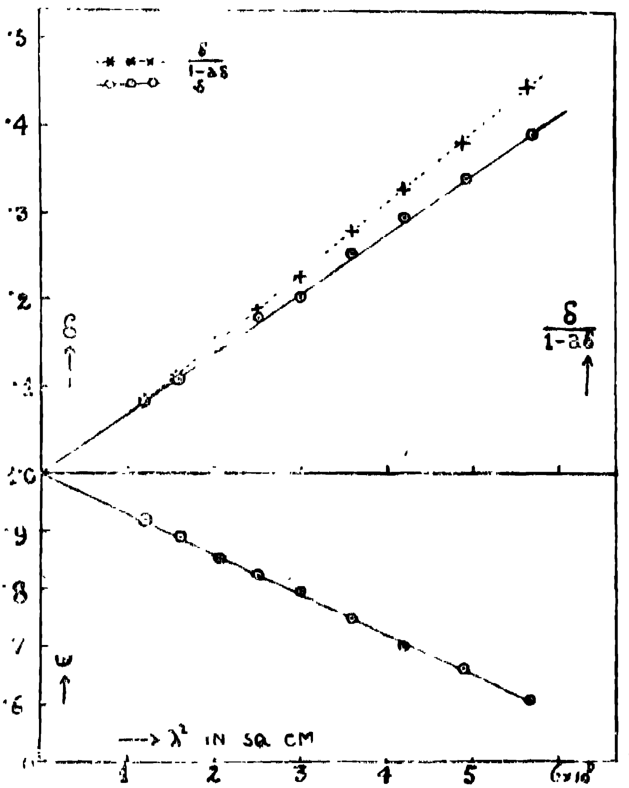

FIGURE 5

The results are graphically shown in fig. 5. In the diagram the values of ϵ, δ and $\frac{\delta}{1-a\delta}$ are plotted against the squares of wavelengths employed. It is interesting to find that all the curves are practically straight lines.

DEDUCTIONS FROM THE ABOVE EXPERIMENTAL RESULTS

The multiplying factor μ introduced in the Lorentz expression for the dielectric constant of a frictionless electronic medium can be expressed in the form

$$\mu = \frac{A}{\lambda} \cdot f(t), \qquad \cdots \quad (3)$$

where t is the transit-time of the electrons, λ the wavelength of the measuring field and A a constant. From the expression given in (2) we therefore get

$$\frac{\delta}{1-a\delta} = \frac{\lambda^2 e^2 N}{\pi m c^2}\left(\frac{A}{\lambda}\right). f(t).$$

On neglecting Lorentz term we have

$$\delta = \frac{\lambda^2 e^2 N}{\pi m c^2}\left(\frac{A}{\lambda}\right). f(t).$$

In the experiments the results of which are recorded in the last section, t = const. and N = const. We have also seen from fig. 5 that both δ or ϵ and $\frac{\delta}{1-a\delta}$ when plotted against λ^2 gave straight lines, so that it can be said that $\frac{A}{\lambda}$ = const. In other words it can be concluded that the constant A in the multiplying factor is proportional to the wavelength λ.

DEPENDENCE OF THE DIELECTRIC CONSTANT OF THE ELECTRONIC MEDIUM ON THE TRANSIT-TIME OF THE ELECTRONS

Keeping the thermionic current through the inter-electrode capacity fixed at a certain value and working with a fixed frequency of the measuring field, the effect of varying the time of stay of the electrons on the dielectric constant of the electronic medium was studied. The time of stay was varied by varying the anode or the screen-grid voltage, but the thermionic current through the anode-screen-grid space was kept constant by adjusting the filament current. The higher the voltage V, the smaller is the transit-time t of the electrons. In fact, we can write $t \propto \frac{1}{\sqrt{V}}$, so that when N = const., ω = const., it can be seen that

$$\frac{\delta}{1-a\delta} \propto f(t) \propto f\left(\frac{1}{\sqrt{V}}\right),$$

since $\frac{A}{\lambda}$ = const. or approximately $\Delta C \propto f\left(\frac{1}{\sqrt{V}}\right)$,

where ΔC is the observed change of inter-electrode capacity when the inter-electrode space is filled with electrons. In fig. 6 are shown two curves for two different frequencies of the measuring field. The values of ΔC are plotted against $\frac{1}{\sqrt{V}}$ in this figure.

It is evident that ΔC increased steadily with the diminution of the voltage, *i.e.*, with the increase of the transit-time t.

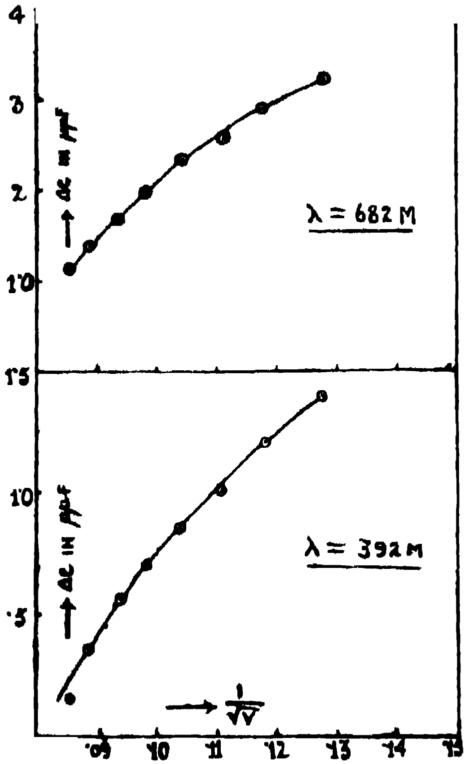

FIGURE 6

DEPENDENCE OF THE DIELECTRIC CONSTANT OF THE ELECTRONIC MEDIUM ON THE MAGNITUDE OF THE MEASURING FIELD

Prasad and Verma[8] reported a parabolic variation in the value of the dielectric constant of the medium with the variation of the magnitude of the measuring field. With ultra-high frequencies the results of some experiments in this laboratory definitely showed that the dielectric constant was independent of the magnitude. It has, however, been recently shown[9] that since in Prasad and Verma's experiments, the adjustment of the balancing condenser (to make up for the change of the inter-electrode capacity) was made till a fixed number of beats were heard per second, the distortion in the receiving set arising out of the non-linear performance of the detector unit was likely to give rise to such an apparent dependence. To test such dependence, if there is really any, the adjustment of the balancing condenser should be made for no-beat. When there is no beat, the complication arising from non-linear distortion is eliminated. Some experiments were therefore performed to examine whether the variation of the magnitude of the measuring field would affect the value of the dielectric constant by following the no-beat technique. The magnitude of the measuring field was varied in these experiments by varying the plate voltage of the valve-oscillator. To obtain an estimate of the voltage of the H. F. field across the inter-electrode capacity, the current in the balancing condenser branch was

measured. This current when multiplied by the reactance of this branch would give the desired H. F. voltage. Since the capacity of the balancing condenser was changed only to a small extent, the voltage could be approximately measured in terms of this current. The thermionic current through the anode=screen-grid space was kept fixed during the test.

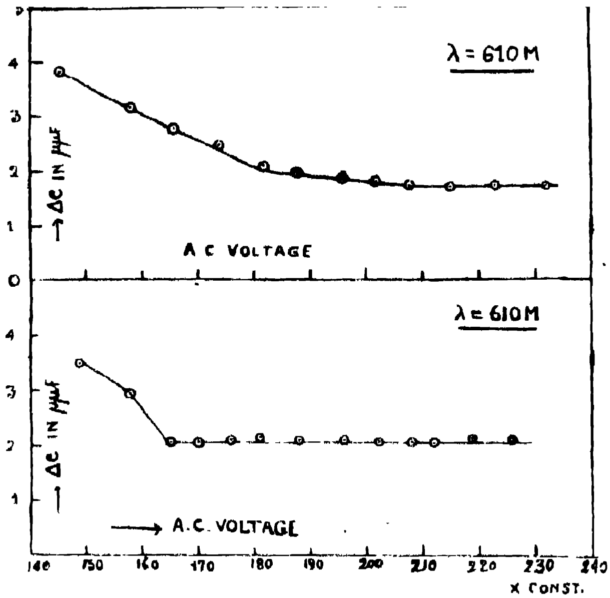

FIGURE 7

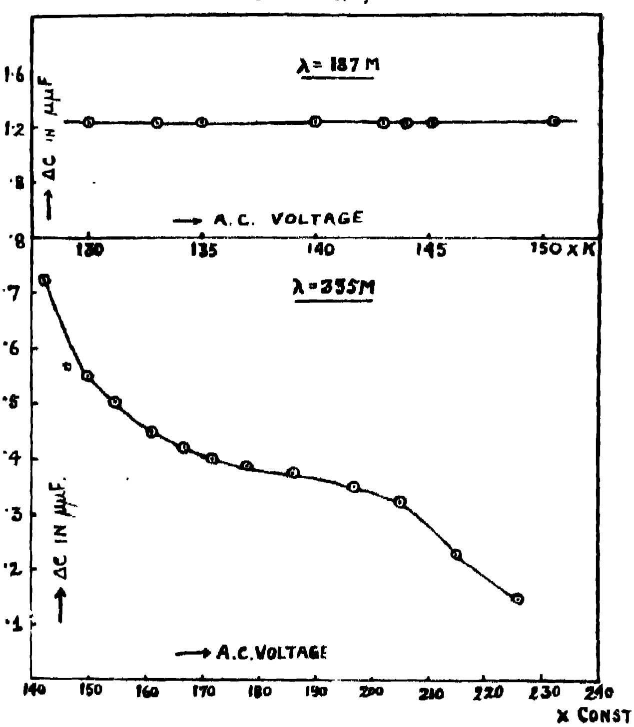

FIGURE 8

In fig. 7 are shown the results of two sets of experiments for $\lambda=610$ m.

It can be seen that for small H. F. voltages of the measuring field, ΔC diminished with the increase of voltage but ultimately it steadied down to a constant value. Similar experiments were performed with higher frequencies. These results are graphically shown in fig. 8.

It is significant that for $\lambda=187$ m. ΔC remained constant throughout the range of H. F. voltages of the measuring field. For $\lambda=335$ m. the diminution persisted even for the higher voltages. The experiments with wavelengths in the neighbourhood of 300 m. were performed many times—but the results were all similar.

The amplitude of the electrons moving under the action of an alternating field is given by $\frac{eF_m}{\omega^2 m}$, where F_m is the peak value of the applied field. As F_m is increased, the amplitude is increased. For the smaller values of F_m the electrons may not be able to reach the anode surface. So long the anode is not reached the conductivity of the space must be small, *i.e.*, the equivalent shunt resistance across it rather higher. This resistance would gradually fall with the increasing value of F_m. Ultimately when the anode is reached by the electrons, this resistance would fall to a constant value. In other words, the conductivity correction $(\Delta C)_\sigma$ for the smaller voltages should be small ; it would gradually increase and attain a constant value for the higher voltages. Since the observed ΔC is equal to $(\Delta C)_\epsilon - (\Delta C)_\sigma$, the observed diminution of ΔC and the ultimate constancy of ΔC with the increasing voltage of the measuring field could be explained. In the case when the diminution of ΔC persisted with the increasing voltage it can perhaps be said that the amplitude of the electrons did not extend sufficiently to reach the anode surface.

SUMMARY AND CONCLUSIONS

In this paper are recorded the results of an investigation on the variation of the effective dielectric constant of an electronic medium in the anode=screen-grid space of a Philips A442 valve under various conditions for medium rodio-frequencies. The measurements of the effective dielectric constant were made, by following the no-beat technique of a double heterodyne method. The corrections for the conductivity of the medium were made in estimating the dielectric constants. The procedure for carrying out these conductivity corrections are fully described.

The experimental results have been analysed following Lorentz's formula for the dielectric constant of a frictionless electronic medium. A multiplying factor μ has been introduced in the expression to obtain the effect of the time of stay of the electrons in the inter-electrode space. The factor has been expressed

in the form $\mu = \frac{A}{\lambda} . f(t)$, where A is a const., t the transit-time and λ the wave-length of the measuring field.

Working with a definite frequency and keeping the transit-time of the electrons fixed, the effective dielectric constant of the electronic medium was found on the whole to decrease almost proportionately with the increase of the thermionic current. This is what is expected from Lorentz's formula.

When the frequency was changed, keeping the thermionic current and the transit-time fixed, the effective dielectric constant of the medium was found to decrease strictly proportionately with the square of the wavelength of the measuring field. In order to fit in with the Lorentz's formula (after introducing the factor μ) it was concluded that the transit-time factor μ must be independent of the wavelength. The constant A should therefore vary directly as the wavelength.

Keeping the thermionic current through the anode=sceen-grid space constant and working with a fixed frequency it was found that the observed change of capacity on filling the inter-electrode space with electrons increased steadily with the increase of the transit-time of the electrons. This meant that the effective dielectric constant of the electronic medium in these experiments decreased steadily with the increase of the transit-time. It is therefore concluded that the multiplying factor μ depends only on the transit-time.

PHYSICS DEPT.,
DACCA UNIVERSITY.

REFERENCES

1 Benner, *Ann. d. Physik*, 5, 3, 993 (1929)

2 Hollmann and Thoma, *Ann. d. Physik*, 5, 32 (1938).

3 Bergmann and Düring, *Ann. der Physik*, ser. V, Vol. i, No. 48, May (1929).

4 Sil, *Phil Mag.*, **16**, 1114 (1933).

5 Khastgir and Imam, *Ind. Jour. Physics*, **11** 37 (1937).

6 Khastgir and Sirajuddin, *Phil. Mag*, **28**, 532, (1939).

7 Hund, Phenomena in high-frequency systems, 1st edition, p. 21 (1936).

8 Prasad and Verma, *Zeits. f. Physik*, *Band*, 99, 7 and 8 heft.

" " " " " 107, 7 and 8 heft.

9 Khastgir and Serajuddin, *Zeits. f. Physik*, **111**, 475 (1939).

DETERMINATION OF THE STRUCTURE OF META-DINITROBENZENE BY PATTERSON FOURIER SUMMATION *

By K. BANERJEE, D.Sc., F.N.I.
Reader in Physics

AND

M. GANGULY, M.Sc.
Bengal Govt. Research Scholar, Dacca University

(Received for publication, May 30, 1940)

ABSTRACT. The structure of meta-dinitrobenzene has been studied by the Patterson Fourier Summation Method. Relative values of the integrated intensities of reflections from the hko planes have been measured from Weissenberg goniometer photographs by the help of a Zeiss microphotometer. By using needle shaped crystals much elongated along the c-axis, a single traversal of the scanning spot of light was found necessary and a considerable economy of labour was thus effected. The absolute intensities were obtained by comparison with reflections from rocksalt in a powder photograph of a mixture of known proportion of metadinitrobenzene and rock-salt. From the projections on the (001) plane of the different interatomic vectors in the unit cell obtained by Patterson Analysis a preliminary determination of the atomic arrangements has been made.

INTRODUCTION

Meta-dinitrobenzene crystallises in the orthorhombic bipyramidal class.[1] The space-group has been determined independently by Hertel and Schneider[2] and by Hendricks.[3] They found that this crystal belongs to the space-group D_{2h}^{16}Pbnm with a unit cell containing 4 molecules having dimensions $a_0 = 13.3$ Å, $b_0 = 14.2$ Å, $c_0 = 3.82$ Å. Thus it was concluded that the molecule had a plane of symmetry parallel to the 001 plane and as the dimension of the c axis is very short the plane of symmetry must be along the benzene ring. This is very unusual for the benzene rings in aromatic compounds. Because none of the aromatic compounds that have been so far studied except this one show a plane of symmetry along the plane of the benzene ring. Further N—O bonds must either lie parallel to the benzene plane or lie symmetrically on the two sides of the N atom in a plane perpendicular to the molecular plane. The former alterna-

* Communication by the Indian Physical Society.

tive is ruled out as it was shown by Hendricks[3] that it is impossible thereby to explain the intensities of the 001 planes. As regards the N-O bonds in para-dinitrobenzene, there is however, a controversy[4] as regards whether the bonds are symmetrical about N, but here the two bonds come out to be symmetrical as a consequence of the space-group. Thus it is very useful to see whether these bonds are similar or not to the N-O bonds in the para-compound. In order to decide this point as well as to determine the structure of a benzene ring having a plane of symmetry along the plane of the ring, a complete analysis of the structure of this compound has been taken up. A projection on the 001 face should show all the different atoms separated out except that the two oxygen atoms attached to a single nitrogen atom will be superposed on each other. So this projection will give us practically the complete structure.

An attempt at determining the x and y co-ordinates of the atoms by a trial and error method proved unsuccessful due to the number of unknown parameters as well as the uncertainties about the atomic structure factors of oxygen and nitrogen. So a Patterson analysis of this projection has been presented in this paper.

EXPERIMENTAL

Meta-dinitrobenzene was crystallised from absolute alcohol. Long, very narrow needle-shaped crystals were obtained, c-axes of which are parallel to the lengths of the crystals. This shape has an advantage in measuring the intensities, as we may consider the intensity of a diffraction spot to be uniform over its length. Such a crystal was mounted on the Weissenberg goniometer with the c-axis along the axis of rotation and at the initial position the x-ray beam was made parallel to the a-axis. These adjustments were made with the help of a Czapski two-circle goniometer. Copper $K\alpha$ radiation was used. The spots were indexed by the help of charts prepared according to Wooster and Wooster's[5] method. Intensities of the spots were measured with the help of a Zeiss microphotometer, by allowing the scanning light to traverse across the centre of the spots. The photometer records were converted to intensities by the help of a standard wedge obtained in the manner of Robinson.[6] Intensity curves were thus obtained from the photometer curves by point to point plotting and the relative values of integrated intensity were determined by finding the areas under the intensity curves.

For measurements of the absolute intensities a powder photograph was taken with a stick prepared with known proportions of meta-dinitrobenzene and rock-salt. The lines (130) and (310) due to the former could be identified uniquely and were well separated from the nearest lines. The integrated intensities of these lines were compared with the (200) and (220) lines of rock-salt. From the

known structure factors of rock-salt the structure factors for these two reflections could be calculated according to the relation

$$\frac{I_m}{I_r} = \frac{\left(\frac{1}{abc}\right)^2 p_m \cdot F_m^{\,2} \cdot \frac{m_m}{\rho_m} \cdot \frac{1+\cos^2 2\theta_m}{\sin 2\theta_m \cdot \sin\theta_m}}{\left(\frac{1}{a_0^3}\right)^2 \cdot p_r \cdot F_r^{\,2} \cdot \frac{m_r}{\rho_r} \cdot \frac{1+\cos^2 2\theta_r}{\sin 2\theta_r \cdot \sin\theta_r}}$$

where $\frac{I_m}{I_r}$ is the ratio of the integrated intensities of the meta-dinitrobenzene line and rock-salt line measured from the powder photograph. a, b, c are the cell dimensions of meta-dinitrobenzene and a_0 is the length of the unit cell of rock-salt. $\frac{m_m}{m_r}$ is the ratio of the masses of the two substances taken in the powder stick.

p = number of equivalent planes.

F = structure factor.

ρ = density.

θ = glancing angle and the subscripts m and r refer to metadinitrobenzene and rock-salt respectively.

The values of the structure factors of (130) and (310) planes thus obtained were utilised in determining the absolute values of the structure factors of all other planes from the relative measurements. The values of the structure factors obtained thus are given in Table I.

TABLE I

Plane	Structure factor	Plane	Structure factor
040	46 3	370	29.0
060	56.7	400	57.2
080	37.0	420	44.2
0(12)0	27.7	430	22.1
120	43.5	450	30.5
130	67 7	510	34.9
140	56.0	520	58.3
160	33.8	530	27.6
210	42.0	540	25.0
220	35.0	560	34.3
230	45.7	570	33.9
240	26.8	580	29.2
250	40.1	600	70.4
270	27.5	620	29.2
310	72.9	710	60.2
330	44.3	720	30.7
340	25.9	800	19.3
350	26 7	(10)00	26.2
360	69.1	—	—

For the Patterson summation a quarter of the cell is taken so that $a/2$ and $b/2$ are the sides. The whole cell can be obtained from this by the appli-

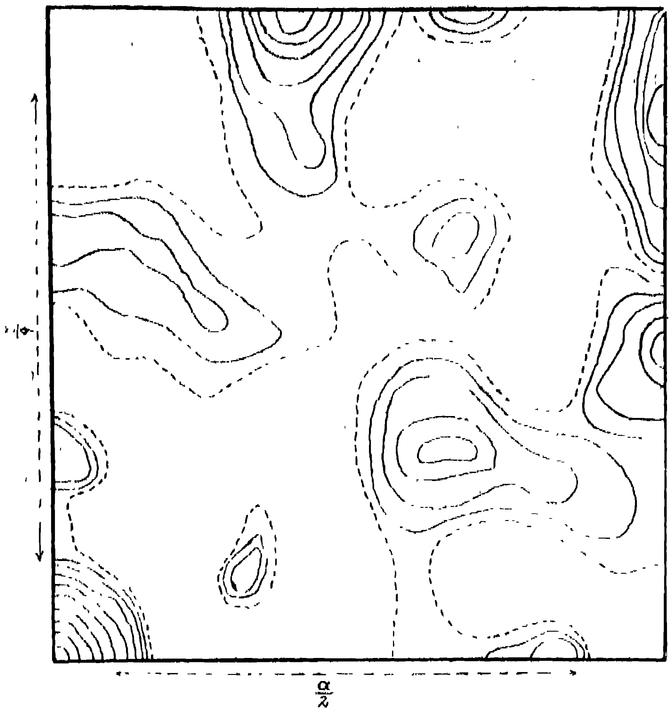

FIGURE 1

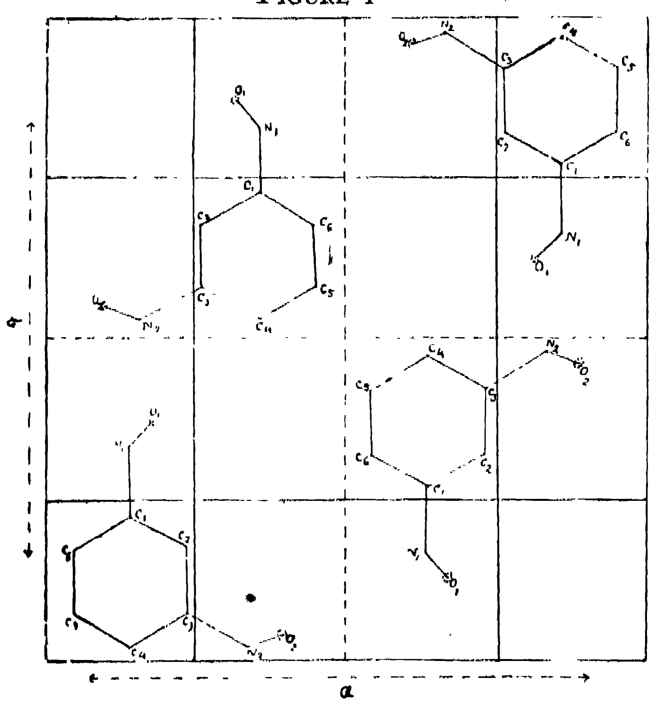

FIGURE 2

cation of the planes of symmetry. Each side was divided into sub-divisions of $a/24$ and $b/24$ and the Patterson densities were calculated according to

$$A_{(x,y)} = \sum^{h=c} \sum_{k=-a}^{k=a} F^2_{(hko)} \cdot e^{2\pi i\left(\frac{hx}{a} + \frac{ky}{b}\right)}$$

where $A\ (x, y)$ is the Patterson sum at the point x, y. By plotting these Patterson sums lines are drawn through points of equal density and are shown in Figure 1.

The peaks of the diagram are then correlated with the different interatomic vectors and the magnitudes of these vectors with their inclinations with the x-axis obtained in this way are given in Table II, the symbols for the different atoms used in this table will be understood from a reference to Figure 2 where is given the arrangement of the meta-dinitrobenzene molecule in the unit cell as can expiain these interatomic vectors :

TABLE II

Interatomic Distance Vectors

[Each of O_1 and O_2 represents the projections of two oxygen atoms]

Atomic pair	Interatomic distance	Angle with 'a' axis
$C_{1a}O_{1a}$; $C_{1d}O_{1d}$	2.2Å	79°
$C_{3c}O_{2c}$; $C_{3b}O_{2b}$	2.2Å	25°
$C_{1a}N_{1a}$; $C_{1b}N_{1b}$; $C_{4c}N_{1c}$; $C_{1d}N_{1d}$	4.3Å	90°
$C_{6b}N_{2b}$; $C_{6c}N_{2c}$	4.3Å	30°
$C_{4a}O_{1a}$; $C_{4d}O_{1d}$	4.8Å	84°
$C_{6b}O_{2b}$; $C_{6c}O_{2c}$	4.8Å	24°
$C_{1a}C_{1b}$; $C_{2a}C_{6b}$; $C_{3a}C_{5b}$; $C_{4a}C_{4b}$; $C_{5a}C_{3b}$; $C_{6a}C_{2b}$; $N_{1a}N_{2b}$; $C_{1c}C_{1d}$; $C_{2c}C_{6d}$; $C_{3c}C_{5d}$; $C_{4c}C_{4d}$; $C_{5c}C_{3d}$; $C_{6c}C_{2d}$; $N_{1c}N_{2d}$	7.5Å	70°
$C_{1a}C_{4c}$; $C_{2a}C_{3c}$; $C_{3a}C_{2c}$; $C_{4a}C_{1c}$; $C_{5a}C_{6c}$; $C_{1b}C_{4d}$; $C_{2b}C_{3d}$; $C_{6a}C_{5c}$; $C_{3b}C_{2d}$; $C_{4b}C_{1d}$; $C_{5b}C_{6d}$; $C_{6b}C_{5d}$	7.5Å	27°
$O_{1a}O_{2c}$; $O_{1b}O_{2d}$	4.3Å	22°
$N_{1a}C_{5c}$; $N_{1b}C_{3d}$; $C_{1a}C_{6c}$; $C_{1b}C_{2d}$	5.6Å	17°
$C_{4a}C_{4c}$; $C_{4b}C_{4d}$; $N_{2a}N_{2c}$; $N_{2b}N_{2d}$	8 9Å	41°
$N_{1b}C_{2d}$; $N_{1a}C_{6c}$; $N_{1d}C_{6b}$; $N_{1c}C_{2a}$	5.4Å	2°
$N_{1a}C_{6b}$; $N_{2d}C_{6c}$	6.3Å	48°
$N_{1a}C_{3b}$; $N_{1d}C_{3c}$	4 0Å	66°
$C_{2c}O_{1d}$; $O_{1a}C_{2b}$	4.5Å	75°

The atomic parameters are deduced as an approximation from this structure and are given in Table III.

TABLE III

Atomic parameters

Atom	x/a	y/b
C_1	0.146	0.224
C_2	0.237	0.174
C_3	0.237	0.076
C_4	0.146	0.0264
C_5	0.055	0.076
C_6	0.055	0.174
N_1	0.146	0.329
N_2	0.303	0.023
O_1	0.172	0.372
O_2	0.386	0.033

Fourier projections on the three crystallographic planes are being attempted on the basis of this result.

Our thanks are due to Prof. S. N. Bose for providing facilities for the work and one of the authors is grateful to the Education Department of the Government of Bengal, for providing him with a scholarship that has enabled him to carry out this work.

REFERENCES

1. P. Groth., *Chem. Krist.*, Vol. IV, 14.
2. Hertel and Schneider, *Z. Physik. Chem.*, **7B**, 188 (1930).
3. S. B. Hendricks, *Journ. Amer. Chem. Soc.*, **53**, 4280 (1931).
4. K. Banerjee, *Phil. Mag.*, **18**, 1004 (1934); R. W. James, G. King and H. Horrocks, *Proc. Roy. Soc.*, **153A** (1936).
5. W. A Wooster and Nora Wooster, *Zeits f. Krist.*, **84**, 327 (1933).
6. B. W. G. Robinson, *Journ. Sci. Instr.*, **10**, 233 (1933).
7. A. L. Patterson, *Phys. Rev.*, **46**, 372 (1934).

A NOTE ON THE REFRACTIVE INDEX OF SHELLAC *

By G. N. BHATTACHARYA, M.Sc.
Indian Lac Research Institute, Ranchi

(*Received for publication, May 1, 1940*)

INTRODUCTION

ABSTRACT. Refractive indices of various samples of shellac, lac constituents, and a few other natural and synthetic resins have been determined using the ordinary type of Abbe Refractometer by a simple technique at different temperatures between 20°C and 90°C. From the curves representing the variation of refractive indices of these with temperature, their softening ranges have been found and implications discussed. The temperature coefficients have also been calculated for the different linear portions. It has been suggested in the paper that the determination of refractive indices of all low melting resins may be rapidly and easily made by adopting this simple technique instead of the hitherto followed lens and reflection-type refractomer methods. Houwink's observation that the refractive index of shellac increases on polymerisation by heat has also been confirmed.

The refractive index is one of the most important optical properties which are frequently used for the identification of various solids, liquids and gaseous substances or for the testing of their purity. The appearance of varnish films and paint coatings depends to a large extent on this important characteristic. The relative refractive indices of some fillers used in lacquer and rubber industries are responsible for their transparency. In fact, even most of the non-crystalline substances as for example, artificial silk fibres, wool, cotton, pigments, etc., are also subjected to an examination in regard to their refractive indices.

Bradley [1] has shown the importance of the application of refractive index in the case of resins. He used oblique illumination immersion method and found out correlation of this characteristic of resins with their general physical and chemical properties as a basis for their identification. By using a crystal refractometer Greger [2] also correlated refractive indices of resins with their general physical properties, as for example, density, hardness, melting point, solubility, etc. But the absence of an accurate and easy method, such as the use of a compact and full-proof instrument like the Abbe Refractometer, has been regretted by many workers.[3] Hanstock,[4] therefore, devised a simple method of determining refractive indices of resins by measuring the focal length of a combination of

* Communicated by the Indian Physical Society.

two convex lenses and interposing later on the resinous substance in the form of a concave lens cast between the above two convex lenses. Houwink[5] made use of the immersion method and determined the refractive indices of many synthetic and a few natural resins before and after their polymerisation by heating. His study has thrown some light on the structure of these substances. The Hanstock lens method has been used by Thakur and Aldis[6] as well as Verman[7] for a comprehensive study of various lac samples and their constituents. But, though the lens method is simple, however, in principle, some have admitted that it is 'cumbersome' for occasional examination. Very recently West[8] has published several methods of increasing the distinctness of the border line in the field of view of the Abbe Refractometer when the reflection method is used for the measurement of refractive index of resins and plastic bodies. To increase the contrast between the two halves of the field of view he has used polarised light, a polarizing screen between the source of illumination and the front prism as as well as a cap analyser over the eye piece. Though he has claimed some practical advantage for this polarising method, there cannot be any doubt about the superiority of the method of measurement by the transmitted light in the Abbe Refractometer. The object of the present paper is to show that the standard type of the Abbe refractometer can be used for the determination of the refractive index of all low melting resins, natural or synthetic, by a simple technique to eliminate the obvious difficulties, and also to provide correct data for various lac samples corresponding to sodium light at different temperatures. The range through which the refractive index of a genuine lac sample varies has been investigated and discussed at length by Thakur and Aldis[6] and so it was not undertaken by the present author.

EXPERIMENTAL

A Zeiss refractometer with heatable prisms was used for the determination of refractive index of various samples of lac and a few other natural and synthetic resins. An arrangement was made for continuously passing water at any desired temperature through the refractometer prisms with the usual spiral heater and adjustable water-pressure regulator, which are generally supplied with the instrument. Any other arrangement, such as, for example, the circulation of a liquid from a thermostat through the prisms, might have been used. The thermometer usually supplied with the instrument has a graduation up to 75°C. This was replaced by an ordinary thermometer reading up to 100°C.

A small quantity of the resin was then slowly melted on a crucible and carefully applied on the surface of the lower prism, which was kept at or slightly above the melting point of the resin. It has been found that at this temperature the substance spreads itself quite satisfactorily and small air bubbles that may sometimes get entangled in the molten resin during application on the prism

surface are easily eliminated if some time (1 or 2 mins.) is allowed to elapse before the prisms are closed. Readings may be taken at any lower temperature now, provided the cooling is gradual and slow. A sudden cooling may produce fine cracks in the resin film resulting in the indistinctness of the line of separation. Moreover, this may put excessive strain on the expensive prisms, though gradual heating or cooling will not affect them. A strong source of illumination facilitates easy and rapid working. A 100-watt, 220-volt opal glass lamp and, also, Bausch and Lomb microscope lamp were used successively by the author with success. A piece of black paper as a screen in front of the compensator to shut off extraneous light was found to give better contrast. Refractive indices were thus determined at different temperatures between 20° C and 100° C. In order to open the prisms for cleaning, the temperature was always raised above the melting point of the resin, when these could be opened and cleaned easily with some cotton wool soaked in a suitable solvent.

RESULTS

The results of refractive-index measurement by this method have been shown in Tables I and II. Data on various samples of lac at different temperatures have been incorporated in Table I, whilst those of lac constituents and other resins in Table II. For the sake of comparison with other available data a separate table (Table III) has been compiled with references. Table IV shows the temperature coefficients of refractive indices.

TABLE I

Lac samples	Refractive Index at							
	20° C	30° C	40° C	50° C	60° C	70° C	80° C	90° C
Kusum shellac	1·5224	1·5210	1·5192	1·5170	1·5130	1·5050	1·5014	1·4980
Palas shellac	1·5235	1·5220	1·5200	1·5172	1·5128	1·5075	1·5035	1·5000
Khair shellac	1·5210	1·5195	1·5175	1·5158	1·5116	1·5070	1·5022	1·4982
Ber shellac	1 5236	1·5225	1·5215	1·5195	1·5152	1·5110	1·5070	1·5026
Pakur shellac	1·5236	1·5222	1·5206	1·5175	1·5136	1·5096	1·5054	1·5012
Button lac (R.L.)	1·5242	1·5222	1·5200	1·5165	1·5126	1·5086	1·5042	1·5005
Dewaxed shellac Blonde	2·5228	1·5200	1·5170	1·5132	1·5090	1·5048	1·5015	1·4976
Shellac Std. I.	1·5250	1·5232	1·5212	1·5180	1·5124	1·5080	1·5040	1·5006
Shellac (superfine unarsenicated)	1·5244	1·5222	1·5200	1·5164	1·5110	1·5070	1·5030	1·4992
Shellac (Superfine arsenicated)	1·5242	1·5225	1·5205	1·5172	1·5128	1·5078	1·5036	1·5000
Shellac (Fine grade)	1·5250	1·5232	1·5212	1·5180	1·5136	1·5195	1·5056	1·5018
T. N. Shellac	1·5272	1·5248	1·5225	1·5190	1·5140	1·5100	1·5060	1·5020
T. N. Shellac F. O.	1·5246	1·5230	1·5214	1·5182	1·5145	1·5102	1·5052	1·5010
T. N. Shellac 12%	1·5300	1·5276	1·5250	1·5220	1·5175	1·5126	1·5078	1·5032
Garnet lac	1·5292	1·5275	1·5255	1·5230	1·5190	1·5150	1·5110	1·5070

TABLE II

Samples	Refractive Index at							
	20° C	30° C	40° C	50° C	60° C	70° C	80° C	90° C
Pure lac resin (E.I.)	1·5248	1·5232	1·5218	1·5202	1·5180	1·5156	1·5116	1·5072
Soft lac resin (E.S.)	1·4976	1·4938	1·4900	1·4860	1·4820	1·4780	1·4740	1·4702
Lac Wax	1·4910	1·4880	1·4830	1·4710	1·4564	1·4500	1·4462	1·4430
Gum Elemi	1·5330	1·5285	1·5240	1·5200	1·5160	1·5130	1·5090	1·5055
Gum Dammar	1·5350	1·5340	1·5330	1·5320	1·5305	1·5290	1·5250	1·5210
Teglac No. 15	1·5540	1·5522	1·5500	1·5470	1·5430	1·5400	1·5362	1·5324

TABLE III

Lac sample	Author's data at 20°C	Data collected from other sources		
		Ref. Index	Temp.	Reference
Kusmi shellac	1·5224	1·515—1·518 1·520	23° C —	Thakur & Aldis Verman
Palas shellac	1·5235	1·517 1·516—1·519	18° C 23° C	Hanstock Thakur & Aldis
Dewaxed shellac	1·5228	1·521—1·522 1·519	23° C —	Thakur & Aldis Verman
Garnet lac	1·5295	1·520	18° C	Hanstock
T. N. Shellac	1·5272	1·513 1·54	18° C —	Hanstock Chamot & Mason
E. S. Resin	1·4976	1·503	23° C	Thakur & Aldis
E. I. Resin	1·5248	1·526 1·520	23° C —	Thakur & Aldis Verman
Shellac	1.5210—1·5236	1·524	—	Houwink
Orange superfine shellac	1·5244	1·516	—	Bradley

TABLE IV

Temperature coefficients for lac and other resins

Samples	Temperature coefficient	Range of temperature in °C
Kusum shellac	−0·000175 −0·000300	Bet. 20 and 40 ,, 70 and 90
Palas shellac	−0·000200 −0·000433	,, 20 and 40 ,, 60 and 90
Khair shellac	−0·000175 −0·000433	,, 20 and 40 ,, 60 and 90
Ber shellac	−0·000112 −0·000420	,, 20 and 40 ,, 60 and 90
Pakur shellac	−0·00015 −0·000400	,, 20 and 40 ,, 50 and 90
Button lac (R. L.)	−0·000210 −0·000400	,, 50 and 40 ,, 50 and 90
Dewaxed shellac Blonde	−0·000200 −0·000400	,, 20 and 30 ,, 40 and 90
Shellac Standard I	−0·000190 −0·000400	,, 20 and 40 ,, 60 and 90
Shellac (Superfine unarsenicated)	−0·000210 −0·000400	,, 20 and 40 ,, 60 and 90
Shellac (Superfine arsenicated)	−0·000200 −c·000410	,, 20 and 40 ,, 50 and 90
Shellac (Fine Grade)	−0·000200 −0·000400	,, 20 and 40 ,, 50 and 90
T. N. Shellac	−0·000240 −0·000400	,, 20 and 40 ,, 60 and 90
T. N. Shellac F. O.	−0·000162 −0·000450	,, 20 and 40 ,, 60 and 90
T. N. Shellac 12%	−0·000250 −0·000467	,, 20 and 40 ,, 60 and 90
Garnet lac	−0·000200 −0·000400	,, 20 and 40 ,, 50 and 90
Pure lac resin	−0·000167 −0·000425	,, 20 and 50 ,, 70 and 90
Soft lac resin	−0·000400	,, 20 and 90
Lac wax	−0·000150 −0·000200	,, 20 and 30 ,, 60 and 90
Gum Elemi	−0·000450 −0·000320	,, 20 and 40 ,, 60 and 90
Gum Dammar	−0·000100 −0·000400	,, 20 and 50 ,, 70 and 90
Teglac No. 15	−0·000200 −0·000375	,, 20 and 40 ,, 50 and 90

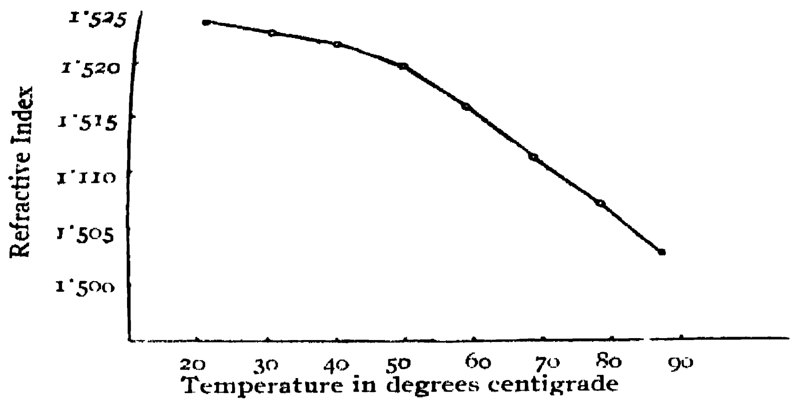

Refractive Index— Temp. Curve for Ber (*Zizyphus Jujuta*) lac

FIGURE 1

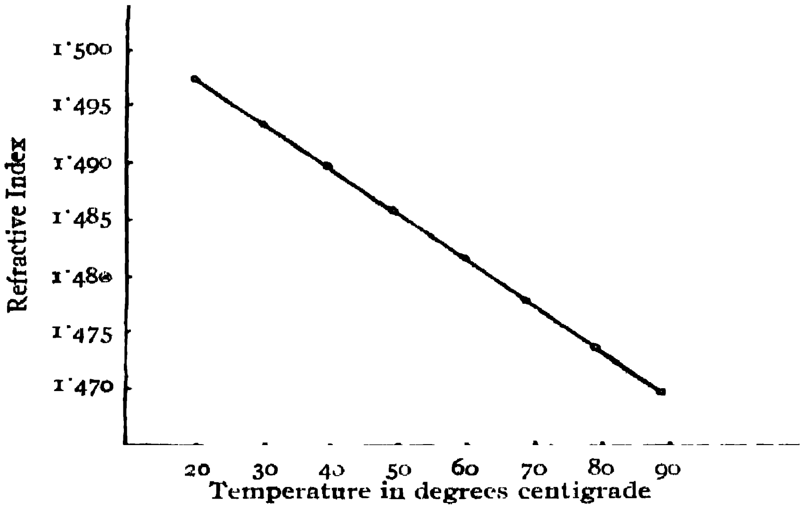

Refractive Index—Temp. Curve for soft lac resin

FIGURE 2

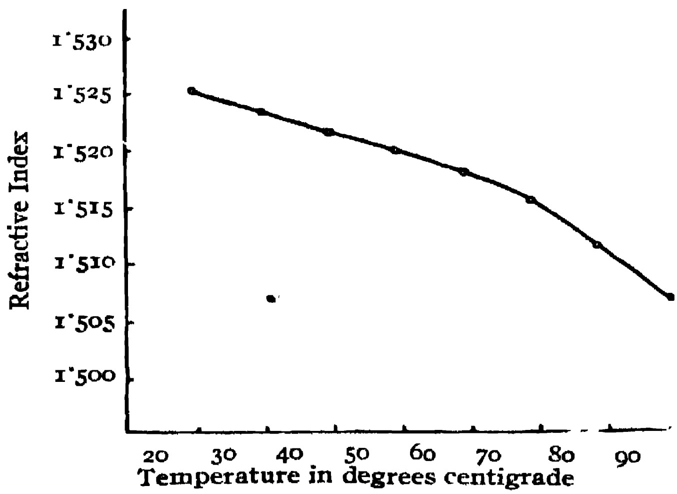

Refractive Index—Temperature Curve for pure lac resin

FIGURE 3

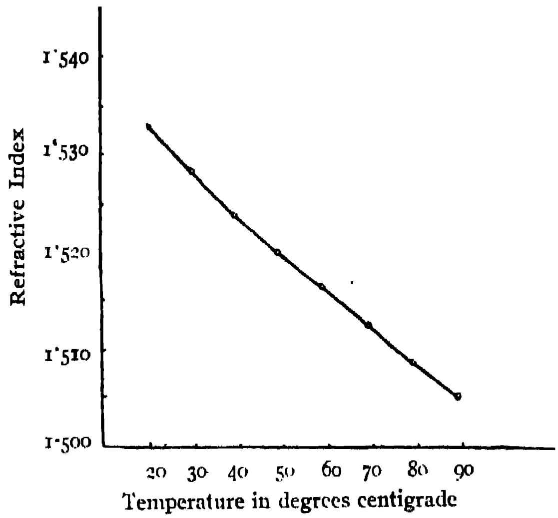

Refractive Index—Temp. Curve for Gum Elemi.

FIGURE 4

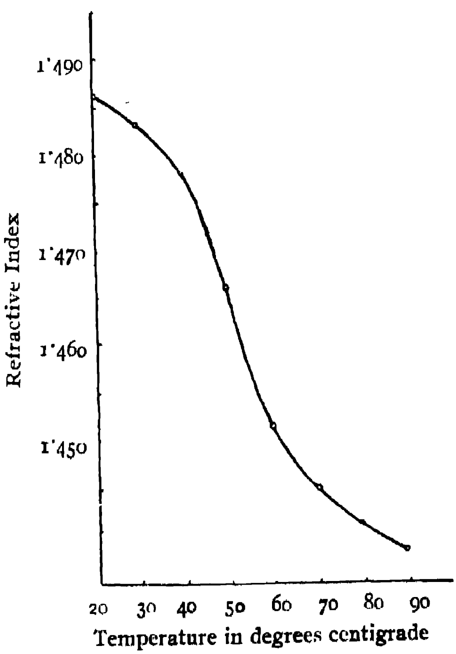

Refractive Index—Temp. Curve for Shellac Wax

FIGURE 5

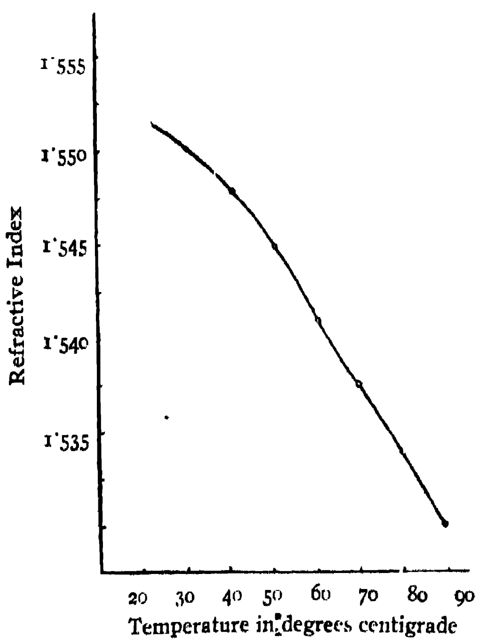

Refractive Index—Temp. Curve for Teglac No. 15

FIGURE 6

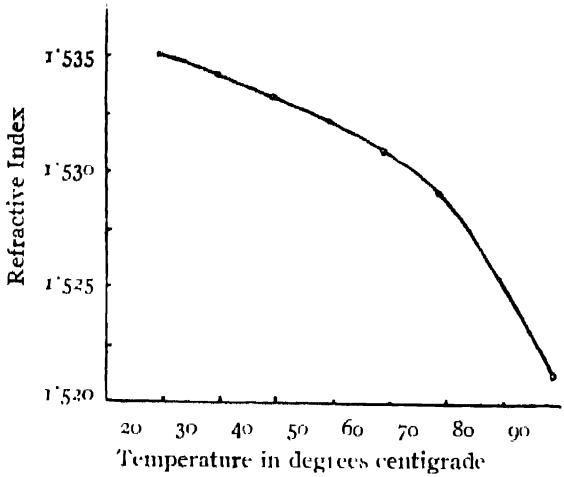

Refractive Index--Temp. Curve for Dammar Gum

FIGURE 7

DISCUSSION

A typical curve representing the temperature variation of refractive index of lac has been shown in Figure 1. The graph is for Ber lac but most of the different varieties of lac examined fall under this group. From this curve it will be seen that there is a bend nearabout the region of 40°C—50°C. This simply shows that the temperature coefficients of refractive indices of lac change nearabout this range, indicating thereby the softening of the substance. The variation of refractive index is almost linear up to the lower limit of this softening range and it follows the same law after the higher limit, too. The soft resin constituent of lac, however, does not show any such bend on its curve, but follows a linear relationship throughout the range of investigation (Figure 2). It is easy to see, therefore, that the soft resin is a pure liquid even at 20°C and remains so throughout the range of temperature of investigation.

The pure resin, on the other hand, softens after 60°C and becomes liquid only after 80°C. (Figure 3).

Thus it is seen that the shellac or the pure resin begins actually to soften at a lower temperature than that found by the standard methods[9] generally used for the determination of the softening point. This fact has also been evidenced by the variation of the specific heat of lac with temperature.[10]

It may be easily seen that the Hanstock lens method has given somewhat lower values for the refactive index than the other methods. This was observed by Verman and he attributed the cause, at least partially, to the use of white light instead of sodium light. This explanation seems reasonable, for, although the lens apparatus was calibrated using a liquid whose refractive index was assumed for sodium light, it could not compensate completely for this discrepancy

owing to the difference in the dispersion co-efficient of a resin and a liquid. That may, therefore, be the reason why the values obtained for refractive index of shellac by Hanstock or Verman or Thakur and Aldis are slightly lower than that found by Houwink or Chamot and Mason[11] or the present author. Houwink's value for the refractive index of shellac obtained by the immersion method coincides admirably with the average value for shellac obtained by the present method using Abbe Refractometer. For a few other resins, too, (both natural and synthetic) whose refractive indices have been measured with the Abbe Refractometer, the values are slightly different from those obtained by the lens method. Dammar Gum and Teg lac No. 15 give slightly higher values whilst the value for Gum Elemi is a bit lower than that obtained by Hanstock. It appears, however, that those substances which are liquid at ordinary temperatures have given slightly lower values by the Abbe Refractometer than those obtained by the lens method (cf. soft resin and Gum Elemi), whilst reverse is the case for other resins. This again suggests that the discrepancy is chiefly due to using white light instead of sodium light.

The temperature coefficient for almost all varieties of shellac is between 1.5×10^{-4} and 2.0×10^{-4} before the softening range and between 3.0×10^{-4} and 4.2×10^{-4} after this range. The average temperature co-efficient for the soft resin and the Gum Elemi is 4.0×10^{-4} throughout the temperature range of investigation. These co-efficients have been shown in a separate table. (Table IV).

The determination of the refractive indices of resins using Abbe Refractometer is, therefore, recommended either before the softening range starts, *i.e.*, below 40°C or after it ends, *viz.*, at about 70°C. The exact softening range will of course depend upon the nature of the particular resin of which the refractive index is to be determined. For all varieties of shellac, however, the higher temperature, *viz.*, about 70°C is very much desirable for the reason that it gives a very sharp, well defined line of demarcation between the two halves of the field of view and takes very much less time in the determination of this constant for routine work. For, this temperature, being near the melting point of practically all varieties of shellac, will serve both for the purpose of film formation on the lower prism of the refractometer as stated before, as well as for the determination of refractive indices. Determination at lower temperatures will mean raising first of all the temperature of the prism to a higher temperature for producing films and then lowering it for actual measurement. For cleaning the prisms again the temperature will have to be raised. As this naturally takes some time for each sample, it is an advantage to measure refractive indices of shellac or other low melting resins at a higher temperature. For hard lac resin or some other polymerised or adulterated lac samples it may be sometimes necessary to carry on the determination at 80°C or so. From the table it will appear

that almost all genuine samples of lac will give a value within the range 1.505 to 1.511 at 70°C and within 1.501 to 1.507 at 80°C. Admixture of rosin always gives a higher value, as will be seen from the values obtained for a sample of shellac marked T.N. 12, containing 12% rosin. Thakur and Aldis similarly obtained a higher value for a sample containing 30% rosin.

Houwink has observed that resins generally give a higher value of refractive index on polymerisation. For a sample of shellac the value increased from 1.524 to 1.535 on heating for 100 hours at 110°C. Verman, on the other hand, found a definite decrease in the refractive index for trichlorethylene-extracted hard lac resin on heating overnight at 120°C. The present author, therefore, tried to determine the refractive index of heat hardened pure lac resin for confirmation of the point. It was found that ether-extracted pure lac resin on being heated at about 100°C for only 6 hours gave a slightly higher value of refractive index, *viz.*, an increased value from 1.5248 to 1.5270.

ACKNOWLEDGMENT

The author is indebted to Dr. H. K. Sen, Director of the Indian Lac Research Institute, for his kind interest in this work.

REFERENCES

1 Bradley, T. F., *Ind. Eng. Chem. Anal. Edn.*, **3**, 304 (1931)

2 Greger, J., *Sitzungs Berichte der K. Akad. der Wissenschaften Wein*, 503 (1919).

3 Morrel, R. S., '*Synthetic Resins & Allied Plastics*' *Ox. Univ. Press*, 1937.

4 Hanstock, R. F., *Res. Assoc. Brit. Paint Col. and Var. Manuf. Tech.*, Paper No. 35, 1932.

5 Houwink, R., '*Physikalische Eigenschaften und Feinbau von Natur und Kunsharzen*' *Akad. Verlag., Leipzig*, 1934

6 Thakur A. K., & Aldis, R. W., *Ind. Lac. Res. Inst. Bull.*, No. 17, 1934

7 Verman, L. C., *Lond. Shellac Res. Bur. Tech.*, Paper No. 10, 1936

8 West, C. D., *Ind. Eng. Chem. Anal. Edn.*, **10**, 627 (1938).

9 *Lond. Shellac Res. Bur. Tech.*, Paper No. 4, 1935; *Official Methods of Analysis, specifications and general information on shellac and bleached shellac U.S. Shell. Imp. Assoc. and Amer. Bleached Shell. Man. Assoc.*, 1934.

10 Bhattacharya, G. N., *Specific Heat of Lac.* (Paper under publication).

11 Chamot & Mason, '*Handbook of Chem. Microscopy*' *John Wiley & Sons.*

HIGH FREQUENCY MEASUREMENTS OF THE AMPLIFICATION FACTOR AND INTERNAL RESISTANCE OF A THERMIONIC VALVE*

By M. KAMESWAR RAO, M.Sc.

(Received for publication, June [illegible])

ABSTRACT. The results of some series of measurements of the amplification factor and the internal resistance of a thermionic valve over a range of radio-frequencies are given in this paper. The measurements of the amplification factor were made by following Miller's method suitably modified. The internal resistance of the valve with and without any fixed high voltage applied to the plate was determined by the distuning method

1. INTRODUCTION

Some measurements of the amplification factor of a thermionic valve in the region of radio-frequencies had previously been reported by Joshi and Saxena [1] Mitra and Sil[2] had also published some work on the internal resistance of a valve for high radio-frequencies and they gave a theoretical interpretation of their work.

The high-frequency measurements undertaken in the present investigation constitute a study of the amplification factor and internal resistance of a thermionic vaive over a wider range of radio-frequencies. Miller's method suitably modified was adopted for the H. F. measurement of amplification factor and for the high-frequency measurements of the internal resistance, the distuning method was employed.

2. HIGH-FREQUENCY MEASUREMENTS OF THE AMPLIFICATION FACTOR OF A VALVE

(a) *Description of apparatus*

An oscillator of the Hartley type was constructed with a suitable inductance coil and a suitable tuning condenser, one or both of which could be replaced to give the desired frequencies. A coupling unit was built separately, consisting of a suitable inductance and a suitable variable condenser. Two leads twisted together carried H.F. currents to the Miller bridge which was used with some modifications for finding amplification factor of the valve. These

* Communicated by the Indian Physical Society.

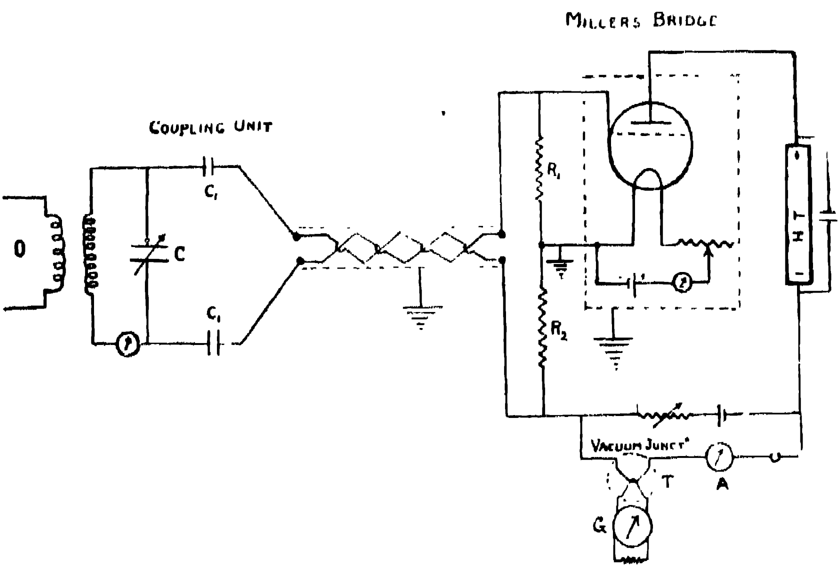

FIGURE 1

leads which were insulated from each other were passed through an earthed tin tube. One end of each of the two leads was connected through a suitable condenser C_1 to the loosely coupled circuit. The experimental arrangement is shown in fig. 1 R_1 and R_2 were the two resistances connected in series with their common joint earthed and connected to the filament negative. One end of R_1 was connected to the grid of the valve. The other end of R_2 was connected through the heater coil of a vacuum thermo-junction T, a D.C. milliammeter A and a key to the negative of the H.T. battery, the positive end of which was connected directly to the plate of the valve. There was an arrangement with a low-tension battery and a variable resistance to balance out the continuous plate current through the heater coil of the vacuum junction as indicated by the milliammeter A. A moving-coil mirror galvanometer G was used in combination with the junction

The resistance R_2 was a metal-film resistance of 4900 ohms with practically no self-capacity. It was kept inside a beaker containing transformer oil to minimise the heating of the resistance. R_1 was a non-inductively-wound P.O. Box resistance. This resistance was adjusted till the deflection in the galvanometer connected with the heater coil of the vacuum junction was minimum. The amplification factor of the valve was then given by

$$\mu_0 = \frac{R_2}{R_1} \qquad \ldots \quad (1)$$

(b) *Measurements of the H.F. amplification factor for various frequencies*

The frequency-range in these measurements was from 149 kc/sec to 3333 kc/sec (*i.e.* from $\lambda = 91$ m. to $\lambda = 760$ m.). The amplification factor of a

Telefunken RE 134 valve was found to increase steadily with the increase of frequency up to about 1600 kc/sec. It was thereafter found to decrease with further increase of frequency. For high radio-frequencies the non-inductively-wound resistance R_1 can never be considered non-inductive. The observed decrease of the amplification factor may be attributed to this cause. Measurements were not therefore carried for still higher frequencies. The experimental results are shown in fig. 2.

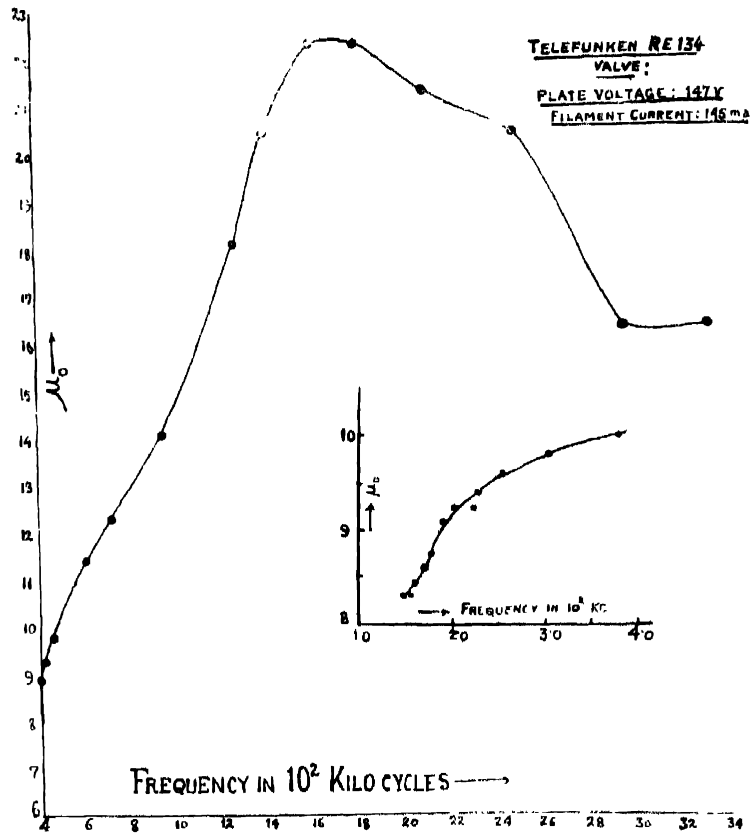

FIGURE

3. HIGH-FREQUENCY MEASUREMENTS OF INTERNAL RESISTANCE OF THE VALVE FOR DIFFERENT FREQUENCIES

The distuning method was employed for the measurement of the internal resistance of the same Telefuken valve. The experimental arrangement is shown in fig. 3. An accurate thermo-galvanometer A and calibrated condensers were used. The condensers were calibrated by a heterodyne wave-meter.

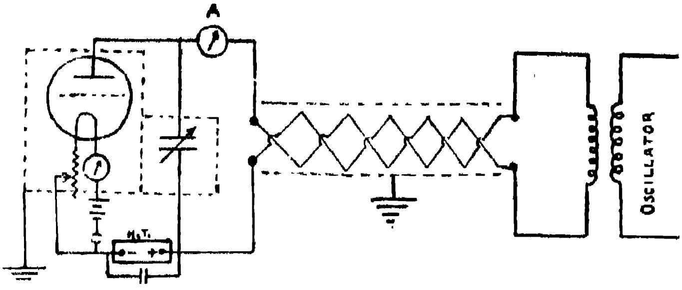

FIGURE 3

First the resistance R of the oscillatory circuit containing the inductance and the variable capacity was determined when the filament of the valve was off. Next, the filament was switched on, so that the capacity was now shunted by the high resistance of the valve. The resistance R′ of the circuit was then determined. The resistance in ohms was calculated from the usual formula :

$$R_{(ohm)} = 265 \cdot \frac{\lambda_m}{C_0}\left(\frac{C_2 - C_1}{C_0}\right) \qquad \ldots(2)$$

where λ_m is the wavelength in metres, C_1 and C_2 are the capacities when the current is reduced to $\frac{1}{\sqrt{2}}$ times the resonant current and C_0 the resonant capacity. (The capacities are expressed in micro-micro-farads.)

The difference $(R' - R)$ which corresponded to the increase of the series-resistance due to electrons in the inter-electrode space was then converted into its equivalent-parallel-resistance ρ by the formula :

$$\rho = \frac{1}{\omega^2 C_0^2 (R' - R)} \qquad \ldots(3)$$

This gave the internal resistance of the valve. The variation of internal resistance of the valve frequency is shown in fig. 4.

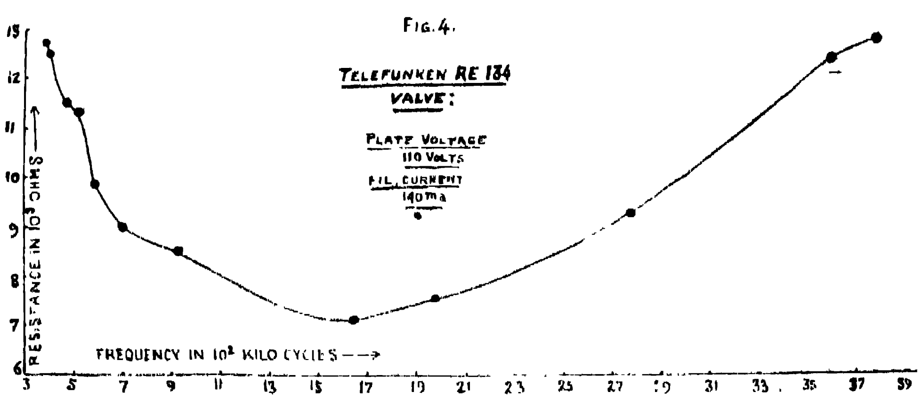

FIGURE 4

It is significant that the internal resistance of the valve was found at first to diminish with frequency till about 600 kc. and then it was found to increase again with further increase of frequency. It should be pointed out that the amplification factor of the same valve was found to increase steadily with frequency up to about the same frequency.

Another series of experiments for determining the internal resistance of a Philips B 406 valve *without applying any voltage to the plate of the valve* was carried out. The range of frequency employed in these measurements was from 165 kc./sec. to 12000 kc./sec. These results are illustrated in figs. 5 and 6.

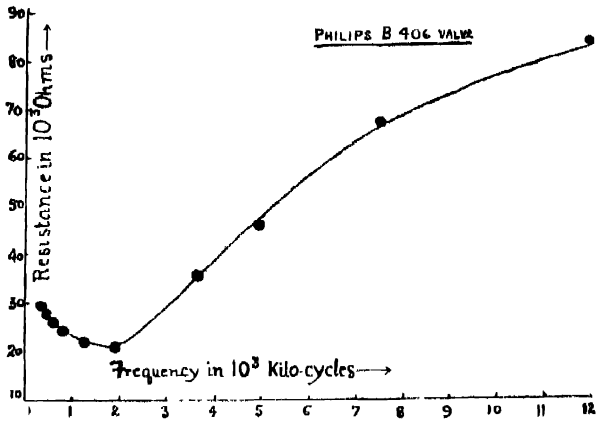

FIGURE 5

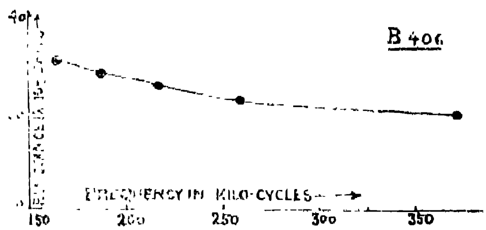

FIGURE 6

Comparing these results with Mitra and Sil's measurements it can be said that the nature of variation of the internal resistance observed by them was, on the whole, similar to that observed in the present work. The difference lay in the fact that the internal resistance of the valve in these experiments diminished steadily, though slowly, with frequency, whereas in the same range of frequencies the internal resistance of the valve used by Mitra and Sil was found practically constant.

4. SUMMARY

The H.F. amplification factor of a Telefunken RE 134 valve was measured and found to increase steadily with frequency up to a certain value of the

frequency, after which it was found to diminish with further increase of frequency. The measurements of the internal resistance of the same valve (with a fixed plate voltage) showed that at first it diminished with the increase of frequency and that subsequently it increased steadily with further increase of frequency. The internal resistance of a Philips B 406 valve (without any applied voltage to the plate of the valve) was also measured for a wide range of frequencies. The nature of the variation with frequency in this case was similar to that in the previous case (when a fixed voltage was applied to the plate).

The measurements of the internal resistance of the valve for radio frequency were carried out by following the distuning method. The measurements of amplification factor were made by the method of Miller.

REFERENCES

[1] Joshi and Saxena, *Science and Culture*, **3**, 569 (1939).
[2] Mitra and Sil, *Phil. Mag.*, **13**, 1081 (1932).

" ON THE ORIGIN OF SOLAR SYSTEM "*

By P. L. BHATNAGAR
Mathematics Department, Allahabad University

(Received for publication, May 30, 1940)

ABSTRACT. The paper deals with the tidal theories of the origin of the Solar System. The author has shown in §2 to §5 that in *two-body problem* there is no possibility for the formation of the planetary ribbon, from which the present planets are supposed to have been developed, by a close encounter or a grazing collision between two stars of usual masses.

In §6 and the following sections, the author has examined mathematically the theory extended by Lyttleton to explain the origin of planets and has proved that in the most favourable situation for the formation of the planetary ribbon in the *three-body problem*, at the middle of the collision between the sun's companion and a visiting star, the sun would come so near to its companion and hence to the visiting star that a very close encounter or collision between them can hardly be avoided.

§1. From time to time, several theories have been suggested to account for the peculiar dynamical arrangement of bodies which constitute the solar system. But when these theories are tested in the light of the distribution of angular momentum in the system, none is found to bear the test and a new theory was expected to come forth which may explain this aspect of the solar system also. H. N. Russell, along with several other theories, suggested [1] "that our sun might have been a binary star having a companion much smaller than itself which had been revolving about the sun at a distance comparable with major planets, and that the collision between this body and a passing star broke this companion into fragments from which the present planets were developed." He gave up the hypothesis thinking that it was not possible to account satisfactorily for the ionisation of the companion from the sun and the ultimate formation of the terrestrial planets.

Lyttleton [2] tried to give a mathematical treatment to Russell's suggestion that the sun had once been a component of a binary star whose companion had been removed by a close encounter with a passing star. He also studied the particular case where the masses of these three stars were taken to be equal. He studied mainly the ionisation of the companion from the sun and assumed that "the mechanism which effects this disruption also produces the planets giving them widely varying angular momentum per unit mass and possibly causing them to proceed round the sun in the same general direction more or less in a plane."

* Communicated by the Indian Physical Society.

Luyten and Hill studied[3] in detail the two cases, *viz.*, where the masses of all the three stars are equal and where the intruding star was less massive than the sun. They pointed out that the two important factors were over-looked by Lyttleton, *viz.*, (1) kinetic energy required to form the planets is very large and the intruding star must have had an initial velocity of about 100 km./sec. at least relative to the sun at a great distance from the binary system which is of rare occurrence in nature and (2) that Lyttleton assumed that the whole of the planetary ribbon was available for the capture by the sun, whereas the calculations show that only 6% of the whole length of the ribbon could be captured if at all possible and, in view of these circumstances, the theory is untenable.

To avoid the requirements of very large velocities of the intruding star, Lyttleton[4] put forward a new hypothesis that the intruding star was much more massive than the sun. In a recent paper[5], Luyten has criticised this hypothesis of more massive intruder and suggested that it is exceedingly improbable that the sun could capture any part of the ribbon without itself being captured by the intruder, and that "in the situation most favourable to capture, the sun must have been running roughly parallel to the filament for some time and must have suffered a close approach or a collision with the intruder.

The whole problem is very complicated on account of the fact that it involves the consideration of the problem of three bodies in the beginning and after collision, a consideration of multiple bodies. The above-mentioned treatment by Lyttleton, Luyten and Hill, as it stands, lacks in Mathematical analysis. Lyttleton assumes that the sun remains from the beginning to the end of the encounter at the same mutual distance from the companion. In a recent paper, Luyten has criticised Lyttleton's vector diagram and pointed out the errors, but his criticism also is more or less speculative in character. In the present paper the author has tried to study the change in the velocity and position of the sun during this catastrophe from the mathematical point of view.

Since the time the tidal theory has been suggested, the possibility of a close encounter or a grazing collision resulting in the production of a material ribbon, from which the present planets were formed, was assumed. Before discussing the main problem, the validity of this assumption is tested.

§2. *Tidal Force* :—Let S_1 and S_2 be two stars whose elements are given below:—

	S_1	S_2
Mass	M_1	M_2
Undisturbed mean radius	$R_1 = \sqrt[3]{\dfrac{3M_1}{4\pi\rho_1}}$	$R_2 = \sqrt[3]{\dfrac{3M_2}{4\pi\rho_2}}$
Mean density	ρ_1	ρ_2.

Distance between S_1 and $S_2 = d$.

Let $M_2 = nM_1$, $d = qR_1$ and $r = pR_1$.

Also let ABCD (diagram I) be the section of S_1 by the relative orbital plane of S_1 and S_2, which we take to be the plane $\phi = 0$.

$$F_1 = \text{attraction at } P' (r, \theta, 0) \text{ due to } S_2$$

$$= \frac{M_2G}{d^2 + r^2 - 2rd\cos\theta},$$

regarding S_2 to be spherical.

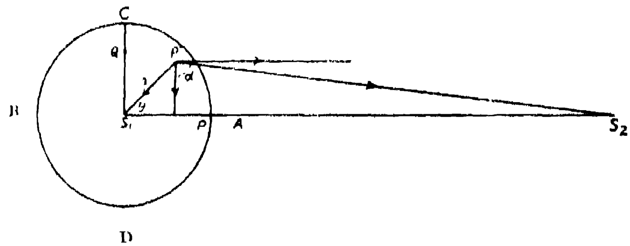

DIAGRAM I

$$F = \text{attraction at } S_1 \text{ due to } S_2 = \frac{M_2G}{d^2},$$

$$\text{component of } F_1 \text{ parallel to } S_1S_2 = \frac{M_2G\,(d - r\cos\theta)}{(d^2 + r^2 - 2rd\cos\theta)^{\frac{3}{2}}} \qquad \ldots \quad (1)$$

$$\text{and component of } F_1 \text{ perpendicular to } S_1S_2 = \frac{M_2G\,(r\sin\theta)}{(d^2 + r^2 - 2rd\cos\theta)^{\frac{3}{2}}}. \qquad \ldots \quad (2)$$

Therefore the tide-generating force at P′ consists of two components: one parallel to S_1S_2 and equal to

$$\frac{M_2G\,(d - r\cos\theta)}{(d^2 + r^2 - 2rd\cos\theta)^{\frac{3}{2}}} - \frac{M_2G}{d^2}$$

and other perpendicular to S_1S_2 and equal to

$$\frac{M_2G\,r\sin\theta}{(d^2 + r^2 - 2rd\cos\theta)^{\frac{3}{2}}}$$

$$\text{Therefore } T = M_2G\sqrt{\frac{1}{d^4} + \frac{1}{(d^2 + r^2 - 2rd\cos\theta)^2} - \frac{2(d - r\cos\theta)}{(d^2 + r^2 - 2rd\cos\theta)^{\frac{3}{2}}}} \quad (3)$$

which acts in a direction making an angle α with the perpendicular direction to S_1S_2, such that

$$\tan\alpha = \frac{d^2(d - r\cos\theta) - (d^2 + r^2 - 2rd\cos\theta)^{\frac{3}{2}}}{d^2 r\sin\theta} \qquad \ldots \quad (4)$$

When r/d is small we may put

$$T = \frac{M_2 G r}{d^3} \sqrt{1 + 3\cos^2\theta}$$

and
$$\tan \alpha = 2\cot\theta - \frac{3r}{2d} \sin\theta.$$

The component of T along $S_1 P' = T \sin(\alpha - \theta)$.

The force of gravity at P′ due to $S_1 = \frac{M_1 G r \kappa}{R_1^3}$,

where κ is a function of θ (independent of r) depending on the degree of distortion of S_1.

The component of the tidal force balances the gravity at P′

if
$$T \sin(\alpha - \theta) = \frac{M_1 G r \kappa}{R_1^3},$$

i.e., if

$$M_2 G \sin(\alpha - \theta) \sqrt{\frac{1}{d^4} + \frac{1}{(d^2 + r^2 - 2rd\cos\theta)^2} - \frac{2(d - r\cos\theta)}{(d^2 + r^2 - 2rd\cos\theta)^{\frac{3}{2}}}} = \frac{M_1 G r \kappa}{R_1^3}$$

which may be put in the form

$$p = n \sin(\alpha - \theta) \sqrt{\frac{1}{q^4} + \frac{1}{(q^2 + p^2 - 2pq\cos\theta)^2} - \frac{2(q - p\cos\theta)}{(q^2 + p^2 - 2pq\cos\theta)^{\frac{3}{2}}}} \quad \dots (7)$$

where
$$n = \frac{n}{\kappa} \text{ (function of } \theta) \quad \dots (8)$$

and
$$\tan\alpha = \frac{q^2(q - p\cos\theta) - (q^2 + p^2 - 2pq\cos\theta)^{\frac{3}{2}}}{q^2 p \sin\theta}. \quad \dots (9)$$

Let us now put $\theta = 0$. Then the points of equality of the tidal force and the gravitational force on $S_1 S_2$ are given by

$$\frac{1}{(q - p)^2} - \frac{1}{q^2} = \frac{p}{n}. \quad \dots (10)$$

The three roots of (10) are

$$p_0 = 0 \quad \text{(centre)},$$

$$p_1 = q - \frac{n}{2q^2}\left\{1 - \sqrt{1 + \frac{4q^3}{n}}\right\},$$

$$p_2 = q - \frac{n}{2q^2}\left\{1 + \sqrt{1 + \frac{4q^3}{n}}\right\}.$$

Let $2n > q^3$.

Then, if $2n > 4q^3$, one root is positive and the other negative ; the negative root is less than the positive one in magnitude ; if $2n < 4q^3$, the negative root is greater than the positive root in magnitude.

Let $2n < q^3$. Then both the roots are positive.

We shall now consider the variation in the difference of the tidal force and gravitational force along the radious of S_1 directed towards $S_2°$. Let

$$y = M_2G\left[\frac{1}{(d-r)^2} - \frac{1}{d^2}\right] - \frac{M_1G\gamma\kappa}{R_1^3}.$$

Putting $\frac{M_1Gk}{R_1^2} = g$ and then $y = g z$, we have

$$Z = n\left[\frac{1}{(q-p)^2} - \frac{1}{q^2}\right] - p.$$

Differentiating with respect to p we have

$$\frac{dz}{dp} = \frac{2n}{(q-p)^3} - 1.$$

Hence z increases with p if $2n > (q-p)^3$ and decreases with the increasing p if $2n < (q-p)^3$. These inequalities are all the more satisfied if $2n > q^3$ and $2n < (q-p_1)^3$ respectively, where p_1 is the greatest value of p.

The complete tidal disruption of S_1 would be possible only in the first case, *i.e.*, when $2n > q^3$ because in that case the tidal force on the material everywhere on the axis would be directed outwards ; whereas in the case $2n < (q-p_1)^3$, there cannot be even the slightest shedding of material from S_1. For the partial shedding-off of the material from S_1 the value of n should be between $\frac{1}{2}q^3$ and $\frac{1}{2}(q-1.65396)^3$, where p_1 has been taken equal to 1.65396 corresponding to the critical [6] eccentricity .882579 required for the disruption of S_1. In the following tables the limiting values for n have been collected for different values of q.

TABLE I

If S_1 is in form of a sphere			If S_1 is a critical spheroid	
$n <$	$n >$	q	$n <$	$n >$
4	·5	2	1.947	.0101
32	13·5	4	15·578	3·143
108	62.5	6	52·574	19.980
256	171 5	8	124.621	62.206
500	364.5	10	243.400	141.501
864	665·5	12	420.595	269·552
1462	1098.5	14	711.702	458.040

In these calculations we have put $p_1 = 1$ in case of the spherical star

and $\quad p_1 = 1.65396$ and $k = \frac{3}{2} \cdot \frac{1-e^2}{e^3} \cdot \left[\log \frac{1+e}{1-e} - 2e \right]^{-1}$

$$= .4868, \text{ taking } e = .8826.$$

TABLE II

n	η	$p=0$	.2	.4	.6	.8	1.0	1.2
10	4.868	$z=0$	.1325	−.2534	−.3590	−.4485	−.5139	−.5490
27	13.1436	0	−.0178	−.0042	.0483	.1491	.3125	.5577
32	15.5776	0	.0160	.0691	.1683	.3248	.5555	.8832

In the graph I curves have been drawn for three values of n showing the behaviour of z as p is increased, taking $a = 4$.

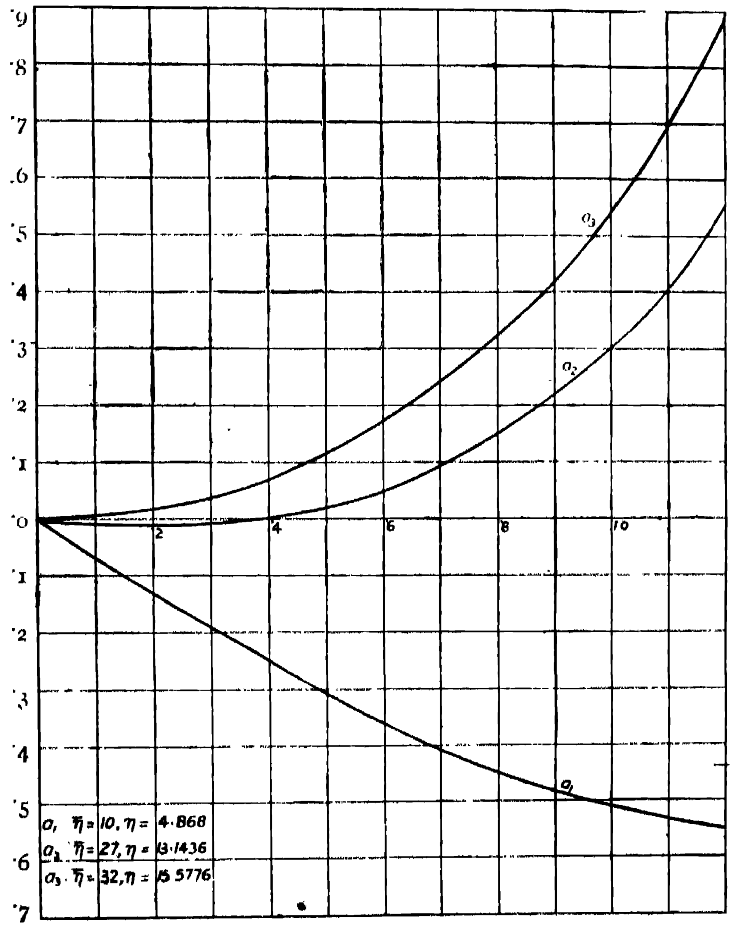

GRAPH I

When the star is the spheroid $\frac{x^2}{a^2} + \frac{y^2+z^2}{b^2} = 1$ $(a > b)$, then $k = +\frac{3}{2} R_1{}^3 \int_0^\infty \frac{du}{(a^2+u)^{\frac{3}{2}}(b^2+u)}$

$$= \tfrac{3}{2} R_1{}^3 \cdot \frac{1}{a(a^2-b^2)^{\frac{3}{2}}} \cdot \left[a \log \frac{a+\sqrt{a^2-b^2}}{a-\sqrt{a^2-b^2}} - 2\sqrt{a^2-b^2} \right] = \tfrac{3}{2} \cdot \frac{1-e^2}{e^3} \cdot \left[\log \frac{1+e}{1-e} - 2e \right].$$

In a_3, since at every point along S_1A the tidal force is greater than the gravity, the acceleration at every point would be directed away from the centre S_1 and the stellar material would move outward resulting in ejection, because the action of the fluid pressure is always to encourage the ejection. In a_2, up to $p=.418$ the gravity is greater than the tidal force and after that the latter is greater than the former and thus the acceleration at every point corresponding to greater values of p than .418 would be directed away from S_1 and hence a partial ejection may take place. In a_1 ejection does not seem possible.

It should be noted that if S_1 is in the form of a sphere, the same curves correspond to the masses $n=10$, 27 and 32. Thus, if initially S_1 is undistorted, for ejection of the material, S_2, which is supposed to be situated at the same distance $q=4$, should possess comparatively larger masses.

We shall now consider the variation in magnitude and direction of the tidal force acting along an imaginary circular section of S_1 in the relative orbital plane of S_1 and S_2. We shall make use of the approximate formula, since in that case, too, the fundamental characteristics remain unaltered. Formulae (5) and (6) are :

$$T=\frac{M_2Gr}{d^3}\sqrt{1+3\cos^2\theta} \qquad \ldots \quad (5)$$

and

$$\tan\alpha=2\cot\theta-\frac{3}{2}\cdot\frac{r}{d}\cdot\sin\theta. \qquad \ldots \quad (6)$$

Instead of plotting T against θ, we shall plot T′ against θ, where

$$T'=\frac{Td^3}{M_2Gr}.$$

The components of T′ tangential to the circle and along the radius vector are equal to $T'\cos(\theta-\alpha)$ and $T'\sin(\theta-\alpha)$. We shall plot these two components also in the same graph (see graph II).

TABLE III

θ	T′	T′ cos $(\alpha-\theta)$	T′ sin $(\theta-\alpha)$	
0°	2	0	2	Away from the centre.
10°	1.98	.513	1.91	
20°	1.91	.963	1.65	
30°	1.80	1.30	1.25	
40°	1.66	1.48	.750	
50°	1.50	1.48	.240	
60°	1.32	1.30	.230	Towards the centre.
70°	1.16	.963	.647	
80°	1.04	.513	.905	
90°	1.00	.000	1.000	

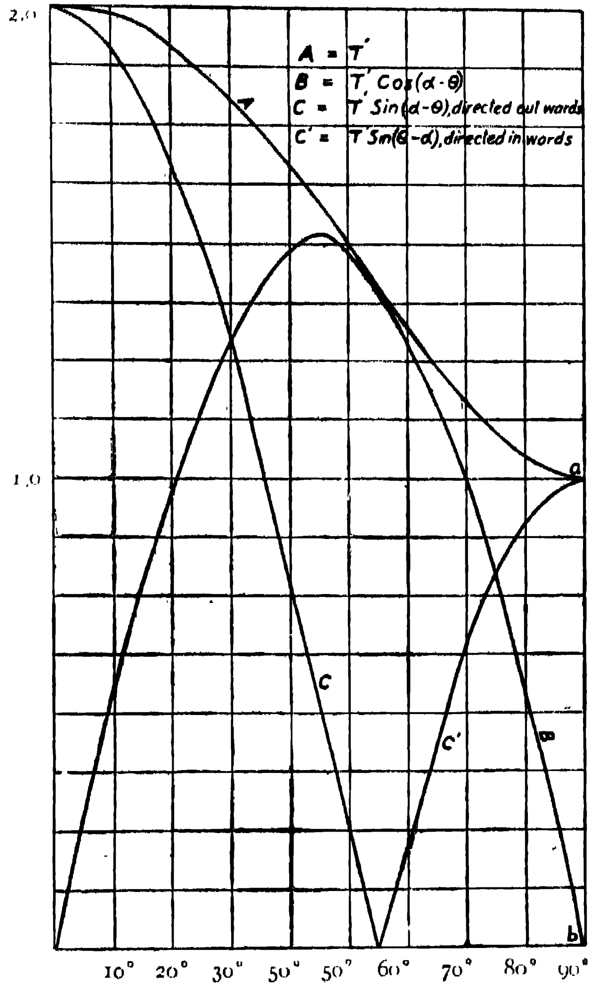

GRAPH II

In preparing the above table we have made use of the formula tan $\alpha = 2 \cot \theta$ instead of the formula (6). If the formula (6) would have been employed then the curve B would not reach the θ-axis, it would have been much above it for $\theta = 90°$ and similarly c' would not join A at $\theta = 90°$. The end points a and b would move towards one another along ab as we consider more and more correct approximate form of the formula (5) and (6).

§3. *Material required to form the ribbon* :—Considering the stars defined in §2, we have

$$M_1 = \text{the mass of } S_1 = \tfrac{4}{3}\pi R_1^3 \rho_1 .$$

As mentioned in §1, the total mass† of the planets $= .0015\ M_\odot$ and that only 6% of the filament by length may be captured in form of the primitive planets if at all. Therefore the total mass that should be ejected from S_1 to form the

† Russell, Dugan and Stewart's "Astronomy," part (*i*), appendix p. (*ii*).

ary ribbon $= .025\ M_{\odot}$, if the mean density of the filament is also equal to the mean density of the star S_1. In general the density of the filament would be much less than that of the parent star, firstly because the material forming the filament would be from the boundary of the star, secondly under the opposing gravitational forces of the two encountering stars the filament would diffuse in the space rapidly and thirdly because the temperature of the filament would be at least few thousand degrees centigrade which would help immensely the diffusion pointed just above. If S_1 possesses mass equal to that of the sun, then the mass of the material that should be ejected out should be equal to $.025\ M_1$

$$= .025 \times \tfrac{4}{3}\pi R_1^3 \rho_1.$$

This material would form a sphere of radius R_0 and mean fluid density ρ_1,

where $$R_0 = .2924\ R_1$$

and hence p_0 must be nearly 1.0692 if S_1 is a critical spheroid or .4152 if the star is spherical, where p_0 is the value of p where $z=0$—of course positive and other than zero. For this to be realised, the masses of S_2 for values of q are obtained in the following table :—

TABLE IV

When S_1 is a sphere		When S_1 is a critical spheroid
n	q	n
2.7843	2	.5757
27 109	4	9 6444
96.923	6	38.979
236 24	8	100.23
469.10	10	205.15
819.42	12	365.26
1311 3	14	592.39

Taking S_1 equal to the sun we find that in order that there may be a possibility for the material, necessary to form the planetary ribbon, to be ejected out, the mass of S_2 for a particular value of q lies between the two limits given in the above table for S_1 would neither be a sphere nor a critical spheroid in general,

§4. *Tidal distortion of a spherical star into a critical spheroid* :—Putting $\theta=\pi/2$ in (3), we get the tidal force at a point like Q. We have at Q

$$T=M_2G\sqrt{\frac{1}{d^4}+\frac{1}{(d^2+r^2)^2}-\frac{2}{d(d^2+r^2)^{\frac{3}{2}}}}$$

and $$\tan\alpha=\frac{d^3-(d^2+r^2)^{\frac{3}{2}}}{d^2r}\quad\text{(from 4).}$$

Hence $$T\cos\alpha=M_2G/(d^2+r^2)^{\frac{3}{2}}$$

$$T\sin\alpha=\frac{M_2G\{d^3-(d^2+r^2)^{\frac{3}{2}}\}}{d^2(d^2+r^2)^{\frac{3}{2}}}.$$

While considering the tidal deformation of S_1 we shall regard S_2 a point mass. Let at any stage of deformation a, b and b be the lengths of the axes of the spheroid to which the star has been deformed under the influence of S_2.

Pressure at S_1 as obtained from the consideration of the equilibrium of the fluid column along S_1A

$$=\int_0^a\left[\left\{\frac{-2\pi G\rho_1ab^2}{a(a^2-b^2)^{\frac{3}{2}}}\left(2\sqrt{a^2-b^2}+a\log\frac{a-\sqrt{a^2-b^2}}{a+\sqrt{a^2-b^2}}\right)\right\}-M_2G\left(\frac{1}{(d-r)^2}-\frac{1}{d^2}\right)\right]dr$$

$$=-\frac{\pi G\rho_1a^2b^2}{(a^2-b^2)^{\frac{3}{2}}}\left\{2\sqrt{a^2-b^2}+a\log\frac{a-\sqrt{a^2-b^2}}{a+\sqrt{a^2-b^2}}\right\}-M_2G\left[\frac{1}{(d-a)}-\frac{1}{d}-\frac{a}{d^2}\right],$$

where the expression within the serpentine brackets arises due to the attraction of the star S_1 and the remaining expression due to the tidal force of S_2.

Similarly the pressure at S_1 as obtained from the consideration of the equilibrium of the fluid column S_1B

$$=\pi G\rho_1ab^4\left[\frac{1}{ab^2}+\frac{1}{2a(a^2-b^2)^{\frac{3}{2}}}\left\{2\sqrt{a^2-b^2}+a\log\frac{a-\sqrt{a^2-b^2}}{a+\sqrt{a^2-b^2}}\right\}\right]$$
$$+M_2G\left[\frac{1}{d}-\frac{1}{\sqrt{d^2+b^2}}\right].$$

These two pressures must be equal. Hence

$$M_2\left[\frac{a}{d^2}-\frac{1}{d-a}+\frac{1}{\sqrt{d^2+b^2}}\right]$$

$$=\frac{3}{4}\frac{M}{a}\left[1+\frac{2a^2+b^2}{2(a^2-b^2)^{\frac{3}{2}}}\left\{2\sqrt{a^2-b^2}+a\log\frac{a-\sqrt{a^2-b^2}}{a+\sqrt{a^2-b^2}}\right\}\right].$$

Now $\quad a=R_1(1-e^2)^{-\frac{1}{3}}$ and $b=R_1(1-e^2)^{\frac{1}{6}}$.

According to the notations given in §2, we can put this equation in the form

$$n\left[\frac{1}{q^2(1-e^2)^{\frac{1}{3}}} - \frac{1}{q-(1-e^2)^{-\frac{1}{3}}} + \frac{1}{\sqrt{q^2+(1-e^2)^{\frac{1}{3}}}}\right]$$

$$= \tfrac{3}{4}(1-e^2)^{\frac{1}{3}}\left[1 - \frac{3-e^2}{2e^3}\left\{2e + \log\frac{1-e}{1+e}\right\}\right]. \quad \ldots \quad (11)$$

When S_2 is at S''_2, the position of S_2 of its nearest approach to S_1 or much before this (such that S_1S_2 is of the order of 20 to 30 solar radii) in the diagram (ii), S_1 must be so much deformed that its eccentricity is greater than the critical value .882579, otherwise there is no chance for ejection of the material (see in §5). In the case when S_1 is deformed to the critical shape the material would be shed away from the star S_1 irrespective of the motion of S_2 on account of the momentum imparted to it by the encounter of these stars We shall now treat the equation (11) numerically. Taking $e = .8826$, we have

TABLE V

$q =$	2	4	6	8	10	12	14	20	30
$n =$	.0,8	2.578	10 557	27.205	55.66	99.1	160 7	484.7	1682

The above table gives the relation between q and n. In order that the spherical star S_1 may be deformed in the form of a spheroid of eccentricity $e = .8826$ due to the tidal action of another star S_2 situated at the distance determined by q, the mass of the latter must be n. It is quite evident from the table (V) that in order that the requisite deformation ($e = .8826$) may be realized from a distance of about 20 to 30 solar radii the mass of S_2 must be unusually enormous.

In §2, §3 and §4 we have considered the tidal distortion of a spherical star and the conditions for its ultimate disruption when the visiting star is stationary so that the tidal forces have got enough time to redistribute the material of S_1 and produce the calculated distortion. It has been shown above that in order to deform S_1 (assumed to be sperical initially) so as to reduce it to the critical spheroid ($e = .8826$) the stationary star situated at the distance of 20 solar radii must possess 485 times the mass of the sun. Similarly, if we take the distance between S_1 and S_2 to be 30 solar radii, the requisite mass of S_2 must be 1682 times the solar mass. By taking M_1 greater than M_0 we shall be able to increase the value of p_0. ; but on account of the increased mass of S_1 we shall require more massive intruder in order to balance the gravitational force of S_1 at that distance even. In order that the tidal force may be greater than the gravitational force on the material of S_1 necessary to form the planetary ribbon when S_2 is at a distance of 8 solar radii, the latter must be about 100 times more massive than

the sun if S_1 is already deformed to the critical eccentricity and about 236 times more massive than the sun if S_1 is spherical. The reduction of the distance between S_1 and S_2 and consequently reducing q, no doubt, reduces the value for the mass of S_2, but on account of the extensions of the stars there is bound to be a very tremendous collision between them in the first place and in the second it will be seen in the discussion of the dynamical problem below that the duration of the effective encounter and the collision is so much reduced by reducing q that the disruption becomes an impossibility unless there is very tremendous collision between the stars and in that case what actually happens cannot be predicted. Thus it can be inferred that in statical problem in order to ensure disruption of S_1 by the tidal action of S_2, situated at suitable distance, the latter must possess unusually great mass.

§5. *Stellar encounter*:—Nearly everybody has assumed the possibility of encounter between two stars resulting in the formation of the planetary ribbon. We shall in the very beginning make an attempt to study if it is at all possible to produce the desired ribbon by a close encounter or a grazing collision between two stars of usual masses and sizes if we take the relative motion of the stars into account.

As we can conclude from the discussions in §2, the greatest tidal forces are excited on S_1 when the passing star is nearest to S_1 and that seems to be the most favourable situation for the removal of the material from the former, in the form of planetary ribbon. It will be seen in the following treatment that the time during which the grazing collision lasts is extremely small. Is it then possible even for those maximum tidal forces which act for a very short time at a particular point of the material of S_1 to produce the desired ribbon? The following treatment shows that the answer is in the negative.

Before proceeding further, it is necessary to define the encounter and its duration. By encounter we mean the close approach of a star within a certain specified distance of another star and the duration of the encounter may then be conveniently defined as the time during which the intruding star is within that specified distance.

In §9, we have calculated the eccentricity of the hyperbolic orbit of the intruding star relative to the other star at least in two cases. In both these cases we find that e is very nearly equal to unity (*viz.*, 1.068 and 1.014). This is quite in keeping with the general consideration of the stellar motions. The stars possess very small *proper motions* but if then any sort of collision is to take place the intruder moves towards the star under its gravitational force and the orbit described under these circumstances must be more or less a parabola. Hence in general we shall assume that during the encounter between the stars, S_2 is describing a parabola under the action of the gravitational force of S_1.

Let us assume that the eccentricity of the hyperbolic orbit described by S_2 relative to S_1 is e. Then the equation to the orbit will be

$$r = \frac{\dfrac{h^2}{M_1+M_2}}{1+e\cos\theta}, \qquad \cdots \quad (12)$$

where h is the areal constant determined later on. At any instant

$$\text{velocity} = \sqrt{\dot{r}^2 + r^2\dot{\theta}^2}$$

$$= \sqrt{\frac{2(M_1+M_2)}{r} + \frac{(M_1+M_2)^2(e^2-1)}{h^2}}. \qquad \cdots \quad (13)$$

If the hyperbolic motion of S_2 relative to S_1 begins when the former is at a distance l_1 from the latter and the velocity of S_2 relative to S_1 at that instant be $\overline{R}_b$, then we have

$$\overline{R}_b^2 = \frac{2(M_1+M_2)}{l_1} + \frac{(M_1+M_2)^2(e^2-1)}{h^2} \qquad \cdots \quad (14)$$

and

$$\frac{h^2}{M_1+M_2} = \frac{(M_1+M_2)(e^2-1)}{\overline{R}_b^2 - \dfrac{2(M_1+M_2)}{l_1}} \qquad \cdots \quad (15)$$

hence (12) can be written as

$$r = \frac{\dfrac{(e^2-1)(M_1+M_2)}{\overline{R}_b^2 - \dfrac{2(M_3+M_2)}{l_1}}}{1+e\cos\theta}. \qquad \cdots \quad (16)$$

Let the shortest distance between S_1 and S_2 be d_1. Then

$$d_1 = \frac{(e-1)(M_1+M_2)}{\overline{R}_b^2 - \dfrac{2(M_1+M_2)}{l_1}} \quad (\theta=0). \qquad \cdots\cdot \quad (17)$$

Therefore

$$e = 1 + \frac{d_1}{M_1+M_2}\left\{\overline{R}_b^2 - \frac{2(M_1+M_2)}{l_1}\right\} \qquad \cdots \quad (18)$$

and

$$r = \frac{(e+1)d_1}{1+e\cos\theta}; \qquad \cdots \quad (19)$$

also

$$\overline{R}_b^2 = \frac{2(M_1+M_2)}{r} + \left\{\overline{R}_b^2 - \frac{2(M_1+M_2)}{l_1}\right\}$$

$$= \frac{2(M_1+M_2)}{r} + \frac{(M_1+M_2)(e-1)}{d_1}, \qquad \cdots \quad (20)$$

where R_b is the velocity of S_2 relative to S_1 at any instant when the former is moving on the hyperbola (19).

As long as the star S_2 is moving towards S_1, it will move on the hyperbola specified by (19) but when S_2 is at the shortest distance from S_1 there may be exchange of material in the case of the grazing collision and in case of an encounter the tidal forces may alter the velocity and the motion may be modified. Hence we assume that the hyperbolic orbit (19) ceases at the perihelion of (19) and S_2 proceeds along a different hyperbola. If we futher assume that this modified hyperbolic motion ends at a distance l_2 from S_1 when S_2 is moving with a velocity $\overline{R}$ relative to the former, the equation to the orbit will be

$$r=\frac{(e_1+1)d_1}{1+e_1\cos\theta} \qquad \ldots \quad (21)$$

and

$$R_a^2=\frac{2(M_1+M_2)}{r}+\left\{R_a^2-\frac{2(M_1+M_2)}{l_2}\right\}$$

$$=\frac{2(M_1+M_2)}{r}+\frac{(M_1+M_2)(e_1-1)}{d_1}, \qquad \ldots \quad (22)$$

where e_1 is the eccentricity of the new orbital hyperbola and R_a the velocity of S_2 relative to S_1 at any instant on it.

Hence the loss of the kinetic energy *

$$=\tfrac{1}{2}\frac{M_1M_2}{M_1+M_2}\left(\overline{R_b}-\overline{R_a^2}\right)+M_1M_2\left(\frac{1}{l_2}-\frac{1}{l_1}\right). \qquad \ldots \quad (23)$$

This kinetic energy is supposed to be utilised in the formation of the planetary ribbon. But later on it will be seen that a major part of this energy is utilised in accelerating the motion of M_0 in the three-body problem dicussed in §6 and the following sections.

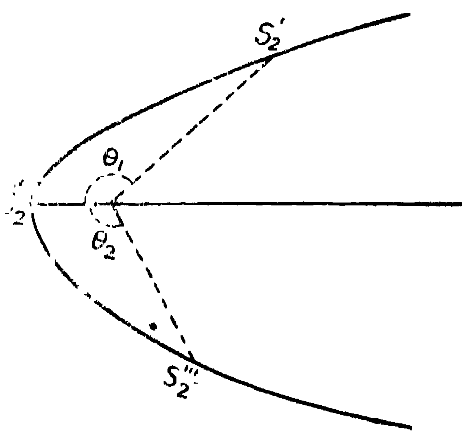

DIAGRAM II

* It may be noted here that we have an additional term in this expression which vanishes when $l_1=l_2$.

In the diagram II when S_2 is at S_2'' it is nearest to S_1 so that $S_1 S_2''=d_1$. $S_2' S_2''$ and $S_2'' S_2'''$ are the branches of the two hyperbolas assumed in (19) and (21) where S_2' and S_2''' are the positions of S_2 where its hyperbolic motion relative to S_1 begins and ends respectively. Let $\overline{T}$ be the total time during which the hyperbolic motion lasts. Then

$$\overline{T}=\frac{d_1^{\frac{3}{2}}}{(M_1+M_2)^{\frac{1}{2}}}\left[(e+1)^{\frac{3}{2}}\int_0^{\theta_1}\frac{d\theta}{(1+e\cos\theta)^2}+(e_1+1)^{\frac{3}{2}}\int_0^{\theta_2}\frac{d\theta}{(1+e_1\cos\theta)^2}\right],$$

where
$$\theta_1=\cos^{-1}\left[\frac{1}{e}\left\{\frac{(e+1)d_1}{l_1}-1\right\}\right]$$

and
$$\theta_2=\cos^{-1}\left[\frac{1}{e_1}\left\{\frac{(e_1+1)d_1}{l_2}-1\right\}\right].$$

Now to simplify the calculations if we assume that $l_1=l_2=l$ (say), $e=e_1=1$ (the justification of this assumption is given above), we have

$$T'=\frac{2\sqrt{2}}{3}\sqrt{\frac{l-d_1}{M_1+M_2}}(l+2d_1), \qquad \ldots \quad (24)$$

where T' is the total time during which S_2 is within the distance l of S_1. Similarly the time T'' taken by S_2 to move from one end of the latus-rectum to the other of the parabolic orbit will be given by

$$T''=\frac{8\sqrt{2}}{3}\cdot\frac{d_1^{\frac{3}{2}}}{\sqrt{M_1+M_2}}; \qquad \ldots \quad (25)$$

also the time taken by S_2 to move from one end of the latus rectum to any position (r, θ) will be given by

$$T=\frac{\sqrt{2}}{3}\cdot\frac{1}{\sqrt{M_1+M_2}}\cdot\left[(2d_1+r)\sqrt{r-d_1}-4d_1^{\frac{3}{2}}\right]; \qquad \ldots \quad (26)$$

Case I: Let $M_1=M_2=M_{\odot}$,

$l_1=10$ astronomical units,

$d_1=1/40$,, ,, ,

and $r=1/2$,, ,, .

Then $T'=3{\cdot}5$ years (approx.),

$T''=15$ hours (,,),

and $T=169$ hours (,,).

Case II: Let $M_1=2M_{\odot}$, $M_2=8\,M_{\odot}$,

$l=10$ astronomical units,

$d_1=1/40$,, ,, .

and $r=1/2$,, ,, .

Then $T' = 1\cdot5$ years (approx.)

$T'' = 6\cdot5$ hours (,,),

and $T = 76$ hours (,,).

We shall refer these cases as case I and case II everywhere in the following treatment.

In the case of the hyperbolic motions, the time would be comparatively less. Also as we increase the masses of the stars the time decreases rapidly. As a matter of fact, T varies inversely as the square root of the sum of the masses of the two stars.

We shall now study the phenomenon of the production of the tides in S_1 under the action of S_2. Let us now imagine that the latter is at a distance d from the former. In such a position the heights h_1 and h_2 of the tides in S_1 at the points nearest and farthest from S_2 would be given by [7]

$$h_1 = \frac{M_2}{M_1} \cdot \frac{R_1^4}{d^3} \cdot \left(\Delta_1 + \frac{R_1}{d} \Delta_3 + \frac{R_1^2}{d^2} \Delta_4 \right) \ldots \quad \ldots \text{ at the nearest pole,}$$

and
$$h_2 = \frac{M_2}{M_1} \cdot \frac{R_1^4}{d^3} \cdot \left(\Delta_2 - \frac{R_1}{d} \Delta_3 + \frac{R_1^2}{d^2} \Delta_4 \right) \ldots \quad \ldots \text{ at the farthest pole,}$$

where Δ's are certain numerical constants.

Similarly the maximum contraction in S_1 will be given by

$$h_3 = \tfrac{1}{2} \cdot \frac{M_2}{M_1} \cdot \frac{R_1^4}{d^3} \cdot \left(\Delta_2 - \tfrac{3}{4} \Delta_4 \frac{R_1}{d} \right) \ldots \quad \text{at the equator.}$$

To the first approximation we may put

$$h_1 = h_2 = \frac{M_2}{M_1} \cdot \frac{R_1^4}{d^3} \cdot \Delta_2$$

and
$$h_3 = \tfrac{1}{2} \cdot \frac{M_2}{M_1} \cdot \frac{R_1^4}{d^3} \cdot \Delta_2$$

and hence

$$h_1 = 2h_3 .$$

In the following tables the heights h_1 of the tides have been collected for different polytropic indices and different values of d :

**Case I* : Taking $R_1 = R_\odot = 7/1500$ astron. unit.

* Here n is quite different from the n used in §2 to §4 to denote $\frac{M_*}{M_1}$.

TABLE VI

d (astron. units).	$n=1$	$n=1.5$	$n=2$	$n=3$	$n=4$
1/30	21.7 10^{-6}	18.7 10^{-6}	16.8 10^{-6}	15.9 10^{-6}	14.7 10^{-6}
1/20	6.2 10^{-6}	5.3 10^{-6}	4.7 10^{-6}	4.3 10^{-6}	4.2 10^{-6}
1/10	0.7 10^{-6}	0.6 10^{-6}	0.5 10^{-6}	0.48 10^{-6}	0.47 10^{-6}
1/5	0.9 10^{-7}	0.8 10^{-7}	0.7 10^{-7}	0.6 10^{-7}	0.6 10^{-7}
3/10	0.3 10^{-7}	0.26 10^{-7}	0.23 10^{-7}	0.20 10^{-7}	0.20 10^{-7}
2/5	0.1 10^{-8}	0.97 10^{-8}	0.86 10^{-8}	0.77 10^{-8}	0.73 10^{-8}
1/2	5.8 10^{-9}	4.9 10^{-9}	4.3 10^{-9}	3.9 10^{-9}	3.8 10^{-9}
1	0.7 10^{-9}	0.6 10^{-9}	0.5 10^{-9}	0.48 10^{-9}	0.47 10^{-9}
5	5.8 10^{-12}	4.9 10^{-12}	4.3 10^{-12}	3.9 10^{-12}	3.8 10^{-12}
10	0.7 10^{-12}	0.6 10^{-12}	0.5 10^{-12}	0.48 10^{-12}	0.47 10^{-12}

TABLE VII

Case II : $R_1=2R_{\odot}$ and $R_2=4R_{\odot}$.

d (astron. units.)	$n=1$	$n=1.5$	$n=2$	$n=3$	$n=4$
1/30	1.39 10^{-3}	1.19 10^{-3}	1.07 10^{-3}	1.02 10^{-3}	0.94 10^{-3}
1/20	0.40 10^{-3}	0.34 10^{-3}	0.30 10^{-3}	0.27 10^{-3}	0.27 10^{-3}
1/10	44.8 10^{-6}	38.4 10^{-6}	32.0 10^{-6}	30.7 10^{-6}	30.1 10^{-6}
1/5	57.6 10^{-7}	51.2 10^{-7}	44.8 10^{-7}	38.4 10^{-7}	38.4 10^{-7}
3/10	19.2 10^{-7}	16.6 10^{-7}	14.7 10^{-7}	12.8 10^{-7}	12.8 10^{-7}
2/5	70.4 10^{-8}	62.4 10^{-8}	55.0 10^{-8}	49.6 10^{-8}	46.4 10^{-8}
1/2	371.2 10^{-9}	313.6 10^{-9}	275.2 10^{-9}	249.6 10^{-9}	243.2 10^{-9}
1	44.8 10^{-9}	38.4 10^{-9}	32.0 10^{-9}	30.7 10^{-9}	30.1 10^{-9}
5	371.2 10^{-12}	313.6 10^{-12}	275.2 10^{-12}	249.6 10^{-12}	243.2 10^{-12}
10	44.8 10^{-12}	38.4 10^{-12}	32.0 10^{-12}	30.7 10^{-12}	30.1 10^{-12}

From the above tables we know that the maximum tides are generated when $n=1$; hence we shall consider the case $n=1$ only.

Let the maximum heights of the tides generated in S_2 be given by h'_1 where

$$h'_1=\frac{M_1}{M_2}\cdot\frac{R_2^4}{d^3}\cdot\left|\Delta_2+\frac{R_2}{d}\Delta_3+\frac{R_2^2}{d^2}\Delta_4\right.$$

Now the distance between the distorted surfaces of the two stars would be zero, if

$$d = R_1 + h_1 + R_2 + h'_1$$

$$= R_1 + R_2 + \frac{M_2}{M_1} \cdot \frac{R_1^4}{d^3} \cdot \left[\Delta_2 + \frac{R_1}{d} \Delta_3 + \frac{R_1^2}{d^2} \Delta_4 \right]$$

$$+ \frac{M_1}{M_2} \cdot \frac{R_2^4}{d^3} \cdot \left[\Delta_2 + \frac{R_2}{d} \Delta_3 + \frac{R_2^2}{d^2} \Delta_4 \right]$$

Knowing R_1, R_2, M_1, M_2 and Δ's we can determine d from this. We find that the distorted surfaces would touch when

Case I : $d = 1/100$ astronomical unit,

Case II : $d = 1/30$,, ,, .

Thus in the case I the tidal elongations of the distorted surfaces touch each other when the distance between the centres of the two stars is about 1/100 astron. unit and in the case II when the distance between them is 1/30 astron. unit. If the distance between them be less than what is mentioned above, there would be a colliding action between the materials of the two stars. In case I as we assumed the shortest distance between the stars to be 1/40 astron. unit even at the perihelion of the relative orbit, the tides would not touch each other. In case II, the material contact or collision lasts as long as the stars remain within a distance of about 1/30 astron. unit of each other, but it must be remembered that mere material contact does not ensure the conditions for ejection and disruption.

We shall now study the effect of the relative motion of the stars on the phenomenon of the tides. For the sake of simplicity we shall regard S_2 at rest and S_1 moving relative to S_2 for the time being. Here it is to be noted that the stars are assumed to be non-rotating.

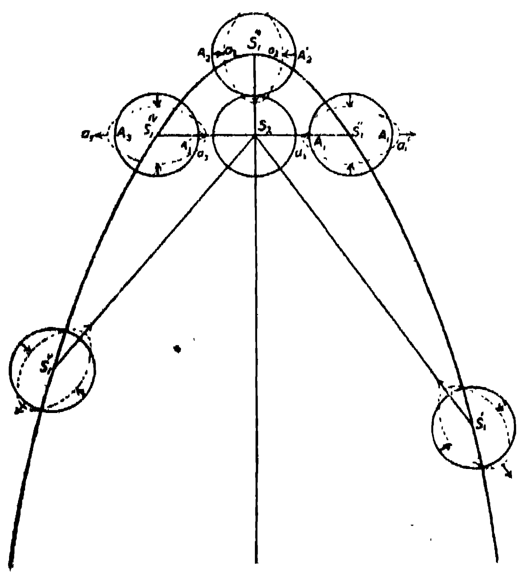

DIAGRAM III

In the diagram III S_1''' is the perihelion and S_1'' and S_1^{IV} are the ends of the latus-rectum. The complete circles represent the sections of the star's undisturbed surface by the relative orbital plane, whereas dotted figures represent the sections of the star's disturbed surface if in every position the tidal forces have got sufficient time to produce the tides.

For any possible formation of the planets, it is necessary only to study what becomes of the planetary ribbon when the stars begin to recede from each other after the closest approach.

During the short interval of a few hours (15 hrs. in Case I and 6.5 hrs. in Case II) the star S_1 moves from the position S_1'' to S_1^{IV} through S_1'''. A_1A_1', $A_2\,A_2'$, $A_3\,A_3'$ stand for the same diameter in the three positions of the star since we have taken the star to be non-rotating. During this time the tidal forces change directions two times (which may be noted at once by marking the direction of the tidal forces at any point such as A or A') and also the points of the maximum tides sweep over the whole section of the surface of S_1 by the relative orbital plane. When the star is at S_1'', A_1 is the point of the maximum tide and the material situated at A_1 moves towards a_1, but before the tidal material has moved over any considerable distance, S_1 moves to S_1''' and the direction of the tidal force at A_2 is reversed ; the matter is given acceleration in the direction exactly opposite to the previous one and the material at A_2 tends to move towards a_2 nullifying the previous motion. But before the material at A_2 moves any considerable distance towards a_2, the star S_1 moves to S_1^{IV}, once again changing the direction of the tidal forces. Thus we can see that the motion of the tidal material will be more or less oscillatory, but its amplitude would be much less than the maximum elongation possible under the circumstances. Thus it can be seen that as long as the star is between S_1'' and S_1^{IV}, there is little or no chance for the formation of the planetary ribbon.

As we have calculated above, when the distance between the stars is greater than 1/100 astron. unit in Case I and 1/30 astron. unit in Case II, even if it be possible for the tides to reach the maximum heights, they would not be able to touch each other and thus no planetary ribbon would be possible after the star has crossed the position S_1^{IV} as we have taken

$$S_2S_1^{IV} = 1/20 \text{ astron. unit.}$$

In order to satisfy the condition for the ejection of the material from S_1 sufficient for the formation of the planets we have to take S_2 to be very massive (rather unusually massive) as pointed out by the calculations in §2, §3 and §4. We have considered these two hypothetical cases because the previous workers (named in §1) have given much discussions to them. If we consider the masses which are required to ensure the conditions for the disruption and ejection of the necessary material the times calculated in these two cases are further diminished and the star S_1 takes much less time in moving from S_1'' to S_1^{IV}. Not only this,

the actual hyperbolic motion would be much faster and the calculated times would be further decreased.

Thus there seems to be absolutely no possibility of the formation of the desired planetary ribbon by a close encounter or the grazing collision between the two stars of usual masses.

§6. Let us now examine the hypothesis mentioned in §1, *viz.*, "that our sun might have been a binary star having a companion.......................and that the collision between this body and a passing star broke the companion into fragments from which the present planets were developed." Once the conclusions of the two-body problem discussed above are accepted it would seem that the discussion of the following three-body problem is superfluous because the formation of the planetary ribbon is fundamental here also but a slight consideration would show that the nearness of the third star would alter the situation to a great deal and under the action of the sun and the intruding star the disruption of the companion star may be facilitated. Hence it is necessary to discuss this aspect of the tidal problem *de novo*.

Let us assume that the masses of the sun, its companion and the intruding star are M_0, M_1 and M_2 respectively and that G is the centre of mass of M_0 and M_1.

Let us choose our axes in space with fixed directions. Let the coordinates of M_0 relative to M_1 be (x, y, z) and those of M_2 relative to G be (x_1, y_1, z_1), then the motion of M_0 relative to M_1 will be given[8] by

$$\frac{d^2x}{dt^2}=\frac{M_0+M_1}{M_0M_1}\cdot\frac{\delta V}{\delta x};\quad \frac{d^2y}{dt^2}=\frac{M_0+M_1}{M_0M_1}\cdot\frac{\delta V}{\delta y};\quad \frac{d^2z}{dt^2}=\frac{M_0+M_1}{M_0M_1}\cdot\frac{\delta V}{\delta z}$$

and that of M_2 relative to G will be given by

$$\frac{d^2x_1}{dt^2}=\frac{M_0+M_1+M_2}{M_2(M_0+M_1)}\cdot\frac{\delta V}{\delta x_1};\quad \frac{d^2y_1}{dt^2}=\frac{M_0+M_1+M_2}{M_2(M_0+M_1)}\cdot\frac{\delta V}{\delta y_1};$$

$$\frac{d^2z_1}{dt^2}=\frac{M_0+M_2+M_2}{M_2(M_0+M_1)}\cdot\frac{\delta V}{\delta z_1},$$

where the gravitational potential V is given by

$$V=\frac{M_0M_1}{r_{0,1}}+\frac{M_1M_2}{r_{1,2}}+\frac{M_2M_0}{r_{2,0}},$$

and $r_{0,1}$ = distance between M_0 and $M_1=\sqrt{x^2+y^2+z^2}$,

$$r_{1,2}=\text{distance between } M_1 \text{ and } M_2=\sqrt{\sum_{x,y,z}\left(x_1+\frac{M_0x}{M_0+M_1}\right)^2},$$

$$r_{2,0}=\text{distance between } M_2 \text{ and } M_0=\sqrt{\sum_{x_1,y_1,z_1}\left(x_1-\frac{M_1x}{M_0+M_1}\right)^2}.$$

Here it is now evident that V is a function of x, y, z ; x_1, y_1, z_1.

Therefore $dV = \sum_{x, y, z} \frac{\delta V}{\delta x} dx + \sum_{x_1, y_1, z_1} \frac{\delta V}{\delta x_1} dx_1$.

Hence $\frac{dV}{dt} = \frac{M_0 M_1}{M_0 + M_1} \sum_{x, y, z} \frac{d^2x}{dt^2} \cdot \frac{dx}{dt} + \frac{M_2(M_0 + M_1)}{M_0 + M_1 + M_2} \sum_{x_1, y_1, z_1} \frac{d^2x_1}{dt^2} \cdot \frac{dx_1}{dt}$.

Integrating we have

$$\tfrac{1}{2} \frac{M_0 M_1}{M_0 + M_1} v^2 + \tfrac{1}{2} \frac{M_2(M_0 + M_1)}{M_0 + M_1 + M_2} v'^2 = V + \text{constant}, \quad \ldots \quad (27)$$

where v is the velocity of M_0 relative to M_1 and v' is the velocity of M_2 relative to G. We have now to determine the constant.

Let us measure the time from the instant when M_2 was at an infinite distance from G and assume that the velocity of M_2 relative to G at that instant was v'_∞. Let us further assume that at that instant M_0 was describing a circular orbit relative to M_1 with a radius a. Therefore

$$\text{constant} = \tfrac{1}{2} \frac{M_2(M_0 + M_1)}{M_0 + M_1 + M_2} v'^2_\infty - \tfrac{1}{2} \frac{M_0 M_1}{a},$$

since the distances $r_{2,0}$ and $r_{1,2}$ were infinite initially and the contribution to V by the terms involving these distances can be neglected.

Thus we have at any subsequent instant

$$\tfrac{1}{2} \frac{M_0 M_1}{M_0 + M_1} v^2 + \tfrac{1}{2} \frac{M_2(M_0 + M_1)}{M_0 + M_1 + M_2} v'^2 - V = \tfrac{1}{2} \frac{M_2(M_0 + M_1)}{M_0 + M_1 + M_2} v'^2_\infty - \tfrac{1}{2} \frac{M_0 M_1}{a}. \quad \ldots \quad (28)$$

Equation (28) may be regarded as the *energy equation*.

§7. After the collision between M_1 and M_2 is over, a ribbon is supposed to be formed between them. Luyten has suggested[9] that "the capture of this ribbon by the sun is not instantaneous and since the portions of the filament most favourable to capture are balanced precariously around the point of equality of the attractions of M_1 and M_2, it would seem that the capture cannot take place until the attraction of the sun on the filament is considerably greater than that of either of the parent stars." It is quite apparent from this that it is necessary for the sun to move roughly parallel to that portion of the filament which is most likely to be captured for considerable time. Now the filament would move in the plane of the relative orbit of M_1 and M_2 and hence the sun should also move in the same plane. This is not possible unless and until the orbital plane of M_0 relative to M_1 and that of M_2 relative to M_1 actually coincide before and after the collision. If we take the orbital plane of M_2 relative to M_1 as the x-y plane, then in the equation (28) the velocity v and v' reduce to velocities in the same plane and hence z is to be taken to be

zero everywhere. It may also be mentioned that at the middle of the collision, the sun should move parallel to the middle of the filament and hence more or less parallel to the star M_2.

When M_2 has come considerably near to the binary system, the circular motion and the distance between the sun and its companion are bound to be disturbed. Let us assume that at some instant the distance between M_0 and M_1 is L and that it is moving with a velocity v relative to M_1 in the direction which makes an angle β with the straight line joining M_1 and M_2. Then the velocity of G at the instant relative to M_1 would be $\frac{M_0 v}{M_0+M_1}$ in the same direction as that

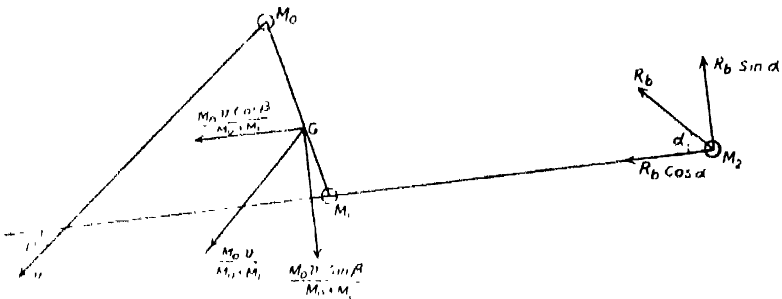

DIAGRAM IV

of the motion of M_0 (see diagram IV). Let us assume that at this instant M_2 is moving relative to M_1 with a velocity R_b and in the direction which makes an angle α with the straight line joining M_1 and M_2. Then the velocity of M_2 relative to G would be given by

$$v'^2 = R_b^2 + \left\{ \frac{M_0 v}{M_0+M_1} \right\}^2 - 2\frac{M_0 R_b v}{M_0+M_1}\cos(\alpha+\beta), \qquad \dots \quad (29)$$

where $\alpha+\beta$ is the angle between the directions of motions of G or M_0 and M_2, each relative to M_1.

As has been pointed out above, at the middle of the collision, M_0 must move parallel to M_2 and hence $\alpha+\beta=0$ at that instant.

In order that the collision between M_1 and M_2 may take place, they have to come so near each other that the motion of M_2 relative to M_1 may be assumed to be solely conditioned by M_1 for some time before the collision. Suppose that when M_2 is at a distance l_1 from M_1, it begins to describe hyperbolic orbit relative to M_1 entirely under the influence of M_1 with a velocity $\overline{R_b}$ $\left(> \sqrt{\frac{2(M_0+M_1)}{l_1}}\right)$. The equation to the orbit, the value of e and R_b, the velocity at any instant would be given by the equations (19), (18) and (20) respectively.

§ 8. Let us now investigate if it is possible for M_0 to continue its circular motion relative to M_1 right up to the instant when M_2 is at a distance l_1 from M_1 and is just beginning to describe a hyperbolic orbit relative to M_1 entirely under the influence of the latter. Now l_1 is so small that the attraction of M_1 on M_2 is appreciably greater than the attraction of M_0 on M_2. Also in order that M_2 may not collide with M_0 and that the hyperbolic motion of M_2 relative to M_1 may be possible, M_0 ought to be clearly out of its way, *i.e.*, ϕ, the angle between the line joining M_0 and M_2 and that joining M_2 and M_1 during this time ought to be greater than $\pi/2$ and less than $3\pi/2$, and the most favourable case is when $\phi=\pi$. In this case l_1 may be taken sufficiently great, say of the order a, at least. For definiteness we assume that $l_1=2a$.

Now α is the angle between the radius vector and the tangent to the hyperbolic orbit of M_2 relative to M_1 and hence is given by*

$$\tan\alpha=\frac{(e+1)\,d_1}{2ae\sin\alpha_0},$$

where α_0 is given by
$$2a=\frac{(e+1)d_1}{1+e\cos\alpha_0}$$

i.e.,
$$\sin\alpha_0=\sqrt{1-\left\{\frac{2a-(e+1)d_1}{2ae}\right\}^2}$$

and therefore
$$\tan\alpha=\frac{(e+1)d_1}{\sqrt{4a^2e^2-\{2a-(e+1)d_1\}^2}}.$$

We have $\beta=\frac{\pi}{2}$, as the orbit of M_0 is circular with respect to M_1 and

$$v^2=\frac{M_0+M_1}{a}$$

also
$$V=\frac{M_0M_1}{a}+\frac{M_2M_1}{2a}+\frac{M_2M_0}{3a},$$

since $\phi=\pi$.

Let v_1' be the value of v' in this position.

* Let the equation to the hyperbola be $r=\frac{l}{1+e\cos\theta}$. In Cartesian co-ordinates this reduces to $y^2-(e^2-1)x^2+2elx-l^2=0$. "$m$" of the tangent at a point $(a_1\cos\alpha_0,\ a_1\sin\alpha_0)$ is given by $m=\tan\theta=\frac{(e^2-1)a_1\cos\alpha_0-el}{a_1\sin\alpha_0}$. α, the angle between the radius vector and the tangent $=\theta-\alpha_0=\tan^{-1}\frac{\tan\theta-\tan\alpha_0}{1+\tan\theta\tan\alpha_0}=\tan^{-1}\frac{l}{a_1e\sin\alpha_0}$.

Substituting these values in (28), (29) and (20), we have

$$\frac{M_0M_1}{2a}+\frac{1}{2}\frac{M_2(M_0+M_1)}{M_0+M_1+M_2}v_1'^2-\left\{\frac{M_0M_1}{a}+\frac{M_1M_2}{2a}+\frac{M_2M_0}{3a}\right\}$$

$$=\frac{1}{2}\frac{M_2(M_0+M_1)}{M_0+M_1+M_2}v_\infty'^2-\frac{1}{2}\frac{M_0M_1}{a}$$

or

$$\frac{1}{2}\frac{M_2(M_0+M_1)}{M_0+M_1+M_2}v_1'^2=\frac{1}{2}\frac{M_2(M_0+M_1)}{M_0+M_1+M_2}v_\infty'^2+\frac{M_1M_2}{2a}+\frac{M_2M_0}{3a} \qquad \dots (30)$$

and

$$v_1'^2=R_b^2+\left\{\frac{M_0}{M_0+M_1}\right\}^2\frac{M_0+M_1}{a}+\frac{2M_0}{M_0+M_1}R_b\sqrt{\frac{M_0+M_1}{a}}\sin\alpha, \qquad \dots (31)$$

as $\beta=\frac{\pi}{2}$,

where
$$\tan\alpha=\frac{(e+1)\,d_1}{\sqrt{4a^2e^2-\{2a-(e+1)d_1\}^2}}$$

or
$$\sin\alpha=\frac{\sqrt{e+1}\,d_1}{2\sqrt{a^2(e-1)+ad_1}} \qquad \dots (32)$$

and
$$R_b^2=\frac{M_1+M_2}{a}+\frac{M_1+M_2}{d_1}(e-1). \qquad \dots (33)$$

Knowing d_1, v'_∞, M_0, M_1 and M_2, we can calculate e from (30), (31), (32), and (33) and thence we can find out R_b and v'_1.

A critical study of these equations (30), (31), (32) and (33) shows that in ordinary circumstances there is absolutely nothing against assuming that right up to the commencement of the hyperbolic motion of M_2 relative to M_1 at a distance of $2a$ from M_1, M_0, which is describing a circular orbit relative to M_1, is moving with the velocity $\sqrt{\frac{M_0+M_1}{a}}$; ϕ may be taken to be π.

Now the problem reduces to the following stage :—

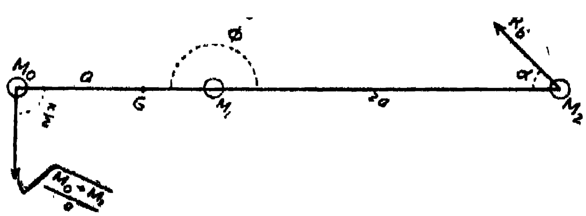

DIAGRAM V

M_0 is describing a circular orbit relative to M_1 with the velocity $\sqrt{\frac{M_0+M_1}{a}}$;

and is situated on the straight line joining M_1 and M_2 as we have taken $\phi=\pi$. M_2 is at a distance $2a$ from M_1 and it just commences its hyperbolic motion relative to M_1 entirely under the influence of the latter with the relative velocity R_b ; the eccentricity e of the relative orbit is known.

Now the theory requires that M_1 is ionized from M_0 due to the encounter and collision and hence at the middle of the collision M_0 must possess some velocity greater than the parabolic velocity at its position relative to M_1 ; for, at this instant, the tidal forces on M_1 reach their maximum and thus this situation is the most favourable for the ionization. We shall suppose that at the middle of the collision, M_0 has got a velocity equal to $\kappa\sqrt{\frac{2(M_0+M_1)}{a_1}}$ where $\kappa\geq$

and a_1 is the distance of M_0 from M_1 at that instant.

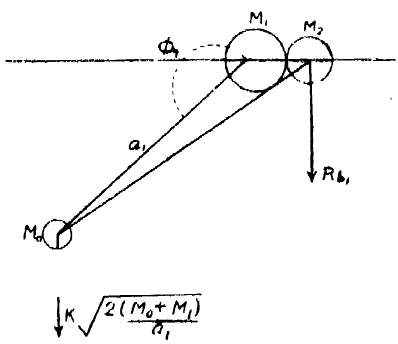

DIAGRAM VI

Now $$V=\frac{M_0M_1}{a_1}+\frac{M_1M_2}{d_1}+\frac{M_2M_0}{\sqrt{a_1^2+d_1^2-2a_1d_1\cos\phi_1}},$$

where ϕ_1 is the angle between the lines of centres of M_0, M_1 and M_1, M_2,

$R_{b_1}^2$ = square of the velocity of M_2 relative to M_1 in this position

$$=\frac{2(M_1+M_2)}{d_1}+\frac{(M_1+M_2)(e-1)}{d_1}\quad\text{from (20)} \qquad \dots (34)$$

$$v^2=\frac{2(M_0+M_1)}{a_1}\kappa \qquad \text{(supposition)}, \qquad \dots (35)$$

$\alpha+\beta=0$,

$v_2'^2$ = square of the velocity of M_2 relative to G in this position

$$=R_{b_1}^2+\left[\frac{M_0}{M_0+M_1}\right]^2\frac{2(M_0+M_1)}{a_1}\kappa^2-\frac{2M_0}{M_0+M_1}R_{b_1}\kappa\sqrt{\frac{2(M_0+M_1)}{a_1}} \qquad \dots (36)$$

and $\frac{M_0M_1}{a_1}(\kappa^2-1)+\frac{1}{2}\frac{M_2(M_0+M_1)}{M_0+M_1+M_2}v'^2_2+\frac{M_0M_1}{2a}$

$$=\frac{M_1M_2}{d_1}+\frac{M_2M_0}{\sqrt{a_1^2+d_1^2-2a_1d_1\cos\phi_1}}+\frac{1}{2}\frac{M_2(M_0+M_1)}{M_0+M_1+M_2}v'^2_\infty \quad \ldots \quad (37)$$

from (28).

Making use of the value of e, as determined previously, in (34), (36) and (37), we can obtain an equation involving M_0, M_1, M_2, κ, a_1, v'_∞, d_1 and a.

Assuming values for M_0, M_1, M_2, a, d_1 and v'_∞, we shall have an equation between κ and a_1. From this we can investigate if it is possible to have any value for a_1 of the order of 10 to 18 astronomical units (the distance between the sun and the major planets) for some reasonable value of $\kappa \geq 1$.

§9. NUMERICAL CALCULATIONS

Case I : Let us assume that

$M_0=M_1=M_2=M_\odot$ mass of the sun

$d_1=1/40$ astron. unit

$a=18$,, ,, ,,

$v'_\infty=70$ Km./sec. $=7/3$ units/sec.,

where 1 unit$=30$ Km.

Substituting these values in (30), (31), (32) and (33), we get

$$v'_1=\sqrt{\frac{67}{12}} \text{ units/sec.} \quad \ldots \quad (30')$$

$$\sin\alpha=\frac{\sqrt{e+1}}{1440\sqrt{e-1+\frac{1}{720}}}, \quad \ldots \quad (32')$$

$$R_b^2=80\left\{e-1+\frac{1}{720}\right\} \quad \ldots \quad (33')$$

and

$$e=\frac{769}{720}-\frac{\sqrt{e+1}}{4320\sqrt{80}}. \quad \ldots \quad (31')$$

Therefore $e=1.068$ (approx.)

and

$$R_b=\frac{\sqrt{50}}{3} \text{ units/sec.}$$

Making use of these values in (34), (36) and (37), we have

$$R_{h_1}=\sqrt{165.44} \text{ units/sec.} \quad \ldots \quad (34')$$

and

$$v_2'=\sqrt{165.44+\frac{\kappa^2}{a_1}-\frac{25.724}{\sqrt{a_1}}\kappa} \quad \ldots \quad (36')$$

Also $$(1.33\,\kappa^2-1)\frac{1}{a_1}-\frac{1}{a\pm.03}-\frac{8.58}{\sqrt{a_1}}\,\kappa+13.36=0 \qquad (37')$$

positive or negative sign being taken according as ϕ_1 is equal to π or 0.

Equation (37′) defines a relation between κ and a_1. The values of a_1 for different values of κ have been tabulated below :—

TABLE VIII

κ	With $+ve$ sign in (37′)	With $-ve$ sign in (37′)
1	$.0011<a_1<.0012$	$.042<a_1<.043$
	$.49<a_1<.50$	$.51<a_1<.52$
2	$1.08<a_1<1.09$	$.033<a_1<.034$
	$.07<a_1<.08$	$1.10<a_1<1.11$
3	$1.99<a_1<2.00$	$2.04<a_1<2.05$
	$.297<a_1<.298$	$.024<a_1<.025$

Case II : Let us assume that

$$M_0=M_\odot,\ M_1=2M_\odot,\ M_2=8M_\odot,$$
$$R_0=R_\odot,\ R_1=2R_\odot,\ R_2=4R_\odot$$

We have taken R_1 and R_2 such as to give sufficient densities to M_1 and M_2 so that ultimately a ribbon of sufficient mass may be formed by a mild collision between M_1 and M_2 (if this be possible). If they are taken large, then to produce a ribbon of desired mass, sufficiently deep collision will be required; here we may put

$$d_1=\tfrac{1}{38}\text{ astron. unit } (R_1+R_2>\tfrac{1}{38}\text{ astron. unit})$$

and $$v'_\infty=70\text{ km./sec.}=7/3\text{ units/sec.}$$

Then from (30), (31), (32) and (33), we have, as in the Case I,

$$e=1.014 \text{ (approx.)}$$

and $$R_b=\sqrt{5.876}\text{ units sec.}$$

Hence we get

$$(2.73\kappa^2-2)\frac{1}{a_1}-\frac{8}{a_1\pm.03}+221=20.12\,\kappa\sqrt{\frac{6}{a_1}}, \qquad \ldots \quad (37'')$$

the positive or negative sign being taken according as ϕ_1 is put equal to π or 0.

The values of a_1 for different values of κ, as obtained from (37″), are tabulated below :—

TABLE IX

κ	With $+ve$ sign in (37″)	With $-ve$ sign in (37″)
1	$0.0002 < a < .00021$	$.000 < a_1 < .0004$
	$0.093 < a_1 < 0.094$	$.0044 > a_1 < .0054$
		$.04 < a_1 < .05$
		$.12 < a_1 < .13$
2	$.008 < a_1 < .009$	$.037 < a_1 < .038$
	$.18 < a_1 < .19$	$.203 < a_1 < .204$
3	$a_1 = .03$	$.035 < a_1 < .036$
	$a_1 - .3$	$.38 < a_1 < .39$

§10. *Conclusion* :—In sections §2 to §5, we have seen that even in the most favourable situations, there is little or no possibility for the formation of the planetary ribbon due to the close encounter or the grazing collision between two stars of usual masses.

Tables VII and IX show that for every value of κ (from 1 to 3) the corresponding values of a_1 are very small. Of these the admissible values are only those which satisfy the equations of conservation of angular momentum also ; but whichever value be selected, at the middle of the collision between M_1 and M_2, the sun M_0 would come so very near to M_1, and hence to M_2 that a collision or a very close encounter can hardly be avoided.

In view of the above facts, we can say that no existing tidal theory can satisfactorily explain the origin of the solar system.

§11. In the end I wish to express my very respectful thanks to Prosessor A. C. Banerji for his keen interest during the preparation of this paper.

NOTE

A month after writing this paper, the important work of Dr. Spitzer was published in the December (1939) issue of the Astrophysical Journal. From astrophysical considerations Spitzer has proved that even if the desired planetary ribbon is assumed to be formed by a close encounter or a grazing collision between two stars, it will be diffused in space without giving birth to the planets. In the present paper the author has shown from purely dynamical considerations that no planetary ribbon can be formed. Thus from entirely different considerations, Dr. Spitzer's work also supports the fundamental conclusion of this paper that the existing tidal theories are unable to explain the formation of the solar system.

REFERENCES

1 Russell, H. N.—" The Solar System and its origin," p. 135 (1935).
2 Lyttleton--M. N., Vol. 96, pp. 559 568 (1936).
3 Luyten and Hill—Astrophysical Journal, Vol. 86, p. 469 (1937).
4 Lyttleton—M. N, Vol 98, p. 536 (1938).
5 Luyten--M. N., Vol. 99, p. 692 (1939).
6 Jeans—" Problems of Cosmogony and Stellar Dynamics," p. 45.
7 S. Chandra Sekhar—M. N, Vol. 93 (1933), p. 455. The numerical values of Δ s depending on the polytropic index *n* are given here.
8 Brown and Shook -" Planetary Theory " (1933), pp. 11-13.
Luyten--M. N., Vol. 99 (1939), p. 692.

ON THE INTENSITY VARIATIONS OF THE DOWN-COMING WIRELESS WAVES FROM THE IONOSPHERE*

By S. R. KHASTGIR, D.Sc. (EDIN.), MEM.I.R.E.
Dacca University

AND

ANIL KUMAR RAY, M.Sc.

(Received for Publication, June 19, 1940)

ABSTRACT. Experiments are described with an aerial system for suppressing the ground-wave. After having suppressed the ground-wave, the variations of the intensity of the down-coming wireless waves were studied. Typical continuous records of the variations of the intensity of such waves are presented. It has been shown that the time-variation of the amplitude of the down-coming waves is consistent with Rayleigh's formula for random scattering. The amplitude variation can therefore be explained as due to the interference of waves scattered from a series of diffracting centres at the ionosphere.

The most probable value of the amplitude of the down-coming wave as obtained from the experimental data on the intensity variations of the same wave was compared with the amplitude of the ground-wave. Between Dacca and Calcutta, the ratio of the vertical electrical forces produced by the ground-wave and the down-coming wave was thus estimated.

I. INTRODUCTION

Appleton and Ratcliffe[1] had previously shown that in the case of reception of wireless signals on a wavelength of about 300 metres at a distance of about 130 km. the observed signal variations were due chiefly to variations in the intensity of the down-coming wave. They had also concluded that the variations in the phase relation between ground- and sky-waves were a secondary cause of fading and that changes in the angle of incidence or polarization of the down-coming waves were not responsible in any marked degree for signal variations. Working on wavelengths between 200 and 500 metres for distances of transmission less than 200 km. Ratcliffe and Pawsey [2] subsequently made a study of the intensity variations of the down-coming wireless waves. Considering the possible causes of intensity variations in the light of their experimental results, they suggested that a major cause of "fading" was the interference at the ground, of waves "scattered" from a series of diffracting centres distributed over some area in the ionosphere. In fact they observed lateral deviations of the wireless waves after reflections from the ionospheric layers. Further experi-

* Communicated by the Indian Physical Society.

ments by Pawsey[3] confirmed these conclusions. He showed that the time-variation of the amplitude of the reflected wave was consistent with the idea of random scattering at the ionosphere.

The object of the present investigation was to undertake a study of the variations of the intensity of the down-coming wave originally coming from the Calcutta V.U.C. station ($\lambda = 370.4$ m.) and received during the night hours at Dacca and to test whether the observed variations could be traced to similar random scattering at the ionosphere. For that purpose in view it was necessary to have the ground-wave suppressed.

RECEIVING SYSTEMS FOR THE ATMOSPHERIC WAVE

(*a*) Aerial system:

The aerial system used in this investigation was similar to that used by Ratcliffe and Pawsey[2]. The system was a combination of a vertical aerial with a triangular loop aerial with only two turns having its plane (which was vertical) lying in the direction joining the transmitter and the receiver (Calcutta and Dacca). The two aerials were coupled as shown in fig. 1 by way of a variable mutual inductance M between two suitable coils L_a and L_b, each one being in series with each of the two aerials. The two coils and the vertical aerial tuning condenser C_a were contained in a properly shielded box. The antenna effect in the loop was eliminated by arranging the loop circuit to be perfectly symmetrical and earthing the mid-point as shown in the figure.

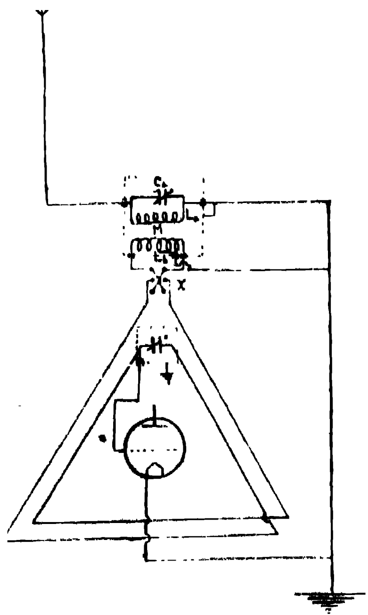

FIGURE 1

(*b*) The Receiver:

The receiving set which was of a regenerative type consisted of a H.F. amplifier, a detector and two L.F. amplifiers. (Fig. 2.) The regeneration was controlled by a variable condenser. A reflecting moving-coil galvanometer was placed in the anode circuit of the detector valve. With the help of a low tension battery and a variable resistance, the no-signal anode current through the galvanometer was balanced out. After suitable adjustments (to be described subsequently) of the suppressed-ground-wave aerial system and carefully tuning the set and adjusting its reaction condenser, the deflections produced in the balanced galvanometer due to the signals were noted. The zero reading was taken on short-circuiting the tuning condenser. A loud-speaker was placed as shown at the output end of the receiver so that the signal could be heard simultaneously with the deflections produced in the balanced galvanometer placed in the anode circuit of the detector valve.

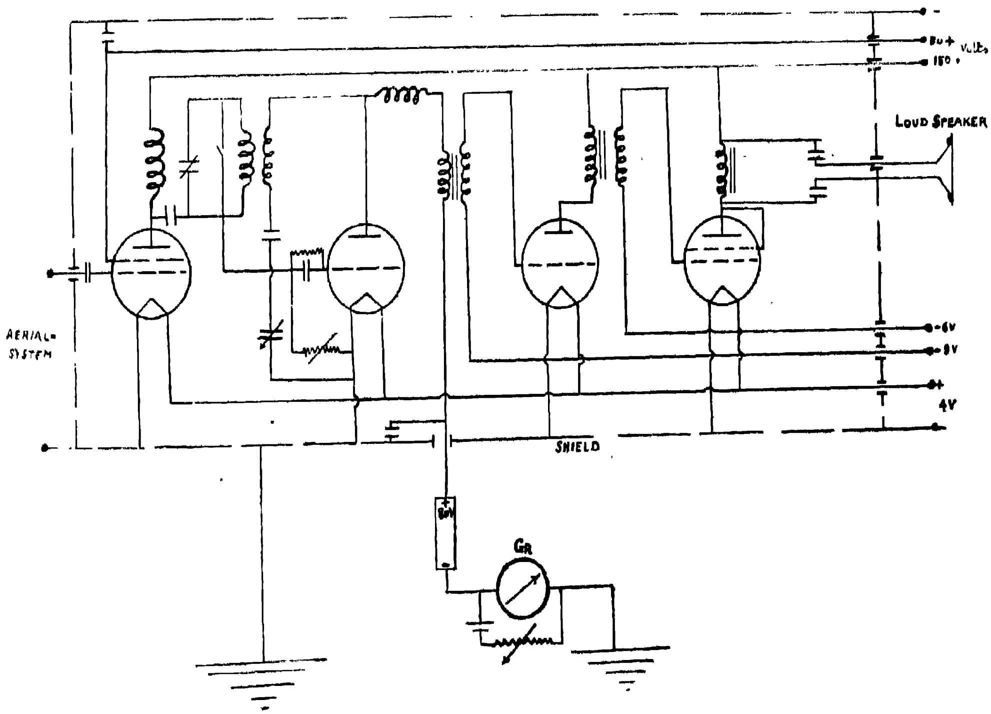

FIGURE 2

3. THEORY AND METHOD OF GROUND-WAVE SUPPRESSION

Let the down-coming wave incident at an angle i have a component of the electric force E_1 in the plane of propagation and let the electric field of the

ground-wave be given by E_0. We shall denote the corresponding magnetic fields by H_1 and H_0. The angular frequency of the fields is denoted by p.

If E_L represent the e.m.f. induced by the wave in the loop-circuit of the suppressed-ground-wave system and E_A the e.m.f. in the vertical aerial, then when the ground-wave alone is present, we have

$$E_L = \alpha \frac{\partial H_0}{\partial t} = jp\beta E_0,$$

where α and β are circuit constants and $E_A = hE_0$, where h is the vertical aerial height.

Here α, β and h are all real quantities.

If Z_L and Z_A are respectively the complex impedance of the loop and the equivalent series circuit of the vertical aerial, the current in the loop circuit is given by

$$i_L = \frac{jpE_0\left\{\beta - \dfrac{Mh}{Z_A}\right\}}{Z_L + \dfrac{p^2M^2}{Z_A}} \qquad (1)$$

If now the value of M is adjusted so that

$$\beta = \frac{M.h}{Z_A} \qquad \ldots \qquad (2)$$

the ground-wave will be completely suppressed. This condition means that the vertical aerial circuit should be tuned. Suppression is, however, independent of the tuning of the loop circuit.

The adjustements for the ground-wave suppression were made during the day when the ground-wave alone was present. The adjustments consisted in

(1) accurately tuning the vertical aerial after having disconnected the loop and also tuning the loop separately with the help of the shielded tuning condenser and in

(2) varying the mutual inductance M after restoring the original connections of the aerial system, till there was no current in the balanced galvanometer and no sound in the loud-speaker.

During the night, when the down-coming wave is present, the loop-circuit current is given by

$$i_L = \frac{2jpE_1\left\{\beta - \dfrac{Mh}{Z_A}\,\mathrm{Sin}\ i\right\}}{Z_L + \dfrac{p^2M^2}{Z_A}} \qquad \ldots \qquad (3)$$

(The ground-reflection coefficient for the medium waves is taken as unity.)

Under the condition of ground-wave suppression set out in (2), *viz.*,

$$\beta = \frac{M.h}{Z_A}$$

we have, therefore,

$$i_L = \frac{2jpE_1\beta(1 - \text{Sin } i)}{Z_L + \dfrac{p^2M^2}{Z_A}} \tag{4}$$

Thus the value of E_1 could be determined in terms of the loop current i_L which again could be derived in terms of the deflection produced in the balanced galvanometer of the receiving set.

4. TESTS FOR GROUND-WAVE SUPPRESSION AND THE RESPONSE CURVES OF THE AERIAL SYSTEM

Tests whether a zero signal was due to a decrease of sensitivity or to the desired balancing of E_A and E_L were made as follows :

(*a*) *A further increase of M caused the signal to reappear* —

This showed that the zero was due to a balance of E_A and E_L, otherwise the signal would continually decrease with further increase of M.

(*b*) *On reversing M* with the help of a commutator arrangement x (shown in figure 1) *a relatively large signal appeared*. This was also an indication to show that the observed suppression was due to the desired balance.

The sensitivity of the suppression arrangement is shown in figure 3. The deflections of the balanced galvanometer of the receiving set were observed for the different dial readings of the vertical aerial coil. In the actual arrangement the loop coil was kept fixed and the vertical aerial coil was tilted to vary the mutual inductance between them. There was no deflection in the galvanometer when the dial reading of the vertical aerial coil was 72.

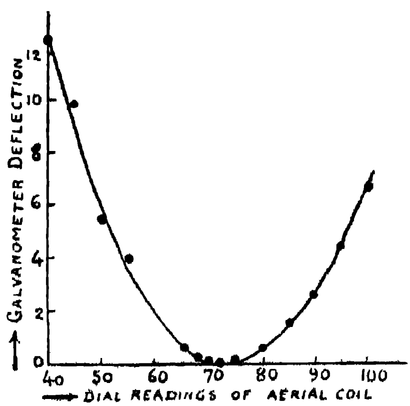

FIGURE 3

5. THE CALIBRATION OF THE RECEIVING SET AND THE CALCULATION OF THE FIELD-STRENGTH

The circuit diagram of the arrangement for calibrating the receiving set is given in figure 4. A current-attenuating-unit was devised. In this arrangement a Hull-cylinder in series with a small fixed condenser C_1 was placed in parallel with a big condenser C_2. This attenuation unit was carefully shielded and was connected as shown in the diagram with a variable condenser C and a coil L which was coupled to the coil of a neighbouring oscillator. An A.C. milliammeter was placed in the main calibration circuit and a similar milliammeter was inserted in the Hull-cylinder branch. By inducing a large current (which was measured) in the main circuit and a corresponding small current (which was also measured) in the Hull-cylinder branch, the current-attenuation-ratio was determined; or, in other words, the current through the Hull-cylinder branch was known as a definite fraction of the main current.

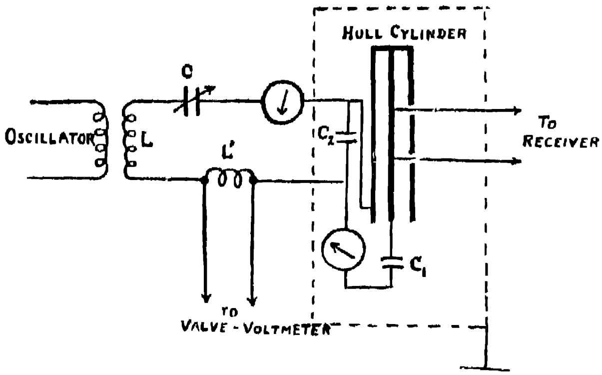

FIGURE 4

A suitable current was then induced into the calibration circuit from the neighbouring oscillator so that the voltage developed across the two tapping points (3 cm. apart) on the Hull-cylinder (from which leads were taken to the input terminals of the receiving set) was of such a value as to produce a deflection in the balanced galvanometer (G_B) of the receiving set comparable with the deflections produced by the night signals received by the suppressed ground-wave aerial system. In fact it was necessary to induce a certain range of small currents for this purpose. The corresponding currents in the Hull-cylinder branch were then evaluated. A small coil L′ was also inserted in the main circuit. Connections were taken from the two ends of this coil to the input terminals of a valve-voltmeter. The balanced galvanometer in the anode circuit of the valve-voltmeter gave perceptible deflections when small currents which did not produce any effect on the A.C. milliammeter in the main circuit were

passed. From the calibration graph of the valve-voltmeter which was drawn for the purpose, the values of the small currents giving rise to these deflections in the galvanometer of the valve-voltmeter could then be obtained. The voltage-drops across the tapping points on the copper rod of the Hull-cylinder from which the leads were taken out were then determined, the inductance of the rod inside the cylinder being given by $L = \log_e \frac{R}{r}$ per cm., where R is the inner radius of the cylinder and r the outer radius of the rod.

The deflections of the balanced galvanometer (G_B) in the receiving set were then observed for a suitable range of known applied voltages and a calibration graph drawn showing these deflections for the different voltages. This calibration graph was utilised for determining the voltages induced across half the loop of the aerial system which produced the observed deflections in the receiver galvanometer (G_B) due to the constantly varying amplitudes of the down-coming wave from the ionosphere.

The field-strength of the down-coming wave was obtained from:

$$E = \frac{7{\cdot}6 . R_A}{A.N.f^2.L_A} . V . 10^{10} \text{ volts/metre} \tag{8}$$

where N = no. of turns of the wire in the loop-aerial.

V = voltage developed across the loop.

A = area of the loop in sq. cm.

R_A = total radio frequency loss-resistance of the loop circuit in ohms.

L_A = inductance of the loop-circuit in henrys, and

f = frequency of the waves in cycles per sec.

On substituting the values of the different quantities used in the present work, the expression would reduce itself to

$$E = 1{\cdot}94V. \tag{9}$$

6. EXPERIMENTAL RESULTS

Variations of the intensity of the down-coming waves

After having suppressed the ground-wave in the daytime, continuous records every half minute of the deflections of the balanced galvanometer in the receiving set connected with the aerial system were taken. Corresponding to these observed galvanometer deflections, the voltages developed across the loop were obtained from the calibration graph mentioned before. From a knowledge of the voltages, the field-strengths were then calculated with the help of (9). The variations of the field-strengths of the down-coming waves received on the nights of 10.3.39. and 11.3.39. are shown in Figure 5.

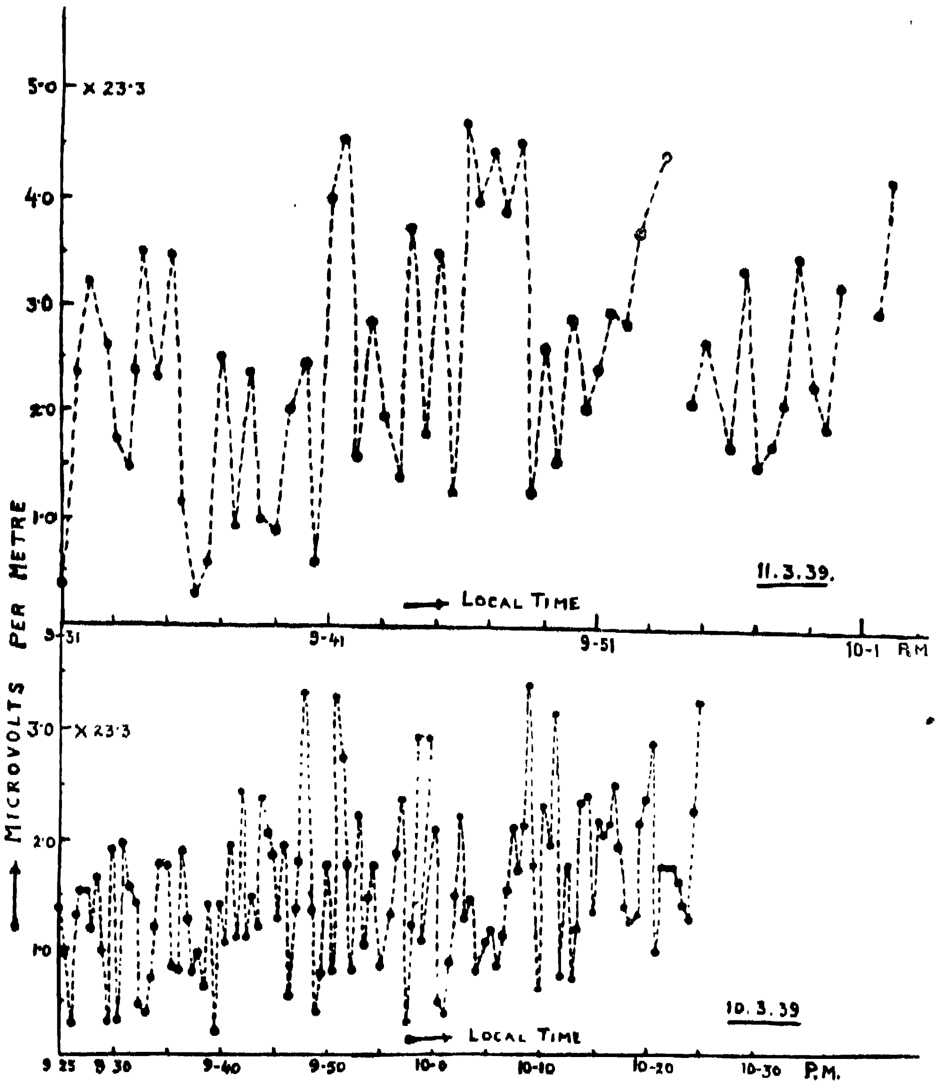

FIGURE 5

7. COMPARISON OF EXPERIMENTAL RESULTS WITH RAYLEIGH'S CALCULATIONS BASED ON RANDOM SCATTERING

If a single down-coming wave is built up of elementary contributions from a series of diffracting centres distributed more or less at random in the ionosphere, the resultant electric field would then be produced by compounding a set of components of random amplitudes and phases. Late Lord Rayleigh[4] deduced an expression for the probability of occurance of any resultant amplitude on the assumption of a large number of components of random phases. The probability is given by the expression :

$$P' = \frac{2}{R^2} \cdot e^{-\frac{r^2}{R^2}} \cdot r,$$

where R^2 is the sum of the squares of the components and $P'.dr$ is the probability of a resultant amplitude between r and $r+dr$. (Here R^2 is not known.)

The distribution of the amplitudes of the down-coming wave was found for each set of our observations and each of the distribution curves was compared with Rayleigh's distribution curve. The whole range of the observed amplitudes was accordingly divided into a number of equal parts, each part being conveniently made equal to $.8k$ where $k = 23.3 \times 10^{-6}$. The number of times the observed amplitude was found to lie between r and $r + .8k$ was then counted and a distribution curve in each case was drawn showing the number of amplitudes lying between r and $r+dr$ against the average value of r. The actual distribution curves for the two sets of observations are shown in Figure 6. In one of the curves, the most probable amplitude of the down-coming wave came out to be 1.2×23.3 or $28\mu V$/metre, whereas in the other curve the most probable value of the amplitude was 2×23.3 or $46.6\ \mu V$/metre.

In constructing the distribution curves according to Rayleigh, the following procedure was adopted :

According to Rayleigh, $$P' = \frac{2}{R^2} \cdot e^{-\frac{r^2}{R^2}} \cdot r.$$

The maximum value of P' corresponds to $R^2 = 2r_m^2$.

This can be derived by differentiating P' with respect to r and putting

$$\frac{dP'}{dr} = 0.$$

Thus $$P' = \frac{r}{r_m^2} \cdot e^{-\frac{r^2}{2r_m^2}}.$$

Here r_m is that value of r for which the number of observations is maximum. Substituting the experimental value of r_m from each distribution curve, the values of P' were calculated for various values of r. These values were afterwards multiplied by a suitable constant to give the best possible fit with each of the observed distribution curves. The computed distribution curves giving the best possible agreement with the actual distribution curves are shown by dotted lines in the same diagrams in Figure 6. It can therefore be said that the intensity variations of the down-coming wave is due largely to irregular scattering at the ionosphere.

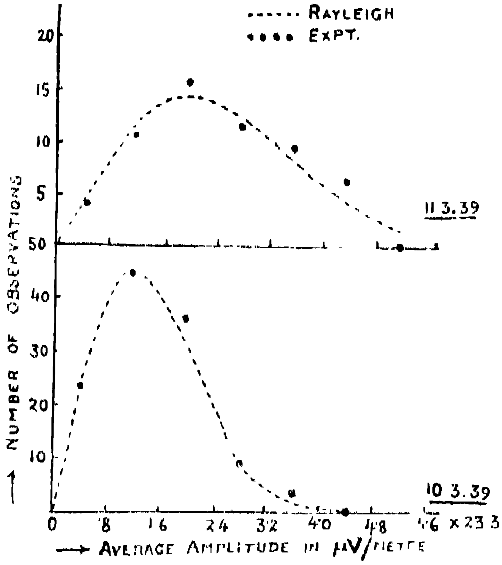

FIGURE 6

8. DETERMINATION OF THE FIELD-STRENGTH OF THE GROUND-WAVE AND OF THE RATIO OF THE VERTICAL ELECTRICAL FORCES PRODUCED BY THE DOWN-COMING WAVE AND THE GROUND-WAVE

Having obtained an estimate of the amplitude (E_1) of the down-coming wave, it was desired to obtain the value of the amplitude (E_0) of the ground-wave from the same transmitting station, so that the determination of the ratio E_1/E_0 could be possible.

The determination of the amplitude of the ground-wave was the same as the measurement of the field-strength of the Calcutta station in daytime when the ground-wave alone was present. For this measurement, observations of the deflections of the receiver galvanometer due to the day-signals from Calcutta were taken using only a loop aerial. After constructing the necessary calibration graphs, the value of the field-strength during the daytime was obtained. The mean field-strength of the ground-wave was found to be equal to 147.6 μV/metre.

Taking 28 μV/metre to be the field-strength of the down-coming wave for one set of observations on 10.3.39, $\frac{E_1}{E_0} = \frac{1}{5}$ and taking 46.6 μV/metre to be the field-strength for the other set of observations on 11.3.39., we have $\frac{E_1}{E_0} = \frac{1}{3}$. Thus, between Dacca and Calcutta, the values of the ratio of the vertical electrical forces produced by the ground-wave and the down-coming wave for these two

sets of observations are 3 and 5. From the analysis of fading observations by Sengupta and Khastgir [5] this ratio has been previously found to be 3 or 4.

REFERENCES

[1] Appleton and Ratcliffe, *Proc. Roy. Soc. A.*, **115**, 29 (1927).
[2] Ratcliffe and Pawsey, *Proc. Camb. Phil. Soc.* **29**, 301 (1933).
[3] Pawsey, *Proc. Camb. Phil. Soc.* **31**, 125 (1935).
[4] Rayleigh, Collected Works, **1**, 445.
[5] Sengupta and Khastgir, *Ind. Jour. Physics*, **10**, 133, (1936).

ON WIDE BAND-PASS EFFECT IN CRYSTALS ASSOCIATED WITH NEGATIVE IMPEDANCE ELEMENTS AND DEVELOPMENT OF WIDE-BAND LOW-LOSS CRYSTAL BAND-PASS FILTERS

By S. P. CHAKRAVARTI

AND

N. L. DUTT

(*Received for publication, June 18, 1940*)

ABSTRACT. The band-pass crystal filters regarded to be the best from band-width point of view are (1) four-terminal lattice filter (consisting of crystals, condensers and coils) and (2) four-terminal resistance compensated filter. The former gives a maximum band width of 5 to 6 Kc/s at the expense of high attenuation in the transmission band. The latter can give a band-width of 10 Kc/s or so with lesser attenuation and is only suitable for use in unbalanced circuits such as for coupling unbalanced tube systems.

The present paper relates to "wide-band band-pass effect" obtained from combination of crystal and stabilized negative impedance elements in two-terminal networks and four-terminal balanced sections whereby new means have been provided to design and construct wide-band band-pass filters and couplings giving band-widths up to 10 Megacycles per second or more with lower attenuation in the transmission band. The best sharpness of cut-off obtainable in these filters is of the same order as in the two-section four-terminal lattice filter consisting of crystals, condensers and coils.

The mechanism of the band-pass action and the application of these wide-band band-pass filters and couplings to multi-channel radio-telephone and television systems are discussed.

1. PIEZO-ELECTRIC CRYSTALS AS ELEMENTS IN WAVE FILTERS

Electric wave-filters must transmit without distortion waves with frequencies lying between two limits say, f_1 and f_2 c. p. s., and attenuate sufficiently all waves with frequencies lying outside the above limits

The "percentage band-width" is given by $(f_2-f_1)/f_m$, and the "percentage separation-ranges" on the two sides are given by $({}_1f_\infty-f_1)/f_1$ and $({}_2f_\infty-f_2)/f_2$ where f_m = mean frequency of the band, and ${}_1f_\infty$ and ${}_2f_\infty$ are frequencies of infinite attenuation adjacent to f_1 and f_2 respectively.

At lower frequencies, a filter made up of coils and condensers can seperate frequencies well because the "percentage band-width" and the "percentage

separation-range" are relatively larger. At high frequencies, the percentage band-width obtained from the same band width is much smaller and the insertion loss for a filter made up of coils and condensers cannot be made to increase faster with frequency than a certain percentage rate due to low 'Q' (*i.e.* reactance/resistance) values of coils and condensers and therefore a sudden frequency discrimination cannot be realised between transmission and attenuation bands.

If elements such as piezo-electric crystal resonators which have large 'Q' values are employed, filters having small percentage band-widths as well as attenuating in small percentage separation-ranges can be constructed.

It is only during last few years that filter sections containing crystal elements have been realized in the pratical field for use in high-frequency systems. Low-pass and high-pass crystal filter sections so evolved have been found to meet the requirements of the field satisfactorily, but the band-pass crystal filter sections are known to present certain limitations which have prevented their use in *wide-band* high-frequency systems.

2. LIMITATIONS OF EXISTING CRYSTAL BAND-PASS FILTERS

The simplest types of band-pass filters use crystal elements and condensers in ladder sections. The crystal elements of high Q value have been used with the best condensers having Q of the order of 10,000. The effect of capacitance connected in series with or parallel to a crystal is in the narrowing of the band-width. The limitations in the ladder type of sections are (1) very small transmission band-width and (2) the position of the attenuation peak frequencies.

By using lattice sections (consisting of crystal elements and condensers only), it is possible (1) to obtain a band-width roughly twice that of the ladder type and (2) to adjust the positions of attenuation peak frequencies with respect to the transmission band. The use of more than four crystals in any network configuration, employing crystal elements and condensers only, does not give larger band-width but contributes to higher attenuation in the transmision band on the other hand.

To obtain a filter section for a wider band-width at the same time maintaining advantages of sharply resonant crystals, lattice section using crystals, condensers and inductances has been developed[1,6]. The comparatively lower Q value of coils used in such a section gives large attenuations in the transmission band. A still wider band-width with somewhat lesser attenuation can be obtained from resistance compensated lattice filters[1] using similar elements.

Comparative figures regarding band-width, percentage band-width, percentage separation-ranges and attenuation in transmission band of some existing types[1] of crystal band-pass filters are given in Table I.

TABLE I

No.	Type	$f_2 \sim f_1$ (Kc/s)	$(f_2 \sim f_1)/f_m$	$({}_2f_m \sim f_2)/f_m$	Attenuation db
	Ladder section (crystals and condensers)	150·12—149·86 =0·26	·0017	·0014	1—2
2	Two Lattice sections (c condensers and coils)	65 3—62·7 =2·6	·04	·03	3·5
3	Do.	499·75—496·85 =2·9	·0058	·02	17·0—17·5
1	Resistance compe lattice section	470—460 =·10	·021	·01	3·5

It will be seen from the Table I that two lattice sections formed of crystals, condensers and coils and connected in tandem suffer from two serious discrepancies :—(1) the maximum band-width obtained is still much narrower for most requirements of communication systems, (2) even for securing that band-width the attenuation in the transmission band becomes large and (3) the attenuation increases as sections are designed for higher and higher frequency range.

The limitations stated above have been found to be removed in the new types of band-pass filters developed for high frequency radio systems as a direct consequence of the "wide band-pass effect" discussed in the following sections. The best sharpness of cut-off obtained in the new type of four-terminal crystal filter is of the same order as the sharpness of cut-off of two-section lattice filter made up of crystals, coils and condensers.

3. BAND-PASS EFFECT IN PIEZO-ELECTRIC CRYSTAL CONNECTED IN SERIES WITH NEGATIVE IMPEDANCE ELEMENT

Quartz crystal (C T) resonator cut in such a way as to have only one frequency of vibration and mounted between electrodes has been used althroughout. The stabilized negative impedance element (N) consists of a screen-grid tube operated under secondary emission condition with condenser (C) and coil (L_2) to block the direct and high frequency currents respectively (Fig. 1). The stability and other properties of the negative impedance element are discussed [2,3] elsewhere and are therefore omitted here.

The attenuation or gain in db caused by the two terminal network consisting of the crystal, the blocking condenser and the negative impedance element has been measured by taking the input and the output voltage across the same impedance (AB and A′B′ respectively) by means of a screened Cambridge thermionic valve-voltmeter.

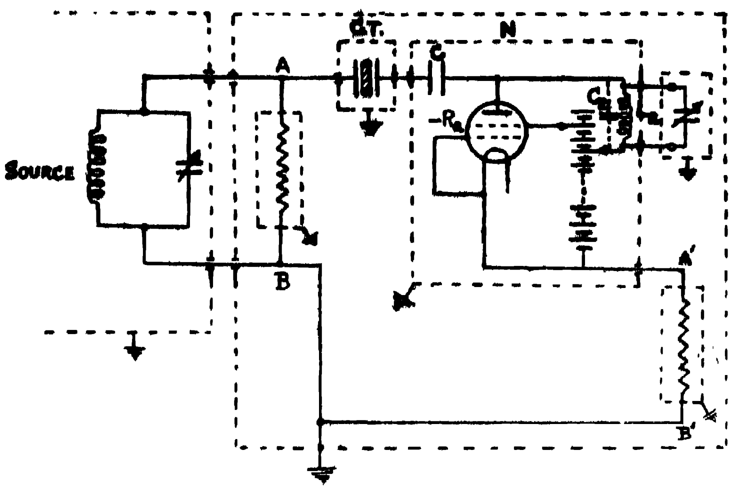

FIGURE 1

CASE I.—NEGATIVE IMPEDANCE ELEMENT DETUNED TO THE CRYSTAL FREQUENCY

Since the negative element (N) (omitting the blocking condenser) is equivalent to the circuit consisting of C_2, L_2, and $-R_a$ connected in parallel where C_2 = the total of the anode—filament capacitance of the tube and the self capacitance of L_2 and $-R_a$ = the negative resistance (at the frequency concerned), it is possible

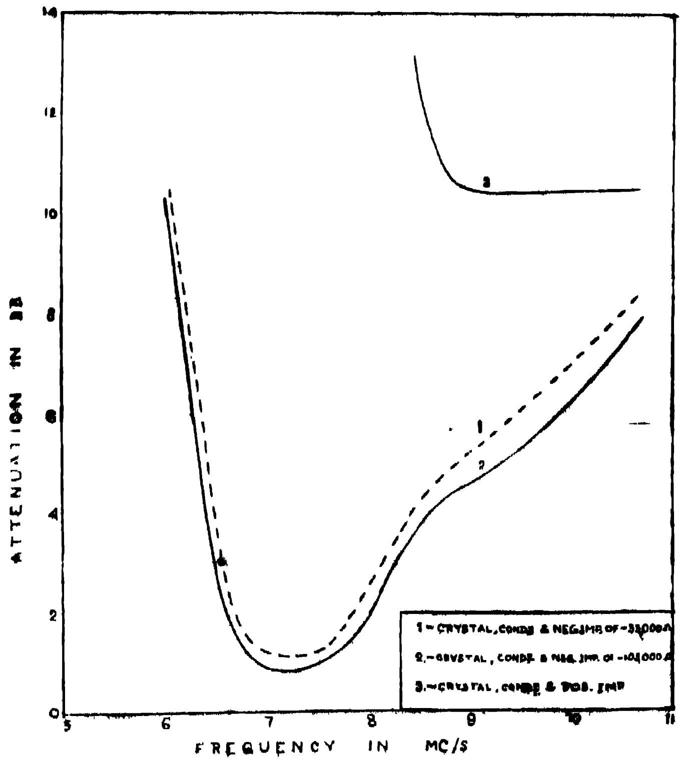

FIGURE 2

either to tune the L_2 C_2 circuit to the crystal frequency by an external screened condenser connected in parallel to L_2 or to leave it as its natural frequency (*i e.*, detuned to crystal frequency).

Fig. 2 shows the attenuation characteristics of the crystal in series with the negative impedance element (including blocking condenser) detuned to the crystal frequency. The attenuation characteristic of the crystal, condenser (of same value as the blocking condenser) and positive impedance of 50,000 ohms connected in series is plotted on the same sheet for comparison.

It will be seen that the crystal connected in series with condenser and positive impedance gives the characteristic of a high-pass filter of cut-of frequency

TABLE II

No.	$-_0R_n$ in series (Ohms)	f_2-f_1 (Mc/S)	$(f_2-f_1)/f_m$	$({}_2f_\infty-f_2)/f_2$	$({}_1f_\infty-f_1)/f_1$	Attenuation in *db*.
1	−33,000	7·9−6·7 =1·2	0.17	0·37	0·30	1·1-2·0
	-105,000	8·0−6·6 =1·4	0·20	0·41	0·30	0·8-2·0

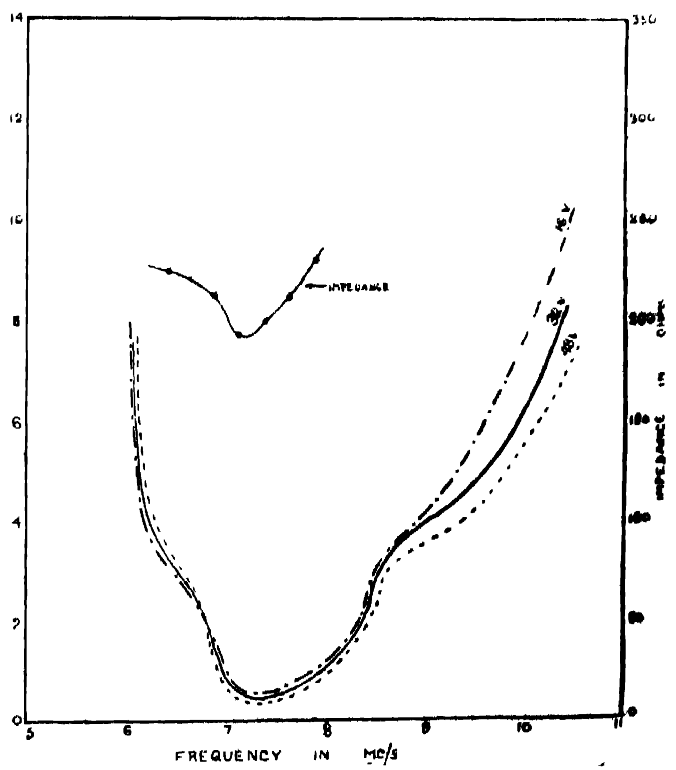

FIGURE 3

8·9 Mc/S whereas the crystal connected in series with negative impedance element (including blocking condenser) gives the characteristic of a wide-band band-pass filter, in which the attenuation in the transmission band is about 9 *db* less than that of the former. Table II shows the properties of band-pass filters so formed under detuned condition. $-_0R_n$ refers to value obtained from static characteristic.

Since capacitance in series or shunt with the crystal reduces the band-width, measurements have been repeated on the crystal in series with the negative impedance element without the blocking condenser. Further, as the omission of the condenser places across the crystal a D. C. voltage equal to the anode voltage, measurements have been repeated with different anode voltages.

Fig. 3 shows that the effect of omitting the condenser is to increase the band-width by about 14% and that of decreasing the anode voltage is to increase the sharpness of cut-off on one side. Measured variation of impedance of the two-terminal network (without blocking condenser) is also shown in Fig. 3.

CASE II. NEGATIVE IMPEDANCE ELEMENT TUNED TO THE CRYSTAL FREQUENCY

Fig. 4 shows the attenuation and impedance characteristics of the network with negative impedance element (without the blocking condenser) tuned to the crystal frequency. Table III shows the properties of band-pass filters so formed under tuned condition.

TABLE III

No.	$-_0R_n$ in series (Ohms)	$f_2 \sim f_1$ Mc/S	$(f_2 \sim f_1)/f_m$	$(_2f_s \sim f_2)/f_2$	$(_1f_s - f_1)/f_1$	Gain in *db*
1	−18,000	7·15-6·4 =0·75	0·110	0·25	0·14	4·5-5·3
2	−33,000	7·2-6·4 =0·80	0·117	0·25	0·14	4·7-5·4
3	−105,000	7·0-6·5 =0·50	0·074	0·21	0.14	5·5-5·9

The effect of tuning the element is therefore (*a*) to reduce the band-width, (*b*) to make the cut-off's sharper and (*c*) to decrease the attenuation in the transmission band.

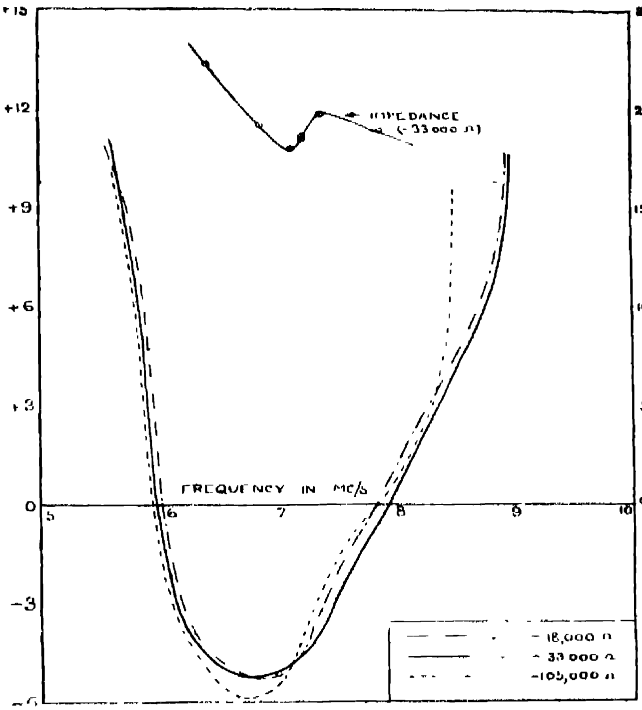

FIGURE 4

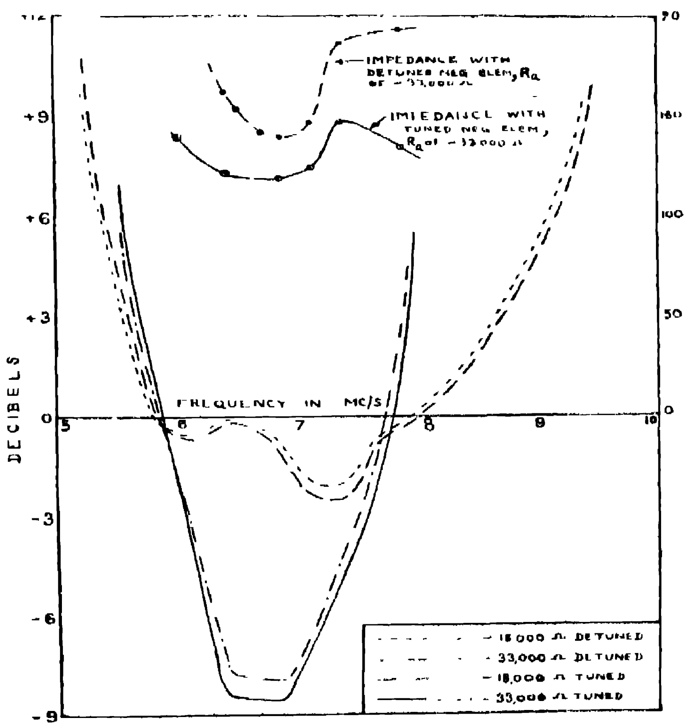

FIGURE 5

4. BAND-PASS EFFECT IN PIEZO-ELECTRIC CRYSTAL CONNECTED IN PARALLEL TO THE NEGATIVE IMPEDANCE ELEMENT

The stabilized negative impedance element (including the blocking condenser) is connected in parallel to the crystal. The blocking condenser cannot be omitted in this case as its absence may short-circuit the anode battery.

Fig. 5 shows the attenuation and impedance characteristics of the network under detuned and tuned conditions. Table IV shows the properties of the band-pass filters so formed under both conditions.

TABLE IV

No		$-_0R_n$ in parallel (Ohms)	$f_2 \sim f_1$ Mc/S	$(f_2 \sim f_1)/f_m$	$(_2f_r - f_2)/f_2$	$(_1f_r \sim f_1)/f_1$	Gain in *db*
(*a*) Detuned Case	1	−18,000	7·8–5·9 1·9	·28	·32	·13	15–2·1
	2	−33,000	7·8–5·9 − 1·9	·28	·32	·13	0·3–2·5
(*b*) Tuned Case	1	−18,000	6·9 − 6·4 −·05	·076	·107	·14	7·8 − 7·95
	2	−33,000	6·85 − 6·4 =0·45	·066	·107	·14	8·4 − 8·6

On comparing the 'parallel arrangement' under detuned condition with the 'series arrangement' under the same condition, it can therefore be said that the former gives (*a*) a larger band-width, (*b*) better sharpness of cut-off on one side, and (*c*) gain in the transmission band instead of attenuation. The effect of tuning the element in the parallel arrangement is similar to that of the 'series arrangement.'

5. BAND-PASS EFFECT IN FOUR-TERMINAL LATTICE SECTIONS CONTAINING PIEZO-ELECTRIC CRYSTAL AND STABILIZED NEGATIVE IMPEDANCE ELEMENT IN SERIES OR PARALLEL IN ONE OR BOTH ARMS

Four-terminal lattice sections consisting of two-terminal networks of the types discussed (in sections 3 and 4) in series and lattice arms have been grouped as follows :—

Class I.—In which piezo-electric crystal and negative impedance element connected in series or parallel are in one of the arms and series or parallel resonant circuit tuned to the crystal frequency or the negative impedance element s in the remaining arm (Fig. 6*a*).

Class II.—In which piezo-electric crystal and negative impedance element connected in series or parallel are in one of the arms and a similar arrangement is in the remaining arm, the frequency of the crystals in series and lattice arms being the same or different (Fig. 6*b*).

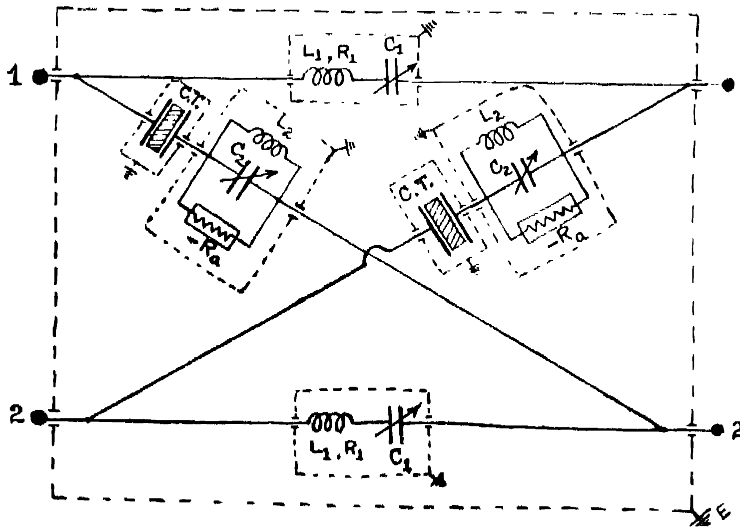

FIGURE 6 (*a*)

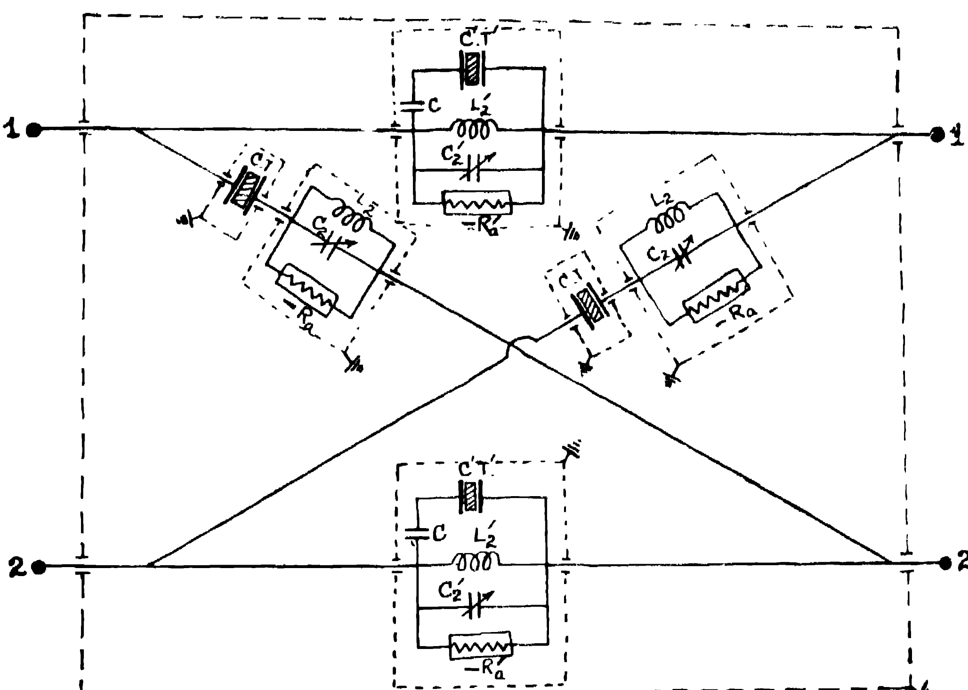

FIGURE 6 (*b*)

In sections of Class I, the negative impedance element can either be tuned to the crystal frequency or the frequency of the resonant circuit or remain

detuned, and in sections of Class II the negative impedance elements can be tuned to frequencies of crystals in the same or other arms or remain detuned.

The present section relates to studies on the sections of Class I only, as little quantitative work could be done on the sections of Class II due to unavailability of desired components, etc., at the present war conditions. It is proposed to publish the studies on the sections of Class II at a later date.

The sections of Class I which have been discussed here consist of :—

(1) Series tuned circuits in the series arms, and the crystal connected in series with the negative impedance element in the lattice arms ; and

(2) Parallel tuned circuits in the series arms, and the crystal connected in parallel to the negative impedance element in the lattice arms.

Fig. 7 shows the attenuation and characteristic impedance measured at different frequencies under different conditions. In the figure, " I " stands for Class I ; (1) and (2) stand for particular sections of Class I referred to above ; and D, T and ST stand for ' detuned,' ' tuned to crystal ' and ' tuned to resonant circuit,' respectively.

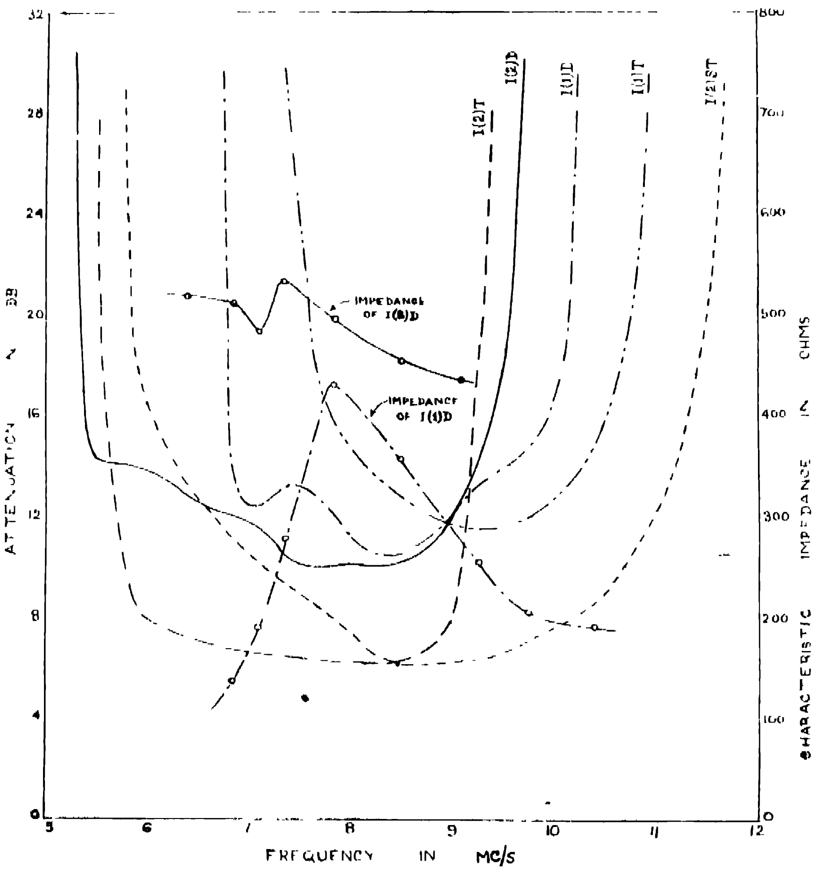

FIGURE 7

Table V shows the properties of the wide-band band-pass lattice filters of Class I so formed. The value of negative resistance (static) has been $-33{,}000$ ohms in all cases.

TABLE V

No	Class and No.	$f_2 \sim f_1$ Mc/S	$(f_2 \sim f_1)/f_m$	$({}_2f_c \sim f_2)/f_2$	$({}_1f_c - f_1)/f_1$	Attenuation in *db*
(*a*) Detuned Case 1	I – (1)	9·7-7·0 = 2·7	0·34	·051	·052	10·4-14·4
2	I – (2)	9·0-5·5 = 3·5	0·50	·083	·045	12·0-14·2
(*b*) Tuned Case (negative element tuned to crystal) 3	I – (1)	10·1-8·5 = 1·6	0·17	·045	·075	11·5-13·0
4	I – (2)	8·9-6·1 = 2·8	0·38	·055	·070	6·2-7·6
(*c*) Tuned Case (negative element tuned to resonant circuit) 5	I – (2)	10·5-7·0 – 3·5	0·41	·068	·00	6·1-10·0

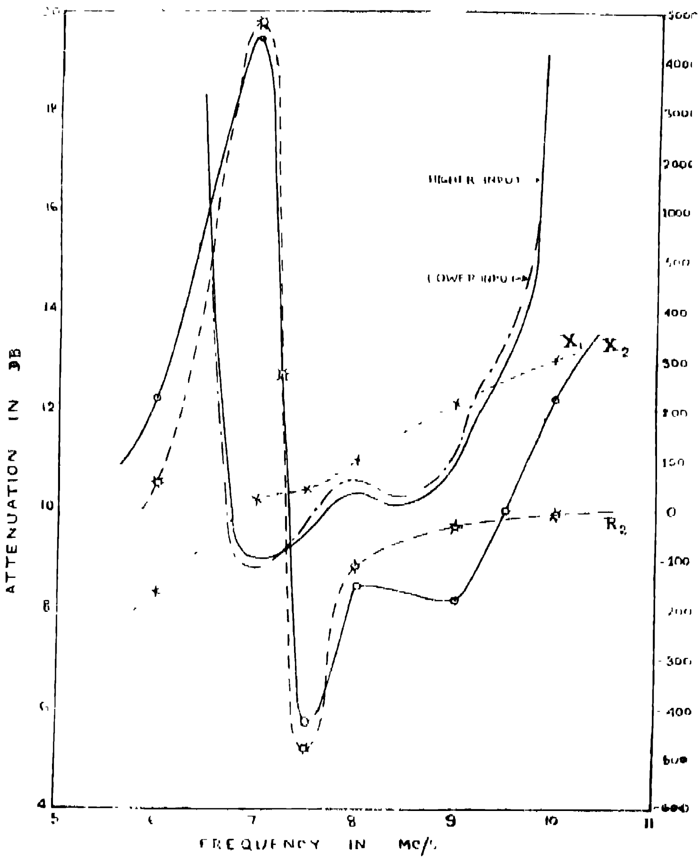

FIGURE 8

To test the linear performance of Class I types of filters discussed above, attenuation-frequency characteristics were taken with different inputs varying over a range of 60 decibels. Fig. 8 shows the curves corresponding to limiting values of input 0.1 and 100 volts for Class I—(1) filter. It will be seen that attenuation is fairly independent of the input for the range of variation.

6 MECHANISM OF THE BAND-PASS ACTION

Two-terminal Network

If the equivalent electric circuit of the crystal mounted between electrodes be a parallel circuit with L_0 and C_0 in series in one arm shunted by C' in another arm, the crystal impedance ${}_cZ_2$ is given by

$$ {}_cZ_2 = \frac{j\left(\omega L_0 - \dfrac{1}{\omega C_0}\right)}{1-\omega^2 L_0 C' + \dfrac{C'}{C_0}} \qquad \ldots \quad (1)$$

R_0 being neglected.

The impedance of negative elements consisting of L_2, C_2 and $-R_a$ in parallel is given by

$$ {}_NZ_2 = \frac{j\omega L_2 R_a}{R_a(1-\omega^2 L_2 C_2) - j\omega L_2} \qquad \ldots \quad (2)$$

If the two impedances are connected, say, in series, the total impedance

$$ Z_2 = \frac{-\dfrac{j}{\omega C_0}(1-\omega^2 L_0 C_0)}{1-\omega^2 L_0 C' + C'/C_0} + \frac{j\omega L_2 R_a}{R_a(1-\omega^2 L_2 C_2) - j\omega L_2} \qquad \ldots \quad (3)$$

The variation of total impedance $|Z_2|$ with frequency is shown in Fig. 3. The mechanism of action lies in the nature of variation of $|Z_2|$ which is minimum at a frequency at or about the middle of the transmission band, increases slightly from this value on both sides over a large frequency range and subsequently increases rapidly on both sides. The variation of $|{}_NZ_2|$ with frequency is largely responsible for giving such a variation of $|Z_2|$. Similar consideration applies when two impedances are connected in parallel.

Four-terminal Lattice Section

If the series arms consist of series resonance circuit (inductance $=L_1$, capacitance $=C_1$ and resistance $=R_1$) and the lattice arms consist of crystal

connected in series with the negative impedance element, the circuit constants being the same as given in above paragraphs, then

$$\text{Reactance in series arm} = jX_1 = j\left(\omega L_1 - \frac{1}{\omega C_1}\right) \quad \ldots \quad (4)$$

Reactance in lattice arm

$$= jX_2 = j \quad \frac{\omega L_0 - 1/\omega C_0}{1 - \omega^2 L_0 C' + C'/C_0} + \frac{\omega L_2 R_a^2 (1 - \omega^2 L_2 C_2)}{R_a^2 (1 - \omega^2 L_2 C_2)^2 + \omega^2 L_2^2} \quad (5)$$

The mechanism of "wide band-pass" action in a four-terminal lattice section of the types discussed is that the reactances in series and lattice arms remain of opposite sign over a *very wide frequency band*—a condition which has been brought about by the negative impedence element. It must be noted however that the resistance components of the impedances in series and lattice arms modify the width of the pass-band as illustrated below.

The resistance component in series arm is R_1 and that in lattice arm is

$$R_2 = -\frac{\omega^2 L_2^2 R_a}{R_a^2 (1 - \omega^2 L_2 C_2)^2 + \omega^2 L_2^2} \quad . \quad (6)$$

The attenuation caused by the positive resistance in series arms will be partially or completely reduced by the gain caused by the negative resistance in lattice arms. The wide band filters are therefore low-loss ones as well.

In Fig. 8 are shown the reactances in series and lattice arms of Class I—1) filter when the negative element is detuned to crystal as well as the resistance component R_2 of the lattice arm (R_1 being negligible). It will be seen that although the reactances remain of opposite signs between 6 and 9.5 Mc/s the resistance component of the lattice arm at 7.3 Mc/s is positive and of large value and at 9.5 Mc/s is negative but of small value. The pass-band from both these considerations is 7.3-9.5 Mc/s, whereas from actual attenuation measurements it is 7.0-9.7 Mc/s.

7. PROPOSED APPLICATION

The wide-band crystal band-pass filters discussed above appear to be well suited for use in wide-band H. F. Systems (*e.g.*, television and multi-channel radio telephony) as (*a*) band-pass couplings between stages of the transmitter and (*b*) band-pass filters in transmitting and receiving equipments.

Multi-channel radio telephone systems on short and ultra-short waves are at present generally designed for two and nine channels respectively. For two-channel system, the total band-width (including both side-bands) is 9 to 10 Kc/s therefore requires no special consideration. For nine-channel system as used by the British Post Office,[7] the carrier frequency is 76 Mc/s and the modulating band arising from nine channels is about 130 Kc/s wide (*i.e.*, 153-283 Kc/s).

Total band-width with two side bands is about 260 Kc/s. Attention has been directed to the design of several units (*e.g.*, modulation transformer, I. F. band-pass filter, I. F. negative feed-back amplifier, etc.) at transmitting and receiving terminals for as effective transmission of this wide-band as possible.

In a modern television transmitter as used by the French Post Office,[4,5] the carrier frequency is 46 Mc/s and the total band-width with two side-bands is 6 Mc/s. Penultimate and final R. F. power stages are designed as "inverted amplifiers" to work without balancing condensers and secure the essential condition for the wide band-width. Further, the penultimate stage is coupled to the final stage through the water cooled resistances for maintaining the load on the former stage fairly constant over the wide band of modulating frequencies.

Performance in the above cases, though satisfactory, is open to improvement in many ways. Most of the difficulties of wide band transmission could be obviated with economy and stability obtained by suitably using the wide-band crystal filters (specially of four terminal type) as band-pass coupling and band-pass filter in equipments. Take, for instance, the transmitting terminal equipment of a 100-channel radio telephone system employing series modulation at the penultimate stage. Fig. 9 shows the schematic diagram. The modulating band which consists of single side-bands of 100 carrier channels with spacings will be 0.5-1.1 Mc/s and the station carrier frequency is 30 Mc/s. Wide-band lattice band-pass filters 0.5-1.1 Mc/s and 28.9-31.1 Mc/s will be necessary at points shown by F_1 and F_2, respectively. Similar filters will be necessary at the receiving terminal.

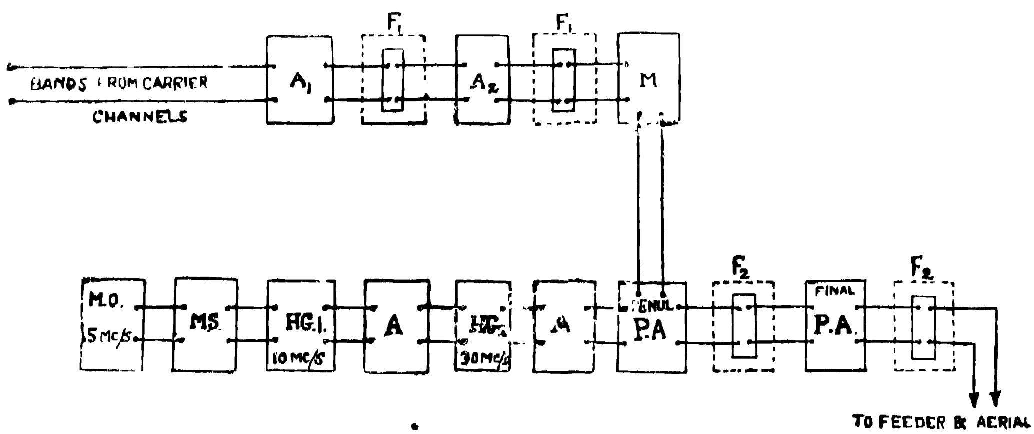

FIGURE 9

A_1 and A_2 = Amplifiers; M = Modulator, M.O. = Crystal controlled Master Oscillator; M.S. = Master Separator and Amplifier; H.G.$_1$ and H.G.$_2$ = Hermonic Generators; A = R.F. Amplifier; P.A. = R.F. Power Amplifiers.

8. CONCLUSION

The following conclusions have been arrived at :—

(1) A piezo-electric crystal connected in series with stabilized negative impedance element, detuned or tuned to the crystal frequency, acts as a two-terminal wide-band band-pass filter of low attenuation or gain in the transmission band.

Effect of tuning the element is (*a*) to reduce the band-width ; (*b*) to make the cut-off's sharper and (*c*) to decrease the attenuation in the transmission band.

(2) A piezo-electric crystal connected in parallel to the stabilized negative impedance element, detuned or tuned to the crystal frequency, acts as a two-terminal wide-band band-pass filter giving larger band-width, lesser attenuation in the transmission band and better sharpness of cut off (on one side) than the series arrangement referred to above under (1).

Effect of tuning the element is the same as mentioned above under (1).

(3) A lattice section, in which piezo-electric crystal connected in series with or parallel to stabilized negative impedance element detuned or tuned either to crystal frequency or to frequency of resonant circuit in the other arm is in one of the arms and series or parallel resonant circuit is in the remaining arm, acts as a four-terminal ultra wide-band band-pass filter having attenuation lesser than and sharpness of cut-off almost same as the two lattice sections made up of crystals, condensers and coils.

Effect of tuning the element to frequency of resonant circuit in the other arm is to make the band-width same as or greater than that of detuned case.

(4) For two-terminal filters, the impedance is in general minimum at a frequency within the transmission band and gradually increases on both sides of it.

For four-terminal filters, the characteristic impedance is maximum at a frequency near about the mid-frequency of the transmission band.

(5) The attenuation in the transmission band decreases in general with (*a*) the increase of negative resistance value, and (*b*) the tuning of the negative impedance element.

(6) The variation of attenuation or gain with frequency in the transmission band is in general less when the negative element is tuned than when it is detuned.

(7) The attenuation or gain of four-terminal filters is more or less independent of input at least upto a variation of 60 db. in the input.

9. ACKNOWLEDGEMENT

The whole of the experimental work has been carried out at the Kanodia Electrical Communication Engineering Laboratories, Department of Applied Physics, Calcutta University. The authors desire to thank Prof. P. N. Ghosh for giving them all facilities and taking every kind interest during the progress of the work.

REFERENCES

[1] Mason, *Bell System Tech. Journals*, July 1934 and October (1937).
[2] Chakravarti, *Phil. Mag.*, July (1938).
[3] Chakravarti, *Phil. Mag.*, (proofs returned in April 1940)
[4] Mallin and Rabut, *Electrical Communication*, April (1939).
[5] Wheeler, *Proc. I.R.E.*, July (1939)
[6] Stanesby and Broad, *P.O.E.E.J.*, January (1939).
[7] Mirk, *P.O.E.E.J.*, April (1938)

AN APPARENT INFLUENCE OF THE EARTH ON SOLAR PROMINENCES

BY A. K. DAS

AND

B. G. NARAYAN

(*Received for publication, June 22, 1940*)

ABSTRACT. In this paper a statistical study has been made of Kodaikanal observations of solar prominences during the period 1913-37 and it has been found that the annual variations of the mean daily areas, the mean daily heights and of the mean daily bases of prominences at the limb correspond to the variation of the earth's distance from the sun in the course of the year. In particular it has been found that the maximum of the mean daily area at perihelion and the minimum at aphelion differ from each other by about 9.6 per cent of the maximum. This has been shewn to be evidence of the existence of a terrestrial influence on solar prominences. The effects of planets other than the earth have also been examined and it has been concluded that they cannot be appreciable. It has been tentatively suggested that the observed influence of the earth on prominences may well be the result of a tide-raising force which varies inversely as the cube of the distance between the earth and the sun.

The possibility of an influence of the earth and of other planets on solar prominences has been considered by several workers[1-7] in the past; their methods of investigation have been varied, but they have been concerned chiefly with the distribution of the numbers and areas of sunspots and of faculae on the eastern and western sides of the central meridian and the numbers and areas of prominences on the eastern and western limbs of the sun. These investigations have, however, led to conflicting results and in most cases their results cannot be regarded as conclusive. It is not easy to decide whether this inconclusiveness is due to the insufficiency of the observational material used or due to other causes. In any case it seemed to us desirable to investigate the problem afresh by examining a uniform series of data of prominence areas extending over as long a period as possible and by employing a somewhat different method.

EARTH'S INFLUENCE AND DISCUSSION OF AVAILABLE PROMINENCE DATA

If the earth exercises any influence on solar phenomena it is most likely to be of a gravitational nature and one may reasonably expect this influence to manifest itself most when the earth is nearest to the sun and least when it is farthest away from it. During the course of its annual revolution the earth comes nearest to the sun in January and goes farthest from it in July at the

epochs of perihelion and aphelion respectively. We may accordingly expect the areas of prominences to show a maximum in January and a minimum in July or *vice versa* according as the earth exercises an enhancing or a deterring influence on them. It is this aspect of the problem which has been particularly considered in the present study. We have exclusively used observational data derived from the records of the Solar Physics Observatory, Kodaikanal. Daily photographs of prominences in the calcium K line taken with a Cambridge spectroheliograph are available at this observatory from the year 1905 onwards. From these, the profile areas of prominences are measured in square minutes and tabulated for each month. The numeration of prominences is admittedly an arbitrary procedure and there must often be a great deal of uncertainty as to whether a prominence is one or several. For this reason the profile areas of prominences have been considered to be a more reliable measure of prominence activity than the numbers, and accordingly this investigation confines itself to the data of the areas of prominences for the period (1913-37).*

TABLE I

Mean daily areas of prominences in square minutes

Year	Jan.	Feb.	Mar.	Apr	May	Jun	Jul	Aug.	Sep	Oct	Nov.	Dec.
1913	2·03	2·77	2·77	2·35	1·91	1·65	1·93	1·44	1·95	1·71	1·94	2·13
14	3·09	3·78	2·15	3·00	2·65	2·98	2·27	3·35	2·55	3·06	3·76	4·47
15	4·37	3·89	7·07	6·08	5·64	3·82	3·65	6·02	4·82	6·68	4·45	4·22
16	5·08	3·88	2·93	3·02	3·63	3·65	2·90	3·18	2·96	3·09	3·97	5·62
17	4·04	6·68	5·43	5·39	5·04	4·35	4·10	5·52	3·60	4·45	6·45	5·43
18	6·15	4·91	5·59	4·56	3·77	4·06	4·37	3·68	3·13	2·00	2·41	2·54
19	3·02	3·46	3·69	3·77	3·39	2·66	3·76	3·63	3·82	4·51	4·15	4·27
20	4·37	3·86	4·39	4·70	4·83	3·70	3·08	3·31	4·16	4·83	4·30	5·42
21	4·74	5·37	4·61	4·90	4·63	3·32	3·25	2·82	4·05	3·96	3·75	3·46
22	2·99	3·21	3·45	3·68	3·07	·46	2·93	2·25	2·05	2·56	3·74	4·74
23	5·30	5·00	4·65	4·73	3·90	3·90	4·20	3·40	4·10	4·10	5·00	3·94
24	5·40	5·66	4·43	4·67	4·20	5·10	4·70	5·00	4·60	6·70	6·30	5·40
25	5·03	5·26	4·49	4·80	5·60	7·10	6·40	5·50	6·30	7·70	7·80	7·84
26	8·76	8·40	9·13	7·04	7·90	7·80	6·30	6·10	8·00	7·70	7·69	7·03
27	8·20	7·00	8·16	7·80	7·50	7·80	7·20	5·20	6·00	5·10	4·35	5·64
28	5·97	6·40	8·39	7·70	8·40	5·00	7·20	7·10	8·20	7·10	8·13	5·47
29	7·22	6·24	6·38	3·70	·80	2·00	3·40	3·90	6·20	5·00	6·04	5·64
30	5·10	5·60	4·89	5·39	6·30	4·20	3·80	2·60	2·90	3·70	2·71	4·10
31	4·20	4·77	4·19	4·30	4·40	3·50	4·40	4·70	4·50	4·90	3·24	2·76
32	3·00	3·00	3·10	2·52	2·10	2·00	1·80	1·60	1·80	1·50	1·71	2·00
33	2·10	1·70	1·92	2·73	2·20	2·40	2·80	1·80	2·20	2·50	3·02	2·44
34	2·70	3·10	2·70	3·65	5·10	4·10	5·50	4·20	4·10	3·70	3·86	3·04
35	4·40	4·50	4·50	4·60	*4·70	4·50	4·60	5·10	5·60	3·10	6·16	6·15
36	7·28	6·83	6·24	7·26	7·95	6·37	4·97	5·61	7·34	8·12	10·14	7·13
37	8·27	8·27	7·01	6·95	7·91	5·40	6·50	7·59	6·69	7·34	5·30	6·09
Mean	4·68	4·94	4·89	4·81	4·78	4·25	4·24	4·30	4·50	4·64	4·82	4·72

* We have not made use of the data available for the period 1905-12 for reasons given later in this paper.

In Table I are given the mean daily areas of prominences for each month of the year for the period 1913-37 and the means for the whole period are given in the last row of the table. The mean daily areas have been derived by dividing the total areas of prominences measured from the photographs for the month by the number of effective days in the month. The effective days have been calculated by giving suitable weights to the photographs taken on days of bad observing conditions according to their quality. The photographs taken on days of bad observing conditions have their effective days estimated as $\frac{3}{4}$, $\frac{1}{2}$ or $\frac{1}{4}$ of a perfect day of observation according to the quality of the sky and the definition at the time of the photograph. This procedure of allowing for unfavourable weather conditions has been followed at the Kodaikanal Observatory for many years and has proved to be a satisfactory method of arriving at reliable daily areas of prominences and of dark markings.§

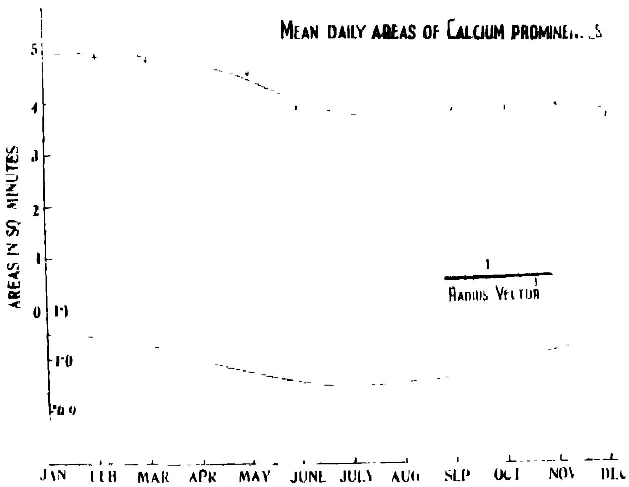

FIGURE 1

The means of Table I are represented diagrammatically in Fig. 1 from which it is evident that the maximum occurs in January and the minimum in July. This suggests that the earth enhances the areas of prominences in January when it is at perihelion and decreases them in July when it is at aphelion. A similar

§ From the year 1923, under the auspices of the International Astronomical Union whenever daily photographs are incomplete or wanting at Kodaikanal, photographs are obtained from other observatories, such as Meudon, Paris, Mt Wilson, Cambridge, etc., for completing the records. Owing to the monsoon conditions prevailing at Kodaikanal during the second half of the year a larger number of photographs from abroad is obtained for that half of the year than for the first half. It is found that the incorporation of the supplementary data derived from the photographs supplied by the co-operating observatories does not alter to any appreciable extent the values of the mean daily areas obtained from Kodaikanal records alone by the method indicated above.

TABLE II

Year.	A	B	C	A_1	B_1	C_1			
	Mean daily areas in Decr. & Jany. in sq. mms.	Daily areas —the mean $(x-\bar{x})$	$(x-\bar{x})^2$	Mean daily areas in June & July in sq. mms.	Daily areas —the mean $(x_1-\bar{x}_1)$	$(x_1-\bar{x}_1)^2$	$A-A_1$	$\{(A-A_1)-\overline{(A-A_1)}\}$	$\{(A-A_1)-\overline{(A-A_1)}\}^2$
1913	2·54	−2·36	5·5676	1·78	−2·55	6·5025	+0·76	+0·194	0·0376
14	3·67	−1·23	1·5129	2·72	−1·61	2·5921	+0·95	+0·386	·1490
15	4·74	−0·16	0·0256	3·74	−0·59	0·3481	+1·00	+0·434	·1884
16	5·33	+0·43	0·1849	3·23	−1·10	1·2100	−2·10	+1·534	2·3532
17	5·21	+0·31	0·0961	4·22	−0·11	0·0121	+0·99	+0·424	·1798
18	4·59	−0·31	0·0961	4·52	+0·19	0·0361	+0·07	−0·496	·2451
19	3·59	−1·31	1·7161	3·12	−1·21	1·4641	+0·47	−0·096	·0092
20	4·94	+0·04	0·0016	3·41	−0·92	0·8464	+1·53	+0·964	·9293
21	4·06	−0·84	0·7056	3·29	−1·04	1·0816	+0·77	+0·204	·0415
22	3·88	−1·02	1·0404	2·65	−1·68	2·8224	−1·23	+0·664	·4409
23	4·96	+0·06	0·0036	4·07	−0·26	0·0676	+0·89	+0·324	·1050
24	5·40	+0·50	0·0250	4·93	+0·60	0·3600	+0·47	−0·096	·0092
25	6·28	+1·38	1·9044	6·78	+2·45	6·0025	−0·50	+0·066	·0044
26	8·22	+3·32	11·0224	7·11	+2·78	7·7284	+1·11	+0·544	·2959
27	6·91	+2·01	4·0401	7·54	+3·21	10·3041	−0·63	+0·064	·0041
28	5·73	+0·83	0·6889	6·63	+2·30	5·2900	−0·90	+0·334	·1116
29	6·54	+1·64	2·6896	3·14	−1·19	1·4161	+3·40	+2·834	8·0316
30	5·00	+0·10	0·0100	3·98	−0·35	0·1225	+1·02	+0·454	·2062
31	3·63	−1·27	1·6129	3·90	−0·43	0·1849	−0·27	−0·296	·0876
32	2·54	−2·36	5·5696	1·93	−2·40	5·7600	+0·61	+0·044	·0019
33	2·26	−2·64	6·9696	2·60	−1·73	2·9929	−0·34	−0·226	·0511
34	2·89	−2·01	4·0401	4·87	+0·54	0·2916	−1·98	−1·114	1·9993
35	5·20	+0·30	0·0900	4·55	+0·22	0·0484	+0·65	+0·084	·0071
36	7·23	+2·33	5·4289	5·72	+1·39	1·9321	+1·51	+0·944	·8911
37	7·12	+2·22	4·9284	7·88	+3·55	12·6025	−0·76	−0·194	·0376
Mean	$\bar{x}=4·902$		60·09	$\bar{x}_1=4·332$		+71·695	$\overline{A-A_1}=+0·566$		+16·4188

result was obtained by Evershed[3] who found a greater excess of eastern preponderance in the case of prominence numbers and areas measured at perihelion than at aphelion; but he apparently did not attach much significance to this observation presumably because he thought that the small order of difference found by him might be due to bad observing conditions obtaining at Kodaikanal during the south-west monsoon period. This doubt may have been justifiable in the case of the smaller amount of observational material Mr. Evershed had at his disposal and also his method of treatment of the problem; but the larger amount of data used in the present study and the method here employed scarcely leave any room for doubt that the maximum in January and the minimum in July shewn in fig. 1 may be due to the influence of varying observing conditions. The data used in this statistical work extend over a period of twenty-five years, which is a fairly long period, but still it seems desirable to ascertain what degree of reliance can be placed on the conclusions drawn from the data used. For this purpose we have made use of Fisher's[8] "'t' significance test." The means of the grouped values given in Table II fulfil the "t" significance test as shewn below :—

$\bar{x} = 4{\cdot}902$	$\bar{x}_1 = 4{\cdot}332$
$\frac{s^2}{n} = \frac{\Sigma(x-\bar{x})^2}{n(n-1)}$	$s = 1{\cdot}729$
$s = 1{\cdot}581$	$t = \bar{x}_1 \sqrt{n_1}/s$
$t = \frac{4{\cdot}902 \sqrt{25}}{1{\cdot}581}$	$= \frac{4{\cdot}332 \times 5}{1{\cdot}729}$
$= 15{\cdot}5$	$= 12{\cdot}50$
$P = < {\cdot}01$	$P = < {\cdot}01$

From the table of "t" values it is found that for both the means where n is equal to 25 observations the high values of t show a P-value of less than ·01 which indicates a high degree of significance. The "t" test applied to the mean of the differences between the daily prominence areas at the two epochs also shows a high degree of significance, the P value being less than ·01 The variation of mean daily areas from the maximum in January to the minimum in July amounts to about 15 per cent. of the maximum. It is to be noted, however, that the earth is at perihelion in the beginning of January and at aphelion in the beginning of July, so that the monthly values of January and July do not exactly represent the earth effect at the two epochs, part of the effect falling within the previous month in each case. We have, therefore, worked out the mean values for the months of December and January and for June and July, the former period (December-January) representing the perihelion epoch and the latter (June-July) the aphelion epoch. The results are collected in Table II. These values should

reflect the earth effect at the perihelion and aphelion epochs more truly. It is found that the fall from the maximum to the minimum now works out to be 12 per cent. of the maximum. This difference will be further reduced if allowance is made for the possible error in the estimation of effective days. It has already been described how the days of observation are converted into effective days in order to eliminate the influence of bad observing conditions on the daily means. Since the mean daily areas of prominences are obtained by the use of effective days, any error in the estimation of effective days should introduce a corresponding error in the mean daily values. The extreme error that is likely to enter in the estimation of effective days is $\pm \frac{1}{4}$ of an effective day in an incomplete day of observation, since the days are estimated as $\frac{3}{4}$, $\frac{1}{2}$ or $\frac{1}{4}$ of a day. Assuming an error of this order the effective days for each month were recalculated and the means of the mean daily areas of prominences were obtained for the values given in Table II. From the recalculated figures it was found that the difference between the mean areas at perihelion and aphelion periods was reduced to 0·6 per cent of the higher value instead of the 12 per cent. previously obtained. The significant fact, therefore, is that there is still a substantial difference between the values at the two epochs of perihelion and aphelion which has to be accounted for.

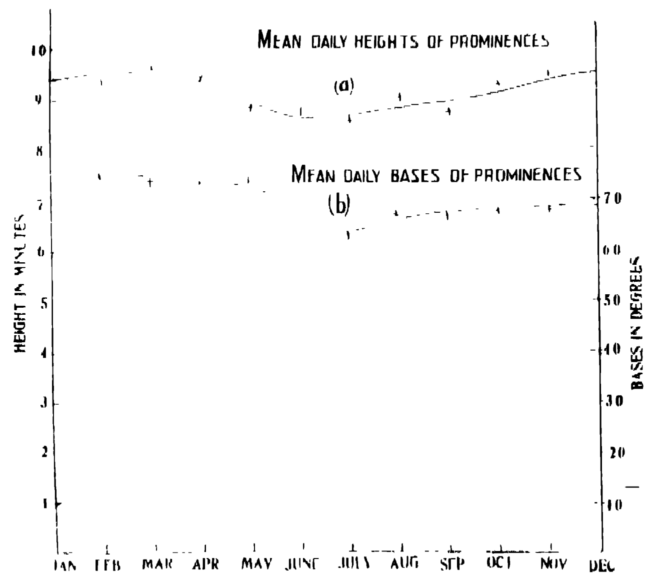

FIGURE 2

The mean daily heights and bases of prominences derivable from Kodaikanal records were also examined as in the case of the areas. Fig. 2 represents diagrammatically the variations of the mean daily heights and bases from month to month. The resemblance between the curves in Fig. 2 and that in Fig. 1 is quite close. Thus it is evident that the annual variations of all the three elements of solar prominences correspond to the annual variation of the relative distance

between the earth and the sun. We now proceed to consider how far this correspondence can be regarded as being due to the influence of the earth alone.

INFLUENCE OF OTHER PLANETS

If the earth is supposed to have an effect on solar phenomena it is to be expected that the other planets may also exercise similar influences. Evershed [3] has shown that of the major planets Venus alone shows an effect similar to that of the earth. On the other hand Royds and Sitaramaiyar [4] state that they do not find any effect of planets or even of the earth on the distribution of numbers of prominences on the east and the west limbs of the sun. Without attempting to reconcile these conflicting views we may take it that, if there is any planetary influence, the greatest positive effect would occur for the outer planets when at opposition and the greatest negative effect when in conjunction with the sun, while for the inner planets the greatest positive effect would occur when at the inferior conjunction and the greatest negative effect when at the superior conjunction. On this assumption the positive and negative effects of the planets on prominence areas at perihelion and aphelion can be calculated from the planetary phenomena occurring near about these epochs. From an examination of planetary phenomena during the years 1913-37 we find that in the months of December and January there occur 3 oppositions and 4 conjunctions of Jupiter, 15 inferior and 12 superior conjunctions of Mercury, while in June and July 5 oppositions and 4 conjunctions of Jupiter, 12 inferior and 14 superior conjunctions of Mercury and 3 inferior and 3 superior conjunctions of Venus occur. If suitable weights according to the tidal force (*vide* Table III quoted from Kodaikanal Observatory Bulletin No. XXXV which gives the different measures of the relative influence of planets on the sun which may be considered) are given to the positive and negative effects it is found that the influences of planets other than the earth at the two epochs are practically equal. The planetary influence does not therefore affect to any appreciable extent the observed difference between the perihelion and aphelion values of prominence areas, which may consequently be taken to represent almost entirely the influence of the earth. In this connection we may note that the planetary phenomena occurring from October to January show that their effect is greater in November than in December ; this may be responsible for inflating the values of mean areas of prominences in November over those of December as can be seen from Table I. We do not however advance this as the only explanation of the peculiarity of the November figures ;—although we consider it to be very probable that prominence areas are affected by the other planets according to their positions favourable or otherwise with reference to the earth, we do not think it possible to determine with any certainty the effect of the planets on prominences from the measures of prominence photo-

graphs taken from the earth, as the effect is likely to be masked by the predominating effect of the earth.

TABLE III

Planets	Effect $\propto M/d$	$\propto M/d^2$	$\propto M/d^3$ (Tidal)	$\propto M/d^4$
Mercury	0·14	0·37	0·95	2·44
Venus	1·12	1·54	2·13	2·95
Earth	1·00	1·00	1·00	1·00
Mars	0·07	0·05	0·03	0·02
Jupiter	60·45	11·62	2·23	0·43
Saturn	9·86	1·03	0·11	0·01

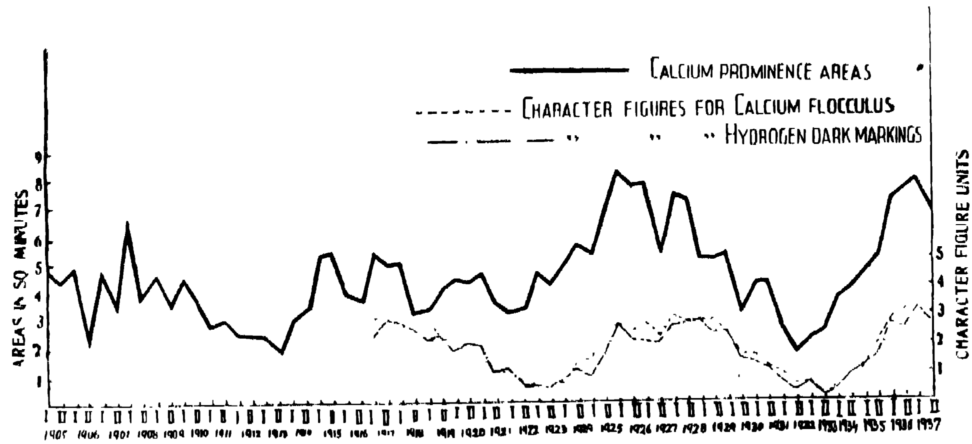

FIGURE

Effect of Variations of Solar Activity on Prominence Data

A diagrammatic representation of the mean daily areas for each half-year for the period (1905-37) (Fig. 3) shows that the values are higher for the first half of the year than for the second half consistently during the period 1905-12 and thereafter the variation of the values is random. This peculiarity suggested that the whole series of prominence observations from 1905 to 1937 was not uniform and it could be split up into two periods, one extending from 1905 to 1912 and the other from 1913 to 1937. Owing to their non-uniformity both the periods could not be combined for this investigation and the data for the shorter period

were not used. The data actually made use of did not suggest the existence of any vitiating influence which might introduce any systematic error; nevertheless it was thought desirable to subject them to further scrutiny in order to see whether the observed variations were due to the variations of solar activity or to any other cause. The Bulletin of Character Figures of solar phenomena published by the International Astronomical Union gives the character figures for each solar phenomenon, such as sunspots, calcium flocculi, hydrogen flocculi, etc., for each month of the year from the year 1917 onwards. These character figures represent the index of solar activity for the concerned solar phenomena In the absence of character figures for calcium prominences the figures for calcium and hydrogen flocculi were chosen and the values for each half-year were plotted alongside the prominence areas for the period 1917-37. From the general agreement of the three curves it can be inferred that the variations of mean areas from half-year to half-year reflect only the variations in solar activity. The variations of prominence areas during the earlier period could not be tested for lack of character figures data

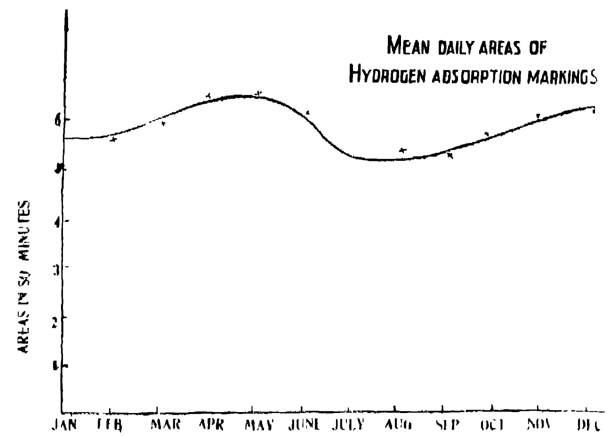

FIGURE 4

Behaviour of Absorption Markings in relation to Earth Effect

As it has been established that the absorption markings are the projections of the overlying prominences on the disc, it is of interest to examine whether the earth influence noticed in prominences is equally observable in the case of the hydrogen absorption markings. Table IV gives the mean daily areas for each month of the hydrogen absorption markings for the years 1917-37 with the exception of 1922. Figure 4 shews the distribution of mean areas from month to month. The trends of the curves in figure 1 and figure 4 are by no means similar. In Figure 4 there are two maxima and two minima,

TABLE IV

Mean daily areas of Hydrogen absorption markings in square minutes

Year	Jan	Feb	Mar.	Apr.	May	Jun	Jul.	Aug.	Sep.	Oct	Nov.	Dec
1917	3·34	4·15	4·65	3·72	5·20	4·40	4·93	6·44	5·18	6·06	6·07	6·6[illegible]
18	5·77	4·06	5·73	6·23	6 69	10·30	3·42	5·18	4·99	4·64	6·79	7·[illegible]
19	5 39	3·58	7·46	6·44	6 87	3·40	6·26	4·41	5·80	5·10	8·00	5·5[illegible]
20	6 76	6·02	4·42	0 80	6·84	9·64	5·20	11·72	5·31	8·75	5·40	11 95
21	6·10	4 73	11·60	4 27	7·10	13·1[illegible]	2·25	5·30	5·25	3·02	4·60	3·03
22	—	—	—	—	—	—	—	—	—	—	—	—
23	2 19	2·12	1·82	1·64	0 08	0·80	0·52	0·41	0·68	2·60	2·05	3·20
24	2·70	2·40	2·65	1·95	2·10	3·10	5·00	4 50	3·80	5·36	3·20	2·70
25	3·44	2·23	2·90	2·72	3·84	3·02	3 05	4·00	5·64	5·60	6·60	5·73
26	8·00	12·10	10·0[illegible]	10·02	8 00	5·87	6·70	6·53	5·24	4·60	5 49	7·30
27	5·90	6 75	5·57	10·70	8·40	4·00	5 30	4 40	5·01	5·30	5 60	4·23
28	4·80	5·00	5·00	6·21	6·38	8·35	7·32	5·97	8·26	7·15	8·03	7·20
29	9·00	8·58	7·05	7 91	4·64	4·80	5·43	5·85	6·39	6·56	7 08	7·28
30	6·81	5·40	6·81	7·37	7 34	5·65	5·01	3·85	3·01	2 71	3·92	5·26
31	2·74	2·47	2·90	3·89	4 41	4·08	3·36	3 25	3·10	4·15	3 14	2·49
32	2·4[illegible]	3·41	2·65	3·0[illegible]	1·91	1·95	1·97	1·75	1·29	1·05	0 60	1·27
33	1·80	1·64	2·16	2·27	2·13	1·90	1·94	1·86	1·37	1·62	1·14	0·90
34	0·91	1·70	1·62	2·93	3·66	4·08	4·04	3·05	4·15	3·65	5·80	3·64
35	3·56	3·18	5·93	7·40	7·39	5·92	7·84	7 32	7·10	10·50	10·03	12·90
36	12·31	15·60	12·40	17·06	18·90	13·20	12·00	11·80	12·00	15·10	17·11	13·71
37	19·02	17 82	16·48	15·20	17·00	14·41	13·38	13·55	14·10	12·23	11·55	13·10
Mean for 20 yrs.	5·58	5·65	5·00	6·44	6 40	6·10	5·25	5·46	5·40	5 79	6·19	·266

and though the primary minimum occurs in July, the primary maximum occurs in April-May. It seems possible that this behaviour of the Hα dark markings may be due to complications introduced by the semi-annual periodic variation of the heliographic latitude of the earth which ought to have an influence on the markings. In fact, there should be a semi-annual variation in the mean areas of the markings in the northern and southern hemispheres according as the position of the earth varies from north to south or *vice versa*. This aspect of

the problem has been discussed by Evershed and Chidambara Iyer[7]. The areas of markings in the northern and southern hemispheres were therefore worked out separately and the distributions in the different months of the year for each hemisphere were plotted in curves. The distribution of areas in the southern hemisphere was found to agree with the theoretical curve, but there was no agreement between the observed distribution and the theoretical curve in the northern hemisphere. A similar separation of areas of prominences between the northern and southern hemispheres was made and the distribution in both the hemispheres was found to be similar to that represented in figure 1 and not to the theoretical curves showing the combined effects of the earth's orbital motion and the variation of the heliographic latitude of the earth in the course of the year. It was therefore concluded that the variation of heliographic latitude of the earth has no effect on the areas of prominences, while it may have some effect on the markings but that effect is not adequate to explain the peculiarities of the distribution of the areas as shown in figure 4.

The dissimilarity in the annual variation of the areas of prominences and of the areas of dark markings should not be taken to signify that there is an intrinsic difference between the behaviours of prominences at the limb and prominences on the disc in regard to the earth effect here considered. The cause of the apparent disparity most probably lies in the inherent indefiniteness of the quantity we call the area of a dark marking. The areas of all prominences at the limb are measured under identical conditions, namely in a plane at right angles to the surface of the sun, and therefore the mean daily areas derived from them are definite quantities. The areas of dark markings, on the other hand, depend upon the longitudes at which they exist as well as on other variable factors; consequently the mean area of dark markings for any given day is derived from measures made under various conditions which introduce a good deal of indefiniteness in the value of the daily mean area. This indefiniteness is further accentuated by the existing practice of applying foreshortening corrections of doubtful applicability, for in the course of its passage across the disc a dark marking presents an intricately varying area, which depends not only upon the variation of the projection of the height of the prominence concerned but also upon other variables; in no position on the disc does the area of a dark marking have a definite relation to the area of the corresponding prominence at the limb. One can easily recognise several other aspects in which the area of a dark marking accessible to measurement is quite unsuitable, compared to the area of the corresponding prominence at the limb, as an index of earth effect. For example, the volume of matter existing as prominences over the whole disc including the limb at any epoch and particularly its annual variation should furnish a reliable clue for the detection of an earth influence. Since the depth of a prominence is small compared

to its height and base, the areas of prominences at the limb give a fairly dependable indication of the volume of matter existing as prominences. The areas of dark markings, on the other hand, can give no such reliable indication of the amount of matter existing as prominences on the disc; for, as Royds[1] has shown, only a fraction of the total quantity of prominence matter absorbs the radiation from the photosphere, the effective part of a prominence in the production of a dark marking being a layer extending from a height of 28 sec. to 33 sec. which may be cool enough to absorb photospheric light. It is also a fact of common observation that all prominences which are observed at the limb do not give rise to dark markings on the disc. It is clear therefore that the mean daily areas of dark markings cannot be as good an index of the volume of matter existing as prominences on the day concerned as the mean daily areas of prominences at the limb. For the reasons enumerated above it is evident that one can scarcely expect to find a similarity of distribution between the areas of prominences and of absorption markings during the different months of the year.

Cause of Earth's Influence

So far it has been our object to eatablish that there is a genuine influence of the earth on solar prominences. We now proceed to consider the cause of this phenomenon. The mean distance of the earth from the sun is 92 million miles and the difference between the distances at perihelion and aphelion is about 3 million miles. The distances between the earth and the sun at perihelion and aphelion may be taken to be approximately 90.5 and 93.5 million miles respectively. If the earth effect varies directly as its mass and inversely as some power of the distance, the ratio of the effects at the two epochs of perihelion and aphelion varies inversely as the ratio of the powers of the distances. If d_1 and d_2 and r_1 and r_2 represent the distances and the mean daily areas of prominences at perihelion and aphelion respectively, the ratio of the earth effects on prominence areas at the two epochs is given by

$$r_2/r_1 = d_1/d_2 \text{ or } d_1^2/d_2^2 \text{ or } d_1^3/d_2^3 \text{ or } d_1^4/d_2^4 \quad - \quad \text{etc.}$$

$$\text{or } \frac{4{\cdot}332}{4{\cdot}902} = \frac{90{\cdot}5}{93{\cdot}5} \text{ or } \frac{(90.5)^2}{(93{\cdot}5)^2} \text{ or } \frac{(90.5)^3}{(93{\cdot}5)^3} \text{ or } \frac{(90.5)^4}{(93{\cdot}5)^4} \quad \text{etc.}$$

$$\text{or } {\cdot}884 \quad {\cdot}969 \quad {\cdot}937 \quad {\cdot}907 \quad {\cdot}877 \quad \text{etc.}$$

The ratio r_2/r_1 lies between ·907, and ·877, which shows that the earth effect actually observed varies inversely as some power of the distance intermediate between the third and the fourth. Although this does not justify the conclusion that the earth effect on solar prominences which emerges from the present study

is an entirely tidal effect, it would appear that the magnitude of this effect could be accounted for by tidal force with fair approximation.

In conclusion we may mention that the majority of the previous workers ave found a suppressing influence of the earth on solar prominences whereas Evershed and Chidambaraiyar have found evidence for the earth exerting an nhancing influence. The result of the present investigation gives further evidence in support of the latter view.

It is a pleasure to thank Dr. A. L. Narayan and Mr. P. R. Chidambaraiyar for their kindness in reading the manuscript of this paper and for their criticisms.

SOLAR PHYSICS OBSERVATORY,
KODAIKANAL.

REFERENCES

1 Sykora, Mem Spett. Ital., **26**, 161 (1897).
2 Mrs. Maunder; M.N.R.A.S., **67**, 451 (1907).
3 Evershed, Kodai Obs. Bull. No. 28.
4 Royds and Sitaramayya; Kodai Obs. Bull. No. 35.
5 Pocock; M.N.R.A.S., **79**, 54 (1918).
6 Maunder; M.N.R.A.S., **80**, 724 (1920).
7 Evershed and Chidambara Iyer; Kodai Obs. Bull. No. 67.
8 R. A. Fisher; Statistical Methods for Research Workers, p. 104.
Royds, Kodai Obs. Bull. No. 89.

VARIATION OF FIELD-STRENGTH IN THE VICINITY OF AN ULTRA-SHORT-WAVE HORIZONTAL TRANSMITTING AERIAL *

By S. S. BANERJEE, D.Sc.,
Benares Hindu University

AND

PARMANAND, M.Sc.
Upper Air Observatory, Agra

(*Received for publication, July 2, 1940*)

ABSTRACT. The intensity of radiated field-strengths in the neighbourhood of an ultra-short-wave horizontal transmitting aerial has been determined and its variation with different angular directions with respect to the aerial has been studied. For the purpose of radiation a modulated valve oscillator generating waves of 6.1 metres in length was employed along with a half-wave horizontal aerial. A calibrated ultra-short wave receiver was used for the determination of field-strengths. The observed values of field-strengths were compared with those calculated mathematically. In order to study the directional quality of such an aerial the angular tracks of maximum and minimum amount of energy-flow have been determined by theoretical calculations and the results were verified by experimental observations. It has been observed that aerials of different lengths will radiate the energy along different channels and a typical record of observations for the intensity measurements has been shown with a half-wave radiator.

INTRODUCTION

Wireless communications with ultra-short waves have now grown to be fairly common due to their application in television, aircraft communications, upper-air weather observations, and various others. Due to the small size of these waves, special types of aerials have to be designed and hence the study of the variation of radiated field-strength in the neighbourhood of such aerials would be of great importance to the radio engineer. Such investigations have been made by various workers [1,2,3] with comparatively larger wavelengths and mostly with vertical aerials. In the present communication the intensity of the radiated field in the vicinity of an ultra-short-wave horizontal transmitting aerials was determined and the mode of its variation around the aerial has been investigated. A modulated oscillator was used to generate waves of 6.1 metres in length for

* Communicated by the Indian Physical Society.

the purpose. A regenerative ultra-short wave receiver was constructed to receive the signals generated by the oscillator. The generator was connected with a half-wave horizontal aerial which was placed in a fixed direction and the receiver was moved along the circumference of a circle with the input end of the transmitting aerial at the centre. The field-strengths were measured at different angular directions with respect to the orientation of the transmitting aerial. The observed field-strengths have been verified by the values of the same calculated mathematically. While moving round the aerial, several positions of maximum and minimum values of the field-strengths are obtained which have also been confirmed by theoretical calculation after finding out the proper conditions for the same. For the determination of absolute field-strengths, the receiver was calibrated, the method of which has been described in subsequent sections.

THEORY

Suppose OP in fig. 1 represents the horizontal radiating aerial and ABC is the circumference of a circle along which the receiver is moved in order to determine the field-strengths. The input end O of the aerial is situated at the centre of the circle. Let A be a point at which the signal-strength is to be determined, r_1 and r_2 are the distances from the ends O and P of the aerial to the point A respectively. The length of the radiating aerial is denoted by l.

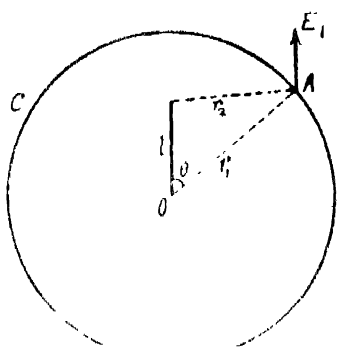

FIGURE 1

It has been shown by Carter [4] that the electric field-strength at any point in the vicinity of a straight radiating aerial and in the direction parallel to the length of the radiator is given by

$$E_l = j30I \left[\frac{e^{-jmr_2}}{r_2}(-1)^n - \frac{e^{-jmr_1}}{r_1} \right] \text{ volts/cm.} \qquad \dots \quad (1)$$

where I is the current in amperes flowing through the aerial, $m = 2\pi/\lambda$, λ being the wavelength radiated, and n is any positive integer depending on the length of the aerial.

Simplifying the above equation (1), we get,

$$E_\ell = -30I\left[j\left\{\frac{\cos(mr_2)}{r_2} + \frac{\cos(mr_1)}{r_1}\right\} + \left\{\frac{\sin(mr_2)}{r_2} + \frac{\sin(mr_1)}{r_1}\right\}\right] \text{volts/cm.} \quad \dots \quad (2)$$

From fig. 1, it will be seen that

$$r_2^2 = l^2 + r_1^2 - 2lr_1\cos\theta,$$

where θ is the angle between r_1 and OP. Substituting this value of r_2 in equation (2) and neglecting the imaginary terms, we get

$$E_\ell = -30I\left[\frac{\sin(m\sqrt{l^2+r_1^2-2lr_1\cos\theta})}{\sqrt{l^2+r_1^2-2lr_1\cos\theta}} + \frac{\sin mr_1}{r_1}\right] \text{volts/cm.} \quad \dots \quad (3)$$

The present investigation was carried out with radiating aerials half wave-length long and the field-strengths were determined along the circumferences of concentric circles of various radii. A typical calculation for a circle of radius $3\lambda/4$ is shown below.

For calculation of field-strengths at the distances of $3\lambda/4$ from the input end of the radiating aerial in different directions, $\lambda/2$ is substituted for l and $3\lambda/4$ for r_1 in equation (3) and thus we get

$$E_\ell = -\frac{30I}{\lambda}\left[\frac{\sin 2\pi\sqrt{\frac{13}{16}-\frac{3}{4}\cos\theta}}{\sqrt{\frac{13}{16}-\frac{3}{4}\cos\theta}} - \frac{4}{3}\right] \text{volts/metre} \quad . \quad (4)$$

when λ is measured in metres.

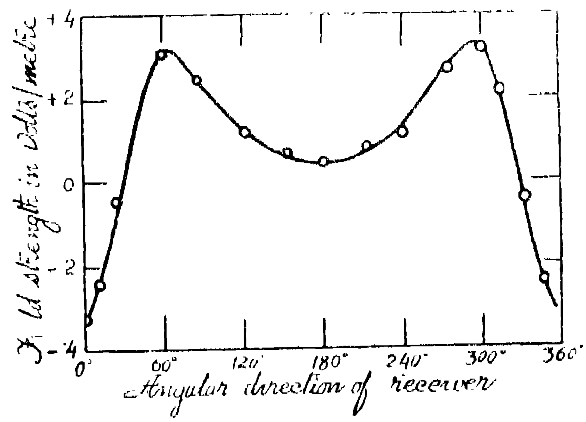

FIGURE 2

Various values of the field-strengths E_ℓ have been calculated for different angular directions indicated by θ in equation (4) and they are shown in Table I, below. For the sake of convenience of indicating the directions of maximum and minimum values of field intensity the variation of field strength with angular

directions has been depicted graphically in fig 2, which will be compared with such curves obtained experimentally shown later.

TABLE I

Angular direction of the receiver	Calculated field-strengths in volts/metre	Angular direction of the receiver	Calculated field-strengths in volts/metre
0°	−0.334	180°	0.064
10°	−0.290	210°	0.067
15°	−0.240	240°	0.105
20°	−0.170	270°	0.218
30°	−0.010	300°	0.328
45°	0.210	330°	−0.010
60°	0.328	340°	−0.170
90°	0.218	345°	−0.240
120°	0.105	350°	−0.290
150°	0.067	360°	−0.334

The approximate angular directions for maximum and minimum amounts of energy-flow will appear from the curve shown in fig. 2, the exact directions, however, were obtained by differentiating equation (4) and subsequently equating the expression obtained to zero.

Thus we get from equation (4)

$$\frac{dE_t}{d\theta}=\frac{30I}{\lambda}\left[\frac{\cos 2\pi\sqrt{\frac{13}{16}-\frac{3}{4}\cos\theta}\times\frac{3\pi}{4}\sin\theta-\frac{3}{8}\left(\frac{13}{16}-\frac{3}{4}\cos\theta\right)^{-\frac{1}{2}}\sin\theta\times\sin 2\pi\sqrt{\frac{13}{16}-\frac{3}{4}\cos\theta}}{\frac{13}{16}-\frac{3}{4}\cos\theta}\right] \quad \ldots (5)$$

Equating the right-hand expression of the above equation to zero, we get for the condition of maximum or minimum field-strengths,

$$3\pi^2\cos\theta+\tan^2 2\pi\sqrt{\frac{13}{16}-\frac{3}{4}\cos\theta}\,\cos\theta=\frac{13\pi^2}{4}. \quad \ldots (6)$$

Now, the above equation is satisfied for five values of θ, *viz.*, 19°40′, 66°38′, 160°20′, 293°22′ and 340°20′. In order to distinguish the angles

corresponding to maximum and minimum values of field-strengths, equation (5) is differentiated once more and the positive or negative values of $d^2E_1/d\theta^2$ are determined for those angles.

Thus from equation (5) we get,

$$\frac{d^2E_1}{d\theta^2} = -\frac{3\pi}{4A}\cos\theta\cos 2\pi\sqrt{A} + \frac{3}{8A^{\frac{3}{2}}}\left\{\frac{3\pi^2}{2}\sin^2\theta\sin 2\pi\sqrt{A} + \cos\theta\sin 2\pi\sqrt{A}\right\}$$

$$+\frac{27\pi}{32A^2}\sin^2\theta\cos 2\pi\sqrt{A} - \frac{27}{64A^{\frac{5}{2}}}\sin^2\theta\sin 2\pi\sqrt{A} \quad .. \quad (7)$$

where $\qquad A = \frac{13}{16} - \frac{3}{4}\cos\theta.$

From equation (7) it can be shown that the angles 19°40′, 160°20′ and 340°20′ correspond to the minimum values of field-strengths and the angles 66°38′ and 293°22′ correspond to the maximum values.

The angular directions for the maximum and minimum radiation of energy will also be clear from fig. 2. It may be noted from fig. 2 that the highest value of the radiated field-strength is indicated only at 0° and 360° and as these angles do not correspond to maximum or minimum value of the field-strength, they do not satisfy equation (6). These mathematically calculated values of the angular directions were verified by experimental observations recorded in the next section.

EXPERIMENTAL ARRANGEMENT AND OBSERVATIONS

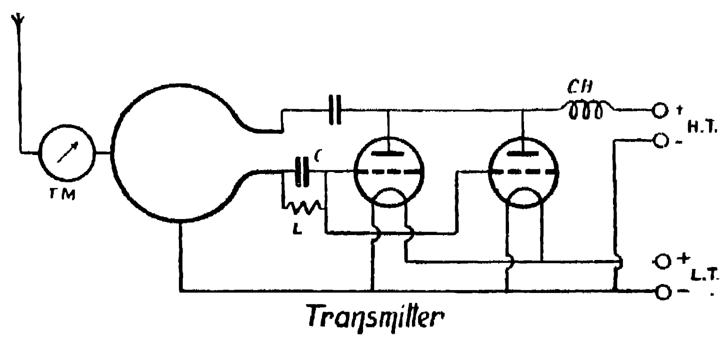

FIGURE 3

Transmitter. A parallel-fed modulated oscillator of Hartley type was built with two valves in parallel. The chematic diagram of this is shown in fig. 3. A constant modulation was effected by a leak L and a condenser C in the grid circuit. An ultra-short-wave choke CH was connected in the anode circuit. Aerial current was measured by a thermo-milliammeter TM. The oscillator could generate wave 6.1 metres in length. The aerial consisted of

straight bare copper wire half wave-length long. The wave-length emitted by the oscillator was measured by a pair of Lecher wires and a thermo-galvanometer.

Receiver. The receiver for the measurement of the intensities of the radiated fields consisted of a leaky grid detector with reaction and a low frequency amplifier as shown in fig. 4. The regenerative type of receiver

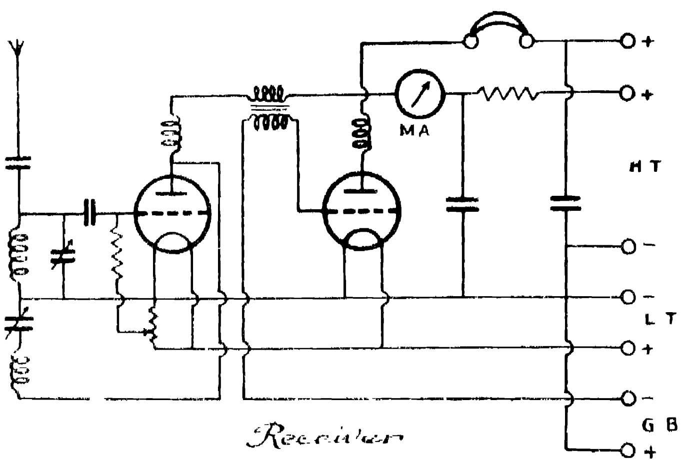

FIGURE 4

was specially preferred to a super-heterodyne or super-regenerative type for the convenience of calibration and stability at ultra-high frequencies. A milli-ammeter MA indicated the change in the plate current of the detector for calculating the field-strengths. The receiving aerial was of a similar type as employed in the transmitter but of a smaller length. The receiver was carefully screened and for the measurement of absolute values of field-strengths radiated it was calibrated. The usual method of calibration of such a receiver is inapplicable in the present investigation as the dimensions of the receiving loop would be comparable with the wavelength radiated for observations and hence the following method of calibration was adopted. The receiver was kept at a known distance from the transmitter and the transmitting aerial was excited by passing current through it which was recorded in the thermo-milliammeter. The radiated signal from the transmitting aerial was tuned by the receiver and the changes in the plate current of the detector was noted and the sound in the headphones in the second stage of the receiver was also heard. This observation was repeated with different independent values of currents flowing through the transmitting aerial. From the knowledge of the current flowing through the transmitting aerial the field-strength at the receiver was calculated from equation (3) given in the previous section. The calibration curve showing the field-strength for any value of the change of plate current under proper conditions is shown in fig. 5. Thus knowing the change in plate current when the receiver is tuned at any distance, the field-strength could

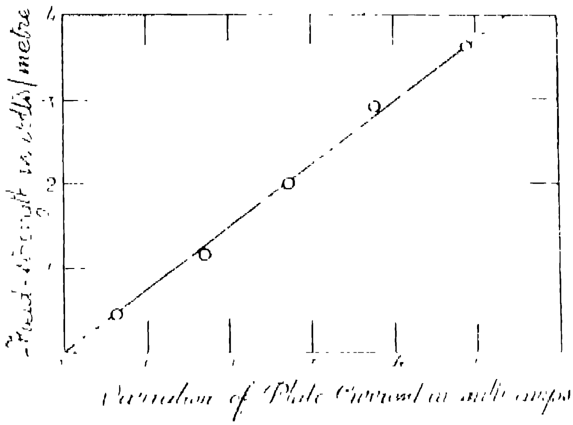

FIGURE 5

be readily obtained from the graph. The relative field-strengths were often checked by the headphones connected in the output of the receiver. The ultra-short-wave transmitter with the horizontal aerial was placed in an open space sufficiently above the ground. The signal strengths were measured at various points which were at distance of three-fourths of a wavelength in different directions from the transmitter. The various directions in which the observations were recorded were indicated by the angle which that direction made with the transmitting horizontal aerial. The receiving aerial was placed at the same height as the transmitting one and was always oriented in the direction parallel to the radiating aerial.

Table II below gives the values of the field-strengths experimentally observed in different directions from the transmitter. First column of the table shows the angular direction of the receiver from the transmitter and the second column indicates the corresponding observed field-strengths.

TABLE II

Angular direction of the receiver	Observed field-strengths in volts/metre	Angular direction of the receiver	Observed field-strengths in volts/metre
0°	0.335	180°	0.060
10°	0.288	210°	0.070
15°	0.244	240°	0.104
20°	0.165	270°	0.244
30°	0.010	300°	0.324
45°	0.210	330°	0.010
60°	0.324	340°	0.165
90°	0.244	345°	0.244
120°	0.104	350°	0.288
150°	0.070	360°	0.335

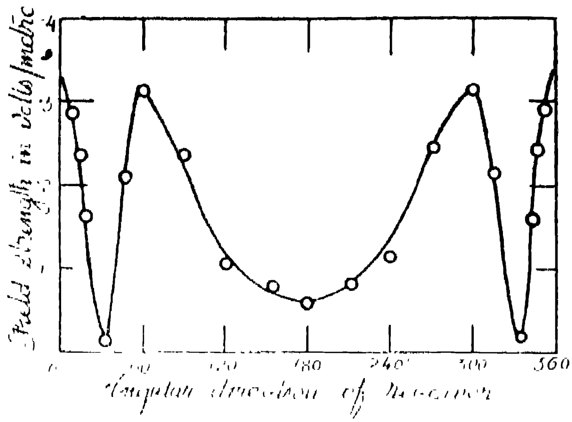

FIGURE 6

Fig. 6 shows the variation of the radiated field-strengths with different angular directions from the transmitter. It will be observed that the curve shown in fig. 6 will agree very closely with that shown in fig. 2 in the previous section, if we neglect the negative sign of the field-strengths in the latter. This will be also clear if the numerical values of the calculated and observed field-strengths, shown in Table I in the last section and Table II above, be compared without any reference to the direction of the fields.

SUMMARY AND CONCLUSION

Field-strengths in the vicinity of an ultra-short-wave horizontal aerial have been calculated and experimentally measured by means of a calibrated receiver. The directions of maximum and minimum amounts of energy-flow have been also determined by theoretical calculation and experiments. The transmitter consisted of a modulated valve oscillator with a half-wave radiating aerial, generating waves 0.1 metres long. The receiver consisted of a leaky grid regenerative detector and a low-frequeny amplifier. It has been concluded that the directions of maximum and minimum amounts of radiated energy from such an aerial depends on the lengths of the aerials employed, and the observations for a half-wave aerial have been recorded.

The authors desire to express their hearty thanks to Dr. B. Dasannacharya, Head of the Department of Physics for imparting an accommodation to carry out the experimental part of the above investigation and also for providing other necessary facilities.

WIRELESS SECTION,
PHYSICS DEPARTMENT,
BENARES HINDU UNIVERSITY.

REFERENCES

1 A. Meissner, *Proc. Inst. Rad. Eng.*, **15**, 928 (1927).
F. R Stansel, *Proc. Inst. Rad. Eng.*, **24**, 802 (1936)
3 F. K. Niessen, *Ann. der Phys.*, **33**, 404 (1938).
4 P. S. Carter, *Proc. Inst. Rad. Eng.*, **20**, 1004 (1932).

ASSOCIATION OF ACETIC ACID IN NON-AQUEOUS SOLVENTS*

By P. KOTESWARAM **

(Received for publication, July 2, 1940)

Plate XI

ABSTRACT. After a review of the work on acetic acid in water, the necessity for the study of this substance in non-aqueous solvents is stressed. Investigations were made with both polar and non polar liquids as solvents for this acid. The changes in Raman frequencies of this liquid in mixtures with chloroform, nitrobenzene, ethyl ether, acetone and methyl-ethyl ketone are described. No changes are perceptible in solutions with chloroform. This is explained on the basis of the absence of either a donor or an acceptor atom in this solvent, which is therefore supposed not to have any influence on the acid. The other four substances, on the other hand, bring about distinct shifts in the C=O frequency in particular. This is attributed to the presence of the donor atom O in these molecules, which is in a position to associate with the acceptor H in the acid molecules. Such an association can bring about the splitting of the associated molecules of the acid also, which therefore results in the change of the Raman frequencies of the acid. A new line with frequency 1760 cm.$^{-1}$ is ascribed to the free C=O bond in the acid which arises out of the disruption of the acid complexes into simpler molecules and which remains free in the new complex formed with the solvent, as there is no acceptor H in the molecules of these solvents to get associated with the O in it

INTRODUCTION

In a previous publication,[1] the author studied the Raman spectrum of acetic acid at different concentrations in water and found that the principal C=O band of the acid with its intensity maximum at 1670 gradually shifted with dilution towards higher frequencies. At 25% concentration of the acid, it was found that the intensity maximum of the C=O band was about 1710. By a study of the effect of temperature on the acid, it was found that by increasing the temperature the intensity maximum again shifted in the same direction It was pointed out that the appearance of the band at 100°C in the pure acid was similar to that at 95% concentration of the acid in water. These results were attributed to the breaking up of the initially associated molecules of the acid into lower polymers at higher temperatures and at higher dilutions. Similar results obtained with formic and benzoic acids in aqueous solutions were explained similarly.[2,3]

* Part of the thesis approved for the D.Sc. Degree of the Madras University. This work was done under the direction and guidance of Dr. I. Ramakrishna Rao, Andhra University, Waltair.

** Communicated by the Indian Physical Society.

While these changes were observed in aqueous solutions, the acid showed no change in solvents like benzene and carbon-tetra chloride. The two non-aqueous solvents chosen having been non-polar, the dissociating effect in aqueous solutions was attributed to the polar solvent, water.

A further elucidation of the phenomenon was necessary for a complete understanding of the phenomenon of association in acetic acid and hence the author studied the Raman spectrum of the acid in other non-aqueous polar solvents. The results obtained are detailed below.

EXPERIMENTAL

The usual experimental arrangements for obtaining Raman spectra of liquids described already in the author's previous communication[1] were used. The liquids under study were distilled in vacuum and rendered free from water to eliminate its effect. Transferring of solutions was done without disturbing the arrangement. Thus the slit of the spectrograph was kept at the same constant width throughout the investigations.

RESULTS

Polar liquids can be broadly classified as normal and abnormal. Among these, normal liquids are those, which, though polar, are not associated. Abnormal liquids are highly associated and show abnormal physico-chemical properties. The fatty acids, alcohols and water are prominent examples of abnormal liquids, while almost all other polar liquids are normal—acetone, ether, nitrobenzene, etc. But some of these normal liquids have got a strong tendency to associate with other molecules. A molecule having a 'donor' atom has got affinity for one having an 'acceptor' atom and forms a donor-acceptor link with it. An associated liquid has got both a donor and an acceptor and hence co-ordination or hydrogen bond formation (as the American school calls it) takes place and the molecules associate.

The effect of chloroform, nitrobenzene, diethyl-ether, acetone, and methyl-ethyl ketone on acetic acid was studied with a view to observe the changes in the polymerisation of the acid. Of these, nitrobenzene has the highest dipole-moment about 4×10^{-18} e.s.u. and the rest of the solvents have moments ranging from 1·55 for ether to 2·5 for acetone.

The following results were obtained: the first three solutions were 50 : 50 mixtures by volume.

1. *Solution in chloroform.*

There are no prominent changes in the Raman lines of acetic acid in chloroform.

In Nitrobenzene.

The C − C line of acetic acid at $\Delta\nu = 893$ is unchanged. The C = O line at 1670 rendered less diffuse and another line at about 1700 makes its appearance. Both these lines are not very clear on the plate due to the continuous spectrum which developed during the exposure.

3. *In Ether.*

The C − C line in the pure acid has a faint component at about 872, which is not visible with ordinary exposures. In the solution in ether, this line accompanying the 893-line increases in intensity such that it is clearly seen, comparable in intensity to the strongest 893-line. The C = O line at 1670 gets more diffuse than in the pure acid and two diffuse lines, with intensity maxima at 1685 and 1750 can be clearly seen.

4. *In Acetone.*

The most prominent changes are undergone by acetic acid in mixtures of acetone and of methyl-ethyl ketone with the acid. Three different concentrations, 75%, 50%, and 25% of the acid in the mixture have been studied.

Conspicuous changes are observed on the following lines:

C − C line.—As in the case of solution in ether, the low-frequency companion at 872 makes its appearance in a 75% solution, and as the concentration of the acid in the mixture decreases, the low-frequency component increases in intensity, till at 25% concentration, it is more intense than the 893-line itself. There is no line in acetone in that region and hence the effect can be attributed only to acetic acid molecules (Fig. 1) (Plate XI). In the microphotometric curves given in fig. 1 the increase in intensity of the 872-line at higher concentrations is clearly seen.

C = O line.—In pure acetic acid, the C = O frequency is about 1670. In pure acetone it is about 1712. In the mixture the 1670-line maximum is seen proceeding towards higher frequencies with dilution till it gets blended with the acetone line. In addition, a line at 1760 which is quite sharp, makes its appearance. This line is present at all the three concentrations studied.

$\Delta\nu = 623$.

This line also seems to change in a manner similar to the C − C line at 893. In the pure acid, it has got a low-frequency component at 601, but the component is too feeble to be visible with ordinary exposures. But as the concentration of acetic acid in the mixture decreases, the intensity of its low-frequency component increases correspondingly.

5. *In Methyl-ethyl ketone.*

The effect in methyl-ethyl ketone is similar to that in acetone. As before, there is a clear splitting of the 893-line and an increase in the intensity of its low-

frequency component with increasing dilution of the acid in the solvent (Fig. 1). The line at 1670 shifts towards higher frequencies till it gets blended with the C=O line of the ketone at 1715 and the new line at 1760 also makes its appearance. The effect on the line 623 could not be studied due to the presence of another ketone line close to it.

Comparison of these results with those obtained by dilution in other Solvents.

For a proper understanding of the behaviour of acetic acid molecules in the different solvents studied, a comparison of the results obtained with other solvents also is necessary. We shall first take the C=O line at 1670 which is bound to be affected most by polymerisation or depolymerisation.

In non-polar solvents, benzene and carbon-tetrachloride, this line is unaffected. Among other solvents, chloroform does not seem to have any perceptible effect on it. Nitrobenzene splits it into two components, one at 1670 and another at 1760 The same is the case with ether but the 1670-line shifts slightly towards higher frequencies and both the lines are very diffuse unlike what they are in nitrobenzene solution. In ketones (acetone and methyl-ethyl ketone) as solvents, we again see the 1670-line shifting towards higher frequencies and the 1760-line appearing. The actual position of the shifted 1670-line and its spectral characteristics cannot be estimated on account of the superposition of the 1715-line of the ketone on it. While in all these polar solvents, a clear distinct line at 1760 is obtained, it is significant that in water alone, no such line at 1760 is found even at a dilution of 25%. In aqueous solutions, the 1760-line gets more and more diffuse and shifts gradually towards higher frequencies.[2] At no stage can two distinct lines, either sharp and separate as in nitrobenzene or diffuse and yet discreet as in ether, be obtained.

With regard to other lines, there is again a difference in their behaviour in water and in the other polar solvents. The 620- and 893-lines are unaffected in solutions in non-polar solvents and in chloroform In nitrobenzene there does not seem to be any conspicuous change. But in ether both of them double up with low-frequency components at 601 and 872 respectively. In acetone and methyl-ethyl ketone, the same is the case and we find that as the concentration of the acid in the solution diminishes, the low-frequency lines become more intense till at 25% acid in acetone, the 872-line outshines its companion. The reverse happens in aqueous solutions The lines tend to become more diffuse with decreasing concentration, the low-frequency component disappearing even at high concentrations. This is again a conspicuous difference between aqueous and non-aqueous solutions of the polar type.

DISCUSSION

To understand the changes listed above, we must first get an idea of the molecular structure of the acid and that of the solvent used. As we already know,

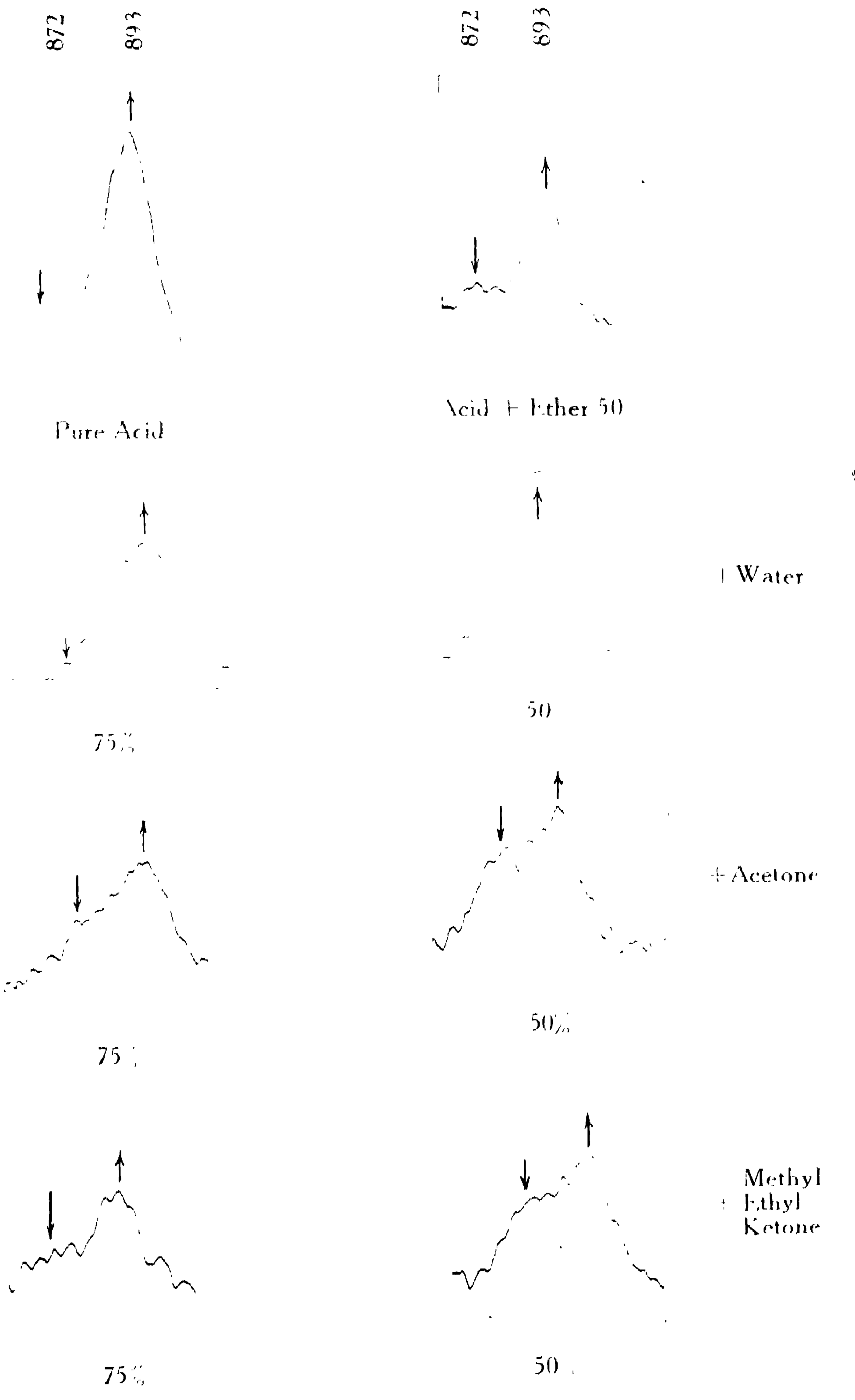

Fig. 1. C-C Lines of Acetic Acid in different Solvents

the acid is an associated liquid, mostly containing dimers of the type

$$H_3C\text{-}C\left\langle\begin{matrix}O\ldots HO\\ OH\ldots O\end{matrix}\right\rangle C\text{-}CH_3$$

There is no definite evidence for the existence or non-existence of other more complicated molecules or less complicated ones. The solvents employed in these investigations are of three types: (1) non-polar, (2) polar and normal and (3) polar and abnormal or associated. In the first case no changes are observed, showing that the acid molecules remain as they are This observation is in consonance with existing physico-chemical data which gives abnormal values for the molecular weights of acetic acid in non-polar solvents like benzene.

In polar solvents, changes are observed, showing thereby that the molecular structure of the acid is affected. The following changes may take place :

(*i*) Breaking up of associated molecules into simpler ones.

(*ii*) Formation of complexes between the solvent molecules and the simple molecules so liberated.

Thus, in general, there is the possibility of such a solution containing the following types of molecules : (I) unbroken molecular aggregates of the pure acid, (II), lower polymers like monomers and (III) complexes formed with the solvent. An explanation of the changes observed in the Raman spectrum of the acid in the different polar solvents is bound to be dependent upon the factors outlined above.

Next we should consider the effect of these changes upon the frequencies of the particular oscillations studied. The author has already pointed out that the effect of association on the C=O line is to reduce its frequency and the effect of depolymerisation is to increase it, if the co-ordination or the formation of the hydrogen bond takes place on the O in C=O.[1, 2, 3] Based upon this factor, it was argued that in aqueous solutions of acetic, formic and benzoic acids, the increase in frequency of the C=O band is due to the formation of lower polymers. Association can take place not only through the O in C=O, but through H in OH which can act as an acceptor. It is only in the case of similar molecules, *i.e.*, in the case of molecular polymers of the pure acid alone, that both the donor and acceptor atoms are linked up through hydrogen bonds. If, on the other hand, a different molecule, say ether or acetone, forms a complex with the acid, then its donor atoms link up only with the acceptor atoms in the acid, *viz.*, with the H in OH. Thus, the C=O is unlinked, its external binding through the hydrogen bond is released, and the effect on it, if any, of the hydrogen bond at the end of the H in OH may not be towards diminishing it. Hence, again, there is an increase in the frequency of the C=O, if a molecular complex is formed between the acid molecule and another molecule having a donor atom.

The changes undergone by the Raman lines of acetone and methyl-ethyl ketone in acetic acid are discussed in another paper.[5] The effect of acetone, methyl-ethyl ketone and ether on the acid seems to be to break up the associated molecules (probably dimers) into their monomers and form complexes with them of the types

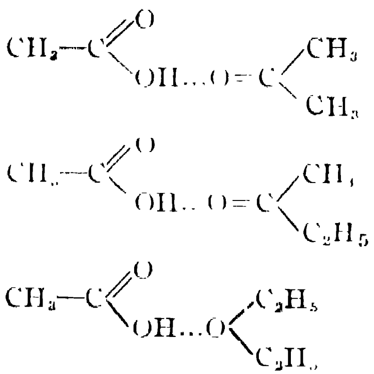

In all these, the C=O linkage of the acid is unattached and hence the 1760-line may probably be due to this. That it may not be due to the C=O in acetone or methyl-ethyl ketone is shown by the fact that the line is present in solutions in ether as well as in nitrobenzene.

The C—C binding in these cases seems to be affected by the formation of these complexes. Hence the appearance of the new line at 872. The fact that the line increases in intensity with increasing dilution of the acid shows that at greater dilutions more and more molecules of the acid are broken up and link themselves to the solvent to form complexes. The changes in the 620-line are explained similarly. The author attributed[1] this line to an external oscillation of the carboxyl group. If this group is attached to an external molecule, the line is bound to be displaced and the doubling is caused by the presence of attached and unattached molecules in the mixture. Further confirmation of this is found in the fact that these low-frequency components appear in the pure state of the acid, while they disappear at greater dilutions in water. The fact that the 893-line is not doubled in solutions of acetic acid in nitrobenzene is probably due to the non-formation of complexes. The effect of nitrobenzene may be merely to break up the dimers into monomers on account of its large dipole moment. The NO_2-line of nitrobenzene is itself unshifted and hence this conjecture. Chloroform does not seem to have any effect at all on the acid. Probably the effect of the dipole interaction is too feeble to break the dimers of the acid.

The effect of water on the acid is distinctly dissimilar to that of all the previous solvents studied. While there is the appearance of two distinct lines for the frequencies 620, 893 and 1670 in all the other polar solvents, in water there is a gradual shifting of the maximum of the 1670-band towards 1710 at higher dilutions and the other lines merely get diffuse, the low-frequency compo-

nents disappearing. This, as has been already pointed out, seems to be due to the breaking up of the higher polymers into lower ones. The fact that the low-frequency components of the 620- and 893-lines which are characteristic of the higher polymers disappear in aqueous solutions, lends support to this view. But it may be argued, why don't water molecules link themselves up with the monomers so formed and form complexes as in the case of solutions in acetone and methyl-ethyl ketone? If they should link up to the C=O, the C=O frequency must be diminished. But in fact it increases. The lines characteristic of the higher polymers of the complexes formed with the monomers, *viz.*, the low-frequency components of the 620- and 893-lines are absent in aqueous solution. Hence it is evident from the data that hydrates with water do not seem to be formed. There is another way of linking in order to form a hydrate The H in OH in acetic acid may act as an acceptor and the O in water may be the donor. Then the structure of the hydrate resembles that of the acetonate given already and hence the 1760-line must be expected. Also the low-frequency components of the lines 620 and 893 must make their appearance as in the case of other solvents. Experiment shows that there is no trace of a separate and distinct 1760-line and that the 601- and 872-lines actually disappear in aqueous solutions. Moreover, physico-chemical data of Jones and his co-workers point out to the non-existence of hydrates of acetic acid in aqueous solutions.[4] Hence the changes of the Raman lines of acetic acid in aqueous solutions seem to be due only to a depolymerisation of the acid in the soivent, as pointed out elsewhere.[5]

Probably a distinction can be drawn between the effect of other polar solvents and that of water In the case of water, we are treating with an abnormal and associated liquid. It is well known that the effect of one associated liquid on another is towards mutual depolymerisation. Each tends to diminish the association of the other. Probably that is so in mixtures of fatty acids and water.

The extreme diffuseness not only of the C=O line but of every other line in aqueous solutions appears to be due to the fluctuations of the polarisation field of the water envelope round each molecule in general. The effect of this field and its fluctuations is maximum in the case of water as compared to the other polar solvents, probably on account of the small size of the molecule.

REFERENCES

1 P. Koteswaram, *Zeits. f. Physik*, **110**, 118 (1938).

2 ,, *Jour. Chem Phys.* **7**, 88 (1939).

3 ,, *Zeits. f. Physik*, **112**, 395 (1939).

4 H. C. Jones, "*Hydrates in solutions*", Publications of the Carnegie Institute of Washington,-Feb. 1907, p. 110.

5 Paper No. 36, this journal

MOLECULAR ASSOCIATION IN ACETONE AND METHYL-ETHYL KETONE*

By P. KOTESWARAM.**

(*Received for publication, July 2, 1940*)

Plate XXII

ABSTRACT. The Raman spectrum of acetone is studied in different solvents: water, methyl alcohol, phenol and acetic acid at different concentrations. In all these cases, the C–O line of acetone is found to shift towards smaller frequencies, while its C–C line and some of the deformation frequencies are found shifting towards higher frequencies. In acetic acid, a new line at 1760 cm.$^{-1}$ is obtained. These results are explained on the basis of the formation of hydrates in water, and complexes between the acetone molecules and those of the solvent in which it is dissolved. While these solvents produce such conspicuous changes, non-polar solvents like benzene and carbon-tetrachloride and normal polar solvents like ether and chloroform do not produce any effect on the Raman spectrum of acetone. Thus acetone seems to associate only with molecules having an acceptor atom. Similar results obtained with methyl ethyl ketone are similarly explained.

MOLECULAR ASSOCIATION IN ACETONE AND METHYL-ETHYL KETONE

INTRODUCTION

The application of Raman effect to the problem of molecular association has been the subject of recent investigations by the author. Ramakrishna Rao[1] first applied it to the study of water and interpreted the structural variations of the Raman water band with temperature as being due to the changes in the relative intensities of its three maxima which are themselves due to the presence of polymers of the type $(H_2O)_3$, $(H_2O)_2$ and H_2O. An application of the same method to heavy water by Ramakrishna Rao and the author [2] revealed similar intensity variations in its Raman band with temperature and these variations were again explained as due to the change in the equilibrium between three types of polymers in heavy water also $(D_2O)_3$, $(D_2O)_2$ and D_2O. Extending the work to other associated liquids, the author studied the Raman spectra of acetic,[3] formic and benzoic acids [4] in their solutions in water and at different temperatures. The intensity maximum of the band due to the carbonyl frequency in all the acids studied was found to be shifting towards higher frequencies on dilution in aqueous solutions and with increased tempera-

* Part of the thesis approved for the D.Sc degree of the Madras University.

** Communicated by the Indian Physical Society.

tures. These results were explained on the assumption that the molecules of the fatty acids are initially associated and that they break up at higher temperatures into their lower polymers as in the case of water and heavy water and also that they depolymerise in the presence of a highly associated solvent like water.

To study the behaviour of acetic acid in other solvents also, the Raman spectra of this substance in mixtures with both polar and non-polar liquids were taken.[5] Therein it was found that in non-polar solvents like benzene and carbon tetrachloride, acid molecules are not affected, the Raman spectrum of the mixture being just a superposition of the spectra of the individual components. But in other polar solvents, nitrobenzene, ether, acetone and methyl-ethyl ketone, the C=O line consisted of two definite lines, one at 1670 as in the pure acid and another at 1760, which was attributed to the externally unattached C=O in the complex formed between the acid and the solvent. Further evidence for the formation of the complexes was got by a study of the acetone lines which are themselves affected in the presence of acetic acid. A detailed study of the behaviour of acetone and methyl-ethyl ketone, not only in solutions in acetic acid but in a number of other solvents, gives an insight into the capacity of these ketones to associate with other dissimilar molecules.

EXPERIMENTAL

The experimental arrangement used was the usual Wood's tube with a Wolm trough. $NaNO_2$ solution was used to filter off 4046-line of the mercury arc and the other lines of lower wavelengths. The liquids were rendered free from water and vacuum-distilled.

RAMAN SPECTRUM OF ACETONE

The Raman spectrum of acetone was investigated by a large number of workers, prominent among them being Dadieu and Kohlrausch[6], Whitelaw[7], Ganesan and Venkateswaran[8], Dillon Dicknisen[9], Sirkar[10], Edsall[11] and Engler[12]. Bates, Anderson and Halford[13] studied Dentero-acetone. As acetone gives sharp lines, there are no discrepancies with regard to its Raman frequencies. Kohlrausch gives the Raman frequencies for the liquid as the mean of the frequencies observed by a number of workers. The intensities of the lines are mentioned in brackets opposite each frequency. 376(2), 490(1), 526(3), 788(10), 901(0), 925(1b), 1060(3), 1194(3), 1223(5), 1340(0), 1430(5b), 1712(5) 2925(10), 2969(2), 3003(2).

Edsall worked with aqueous solutions of acetone and found no shifts in the frequencies. Whiting and Martin[14] working with acetone and carbon disulphide mixture detected no effect.

Gordy,[15] working in the infra-red region, reported a shift of C=O absorption in acetone towards longer frequencies in heavy water and chloroform solutions.

He could not study the effect of water upon the C=O frequency due to the superposition of the absorption band of water in the same region. In a recent publication[16], he found a new absorption frequency at 4μ in mixtures of acetone and chloroform and attributed it to the frequency due to the hydrogen bond −H...O−, between the O in C=O and H in C−H in chloroform. This he claimed as the first discovery of the direct spectrum of the hydrogen bond, all other evidences being indirect, based upon the changes in the frequencies of the bands closest to that of hydrogen.

RAMAN SPECTRUM OF METHYL-ETHYL KETONE

The Raman spectrum of this liquid was studied by Dadieu Kohlrausch[6], Whitelaw,[7] Ganesan and Venkateswaran[8] and Kohlraunch and Koppl[17]. Due to discrepancies in the measurements by various workers, the author again measured the frequencies, and the results obtained by the different authors are given below.

TABLE I

Ganesan and Venkateswaran	Whitelaw	Kohlrausch and Koppl	Author
—	310(1)	256(1)	—
408(2)	406(0)	408(3)	408(4)
560(2)	593(2)	592(3)	590(4)
766(4)	764(6)	763(7)	765(10)
964(1)	955(0)	947(1b)	950(1)
—	—	1001(1b)	1000(1)
1093(1)	1085(4)	1088(3)	1090(1)
1176(0)	1165(0)	1105(½)	1108(4)
1207(0)	1213(0)	—	1220(1)
—	—	1247(½)	1250(1)
1375(1)	1356(1)	—	1357(3)
1431(3)	1436(2)	1412(3b)	1420(5)
—	—	1450(3b)	1450(5)
1729(2)	1734(3)	1711 ± 10(3b)	1712(7)
2876(2)	—	—	2915(3)
2936(4)	2928(6)	2917(10b)	2925(8b)
3651(1)	2948(3)	2980(6b)	2975(2)

EFFECT OF DIFFERENT SOLVENTS ON THE RAMAN SPECTRUM OF ACETONE

Different solvents were chosen for studying their effect on the molecules of acetone. They are (*i*) non-polar—benzene and carbon-tetrachloride, (*ii*) polar and normal chloroform, ether, (*iii*) polar and abnormal—water, methyl alcohol, phenol and acetic acid. The results obtained in all these cases are given below.

(*i*) *Non-Polar* : Benzene and carbon-tetrachloride has no effect on the Raman spectrum of acetone as was the case on acetic acid. This is in accordance with Whiting and Martin's observation that carbon-disulphide also had no effect on acetone.

(*ii*) *Polar and Normal* : Among the normal polar solvents studied, ether and chloroform differ in the fact that ether does not have a hydrogen atom to link up to the O in C=O in acetone. Both the liquids, acetone and ether, have donor atoms O. Hence there was naturally no effect of either of the molecules on the other. In the case of chloroform, it has got a hydrogen atom linked up to the carbon and recent solubility and infra-red data point out the possibility of the H in chloroform having acceptor properties. In fact, Gordy reported the absorption due to the hydrogen band between O in C=O in acetone and the H in chloroform. But even prolonged exposures with mixtures of acetone and chloroform did not give any trace of a line or band in the region 4μ ($\Delta\nu$=2500) as indicated by Gordy or in the region of the familiar OH band ($\Delta\nu$=3200–3600). The spectrum of the mixture was just the superposition of the spectra of the individual components as in the previous case. There was no shift of any of the acetone lines or of the chloroform lines as reported by Gordy in the infra-red region.

(*iii*) *Polar and Abnormal* : This class of liquids brought about conspicuous changes in the Raman spectra of acetone. The results with each one of the liquids are given *seriatum* :

(1) *Water* : Edsall reported no shifts of the C=O line in solutions of acetone in water. But the author observed shifts not only of the C=O line but of a number of other lines of acetone. Raman spectra of solutions containing 90%, 75%, 50% and 25% by volume of acetone in water were compared with that for the pure liquid and the following changes were observed in dilute solutions :—

(*a*) The line 1712 attributed to the C=O frequency, definitely shifted gradually to smaller frequencies with increasing concentration of water.

(*b*) The line 788 attributed to the C–C oscillation shifts gradually to longer frequencies.

(*c*) The lines 530, 1069, 1223, 1340 shift to longer frequencies with increasing dilution.

(*d*) The line 370 becomes very weak at higher dilutions.

788 1712

g. 1 (a)

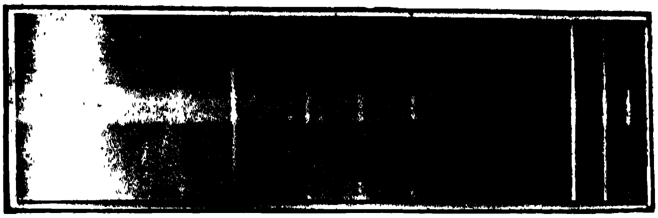

Acetone pure

75% + Water 25%

788 1712

Fig. 1 (b)

Acetone 25
+ Water 75

1712

Fig. 1 (c)

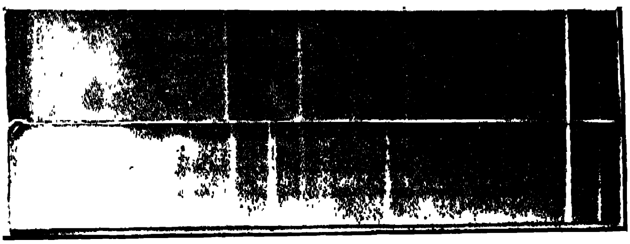

Pure Acetone

Acetone 34%
+ Phenol 68%

Fig. 1 (d)

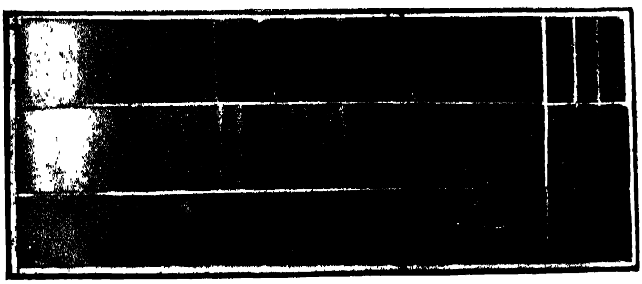

Acetone Pure

Acetone 50
+ Acetic Acid 50

Acetic Acid Pure

ure

30

765 1712

Fig. 1. Acetone in different Mixtures.
Fig. 2. Methyl Ethyl Ketone + Water

Figure 1 (*a*) gives the Raman spectra of pure acetone as compared with that of a 75% solution in water. 1 (*b*) compares pure acetone with a 25% solution.

The following table gives the approximate frequencies of the C–C and the C=O lines at the different concentrations :—

TABLE II

C–C and C=O frequencies of Acetone in Aqueous Solutions

Percentage of acetone	C–C	C–O
Pure	788	1712
90%	793	1706
75%	796	1704
50%	799	1702
25%	800	1696

Measurements are from microphotometric curves under high magnification.

(2) *Methyl Alcohol* : Methyl alcohol did not produce as pronounced an effect as in the case of water. But a slight shift in the C=O line at 1712 towards shorter frequencies is perceptible. In the microphotometric curve of the Raman spectrum of a 50:50 mixture, the C=O line shows a structure with two peaks. The 1223-line shows a distinct shift at higher dilutions.

(3) *Phenol* : Phenol produces very conspicuous shifts on the lines of acetone. Four different concentrations were studied with increasing proportions of phenol by weight, (*viz.*) 53%, 40%, 34% and 13% of acetone in the mixtures. The percentages are by weight. In the solutions, the C=O band at 1712 again definitely shifts to shorter frequencies and the C–C line at 788 shifts to longer frequencies. Observations of the shifts of the C–C line are difficult due to the presence of the 812-line of phenol close to it and to the high-frequency side of it, but a closer scrutiny reveals the shift in this line. Among the other lines, the shift in the 530-line cannot be observed on account of the superposition of a line due to phenol, and the 1223-line gets more diffuse and shows a large shift towards higher frequencies. This is due to the superposition of the 3050-line of phenol excited by the 4046-mercury-line, which is transmitted feebly through the sodium-nitrite filter. The 1340-line seems to be suppressed in solutions. Figure 1 (*c*) compares the Raman spectrum of pure acetone with that of a mixture containing 34% acetone and 68% of phenol.

(4) *Acetic Acid* : Acetic acid again produces pronounced effects on the Raman spectrum of acetone. The effect of acetone on the Raman pectrum of acetic acid has been discussed in a previous publication.[5] The effect

of acetic acid on acetone is given here. Three concentrations 75%, 50%, and 25% by volume of acetone in the solutions were studied. The effect on the C=O line of acetone cannot be studied with precision due to the superposition of the shifted C=O line of acetic acid on it, but a perusal of the spectra and their microphotometric traces points out to the probability of the C=O line having shifted towards low frequencies as in the other cases described above. But the shifting of the C—C line at 788 towards higher frequencies is quite clear and the effect can be traced to acetone alone, as there is no acetic-acid line in that region. Figure 1 (*d*) gives the Raman spectra of acetone, acetic acid and a 50:50 mixture of acetone and acetic acid. The new line at 1760 makes its appearance in all the three concentrations. It is marked by an arrow in figure 1 (*d*) It is very clear in the 50:50 mixture by volume. The lines 530, 1069, 1223, and 1340 have shifted to longer frequencies. The effect can be taken to be that of acetone as in the 50% mixture, the time of exposure being reduced in order not to excite the feeble lines of acetic acid in that region.

SUMMARY OF THE RESULTS

(1) In solutions of acetone in non-polar solvents like benzene and carbon-tetrachloride, the Raman lines are unaffected, the spectrum of the mixture being an exact superposition of the spectra of the individual compenents.

(2) Similar is the case in solutions of acetone in normal polar solvents—chloroform and ether. The acetone lines are unaffected by the presence of the solvent.

(3) Water, methyl alcohol, phenol and acetic acid produce distinct changes in the Raman spectrum of acetone, the main alterations being a shift of the 1712-line towards shorter frequencies, and a corresponding shift of the 788-line towards higher frequencies. The lines 530, 1069, 1223, and 1340 shift towards higher frequencies in mixtures of acetone with water and acetic acid, while in methyl alcohol, the 1223-line shifts towards higher frequencies. In phenol it is not possible to study these lines on account of their very feeble excitation and due to their superposition on the phenol lines. The shift is progressive in all these solutions, higher dilutions producing greater shifts.

EFFECT OF SOLVENTS ON METHYL-ETHYL KETONE

Similar results were obtained with methyl-ethyl ketone. Non-polar solvents like benzene and carbon-tetrachloride and normal polar solvents like ether and chloroform do not produce any effect on the ketone. The effect of water and acetic acid is exactly similar to that on acetone. Fig. 2 gives the effect produced by water in a 30% solution of the ketone (by volume). The C=O line at 1712 is again shifted to lower frequencies. The C−C line at 765 is shifted to higher

frequencies. The 590-line is also slightly shifted to higher frequencies and the effect of the other lines could not be studied due to their feebleness.

The effect of acetic acid on the ketone is again similar to that on acetone The low-frequency shift of the 1712-line cannot be studied distinctly on account of the superposition of the shifted C=O of the acetic acid. The effect on the C—C 765-line, (*viz.*) its high-frequency shift, is detectable. The new line at 1760 can be seen in a mixture of the ketone in the acid (50 : 50 by volume).

DISCUSSION OF THE RESULTS

The results outlined above point out to a definite change in the molecular structures of acetone in abnormal polar solvents like water, methyl alcohol, phenol, acetic acid, while no such change is noticed in non-polar solvents like benzene and carbon-tetrachloride and in polar normal solvents like ether and chloroform. That the non-polar solvents do not have any effect on the solutes (the words solvent and solute are used merely to indicate the two components of the mixture with no special significance such as that the solvent is the larger component by weight or by volume) is well-known and is explained by the fact that they cannot have any dipole interaction producing molecular association or dissociation on the solute for the simple reason that they do not possess any dipoles. In the case of polar normal liquids, the behaviour of ether is again plain as molecular association can take place only when a donor and an acceptor atoms are present in the mixture. Both ether and acetone have donor atoms and hence there cannot be a hydrogen bonding between them. Recent infra-red data by Gordy and his co-workers and the solubility data of Gladstone and others led to the supposition that chloroform can form hydrogen bonds through its hydrogen acting as an acceptor. As has been stated already, Gordy claimed to have recorded the hydrogen bond between acetone and chloroform But the author's work on Raman spectra does not lend suport to the conclusion. Even supposing that the band excited by the hydrogen bond is infra-red active and Raman inactive, there must be a pronounced effect on the C=O oscillation in acetone. In fact Gordy reports a shift in the C=O towards higher frequencies. But no such shift is observed by the author in the Raman spectrum of the mixture of acetone and chloroform.

On the other hand, abnormal liquids like water, phenol, acetic acid, and methyl alcohol produce marked changes on the Raman spectrum of acetone. The shift of the C=O line towards shorter frequencies is very significant. In previous publications,[3,4] it was argued that association must bring about a decrease in the frequency of the C=O bond. The effect of the external attachment like the hydrogen bond was pointed out to be towards a diminution of the C=O binding. The fact that water of crystallisation diminishes the frequency of the NO_3-ion in a number of nitrates was also pointed out in support of the contention. In the present work, there is direct evidence of such

a diminution of the C=O frequency by an external attachment. The strong donor O of the C=O in acetone seems to form a hydrogen bond with the H in OH of the solvent, and hence the diminution of the C=O frequency. But Gordy reports a shift of the C=O to higher frequencies in mixtures of acetone in heavy water. The author's results in water mixtures are again in contrast to this observation.

Another very remarkable change is noticeable in solutions of acetone in abnormal solvents in the C—C line. This line at 788 shifts to higher frequencies in solutions in water, phenol, methyl alcohol and acetic acid. This change is also attributable to the formation of the complex. Probably the effect of the external hydrogen bonding upon this frequency is to increase it, as compared to the decrease in the C=O frequency. The molecular oscillations in these cases can be represented as follows :

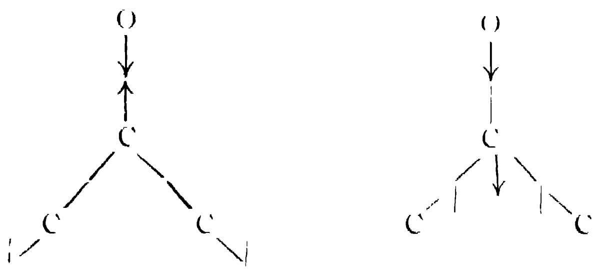

$\omega_1 = 1712$ $\omega_2 = 788$

For the same external force field, if ω_1 diminishes, ω_2 may increase on account of the differing nature of the two oscillations. Kohlrausch and Koppl attribute the values 370, 530, and 1069 to deformation frequencies ω_5, ω_3 and ω_4 respectively. As it is not proposed to get into the discussion about the assignment of the frequencies in this paper, it is merely stated that the shifts in frequencies 530, 1069, 1223, and 1340 are all due to the formation of the complex itself, the deformation frequencies as well as the higher overtones also being affected in addition to the symmetrical and antisymmetrical oscillations.

A perusal of the microphotometric curves of the Raman spectra of acetone at different dilutions and a comparision of the same with the curves for the C=O frequencies in acetic acid and in formic acid at different dilutions shows that in all these cases the shift of the intensity maximum is progressive. In the case of acetic and formic acids, the shift of the C=O is towards longer frequencies and, in the case of acetone, it is towards shorter frequencies in aqueous solutions. The two progressive shifts in opposite directions suggest two opposing effects on the molecular structure. While in the one case, acetic and formic acids, it is towards a strengthening of the C=O bond probably caused by the breaking up of the higher polymers into lower ones, in the case

of acetone, the shift indicates a weakening of the bond, caused by an external attachment and hence by the association of acetone with water. There is another argument. Supposing that the high-frequency shift of the C=O in fatty acids in aqueous solutions is due to hydrate formation, then the low-frequency shift in acetone solutions must be due to the breaking up of the complexes. Acetone is a normal liquid and no complexes exist in the pure state. Hence, the low-frequency shift in acetone must be due to the formation of a hydrate and correspondingly the high-frequency shift in the fatty acids to the breaking up of the associated complexes.

The progressive nature of the shift can be easily understood, as with increasing dilution, the percentage of complexes in the mixture increases and hence, the intensity maximum of the band shifts progressively towards the direction of the frequency of the C=O in the complex.

Another distinguishing feature in aqueous solutions of both the fatty acids and of acetone is that, though it is the intensity maximum that shifts, the total width of the band remains more or less the same In the case of acetic acid, the band is broad even in the pure state, and it remains so at almost all the dilutions studied, except at every high dilutions when it shows a tendency to sharpen. In the case of acetone, the C=O oscillation is revealed by a slightly diffuse line and it remains so at all dilutions.

Thus the main part of the evidence for the formation of association complexes is :

(1) The shift towards low frequencies of the C=O line in acetone.

(2) The corresponding shift towards higher frequencies of the C—C line.

(3) Shifts of the other lines, 530, 1069, 1223 and 1340, towards higher frequencies.

In cases like acetic acid where the shift of the C=O line cannot be clearly detected, the other two evidences help to postulate the possibility of the complex-formation. The shifting of the C—C line and the other deformation frequencies in acetone-acetic acid mixtures, in addition to the evidence of the C=O line itself which can be seen shifted to lower frequencies in plates which are not sufficiently exposed to record the acetic acid lines clearly, points out to the formation of an associational complex with the acid as with the other solvents—water, methyl-alcohol, and phenol. Thus the C=O line at 1760 is attributed to the externally unattached C=O of the complex. Detailed reasons for doing so are explained *elsewhere*.* [5]

The next problem is whether acetone breaks up the association of the solvent and attaches itself to the monomers liberated or whether it attaches itself to the higher polymers themselves. In acetic acid, this question can be partially answered. In the dimer or in any higher complex, both the donor and

acceptor atoms are closed up within a ring structure with hydrogen bonds interposed as follows :

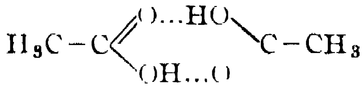

For the acetone to associate with the acid molecule, it must necessarily break up the polymer in order to liberate the H. Thus association may take place between acetone and the monomer of the acid liberated, as follows :

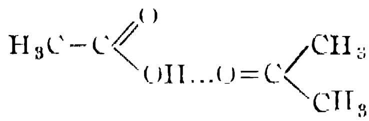

This breaking up of the higher polymers into lower ones has also been inferred from the fact that the C=O line of acetic acid shifts towards higher frequencies in acetone solutions as in the case of dilution in water and at higher temperatures. In other solvents it is not easy to detect the same effect, since they do not form closed-ring structures even on association, both the donor and the acceptor atoms being at either end of the polymer and free to associate. A study of the water band in acetone solutions by Sambasiva Rao[18] revealed a sharpening of this band indicating that the higher polymers $(H_2O)_3$ break up into lower ones $(H_2O)_2$ and H_2O. But the water band is a composite one involving also that excited by the water that has hydrated with the acetone molecules.

EFFECT ON METHYL-ETHYL KETONE

The effect of normal and abnormal solvents on methyl-ethyl ketone is exactly similar to that on acetone. Dilution brings about a shift of the C=O line towards higher frequencies. Solution in acetic acid also gives rise to similar changes. Hence the ketone seems to form complexes with acetic acid as in the case of acetone.

This work was done in 1939 in the Physics Laboratories of the Andhra University, Waltair, under the direction of Dr. I Ramkrishna Rao, to whom the author desires to express his gratitude.

REFERENCES

1 I. Ramkrishna Rao, *Proc. Roy Soc. A*, **92**, 406 (1931).

2 I. Ramkrishna Rao and P. Koteswaram, *Nature*, **141**, 331 (1938). *Ind. Jour, Phys.*, **12**, 63 (1938).

[3] P. Koteswaram, *Zs. f. Physik*, **110**, 118 (1938)

[4] ,, *Jour. Chem. Phys.*, **7** (1939)

[5] ,, *Current Science*, **8**, 70 (1939)

[6] A. Dadieu and K. W. F. Kohlrausch, *Monatshefte fur Chem.* **52**, 220 (1929), **56**, 401 (1930).

[7] N. G. Whitelaw, *Phys. Rev.*, **34**, 376, (1929)

[8] Ganesan and Venkateswaran, *Ind. Jour. Phys.*, **4**, 106 (1929).

[9] Dillon and Dickinson, *Proc. Nat. Acad. of Sciences Amer.* **15**, 699 (1929)

[10] Sirkar, *Ind. Jour. Phys.*, **7**, 61, 257 (1932)

[11] Edsall, *Jour. Chem. Phys.*, **4**, 1 (1935)

[12] Engler, *Z. fur. Phys., Chem.*, *B***32**, 471 (1936).

[13] Bates, Anderson and Halford, *J. Chem. Phys.*, **4** 535 (1936).

[14] Whiting and Martin, *Trans. Roy. Soc. Canada*. **25**, 87 (1931).

[15] W. Gordy, *J. Amer. Chem. Soc.*, **60**, 605 (1938)

[16] ,, *Nature*, 142, 831 (1938).

[17] K. W. F. Kohlrausch and F. Koppl. *Z. Phys. Chem.* *B***24**, 370 (1933).

[18] C. Sambasiva Rao, *Phil. Mag.*, **20**, 587 (1935).

[*] Paper No. 34, this Journal

MOLECULAR ASSOCIATION AS STUDIED BY RAMAN EFFECT*

By P. KOTESWARAM**

(Received for publication, July 2, 1940)

ABSTRACT. From a study of molecular association between similar and dissimilar molecules in a number of liquids and their mixtures, certain general conclusions are drawn as to the cause of molecular association. It has been found that, for association between two molecules, one must have a donor atom and the other an acceptor. Mere polar nature of a molecule does not facilitate association. The extent of depolymerisation of liquids on mixing is also investigated.

INTRODUCTION

Since very early times, different methods were employed for the study of molecular association in substances. Physico-chemical data based upon the elevation of boiling points and the depression of freezing points, or on the determination of surface tension and other physical constants, are subject to limitations peculiar to the constants determined and hence association factors based upon these determinations were all approximate Another relevant factor to be considered is that it is the abnormality in obeying some empirical rule which is found to hold good in a number of substances, that indicates that their molecules are associated and which gives an idea of the degree of association. These methods can in general be described as statistical, depending upon the behaviour of the substance in bulk.

With the development of newer physical methods like the determination of dielectric constants and dipole moments, X-ray and electron diffraction methods, and infra-red investigations, a direct approach is made to the molecule with a view to study its behaviour. The advent of Raman effect takes us direct to the molecule as the spectral lines recorded are due to the vibrations of individual molecules. Thus the effect of environment on the vibrations of the molecules manifests itself by producing changes in the frequencies and intensities of these lines. It is this factor that is most helpful in the study of molecular association by this method. With the presence of another molecule attached by a weak valency bond to one of its constituent atoms, the vibrations of every molecule are bound to be affected and the effects revealed as shifts

* Adapted from the thesis approved for the D.Sc. degree of the Madras University.

** Communicated by the Indian Physical Society.

in the Raman lines. What happens in every individual molecule is more or less visualised in the Raman spectra and, thus, this method gives us a direct evidence about the existence or otherwise of association. To distinguish this method from other physico-chemical methods, one relevant example may be given. In a non-polar solvent, the molecular weight of an associated solute depends upon its concentration to a certain extent. This is not due to any breaking up of the associated molecules in the solvents at low concentrations, but to other influences the nature of which is still uncertain. No such anomaly is presented in Raman spectra, the spectral lines undergoing no change with concentration of the associated substance in non-polar solvents.

One of the limitations of this method is that it may not be possible to determine the actual degree of association in a substance at a particular concentration, but by a comparison of the intensities of individual components attributed to various polymers, an attempt can be made to determine their percentage in a liquid. Typical examples are the work of Ramakrishna Rao in water,[1] in which he evaluated the relative proportions of the three types of polymers at different temperatures in water and the work of Ramakrishna Rao and the author [2] in heavy water. But even here, a determination of the absolute percentages cannot be made, only an estimate of the relative proportions at the different states being possible.

The work of the author in this field can be divided into two parts: 1. Association between similar molecules and 2. Association between dissimilar molecules.

(1) *Association between similar molecules*

The behaviour of water at different temperatures is the starting point for these investigations. Ramakrishna Rao's[1] work on its Raman band and his observations that it consists of three distinct maxima attributable to H_2O, $(H_2O)_2$, $(H_2O)_3$ molecules respectively and his determinations of the relative proportions of the different polymers at different temperatures by a comparison of the intensities of the three components of the band led to the natural extension of the work to heavy water.[2] Heavy water also is found to give rise to a broad Raman band with three distinct maxima at 2394, 2534, and 2674 cm^{-1}. With increasing temperature, as in the case of ordinary water, the band is found to undergo structural variations indicating a decrease in the intensity of the low frequency component 2394 and a corresponding increase in intensity of the high-frequency component 2674, the middle component 2534 remaining more or less unchanged in intensity. The third component 2674 being very close to the frequency of the heavy water vapour line, is naturally attributed to single D_2O molecules and the other two components to $(D_2O)_2$ and $(D_2O)_3$ molecules for reasons analogous to those for ordinary water. The decrease in the intensity of the low-frequency component at 2394 with increasing

temperature is explained as due to the decrease in the proportion of the $(D_2O)_3$ molecules and the increase in the intensity of the high-frequency component is attributed to the corresponding increase in the proportion of the D_2O molecules.

The fatty acids were studied next by the same method, the substances selected being acetic,[3] formic and benzoic acids [4] The C=O oscillation in these compounds is found to undergo conspicuous changes under different conditions. The effect of increased temperature on the three acids studied is to shift the maximum of the C=O frequency towards higher values. This result which is analogous to that in water and heavy water is explained as due to the breaking up of the associated molecules in the fatty acids into simpler ones. Dilution in water also produces distinct shifts of the C=O band towards higher frequencies, an effect which is attributed to the breaking up of the associated fatty acid molecules into simpler ones The effect on methyl alcohol in aqueous solutions is dissimilar to that of acetic acid, the C–O line of the alcohol shifting to shorter frequencies unlike the C=O line of the acid. No definite conclusions can be arrived at in the case of methyl alcohol till a study of the OH band of the alcohol is made in a number of associating solvents.

(2) *Association between dissimilar molecules*

The molecules of the liquids described in the previous section are all associated among themselves and seem to break up at higher temperatures and at higher dilutions in polar solvents like water. There is another type of liquids which are normal by themselves, but which have a strong tendency to associate with other suitable molecules. Thus there is the possibility of association being produced between the solvent and the solute.

The effect of a number of solvents on acetone [5] was studied with a view to detect any association between acetone molecules and those of the solvent. The C=O line of acetone is the one observed to undergo conspicuous changes. In addition, the C–C line is also affected. Non-polar solvents like benzene and carbon-tetrachloride and polar normal solvents like ether and chloroform do not produce any effect on the acetone lines. Water, methyl alcohol, phenol and acetic acid produce shifts in the C=O line towards smaller frequencies and in the C–C line towards larger frequencies. A number of deformation oscillations are also shifted towards higher frequencies. Similar results are obtained in the case of methyl-ethyl ketone These results are explained as due to the formation of complexes between the ketone and the other component in the solution studied, *viz.*, water, methyl alcohol, phenol, and acetic acid.

The Raman spectra of mixtures of acetic acid and acetone [6] and also of acetic acid and methyl-ethyl ketone [7] contain a new line at 1760, not present

either in the pure ketone or in the pure acid. Moreover, the C–C line of the ketone shifts to longer frequencies as in the case of mixtures of the ketone with water and phenol while the C–C line of the acid at 898 doubles up at higher dilutions, its low-frequency component at 872 increasing in intensity with a corresponding decrease in the intensity of the line 898. This significant change is also observed in solutions of acetic acid in ether. But nitrobenzene does not produce a change in the C–C line but as in the case of solutions of acetic acid in acetone, methyl-ethyl ketone and ether, solutions in nitrobenzene reveal the new line at 1760. Chloroform does not produce any conspicuous shifts and non-polar solvents like benzene and carbon-tetrachloride do not produce any effect on the acetic acid lines. The changes observed in the Raman frequencies of acetic acid in solutions in ketones and in ether are explained by the formation of complexes of the type

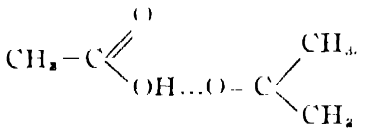

by the hydrogen bonding between the O of the ketone and the H of the OH in the acid. The 1760-line is attributed to the externally unattached C=O in the acid molecule in the complex. The low-frequency components of the 893- and the 620-lines which are feeble in the pure acid are pointed out as lending additional support to the concept of the association between acetic acid and the ketone or ether. In nitrobenzene, the absence of these components and the presence of the 1760-line is explained on the assumption that the associated molecules in the pure acid are merely broken up in solution, unaccompanied by association with molecules of nitrobenzene.

Acetic acid is thus found exhibiting two different properties. It does not seem to hydrate with water, the effect seeming to be merely towards a breaking up of the higher polymers into lower ones, whereas in acetone, methyl ethyl ketone and in ether it seems to combine with them to form complexes. Reasons for supposing that it does not hydrate with water are: the high-frequency shift of the C=O line, the absence of the 1760-line characteristic of the complexes and the absence of the low-frequency components of the 620- and the 898-lines also characteristic of the complexes, in aqueous solutions.

CONCLUSIONS

The foregoing work leads to the following generalisations with regard to molecular association in liquid.

(1) The mere polar nature of molecule does not give it associating properties, *e.g.*, chloroform and nitrobenzene.

(2) The substance must have both a donor and an acceptor atom for association in the pure state, *e.g.*, water and fatty acids.

(3) Molecules having only a donor or an acceptor atom cannot associate with those of the same type, *e.g.*, acetone. But they can form complexes with those having an acceptor or a donor atom, *e.g.*, acetone + water, acetone + phenol, acetone + acetic acid, etc.

(4) Non-polar liquids do not have any effect on polar solvents either normal or associated, *e.g.*, benzene + acetone, benzene + acetic acid.

(5) Polar normal liquids not having a donor or an acceptor atom do not have any effect on other polar liquids whether they have a donor or an acceptor, *e.g.*, chloroform + acetone, ether + acetone.

(6) Normal polar liquids which have a high dipole moment seem to split up associated liquids without combining with them to form complexes, *e.g.*, nitrobenzene + acetic acid.

(7) Two associated liquids seem to have mutual splitting effect on each other, there being no evidence for cross-association. These conclusions confirm the results from other physico-chemical methods.

The author's thanks are due to Dr. Ramakrishna Rao under whose guidance the work was done and to the authorities of the Andhra University for the facilities given.

REFERENCES

[1] *Proc. Roy. Soc., A*, **130**, 498 (1931).
[2] *Ind. Jour. Phys.*, **12**, 63 (1938).
[3] *Zeits. f. Physik.*, **110**, 118 (1938).
[4] ,, ,, **112**, 395 (1939).
[5] *loc. cit.*
[6] *Current Science*, **8**, 70 (1939).
[7] *loc. cit.*

FREQUENCY CHANGES IN THE RAMAN SPECTRUM OF SULPHURIC ACID

By N. RAJESWARA RAO, M.Sc.*
Andhra University, Waltair

(Received for publication, July 6, 1940)

ABSTRACT. Changes in the frequency of the Raman lines of sulphuric acid with dilution are measured. The low-frequency bands 415 and 570 are shifted away from the Rayleigh line, and the 913-line shifts towards it, with increasing dilution. The 1040 first decreases in Raman frequency with dilution, and, on further dilution, its frequency is increased, while the 984 line remains unchanged. In solution of acid sulphate, the 913, 1040 and 984 have less frequency as compared with equivalent solution of sulphuric acid. Besides, all the lines are diffuse and broad in intermediate concentrations.

The changes in the low-frequency bands are attributed to the changes in the relative abundance of H_2SO_4, HSO_4 and SO_4 radicals in solution with change in concentration. The behaviour of 913 is attributed to the relative abundance of H_2SO_4 and HSO_4 radicals, each of which contributes a component to this band. The 984- and 1040-lines owe their behaviour to the combined effects of (1) ions surrounding each of SO_4 or HSO_4 ions and (2) hydration. The lower frequency in the acid sulphate solution as compared to the equivalent acid solution, is attributed to the predominence of hydration over the effect of surrounding ions, due to the smaller percentage of H ions in the former.

INTRODUCTION

In a previous communication,[1] the author reported investigations on the progressive dissociation of sulphuric acid with dilution, from a study of the intensity changes in the Raman lines of this substance with change in concentration. Equally interesting are the changes in the Raman frequencies of this substance with dilution.

A characteristic feature of sulphuric acid is that all its Raman lines are broad and diffuse. This is the reason why the values for the frequencies of the lines and their changes on dilution, given by various authors differ to a large extent. Also, the continuous spectrum which is superposed on the Raman lines adds to the difficulties in locating the maxima and extents of the bands. Nisi [2] reported that the Raman lines suffer a general shift towards higher frequency on dilution and explained the result as due to the hydration of the molecules. Specchia [3] observed a similar result. Ramakrishna Rao,[4] while agreeing that the low-

* Communicated by the Indian Physical Society.

frequency bands with maxima 385-450 and 543-608 shift away from the Rayleigh line on dilution, expressed doubt as regards the increase in the frequencies of the 913-860 and 1040-1037 lines since they are of the same order of magnitude as the experimental error. Woodward and Horner [5] stated that all the bands, except the 910-860, are shifted towards higher Raman frequency and their observations are in conformity with those of Bell and Jeppesen.[6] On the other hand, Bell and Fredrieson,[7] working with a grating, observed no shifts except in the case of 543·608. But, none of the above authors explained these shifts. The present work is an attempt in this direction.

EXPERIMENTAL

To remove the intense continuous spectrum that is present in the Raman spectra of solutions of sulphuric acid, the acid is treated with a few drops of pure nitric acid and heated to about 200°C for about half an hour, following the suggestion made by Medard.[8] With the acid treated like this, clear spectra are obtained. In order to facilitate clear observation of the shifts, the spectra are taken using a Hartman diaphram. The experimental arrangement is the same as described in the previous communication.[1] Since the Raman lines are broad and diffuse, it is difficult to locate their maxima by a micrometer. Therefore, microphotometric curves are taken for the spectra and the frequencies of the maxima measured by using the Hartman dispersion formula. The values of the frequencies of the Raman lines and their widths at various concentrations are given in the following table.

TABLE GIVING THE FREQUENCIES OF THE RAMAN LINES IN SOLUTIONS OF SULPHURIC ACID, ACID-SULPHATE AND SULPHATE

Concentration in gm. moles.	A			B			C			D			E
	Extent	Max	Width	Extent	Max	Width	Extent	Max	Width	Extent	Max.	Width	Max.
16 5	390—450	410, 385	69	488—600	543	112	884—937	913	53	1005—1059	1040	54	
14.5	369—482	400	113	525—625	552	100	871—937	910	66	994 1066	1036	72	
12.5	369—494	408	125	525—620	570	95	852—937	905	85	998—1091	1030	93	
10 5	369—478	408	109	525 620	570	95	862—926	899	64	963—1080	1030	117	984
7 5	380—467	415	87	536—620	578	95	862—930	887	68	1001—1080	1035	79	984
1.5	380—467	415	87	536—620	578	95	858—879	866	21	1001—1055	1039	54	984
3.0	380—467	415	87	536—620	578	95	858—879	866	21	1001—1055	1039	54	984
$KHSO_4$ 3.0	373—452	415	79	536—620	578	95	858—879	860	21	1001—1055	1037	54	980
$(NH_4)_2SO_4$ 3.0	408—462	450	54	586—640	608	54	...	...	...	...	...	...	980

In the above table, the first column gives the concentration in gram. moles of the acid in 1000 c.c. of the solution. Each of the other columns, allotted for each of the lines, is subdivided into three, the first division giving the extent of the band, the second the Raman frequency of the maximum and the third the width of the band.

RESULTS AND THEIR EXPLANATION

For the sake of convenience, the Raman lines are lettered from A to E, A and B representing the low-frequency bands 385-450 and 543-608 C, D and E correspond to 913-860, 984-980 and 1040-1039, respectively. The other bands, *viz.*, 1171 and 1365, are very diffuse and feeble and disappear very quickly on dilution, and hence no attempt is made to measure their changes in frequency with dilution.

A.—Raman frequency 385-450

This band is found in the spectra taken with all the substances containing SO_4 radical, and hence is regarded as characteristic of it. It has a clear doublet structure at the highest concentration with maxima at 385 and 410. Bell and Jeppesen,[6] who have worked with 100% acid report that this structure is very prominent with the purest acid. In the spectra taken with dilute solutions of sulphuric acid and of acid sulphates there is only one diffuse band with its maximum at 415, and in sulphate solutions at 450. Therefore, it is concluded by Ramakrishna Rao [4] and Woodward and Horner [5] that 385-410, 415 and 450 are respectively characteristic of H_2SO_4, HSO_4 and SO_4 radical, respectively.

With increasing dilution the band is observed to be shifting away from the Rayleigh line and it is explained by Ramakrishna Rao [4] and Woodward and Horner [5] as due to the fact that with decreasing concentration, the H_2SO_4 molecules dissociate to HSO_4' and H^+ ions which brings about a diminution of intensity of the doublet on which is superposed the higher-frequency band excited by HSO_4 ions.

B.—Raman frequency 543-608

Like A, this band is also taken as characteristic of SO_4 radical for the same reason. In the pure acid, it has a single maximum at 543. With dilution, it behaves in a similar manner and just for the same reasons as in the case of A.

Bell and Jeppesen[6] objected to the above explanations Working with a large number of concentrations of the acid at intervals of 5%, they failed to observe at any concentration, a separation, of the two components due to HSO_4 and H_2SO_4 radicals. But, in view of the width and the closeness of the bands, no such separation can be expected. There can be only a shift in the resultant

maximum and an increase in the width of the band as a result of the superposition of the components due to H_2SO_4 and HSO_4. This is what is actually observed.

C:—Raman frequency 913-860

This band is found to be very intense in the spectra taken with very concentrated solutions of the acid and as the concentration of the acid is diminished, its intensity diminishes more than in proportion to dilution. Hence it is attributed to the undissociated H_2SO_4 molecules.

But, in the spectra taken by the author, this band persists, though with much less intensity, even in dilute solutions and also in solutions of $KHSO_4$ but with a slight decrease in Raman frequency, a fact which has not been observed by any of the previous authors.

The band exhibits conspicuous changes in the frequency. Its width is 51 wave numbers in the highest concentration, and its maximum is at 913 But, as the dilution is increased, the maximum shifts towards lower-frequency and the higher-frequency portion of the band gets feebler. With increasing dilution, it becomes narrow with a width of 21 cm. which is the same as in $KHSO_4$ solution.

The behaviour of this band can be easily understood, if it is taken as composed of two components, a strong one with higher-frequency contributed by the H_2SO_4 molecules and feeble one contributed by HSO_4 ion. As the concentration of the acid decreases, the high-frequency component decreases in intensity, but, since the H_2SO_4 component is very strong compared to the HSO_4 component, the intensity of the band as a whole becomes feeble and gives the impression that the band is excited entirely by the H_2SO_4 molecules. In the intermediate dilutions, where both types of molecules are present, the band is naturally very broad and in the very low concentrations where the H_2SO_4 component is absent, the band is narrow and is shifted towards lower frequency.

D:—Raman frequency 1040

This band is taken to be characteristic of HSO_4^- ion. It is very broad in solutions of moderate concentration of the acid, while in very concentrated solution it is less wide and in dilute solutions it is fairly sharp. Also, the maximum of the band shifts slightly but definitely towards lower frequency from high concentrations to moderate concentrations and shifts again from moderate concentration to dilute solutions. And in solution of acid sulphate it is of slightly lower frequency than in sulphuric acid of the same molecular concentration.

The larger diffuseness of this line in intermediate concentrations of the acid is in conformity with similar behaviour revealed in the course of investigations in this laboratory in general, by Raman frequencies of electrolytes, in the

intermediate concentrations, at which the band is usually most diffuse, and this is apparently due to the large ionic concentration of oppositely charged ions in the neighbourhood of each ion giving rise to the Raman frequency under consideration. In crystals, the line is the sharpest and of the highest frequency, when there is no water of hydration. In crystals, the disposition of the cation with respect to the axis of symmetry of the anion is the same for all the anions So, from solution to crystal there is only an increase in frequency without increase in diffuseness. But in intermediate concentrations of the acid solutions, where the number of cations surrounding each anion is the greatest, the relative disposition of the ionic field and the axis of symmetry of the anion is probably different for different ions, and hence, the Raman frequency may change slightly from ion to ion and this probably is the cause for diffuseness of the line in the intermediate concentrations.

As regards the change of Raman frequency, there are in general two causes giving rise to it (1) the surrounding ions and (2) water of hydration. The former have a tendency to increase the Raman frequency, while the latter diminishes it. In solutions of sulphuric acid, both these factors influence the Raman frequency, and the actual frequency at any concentration is due to the resultant of these two effects. It is difficult, however, to determine in the case of the changes exhibited by HSO_4 ions what part of the change is due to ionic influence and what part due to hydration, on account of the complications arising out of the superposition of the two effects.

The lower frequency of the band in acid-sulphate solutions, as compared with that of the acid of the same molecular concentration, seems to be due to the fact that there are less number of $H^{\cdot}$ ions in the former. The hydrogen ions, in virtue of their lightness and smallness in size, can approach the negative ions much closer and hence can exert more influence than the heavy potassium ion can. Hence, in solutions of acid-sulphates, the effect of hydration is more predominent which, therefore, brings about a shift in the line towards lower frequency.

E:—Raman frequency 984

This line which is characteristic of SO_4'' ion, is very strong in solutions of sulphates and in dilute solutions of bisulphates. In solutions of sulphuric acid, it appears very feeble even in very dilute solutions. In high concentrations, the line appears very feeble and on it is superposed a part of the 1040-band. So, it is very difficult, either to locate the maximum in a microphotometric record or observe it by a micrometer. Therefore, nothing can be said regarding its changes in the frequency on diluting the acid. On comparing the line in the acid and acid-sulphate of the same molecular proportion, it is found that it is of slightly less frequency in acid-sulphates.

In solutions of the acid, probably the effect of ionic influence is just neutralised by that of hydration, so that there is no change in the frequency of this line. The lower frequency in solutions of acid-sulphates when compared with that of the acid is similar to that suffered by the HSO_4 ion probably due to the same reasons.

It is generally contended [9] that the greater is the chance for hydration of an ion in solution, (1) the larger the ionic charge, (2) the smaller the size in the case of cations (3) the larger the size in the case of anions. Also, oxygen is a better donor of electrons than hydrogen is an acceptor. Therefore, the anions in general are less hydrated than the cations.

But, in the present case, the HSO_4' ion is sufficienty large and contains many donor oxygens and hence is capable of being hydrated. The SO_4 ion contains 4 donor oxygens and doubly charged and hence is more easily hydrated than the HSO_4' ion. This is probably the reason why the shift of the E line from the acid to acid-sulphate is larger than the shift of the D line. The above view is supported by the fact that the crystals of sulphates are invariably hydrated with an odd number of H_2O molecules, *e.g.*, $LiSO_4$, $1H_2O$, Na_2SO_4, $7H_2O$, $CuSO_4$, $5H_2O$, etc., shows that to the SO_4 ion is attached one molecule of water and it is supposed [9] to form a stable hexagonal ring of the constitution given below

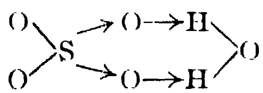

Finally, the author takes great pleasure in recording his grateful thanks to Dr. I. Ramakrishna Rao, under whose direction the present work is done.

REFERENCES

1 N. R. Rao, *Ind. J. Phys.*, **14**, 143 (1940).
2 Nisi, *Jap. J. Phys.*, **5**, 119 (1932).
3 Specchia. '*Atti Accad. Lincei*,' **13**, 754 (1931).
4 I. R. Rao, *Ind. Jour. Phys.*, **8**, 123 (1933).
5 Woodward and Horner, *Proc. Roy Soc.*, A, **44**, 129 (1934).
6 Bell and Jeppesen, *J. Chem. Phys.*, **2**, 711 (1934).
7 Bell and Fredrickson, *Phys. Rev*, **37**, 1562 (1931).
8 Medard, *Compt Rend.*, **197**, 582 (1933).
9 *The electronic theory of Valency* by N. V. Sidgwick, Chapter XI.

EFFECT OF TEMPERATURE ON THE RAMAN SPECTRUM OF GLYCERINE *

By A. L. SUNDARA RAO, M.Sc.
Andhra University, Waltair

(*Received for publication, July 6, 1940*)

ABSTRACT The Raman spectrum of Glycerine was photographed and it revealed 16 Raman lines. The frequencies of the lines are 419, 479, 549, 674, 820, 850, 919, 977, 1054, 1112, 1247, 1300, 1370, 1468, (?), 1463, 2889, 2949. A general assignment of frequencies as due to the C-C, C-O, C-H and δ(C-H) oscillations has been made. The effect of temperature on the Raman spectrum of Glycerine has been investigated. The line 674 becomes more diffuse at higher temperatures and increases in frequency by 20 cm^{-1} at 100°C. The 820 component accompanying the 850 line disappears at the higher temperature. These changes which are similar to those with solution in water are explained as due to depolymerisation of Glycerine complexes.

In the course of a general investigation of the Raman spectra of polybasic alcohols, glycerine was taken for examination. Among the various workers who have studied the Raman spectrum of this substance, mention must be made of Bar [1] and more recently Saxena[2]. The latter has studied the effect of dilution with water at two different concentrations and has observed that the 674 cm^{-1} line becomes more diffuse at higher dilutions and the intensity maximum is shifted by 15 cm^{-1}.

EXPERIMENTAL

In the present investigation the author has repeated the work of Saxena (*loc. cit.*) at the dilutions of 75% and 25% and verified his conclusions. It was thought desirable to see the effect of temperature on the Raman spectrum of glycerine with a view to understanding the cause of the changes with dilution and so the present work was undertaken.

The Wood's tube containing glycerine was placed inside a cylindrical electrical heater 5cm in diameter and 28cm long, open at either end. The heater was provided with a window 2 × 14cm long for allowing the incident radiation. The light from a mercury arc was focussed by a 9″ glass condenser on to the tube containing glycerine. A solution of sodium nitrite was placed between the condenser and the scattering medium. This served to eliminate the 4046 line of the mercury arc and to reduce to a marked extent the continuum lying between 4358 and 4916.

A two prism spectrograph of high light gathering power was used and an exposure of 10 hours was found sufficient to photograph the entire Raman

* Communicated by the Indian Physical Society.

spectrum. A comparison spectrum of copper was given on the same plate using a Hartman's diaphram and the wavelengths determined by measuring on a Hilger comparator.

RESULTS

The results of the investigation are given in Table I, along with the frequencies reported by Bar and Saxena for purposes of comparison The assignment of frequencies to the respective valence bonds are given in Column IV of the Table.

Many of the new frequencies reported by Saxena could not be confirmed by the author, inspite of the clear spectra that were obtained. It is surprising that no trace of the OH band could be found by the author in the case of glycerine even after prolonged exposure for 50 hours.

Effect of Dilution and Temperature

The effect of hydrogen bond formation is to create polymers in a liquid and the greater the number of hydroxyl groups present in a molecule the larger is the size of the polymer formed and the greater the degree of association

On dilution, the association breaks down and as a result some frequencies might be expected to get weakened or modified. In acetic acid, Leitmann and Ukholin[3] and Koteswaram[4] have observed that the 620 line diminishes in intensity with dilution and Koteswaram further reports that the 872 line also disappears at higher temperatures.

In glycerine the lines 604, and the 820 component accompanying the 850 line show a similar behaviour. The 674 line gets weaker and diffuse on dilution and the frequency increases by 20 cm^{-1}. The increase of temperature from 30° to 100°C has a similar effect. The feeble line of Raman frequency 820 either disappears or becomes too feeble to be perceptible in the spectrum of glycerine taken at 100°C.

Koteswaram (*loc. cit.*) in his work with acetic acid pointed out that the Raman line at 1700 corresponding to the C=O oscillation increases in frequency with dilution and with increased temperature. He explained this as due to the depolymerisation of the acid When one molecule is associated with another, the valency bond between atoms in any group within the molecule or that between two groups in the molecule are likely to be weakened. Thus the Raman frequency corresponding to any oscillation in an associated molecule, particularly the oscillation of a bond nearest to the associated molecule or molecules, should be smaller in the associated state than in the depolymerised one. The 674 line in glycerine must be due to an external oscillation in its molecule. In the pure state and at lower temperatures, there is possibly association. In solutions in water and at higher temperatures, there is depolymerisation, on account of which this external bond between two groups (it is difficult to definitely assert to which pair of groups this oscillation corresponds) is

strengthened with a consequent increase in the corresponding Raman frequency. The increased diffuseness of this line with dilution or with increase of temperature indicates that there may be superposition of two lines—one corresponding to the associated molecules in the pure liquid at the lower temperature and the other due to the depolymerised molecules in solution or at higher temperatures.

The feeble 820 line may be due to the C-C oscillations of the associated molecules and therefore naturally disappears at higher temperatures or in solutions as these molecules giving rise to this line are depolymerised.

TABLE I

Raman Frequencies of Glycerine

Bar (1933)	Saxena (1939)	Author	Assignment and Remarks
	328(1)		
	370(½)		
427	419(3) br	419(3) br	
	434(½) s		
497	480(6) br.	479(5) br.	
553	540(1)	540(1)	
684	674(2)	671(2)	Becomes more diffuse at higher dil and at higher temperatures
822	817(3) s	820(3) s	Disappears at higher temperatures
850	847(6)	850(6)	C-C
	862(2) s		
919	919(5) br	919(5)	
977	975(2) s	977(2)	
1055	1048(8) br	1054(8) v br	C-O
	1085(2)		
1108	1112(5) s	1112(7) v br.	
	1104(1)		
1242	1246(2) v br	1247(3) br	
	1300(1) s	1300	A broad band extending over 100 cm⁻¹ containing three maxima
	1378(0)	1370	
		1408	
1471	1466(8) s	1463(10) s	δ(C-H)
2888	2880(12) br.	2889(12) br	Valence (C-H)
2947	2955(12) v br	2940(12) v br	

The author's grateful thanks are due to Dr. I. Ramakrishna Rao for his helpful guidance throughout the progress of this investigation

REFERENCES

1 Bar. *Zeits. f. Physik.*, **81**, 785, 1933.
2 Saxena. *Proc. Ind. Acad. Sci. Sec. A.*, **10**, 333, 1939
3 Leitmann and Ukholin. *J. Chem. Phys.*, **2**, 825, 1934.
4 Koteswaram. *Zeits. f. Physik*, **110**, 118, 1938

THE MOTION OF GASES IN THE SUN'S ATMOSPHERE

PART I. ON THE MECHANISM OF FORMATION OF SOLAR DARK MARKINGS

By A. K. DAS

(Received for publication, June 20, 1940)

ABSTRACT. In this paper the dynamics of a mas of gas ejected from the body of the sun has been studied and the equations of motion of a material particle in a system of rotating coordinates with origin on the surface of the sun have been derived for two cases (1) when the particle is ejected from the photospheric or any other level where the angular velocity of rotation is the same as that observed on the sun's surface and (2) when the particle is ejected from a level where the angular velocity is higher than the angular velocity at the surface. The set of equations for case (2) have been shown to be applicable to a mass of gas ejected from the interior of the sun, that is from levels below the photosphere. Since prominences are formed, according to the growing view held at present by many solar physicists, by the gases ejected from the sub-photospheric levels, these equations should explain at least the broad features of prominences and dark markings. It has been shown in this paper that many of the hitherto ill-explained or un-explained features of dark markings, in particular, can be quantitatively explained on the basis of the above equations. Indications have also been given how these equations should be equally useful in the understanding of several other solar phenomena not dealt with in this paper.

The phenomena revealed by spectroheliograms and photoheliograms are so varied that up till now it has not been possible to construct a unified theory which can account perfectly satisfactorily for all the peculiarities observed on the solar disc. Even the most striking feature of the monochromatic disc photographs, namely, the granulations does not seem to be thoroughly understood, although it is evident from the works of Deslandres, Unsold and others that these granulations which give rise to the "photospheric network" must be the result of convection. In the present state of our knowledge the only way to progress appears therefore to be to restrict one's attention to some of the most salient features and to try to evolve a simple hypothesis which can yield these observed properties through straightforward deduction. In this paper attention is confined to some features of the H_α dark markings and a mechanism is put forward to explain these hitherto ill-explained, and in some cases unexplained, features. The proposed mechanism appears to be quite general and helps the understanding of certain other solar phenomena* which are not very

* These will be considered in the later papers of this series.

easily understandable on the basis of existing solar theories. The following features of the dark markings are considered in the present paper :

(a) the predominantly linear appearance of the dark markings, which led Deslandres to call them "filaments" ;

(b) the tendency of the direction of the dark markings to change from a direction along a meridian in equatorial regions by steadily inclining more and more towards the east until in latitudes higher than about $35°$ the markings lie nearly along a parallel of latitude ;

(c) the tendency of high latitude dark markings to have their directions nearly parallel to the parallels of latitude even at their first appearance ;

(d) the predominantly westward tilt of the tops of dark markings of the low and middle latitudes, the average inclination of a dark marking to the vertical being of the order of $10°$;

(e) the tendency of dark markings to be short in length in the equatorial regions.

It is well established that dark markings are caused by the absorption of photospheric light by the masses of gas which exist as prominences over the solar disc. The appearance of any dark marking is therefore determined by the way in which the absorbing gas is distributed in the prominence concerned and consequently in order to understand the features of the dark markings enumerated in the foregoing paragraph we must form a correct picture of the mode of formation of a prominence. For this purpose an examination of disc photographs is not very helpful although in some cases the dark markings, particularly those of very high latitudes, indicate how the gases responsible for the absorption of photospheric light have emerged from the photosphere. But even a casual examination of limb photographs cannot fail to show that the mass of gas forming a prominence has been ejected from a limited area of the disc. It is therefore natural to assume that a stable prominence is usually formed by a jet of gas issuing from a very small disturbed area of the photosphere or even from below the photosphere. If this hypothesis regarding the mode of formation of a prominence be true, we should be able to understand a good deal of the peculiarities of prominences and consequently of dark markings by considering the dynamics of a jet of gas ejected from the body of the sun. A complete solution of this dynamical problem is highly complicated, but fortunately we can draw several useful conclusions from quite elementary considerations. The problem is strictly one of hydrodynamics, but simple considerations of particle dynamics appear to be sufficient for the purposes of preliminary investigation.

Our problem in its simplified form is the consideration of the motion of a particle ejected from the body of the sun which we regard as a rigid sphere

rotating about its polar axis. The equations of motion of a material particle of

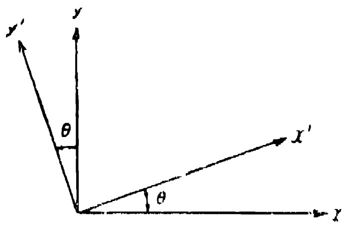

FIGURE 1

mass m in a system of stationary, rectangular coordinates x, y, z are

$$X = m.\frac{du}{dt} = m.\frac{d^2x}{dt^2},$$

$$Y = m.\frac{dv}{dt} = m.\frac{d^2y}{dt^2}, \qquad \ldots \quad (1)$$

$$Z = m.\frac{dw}{dt} = m.\frac{d^2z}{dt^2},$$

where X, Y, Z, are components of the force causing the motion of the particle and u, v, w, are the components of the velocity in the directions x, y, z, respectively. But the gases on the sun move with respect to a rotating system of coordinates, and therefore in order to approximate to solar conditions we have to consider the motion of our particle in a coordinate system x', y', z', rotating with a constant angular velocity ω equal to the angular velocity of the sun as observed on its surface. Let the origin of our rotating system coincide with that of the stationary system of coordinates and let the axis of rotation z' coincide with the z-axis of the stationary system. We note that the rotation of the sun is counterclockwise if we look towards the equator from the north pole of the sun ; ω is therefore positive.

Now if θ is the angle between the x-axis and the x'-axis then we have (see Fig. 1)

$$\left.\begin{array}{lll} \alpha_1 = \cos\theta, & \beta_1 = \sin\theta, & \gamma_1 = 0 \\ \alpha_2 = -\sin\theta, & \beta_2 = \cos\theta, & \gamma_2 = 0 \\ \alpha_3 = 0, & \beta_3 = 0, & \gamma_3 = 1 \end{array}\right\} \qquad \ldots \quad (2)$$

where α_1, β_1, γ_1, α_2, β_2, γ_2, α_3, β_3, γ_3 are the direction-cosines of the three rotating axes with respect to the stationary axes. We know that according to the general rules of transformation from a stationary system of coordinates x, y, z to a system of coordinates in relative motion x', y', z', the following relations must hold :

$$\left.\begin{array}{l} x' = \alpha_1(x - x_0) + \beta_1(y - y_0) + \gamma_1(z - z_0) \\ y' = \alpha_2(x - x_0) + \beta_2(y - y_0) + \gamma_2(z - z_0) \\ z' = \alpha_3(x - x_0) + \beta_3(y - y_0) + \gamma_3(z - z_0) \end{array}\right\} \qquad \ldots \quad (3)$$

and

$$\begin{aligned} X' &= \alpha_1 X + \beta_1 Y + \gamma_1 Z \\ Y' &= \alpha_2 X + \beta_2 Y + \gamma_2 Z \\ Z' &= \alpha_3 X + \beta_3 Y + \gamma_3 Z \end{aligned} \quad \cdots \quad (4)$$

where x_0, y_0, z_0 are the coordinates of the origin of the primed system and X, Y, Z and X′, Y′, Z′ are the components of the force in the two systems respectively. In the case under consideration $x_0 = o$, $y_0 = o$, $z_0 = o$; therefore we have from (2) and (3)

$$\left.\begin{aligned} x' &= x \cos\theta + y \sin\theta \\ y' &= -x \sin\theta + y \cos\theta \\ z' &= z. \end{aligned}\right\} \quad \cdot \quad (5)$$

Putting $\theta = \omega t$ and differentiating with respect to t we have from (5)

$$\left.\begin{aligned} u' &= u \cos\theta - x \sin\theta . \frac{d\theta}{dt} + v \sin\theta + y \cos\theta . \frac{d\theta}{dt} \\ &= u \cos\theta + v \sin\theta + (y \cos\theta - x \sin\theta) . \frac{d\theta}{dt} \\ v' &= -u \sin\theta - x \cos\theta . \frac{d\theta}{dt} + v \cos\theta - y \sin\theta . \frac{d\theta}{dt} \\ &= -u \sin\theta + v \cos\theta - (x \cos\theta + y \sin\theta) . \frac{d\theta}{dt} \\ w' &= w, \end{aligned}\right\} \quad (6)$$

whence by using (5) we get

$$\left.\begin{aligned} u' &= u \cos\theta + v \sin\theta + \omega y' \\ v' &= -u \sin\theta + v \cos\theta - \omega x' \\ w' &= w. \end{aligned}\right\} \quad (7)$$

Differentiating (7) with respect to t we have

$$\begin{aligned} \frac{du'}{dt} &= \frac{du}{dt} . \cos\theta - u \sin\theta . \frac{d\theta}{dt} + \frac{dv}{dt} . \sin\theta + v \cos\theta . \frac{d\theta}{dt} + \omega v' \\ &= \frac{du}{dt} \cos\theta + \frac{dv}{dt} . \sin\theta + \omega(v' - u \sin\theta + v \cos\theta) \\ \frac{dv'}{dt} &= -\frac{du}{dt} . \sin\theta - u \cos\theta . \frac{d\theta}{dt} + \frac{dv}{dt} . \cos\theta - v \sin\theta . \frac{d\theta}{dt} - \omega u' \\ &= -\frac{du}{dt} \sin\theta + \frac{dv}{dt} \cos\theta - \omega(u' + u \cos\theta + v \sin\theta) \\ \frac{dw'}{dt} &= \frac{dw}{dt} , \end{aligned}$$

whence using (7) we have

$$
\begin{aligned}
\frac{du'}{dt} &= \frac{du}{dt}.\cos\theta + \frac{dv}{dt}.\sin\theta + 2\omega v' + \omega^2 x' \\
\frac{dv'}{dt} &= -\frac{du}{dt}.\sin\theta + \frac{dv}{dt}.\cos\theta - 2\omega u' + \omega^2 y' \qquad (8) \\
\frac{dw'}{dt} &= \frac{dw}{dt}
\end{aligned}
$$

Multiplying equations (8) by m we obtain by virtue of the relations (4) and (1) and by ignoring the primes since only primed quantities occur

$$
\left.
\begin{aligned}
m\frac{d^2x}{dt^2} &= X + 2m\omega v + m\omega^2 x \\
m\frac{d^2y}{dt^2} &= Y - 2m\omega u + m\omega^2 y \\
m\frac{d^2z}{dt^2} &= Z\,.
\end{aligned}
\right\} \qquad (9)
$$

These are the equations of motion of a material particle in a rotating system of coordinates, but we notice that the equations (9) refer to the motion of a particle on a rotating sphere the centre of which coincides with the origin of the system of coordinates. In order to make the equations comparable with observation we have to transform them to a rotating system of coordinates whose origin is at some point on the surface of the rotating sphere.

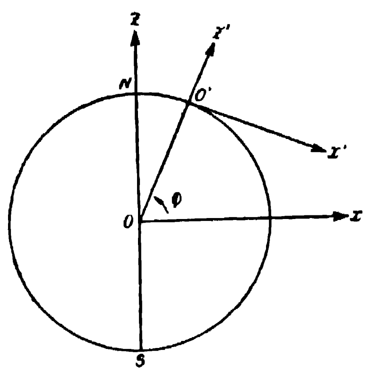

FIGURE 2

Let o' be a point on the surface of the sphere which we choose as the origin of our system of rotating co-ordinates. For simplicity let o' be on the $x-z$ plane which is the plane of Fig. 2, and let the z'-axis point radially outwards, the y'-axis parallel to the y-axis, *i.e.*, towards the back of the paper, so that the x'-axis lies in the plane of the paper. Now, since the z-axis coincides with the axis of

rotation, the x-axis represents the equator. Then in the co-ordinate system with origin at o' the positive z'-axis points vertically upwards, the positive y'-axis is towards the west * and the positive x'-axis points towards the south. Also the angle ϕ between the equator and the radius oo' represents the heliographic latitude, positive for the northern and negative for the southern hemisphere of the sun. The coordinates of o' in the previous system are

$$x_0 = R\cos\phi, \quad y_0 = o, \quad z_0 = R\sin\phi,$$

where R is the radius of the rotating sphere (sun). Also the direction cosines of the primed axes (*i.e.*, of the system with origin at o') with respect to the unprimed axes (*i.e.*, of the system with origin at o) are

$$\begin{array}{lll} \alpha_1 = \sin\phi, & \beta_1 = o, & \gamma_1 = -\cos\phi, \\ \alpha_2 = o, & \beta_2 = 1, & \gamma_2 = o, \\ \alpha_3 = \cos\phi, & \beta_3 = o, & \gamma_3 = \sin\phi. \end{array}$$

Now, since the new system is rigidly fixed to the former system of co-ordinates, *i.e.*, x_0, y_0, z_0 and the nine direction cosines are independent of the time t, the following relation must hold

$$\frac{du'}{dt} = \alpha_1 \frac{du}{dt} + \beta_1 \frac{dv}{dt} + \gamma_1 \frac{dw}{dt}.$$

Therefore we have

$$\frac{du'}{dt} = \frac{du}{dt}\sin\phi - \frac{dw}{dt}\cos\phi,$$

$$\frac{dv'}{dt} = \frac{dv}{dt}$$

$$\frac{dw'}{dt} = \frac{du}{dt}\cos\phi + \frac{dw}{dt}\sin\phi.$$

Multiplying these equations by m and using the values of $\frac{du}{dt}$, $\frac{dv}{dt}$, $\frac{dw}{dt}$ from the equations(9) and by expressing all unprimed quantities in terms of the primed quantities with the help of the general relations

$$x - x_0 = \alpha_1 x' + \alpha_2 y' + \alpha_3 z'$$
$$y - y_0 = \beta_1 x' + \beta_2 y' + \beta_3 z'$$
$$z - z_0 = \gamma_1 x' + \gamma_2 y' + \gamma_3 z'$$

* Our coordinate system is right-handed and when we say east or west we always refer to geographical east and west. But when we say 'southward' we refer to the south pole of the sun, that is to say, in northern hemisphere 'southward' means a direction along a meridian from the north pole to the equator of the sun.

$$
\begin{aligned}
u &= \alpha_1 u' + \alpha_2 v' + \alpha_3 w' \\
X &= \alpha_1 X' + \alpha_2 Y' + \alpha_3 Z' \\
Y &= \beta_1 X' + \beta_2 Y' + \beta_3 Z' \\
Z &= \gamma_1 X' + \gamma_2 Y' + \gamma_3 Z'
\end{aligned}
$$

which must hold between the two systems of coordinates we have

$$
\begin{aligned}
x &= R\cos\phi + x'\sin\phi + z'\cos\phi \\
y &= y' \\
u &= u'\sin\phi + w'\cos\phi \\
v &= v' \\
X &= X'\sin\phi + Z'\cos\phi \\
Y &= Y' \\
Z &= -X'\cos\phi + Z'\sin\phi\ .
\end{aligned}
$$

Now since only primed quantities occur in the equations, we can drop the primes altogether and write in the following most general form the equations of motion of a material particle moving with respect to a system of coordinates with origin on the surface of the sun and rotating with the sun :

$$
\left.
\begin{aligned}
&\text{Equatorwards} \\
&m\frac{d^2x}{dt^2} = X + 2m\omega v\sin\phi + m\omega^2\sin\phi(R\cos\phi + x\sin\phi + z\cos\phi) \\
&\text{Westwards} \\
&m\frac{d^2y}{dt^2} = Y - 2m\omega(u\sin\phi + w\cos\phi) + m\omega^2 y, \\
&\text{Upwards} \\
&m\frac{d^2z}{dt^2} = Z + 2m\omega v\cos\phi + m\omega^2\cos\phi(R\cos\phi + x\sin\phi + z\cos\phi).
\end{aligned}
\right\} \quad \ldots \quad (10)
$$

If we restrict ourselves to small regions of the sun's surface as we shall when considering dark markings and prominences, the terms containing x, y and z can be neglected in comparison with those containing R and the equations (10) can be simplified as follows :

$$
\left.
\begin{aligned}
&\text{Equatorwards} \\
&m\frac{d^2x}{dt^2} = X + 2m\omega v\sin\phi + m\omega^2 R\sin\phi\cos\phi \\
&\text{Westwards} \\
&m\frac{d^2y}{dt^2} = Y - 2m\omega(u\sin\phi + w\cos\phi) \\
&\text{Upwards} \\
&m\frac{d^2z}{dt^2} = Z + 2m\omega v\cos\phi + m\omega^2 R\cos^2\phi
\end{aligned}
\right\} \quad \ldots \quad (11)
$$

These equations show that in addition to the forces X, Y, and Z which are responsible for the initial motion of the particle there appear other forces which modify the motion. These additional forces are clearly apparent or subjective forces, for they become zero if the particle is at rest or if the angular velocity of the sun's rotation becomes nil. The first of the equations (11) shows that the particle has a southward acceleration $2\omega v \sin\phi$ proportional to its westward component of velocity and to the angular velocity of rotation of the sun. This means that if the particle tries to move from east to west it is affected by an apparent force which deflects its path towards some point south of west. The southward acceleration also contains a term $\omega^2 R \sin\phi\cos\phi$ which for a given latitude ϕ depends only on the angular velocity of rotation of the sun and therefore acts upon the particle even when it is not impelled to move by the force X. This term is clearly the equatorward component of the centrifugal force due to the sun's rotation and it must exist so long as we can regard the sun as a sphere without any flattening at the poles like the earth. It may be noted that all measurements of the solar disc have failed to reveal any departure from the perfectly circular shape. We shall not consider the possible reasons for this perfect symmetry of the sun's shape, but accept it as an observed fact. An uncompensated equatorward force $\omega^2 R \sin\phi\cos\phi$ must therefore act on a particle on the sun. If the particle is embedded in the dense layers of the sun's atmosphere the effect of this force may be observable only as a very slow equatorward drift of the particle. The slow equatorward movement of sunspots and of the prominences of the sunspot belt may be due to the effect of this force. If the particle happens to be in the thinner regions of the solar atmosphere, for example in the coronal atmosphere, this force may be expected to produce a considerable equatorward velocity of the particle.

The second of equations (11) shows that the westward acceleration $\frac{d^2y}{dt^2}$ contains two terms $-2\omega u \sin\phi$ and $-2\omega w \cos\phi$. The first term means that the particle has an eastward acceleration due to a deflective force proportional to the angular velocity of the sun's rotation and to the southward component of its velocity. Hence if the particle tries to move along a meridian from higher to lower latitudes, its path is deflected *towards the east* and therefore makes an angle with the meridian. The second term indicates that the particle is acted upon by a deflective force proportional to the vertical component of its velocity and to the angular velocity of the sun's rotation or, in other words, if the particle tries to move vertically upwards its path is deflected *towards the east* and therefore makes an angle with the vertical. From the third of equations (11) we see that the particle is acted upon by a deflective force $2\omega v \cos\phi$ which deflects its horizontal east-west trajectory upwards or away from the surface of the sun. The vertical

acceleration $\frac{d^2z}{dt^2}$ also contains a term $\omega^2R\ \cos^2\phi$, which is clearly the vertical component of the centrifugal force due to the sun's rotation. This term must be responsible for causing a variation in the actual gravity on the sun from the equator to the poles. But this term will play no part in the considerations set forth in this paper, since we shall assume according to the usual practice that in prominences gravity is compensated by radiation pressure under normal conditions. The above equation of motion also shows that a particle moving from west to east is forced downwards by an apparent deflective force $-2\omega v\ \cos\ \phi$ and conversely an east-to-west trajectory is deflected upwards by an apparent force $2\omega v\ \cos\ \phi$. This may be responsible for the curving back of the tops of some prominences to the surface of the sun and for the occurrence of spiral motion observed in some cases. The force $2\omega\omega\ \cos\ \phi$ clearly sets a limit to the length of a marking. We can now examine the effect of the equations of motion (11) on a mass of gas ejected from some layer of the solar envelope or from the photosphere. The process responsible for the ejection of the gas does not matter for the purposes of the present paper, but we may perhaps regard it as a sudden and temporary increase of radiation in a limited region of the layer concerned. Since under normal circumstances the effect of gravity is compensated by radiation pressure this sudden increase in radiation will lead to the ejection of a mass of gas in the form of a jet. The velocity with which the jet will travel outwards will obviously depend upon the actual increase in radiation and upon the friction between the rising mass of gas and the surrounding atmosphere. It seems reasonable to expect that this increase of radiation has an average value and therefore the rising mass of gas will emerge into the coronal atmosphere with a sort of normal velocity determined by the viscosity of the solar material which it has traversed during the travel. Now, experimental measurements of the angular velocity of the sun's rotation at the photosphere and in different levels of envelope have shown very little variation of angular velocity with elevation, so that we may take ω to have a practically constant value over the whole region from the photosphere to the corona. Therefore a mass of gas emerging from any part of this region will have the same initial angular velocity ω as the sun's surface and therefore its motion will be determined by the equations (11). Accordingly it will be deflected from the vertical towards the east and its equatorward motion under the action of the propelling force $\omega^2R\ \sin\ \phi.\cos\ \phi$ will follow a trajectory inclined to the meridian towards the east. This conclusion is, however, directly opposed to observational data according to which the top of a dark marking is inclined towards the west with respect to the vertical and also the inclination of a dark marking to the meridians is such that its equatorial end lies to the west of the polar end. Now, Perepelkin[1] has concluded that the quiescent prominences form in the low layers of the sun. It seems to us very likely that the eruption which supplies the material for the

formation of a prominence has its seat in the interior of the sun below the photosphere. We therefore assume that the mass of gas which gives rise to an ordinary dark marking originates in the interior of the sun where the angular velocity is very high and that on reaching the coronal region it still has an angular velocity ω' much higher than the angular velocity ω of the sun's surface. When a mass of gas emerges from the interior with the angular velocity ω' it will have, relatively to the sun's surface, an angular velocity $\omega'-\omega$ in the same direction in which the sun's surface, is observed to rotate. The dynamical situation will therefore be equivalent to the motion of a particle with respect to a system of coordinates rotating with an angular velocity $-(\omega'-\omega)$. The appropriate dynamical equations are obtained directly from (11) by making the necessary substitution and we have

Equatorwards

$$m\frac{d^2x}{dt^2}=X-2m(\omega'-\omega)v\sin\phi+m(\omega'-\omega)^2R\sin\phi\cdot\cos\phi, \quad (a)$$

Westwards

$$m\frac{d^2y}{dt^2}=Y+2m(\omega'-\omega)(u\sin\phi+w\cos\phi), \quad (b) \qquad \ldots \quad (12)$$

Upwards

$$m\frac{d^2y}{dt^2}=Z-2m(\omega'-\omega)v\cos\phi+m(\omega'-\omega)R\cos^2\phi. \quad (c)$$

From these equations it is evident that the deflection of the uprising jet of gas from the vertical and from the meridians is in agreement with observational data so far as the direction of inclination is concerned. We now proceed to examine how far the inclination derived from equations (12) agree quantitatively with observed values.

The jet of gas may be expected to travel through the coronal atmosphere with a steady velocity horizontally and perhaps also in the upward direction; in fact, if the jet is to make a definite angle with the vertical and with the meridians, it must move with a steady velocity. We note that the constancy of speed implies that all the forces acting on the moving mass of gas mutually

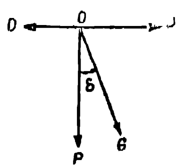

FIGURE 3

balance each other. Let G be the force (per unit mass) which is responsible for the equatorward motion of the gas acting in the direction OG (see Fig. 3) and let OP represent the direction in which the jet actually travels so that $\widehat{GOP}$ is

the angle we want to determine. We assume that the curvature of the trajectory is negligible, that is, the jet moves practically in a straight line. Now the deflective force $2(\omega'-\omega).u \sin\phi$, u being the equatorward velocity, must act at right angles to the direction OP, that is, in the direction OD. We resolve the force G into two components in the directions OP and OB. Then in the steady state the component along OB must be balanced by the deflective force along OD and the component along OP must be balanced by the force of frictional resistance which, as usual, is given by $P=f.v$, where v is the velocity of the moving body and f is the coefficient of friction. Accordingly we have the following relation on putting $v=u$

$$G.\sin\delta=2(\omega'-\omega)\,u\sin\phi \qquad [\textit{vide } \text{eqn. } (12)\,(b).]$$
$$G.\cos\delta=f.u,$$

whence we obtain

$$\tan\delta=\frac{2(\omega'-\omega)\sin\phi}{f}. \qquad \ldots \quad (13)$$

In order to evaluate δ numerically from (13) we must know the numerical value of the frictional constant. We can estimate the magnitude of the frictional constant in the following way. We assume the moving mass of gas to be a sphere of radius r and its velocity u. Then, according to the well-known law of Stokes the gas sphere will experience a total resistance $\overline{P}=6\pi\eta_k r u$, where η_k is the coefficient of viscosity of coronal matter, while moving through the coronal atmosphere. Therefore

$$f=6\pi\eta_k r/\tfrac{4}{3}\pi r^3\rho_p=\frac{9\eta_k}{2r^2\rho_p}. \qquad \ldots \quad (14)$$

Now η_k can be estimated with the help of Jeans's theory,[3] according to which the viscosity of stellar matter is given by $\eta=\frac{4}{15}.\frac{aT^4}{k\rho c}$, where $k=\frac{c\rho}{\mu T^{3\cdot5}}\left(1+\frac{h\nu}{RT}\right)$ as given by Kramers's theory of electron capture. The temperature of coronal matter (in the region where prominences appear) may be taken to be about 10^{-4} times the central temperature of the sun. The density of coronal matter (ρ_k) may be taken as about 10^{-3} times the density of prominence matter ρ_p. Now a prominence, which is composed almost entirely of atomic hydrogen with a very slight admixture of metals and rare gases, contains about 10^{13} atoms of hydrogen per cubic centimetre; therefore, $\rho_p=1\cdot7\times10^{-11}$ gm./cm.^{3}, taking the mass of a hydrogen atom to be $1\cdot7\times10^{-24}$ gm. Hence we have $\rho_k=1\cdot7\times10^{-14}$ gm./cm.^{3} which is about 3×10^{-16} times the central density of the sun. Using these values of temperature and density in Jeans's formula we obtain $\eta_k=10$ times the viscosity at the centre of the sun. The same formula gives $\eta=12\cdot2$ at the centre of the sun. Therefore, $\eta_k=122$. Substituting this value of η_k in (14) we have

$$f=\frac{9\times122}{2\times10^{18}\times1\cdot7\times10^{-11}}$$
$$=3\cdot2\times10^{-5}, \qquad \ldots \quad (15)$$

putting $r=10^9$ cm. The reason for putting $r=10^9$ cm. is that the radius of the mass of gas ejected should be approximately the same as that of an average area of the sun's surface affected by an eruption and that the latter quantity appears to be of the order of 10^9 cm. In order to evaluate δ numerically we must know the numerical value of ω' which is the only unknown left in equation (13), ω being known from observation. In a well-known paper Jeans[3] has shown that the flow of radiation outwards from the interior of a star behaves like a convection current of matter and in fact the viscosity arising from the flow of radiation is more important than material viscosity. It therefore follows that there must be a steady decrease in the angular velocity of rotation from the centre of a star to its surface, but there will be a tendency for the interior of the star to attain a uniform angular velocity of rotation ω^* which must satisfy the relation† $\varpi^2\omega^{2*}=$const. As most of the mass of a star is contained in a sphere of radius barely $\frac{1}{3}$ the radius of the star the average velocity of rotation should be about 10 times the velocity of rotation observed on the surface. In the case of the sun[4] the average period of rotation should therefore be from 2 to 3 days. It is to be noted however that the relation $\varpi^2\omega^*=$const. requires that ω^* should increase from the equator to the poles which is contrary to what is observed on the surface of the sun. Nevertheless this contradiction between theory and observation does not mean that the interior of the sun does not rotate in the way required by theory. The decrease of angular velocity from the equator to the poles, the so-called polar retardation, observed on the surface of the sun may be due to the superposition of a subsidiary mechanism. In fact such a mechanism has been indicated by Eddington.[5] According to Eddington the sun does not satisfy *v.* Zeipel's theorem. A departure from *v.* Zeipel's theorem causes the temperature to rise at the equator and fall at the pole or conversely, so that a pressure gradient is established along the meridians and circulatory currents are initiated in the meridian planes. These primary meridional currents must, however, be deflected to the east or west and tend to become parallel to the parallels of latitude with increasing latitude. These circulatory currents are, according to Eddington, responsible for the polar retardation of rotational velocity as observed on the surface of the sun. It seems likely that these currents would be confined to the upper levels and would not extend much below the photosphere. The interior of the sun will rotate according to the law $\overline{\varpi}^2\omega^*=$const. We assume that the gas, which ultimately forms into prominences and dark markings, originates in some level below the level of the circulatory currents. At this level we shall have

$$\varpi^2\omega^*=\varpi_0^{\,2}\omega_0^*$$

or,

$$R^{*2}\cos^2\phi.\omega^*=R^{*2}\omega_0^*$$

† ϖ is the distance from the axis of rotation.

or, $$\omega^* = \omega_0^* \sec^2 \phi \qquad 16)$$

where ω^* is the angular velocity at latitude ϕ, ω_0^* is the angular velocity at the equator and R^* is the radius of the sun at the level concerned. Now, ω' is sure to be smaller than ω^*. Let us put $\omega' = \frac{1}{n} . \omega^*$, where n is a number greater than 1. Then, using this relation and substituting (16) in equation (13), we have

$$\tan \delta = \frac{2}{f} \left(\frac{1}{n} \omega_0^* \sec^2 \phi - \omega \right) \sin \phi$$

or $$\tan \delta = \frac{2}{f} \left(\frac{1}{n} \omega_0^* \tan \phi . \sec \phi - \omega \sin \phi \right). \qquad \ldots \quad (17)$$

Since the average angular velocity of the interior of the sun is about 10 times the angular velocity of rotation observed on the surface of the sun we may put on the average $\frac{1}{n} \omega_0^* = 10\ \omega_0$. Then using the value of f from (15) and the values of ω at different latitudes from d' Azambuja's empirical formula we can evaluate δ for different latitudes from equation (17). The results of these computations are set forth in column 4 of the following table.

TABLE

Latitude (ϕ)	$\omega \times 10^5$ sidereal	δ (observed)	δ (theoretical)
0°	0.292		0°
		4°	
5°	0,291		8°
		11°	
10°	0.291		16.°3
		17°	
15°	0.290		24°·7
		28°	
20°	0.288		32°·7
		44°	
25°	0.286		40°·7
		45°	
30°	0.283		48°
		58°	
35°	0.281		55°·3
		61°	
40°	0·278		61°·8
		73°	
45°	0·276		67°·5
		70°	
50°	0·273		72°·8
		67°	
55°	0·270		77°·2
		73°	
60°	0·267		80°

For comparison with observation the values of δ derived by Royds and Salaruddin [6] from the measurement of dark markings as recorded in the Meudon charts for a complete 11-year cycle from 1923 to 1933 are given in column 3. Column 2 of the table gives the values of $\omega \times 10^5$ for different latitudes as computed from d'Azambuja's formula. It is clear from the table that the theoretically calculated values of the inclination of dark markings to the meridians agree exceedingly well with those derived from observation. This close agreement between theory and observation shows up very strikingly in

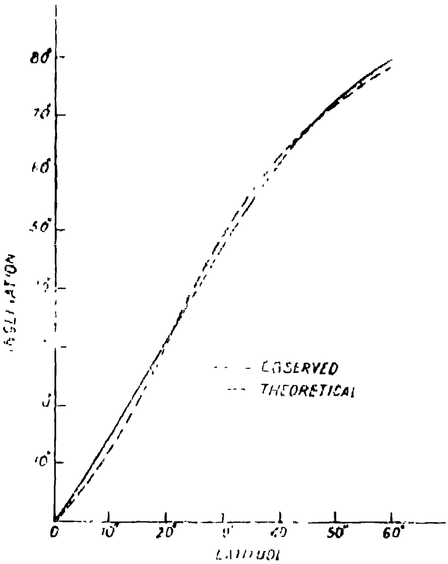

FIGURE 4

Fig. 4. It is evident therefore that the mechanism considered in this paper is perfectly capable of explaining qualitatively as well as quantitatively the westward inclination of dark markings to the meridians and its variation with latitude, which are two of the most striking features of dark markings and which have so far received no satisfactory explanation. Another puzzling feature, namely that a suddenly appearing dark marking has, almost at its first appearance, its direction inclined to the meridian at an angle appropriate to the latitude of its occurrence, is an obvious consequence of the present theory.

We have already seen that, according to the mechanism here considered, the height of a prominence or dark marking should be inclined to the west of the vertical which is in qualitative agreement with the observation of Mlle Roumens [7] of the Meudon observatory. Mlle Roumens obtained an average tilt of 10°W which is the average value derived from measurements of 171 dark markings in low and middle latitudes. Apparently she finds various inclinations, but she mentions that the inclinations show a peak at 7° and another more pronounced one at 22°, that is to say, the value of the inclination to the vertical is more

often 22° than 7°. For comparison with these observations we can calculate the angle δ which the height of a dark marking should make with the vertical in the same way as for the meridional inclination. δ will again be given by the formula (13) in which $\sin\psi$ has now to be replaced by $\cos\psi$ [*vide* eq. (12) (*d*)]. The value of δ thus calculated comes out to be of the order of 50° to 60° which is much larger than the observed value. The reason for this discrepancy is probably that the assumption of steady motion which lies at the basis of the theoretical derivation is not justified in the case of the upward motion. This is perhaps also what is to be expected. The frequent occurrence of streamers in prominences is probably to be looked upon as a result of the unsteadiness of the upward motion. Arguments, both theoretical and experimental, in favour of this conclusion have been given by H. Zanstra in a very recent paper.[8] If the outward radial motion is unstable, there can be no steady inclination between the height of a dark marking and the vertical; but there will still be a rough average inclination for a given time during which the upward motion has existed. Let a jet of gas emerge out of the chromosphere at the equator with a velocity 2V and rise to the height of a typical prominence, namely about 50000 km. At that height its upward velocity is nil, so that the average upward velocity of the jet during the ascent is V. Then from the second of the equation (12) we have

$$\frac{d^2y}{dt^2}=2(\omega_0'-\omega_0).V=18\,\omega_0 V.$$

Integrating this equation we get

$$y=9\omega_0 V t^2. \qquad \ldots \quad (18)$$

Now, according to Pettit the most frequent radial velocities measured in quiescent prominences range from 5 km./sec. to 10 km./sec. and velocities higher than 15 km./sec. are infrequent. We may therefore take 5 km./sec. to be the average valocity with which the jet of gas responsible for the formation of a dark marking travels through the coronal atmosphere. Then $t=50000/5$ secs. $=10^4$ secs. Using these values of V and t and the value of ω_0 from the table above we get from (18) the westward displacement of the top of an average dark marking :

$$y=13150 \text{ km}.$$

Then the inclination to the vertical is given by

$$\tan\delta=\frac{13150}{50000}=0{\cdot}263$$

or

$$\delta=14^\circ{\cdot}75.$$

This rough estimate of the average inclination of a dark marking or prominence is in quite satisfactory agreement with the value derived by Mlle Roumens from observation.

It may be noted in this connection that the mechanism here considered also gives an indication of the magnitude of the breadth of a dark marking. If the whole of the jet above the chromosphere is effective in absorbing photospheric radiation then obviously the breadth of the dark marking should roughly be the westward displacement of the top from the vertical *plus* the diameter of the jet. At the equator the westward displacement for a typical prominence is of the order of 13000 km., so that the breadth of the corresponding dark marking should be of the order of 33000 km. taking the radius of the jet to be about 10^9 cm. or 10000 km. The ratio of height to breadth at the equator will therefore be approximately 1·5 : 1. But this ratio cannot be the same at all latitudes, since the westward inclination to the vertical increases from the equator towards the higher latitudes. In fact, the westward displacement at any latitude ϕ is given by

$$(\omega_0' \sec \phi - \omega \cos \phi)\, Vt^2.$$

Consequently the breadth of a dark marking should increase as we proceed from the equator towards the higher latitudes so that the ratio of the height to breadth would decrease with increasing latitude. But beyond a certain latitude where the length of a dark marking is practically parallel to the parallels of latitude the breadth will be about the same as the diameter of the jet, since the westward tilt of the dark marking and the length of the dark marking will practically lie in a vertical plane normal to the meridians. At high latitudes therefore, the breadth of a typical dark marking would be of the order of 20000 km., which is in fair agreement with observation, and the ratio of the height to breadth would be of the order of 2·5 : 1. Now the equatorward force $(\omega' - \omega)^2$ R $\sin \phi \cos \phi$ is zero at the equator and increases with the latitude; consequently the length (by which we mean the extension across the parallels of latitude) of the marking will be equal to the diameter of the jet or about 20000 km., so that its breadth (by which we mean its extension across the meridians) will be greater than its length. This means that at the equator the marking will appear to be parallel to the equator, and slightly above the equator the marking will tend to be as long as it is broad. From a consideration of the variation of the force $2(\omega' - \omega)v \cos \phi$ [*vide* eq.(12)(*c*)] along with the variation of the force $(\omega' - \omega)^2$ R $\sin \phi \cos \phi$, it follows also that the length of a dark marking should increase as we proceed from the equator towards higher latitudes. In general, at least at the middle and high latitudes, the length of a dark marking can be expected to be much greater than its breadth, thus accounting for the predominantly linear appearance of dark markings. It is difficult to estimate the order of magnitude to be expected for the ratio of the length to breadth of a dark marking formed by a single jet, but it seems likely that even at high latitudes it will not exceed 5 : 1 or 6 : 1. The extraordinarily long markings of high latitudes appear however to be produced by a numbar of jets arranged along a parallel of latitude ; in such cases the ratio of the length to breadth

would be several times more. It is a curious fact that the several jets should arrange themselves along a parallel of latitude at high latitudes the reason for which is not clear; but it seems possible that jets have a tendency to form along the paths of the internal circulating currents which of course must be parallel to the parallels of latitude at high latitudes and become more and more parallel to the meridians as we approach the equator practically in the same way as the directions of dark markings do. This may be the reason why several jets form along the length of a long dark marking; if that be so, the occasional formation of extraordinarily long markings becomes understandable.

In conclusion, I wish to emphasise that the object of the present investigation has been rather to evolve a self-consistent hypothesis capable of accounting for some of the major peculiarities of solar dark markings than to develop a complete theory. My thanks are due to Dr. C. W. B Normand, C.I.E., Director-General of Observatories in India, a discussion with whom about the peculiarities of dark markings led me to undertake this investigation.

ADDENDUM

This paper was written in June, 1939; but its publication has so far been postponed as certain points arising out of the mechanism suggested herein needed consideration. In the mean time Mr. P. R. Chidambara Iyer of this observatory has rightly pointed out to me in a discussion in a different connection that he has held for a long time that a dark marking having an inclination to the meridians attains its minimum area only when its direction is radial to the disc and not when it is at the central meridian. This certainly throws doubt on the validity of Mlle Roumens' conclusion that prominences have a predominantly westward tilt to the vertical. This doubt has been clearly raised by Waldmeier in a very recent paper (*Astro. Mitteilungen, Zürich*, 1939) which has just come to my notice. According to Waldmeier the fact that a dark marking has a minimum area at an eastern longitude and not at the central meridian is a necessary consequence of the inclination of the dark marking to the meridians. Against this one may point out that Mr. M. Salaruddin has found (*K. O. B.*, Vol. IV, No. 96, p. 297) that dark markings without any inclination to the meridians show a preponderance of western areas over eastern areas. This dissymmetry points to the existence of a west tilt. It seems probable that the observed dissymmetry in the case of the markings inclined to the meridians is due jointly to the causes envisaged by Roumens and by Waldmeier. This point is under examination. Should the existence of the west tilt be definitely established, it would find a plausible theoretical cause in the mechanism proposed in the present paper.

SOLAR PHYSICS OBSERVATORY,
KODAIKANAL.
December, 1939.

REFERENCES

[1] Perepelkin, *Poulkovo Observatory Circular*, No. 1, 1932.
[2] Eddington, *Der Innere Aufbau der Sterne*, Berlin 1928, p. 348.
[3] Jeans *M.N.R.A.S.*, Vol. 86, pp 328 44 (1926).
[4] Eddington, *Der Innere Aufbau der Sterne*, Berlin, 1928, p. 349
[5] Eddington, *Observatory*, Vol 48, p 73, March, 1925.
[6] Kodai, *Obs. Bull.*, No. 111, 1937, pp. 407-11.
[7] Mlle Roumens *C.R.*, Tome 201, p 127 (1935).
[8] Zanstra, *M.N.R.A.S.* Vol. 99, 1939, pp. 499-524.

A NOTE ON THE ENERGY AND WAVELENGTH MAXIMA IN FERMI-DIRAC AND BOSE-EINSTEIN DISTRIBUTIONS*

BY A. G. CHOWDHURI
University of Delhi

AND

B. N. SINGH

(*Received for publication, July 4, 1940*)

During recent years there have been a number of physical and astrophysical applications of quantum statistics. In the present note we shall consider the properties of the Fermi-Dirac and Bose-Einstein distribution laws which correspond to the Wien's displacement law in the case of black-body radiation. It is useful sometimes to know the value of the energy corresponding to the maximum in the energy-distribution curve of the particles in the assembly or the value of the de Broglie wavelength corresponding to the maximum in the distribution with respect to the wavelength associated with the particles. These are given in the present paper for the various cases of degeneracy and non-degeneracy.

The number of photons of black-body radiation lying within the energy range ϵ to $\epsilon+d\epsilon$ at temperature T is given by Planck's law

$$n(\epsilon)d\epsilon=\frac{8\pi\nu^2}{c^3}\cdot\frac{1}{e^{h\nu/kT}-1}\,d\nu$$

$$=\frac{8\pi}{c^3h^3}\cdot\frac{\epsilon^2}{e^{\epsilon/kT}-1}\,d\epsilon,$$

so that

$$E(\epsilon)d\epsilon=\frac{8\pi\epsilon^3}{c^3h^3(e^{\epsilon/kT}-1)}\,d\epsilon,$$

where $E(\epsilon)d\epsilon$ is the energy per unit volume of the photons lying in the energy range ϵ to $\epsilon+d\epsilon$.

$E(\epsilon)$ is maximum for $\epsilon=\epsilon_m$, where ϵ_m is given by

$$\frac{dE(\epsilon)}{d\epsilon}=0,$$

which gives

$$1=e^{\epsilon_m k/T}\left(1-\frac{\epsilon_m}{3kT}\right)$$

* Communicated by the Indian Physical Society.

or $$\frac{\epsilon_m}{kT} = 2{\cdot}822.$$

If we consider the photon distribution from the standpoint of wavelength instead of energy, we have for the energy of photons in the wavelength interval λ to $\lambda + d\lambda$

$$E(\lambda)d\lambda = \frac{8\pi ch}{\lambda^5(e^{ch/\lambda kT} - 1)} d\lambda$$

and $E(\lambda)$ is maximum for $\lambda = \lambda_m$, where λ_m is given by

$$\frac{dE(\lambda)}{d\lambda} = 0,$$

which gives $$e^{-ch/\lambda_m kT} = 1 - \frac{1}{5}\frac{ch}{\lambda_m kT}$$

or $$\frac{\lambda_m kT}{ch} = \frac{1}{4{\cdot}965}.$$

We shall now discuss the case of Fermi-Dirac statistics. The energy-distribution law in the completely non-relativistic case $\left(\frac{mc^2}{kT} >> 1\right)$ is

$$E(\epsilon)d\epsilon = \frac{2\pi g(2m)^{\frac{3}{2}}}{h^3} \cdot \frac{\epsilon^{\frac{3}{2}}}{\frac{1}{A}e^{\epsilon/kT} + 1} d\epsilon,$$

where $E(\epsilon)d\epsilon$ is the energy per unit volume of the particles lying in the energy range ϵ to $\epsilon + d\epsilon$.

Differentiating the above with respect to ϵ and equating to zero we get for ϵ_m, the value of ϵ corresponding to the maximum of the distribution curve,

$$e^{\epsilon_m/kT}\left(\frac{2}{3}\frac{\epsilon_m}{kT} - 1\right) = A \qquad \ldots \quad (1)$$

or $$e^x\left(\frac{2x}{3} - 1\right) = A \qquad \text{where } x = \frac{\epsilon_m}{kT}.$$

However, if we consider the energy distribution in terms of wavelength, we have

$$E(\lambda)d\lambda = \frac{2\pi g h^2}{m\lambda^6} \frac{1}{\frac{1}{A}e^{h^2/2mkT\lambda^2} + 1} d\lambda.$$

Putting $$\frac{dE(\lambda)}{d\lambda} = 0$$

we obtain $$e^{\frac{1}{y^2}}\left(\frac{1}{3y^2} - 1\right) = A \qquad \ldots \quad (2)$$

where $$y^2 = \frac{2\lambda_m^2 mkT}{h^2}.$$

The Fermi-Dirac distribution law for the relativistic case $\left(\frac{mc^2}{kT} << 1\right)$ is

$$E(\epsilon)d\epsilon = \frac{4\pi g}{c^3 h^3} \frac{\epsilon^3}{\frac{1}{A} e^{\epsilon/kT} + 1} d\epsilon$$

and this will have a maximum at $\epsilon = \epsilon_m$, where ϵ_m is given by

$$e^x \left(\frac{x}{3} - 1\right) = A, \qquad \dots \quad (3)$$

x being equal to ϵ_m / kT.

As before, if we consider it from the wavelength standpoint, we get

$$E(\lambda)d\lambda = \frac{4\pi ghc}{\lambda^5} \frac{1}{\frac{1}{A} e^{hc/\lambda kT} + 1} d\lambda$$

which will have a maximum at $\lambda = \lambda_m$ where λ_m is given by

$$\frac{dE(\lambda)}{d\lambda} = 0$$

i.e., $$e^{\frac{1}{z}} \left(\frac{1}{5z} - 1\right) = A \qquad \dots \quad (4)$$

where $$z = \frac{\lambda_m kT}{hc}.$$

The equations (1), (2), (3) and (4) have been solved graphically and positions of the maxima due to the variation in A are shown in figures 1 and 2.

In figure (1) are shown curves for the non-degenerate case ($0 < A < 1$) and the details are as follows—

curve (*a*) shows $y = \frac{\lambda_m \sqrt{2mkT}}{h}$ against A for non-relativistic case,

curve (*b*) shows $z = \frac{\lambda_m kT}{hc}$ against A for relativistic case,

curve (*c*) shows $x = \epsilon_m / kT$ against A for non-relativistic case,

curve (*d*) shows $x = \epsilon_m / kT$ against A for relativistic case

In figure (2) are shown curves for the degenerate case ($1 < A < \infty$).

curve (*a*) shows $y = \frac{\lambda_m \sqrt{2mkT}}{h}$ against A for the non-relativistic case,

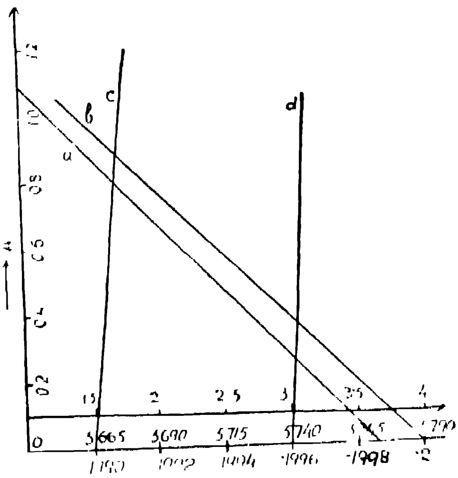

FIGURE 1

The uppermost scale x refers to curves c and d.
The middle scale y refers to curve a.
The lowermost scale z refers to curve b.

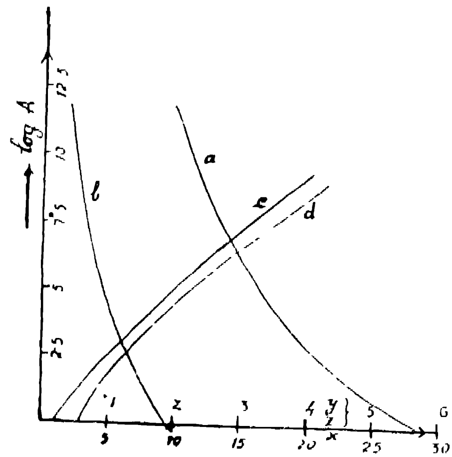

FIGURE 2

The upper scale for y, z refers to curves a and b.
The lower scale for x refers to curves c and d.

curve (b) shows $z = \dfrac{\lambda_m kT}{hc}$ against A for the relativistic case,

curve (c) shows $x = \epsilon_m / kT$ against A for the non-relativistic case,
curve (d) shows $x = \epsilon_m / kT$ against A for the relativistic case.

The ordinate in figure 1 represents A and that in figure (2) log A. The abscissa represents x, y or z as the case may be.

Table 1 shows the limits of the values of x, y and z as A varies from 0 to 1 in the non-degenerate case and from 1 to ∞ in the degenerate case.

TABLE I

Non-relativistic case $\left(\dfrac{mc^2}{kT} >> 1\right)$

	Range of ϵ_m / kT	Range of $\dfrac{\lambda_m \sqrt{2kT}}{h}$
Degenerate case, A varies from 1 to ∞	1·756 to ∞	0·5652 to 0
Non-degenerate case, A varies from 0 to 1	1·5 to 1·756	0·5774 to 0·5652

Relativistic case $\left(\frac{mc^2}{kT} << 1\right)$

	Range of ϵ_m/kT	Range of $\lambda_m kT/hc$
Degenerate case, A varies from 1 to ∞	3·13 to ∞	0·1994 to 0
Non-degenerate case, A varies from 0 to 1	3·0 to 3·13	0·2 to 0·1994

Thanks are due to Dr. D. S. Kothari for his interest in the work.

A PRECISION DIRECT-READING SPECTROPHOTOMETER*

By Dr. A. L. NARAYAN

AND

C. K. ANANTHASUBRAHMANYAM

(*Received for publication, July 10, 1940*)

Plate XIII

ABSTRACT. The experimental errors inherent in photographic photometry are discussed and a direct reading spectrophotometer for the visible especially adapted to the study of line contour and absorption and fluorescence spectra is described. Because of the higher resolution of which it is capable the method permits a more precise and complete analysis of absorption and fluorescence spectra by revealing the fine structure too small to be detected by the usual methods. A test of the instrument was carried out by determining the intensities of the lines 4078 and 4047 from Hg arc and the energy distribution in the $H\beta$ of the solar spectrum. The system is distinguished by high sensitivity and easy adjustment and it dispenses with the labour involved in photographic photometry.

Nearly all attempts to measure intensities of spectral lines depend first on obtaining a photograph of the spectrum and then interpreting the varying densities in the plate in terms of intensities. The method involves very careful calibration of the photographic plates. Photography as an intermediate step introduces several undersirable complications and intricacies. The experimental errors inherent in the photographic method are rather difficult to estimate and are at best only approximate. It is difficult in a given case to say just what part of the error can be attributed to the different sources of error and what part to the particular method in question. Further it would be difficult to apply this method in some cases where the intensity range is large.

Within the last few years much attention is given to the problem of measuring intensity distribution in spectral lines directly and attempts have been made by several investigators in this direction. The advantages of this method are obvious because many troublesome problems whose solutions lead always to sensible errors are eliminated. If we are to gain an accurate knowledge of the physical conditions governing the process of absorption and emission, the necessity for such measures is clear. In collaboration with H. Grenat, d' Azambuja[1] at Meudon and Dunham[2] at the Mt. Wilson Observatory have undertaken research as early as 1934 for the purpose of directly measuring intensity

* Abstract of this paper was read before the Physics section of the Indian Science Congress at Madras in January, 1940.

distribution in spectral lines and determining the absorption line profiles in the solar spectrum. Dr. Dunham who was recently working on the same problem at the University Observatory, Oxford, is reported to have succeeded in measuring the profiles of H α and D lines in the solar spectrum using a null photoelectric method. Dr. Brück[3] working at the Solar Physics Observatory, Cambridge, developed a recording photoelectric microphotometer operating directly in the solar spectrum. All these observers have used the same general method namely the photometric measurement of high dispersion solar spectrograms by the use of a photoelectric cell and a thermionic amplifier, specially designed valves being employed for the purpose. The very feeble current generated as a result of the light falling upon the photocell is amplified about a million times.

With most standard vacuum tubes the emission of the oxide coated cathode is unstable and the grids are not sufficiently insulated. Further, fluctuations in the plate current prevent us from reaching the highest sensitivity. Tubes have been designed in recent years the grid filament resistance of which is very high. They require an anode voltage of only 8 to 10 volts. The mounting of the electrodes also is such as to ensure low surface leakage. The low filment and low anode voltage for which the valves are designed, have a distinct practical advantage, it being a simple matter to maintain steady filament and anode currents. The outstanding examples of these tubes are G. E. Pliotron F P 54 developed by Metcalfe and Thomson[4] and the electrometer Triode[5] manufactured by the G. E. C. London. All these tubes have amplification factors less than one and depend for their usefulness on the very high input resistance. The use of one of these low grid current vacuum tubes is undoubtedly an excellent method for measuring light intensities directly.

In attempting to develop a method for the purpose of recording profiles of Fraunhofer lines without recourse to photography, on account of the excessive cost of and the difficulty of getting in war time the specially designed valves, it seemed to us particularly important, the possibility of using an ordinary valve in the amplification circuit to obtain the desired sensitivity. It has been noted by various authors[6] that the input resistance of an ordinary valve can be greatly increased by a special use of its grids together with greatly reduced voltages. Further, for good insulation the lead from the control grid must emerge through the top of the tube rather than through the base.

During the past 15 months we have carried out an extensive study of the amplification of photoelectric currents and their application to spectrophotometry. After a complete study of these problems, attention was directed to the design and construction of a precision photoelectric spectrophotometer suitable for the measurement of intensities of spectral lines directly. Attempts in this direction have been so successful that it seemed worth while to publish a description of the arrangement.

Since there is considerable variation in the characteristics of individual vacuum tubes, several standard tubes were tested to determine their behaviour under the operating conditions and 1 A 6 was finally selected as it was found most satisfactory. For the amplifier circuit while any of the conventional circuits could be employed, the Dubridge[7] circuit seemed most suitable by virtue of its simplicity of construction and operation. The diagram of the circuit is shown in fig. 1. 1 A 6 is a multielectrode valve having five grids in addition to plate and filament. The two grids Nos. 3 and 5 are connected together and used as a plate while Nos. 1 and 4 are used as space charge grid and control grid respeciively. Grid No. 2 and the plate are superfluous and are directly connected together to the earthed end of the battery. As a result of the high insulation resistance and the reduced voltages used, the input resistance rose to about 10^{13} ohms.

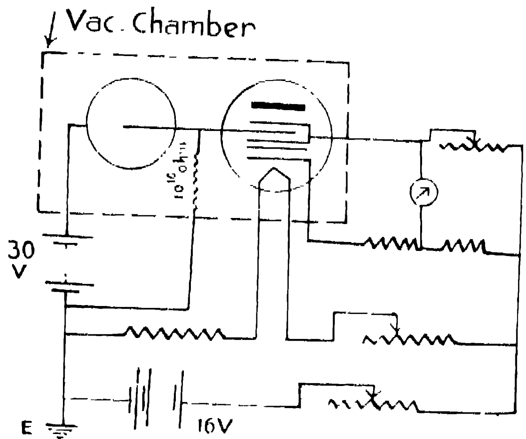

FIGURE 1

It has been shown by L. R. Hafstad[8] that improved stability can be obtained by mounting the photocell and the amplifier in an evacuated container. This precaution practically eliminates the surface leakage from the amplifier tube and the photocell as well as the tendency of the leads to pick up stray ions. The tube, grid leaks and the photocell are therefore enclosed in a heavy cast iron cylinder* which is evacuated and kept dry by a drying agent in a bottle in the pumping lead. It served as an electro-magnetic shield and permitted the photocell and the selective slit to be placed at any point in the spectrum. The vacuum cylinder is 6″ in diameter and 10″ in height and is closed by two end plates. All the parts are mounted on an ebonite base attached to the plate which closes the lower end and the wires necessary for the operation of the amplifier are brought out through sealed insulating bushings and connected by a shielded flexible cable to the control panel. In this way not only the highest insulation is maintained about the most essential points but also the grid leak resistance remains constant.

* This cylinder was kindly made for the authors by the Andhra Scientific Instrument Co.

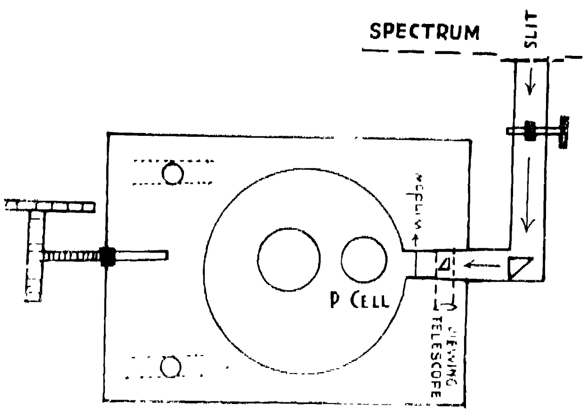

FIGURE 3

A photograph of the actual set up attached to the 20 foot Littrow spectrograph and a schematic drawing of the instrument are given in figs. 2 and 3. The cylinder is provided on one side with a window fitted to a short projecting tube. Over this is fitted the tube T with a slit S which admits the radiation from the selected line to the photocell. The tube carrying the slit has a rack and pinion motion enabling it to be placed in the focal plane of the spectrograph. It is found difficult to seal vacuum tight with sealing wax or to have rubber gaskets as they would perish with time. Instead the cylinder is ground well with the *two* end plates and vacuum grease is applied to the rims. When the pump begins to work the grease spreads itself and is found that the vacuum keeps over-night with very little leakage.

The most important part of the photometer is the arrangement by which the vacuum chamber with the attached slit is moved along the spectrum in a direction parallel to the dispersion. The cylinder is mounted on a heavy steel carriage to the underside of which are fixed hardened steel plates with '$\wedge$' faces resting on hard steel balls carried by sleeves fixed to an iron base. The base is fitted with levelling screws so that the centre of the photometer slit can be brought on to the middle of the spectrum. The carriage is fitted with a micrometer screw which gives a direct traverse of 5 cm. The screw is of pitch 1 mm and is provided with a divided head. The whole arrangement is placed on a heavy iron bracket fixed to one side of the stone pillar at the camera end of the spectrograph.

The resistance leaks employed in these measurements consisted of Xylol-alcohol mixtures* contained in soft glass tubes and Indian-ink lines drawn on strips of good drawing paper and enclosed in glass tubes. To avoid external leakages the outer surface is coated with ceresin wax and the resistances supported

* These were kindly made for the authors by Dr. S. Ramachandra Rao of the Annamalai University to whom their grateful thanks are due.

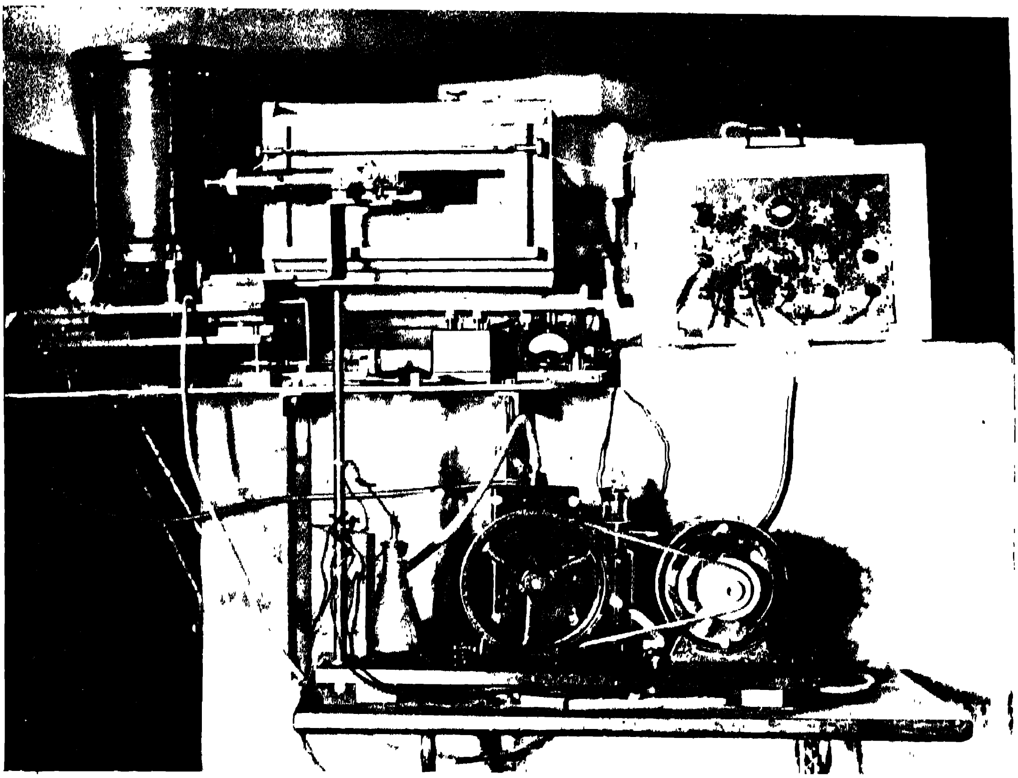

Figure 2

on connecting wires. When an attempt was made to increase the sensitivity of the instrument by placing high grid leak resistances of the order of 10^{12} ohms great difficulty was experienced. If rapid measurement are required the resistance cannot be increased above 10^{10} ohms.

Before making the observations it is necessary to adjust the photometer slit to exact parallelism with the spectral lines. This parallel alignment is checked as follows. In front of the window through which the light passes just before reaching the photocell, a small right-angle prism and a viewing lens may be inserted and the necessary adjustment is made by widening the photometer slit and turning it through the required angle. After the slit is thus adjusted, the prism and viewing lens are removed and the light path is cleared. The outline of the profile can now be easily obtained by shifting the selective slit in front of the spectrum by means of the micrometer screw.

The accuracy of the results obtained depends on how strictly the proportionality holds between the photoelectric current and the intensity of the light incident on the photocell. Before undertaking any intensity measurements it was necessary to investigate the extent to which this relation is satisfied. This was done in the following manner. Neutral perforated screens were used to diminish the intensity of light admitted into the spectrograph by known amounts. These screens each contained symmetrically placed holes of diameters 3·1, 2·5, 1·9, 1·5, 1·3, and 0·6 cm. These were in turn calibrated with a vacuum thermopile and galvanometer as this combination responds linearly to light of different intensities. The proportionality was further assured by using light of low intensity and by causing the amplification system to operate upon the straight portion of the grid bias plate current curve. It has been found that with these precautions, there exists a strictly linear relation between the incident light and the galvanometer deflection.

In order to test the performance of the instrument, some preliminary measurements were carried out with a home-made Hg arc. The observations were made with the horizontal Littrow prism spectrograph of 21 ft. focal length with optical parts of glass. Since stray radiation due to reflection and scattering by optical parts is a troublesome source of error in this type of work, special precautions were taken to reduce it to a minimum. All the inner parts of the spectrograph were painted dull black and several diaphragms were mounted inside so that there is almost no chance for any radiation to be reflected into the spectrum from the inner walls of the spectrograph. A double monochromator which allows only a small region of wavelengths to enter into the spectrograph and removes all unwanted light, was used to improve the purity of the spectrum. In a single monochromator the stray light caused by reflection and scattering in the various parts of the instrument is inevitable. Light from the Hg arc was sharply focussed on the slit of the monochromator and a series of readings were

taken for various widths of the slit for different voltages. The results obtained are given in Table I.

TABLE I

Volatage applied	Slit width	Galvanometer deflection	
		λ 4077·8	λ 4046·6
65	0·08 mm.	19	21
	0·16	32	40
75	0·08	20	23
	0·16	35	43
95	0·08	23	24
	0·16	38	44

We have recently used the instrument for measuring the energy distribution in the $H\beta$ of the solar spectrum. By means of the micrometer screw the selective slit was placed in succession at different points on the line and the galvanometer deflection observed in each case. The results are given in Table II. When the line is thus scanned and allowance is made for the systematic and accidental errors, by plotting deflections against distances the observed profile was obtained. The equivalent width found by measuring the area of the profile is 2·1 Å and the central intensity 18 per cent, which compares very well with Unsold's[9] values.

TABLE II

$H\beta$ line λ 4861·34

Distance from center in mm.	4·5	3·5	3·0	2·5	2·0	1·5	1·0	0	0·5	1·0	1·5	2·0	2·5
Deflection	35	34	33	32	30	28	23·5	7	12	20	25	28	31

Distance from center in mm.	3·0	3·5	4·0
Deflection	34	34	36

It must be understood that these observations are of a preliminary nature and were made solely as a test of the method. The test while not sufficiently rigorous showed that the circuit functions satisfactorily when the grid leak used in below 10^{10} ohms. As compared with the method of photographic spectrophotometry the enormous gain in time obtained with the present instrument is obvious. It possesses apart from high speed, great sensitivity and easy adjustment. And

the device is rapidly adaptable for photographic recording. These as well as other minor advantages should make the device a valuable aid in direct measurement of light intensities. In the case of 1 A 6 it is not practicable to use higher than 10^{10} ohms as the resistance of the input circuit approaches the unshunted resistance of the tube. Further work is in progress. A number of improvements which became evident in the course of the present study are being introduced and 1 A 6 is being replaced by an electrometer type valve which is just received, so as to increase the over-all sensitivity of the instrument. The method will be subjected to a severe test and the relative merits of the null and deflection methods together with the observations of line profiles will be discussed in a later paper.

We have great pleasure in expressing our thanks to Mr. J. M. Sil, B.Sc (Eng.) of the Indian Meteorological Department for technical advice and assistance in making the mechanical parts and to Mr. N. S. Subba Rao, M.A., of the Annamalai University for much valuable advice in building the amplifier circuit.

SOLAR PHYSICS OBSERVATORY,
KODAIKANAL.

REFERENCES

[1] *Tr. I. A. U.*, **5**, 71 (1935).

[2] *Phy. Rev.*, **44**, 329 (1933); *M.N.*, **100**, 282 (1940).

[3] *M.N.*, **99**, 608 (1939).

[4] *Phy. Rev.*, **36**, 1489 (1930).

[5] *G. E. C. Journal*, **6**, 4 (1935)

[6] G. H. Gabas & M. L. Pool, *R.S.I.*, **8**, 196 (1937); H. Tatel & others, *R.S.I.*, **9**, 229 (1938).

[7] *R.S.I.*, **4**, 532 (1933).

[8] *Am. Phy. Soc.*, April (1932).

[9] *Zeit. f. Astrophys*, **2**, 199 (1931)

EVAPORATION FROM EARTHEN JUGS

By HAZARI LAL GUPTA, ABINASH CHANDRA JAIN

AND

NARENDRA NATH KHANNA*
University of Delhi

(Received for publication, July 25, 1940)

ABSTRACT. The thermodynamical theory of the wet-bulb thermometer is extended to evaporation from earthen jugs, and some of the theoretical deductions are verified by experiment It is found that the time during which a given quantity of air becomes saturated at the temperature of the jug by coming in contact with it is independent of the temperature of the jug.

When water is kept in an earthen pot, due to the cooling produced by evaporation and the poor thermal conductivity of the clay, its temperature reaches to within half a degree of the temperature of the wet-bulb thermometer. The wet-bulb temperature represents the lowest attainable by cooling due to free evaporation in the atmosphere.

The cooling of water in an earthen jug is very similar to the cooling of the wet-bulb thermometer and in fact the thermodynamical theory[1] of the latter can be applied to the former. This is done in the present paper and the experimental results are found to be in accord with the theory.

Let us consider water contained in a porous pot or earthen jug, heated electrically by passing a current I in a coil of resistance R and let T denote the temperature (in degree Kelvin) that is attained in the steady state. T' and T'' denote the absolute temperature of the dry- and wet-bulb thermometers respectively, and x', x'', and x the humidity mixing ratios for the normal air, the air saturated at the wet-bulb temperature T'' and the air saturated at the temperature T of the pot respectively. The normal air contains x' grams of water vapour per gram of dry air, and suppose it takes time τ_0 seconds for $(1+x')$ grams of normal air to come in contact with the jug and become saturated at its temperature, *i.e.*, the amount of water vapour associated per gram of dry air increases from

* Communicated by the Indian Physical Society.

x' to x. The amount of heat given out in the process by $(1+x')$ grams of air is $(c_p + x'c'_p)$ $(T'-T)$, where c_p is the specific heat at constant pressure for air and c'_p, for water vapour, and the heat produced in the coil is $RI^2\tau_0/4\cdot2$. If L denote the latent heat of evaporation, the heat required for the evaporation of $(x-x')$ grams of water is $L\,(x-x')$, and we have

$$L(x-x') = (c_p + x'c'_p)\,(T'-T) + \frac{RI^2\tau_0}{4\cdot2} \qquad \ldots \quad (1)$$

As c_p/c'_p is about 2 and x' rarely exceeds 0·025, $x'c'_p$ may be neglected compared to c_p in the first factor on the right hand side of eq. (1). Again as a fairly good approximation we may substitute

$$x = \epsilon\frac{e}{p-e} \sim \frac{\epsilon e}{p}; \qquad \ldots \quad (2)$$

$$x' = \epsilon\frac{e'}{p-e'} \sim \frac{\epsilon e'}{p} \qquad \ldots \quad (2A)$$

where e' is the vapour pressure of normal air, e the saturated vapour pressure for temperature T, p the total pressure and ϵ the ratio of the densities of water vapour and dry air at the same temperature and pressure. We thus obtain

$$\frac{\epsilon L}{p}\,(e-e') = c_p(T'-T) + \frac{RI^2\tau_0}{4\cdot2}$$

or

$$\left(T + \frac{\epsilon L e}{p.c_p}\right) - \left\{\frac{e'L\epsilon}{p.c_p} + T'\right\} = \frac{RI^2\tau_0}{4\cdot2\ c_p}$$

$$\left\{T\frac{c_p.\,p.}{\epsilon L} + e\right\} - \left\{T'\frac{c_p.\,p.}{\epsilon L} + e'\right\} = \frac{pR\tau_0 I^2}{\epsilon L \times 4\cdot2}$$

Substituting $\frac{c_p.\,p.}{\epsilon L} = 0\cdot501$, we finally have

$$(0\cdot501\ T + e) - (0\cdot501\ T' + e') = \frac{pR\tau_0 I^2}{\epsilon L \times 4\cdot2}\,. \qquad \ldots \quad (3)^*$$

The time τ_0 that $(1+x')$ grams of normal air takes to be saturated by coming in contact with the jug will depend on the size of the pores and the surface area exposed for the evaporation of water. The surface exposed for evaporation (as explained below) remains constant during the experiment and it is then found that the relation between $\left\{T\frac{c_p.\,p}{\epsilon L} + e\right\}$ and I^2 is a linear one. This provides

* In the calculations p is taken to be 730 mm.

$c_p = \cdot23$
$\epsilon = \cdot62$
$L = 540$ calories.

us with a verification of the theory of evaporation, and also shows the constancy of τ_0 for a constant surface exposed for evaporation.

The experimental arrangement is illustrated in figure 1. p is a porous pot (of the type used for Leclanche cells of diamater 5·3 cms.) which in some of the experiments had about one half of its surface coated with sealing wax leaving only the portion SS of its surface free for the evaporation of water.

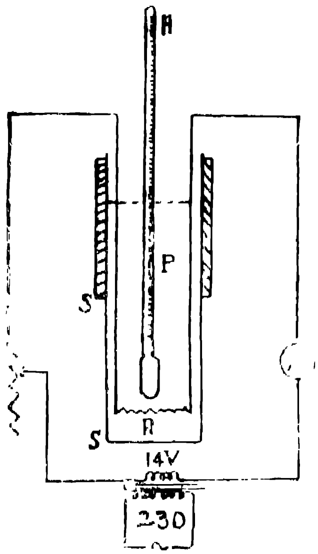

FIGURE 1

At the beginning of the experiment the pot is nearly full of water, but even at the end of the experiment the water level is above the exposed surface SS thus offering a constant surface for evaporation during the experiment. The resistance coil R is of 2·25 ohms. When a current I is passed through the coil,

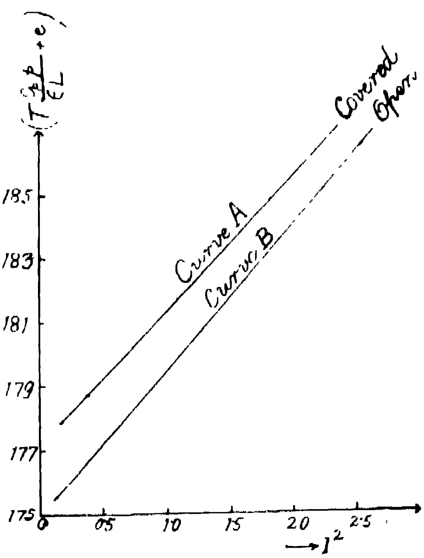

FIGURE 2

after a few minutes the temperature T of the water as indicated by the thermometer H becomes practically steady. Readings are taken for increasing values of I till the temperature T rises above the dry-bulb temperature.

A typical curve for $\left(T \frac{c_p . p}{\epsilon L} + e \right)$ plotted against I^2 is shown in figure 2 (curve A) which shows that the relation between them is linear, thus verifying the thermodynamical theory of evaporation and also the assumption regarding the constancy of τ_0. Experiments were also performed with the pot without the coating of sealing wax, and even here it is interesting to note that the relation observed between $\left(T - \frac{c_p . p}{\epsilon L} + e \right)$ and I^2 is a linear one (curve B, fig. 2). At the start of the experiment, the pot is almost full. At the end of the experiment it is still about two-thirds full. At first sight it would appear that for the uncoated pot the area exposed for evaporation will decrease as the water level sinks in the pot, but, due to capillary action, water creeps along the walls of the pot above the water level inside it, and thus the evaporation-area remains almost constant. However, at the end of the experiment, when the water level has fallen below the top of the pot by about one-third of its length, the points tend to fall below the straight line B. The value of τ_0 can be obtained from the slope of the straight line and we find in the case of figure 2 (curve B) $\tau_0 = 3{\cdot}4$ seconds. The value of τ_0 for a pot, or perhaps better still the value τ_0 for unit area of a porous pot, may be taken as a measure of the "evaporation efficiency" for a pot. It is hoped to undertake such a comparative study for different types of pots at a later date.

Thanks are due to Dr. D. S. Kothari for suggesting the problems and his interest in the work.

REFERENCE

[1] Brunt, Dynamical Meteorology. Hazari Lal and Abinash Chandra, *Ind. Jour. Phys.*, **13**, 395 (1939).

THE EFFECT OF AN ELECTRIC FIELD OF STRENGTH $-1/2aF^2$ ON THE POLARIZABILITY CONSTANT OF THE NORMAL HYDROGEN ATOM*

By WILLIAM H ROBINSON

(*Received for publication, August 30, 1940*)

ABSTRACT. Using the integral for the upper limit of the energy in its lowest state of a system as [1] $\int\phi^* H\phi d\tau$ and applying the variation method along the z axis gives the energy. With a field strength of $-1/2aF^2$, produces a negative polarizability constant for the normal hydrogen atom. The value obtained is $a = -.58047 \times 10^{-24}$ cm.[3] which is in close agreement with that obtained by the second-order perturbation theory.

The electric moment of the induced dipole (charge × distance) is aF, where 'a' is called the 'polarizability' of the atom or ion and F is the strength of the field. Using the integral for the upper limit of the energy in its lowest state of a system as

$$^1E = \int\phi^* H\phi d\tau \qquad \ldots \quad (1)$$

where H is the complete Hamiltonian operator and is expressed as follows

$$H = T(q, p) + V(q) \text{ and } P = \frac{h}{2\pi i}\,\frac{\partial}{\partial q}.$$

For the normal hydrogen atom $1s$, with $n=1$, $L=0$, $m=0$ is given by the wave function

$$\psi_{1s} = \frac{1}{\sqrt{\pi a_0^3}}\, e^{-r/a_0} \qquad \ldots \quad (2)$$

Using the variation method along the z-axis and multiplying eq. (2) by $(1+Az)$,

Letting $$\phi = (1+Az)\psi_{1s} = \frac{1}{\sqrt{\pi a_0^3}}\, e^{-r/a}\,(1+Az) \qquad \ldots \quad (3)$$

where $z = r\cos\theta$

The Hamiltonian operator will be in this case

$$H = -\frac{h}{8\pi^2}\sum \frac{1}{m_i}\,\nabla_i^2 + V \quad \text{and} \quad V = -\frac{e^2}{r} + e.F.z.$$

* Communicated by Prof. K. S. Krishnan, F.R.S.

Using H on equation 3 gives

$$H\phi = -\frac{h^2}{8\pi^2}\sum \frac{1}{m_i}\nabla_i^2\phi + V\phi$$

$$H\phi = -\frac{h^2}{8\pi^2}\left(\frac{1}{m_1}\nabla_1^2\phi + \frac{1}{m_2}\nabla_2^2\phi\right) + V\phi$$

$$H\phi = -\frac{h^2}{8\pi^2}\left(\frac{1}{\mu}\nabla^2\phi\right) \qquad \text{where } \mu = \frac{m_1 m_2}{m_1 + m_2}$$

$$= -\frac{h^2}{8\pi^2}\left[\frac{1}{r^2}\cdot\frac{\partial}{\partial r}\left(r^2\frac{\partial}{\partial r}\right) + \frac{1}{r^2\sin^2\theta}\cdot\frac{\partial^2}{\partial\theta^2}\right.$$

$$\left. + \frac{1}{r^2\sin\theta}\cdot\frac{\partial}{\partial\theta}\left(\sin\theta\frac{\partial}{\partial\theta}\right)\right] - \frac{e^2}{r} + eFr\cos\theta.$$

When we substitute $H\phi$ and ϕ in eq. (1) and evaluate over all space, eq. (1) reduces to

$$E = \int_0^{2\pi}\int_0^{\pi}\int_0^{\infty}\frac{e^{-2r/a_0}}{a_0^{3/2}}(1 + Ar\cos\theta)\left[-\frac{h^2}{8\pi^2\mu}\cdot\frac{1}{r^2}\left\{\frac{1}{a_0^2}\left(r^2 + Ar^3\cos\theta\right)\right.\right.$$

$$\left. - \frac{1}{r^2 a_0}(2r + 3r^2\cos\theta) + \frac{2rA\cos\theta}{r^2} - r^2\left(\frac{1}{a_0}\right)A\cos\theta\right\} - \frac{2Ar\sin\theta\cos\theta}{r^2\sin\theta}$$

$$\left. - \frac{e^2}{r}(1 + Ar\cos\theta) + eFr\cos\theta\,(1 + Ar\cos\theta)\right] r^2\sin\theta\, dr d\phi. \quad \cdots \quad (4)$$

With the following integrals and their values,

$$\int_0^{\pi}\sin\theta\, d\theta = 2,\quad \int_0^{\pi}\sin\theta\cos\theta\, d\theta = 0,\quad \int_0^{\pi}\sin\theta\cos^2\theta\, d\theta = 2/3 \text{ and}$$

$$\int_0^{\infty}\sin\theta\cos^3\theta\, d\theta = 0 \quad \text{substituted in eq. (4) gives}$$

$$E = \frac{2}{a_0^3}\int_0^{\infty} e^{-2r/a_0}\left[-\frac{h^2}{8\pi^2\mu}\left(\frac{2}{a_0^2} - \frac{4}{a_0 r}\right) - \frac{2e^2}{r} + 2/3\, eFr^2 A\right.$$

$$\left. - \frac{h^2}{8\pi^2\mu}\left(\frac{2/3A^2r^2}{a_0^2} - \frac{2A^2r^2}{a_0} - \frac{8A^2}{3} - \frac{2A^2 r}{3a_0}\right) - \frac{2e^2A^2r}{3} + \frac{2eFr^2}{3}\right] dr$$

which reduces to the following, when the integrals of this form

$$\int_0^{\infty} e^{-2r/a_0} r^n dr = \left(\frac{a_0}{2}\right)^{n+1} \lfloor n \quad \text{are evaluated for values of } n = 1,\ 2,\ 3 \text{ and } 4.$$

Their values are respectively $\frac{a_0^2}{4}$, $\frac{a_0^3}{4}$, $\frac{3a_0^4}{8}$, $\frac{3a_0^5}{4}$.

Therefore a reduced form of equation (4) is as follows,

$$E=\left[\frac{h^2}{8\pi^2\mu a_0^2}-\frac{e^2}{a_0}+2eFAa_0^2+\frac{h^2A^2}{8\pi^2\mu}-\frac{e^2A^2a_0^2}{2}\right]. \qquad \ldots \quad (5)$$

Since it is not convenient to normalize ϕ we can divide eq. (1) by

$$\int\phi^*\phi d\tau$$

and E will retain its validity.

Evaluating $\int\phi^*\phi d\tau$ and integrating over all space,

$$\int\phi^*\phi d\tau=\int_0^\pi\int_0^{2\pi}\int_0^\infty\frac{e^{-2r/a_0}}{\pi a_0^3}\;(1+rA\cos\theta)^2r^2\sin\theta d\theta d\phi dr$$

$$=2\int_0^\infty\frac{e^{-2r/a_0}}{a_0^3}\,r^2dr+\frac{2}{3}\int_0^\infty\frac{e^{-2r/a_0}}{a_0^3}\,A^2r^4dr$$

$$=(1+a_0^2A^2). \qquad \ldots \quad (6)$$

Dividing eq. (5) by eq. (6) and letting $h^2=4\pi^2a_0\mu e^2$, E has the form

$$E=\frac{1}{1+a_0^2A^2}\left(-\frac{e^2}{2a_0}+2eFa_0^2A\right). \qquad \ldots \quad (7)$$

Differentiating eq. (7) with respect to A and equating it to zero gives the equation

$$-2a_0^3FA^2+eA+2Fa_0=0. \qquad \ldots \quad (8)$$

Solving for A and omitting $16F^2a_0^4$, because it is small in comparison to the 'e' term, leaves

$$A=\frac{e}{2a_0^3F}.$$

Substituting this value of A in eq. (7) reduces it to the following

$$E=\frac{4a_0^4F^2}{4a_0^4F^2+e^2}\left(\frac{e^2}{2a_0}\right). \qquad \ldots \quad (9)$$

Since E is given equal to $-1/2aF^2$, equation (9) gives

$$a=-4a_0^3,$$

and then taking the radius of the orbit in the normal hydrogen atom, referred to the center of mass as[2] $a_0 = .5282 \times 10^{-8}$ cm., gives $a = -.58947 \times 10^{-24}$ cm.[3]

Therefore, such a field strength produces a negative 'a' which shows that the induced dipole is in the opposite direction to the field instead of in the same direction This value of 'a' obtained here is in close agreement with that obtained by the first- and second-order perturbation theory applied to the Stark effect of the hydrogen atom by Epstein,[3] Wentzel,[4] and Waller.[5]

PHYS. DEPT. NCC. N, 1 (1940),
NORTH CAROLINA COLLEGE,
DURHAM, N.C., U.S.A.

REFERENCES

1 C. Eckart, *Phys. Rev.*, **36**, 878 (1930)

2 R. T. Birge, *Rev. Mod. Phys*, **1**, 1 (1929) , *Phys Rev.*, **40**, 228 (1932).

3 P. S. Epstein, *Phys. Rev.*, **28**, 695 (1926).

4 G. Wentzel, *Z. f. Phys*, **38**, 518 (1926)

5 I. Waller, *Z. f. Phys.*, **38**, 635 (1926).

A NOTE ON A NEW METHOD FOR THE DETERMINATION OF 'J'*

By A. G. CHOWDRI

AND

D. S. KOTHARI
(University of Delhi)

(*Received for publication, July 6, 1940*)

ABSTRACT. The paper describes a modification of Laby and Hercus's method. The rotating magnetic field is here replaced by a non-rotating magnetic field. The angular velocity in Laby's method here corresponds to a factor RX/L, where R is the resistance, L the self-inductance and X is a length.

§1. The most accurate determination of the mechanical equivalent of heat that we have at present is due to Laby and Hercus.[1] In this method work is done electrically but measured mechanically. A metallic continuous-flow calorimeter is suspended by a torsion wire between the poles of a powerful electromagnet, the magnetic field being normal to the axis of suspension of the calorimeter. A rotating magnetic field is produced by rotating the electromagnet, and the calorimeter is prevented from following the motion of the electromagnet by applying a suitable mechanical couple C. If the rate of rotation of the electromagnet be n turns per second, then the work done per second is $2\pi nc$, and

$$2\pi nc = Jws(\theta_2 - \theta_1), \quad \ldots \quad (1)$$

where w is the rate of flow of water through the calorimeter, θ_2 the temperature of water at exit, θ_1 the temperature at entrance and s the mean specific heat of water for the temperature range θ_1 to θ_2.

The present experiment is a variation of Laby's method in that the rotating magnetic field in Laby's method is here replaced by a linear oscillatory field. The theory of the method is straightforward and is as follows :—

§2. Let us consider (figure 1) a metallic ring S suspended in the magnetic field of the electromagnet L which is supplied with an alternating current. Let M

* Communicated by the Indian Physical Society.

be the mutual inductance* between the ring and the magnet, L the self-inductance and R the resistance of the ring,

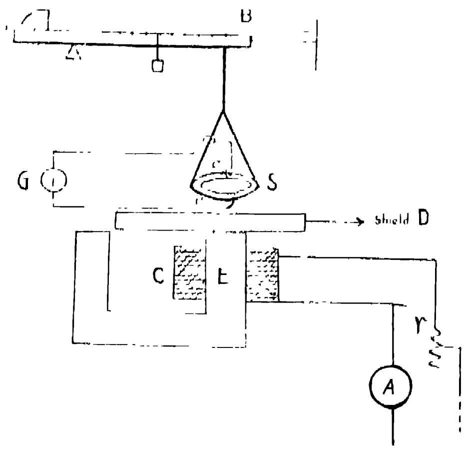

FIGURE 1

It represents the sketch of apparatus. The letters are explained in the text.

then we have $$i_1 Rt + jL\omega i_1 = -jM\omega i \quad \ldots \quad (2)$$

where i_1 is the current induced in the ring, i the current of frequency $2\pi\omega$ flowing in the electromagnet, and $j=\sqrt{-1}$. Solving equation (2) for i_1, we have

$$i_1 = \frac{-M\omega i_0 \sin(\omega t - \phi)}{\sqrt{(R^2 + L^2\omega^2)}}, \tag{3}$$

where $$i = i_0 \sin \omega t, \tag{4}$$

and $$\tan \phi = R/L\omega. \tag{5}$$

The rate of heat generation in the ring will, therefore, be

$$W = R\overline{i_1^2}, \tag{6}$$

where $\overline{i_1^2}$ is the average value of i_1^2.

Substituting (3) in (6) we obtain

$$W = \frac{RM^2\omega^2}{(R^2 + L^2\omega^2)} I^2, \tag{7}$$

where I is the r.m.s. value of the current in the electromagnet.

* Because of the iron core of the electromagnet, M will be a function of the current i in the magnet.

The force F experienced by the ring in the direction of x will be

$$F = -\frac{\partial}{\partial x}(Mii_1), \qquad \ldots \quad (8)$$

which with the help of (3) reduces to

$$F = \frac{\partial}{\partial x}\left[\frac{M^2\omega i_0^2 \sin(\omega t+\phi)}{\sqrt{(R^2+L^2\omega^2)}} \sin \omega t\right] \qquad \ldots \quad (9)$$

The average value of F is therefore

$$\bar{F} = \frac{I^2\omega \cos\phi}{\sqrt{(R^2+L^2\omega^2)}} \frac{\partial M^2}{\partial x}, \qquad \ldots \quad (10)$$

which on substituting for $\cos\phi$ from (5) gives

$$\bar{F} = \frac{L\omega^2 I^2}{R^2+L^2\omega^2} \frac{\partial M^2}{\partial x}. \qquad \ldots \quad (11)$$

Combining (7) and (11) we finally have

$$\frac{\partial W}{\partial x} = \bar{F}.R/L, \qquad \ldots \quad (12a)$$

and

$$W(x) = R/L \int_x^{\infty} \bar{F}\, dx. \qquad \ldots \quad (12b)^*$$

§3. The apparatus is shown in fig. 1 The copper ring S of about 6 cm. diameter and 50 gm. in weight is suspended from the beam of a Cenco Trip-scale Balance B. E is the electromagnet which is connected to the A. C. mains through the adjustable resistance r and the ammeter A in series. The electromagnet used in the experiment consisted of the open core of a Leybold's dismountable type transformer which was used with its coil C of 600 turns. The separation between the ring and the magnet was altered by moving the ring. The vertical force acting on the ring was measured at constant current in the magnet for different values of the distance (x) between the ring and the magnet.

* In comparing this equation with eq. (1) we find that the angular velocity ω in eq. (1) corresponds here to $\frac{dx}{L/R}$, L/R being of the dimension of time.

The heat generated in the ring raises its temperature, and when the steady state is attained the rate of heat-generation will be proportional to the excess of temperature of the ring over the surroundings, provided the excess is small, as was the case in the experiment. The temperature of the ring is measured by the copper-constantan thermo-couple c.c. The E.M.F. developed in the couple is measured by a mirror galvanometer G of voltage sensitivity of about 10^{-5} volts per scale division. The galvanometer deflection θ is proportioned to the excess of the temperature of the ring over the surroundings. The shield D in figure 1 was placed to prevent the heat generated in the electromagnet from affecting the ring.

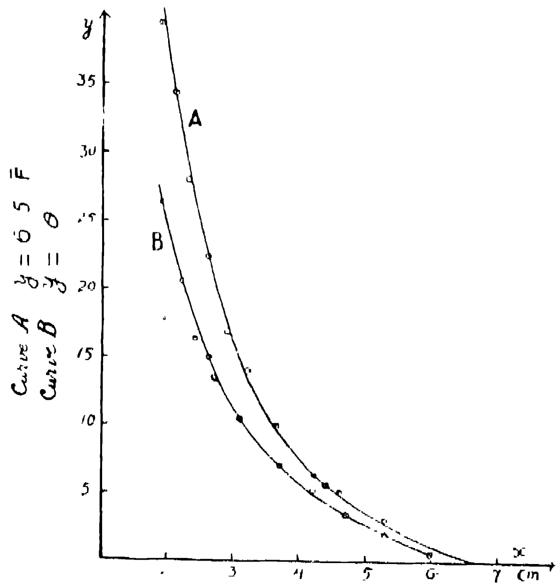

FIGURE 2

The curve A represents the relation between the force F and the distance x. The ordinate is 6.5 times the force in gram-weights.

The curve B shows the galvanometer deflection θ against the distance x.

In figure 2, some typical results are shown. The curve A represents the force F (in gram-weights) against the distance x. The curve B shows the galvanometer deflection θ against x. In both cases the current was $= 2{\cdot}9$ Amperes. The relation (12b) requires that $W(x)$ or the deflection $\theta(x)$ corresponding to it should be proportional to $\int_x^{\infty} \bar{\text{F}}\, dx$. In figure 3, $\theta(x)$ is represented against the

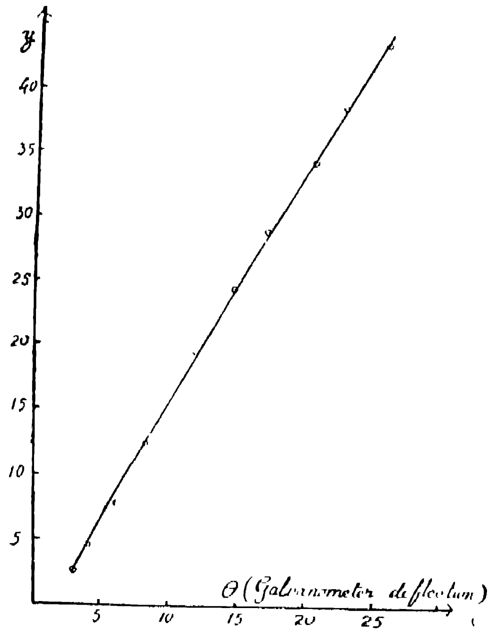

FIGURE 3

In this figure the ordinate represents the integral $\int_x^{\infty} \bar{F}\, dx$, and the abscissa the galvanometer diflection θ corresponding to distance x.

integral $\int_r^{\infty} F\, dx$. The observed points lie practically on a stright line as required by the theory of the experiment. The value of J can be calculated from figure 3 and equation (12), if we know the calibration curve of the thermocouple, the thermal capacity of the ring, its resistance and self-inductance. The approximate values for the various quantities are easily determined though their accurate determination is not an easy matter. However, these details will not be considered in this paper, but all the same, it is of some interest to note this variant of Laby and Hercus method.

PHYSICS DEPARTMENT,
UNIVERSITY OF DELHI.

REFERENCE

1 Laby and Hercus, *Phil. Trans.*, 227, 63 (1927). [See, Saha and Srivastava : A Treatise on Heat, pp. 101-111].

ASSOCIATION OF ACETIC ACID IN NON-AQUEOUS SOLVENTS*

By P. KOTESWARAM **

(Received for publication, July 2, 1940)

Plate XI

ABSTRACT. After a review of the work on acetic acid in water, the necessity for the study of this substance in non-aqueous solvents is stressed. Investigations were made with both polar and non polar liquids as solvents for this acid. The changes in Raman frequencies of this liquid in mixtures with chloroform, nitrobenzene, ethyl ether, acetone and methyl-ethyl ketone are described. No changes are perceptible in solutions with chloroform. This is explained on the basis of the absence of either a donor or an acceptor atom in this solvent, which is therefore supposed not to have any influence on the acid. The other four substances, on the other hand, bring about distinct shifts in the C=O frequency in particular. This is attributed to the presence of the donor atom O in these molecules, which is in a position to associate with the acceptor H in the acid molecules. Such an association can bring about the splitting of the associated molecules of the acid also, which therefore results in the change of the Raman frequencies of the acid. A new line with frequency 1760 cm^{-1} is ascribed to the free C=O bond in the acid which arises out of the disruption of the acid complexes into simpler molecules and which remains free in the new complex formed with the solvent, as there is no acceptor H in the molecules of these solvents to get associated with the O in it.

INTRODUCTION

In a previous publication,[1] the author studied the Raman spectrum of acetic acid at different concentrations in water and found that the principal C=O band of the acid with its intensity maximum at 1670 gradually shifted with dilution towards higher frequencies. At 25% concentration of the acid, it was found that the intensity maximum of the C=O band was about 1710. By a study of the effect of temperature on the acid, it was found that by increasing the temperature the intensity maximum again shifted in the same direction. It was pointed out that the appearance of the band at 100° C in the pure acid was similar to that at 95% concentration of the acid in water. These results were attributed to the breaking up of the initially associated molecules of the acid into lower polymers at higher temperatures and at higher dilutions. Similar results obtained with formic and benzoic acids in aqueous solutions were explained similarly.[2,3]

* Part of the thesis approved for the D.Sc. Degree of the Madras University. This work was done under the direction and guidance of Dr. I. Ramakrishna Rao, Andhra University, Waltair.

** Communicated by the Indian Physical Society.

While these changes were observed in aqueous solutions, the acid showed no change in solvents like benzene and carbon-tetra chloride. The two non-aqueous solvents chosen having been non-polar, the dissociating effect in aqueous solutions was attributed to the polar solvent, water.

A further elucidation of the phenomenon was necessary for a complete understanding of the phenomenon of association in acetic acid and hence the author studied the Raman spectrum of the acid in other non-aqueous polar solvents. The results obtained are detailed below.

EXPERIMENTAL

The usual experimental arrangements for obtaining Raman spectra of liquids described already in the author's previous communication[3] were used. The liquids under study were distilled in vacuum and rendered free from water to eliminate its effect. Transferring of solutions was done without disturbing the arrangement. Thus the slit of the spectrograph was kept at the same constant width throughout the investigations.

RESULTS

Polar liquids can be broadly classified as normal and abnormal. Among these, normal liquids are those, which, though polar, are not associated. Abnormal liquids are highly associated and show abnormal physico-chemical properties. The fatty acids, alcohols and water are prominent examples of abnormal liquids, while almost all other polar liquids are normal—acetone, ether, nitrobenzene, etc. But some of these normal liquids have got a strong tendency to associate with other molecules. A molecule having a 'donor' atom has got affinity for one having an 'acceptor' atom and forms a donor-acceptor link with it. An associated liquid has got both a donor and an acceptor and hence co-ordination or hydrogen bond formation (as the American school calls it) takes place and the molecules associate.

The effect of chloroform, nitrobenzene, diethyl-ether, acetone, and methyl-ethyl ketone on acetic acid was studied with a view to observe the changes in the polymerisation of the acid. Of these, nitrobenzene has the highest dipole-moment about 4×10^{-18} e.s.u. and the rest of the solvents have moments ranging from 1·55 for ether to 2·5 for acetone.

The following results were obtained : the first three solutions were 50 : 50 mixtures by volume.

1. *Solution in chloroform.*

There are no prominent changes in the Raman lines of acetic acid in chloroform.

In Nitrobenzene.

The C – C line of acetic acid at $\Delta\nu = 893$ is unchanged. The C = O line at 1670 rendered less diffuse and another line at about 1760 makes its appearance. Both these lines are not very clear on the plate due to the continuous spectrum which developed during the exposure.

3. *In Ether.*

The C – C line in the pure acid has a faint component at about 872, which is not visible with ordinary exposures. In the solution in ether, this line accompanying the 893-line increases in intensity such that it is clearly seen, comparable in intensity to the strongest 893-line. The C = O line at 1670 gets more diffuse than in the pure acid and two diffuse lines, with intensity maxima at 1685 and 1750 can be clearly seen.

4. *In Acetone.*

The most prominent changes are undergone by acetic acid in mixtures of acetone and of methyl-ethyl ketone with the acid. Three different concentrations, 75%, 50%, and 25% of the acid in the mixture have been studied.

Conspicuous changes are observed on the following lines :

C – C line.—As in the case of solution in ether, the low-frequency companion at 872 makes its appearance in a 75% solution, and as the concentration of the acid in the mixture decreases, the low-frequency component increases in intensity, till at 25% concentration, it is more intense than the 893-line itself. There is no line in acetone in that region and hence the effect can be attributed only to acetic acid molecules (Fig. 1) (Plate XI). In the microphotomeric curves given in fig. 1 the increase in intensity of the 872-line at higher concentrations is clearly seen.

C = O line.—In pure acetic acid, the C = O frequency is about 1670. In pure acetone it is about 1712. In the mixture the 1670-line maximum is seen proceeding towards higher frequencies with dilution till it gets blended with the acetone line. In addition, a line at 1760 which is quite sharp, makes its appearance. This line is present at all the three concentrations studied.

$\Delta\nu = 623$.

This line also seems to change in a manner similar to the C – C line at 893. In the pure acid, it has got a low-frequency component at 601, but the component is too feeble to be visible with ordinary exposures. But as the concentration of acetic acid in the mixture decreases, the intensity of its low-frequency component increases correspondingly.

5. *In Methyl-ethyl ketone.*

The effect in methyl-ethyl ketone is similar to that in acetone. As before, there is a clear splitting of the 893-line and an increase in the intensity of its low-

frequency component with increasing dilution of the acid in the solvent (Fig. 1). The line at 1670 shifts towards higher frequencies till it gets blended with the C=O line of the ketone at 1715 and the new line at 1760 also makes its appearance. The effect on the line 623 could not be studied due to the presence of another ketone line close to it.

Comparison of these results with those obtained by dilution in other Solvents.

For a proper understanding of the behaviour of acetic acid molecules in the different solvents studied, a comparison of the results obtained with other solvents also is necessary. We shall first take the C=O line at 1670 which is bound to be affected most by polymerisation or depolymerisation.

In non-polar solvents, benzene and carbon-tetrachloride, this line is unaffected. Among other solvents, chloroform does not seem to have any perceptible effect on it. Nitrobenzene splits it into two components, one at 1670 and another at 1760. The same is the case with ether but the 1670-line shifts slightly towards higher frequencies and both the lines are very diffuse unlike what they are in nitrobenzene solution. In ketones (acetone and methyl-ethyl ketone) as solvents, we again see the 1670-line shifting towards higher frequencies and the 1760-line appearing. The actual position of the shifted 1670-line and its spectral characteristics cannot be estimated on account of the superposition of the 1715-line of the ketone on it. While in all these polar solvents, a clear distinct line at 1760 is obtained, it is significant that in water alone, no such line at 1760 is found even at a dilution of 25%. In aqueous solutions, the 1760-line gets more and more diffuse and shifts gradually towards higher frequencies.[2] At no stage can two distinct lines, either sharp and separate as in nitrobenzene or diffuse and yet discreet as in ether, be obtained.

With regard to other lines, there is again a difference in their behaviour in water and in the other polar solvents. The 620- and 893-lines are unaffected in solutions in non-polar solvents and in chloroform In nitrobenzene there does not seem to be any conspicuous change. But in ether both of them double up with low-frequency components at 601 and 872 respectively. In acetone and methyl-ethyl ketone, the same is the case and we find that as the concentration of the acid in the solution diminishes, the low-frequency lines become more intense till at 25% acid in acetone, the 872-line outshines its companion. The reverse happens in aqueous solutions The lines tend to become more diffuse with decreasing concentration, the low-frequency component disappearing even at high concentrations. This is again a conspicuous difference between aqueous and non-aqueous solutions of the polar type.

DISCUSSION

To understand the changes listed above, we must first get an idea of the molecular structure of the acid and that of the solvent used. As we already know,

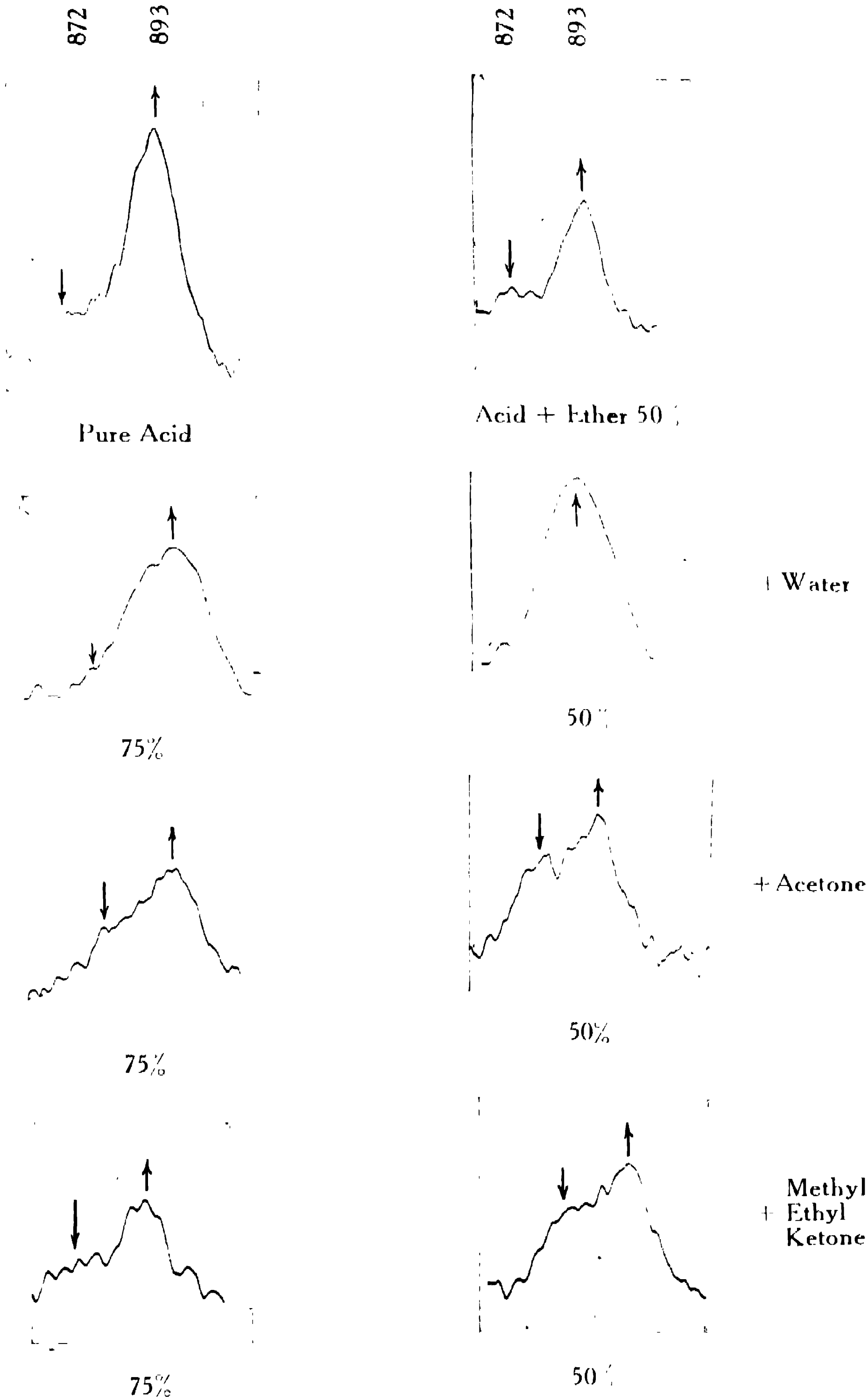

Fig. 1. C-C Lines of Acetic Acid in different Solvents

the acid is an associated liquid, mostly containing dimers of the type

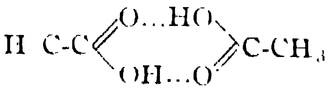

There is no definite evidence for the existence or non-existence of other more complicated molecules or less complicated ones. The solvents employed in these investigations are of three types: (1) non-polar, (2) polar and normal and (3) polar and abnormal or associated. In the first case no changes are observed, showing that the acid molecules remain as they are This observation is in consonance with existing physico-chemical data which gives abnormal values for the molecular weights of acetic acid in non-polar solvents like benzene.

In polar solvents, changes are observed, showing thereby that the molecular structure of the acid is affected. The following changes may take place :

(*i*) Breaking up of associated molecules into simpler ones.

(*ii*) Formation of complexes between the solvent molecules and the simple molecules so liberated.

Thus, in general, there is the possibility of such a solution containing the following types of molecules : (I) unbroken molecular aggregates of the pure acid, (II), lower polymers like monomers and (III) complexes formed with the solvent. An explanation of the changes observed in the Raman spectrum of the acid in the different polar solvents is bound to be dependent upon the factors outlined above.

Next we should consider the effect of these changes upon the frequencies of the particular oscillations studied. The author has already pointed out that the effect of association on the C=O line is to reduce its frequency and the effect of depolymerisation is to increase it, if the co-ordination or the formation of the hydrogen bond takes place on the O in C=O.[1, 2, 3] Based upon this factor, it was argued that in aqueous solutions of acetic, formic and benzoic acids, the increase in frequency of the C=O band is due to the formation of lower polymers. Association can take place not only through the O in C=O, but through H in OH which can act as an acceptor. It is only in the case of similar molecules, *i.e.*, in the case of molecular polymers of the pure acid alone, that both the donor and acceptor atoms are linked up through hydrogen bonds. If, on the other hand, a different molecule, say ether or acetone, forms a complex with the acid, then its donor atoms link up only with the acceptor atoms in the acid, *viz.*, with the H in OH. Thus, the C=O is unlinked, its external binding through the hydrogen bond is released, and the effect on it, if any, of the hydrogen bond at the end of the H in OH may not be towards diminishing it. Hence, again, there is an increase in the frequency of the C=O, if a molecular complex is formed between the acid molecule and another molecule having a donor atom.

The changes undergone by the Raman lines of acetone and methyl-ethyl ketone in acetic acid are discussed in another paper.[5] The effect of acetone, methyl-ethyl ketone and ether on the acid seems to be to break up the associated molecules (probably dimers) into their monomers and form complexes with them of the types

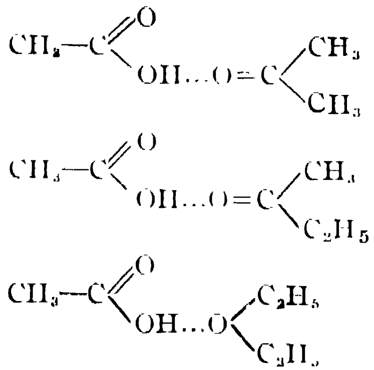

In all these, the C=O linkage of the acid is unattached and hence the 1760-line may probably be due to this. That it may not be due to the C=O in acetone or methyl-ethyl ketone is shown by the fact that the line is present in solutions in ether as well as in nitrobenzene.

The C–C binding in these cases seems to be affected by the formation of these complexes. Hence the appearance of the new line at 872. The fact that the line increases in intensity with increasing dilution of the acid shows that at greater dilutions more and more molecules of the acid are broken up and link themselves to the solvent to form complexes. The changes in the 620-line are explained similarly. The author attributed[1] this line to an external oscillation of the carboxyl group. If this group is attached to an external molecule, the line is bound to be displaced and the doubling is caused by the presence of attached and unattached molecules in the mixture. Further confirmation of this is found in the fact that these low-frequency components appear in the pure state of the acid, while they disappear at greater dilutions in water. The fact that the 893-line is not doubled in solutions of acetic acid in nitrobenzene is probably due to the non-formation of complexes. The effect of nitrobenzene may be merely to break up the dimers into monomers on account of its large dipole moment. The NO_2-line of nitrobenzene is itself unshifted and hence this conjecture. Chloroform does not seem to have any effect at all on the acid. Probably the effect of the dipole interaction is too feeble to break the dimers of the acid.

The effect of water on the acid is distinctly dissimilar to that of all the previous solvents studied. While there is the appearance of two distinct lines for the frequencies 620, 893 and 1670 in all the other polar solvents, in water there is a gradual shifting of the maximum of the 1670-band towards 1710 at higher dilutions and the other lines merely get diffuse, the low-frequency compo-

nents disappearing. This, as has been already pointed out, seems to be due to the breaking up of the higher polymers into lower ones. The fact that the low-frequency components of the 620- and 893-lines which are characteristic of the higher polymers disappear in aqueous solutions, lends support to this view. But it may be argued, why don't water molecules link themselves up with the monomers so formed and form complexes as in the case of solutions in acetone and methyl-ethyl ketone? If they should link up to the C=O, the C=O frequency must be diminished. But in fact it increases. The lines characteristic of the higher polymers of the complexes formed with the monomers, *viz.*, the low-frequency components of the 620- and 893-lines are absent in aqueous solution. Hence it is evident from the data that hydrates with water do not seem to be formed. There is another way of linking in order to form a hydrate. The H in OH in acetic acid may act as an acceptor and the O in water may be the donor. Then the structure of the hydrate resembles that of the acetonate given already and hence the 1760-line must be expected. Also the low-frequency components of the lines 620 and 893 must make their appearance as in the case of other solvents. Experiment shows that there is no trace of a separate and distinct 1760-line and that the 601- and 872-lines actually disappear in aqueous solutions. Moreover, physico-chemical data of Jones and his co-workers point out to the non-existence of hydrates of acetic acid in aqueous solutions.[4] Hence the changes of the Raman lines of acetic acid in aqueous solutions seem to be due only to a depolymerisation of the acid in the soivent, as pointed out elsewhere.[5]

Probably a distinction can be drawn between the effect of other polar solvents and that of water. In the case of water, we are treating with an abnormal and associated liquid. It is well known that the effect of one associated liquid on another is towards mutual depolymerisation. Each tends to diminish the association of the other. Probably that is so in mixtures of fatty acids and water.

The extreme diffuseness not only of the C=O line but of every other line in aqueous solutions appears to be due to the fluctuations of the polarisation field of the water envelope round each molecule in general. The effect of this field and its fluctuations is maximum in the case of water as compared to the other polar solvents, probably on account of the small size of the molecule.

REFERENCES

1 P. Koteswaram, *Zeits. f. Physik*, **110**, 118 (1938).

2 ,, *Jour. Chem. Phys.* **7**, 88 (1939).

3 ,, *Zeits. f. Physik*, **112**, 395 (1939).

4 H. C. Jones, "*Hydrates in solutions*", Publications of the Carnegie Institute of Washington, Feb. 1907, p. 110.

5 Paper No. 36, this journal

SPECIFIC HEAT OF LAC

By G. N. BHATTACHARYA
Indian Lac Research Institute, Ranchi

(*Received for publication, July 24, 1940*)

ABSTRACT. Specific heats of different varieties of lac and lac constituents have been determined with a vacuum calorimeter which in principle is the same as was employed by Nernst and Lindemann for poor heat-conductors. The constructional details of the calorimeter have been described in the paper The first series of experiments show that the specific heat of shellac practically remains constant over the temperature range of 10°C to 40°C and the value obtained is between 0·36 and 0·38 cals./gm./°C. Higher and higher values are obtained as determinations are made at higher and higher temperatures. Seedlac, in general, has a slightly higher value of specific heat than shellac owing probably to the presence of slightly higher percentage of water. Heat-hardened lac has been found to give a lower value of specific heat due to the elimination of water during the hardening process. It has been noticed that lac begins to absorb heat of fusion even at so low a temperature as 40°C which is ordinarily believed to be far away from its softening range of temperature.

INTRODUCTION

An elaborate study has been made on the thermal properties of most of the synthetic resins, but since lac is a natural resin and as such it cannot be a very standardised product, adequate attention was not paid to a careful study of its thermal properties so far. Some data on its thermal conductivity,[1] thermal expansion,[2] softening and melting points[3] and fluidity[4] are available. But no record of the specific heat of lac is available till now. Verman[5] pointed out that the study of this property at different temperatures might be useful in obtaining an idea of the change which lac undergoes on heating.

The problem of storing lac for a long period without having its thermal and electrical properties appreciably altered is engaging the attention of shellac-manufacturers. Cold storage of lac is being considered by some as a probable solution. Data on the specific heat of lac will be very useful for this purpose.

The object of the investigation was to supply specific heat data sufficiently accurate for ordinary purposes but not such as would have necessitated extreme precautions and very elaborate arrangements. This was in order to simplify unnecessary complications considering the nature of purity that we can ordinarily expect from a sample of shellac. Though, therefore, a vacuum calorimeter was finally used in these investigations, the use of a calibrated thermo-couple for the measurement of temperature or of potentiometric evaluation of voltage and current that is usually associated with such a calorimeter has been purposely omitted.

It should be clearly understood, however, that for substances, like resins, which have a softening range of temperature but no definite melting point, the determination of specific heat could be done only at temperatures tolerably removed from the softening range as otherwise latent-heat factors would vitiate the results.

EXPERIMENTAL

Preliminary Experiments

Ordinary calorimetric method was first used for the determination of specific heat of lac, the calorimeter being a well-insulated double-walled one and paraffin oil the calorimetric liquid. Lac in the form of powder was enclosed in a small flat copper container and was never heated above 45°C in order to keep it far below its softening point. Determination was made within two ranges of temperature, *viz.*, between room temperature and 45°C and between room temperature and 0°C. For the higher range of temperature samples were heated having been suspended inside a wide tube surrounded by a jacket through which hot water at some definite temperature could be circulated. For the lower range of temperature, however, the jacket could be filled with crushed melting ice and a small cruicible containing fused calcium chloride was placed on the bottom cork closing the inner tube in order to absorb moisture from the enclosed air. Determination of specific heat was made in the usual way by noting the rise or fall of temperature of paraffin oil and applying proper corrections.

The values obtained in this way for a few samples of shellac were near about 0·5 cals./gm./°C within the higher range of temperature and about 0·3 to 0·4 for the lower range. As this difference was large, the use of a more accurate method of determining specific heat at different temperatures was considered necessary in order to ascertain to what extent the effect of temperature was responsible for it.

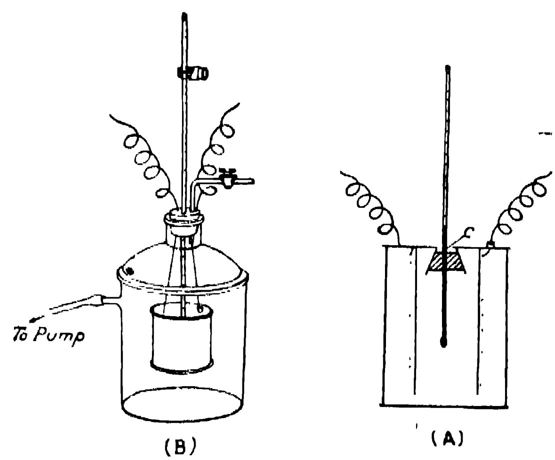

FIGURE I
Vacuum Calorimeter

For this purpose a vacuum calorimeter, which was essentially the same as used by Nernst and Lindemann [6] for the determination of specific heat of poor heat conductors at low temperatures, was employed. The diagrammatic sketch of the design has been shown in Figure 1(A). The outer cylindrical can having a length of 9·5 cms. and a diameter of 3·5 cms. was made of thin sheet copper and the inner tube, which was fixed on the top cover coaxially with the outer cylinder, was also made of the same material having a diameter of exactly half of the outer one. A heating coil of S.W.G. No. 36 constantan wire having a resistance of 5·70 ohms was wound on the inner tube using a thin mica sheet as insulation. One terminal of the coil was soldered to the body of the calorimeter, while the other was brought out through a small hole on the cover having been properly insulated by varnished cotton sleeve and sealed in some insulating cement. A long thermometer, graduated to tenths of a degree and which could easily be read to an accuracy of 1/20th of a degree by clamping a reading lens on it, was fixed along the axis of the cylinders through a rubber cork fitted on a conical hole on the top as shown at C in the figure. A thin layer of paraffin was applied on the cork to make the lid vacuum-tight. The bottom lid could be unsoldered for the purpose of filling the calorimeter. The capacity of the vessel was about 65 c.c. The calorimeter was placed inside a small Witt's filtering vessel, the thermometer projecting outside. The vessel could be evacuated to a low vacuum in order to reduce as much as possible loss or gain of heat from the calorimeter to its surroundings by gaseous conduction or convection. The whole assemblage could be placed inside a big thermostat whose temperature could be kept constant to within 0·1°C throughout the range of investigation.

Method of Determination

The procedure was to fill the calorimeter with the substance in the form of powder and solder the bottom lid so as to make it vacuum-tight. A thin coating of collodion was sometimes applied on the soldered portion for this purpose. The assemblage was then put in the thermostat to attain its temperature. When the thermometer in the calorimeter registered the temperature of the thermostat, the space surrounding the calorimeter was evacuated to a low vacuum. A low current was then passed from a 4-volt lead storage battery of large capacity through the heating coil for some definite time and the temperature noted at the end of every minute during heating and every half minute after that for the purpose of applying radiation corrections.

Calibration

The calorimeter was very carefully calibrated with Schering's pure aluminium metal powder and subsequently its heat capacity thus obtained used in the

determination of specific heat of copper dust and graphite powder. The results obtained agreed to within 5% of their values given in the International Critical Tables.[7] Pure Naphthalene was also used as it had been employed by many previous workers[8] for the calibration of a vacuum calorimeter, and as it is also a poor conductor of heat like shellac. The result was satisfactory and was accurate within the limits of error stated above. The heat capacity of the calorimeter was 14·3 calories/°C.

RESULTS

For a few samples of lac the time of heating was 15 minutes for the first series of experiments and the rise of temperature about 4°C. The heating current was kept constant at 0·35 ampere throughout the experiment. The results of such determinations have been shown in Table I. It will be seen from the table that lac generally begins to absorb heat of fusion from about 40°C and therefore

TABLE I

Sample	Wt taken in gms	Range of temperature in degrees centigrade	Sp. ht. in cals./gm./°C.	Sample	Wt. taken in gms.	Range of temperature in degrees centigrade	Sp. ht in cals./gm./°C.
Kusum shellac	60·3	10—15	0·37	Heat-hardened shellac.	58·3	10—15	0·33
		15—20	0·37			15—20	0·33
		20—25	0·37			20—25	0·34
		25—30	0·37			25—30	0·33
		30—35	0·38			30—35	0·34
		35—40	0·38			35—40	0·35
		40—45	0·44			40—45	0·34
		45—50	0·56			45—50	0·36
Palas shellac	59·5	10—15	0·35	Chemically hardened shellac (shellac exposed to HCl vapour).	55·2	10—15	0·36
		15—20	0·36			15—20	0·36
		20—25	0·36			20—25	0.35
		25—30	0·36			25—30	0·36
		30—35	0·35			30—35	0·36
		35—40	0·37			35—40	0·37
		40—45	0·42			40—45	0.39
		45—50	0·55			45—50	0·43

the apparent specific heat is high at higher temperatures. As a result of this finding specific heat was determined for a number of samples between the range 10°C and 30°C. The time of heating was between 1 hr. and 1½ hrs. for different samples for this range of temperature. Table II shows these results. The input energy could be measured within an accuracy of 1% and the temperature within 1½%. Taking into consideration the accuracy of radiation corrections, the results are not generally claimed to be more accurate than within 5%. In the worst cases, the error may be slightly more. For ordinary purposes, however, this accuracy is considered sufficient.

TABLE II

Sample	Range of temperature 10°C—30°C		Sample	Range of temperature 10°C—30°C	
	Wt. taken in gms.	Sp. ht. in cals./gm/°C.		Wt. taken in gms.	Sp. ht. in cals./gm/°C.
Kusum shellac	60·3	0·37	Pure lac resin (extracted by A-U method)[9].	57·8	0·34
Kusum seedlac	58·8	0·40			
Palas shellac	59·5	0·36	Soft resin (Ether-soluble).	102·4	0·48
Palas seedlac	61·1	0·40			
Khair shellac	59·2	0·37	Shellac wax	76·5	0·43
Khair seedlac	60·8	0·41	Heat-hardened shellac.	58·2	0·34
Pure lac resin (Ether-insoluble).	58·2	0·34	Heat-hardened pure lac resin.	54·6	0·32
			Chemically hardened shellac.	55·2	0·36

DISCUSSION

Comparing the values of specific heat for some other plastics[10] it is found that shellac has almost an identical value. For example, 'Pyroxylin' (Nitro-cellulose plastic) gives for its specific heat 0·34 to 0·38, phenol resins give 0·33 to 0·37, gutta-percha and balata 0·402 and vulcanised-rubber 0·415. For shellac wax, however, the value obtained is definitely lower than that for paraffin wax (mineral wax, sp. ht. 0·69) between the same range of temperature and even slightly lower than that for beeswax (animal wax, sp. ht. 0·477) between 20°C and 30°C.

It will be seen that the values of specific heat of heat-hardened shellac and heat-hardened pure lac resin are lower than those of ordinary shellac and pure

lac resin. This may be explained by supposing that during the process of hardening by heat both shellac and pure lac resin lose some amount of water and form into a condensation product.[11, 12] So naturally the amount of heat required to raise its temperature through one degree may be expected to be less according to Kopp-Neumann law as the specific heat of water is sufficiently high. This explanation gains further support from the fact that the specific heat of chemically hardened shellac is not so low, as there the hardening process is considered to be one of polymerisation without elimination of water.[13]

To calculate the amount of water that is lost by heat-hardening, one of the pure lac resin samples of which the specific heat was determined first, was heated at about 120°C for 15 hours and the specific heat was then determined again. It was found that the value of specific heat fell from 0·34 to 0·32 A sample of Kusum shellac similarly showed a reduction of specific heat, from 0·37 to 0·34. But, as the difference in specific heat was of the same order as the possible experimental error, no definite conclusions could be drawn from the calculations following Kopp-Neumann law.

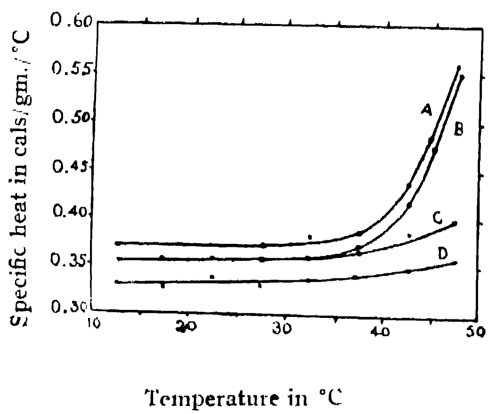

FIGURE 2

Specific heat of lac at different temperatures —
A—Kusum Shellac
B -Palas Shellac
C—Chemically hardened shellac
D—Heat-hardened shellac

It is evident from Table I that the specific heat of lac samples does not show much variation between the temperatures 10°C and 35°C but higher and higher values are obtained as determinations are made at higher and higher temperatures. Figure 2 shows this variation. This simply means that lac begins to absorb a small amount of heat even at so low a temperature as 40°C though this temperature is far removed from its ordinarily believed 'softening range' (56°-75°C).[14] The study of the variation of refractive index of lac with temperature[15] also

revealed similar changes near about the same temperature. On a study of the coefficient of cubical thermal expansion of shellac determined at different temperatures over the range −80°C to 200°C, Samsoen [2] found out a transition temperature at about 46°C. The expansion-coefficient above 46°C was about four times the value below it. He also found out such characteristic temperatures in the case of many other amorphous substances such as, glass, tar, rosin, etc., and has shown that other physical properties of these substances also undergo a sudden change near about their respective transition temperature. Such temperatures have been observed for many other substances by other workers [16] also. These specific-heat experiments, however, confirm Samsoen's observation regarding the transition temperature of shellac near about 46°C. Apparent higher values of specific heat at increased temperatures, therefore, indicate merely the influence of latent heat. In other words, when lac is heated physical changes begin to take place long before they are detected by the standard methods [17] for the determination of softening points. The softening point as determined by these methods, therefore, denotes a definite stage during the softening process, but it does not really indicate the starting of it. The large difference obtained for the specific-heat values between the two temperature ranges in the preliminary investigations was therefore the result of slight softening at the higher range of temperature. Tamman's [3] observation that shellac loses its brittleness at about 30°·5C and the softening range is between 30°·5C and 56°·5C is supported by these experiments.

The slightly higher values of specific heat in the case of seedlac than for shellac may be accounted for by the presence of slightly higher percentage of water and by the absence of any heat treatment during manufacture. The apparent change of specific heat with temperature in the case of hardened lac has been found to be small, as might be expected since their softening points are high. The specific heat of shellac is intermediate between those of soft resin and pure lac resin and it agrees well with the calculated value considering lac as composed of about 75% pure lac and 25% soft lac.

ACKNOWLEDGMENT

The author wishes to express his gratitude to Dr. H. K. Sen, Director of this Institute, for his kind interest in the work and to Prof. H. E. Watson of the University College, London, for some suggestions and helpful criticisms.

REFERENCES

1 Lee, C. H., *Phil. Trans. Roy. Soc.* (London), 481, **A183**, 1892 and 399, **A191**, 1898; Symons, H.D., & Miles Walker, *J.I.E.E.*, 674, **48**, 1912.

2 Samsoen, M.O., *Compt. Rend.*, 517, **182**, 1926. *Ann. des Phys.*, 85, **9**, 1928, & *Bull. de la Soc. d' Enc. l' Ind. Nat.*, 185, **128**, 1929.

[3] Tamman, G., *Der Glasszustand*, 1933.

[4] Houwink, R., *Physikalische Eigenschaften und Feinbau von Natur und Kunsharzen*, 1934.

[5] Verman, L.C., *Lond. Shell. Res. Bur. Tech.* Paper No. 4, August, 1935.

[6] Nernst and Lindemann, *Ann. d. Phys.*, 595, **36**, 1911; Glazebrook, R. T., *Dictionary of App. Phys.*, 40, **1**, 1922; Nernst R. T., *New Heat Theorem*, pp. 37-49.

[7] Lingi Rolla and Giorgio Piccardi, *Int. Crit. Tables*, 92-94, **5**, 1929.

[8] Southard, J. C., and Brickwedde, F. G., *J.A.C.S.*, 4378, **55**, 1933; Hoffmann, Parks and Daniels, *J.A.C.S*, 1555, **52**, 1930; Andrews, Lynn, and Johnston, *ibid*, 1274, **48**, 1926. Dewar, *Proc. Roy. Soc.* (London) 325, **A76**, 1905.

[9] Venugopalan, M., and Sen, H. K., *J. Soc. Chem. Ind*, 371, **57**, 1938.

[10] Randolf, A. F., *Int. Crit. Tables*, 296 and 294, **2**, 1927; Whitby, G. S., *Int. Crit. Tables*, 269 and 294, **2**, 1927.

[11] Gardner, W. H, and Cross, B. B., *Brit. Plastics and Mould Prod. Trad.*, 514, **6**, 1935.

[12] Gardner, W. H., *Physics*, 306, **7**, 1936.

[13] Harries, C, and Nagel, W., *Kolloid Zeit.*, 248, **33**, 1923.

[14] *Ind Lac. Res. Inst. Tech*, Note No. 1, 1937.

[15] Bhattacharya, G. N., *Ind. J. Phys.* 237, **14**, 1940.

[16] Tools, A. Q., and Valasek, J, *Bur. Std. Sc*, Paper No. 358; Parks, G. S., Hoffmann, H M, and Cattoir, F R., *J Phys Chem.*, 1366, **32**, 1928.

[17] Gardner, H. A., *Physical and Chemical Examination of paints, varnishes and lacquers*, 1939; Verman, L. C., *Lond. Shell. Res. Bur. Tech*, Paper 4, 1935.

THE FIRST SPARK SPECTRUM OF TELLURIUM

Part I

By K. R. RAO

AND

M. GOURINATHA SASTRY
Andhra University, Waltair

(*Received for publication, July 27, 1940*)

ABSTRACT. Based on an extensive experimental study of the Emission spectrum of Tellurium, the general features of the structure of the first spark spectrum of the element have been identified. A related system of quartet and doublet terms has been set up, involving the characteristic terms of the 5s, 6s and 6p electron configurations of the singly ionised atom of Tellurium. The ionisation potential of Te II is derived to be 21·5 volts approximately.

INTRODUCTORY

In three previous papers,[1] the analyses of the higher spark spectra of Tellurium Te VI, Te V, Te IV and Te III were published. The present paper is a continuation of the above work and deals with the structure of the first spark spectrum of the element due to the singly ionised atom. A preliminary notice of the work appeared in 'Nature.'[2]

EXPERIMENTAL

The experimental work consisted in an extensive investigation of the spectrum of Tellurium as excited especially in condensed discharges through Tellurium vapour contained in quartz capillary tubes and in vacuum sparks between Aluminium Electrodes tipped with Tellurium. The measurements were made on plates taken with large Glass and Quartz Spectrographs for the visible and ultra-violet and with a tangential incidence 5-ft. Concave Grating Instrument in the vacuum region. A full account of this experimental work was already given in the papers referred to above.

PREDICTED TERMS

The singly ionised Tellurium Atom contains 51 outer electrons like the neutral atom of Antimony and the more important spectral terms theoretically

deduced as characteristic of such an Electron Configuration are briefly given below :

Term Prefix	Predicted Terms		
	Limit ^3P	^1D	^1S
5p	^4S	^2D	^2P
6s	^4P ^2P	^2D	^2S
6p	^4D ^4P ^4S	^2F ^2D	^2P
	^2D ^2P ^2S	^2P	

All the above terms have been identified with the exception of a few doublets based on the ^1D and ^1S states of the ion.

ANALYSIS

The identification of the various multiplets has been based primarily on the detection of the fundamental resonance combination 5p $^4S-6s\,^4P$ consisting of the three lines in the vacuum grating region $\nu\nu$ 86094, 82742 and 78447. All the lines in the region where this group might be expected have been very closely scrutinised and no alternative choice of this group could be arrived at, consistent with the behaviour of the lines under different experimental conditions and the probable disposition of this group. The choice has been confirmed also by a study of the two available lists of lines of Tellurium in this region, one due to Bloch[3] and another (unpublished) due to Professor R. J. Lang of Edmonton (private communication). It has been possible with the aid of this group to extend the identification to the region of longer wave-lengths and to detect the other multiplets formed by the combination of the 6p terms with 6s ^4P. A related system of doublet and quartet terms has been set up through the discovery of several intercombination lines. The lines so far identified have been presented in the form of multiplets in Table I. For the sake of brevity, all the data, comprising of the wave-numbers, term values, and term intervals are included in a single multiplet table, which is self-explanatory. The wave-lengths of the lines are omitted in this part, as not quite necessary. The numbers in brackets are the usual visual estimates of the intensities of the lines. A complete catalogue of all the lines assigned to Te II will be given in a succeeding part dealing with the identification of the 4d terms and other higher members.

The Term Values quoted in the multiplet table have been calculated, as has been done by one of the authors in Se II,[6] from the two members of the series $6s^4P - mp^4S$, although the absolute values derived thus might be somewhat largely in error. The deepest term $5p\ ^4S$ gives the second ionisation potential of Tellurium to be 21·5 volts approximately.

TABLE I

Multiplets in Te II

5p	$^4S_{1\frac{1}{2}}$ 173801 (*102*|*21*)	$^2D_{1\frac{1}{2}}$ 163580 (27|*33*)	$^2D_{2\frac{1}{2}}$ 160847 (*85*|*36*)	$^2P_{\frac{1}{2}}$ 152281 (*41*|*80*)	$^2P_{1\frac{1}{2}}$ 148101
$6s^4P_{\frac{1}{2}} = 95352·6$	78447(10)	68225(3)	—	—	—
4295·1					
$^4P_{1\frac{1}{2}} = 91057·5$	82742(10)	72519(4)	—	—	—
3353·1					
$^4P_{2\frac{1}{2}} = 87704·4$	86094(6)	—	—	—	—
$^2P_{\frac{1}{2}} = 89246·1$	—	74334(10)	—	63035(10)	—
3870·3					
$^2P_{1\frac{1}{2}} = 85375·8$	88425(4)	78204(3)	75471(8)	66905(4)	62724(5)
$^2D_{1\frac{1}{2}} = 78944·4$	94862(5)	84635(6)	81901(3)	—	69153(3)
$\alpha = 71559$	102245(9)	92023(6)	—	80717(1)	76538(6)
$\beta = 83810$		79767(3)	77036(9)	—	—

TABLE I (*contd.*)

Multiplets in Te II

6p / 6s	$^4D_{\frac{1}{2}}$ 74458·6	1647·4	$^4D_{1\frac{1}{2}}$ 72811·2	6295·8	$^4D_{2\frac{1}{2}}$ 66515·4	$^4D_{3\frac{1}{2}}$	$^4P_{\frac{1}{2}}$ 77008·9	2632·9	$^4P_{1\frac{1}{2}}$ 74376·0	4011·4	$^4P_{2\frac{1}{2}}$ 70364·6	$^4S_{1\frac{1}{2}}$ 65461·6	$^2D_{1\frac{1}{2}}$ 71733·8	$^2P_{\frac{1}{2}}$ 73362·4	5212·0	$^2P_{1\frac{1}{2}}$ 68150·4
$^4P_{\frac{1}{2}}$ = 95352·6	20893·9(5)		22541·6(5)		—	—	18343·2(10)		20976·0(7)		—	29891·3(1)	—	21991·4(5)		—
4295·1																
$^4P_{1\frac{1}{2}}$ = 91057·5	16598·8(1)		18245·8(6)		24541·7(8)	—	14048·2(2)		16681·2(6)		20692·6(10)	25596·3(1)	—	17696·4(10)		22908·1(9)
3353·1																
$^4P_{2\frac{1}{2}}$ = 87704·4	—		14892·3(1)		21188·0(1)	—	—		—		17339·5(5)	22243·6(6)	15971·4(3)	—		19555·6(3)
$^2P_{\frac{1}{2}}$ = 89246·1	—		16436·1(3)		—	—	—		14870·0(0)		—	—	17513·2(10)	15884·6(7)		21097·0(3)
3870·3																
$^2P_{1\frac{1}{2}}$ = 85375·8	—		—		18860·7(4)	—	—		—		15011·5(2)	19912·8(2)	—	—		17227·4(6)

A comparison of the intervals of the deepest terms in the iso-electronic spectra of Sb I[4] and Te II and of As I[5] and Se II[6] is shown in Table II. It provides strong evidence of the correctness of the identification. The usually expected regularity among the term intervals is obvious from the Table.

TABLE II

Term Intervals

Term Interval	As I	Se II	Sb I	Te II
ms $^4P_{\frac{1}{2}}$-$^4P_{1\frac{1}{2}}$	915·8	1483·6	2696·0	4295·1
$^4P_{1\frac{1}{2}}$-$^4P_{2\frac{1}{2}}$	1287·8	1920·7	2387·4	3353·1
$^2P_{\frac{1}{2}}$-$^2P_{1\frac{1}{2}}$	1469·6	2459·7	2400·0	3870·3
mp $^2P_{\frac{1}{2}}$-$^2P_{1\frac{1}{2}}$	461·2	858	2068·8	4180
$D_{1\frac{1}{2}}$-$^2D_{2\frac{1}{2}}$	322·3	616	1341·6	2733
ms $^4P_{2\frac{1}{2}}$-$^2P_{\frac{1}{2}}$	237·7	222·0	—1341·8	—1541·7

REFERENCES

1 K. R. Rao, *Proc. Roy. Soc., A*, **133**, 220 (1930); Krishnamurty, *ibid.*, **151**, 178 (1935); Krishnamurty and K. R. Rao, *ibid.*, **158**, 562 (1937).

2 K. R. Rao, *Nature*, **143**, 376 (1939).

3 Bloch, *Jour. de Phys. Rad.*, **6**, 441 (1935).

4 Lowenthäl, *Zeits. f. Phys.*, **57**, 828 (1929).

5 K. R. Rao, *Proc. Roy. Soc., A*, **125**, 238 (1929).

6 Krishnamurty and K. R. Rao, *Proc. Roy. Soc., A*, **149**, 56 (1935).

INTERFEROMETRIC MEASUREMENTS OF CERTAIN LINES IN THE SPECTRUM OF BROMINE

By M. GOURINATHA SASTRY
Research Scholar, Andhra University, Waltair

(*Received for publication, July 27, 1940*)

Plates XIV and XV

ABSTRACT. Using a Fabry-Perot Etalon in conjunction with a Hilger Quartz Littrow Spectrograph the wave-lengths of nine lines in the spectrum of Bromine II have been measured. Vacuum Copper Arc lines λλ 5153.235 and 4651.124 have been used as standards.

The measured lines include the super-quintet $5s\ {}^5S - 5p\ {}^5P$ of Br II. The intervals of the $5p\ {}^5P$ level are thus determined accurately.

INTRODUCTION

Determination of the wave-lengths of spectral lines to a high degree of accuracy have been successfully carried out by a number of investigators, Babcock, Burns, McLennan, Meggers, Jackson[1] and others using high resolving power apparatus such as the Fabry-Perot Etalon. The fundamental standard of wave-length that is almost invariably adopted is that of the red Cadmium Line λ 6438.4696 and, in terms of this, the wave-lengths of a very large number of Fe, Ne, He, lines have been measured interferometrically for use as subsidiary standards in Spectroscopic work. Besides the use of such measurements as subsidiary standards, accuracy in the determination of wave-lengths is highly desirable in investigations on the Analysis of Spectra and the identification of spectral lines.

In the course of the work on the analysis of the spectrum of Bromine carried out in this Laboratory, the need for accurate wave-lengths of as many lines of Bromine as possible, particularly of those belonging to Br. II, Br. III has been felt. The present paper deals with the measurement of a few lines, as produced in an ordinary vacuum tube and determined by a 10-mm. Fabry-Perot Etalon in conjunction with a Hilger large Quartz Littrow Spectrograph. The general procedure and method of calculation followed in this work are essentially the same as that of Babcock and of MacLennan and described in detail by the latter,[1] in investigations on the Auroral Green Line.

Theory of the wave-length determination :—It can be easily shown from the theory of the Etalon that for two wave-lengths λ_x and λ, the difference $(m+\delta)$ in the order of interference for normal incidence is given by [2]

$$\Delta\nu = (\nu_x - \nu) = \frac{1}{\mu_x}\left[\frac{m+\delta}{2t} - \nu\Delta\mu\right] \qquad \ldots \quad (1)$$

where ν_x and ν are the respective frequencies and μ_x and μ the refractive indices; m and δ are the integral and fractional parts of the order of the interference. In utilising this equation, two lines (the wavelengths of which are known by interferometric methods) are chosen as standards say λ_x and λ. From the calculated values of the refractive indices for the two lines and the approximate value of 2t, the double thickness of the Etalon, supplied by the manufacturers the value of $(m+\delta)$ is first approximately calculated. This, however, gives the value of m, the integral part of the order of interference accurately.

To find δ correctly, the interference patterns for the two standards are measured. If d_p and d_q be the diameters of any two rings p and q of the system formed by the wave-length λ then a is given by [2]

$$a = \frac{(p-1)d_q^2 - (q-1)d_p^2}{d_p^2 - d_q^2} \qquad \ldots \quad (2)$$

with a similar expression for a_x corresponding to λ_x.

Then δ is calculated from the equation

$$\delta = (a_x - a) \quad \text{or} \quad (1 + a_x) - a.$$

Hence knowing $(m+\delta)$ accurately, the value of 2t is determined with precision from equation (1).

The wave-length of any other required line can then be estimated from this value of 2t from the observations of the fringe pattern of that line, using a single standard.

EXPERIMENTAL

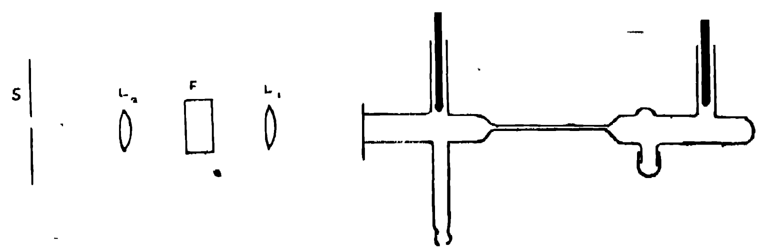

A—Discharge tube
L_1—Collimating lens
F—Fabry-Perot Etalon
L_2—Condensing lens
S—Slit of the spectrograph

FIGURE 1. Optical Arrangement

Fig. a

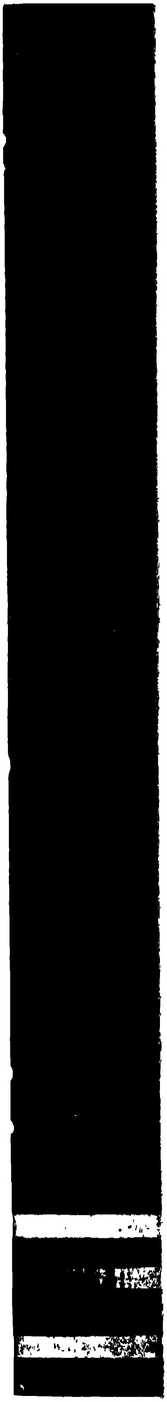

4651·124

5153·235

Fig. b

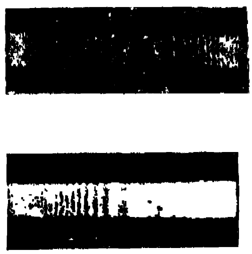

4651·124

5153·235

Fig. a. The patterns of the Vaccum Copper arc Spectrum.

Fig. b. Fringe System of λ 5153·235 and of λ 4651·124 of the Copper arc shown enlarged.

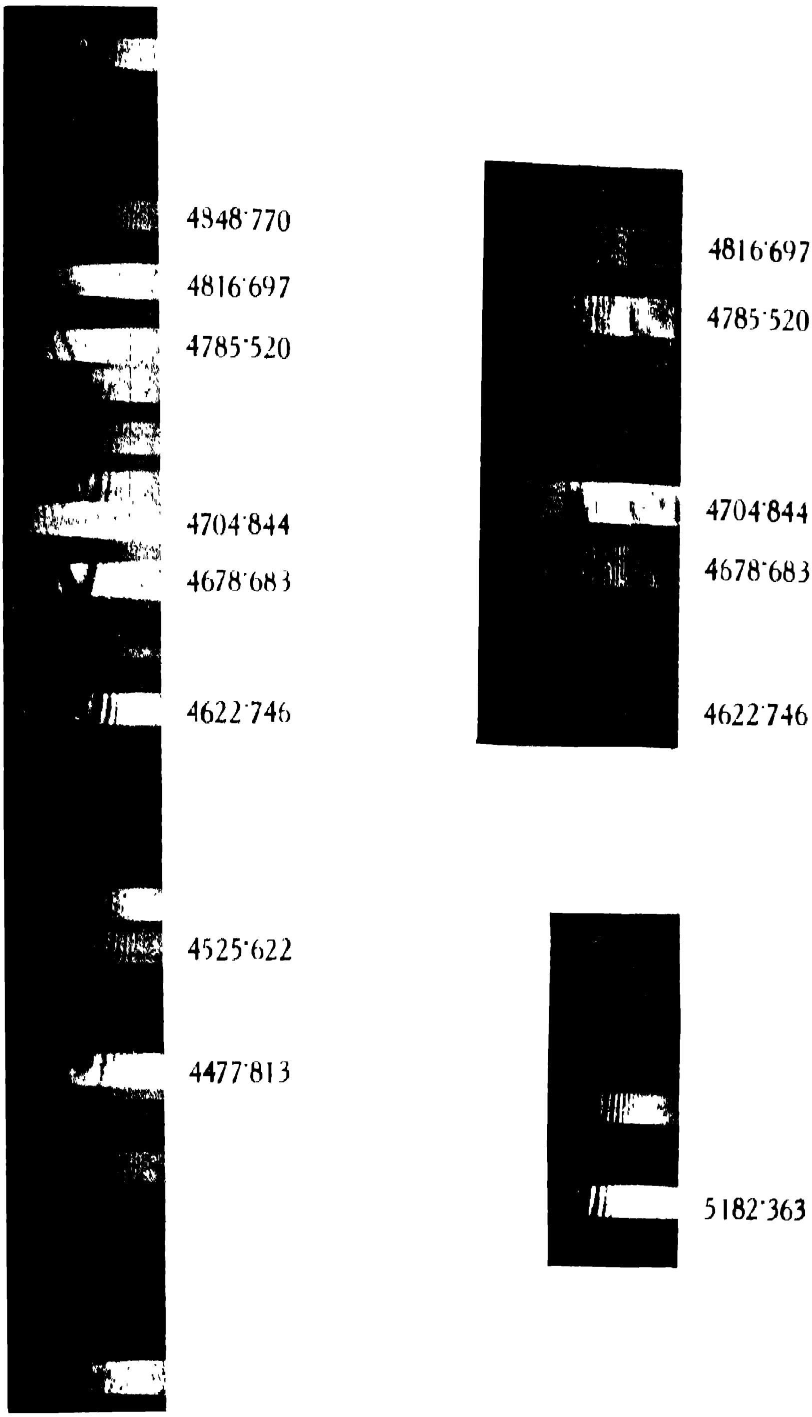

Fig. c. Patterns in the Spectrum of Bromine.

The general optical arrangement is shown diagrammatically in figure 1. Fringe patterns are first obtained for the two lines of Copper λ 5153.235 and λ 4651.124, which served as standards[3] for determining 2t. These lines are excited in a vacuum arc with water-cooled electrodes of about 6 mms. diam. The gap between the electrodes is adjusted to be five to seven milimeters, during the actual exposure. The arc is fed by a current of about 2.5 to 3 amperes from a 220-volt D.C. mains. Light from the arc is rendered parallel by the glass achromatic lens L_1, of about 12 cms. focal length and allowed to strike the parallel faces of the etalon arranged immediately in front of it. On emergence from the plate the light is focussed on to the slit of the spectrograph by another similar lens of shorter focal length. The etalon is so adjusted that the pattern consists of rings on both sides of the centre. With a good alignment of the optical parts exposures of about a minute on Ilford special rapid panchromatic plates gave good pictures of the patterns of the Copper arc lines.

For photographing the Bromine lines an ordinary discharge tube of the H-type is employed. The central capillary portion is about 2 mms. wide and 15 cms long. A bulb at one end of the tube contains a small quantity of copper bromide. Periodic heating of the bulb is found necessary to maintain sufficient pressure of Bromine in the capillary. The discharge tube is continuously evacuated by a Gaede two-stage pump connected to it. To prevent vapours from entering the pump, tubes of calcium chloride, caustic potash and phosphorous pentoxide are inserted between the pump and the discharge tube. The tube is excited by a 1/4 K.W. transformer, the primary being fed by 220 volt A.C. and a current of about .6 to .8 of an ampere. The length of the series spark gap is adjusted for a somewhat low intensity of excitation in order that the lines of Br. II might be emitted strongly. The discharge under these conditions is bluish green. Exposures of 2 to 3 hours are given to bring about the fringe pattern clearly. In all the above experiments the slit of the spectrograph is 0.29 mm. To identify the lines of Bromine, preliminary experiments are made with narrow and wide slit widths to photograph the spectra before and after filling the bulb with copper bromide, using Fe and Cu arc comparison spectra for purposes of measurement.

Plates XIV and XV show the fringe patterns of the copper arc lines 5153 and 4651 and of those of the lines of Bromine that have been measured in this work.

The fringe systems are measured with a Hilger photo-measuring micrometer reading to .001 mm. The point of intersection of the cross-wire has been set symmetrically with respect to the width of the fringe and measurements are made along the length of the diameters of the successive fringes. Each line is measured a number of times in the forward and backward directions ; the average of the readings as measured on three different plates is finally adopted. The results of observation are given in tabular form along with the optical data supplied by the makers of the Etalon in the following section. The calculation of 2t and of the

wave-length of one of the lines of Bromine are shown in detail as a typical illustration of the method. The wave-lengths of the remaining lines which are similarly calculated are entered in the table at the end with the other data. The last column in this table gives the wave-lengths as determined by the use of the second available copper standard to serve as a check on the determination. The agreement between the two independently obtained values is satisfactory.

CALCULATION AND RESULTS

Thickness of the Etalon as supplied by Hilger $=9.924$ mms.

The two Copper Arc standards employed have the values,

$$\lambda = 5153.235 \quad \mu = 1.51229 \quad \nu = 19405.290$$
$$\lambda_x = 4651.124 \quad \mu_x = 1.51578 \quad \nu_x = 21500.175$$
$$\Delta\mu = 0.00349 \quad \Delta\nu = 2094.885.$$

The mean values of a and a_x obtained from the measurement of the fringe systems of two lines are

$$a = .989 \quad a_x = 1.286$$
$$\delta = .297.$$

The integral part deduced from equation (1) is 6436. Hence the value of the double thickness 2t is found to be 1.98463. This value is used in the subsequent calculation.

For the Bromine line the values are,

$$\lambda_x = 4816.71 \qquad \mu_x = 1.51451 \qquad \nu_x = 20761.057.$$

For the Cu standard,

$$\lambda = 5153.235 \qquad \mu = 1.51229 \qquad \nu = 19405.290.$$

Approx. wave-length of Br. lines	Refr. Index	a_x	δ	Approx. $(m+\delta)$	Integral Part m	Final $(m+\delta)$	$\Delta\nu$	Final Wave-Length: Standard $\lambda=5153$	Final Wave-Length: Standard $\lambda=4651$
5182.36	1.51212	1.048	.941	333.931	333	333.941	109.065	5182.362	5182.363
4848.75	1.51427	1.405	.416	3738.688	3738	3738.416	1218.490	4848.770	4848.770
4816.71	1.51451	.629	.640	4160.484	4160	4160.640	1355.818	4816.696	4816.698
4785.50	1.51474	.710	.721	4576.975	4576	4576.721	1491.082	4785.520	4785.519
4704.86	1.51535	.788	.799	5679.585	5679	5679.799	1849.401	4704.844	4704.844
4678.69	1.51556	.981	.992	6045.852	6045	6045.992	1968.256	4678.681	4678.684
4622.75	1.51601	1.278	.289	6843.247	6843	6843.289	2226.869	4622.746	4622.746
4525.60	1.51684	1.354	.365	8276.703	8276	8276.365	2691.117	4525.623	4525.622
4477.80	1.51726	1.528	.539	9005.736	9005	9005.539	2927.043	4477.813	4477.813

Mean values of a obtained from measurements on the diameters of the fringes are

$$\text{for the Cu standard} = .989$$

$$\text{for the Br line} = .629$$

$$\delta = (1 + a_x) - a = .640.$$

The integral part m from equation (1) is 4160.

Hence $$\Delta\nu = 1355.818 \text{ cms.}^{-1}$$

and $$\lambda = 4816.696 \text{ A.U.}$$

The value of same line calculated with the other Copper standard is found to be 4816.698, agreeing very closely with the above.

The above table gives the data obtained with the other lines. The above measurements include those of three lines $\lambda\lambda$ 4816.697, 4785.520, and 4704.844 which form the combination $5s\,^5S_2 - 5p\,^5P_{1,2,3}$ of Br II as identified by Bloch.[4] The intervals $5p\,^5P$ are thus known now accurately to be $^5P_1 - {}^5P_2 = 135.20$, and $^5P_2 - {}^5P_3 = 358.27$ cms.$^{-1}$

The author is indebted to Dr. K. R. Rao for his interest in the work.

REFERENCES

[1] Babcock, *Astrophys. J.*, **57**, 209 (1923); Meggers, *Bureau of Stand. J.*, **18**, 543 (1937); MacLennan and McLeod, *Proc. Roy. Soc.*, **115**, 515 (1927); Jackson, *Proc. Roy. Soc.*, **155**, 407 (1936); *Trans. Roy. Soc.* (Lond.), **111**, 19 (1932).

[2] Williams, *Applications of Interferometry.*

[3] Kayser, *Handbuch* (1932).

[4] Bloch and Lacroute, *Compt. Rend.*, **199**, 41 (1934).

STUDY OF THERMAL NEUTRONS IN THE ATMOSPHERE.*

By S. D. CHATTERJEE

(*Received for publication, September 15, 1940*)

ABSTRACT. The intensity of thermal neutrons in the atmosphere has been measured at the sea-level (Calcutta 70 ft.), and at a higher altitude (Darjeeling 7000 ft.), using a boron-lined proportional counter. A preliminary measurement of the size-frequency distribution of the energies of the disintegration particles from boron by the action of atmospheric neutrons has been carried out at the higher altitude with a boron trifluoride ionisation chamber

1. INTRODUCTION

Various investigators have reported the existence of neutrons associated with cosmic radiation, both at sea-level and at higher altitudes. Locher and Rumbaugh[1] sent up photographic films coated with paraffin during stratospheric flights. They observed proton tracks in the photographic emulsions, which they believed to have been caused by protons knocked out of paraffin by neutrons in the cosmic rays. E. Schopper[2] made a similar observation. Recently, W. Heitler[3,4] and his co-workers have investigated the nature of the radiation producing heavy cosmic-ray particles by means of the photographic plate kept exposed at Jungfraujoch under different thicknesses of lead plate. They come to the conclusion that there are at least two components in the cosmic radiation producing heavy particle, the first of which is very little absorbed in lead and consists very probably of neutrons. The other has a transition curve in lead very similar to that of the soft component of the cosmic radiation (electrons and light quanta). E. Fünfer,[5] using a boron-lined proportional counter and a proportional amplifier, determined the neutron intensity at the sea-level and reported a rapid increase of this intensity with elevation up to the top of Zugspitze, 2650 metres, corresponding to 7·5 metres of water. V. Halban, Kowarski and Magat,[6] measured the neutron intensity at higher altitudes, by studying the radioactivity induced in bromine to altitudes of about 3 metres of water. Recently, Korff[7] has developed new G.-M. counter methods for detecting thermal neutrons in radio-recording unmanned balloon flights, attaining a maximum altitude of ½ metre of water. For the detection of slow neutrons, he used argon-boron trifluoride mixture, which has got the special property of producing big pulses, even when the counter voltage is lowered about 200 volts

* Communicated by the Indian Physical Society.

below the threshold. C. G. Montgomery and D. D. Montgomery[8] used an ionization chamber, enclosed within a glass envelope and filled with BF_3 gas at about the atmospheric pressure. The alpha-particles resulting from the $_5B^{10}$ (n, α) $_3Li^7$ reaction produced voltage pulses which were recorded as galvanometer kicks in a photographic paper. The size-frequency distribution of the pulses was recorded. So far it was assumed that the disintegration of $_5B^{10}$ by slow neutrons took place only according to the reaction $_5B^{10}$ (n, α) $_3Li^7$, but recently Fisk and Maurer,[9] by means of detailed investigation have shown that another energetically possible reaction $_5B^{10}$ (n, p) $_4Be^{10}$ also occurred.

The present experiments were undertaken with the following objects in view :

(*i*) to determine the intensity of thermal neutrons at the sea-level and its variation with higher elevations,

(*ii*) to study the energy-spectrum of the particles produced during the disintegration of boron by slow atmospheric neutrons at high altitudes and to compare the results obtained with those of Fisk and Maurer.

The investigations are being continued, here a report is given of the preliminary results obtained.

II EXPERIMENTAL METHODS AND RESULTS

Two different sets of experiments were undertaken for the above purposes :

(*i*) The neutron intensity measurements at Calcutta (height 70 ft.) and at Darjeeling (height 7000 ft., equivalent water depth 8·1 metres from top of atmosphere), have been done with a boron-lined proportional counter tube and a proportional amplifier. It is proposed to extend the measurements to higher altitudes.

(*ii*) Preliminary measurements on the energy-spectrum have been made only at Darjeeling with an ionization chamber filled with boron trifluoride gas and a linear amplifier.

PROPORTIONAL COUNTER TUBE METHOD

The counter tube consisted of a brass cylinder of thickness 1·5 mm., internal diameter about 8 cms. and effective length 48 cms., with a central thin tungsten wire. The end-pieces consisted of ebonite plates with central plugs of amber and corresponding guard rings. The inner surface of the cylinder was coated with a layer of amorphous boron powder of thickness about 3·0 mgm. per cm^2. Such tubes were filled with argon, argon-tetrachloride and argon-boron trifluoride gaseous mixtures and the regions of proportionality for the tubes filled with the different gas mixtures were investigated. As found out by Korff, the sub-threshold region was found to be extremely narrow in the case of pure argon but spread over a range of voltage about 80 volts in the case of argon-boron

trifluoride mixture over which ionization pulses could be observed. We got a plateau extending about 20 volts over which the number of neutron counts was found to be constant. The pressure used was 8 cms. (5 cms. BF_3 + 3 cms. Argon) and the voltage applied was about 1000 volts. The collecting electrode was directly connected to the grid of a R. C. A. 6J7G tube and subsequent amplification was done by two other stages of pentodes. A neutron in region of boron entering such a counter may cause the disintegration of a $_5B^{10}$ nucleus and the ionisation due to the products will be detected by the proportional amplifier. The pulses could either be heard in a pair of headphones capacitatively coupled or recorded as usual, in a telephone-meter. Counts were taken when the counter with the first vacuum tube was kept inside a metal-lined thin wooden box and again when the entire assembly was placed within a thick borax shield. In our case the residual back-ground count with the borax shield has been found to be very small compared to that found by Fünfer with his boron-lined proportional counter This may be partly due to careful polishing of the internal surface and partly due to the rather thick internal coating of boron (3 mgm./cm.^{2}) which absorbed the alpha-particles due to contamination of the material of the counter. At Darjeeling the counts were taken at the commencement of the monsoon when the humidity was near about 100% and so special precautions had to be taken to avoid spurious counts due to leakage.

TABLE I

	Within borax shield	Without shield	Neutrons per minute
Calcutta (70 ft) ...	0·25 ± 0·02	1·17 ± 0·05	0·92 ± 0·06
Darjeeling (7000 ft) ...	0·4 ± 0·05	3·5 ± 0·2	3·1 ± 0·2

IONISATION CHAMBER METHOD

An ionization chamber was taken in the form of a thin copper cylinder, 42 cms. long and 4·8 cms. in diameter, with a thin central wire as the collecting electrode. The whole system was enclosed in a glass envelope and filled with boron-trifluoride gas at about 57 cms. pressure. A steady potential of 600 volts was supplied to collect the ions. A linear amplifier, the details of whose construction will be described elsewhere, was used for the requisite amplification. The collecting electrode was directly connected to the grid of an electrometer

tube. The voltage pulses caused by the disintegration of boron nuclei, were observed as kicks in a cathode-ray oscillograph. The lengths of the kicks were visually measured with the aid of a ruled transparent screen which could be placed against the fluorescent screen of the oscillograph. Evidently the measurements are not so accurate as those in which the voltage pulses are photographically recorded by a loop oscillograph. Two sets of observations were taken; once when the ionization chamber with its metal container was kept within a thick borax shield and again when the shield was removed. The difference gave the number of disintegrations of boron nuclei produced by atmospheric neutrons. Our ionization chamber being rather small in size, the sea-level intensity cannot be determined with precision. Use has been made of the sea-level data for neutrons obtained by Montgomery and Montgomery using a larger ionisation chamber. Table II gives the neutron intensity as measured at Darjeeling with the ionization chamber.

TABLE II

	Within borax shield	Without shield	Neutrons per minute
Darjeeling (7000 ft.) ...	1.37 ± 0.15	3.80 ± 0.22	2.43 ± 0.25

From Table II we find that the number of counts due to slow neutrons is $(2.43 \pm 0.25) \times 60 = 145.80 \pm 15$ per hour, for an ionisation chamber with an effective volume of 765 cms. and containing BF_3 gas at a pressure of 57 cms. To compare the relative intensity of the slow neutrons at Darjeeling and Calcutta, we proceed as follows:

If n is the number of counts per second of such a counter in the $\frac{1}{v}$ region, n is given by

$$n = \rho \sigma_B v_B . N p_B c_B V.$$

where σ_B is the capture cross-section of ${}_5B^{10}$ for neutrons of velocity v_B.

N is the Loschmidt number.

p_B is the pressure of BF_3 in the counter.

V is the volume of the counter in ccs.

ρ is the density of neutrons per cc. of all velocities within the energy range for which $\frac{1}{v}$ law holds.

We give below in Table III the data for neutron counts obtained by Montgomerys and ourselves.

TABLE III

Investigator	Altitude	Volume of ionisation counter in ccs.	Pressure cms.	No. of counts per hour.
Montgomery and Montgomery[8]	sea-level	1540	74	91 ± 7
Author ...	8·1 metres of water.	765	57	146 ± 15

Converted to the pressure and volume used in Montgomerys' investigation, our No. of counts per hour comes to about 388, and the ratio of the counts at

$$\frac{\text{Darjeeling}}{\text{Calcutta}} = \frac{388}{91} \sim 4.2.$$

Figure 1 depicts the size-frequency distribution of the energies of the disintegration particles from boron by the action of atmospheric neutrons. It is the difference between the size-frequency distribution curves of the particles when the ionization chamber is shielded with borax from that when the shield is uncovered.

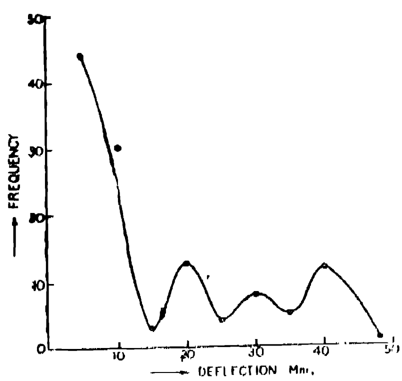

FIGURE 1

Comparison can be made with the energy-distribution curve found by Fisk and Maurer of the disintegration products of boron due to slow neutrons. The positions of the maxima found by them are at 0.4, 2.3, 2.5, 3.5 M. eV. and minima at 1.5, 3.2, 3.7 M. eV. Our energy-distribution curve is roughly in agreement with the above, only we have another maximum near 4.0 M. eV. According to the above investigators, the first maximum is attributed to the emission of protons, due to the process ${}_5B^{10}(n, p){}_4Be^{10}$, and other maxima are due to the emission of α-particles according to the reaction ${}_5B^{10}(n, \alpha){}_3Li^7$.

Further investigation is proceeding with a loop oscillograph for photographically recording the amplitude of deflections in place of visual observations with a cathode-ray oscillograph.

DISCUSSION OF RESULTS

We find the ratio of the intensities of cosmic-ray neutrons with the $\frac{1}{v}$ range of boron for the elevation of Calcutta and Darjeeling (8.1 metres of water) comes out to be

(*i*) with proportional counter $= \frac{3.1}{.92} \sim 3.4$ and

(*ii*) with ionisation chamber taking Montgomery and Montgomery's reading at sea-level, $\frac{388}{91} \sim 4.2$.

According to Korff, the ratio of the neutron intensity at altitude 8.1 metres of water to that at sea-level is about 3.9, which is comparable with our results. In our experiments we think our result with the ionisation-chamber counter to be more accurate than the result obtained with the proportional counter.

ACKNOWLEDGMENT

The author expresses his grateful thanks to Prof. D. M. Bose, Director, Bose Research Institute, for his constant help and guidance.

Bose Research Institute,
93, Upper Circular Road,
Calcutta.

REFERENCES

1 Rumbaugh and Locher, *Nat. Geog. Soc. Contr. Tech. Papers, Stratosphere series* No. 32-36 (1936).
2 E. Schopper, *Naturwiss*, **25**, 557 (1937).
3 W. Heitler, Powell and Fertel, *Nature*, **144**, 283 (1939).
4 W. Heitler, Powell and H. Heitler, *ibid.*, **146**, 65 (1940).
5 E. Fünfer, *Zeits. f. Phys.*, **111**, 351 (1938).
6 Halban, Kowarski and Magat., *C. R.*, **208**, 572 (1939).
7 S. A. Korff., *Rev. Mod. Phys.*, **11**, 213 (1939).
8 C. G. Montgomery and D. D. Montgomery, *Phys. Rev.*, **56**, 10 (1939).
9 Maurer and Fisk, *Zeits. f. Phys.*, **112**, 436 (1939).

ADSORPTION OF MOISTURE FROM THE MOIST AIR BY THE SOILS

BY L. D. MAHAJAN, M.Sc., PH.D., F.INST. P.
Mahendra College, Patiala

(*Received for publication, September 10, 1940*)

ABSTRACT. A method has been devised to study the adsorption of moisture from the moist air by the soils inside the laboratory. Various factors which influence such adsorption have been studied and the following results are obtained :--

(1) The adsorption of moisture from the moist air by the soils increases with the increase of range of humidity. It is comparatively higher in the beginning than in the end. (2) The rate of adsorption of moisture from the moist air increases with the increase of thickness of of the layer of the soil up to a certain limit depending upon the quality of the soil. This rapidly decreases with the depth of the layer from the upper exposed surface. (3) Adsorption increases with the time but the rate of adsorption is high in the beginning and regularly slackens on as the time elapses. It is proportional to the logarithm of the time exposure. (4) Adsorption decreases with the size of the particles or groups of particles (clods) and their proportion in the soil. (5) Adsorption depends upon the physical and chemical constituents of the soil.

The discussion of each factor is given in detail.

INTRODUCTION

Much work has already been done on the soil moisture in the past. In 1934, L. A. Ramdas and M. S. Kati [1] showed that the phenomenon of the evaporation of moisture from a soil surface containing only hygroscopic water and the reverse phenomenon during night exert a controlling influence on the distribution of moisture with height in the air layers and that during the evaporating regime the pressure of the water vapour decreases with height, whereas during the adsorbing regime the pressure of the water vapour increases with height. In 1936, they [2] studied the diurnal variations in the moisture content by two-hourly measurements with representative soils from different parts of the country, the soils being exposed under identical conditions in the Agricultural Meteorological Observatory at Poona. The moisture content of the surface layers of the soil in the bare ground of the same observatory were also measured. Experiments on the adsorption of moisture by dry soils and measurements of various related physical properties of typical soils were also made. In all these cases, the soils have been used as they occur, *i.e.*, without separating them into their components by mechanical or chemical analysis, and the meteorological aspect has been kept in the fore-front.

In order to study the above, the above-mentioned workers and others used such methods where the samples of the soils were kept either outside in the open field or inside the louvered screen. In both these methods the experiments were intended to reveal the phenomenon of adsorption and desorption of moisture under actual field conditions.

But these methods, from the point of view of a physicist, cannot be used for the general study of adsorption of moisture from the moist air by the soils, as in both of these methods, the variation of humidity is at the mercy of the weather and observations have to be extended over a long period, otherwise a great range of variation of humidity is not possible. The humidity cannot be kept constant for any length of time. Besides there is possibility of dust or fine particles of dust which are more or less always hanging in the air, depositing on the samples of the soils.

In order to avoid these difficulties, the author [3] has devised a simple apparatus by which the humidity can be varied within a great range, even from 0 to 100% quite easily and it can, if desired, be kept constant for any length of time. The possibility of the dust particles depositing on the samples of the soils is completely avoided.

With this apparatus, the adsorption of moisture from the moist air by the soils and the exchange of moisture between the earth and the air has been studied *in this laboratory*. The effects of the humidity of the air, the thickness of the layer of the soil, the time for which the soils are exposed to the moist air, the size of the particles of the soil, the quantity of the clods in the soil, and the physical and chemical constituents of the soils on the rate of adsorption of moisture by the soils has been studied and the relations which exist between them have been traced out in the following lines.

THE APPARATUS

In this apparatus, the use of Professor J. B. Seth's method [4] for production of a current of dry or moist air of any desired percentage of humidity has been used. The currents of dry or moist air of suitable strength are sent into a chamber and any constant humidity is regulated. A small quantity of the soil in a dish is kept inside it at almost normal pressure. After keeping it there for some definite time, it is removed and weighed and its hygroscopic or adsorption power is calculated. The pressure inside it is kept constant and is measured with a mercury manometer. This chamber is connected with another similar chamber which in turn is connected with an exhausting pump or an aspirator. Thus the effect of rapid flow of air due to the exhausting pump or any other devise is avoided. In order to record the humidity, a well-tested and calibrated hair hygrometer is kept hanging in the first chamber and for its varification a wet and dry blub hygrometer is kept in the second chamber.

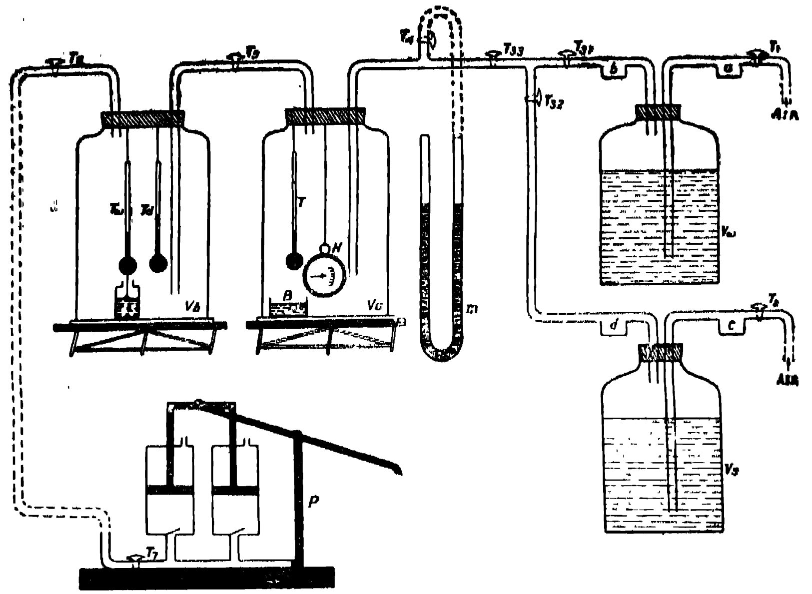

FIGURE I

Construction :—The details of the apparatus are shown in fig. 1 (line sketch), where V_w and V_s are two-litre capacity bottles containing pure water and strong sulphuric acid respectively, m a mercury manometer, and P a double-action exhausting pump. V_a and V_b are two glass chambers without bottoms. At their bottoms are placed two separate glass plates with rubber discs on them which make them fairly air-tight. There are two tubes opening inside the vessel V_a, one being an inlet from the source for a current of dry or wet air and the other an outlet for the enclosed air to the exhausting pump or an aspirator. T_d and T_w are dry and wet bulb thermometers. a, b, c and d are four glass traps on both sides of the liquid bottles in order to avoid the flow of the liquids on either side. T_1, T_2, T_3, T_4, T_5, T_6, and T_7 are stop-cocks fitted at various places to control the current of air and are used according to the needs.

Working :—The double-action air pump is worked so as to create a low pressure in chamber V_b. This causes a current of air to flow from outside through any of the liquids in the vessels V_w and V_s. This current of air passes through the chamber V_a after affecting the pressure of the mercury manometer on its way and fills the low-pressure space in the chamber V_b. If an aspirator is used instead of the exhausting pump, a regular current goes on flowing in from outside to the chamber V_b and also affects the humidity of the air inside the chamber V_a. If humidity is to be decreased, T_2 is opened and T_1 is closed, or if humidity is to be increased, T_2 is closed and T_1 is opened. In the former case the current of air while bubbling through sulphuric acid is devoid of its moisture and lowers the % humidity, while in the latter case the air when bubbling through water carries moisture with it and increases the humidity. If a current of air is regulated any constant humidity for any length of time can be

arranged inside the chambers. Having known the weight of the empty dish B and of the soil in it before placing it inside the chamber and after exposure to the new humidity for any definite period of time, the increase or decrease in weight of the soil for the corresponding variation of humidity can be known. The dish can be taken out of the chamber by removing the bottom plate from below.

OBSERVATIONS

With a few samples of soil taken from the Botanical Garden of this college, several observations have been taken. The effects of various factors which influence the adsorption of moisture from the moist air by the soils have been studied with these samples and a few sets of observations are given below :—

1. HUMIDITY OF THE SURROUNDING AIR

For this purpose a flat-bottomed dish having cross-sectional area 10·36 sq. cms. was filled with a fine soil having layer of thickness 20·6 mm. and was exposed to the moist air of various humidities for a constant period of time 24 hours. The increase in weight for the corresponding increase in humidity was determined in each case. Several sets of observations were recorded and a typical set of observations is given below.

TABLE I

Kind of soil : fine

No.	Initial wt. in gm.	Final wt. in gm.	Initial % Humidity	Final % Humidity	Increase in % Humidity	Increase in wt in gm.
1	61·7125	61·7635	18	22	4	0·0510
2	,,	61·8020	,,	28	10	0·0895
3	,,	61·8955	,,	42	24	0·1832
4	,,	61·9600	,,	55	37	0·2475
5	,,	61·9750	,,	59	41	0·2625
6	,,	61·9945	,,	64	46	0·2820
7	,,	62·0005	,,	80	62	0·2880

The above observations are also shown by a curve in fig. 2 which indicates the behaviour of the fine soil with the increase of humidity of the surrounding air.

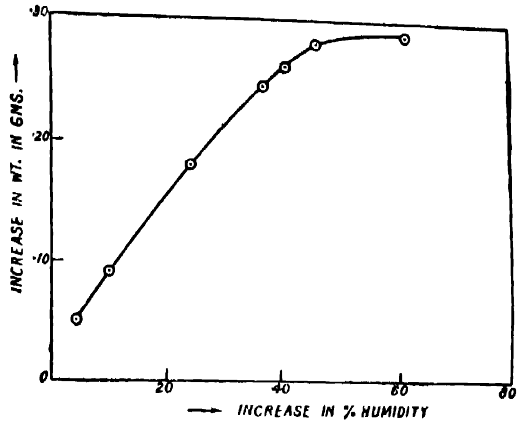

FIGURE 2

Some sets of observations were recorded with the sandy soil which contained about 95% of pure sand. The surface area exposed to the moist air, the thickness of the layer of soil and the time ofexposure were kept the same as in Table I. A set of such observations is recorded below :

TABLE II

Kind of soil : sand

No.	Initial wt. in gms.	Final wt. in gms.	Initial % Humidity	Final % Humidity	Increase in % Humidity	Increase in wt. in gm.
1	82·9550	82·9560	20	26	6	0·0010
2	,,	82·9580	20	28	8	0·0030
3	,,	82·9635	24	36	12	0·0085
4	,,	82·9660	20	37	17	0·0110
5	,,	82·9815	20	55	35	0·0265
6	,,	82·9820	20	64	44	0·0270

The above results are also shown by a curve in fig. 3 which shows the behaviour of the sandy soil with the increase of humidity of the surrounding air. This soil being almost a sand has very little power of adsorption of moisture from the moist air, however for a longer period it may be kept exposed to it.

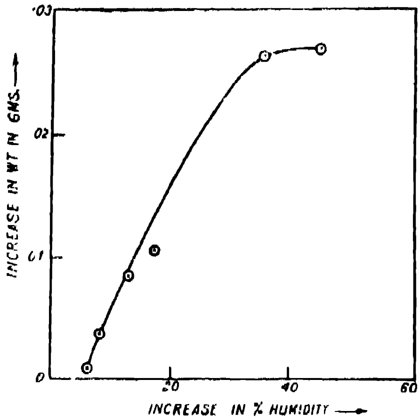

FIGURE 3

Both the above-mentioned curves are of the same shape and indicate that the adsorption of moisture from the moist air by any kind of soil increases with the increase of relative humidity of the surrounding air. The rate of increase in weight, *i.e.*, the adsorption of moisture is comparatively high in the beginning and slow later on. Thus it is evident that the rate of adsorption of moisture slowly decreases with the increase of relative humidity.

2. THICKNESS OF THE LAYER OF SOIL

The effect of the thickness of the layer of the soil was studied by using the same flat-bottomed dish of glass having cross-sectional area 10·36 sq. cm. Time exposure (two hours) and the range of variation of relative humidity (60 to 80%) were kept constant and the thickness of the layer of the soil was varied. With this arrangement several observations were recorded. A set of observations is given below in table III.

TABLE III

Kind of soil : fine

No.	Initial wt. in gms.	Final wt. in gms.	Thickness of layer of soil in mm.	Increase in wt. in gm.
1	8·3050	8·3370	3·0 mm.	0·0320
2	21·8630	21·9310	7·2 ,,	0·0680
3	35·4235	35·5010	11·8 ,,	0·0775
4	61·9750	62·0550	20·6 ,,	0·0800
5	86·0755	86·1660	28·6 ,,	0·0905
6	133·0685	133·1605	44·3 ,,	0·0920

The above results are also shown by a curve in fig. 4 which represents the variation in adsorption with the thickness of the layer of the soil. The amount of moisture adsorbed by any kind of soil increases with the thickness of the layer of the soil up to a certain limit which varies according to the quality of the soil.

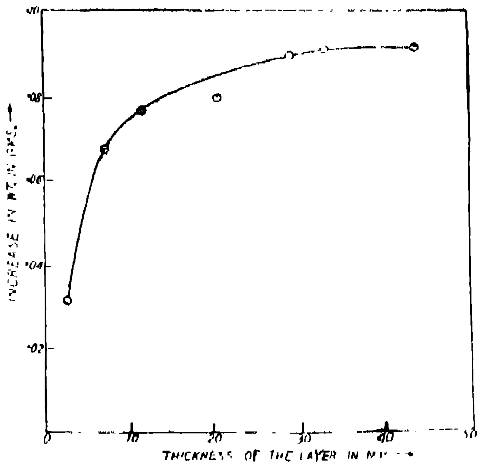

FIGURE 4

The upper layers adsorb much more moisture than the lower layers of the same thickness. The rate of adsorption rapidly goes on decreasing with the depth of the layer from the upper surface which is exposed to the moist air directly, and it is self-evident from the cuive itself. The following data is deduced from the same curve :

The increase in weight for	3 to 10 mm. layer is	0·042	gm.
,, ,, ,, ,,	10 to 20 mm. layer ,,	0·011	gm.
,, ,, ,, ,,	20 to 30 mm. layer ,,	0·005	gm.
,, ,, ,, ,,	30 to 40 mm. layer ,,	0·0015	gm.

The layer which is at a depth of 3 mm. from the directly exposed surface and 7 mm. thick adsorbs 0·042 gm. of moisture from the moist air while a layer which is at a depth of 10 mm. from the exposed surface and 10 mm. thick adsorbs only 0·011 gm. Similarly a layer which is at a depth of 20 mm. and 10 mm. thick adsorbes 0·005 gms. and a layer which is at a depth of 30 mm. and 10 mm. thick adsorbs only about 0·0015 gm. which is negligible. Thus it is quite evident that beyond a depth of about 4 mm. almost no effect of adsorption is noticeable. It is merely the superficial layer which can adsorb the moisture from the moist air and very low layers remain quite unaffected.

3. TIME

The effect of time on adsorption of moisture from the moist air by soils was studied with the same apparatus. The same flat-bottomed dish of glass, having

crosss-sectional area 10·36 sq. cm. was used. The range of variation of humidity (50 to 65%) and thickness of the layer of fine soil (44·3 mm.) were kept constant, while the time period for which a sample of soil was exposed to the moist air was varied. Several sets of observations were recorded and one of those sets is given below :—

TABLE IV

Kind of soil: fine

No.	Initial wt. in gm.	Final wt. in gm.	Time of exposure in minutes	Logarithm of time	Increase in wt. in gm.
1	132·7625	132·8205	12 min.	1·0792	0·0580
2	,,	132·8285	18 ,,	1·2553	0·0660
3	,,	132·8375	30 ,,	1·4771	0·0750
4	,,	132·8695	66 ,,	1·8195	0·1070
5	,,	132·8745	120 ,,	2·0792	0·1120
6	,,	132·8815	180 ,,	2·2553	0·1190

A curve (fig. 5*a*) has been drawn showing the relation between the increase in weight of the soil due to adsorption of moisture from the moist air and the time in minutes. This indicates that the amount of adsorption increases with time but the process of adsorption is rapid in the initial stages and slackens on as the time elapses. In other words the rate of adsorption decreases with time.

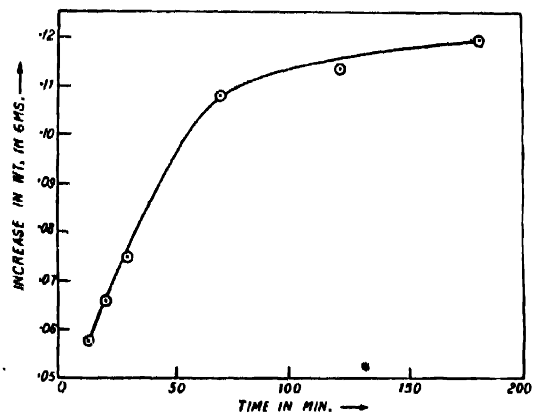

FIGURE 5(*a*)

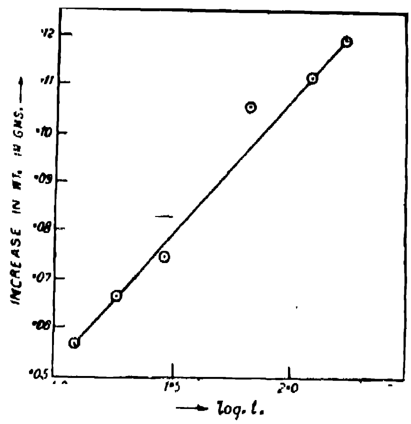

FIGURE 5(*b*)

The study of the relation between these two variable factors shows that if a curve (fig. 5*b*) be drawn between the logarithm of time and increase in weight of the soil a straight line is obtained, which leads to the conclusion that the amount of moisture adsorbed from the moist air by the soils is directly pro-

portional to the logarithm of time for which the soil sample is exposed to the moist air. Thus the relation is logarithmic.

4. SIZE OF THE PARTICLES

In order to study the effect of the size of the particles and groups of particles, *i.e.*, clods of the soil on the adsorption of moisture, the same flat-bottomed dish was used. The range of variation of humidity (80 to 90%) and the thickness of the layer of the soil (16 mm.) were kept constant. Two samples of the soil were used, one being in its natural condition having a large number of thick particles of soil and clods and the other being a finely powdered soil obtained from the natural soil by grinding it. The following sets of observations were recorded :

TABLE V

No.	Kind of soil	Initial wt. in gm.	Final wt. in gm	Time of exposure	Increase in wt. in gm.
1	Finely powdered	81·9825	82·0025	60 min	0·0200
	Natural	79·3390	79·3450	,,	0·0060
2	Finely powdered	81·9825	82·0735	24 hours	0·0910
	Natural	79·3390	79·3980	,,	0·0590
3	Finely powdered	81·9825	82·0695	20 hours	0·0870
	Natural	79·3390	79·3900	,,	0·0510

The above observations show that the adsorption is much smaller in natural soil than in finely powdered soil. In other words, the amount of moisture adsorbed from the moist air decreases with the increase of size of the particles and groups of particles (clods) and also their proportion in the soil.

The reasons for less adsorption in the natural soil possibly appear to be that (*i*) less surface is exposed to the moist air when there are large-sized particles and clods in the soil and (*ii*) the capillary action is much smaller in this case as the interspaces between the particles become large due to large size of the particles.

5. CHEMICAL AND PHYSICAL CONSTITUENTS

The comparison of observations in tables I and II shows that the adsorption of moisture from the moist air is much more in fine clay soil than in the sandy soil. If the quantity of sand in any soil increases, the amount of adsorption decreases in the same ratio. The rate of adsorption of moisture from the moist air also depends on the chemical constituents of the soil.

RESULTS

The following results have been concluded from the study of various factors influencing adsorption of moisture from the moist air by the soils :

1. The adsorption of moisture from the moist air by the soils increases with the increase of range of humidity. It is comparatively higher in the beginning than in the end.

2. The rate of adsorption of moisture from the moist air increases with the increase of thickness of the layer of the soil up to a certain limit depending upon the quality of soil. This rapidly decreases with the depth of the layer from the upper exposed surface.

3. Adsorption increases with time but the rate of adsorption is high in the beginning and regularly slackens on as the time elapses. It is proportional to the logarithm of the time of exposure.

4. Adsorption decreases with the size of the particles or groups of particles (clods) and their proportion in the soil.

5. Adsorption depends upon the physical and chemical constituents of the soil.

CONCLUSIONS

The above-mentioned results throw light on the work done in the past. The study of the comparison of hygroscopic property of the Patiala soil with other Indian soils and the effects of other influencing factors on them is in progress in this laboratory and shall be published in due course of time.

The author is indebted to His Highness's Government, Patiala, for providing facilities to carry out the above work in the Research Laboratory of the Mahendra College, Patiala. My grateful thanks are due to Dr. L. A. Ram Das, Agricultural Meteorologist of the India Meteorological Office, Poona, for providing me with some of his research papers and of various others for reference use only.

PHYSICS RESEARCH LABORATORY,
MAHENDRA COLLEGE, PATIALA,
PATIALA STATE.

REFERENCES

[1] L. A. Ramdas and M. S. Kati, *Ind. Jour. Agri. Science*, Vol. IV, Part 6 (1934).

[2] ,, ,, ,, ,, , *Ind. Jour. Agri. Science*, Vol. VI, Part 6 (1936); L. A. Ramdas and A. K. Mallik, *Current Science*, Vol. VI, No. 9 (1938).

[3] L. D. Mahajan, *Science and Culture*, Vol. VI, p. 120 (1940).

[4] J. B. Seth, *Nature*, Vol. 128, pp. 638-639 (1931).

PENETRATION OF THIN IONOSPHERIC LAYERS *

By A. C. DEB, M.Sc.
Ghose Research Scholar in Physics, Calcutta University

ABSTRACT. Reflection coefficient of a thin ionospheric region, having parabolic ionisation gradient, has been deduced by adapting the B. W. K. method of computation as applied in the case of a parabolic potential barrier. It is found that the reflection co-efficient of such a region is ·5 and not zero at the so-called critical frequency.

Two curves, one for the E- and the other for the F-region have been drawn depicting the variation of reflection coefficient with frequency. It is found that the transition from complete reflection to complete penetration takes place more suddenly for Region F than for Region E. Complete penetration is effected when $\Delta f/\sqrt{f_0}$ is approximately 50 for Region E and 30 for Region F. (f_0 critical frequency, Δf departure of wave frequency from f_0).

INTRODUCTION

According to the Eccles-Larmor formula the refractive index μ of an ionised gas is given by

$$\mu^2 = 1 - \frac{4\pi e^2}{mp^2}N \qquad \ldots \quad (1)$$

where N is the electron density and p the pulsatance of the wave.

It follows that a wave of frequency f incident vertically on an ionospheric region of maximum density N_{max} will either be transmitted or totally reflected by the layer according as f is greater or less than

$$f_0 = \left[\frac{N_{max}e^2}{\pi m}\right]^{\frac{1}{2}} . \qquad \ldots \quad (2)$$

Now in actual experiment it is found that the same wave is reflected both from Regions E and F. This means that there is not total but partial reflection from Region E for frequencies not far removed from the critical frequency. This anomalous result can be explained if it is remembered that the ray treatment of geometrical optics—after which the reflection and penetration condition (2) has been obtained—ceases to be valid when f approaches f_0. This is because [1] when $\mu \rightarrow 0$ the wavelength $\lambda \rightarrow \infty$ and, it is well known that simple treatment of geometrical optics fails when the refractive index of a medium varies appreciably in the distance of a wavelength. The case of the penetration

* Communicated by the Indian Physical Society.

of an ionospheric region, by exploring waves of frequencies near the critical frequency f_0, has therefore to be treated according to wave optics rather than according to geometrical optics. This has been done by several workers[2] and among the recent ones we may mention the work of Saha and Rai. These authors have adapted the famous treatment of Gamow[3] on calculation of the transparency of the potential barrier surrounding an atomic nucleus to the problem of propagation of electromagnetic waves through an ionospheric "electron-barrier." For numerical calculations they have assumed a linear gradient (the outline of the barrier being in the form of an isosceles triangle) and obtained the interesting result that "the amount of energy transmitted falls to half its value for the assumed form of the barrier and for a gradient of electron density characteristic of F layer, if the half breadth of the barrier is about 1·5 km."

Recent observations show that, though the complete form of the electron barrier may not have any simple geometric form, the portion of it near the maximum electron density (which is determinative of the penetration frequency) has the simple form of a parabola. The transparency coefficient of a potential barrier of this form has already been calculated in quantum mechanics by the well-known B. W. K. method and in the present paper this method has been adapted for determining the reflection co-efficients of ionospheric regions having distribution of electron density of similar form.

DISTRIBUTION OF ELECTRON DENSITY

It has been shown by Appleton[4] that according to Chapman's theory of ionised region formation by the action of monochromatic radiation, the electron density N at any level is given by

$$N = N_{max}\left(1 - \frac{Z^2}{4H^2}\right) \qquad \dots \quad (3)$$

where Z is the distance of the level measured from the level of maximum ionisation and $H = \frac{RT}{Mg}$ the "scale height" for the region. This relation is valid for values of Z up to $Z = H$.

The distribution of N with height is thus parabolic near the level of maximum ionisation.

This conclusion has also been confirmed by experiments of Appleton.[5] He compared experimental $P'-f$ curves with those obtained by theoretical calculation made on the assumption of a parabolic gradient and found that the two curves are in substantial agreement.

CALCULATION OF THE REFLECTION COEFFICIENT FOR A PARABOLIC GRADIENT

The equation of a plane wave in a medium of refractive index μ is given by

$$\frac{d^2\psi}{dz^2} = -\left(\frac{2\pi}{\lambda}\right)^2 \mu^2 \psi$$

where λ is the wavelength in vacuum.

For an ionised layer, the refractive index of a wave of pulsatance p is given by equation (1).

If the ionosphere is horizontally stratified and the z-axis is taken in the upward direction then the equation for vertical propagation becomes

$$\frac{d^2\psi}{dz^2} = -\left(\frac{2\pi}{\lambda}\right)^2 \left(1 - \frac{4\pi e^2 N}{mp^2}\right)\psi.$$

The wave-length in the medium is no longer constant and varies as N varies being equal to $\frac{\lambda_{vac}}{\mu}$. Putting $u = \frac{zp}{c}$ and $p_0^2 = \frac{4\pi e^2 N}{m}$, we have

$$\frac{d^2\psi}{du^2} + (1 - p_0^2/p^2)\psi = 0. \qquad \ldots \quad (4)$$

The above equation is for a field-free space. If there be a magnetic field, the equation is profoundly modified. The refractive index becomes complex and is given by the well-known Appleton-Hartree formula. In this case the action of the terrestrial magnetic field may be eliminated by a suitable choice of the direction of propagation of the wave. If the propagation be in a vertical plane in the magnetic equator and the direction of the electric vector of the wave is parallel to the magnetic lines of force then the oscillations of the electrons and ions due to the passage of the wave are not affected. Equation (4) can therefore be applied for the ionospheric exploration by vertical propagation near the magnetic equator when the wave is plane-polarised with the direction of the electric vector north-south.

Now, making the substitutions

$$N = mp_0^2/4\pi e^2$$

$$N_{max} = \frac{mp_{max}^2}{4\pi e^2}$$

and

$$z = cu/p,$$

in equation (3), we derive the relation

$$\frac{p_0^2}{p^2}=\frac{p_{max}^2}{p^2}-\frac{\pi^2 f_0^2 c^2}{H^2 p^4}u^2$$

$$=\frac{p_{max}^2}{p^2}-a^2u^2 \qquad \dots \quad (5)$$

which also is an equation of parabola corresponding to equation (3) with $H^2p^4/\pi^2 f_0^2 c^2$ as the latus-rectum.

Substituting the value of p_0^2/p^2 in equation (4) we get the relation

$$\frac{d^2\psi}{du^2}+(\beta+a^2u^2)\psi=0,$$

where $$\beta=1-p_{max}^2/p^2.$$

The solution of this differential equation giving the equation of reflected and transmitted wave has already been obtained by Kemble with the help of the B. W. K. approximation functions and Krammer's connection formula for the passage of ψ-waves through a potential barrier of parabolic form. Corresponding to the dependence, in quantum mechanics, of the refractive index of the ψ-waves upon the potential, we have the dependence of the same, for the radio-waves in ionosphere, upon the electron density N The potential barrier for ψ-wave thus corresponds to "electron-barrier" for radio-waves.

Without going through the calculations we can therefore write out at once, after Kemble,[6] the expression for T, the transmission coefficient of the radio-waves through the electron-barrier.

For $f<f_0$

$$T=\frac{1}{1+e^{2K}}, \qquad \dots \quad (6)$$

where $$K=\int_{u_1}^{u_2}\sqrt{1-p_0^2/p^2}\,d\xi \qquad \dots \quad (7)$$

and $$\xi=\sqrt{a}\,u.$$

The limits u_1 and u_2 are the values of u where the line $p_0^2/p^2=1$ cuts the electron-barrier. The significance of these limits will be readily understood from a reference to Fig. 1. u_1 represents the distance measured downwards in the

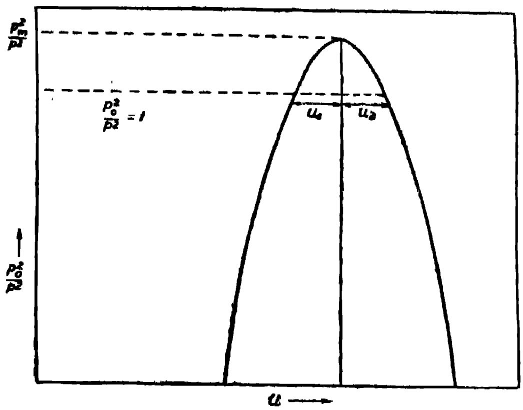

FIGURE 1

ionised layer from the level of maximum ionisation, to the point to which the wave of frequency p would penetrate according to the ray treatment. In other words, u_1 marks the position of the level at which total reflection ought to take place. The wave treatment shows, however, that a fraction of the wave will be transmitted beyond this level and this fraction is given by equation (6). In order to evalute T we have to find the value of the integral (7). If we take the point where the line $p_0^2/p^2=1$ cuts the axis of the parabola as origin, equation (5) may be written as

$$1-p_0^2/p^2=\alpha^2u^2.$$

Hence $$K=\alpha^{\frac{3}{2}}\, 2\int_0^{u_0} u\,du,$$

where $u_0=u_1=u_2$ is the half-breadth of the barrier. Or, since u_0^2 is equal to $\dfrac{\frac{p_m^2}{p^2}-1}{\alpha^2}$,

$$K=\alpha^{-\frac{1}{2}}\,\frac{p_m^2-p^2}{\alpha^2}$$

$$=2\pi\left(\frac{H}{\pi c}\right)^{\frac{1}{2}}\frac{1}{\sqrt{f_0}}\quad\frac{f_0^2-f^2}{f}$$

$$=4\cdot\left[\frac{\pi H}{c}\right]^{\frac{1}{2}}\frac{\Delta f}{\sqrt{f_0}}.$$

For any particular value of H, K can now be calculated for various values of $\Delta f/\sqrt{f_0}$ and the transmission coefficient determined therefrom. Fig. 2 shows

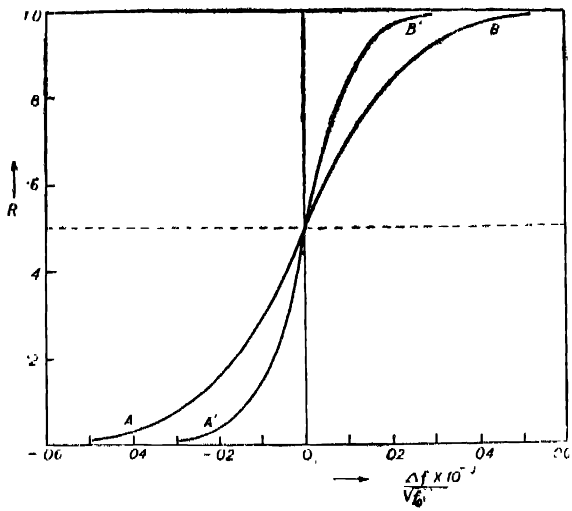

FIGURE 2

how reflection coefficient $R(=1-T)$ varies with the departure of the exploring frequency from the critical frequency f_0. The values of H^7 assumed for the calculation, are 11·4 km. for E-region (curve AB) and 50 km. for the F-region (curve A′B′). It shows how the reflection coefficient varies when the frequency of the exploring waves is decreased below the frequency of penetration.

For $f > f_0$, that is, for the case when the exploring wave frequency is *increased above* the penetration frequency, we are required to find out the value of u_0 when $p^2 > p_m^2$. In this case the line $p_0^2/p^2 = 1$ cuts the parabola in two imaginary points. u_0 being then imaginary, u_0^2 is real and negative and so also $K = u_0^{\frac{3}{2}} a^2$. Instead of (6) we now have

$$T = \frac{1}{1+e^{-2k}},$$

and the portion of the curve in Fig. 2, depicting the variation of $\Delta f/\sqrt{f_0}$ with R for the case $f > f_0$, can therefore be obtained by simply plotting R for Δf negative.

CONCLUSION

From the curves in Fig. 2 it is seen that the reflection coefficient is not zero for the so-called critical frequency. For the two cases considered it becomes so only when the frequency has been increased above the critical value by about 50 and 30 times of the square-roots of the critical frequencies. This shows that the reading of critical frequency from the $P'-f$ curve in the usual way, *i.e.*, by noting the frequency at which reflection from the ionised region ceases, entails a certain percentage of error.

A comparison of the two curves, for H = 11·4 km. and for H = 50 km. representing E- and F-regions respectively, shows that for a region which is more diffuse, a smaller percentage departure from f_0 is needed for complete penetration. In other words, for a difuse region, the transition from complete reflection to complete transmission is sharper.

ACKNOWLEDGMENT

The investigation was undertaken at the suggestion of Prof. S. K. Mitra to whom I express my sincere thanks for constant help and guidance.

WIRELESS LABORATORY,
UNIVERSITY COLLEGE OF SCIENCE,
92, UPPER CIRCULAR ROAD,
CALCUTTA

REFERENCES

[1] Appleton, *Reports on the Progress of Physics*, Vol. II, 133 (1936).

[2] Hartree, *Proc. Camb. Phil. Soc.*, **25**, 97 (1929); Saha and Rai, *Proc. Nat. Inst. Sci. India*, **3**, 359 (1937).

[3] Gamow, Atomic Nuclei and Nuclear Transformation (*Oxford University Press*), 94 (1937).

[4] Appleton, Naismith and Ingram, *Proc. Roy. Soc.* A, **51**, 81 (1939).

[5] Appleton, *Proc. Roy. Soc.* A., **162**, 451 (1937).

[6] Kemble *Phys. Rev.*, **48**, 549 (1935)

Appleton, *Q. Jour. Roy. Met. Soc.*, **65**, No. **281**, 324 (1939).

JOULE-THOMSON AND JOULE EFFECTS FOR BOSE-EINSTEIN AND FERMI-DIRAC GAS*

By B. N. SINGH
University of Delhi

(*Received for publication, July 25, 1940*)

ABSTRACT. The paper gives results for the Joule-Thomson effect and adiabatic process for a degenerate Bose-Einstein gas. A general formula for non-degenerate matter (both Fermi-Dirac and Bose-Einstein) is given and the region of transition from degeneracy to non-degeneracy in the Bose-Einstein gas is discussed in detail.

The second part of the paper discusses the Joule effect for the various cases of matter obeying either statistics.

Various properties of degenerate matter (degenerate in the sense of Fermi-Dirac and Bose-Einstein statistics) have been investigated in the last decade and a half, and the results have found numerous applications in various physical and astrophysical problems. Recently Kothari [1] discussed the Joule-Thomson effect and adiabatic process for a non-relativistic Fermi-Dirac degenerate gas, and Srivastava [2] has considered the non-relativistic non-degenerate cases of Fermi-Dirac statistics. Gogate [3] has extended the discussion to relativistic Fermi-Dirac degenerate and non-degenerate gas. However, the dicussion of Joule-Thomson effect and adiabatic process is incomplete, because the degenerate Bose-Einstein case has not been treated so far. London's theory of liquid He II has revived the interest in the properties of Bose-Einstein degenerate gas. The first part of the present paper deals with the Joule-Thomson effect and adiabatic change in Bose-Einstein gas. A general result for non-degeneracy has also been derived. In the second part the Joule effect has been calculated for both the statistics. It has been shown for both the phenomenon of Joule-Thomson effect and Joule effect that a Fermi-Dirac gas always gets heated and a Bose-Einstein gas is always cooled. For matter obeying Bose-Einstein statistics the region of transition from degeneracy to non-degeneracy has been studied in detail.

PART I—JOULE-THOMSON EFFECT

The non-degenerate case as mentioned already has been treated by Srivastava but here we shall derive a series expansion for the change in temperature produced by the throttling process.

* Communicated by the Indian Physical Society.

Classical thermodynamics gives the well-known relation

$$\left(\frac{\partial T}{\partial p}\right)_H = \frac{T\left(\frac{\partial V}{\partial T}\right)_p - V}{C_p} \qquad \dots \quad (1)$$

Let us consider an assembly of N particles occupying a volume V. Taking into account relativity mechanics the number of particles possessing the kinetic energy ϵ and lying in the range ϵ to $\epsilon + d\epsilon$ is given by

$$N(\epsilon)d\epsilon = \frac{a(\epsilon)}{\frac{1}{A}e^{\epsilon/kT} + \beta}, \qquad \dots \quad (2)$$

where $$a(\epsilon) = \frac{4\pi gV}{c^3h^3}(\epsilon^2 + 2mc^2\epsilon)^{\frac{1}{2}}(\epsilon + mc^2)d\epsilon.$$

Hence E the total kinetic energy for the assembly is given by

$$E = \int_0^\infty \frac{4\pi gV}{c^3h^3} \frac{(\epsilon^2 + 2mc^2\epsilon)^{\frac{1}{2}}(\epsilon + mc^2)\epsilon}{\frac{1}{A}e^{\epsilon/kT} + \beta} d\epsilon. \qquad \dots \quad (3)$$

However, considerable simplification is achieved by considering two extreme cases : (*i*) *completely non-relativistic case* and (*ii*) *completely relativistic case*. Equation (3) then reduces to

$$E = CV(kT)^{s+1} \int_0^\infty \frac{u^s}{\frac{1}{A}e^u + \beta} du, \qquad \dots \quad (4)^*$$

and also, if N denotes the total number of particles in the assembly (we shall take N to be equal to the Avogadro number, *i.e.*, $R = kN$), we have

$$N = CV(kT)^s \int_0^\infty \frac{u^{s-1}du}{\frac{1}{A}e^u + \beta} \qquad \dots \quad (4a)^*$$

where $u = \frac{\epsilon}{kT}$. In the non-relativistic case

$$s = 3/2 \quad \text{and} \quad C = \frac{2\pi g(2m)^{\frac{3}{2}}}{h^3}, \qquad \dots \quad (5)$$

and in the relativistic case

$$s = 3 \quad \text{and} \quad C = \frac{4\pi g}{c^3h^3}. \qquad \dots \quad (6)$$

* These follow immediately by assuming a general distribution law of the form

$$N(\epsilon)d\epsilon = CV(kT)^s \frac{u^{s-1}}{\frac{1}{A}e^u + \beta} du.$$

TABLE I

		Fermi-Dirac Statistics	Bose-Einstein Statistics
Non-degeneracy	(1) Non-relativistic	$E_+ = \frac{3}{2}RT\left[1+\frac{A_0}{2^{\frac{5}{2}}}-A_0^2\left(\frac{2}{3^{\frac{5}{2}}}-\frac{1}{4^{\frac{3}{2}}}\right)+A_0^3\left(\frac{3}{4^{\frac{5}{2}}}+\frac{5}{2^{\frac{11}{2}}}-\frac{3}{6^{\frac{3}{2}}}\right)\ldots\ldots\right]$	$E_- = \frac{3}{2}RT\left[1-\frac{A_0}{2^{\frac{5}{2}}}-A_0^2\left(\frac{2}{3^{\frac{5}{2}}}-\frac{1}{4^{\frac{3}{2}}}\right)-A_0^3\left(\frac{3}{4^{\frac{5}{2}}}+\frac{5}{2^{\frac{11}{2}}}-\frac{3}{6^{\frac{3}{2}}}\right)\ldots\ldots\right]$
	(2) Relativistic	$E_+ = 3RT\left[1+\frac{A_0^R}{2^4}-A_0^{R^2}\left(\frac{2}{3^4}-\frac{1}{4^3}\right)+A_0^{R^3}\left(\frac{3}{4^4}+\frac{5}{4^5}-\frac{3}{6^3}\right)\ldots\right]$	$E_- = 3RT\left[1-\frac{A_0^R}{2^4}-A_0^{R^2}\left(\frac{2}{3^4}-\frac{1}{4^3}\right)-A_0^{R^3}\left(\frac{3}{4^4}+\frac{5}{4^5}-\frac{3}{6^3}\right)\ldots\ldots\right]$
Degeneracy	(1) Non-relativistic	$E_- = \frac{2\pi gVh^2}{5m}\left(\frac{3n}{4\pi g}\right)^{\frac{5}{3}}\left[1+\frac{5\,2^{\frac{2}{3}}\pi^{\frac{4}{3}}}{3^{\frac{7}{3}}A_0^{\frac{4}{3}}}+\ldots\ldots\right]$	$E_- = \Gamma\frac{5}{2}CV(kT)^{\frac{5}{2}}\zeta(\frac{5}{2})$
	(2) Relativistic	$E_- = \pi gchV\left(\frac{3n}{4\pi g}\right)^{\frac{4}{3}}\left[1+\frac{\pi^2 2^{\frac{1}{3}}}{3^{\frac{5}{3}}(A_0^R)^{\frac{2}{3}}}+\ldots\ldots\right]$	$E_- = \Gamma 4\, CV(kT)^4\zeta(4)$.

where, $A_0 = \frac{nh^3}{g(2\pi mkT)^{\frac{3}{2}}}$, $A_0^R = \frac{n}{8\pi g}\left(\frac{ch}{kT}\right)^3$, and $\zeta(k) = 1+\frac{1}{2^k}+\frac{1}{3^k}+\frac{1}{4^k}\ldots\ldots$

The results of integration of equation (4) for the different cases of degeneracy and non-degeneracy are shown in Table 1.

In the non-degenerate case, *i.e.*, $\Lambda \ll 1$, and we have, by integrating equation (4)* and (4a),

$$E_+ = sNkT[1 + a\beta A_1 - b\beta^2 A_1^2 + c\beta^3 A_1^3 \ldots\ldots\ldots], \qquad \ldots \quad (7)$$

where $a = \frac{1}{2^{s+1}}$, $b = \left(\frac{2}{3^{s+1}} - \frac{1}{4^s}\right)$, $c = \frac{3}{4^{s+1}} + \frac{5}{2^{3s+1}} - \frac{3}{6^s}$,

and $$A_1 \equiv \frac{N}{\Gamma sCV(kT)^s} = \sum_{n=1}^{n=\infty} \frac{A^n}{n^s}(-\beta)^{n-1}. \qquad \ldots \quad (8)\dagger$$

Equation (7) gives the general expression for energy in non-degeneracy and by giving appropriate values to β and s we obtain the different cases, *viz.*,

(*i*) $\beta = +1$, $s = \frac{3}{2}$ *completely non-relativistic* Fermi-Dirac non-degenerate case.

(*ii*) $\beta = +1$, $s = 3$ *completely relativistic* Fermi-Dirac non-degenerate case.

(*iii*) $\beta = -1$, $s = \frac{3}{2}$ *completely non-relativistic* Bose-Einstein non-degenerate case.

(*iv*) $\beta = -1$, $s = 3$ *completely relativistic* Bose-Einstein non-degenerate case.

We have, since‡ $E = spV$, $\qquad \ldots \quad (9)$

$$p_+ = \frac{RT}{V}[1 + a\beta A_1 - b\beta^2 A_1^2 + c\beta^3 A_1^3 + \ldots\ldots\ldots] \qquad \ldots \quad (10)$$

and, as from (8) we have

$$\left(\frac{\partial A_1}{\partial T}\right)_v = -\frac{s}{T}A_1,$$

we obtain $C_{v+} = \left(\frac{\partial E_+}{\partial T}\right)_v$

$$= Rs[1 - (s-1)a\beta A_1 + (2s-1)b\beta^2 A_1^2 - (3s-1)c\beta^3 A_1^3 \ldots\ldots] \ldots \quad (11)$$

where $R = Nk$.

* The suffix + attached to a quantity denotes its value in the non-degenerate case. The suffix − represents the degenerate case.

† A_1 becomes equal to A_0 of the previous papers in the non-relativistic case, and in the relativistic case to A_0^R.

‡ For an ideal gas we have the usual relations, $E = \frac{3}{2}pV$ in the non-relativistic case and $E = 3pV$ in the relativistic case.

Again, since

$$\left(\frac{\partial V}{\partial T}\right)_p = -\frac{\left(\frac{\partial p}{\partial T}\right)_v}{\left(\frac{\partial p}{\partial V}\right)_T}, \quad \ldots \quad (12)$$

we have substituting from (10)

$$\left(\frac{\partial V}{\partial T}\right)_p = \frac{V}{T}\left[\frac{1-(s-1)a\beta A_1+(2s-1)b\beta^2A_1^2-(3s-1)c\beta^3A_1^3\ldots\ldots\ldots}{1+2a\beta A_1-3b\beta^2A_1^2+4c\beta^3A_1^3\ldots\ldots\ldots\ldots\ldots\ldots}\right],$$

or $$\left(\frac{\partial V}{\partial T}\right)_p = \frac{V}{T}\left[1-(s+1)a\beta A_1+(2s+2)(a^2+b)\beta^2A_1^2 - (s+1)(4a^3+7ab+3c)\beta^3A_1^3+\ldots\ldots\ldots\right]. \quad \ldots \quad (13)$$

But we have, $$C_p - C_v = T\left(\frac{\partial p}{\partial T}\right)_v\left(\frac{\partial V}{\partial T}\right)_p, \quad \ldots \quad (14)$$

and hence using (9) and (13), we have

$$C_p = C_v\left\{1+\frac{T}{sV}\left(\frac{\partial V}{\partial T}\right)_p\right\}, \quad \ldots \quad (14a)$$

or $$C_{p_1} = C_{v_1}\frac{(s+1)}{s}\{1-a\beta A_1+2(a^2+b)\beta^2A_1^2-(4a^3+7ab+3c)\beta^3A_1^3\ldots\} \quad (15)$$

And therefore from equations (1), (11), (13) and (15) we obtain

$$\left(\frac{\partial T}{\partial p}\right)_H = -\frac{V}{R}\left[\frac{a\beta A_1-2(a^2+b)\beta^2A_1^2+(4a^3+7ab+3c)\beta^3A_1^3\ldots\ldots\ldots}{\{1-a\beta A_1+2(a^2+b)\beta^2A_1^2+\ldots\}\{1-(s-1)a\beta A_1+(2s-1)b\beta^2A_1^2\ldots\}}\right]$$

$$= -\frac{V}{R}\left[a\beta A_1+\{(s-2)a^2-2b\}\beta^2A_1^2+\{(s^2-3s+3)a^2-2(2s-3). +3c\}\beta^3A_1^3\ldots\ldots\ldots\right]. \quad (16)$$

This is the general result for the non-degenerate case and, to a first order, this gives the same results as obtained by Srivastava and Gogate (*loc. cit.*).

We now confine ourselves to the Bose-Einstein statistics only ($\beta=-1$). The non-degenerate case of Bose-Einstein statistics extends right up to $A_1=\zeta(s)-0$, for the degenerate case A_1 being equal to or greater than $\zeta(s)$. However, for $A_1=\zeta(s)-0$ the series in equation (16) is not sufficiently convergent to give accurate results. We have, therefore, to use a direct method to determine the limiting value of $\left(\frac{\partial T}{\partial p}\right)_H$ and its rate of change with respect to A_1 at $A_1=\zeta(s)-0$. This is done as follows.

From equation (4), we have, since $\beta = -1$

$$E_{+} = \frac{RsT}{A_1} \sum_{n=1}^{n=\infty} \frac{A^n}{n^{s+1}}, \qquad \dots (17)$$

where
$$A_1 = \frac{N}{\Gamma s C V (kT)^s} = \sum_{n=1}^{n=\infty} \frac{A^n}{n^s}, \qquad \dots (18)$$

and therefore,
$$\frac{T}{sV}\left(\frac{\partial A}{\partial T}\right)_v = \left(\frac{\partial A}{\partial V}\right)_T. \qquad \dots (18a)$$

This gives
$$\left(\frac{\partial A_1}{\partial T}\right)_v = \frac{-sA_1}{T}, \quad \left(\frac{\partial^2 A_1}{\partial T^2}\right)_v = \frac{s(s+1)A_1}{T^2} \qquad \dots (19)$$

and
$$\left(\frac{\partial A_1}{\partial T}\right)_v = \sum \frac{A^{n-1}}{n^{s-1}} \left(\frac{\partial A}{\partial T}\right)_v, \qquad \dots (20)$$

also from (18),
$$\left(\frac{dA}{dA_1}\right)_1 = \frac{1}{\zeta(s-1)}, \qquad \dots (20a)$$

where the *suffix 1 attached to a function denotes its value* at* A $= \zeta(s) - 0$. If T_0 is the value of T at this point, then we have

$$\left(\frac{\partial A_1}{\partial T}\right)_{1v} = \frac{-s\zeta(s)}{T_0}, \qquad \dots (21)$$

and from (19) and (20a) we obtain

$$\left(\frac{\partial A}{\partial T}\right)_{1v} = -\frac{s}{T_0}\,\frac{\zeta(s)}{\zeta(s-1)}. \qquad \dots (22)$$

We can now derive an expression for Cv_1. From equation (17) we have

$$C_{v+} = \left(\frac{\partial E_+}{\partial T}\right)_v = R\left\{\frac{(s+1)s}{A_1}\sum \frac{A^n}{n^{s+1}} + \frac{sT}{A_1}\left(\frac{\partial A}{\partial T}\right)_v \sum \frac{A^{n-1}}{n^s}\right\}, \qquad \dots (23)$$

or, from (20),
$$C_{v+} = Rs\left\{\frac{(s+1)}{A_1}\sum \frac{A^n}{n^{s+1}} - s\sum \frac{A^{n-1}}{n^s} \Big/ \sum \frac{A^{n-1}}{n^{s-1}}\right\}, \qquad \dots (24)$$

and, therefore,
$$Cv_1 = Rs\left\{(s+1)\frac{\zeta(s+1)}{\zeta(s)} - \frac{s\zeta(s)}{\zeta(s-1)}\right\}. \qquad \dots (25)$$

We shall now determine Cp_1. The relation between C_p and C_v is given by (14a).

Since A is a function of T and V, we have

$$\left\{\frac{\partial A}{\partial T}\right\}_p = \left\{\frac{\partial A}{T}\right\}_v + \left\{\frac{\partial A}{\partial V}\right\}_T \left\{\frac{\partial V}{\partial T}\right\}_p. \qquad \dots (26)$$

* There should not be any confusion as regards A_1 which has already been defined by equation (8).

The values of $\left\{\frac{\partial A}{\partial V}\right\}_{1T}$ and $\left\{\frac{\partial A}{\partial T}\right\}_{1v}$ are obtained from equations (18*a*) and (22).

In order to obtain $\left\{\frac{\partial A}{\partial T}\right\}_{p}$, we make use of the equation

$$p_1 = \frac{C(kT)^s}{s} \int \frac{\epsilon^s d\epsilon}{\frac{e^{\epsilon/kT}}{A} - 1} \qquad \ldots \quad (27)$$

which follows from (4) and (9). Differentiating this with respect to T and keeping p constant, we have

$$\frac{(s+1)}{T} \Gamma_{s+1} \Sigma \frac{A^n}{n^{s+1}} + \frac{s}{A} \left\{\frac{\partial A}{\partial T}\right\}_p \Gamma_s \Sigma \frac{A^n}{n^s} = 0. \qquad \ldots \quad (28)$$

When $A_1 = \zeta(s) - o$, we have, $\left\{\frac{\partial A}{\partial T}\right\}_{1p} = \frac{-(s+1)}{T} \frac{\zeta(s+1)}{\zeta(s)}. \qquad \ldots \quad (29)$

Substituting the values of $\left\{\frac{\partial A}{\partial V}\right\}_{1T}$, $\left\{\frac{\partial A}{\partial T}\right\}_{1v}$ and $\left[\frac{\partial A}{\partial T}\right\}_{1p}$ in (26),

we obtain*
$$\left\{\frac{\partial V}{\partial T}\right\}_{1p} = \frac{V}{T_0} \left\{\frac{(s+1)\,\zeta(s+1)\,\zeta(s-1)}{[\zeta(s)]^2} - s\right\}, \qquad \ldots \quad (30)$$

and hence, from (14*a*), $C_{p_1} = \frac{s+1}{s} \frac{\zeta(s+1)\,\zeta(s-1)}{[\zeta(s)]^2} C_{v_1}. \qquad \ldots \quad (31)$

Therefore, substituting the above result in equation (1) and using (25), we finally obtain

$$\left\{\frac{\partial T}{\partial P}\right\}_{1H} = \frac{V}{R} \frac{\zeta(s)}{(s+1)\,\zeta(s+1)} \left[1 - \frac{1}{\frac{(s+1)\,\zeta(s+1)\,\zeta(s-1)}{[\zeta(s)]^2} - s}\right], \qquad \ldots \quad (32)$$

$$= \begin{cases} 0{\cdot}7844 \dfrac{V}{R} \text{ for } s = 3/2, \\[2ex] 0{\cdot}1338 \dfrac{V}{R} \text{ for } s = 3. \end{cases} \qquad \ldots \quad (32a)$$

The rate of change of $\left\{\frac{\partial T}{\partial p}\right\}_{H}$ with respect to A_1 is determined in a similar way.

* $\left(\frac{\partial V}{\partial T}\right)_p$ could also be obtained by differentiating p obtained from equations (9) and (4) and using (12).

From equations (26), (28), (20) and (18a), we have

$$\left(\frac{\partial V}{\partial T}\right)_p = \frac{V}{T}\frac{(s+1)\sum\frac{A^n}{n^{s+1}}\sum\frac{A^n}{n^{s-1}}}{A_1^2} - \frac{Vs}{T}, \qquad (33)$$

and substituting this in equation (14a), we have

$$C_{p+} = C_{v+}\left[\frac{s+1}{s}\frac{\sum\frac{A^n}{n^{s+1}}\sum\frac{A^n}{n^{s-1}}}{A_1^2}\right]. \qquad \dots (34)$$

Therefore equations (1), (33) and (34) give

$$\left(\frac{\partial T}{\partial p}\right)_H = \frac{V}{R}\frac{1-A_1^2\bigg/\sum\frac{A^n}{n^{s+1}}\sum\frac{A^n}{n^{s-1}}}{\frac{(s+1)}{A_1}\sum\frac{A^n}{n^{s+1}} - sA_1\bigg/\sum\frac{A^n}{n^{s-1}}}. \qquad \dots (35)$$

The above relation after differentiation with respect to A_1 and simplification with the help of equation (20a), leads to

$$\left[\frac{d\left\{\left(\frac{\partial T}{\partial p}\right)_H R/V\right\}}{d\,A_1}\right]_1 = \left[\left\{(s+1)\frac{\zeta(s+1)}{\zeta(s)} - \frac{s\zeta(s)}{\zeta(s-1)}\right\}\left\{\frac{[\zeta(s)]^2\,\zeta(s-2)}{\zeta(s+1)\,[\zeta(s-1)]^3}\right.\right.$$

$$+\frac{[\zeta(s)]^3}{[\zeta(s+1)\,\zeta(s-1)]^2} - \frac{2\zeta(s)}{\zeta(s+1)\,\zeta(s-1)}\Big\}\{\dots\}^{1} - \frac{[\zeta(s)]^2}{\zeta(s+1)\,\zeta(s-1)}\Big\}\Big\{\frac{s\,\zeta(s)\,\zeta(s-2)}{[\zeta(s-1)]^3}$$

$$\left.-\frac{(s+1)\zeta(s+1)}{[\zeta(s)]^2}+\frac{1}{\zeta(s-1)}\right\}\Bigg]\left[(s+1)\frac{\zeta(s+1)}{\zeta(s)} - \frac{s\zeta(s)}{\zeta(s-1)}\right]^{-2}$$

$$= \begin{Bmatrix} 0{\cdot}5503 & \text{for} & s=3/2, \\ \infty & \text{for} & s=3. \end{Bmatrix}. \qquad \dots (36)^*$$

We shall now take up the degenerate case of the Bose-Einstein statistics. This is characterised by $A=1$ and $A_1 \overline{=} \zeta(s)$. Attaching the suffix $-$ to denote the value of the functions in the degenerate case, we have for the total energy E_-, by integrating equation (4),

$$E_- = s\Gamma\overline{s+1}CV(kT)^{s+1}\zeta(s+1) \qquad \dots (37)$$

and from equation (9)

$$p_- = \Gamma\overline{s}C(kT)^{s+1}\zeta(s+1) \qquad \dots (38)$$

and, therefore, from (37),

$$C_{v-} = \Gamma\overline{s+2}C(kT)^s kV\zeta(s+1). \qquad \dots (39)$$

* Noting that $\frac{\zeta(s-2)}{[\zeta(s-1)]^3} = \frac{1}{2\pi}$ in the case of $s=3/2$.

It is clear from equation (38) that the pressure is independent of the volume, and

$$\left(\frac{\partial V}{\partial T}\right)_p = \infty.$$

Therefore,
$$\left(\frac{\partial T}{\partial p}\right)_H = \frac{1 - \dfrac{V}{T\left(\dfrac{\partial V}{\partial T}\right)_p}}{\dfrac{C_p}{T\left(\dfrac{\partial V}{\partial T}\right)_p} + \left(\dfrac{\partial p}{\partial T}\right)_v} = \frac{1}{\left(\dfrac{\partial p}{\partial T}\right)_v},$$

$$= \frac{T}{(s+1)p} = \frac{V}{R}\,\frac{A_1}{(s+1)\,\zeta(s+1)}, \qquad \ldots \quad (40)$$

$$= \begin{cases} 2/5\,\dfrac{T}{p} & \text{for } s = 3/2 \text{ (non-relativistic case),*} \\[2ex] 1/4\,\dfrac{T}{p} & \text{for } s = 3 \text{ (relativistic case).} \end{cases}$$

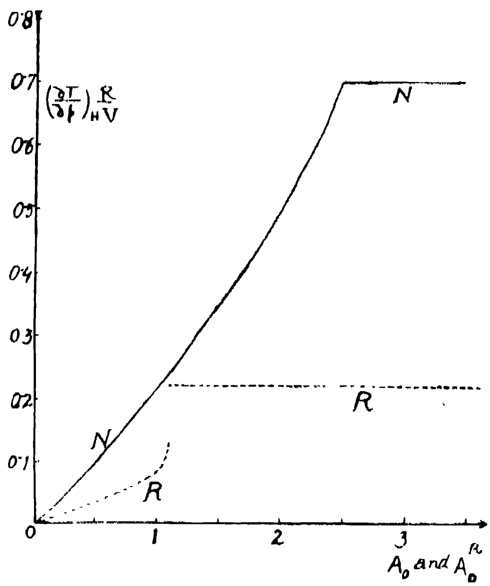

FIGURE 1

Joule-Thomson effect for a Bose-Einstein gas. Curve NN is for the non-relativistic case and RR for the relativistic case.

* These results, however, do not signify that the Joule-Thomson expansion can be used to produce cooling in a Bose-Einstein degenerate gas. For the amount of cooling is just equal to the difference in the temperature on the two sides of the throttle valve which are under different pressures, and the gas undergoing the throttling process simply acquires the temperature determined by the pressure on the side on which it emerges.

Equations (16) and (40) now enable us to obtain the values of $\left(\frac{\partial T}{\partial p}\right)_H$ R/V for the Bose-Einstein gas whether non-degenerate or degenerate. The curve NN in figure 1 shows the variation of $\left(\frac{\partial T}{\partial p}\right)_H$ R/V against A_0 for the non-relativistic case (A_0 denotes the value of A_1 in the non-relativistic case, $s=3/2$; and A_0'' denotes the value of A_1 in the relativistic case, $s=3$). The curve RR refers to the relativistic case, the abscissa for this curve being A_0''. The values of $\left(\frac{\partial T}{\partial p}\right)_H$ R/V at the point $A_1=\zeta(s)-0$ have been obtained from equation (32a) and its slope at $A_1=\zeta(s)-0$ from equation (36). In the non-relativistic case the angle made by the tangent to the curve at $A_0=\zeta(3/2)$ is approximately 28° 50′ and in the relativistic case the angle at $A_0''=\zeta(3)$ is 90°.* It will also be noticed, as is easily shown from equations (40) and (32*a*), that there is no discontinuity in the curve NN at $A_0=\zeta(3/2)$, but there is a discontinuity in the curve RR at $A_0''=\zeta(3)$.

Adiabatic change for a Bose-Einstein degenerate gas :—

In an adiabatic change the entropy remains constant. The entropy S is given by

$$S_-=(s+1)\Gamma s C V k(kT)^s\zeta(s+1). \qquad \dots \quad (41)$$

Consequently in an adiabatic change,

$$VT^s \quad \text{is constant,}$$

i.e.,

$$pV^{\frac{s+1}{s}} \text{ is constant (since } p \propto T^{s+1}). \qquad \dots \quad (41a)$$

PART II—JOULE EFFECT

2. When a gas expands without doing any external work, as in Joule's Experiment, there is no change in the internal energy of the system, *i.e.*,

$$d\bar{E} = 0.$$

Using the well-known thermodynamic relations

$$dQ=dE+pdV$$
$$=C_v dT+l dV,$$

where

$$l=T\left(\frac{dp}{T}\right)_v,$$

* As in the figure the scales of the ordinate and abscissa are in the ratio of 5 : 1, the angles have been drawn equal to 70° and 90° respectively.

† See note on page 462 for definition of A_0.

we obtain, for the Joule effect,

$$\left(\frac{\partial T}{\partial V}\right)_E = \frac{p - T\left(\frac{\partial p}{\partial T}\right)_v}{C_v},$$

and using (9), we have,

$$\left(\frac{\partial T}{\partial V}\right)_E = \frac{p}{C_v} - \frac{T}{sV}. \qquad \dots \quad (42)$$

We shall now consider the non-degenerate case of Fermi-Dirac and Bose-Einstein statistics.

In this case p_+ and C_{v+} are given by equations (10) and (11) and substituting them in (42), we have

$$\left(\frac{\partial T}{\partial V}\right)_E = \frac{T}{V}\left[a\beta A_1 - \{2b - (s-1)a^2\}\beta^2 A_1^2 + \{3c - ab(4s-3) + (s-1)^2 a^3\}\beta^3 A_1^3 \dots\dots\right]. \qquad \dots \quad (43)$$

Considering to a first order only, we obtain, for a non-degenerate gas

(1) in the non-relativistic case

$$\left(\frac{\partial T}{\partial V}\right)_E = \frac{\beta T}{V} \cdot \frac{A_0}{2^{\frac{5}{2}}}, \qquad \dots \quad (44)$$

and (2) in the relativistic case

$$\left(\frac{\partial T}{\partial V}\right)_E = \frac{\beta T}{V} \cdot \frac{A_0^R}{16}, \qquad \dots \quad (44a)$$

where $\beta = 1$ for matter obeying Fermi-Dirac statistics and $\beta = -1$ for matter obeying Bose-Einstein statistics. It is clear from the above, since dV is always positive, that there is a heating effect in the Fermi-Dirac gas whereas a cooling is produced in the Bose-Einstein gas. Also the change is greater, the greater the degree of degeneracy.

(*b*) Now we shall consider degenerate matter. The degenerate case in the two statistics has to be treated separately. First we shall consider the Fermi-Dirac statistics. This is characterised by $A \gg 1$ and $\beta = 1$. The integrations are carried out by using Sommerfelds' formula according to which for large A,

$$\int_0^\infty \frac{u^s}{\frac{e^u}{A} + 1}\, du = \frac{u_0^{s+1}}{s+1}\left[1 + \frac{\pi^2}{6u_0^2}s(s+1) + \dots\right],$$

where $u_0 = \log A$.

Integrating equation (4) for large A, we have

$$E_- = \frac{s}{s+1} NkT(\Gamma s + 1 A_1)^{\frac{1}{s}}\left[1 + \frac{\pi^2}{6}\frac{(s+1)}{(\Gamma s + 1 A_1)^{\frac{2}{s}}} \dots\right],$$

which gives, since $E = spV$,

$$p_- = \frac{NkT}{(s+1)V} (\Gamma \overline{s+1} A_1)^{\frac{1}{s}} \left[1 + \frac{\pi^2}{6} \frac{(s+1)}{(\Gamma \overline{s+1} A_1)^{\frac{2}{s}}} \cdots \right],$$

and

$$C_{v-} = \left(\frac{\partial E_-}{\partial T} \right)_v = \frac{s\pi^2}{3} \cdot \frac{Nk}{(\Gamma \overline{s+1} A_1)^{\frac{1}{s}}} .$$

Substituting these values in equation (42), we have

$$\left(\frac{\partial T}{\partial V} \right)_{E_-} = \frac{T}{sV} \left\{ \frac{3(\Gamma \overline{s+1} A_1)^{\frac{2}{s}}}{(s+1)\pi^2} \cdots - 1 \right\}. \quad \cdots \quad (45)$$

This is the general result for matter degenerate in the sense of Fermi-Dirac statistics. If we have put $s = 3/2$ we obtain to a first order, for the non-relativistic case,

$$\left(\frac{\partial T}{\partial V} \right)_{E_-} = \frac{T}{V} \frac{3^{\frac{4}{3}} A_0^{\frac{4}{3}}}{5 \cdot 2^{2} \pi^{4}} . \quad \cdots \quad (46)$$

On the other hand for the relativistic case ($s =$, we have, to a first order,

$$\left(\frac{\partial T}{\partial V} \right)_{E_-} = \frac{T}{V} \frac{(6A_0^R)^{\frac{2}{3}}}{4\pi^2} . \quad \cdots \quad (47)$$

It is clear from equation (46) and (47) that for a Fermi-Dirac gas there is a heating effect in the degenerate case also, and that this effect is greater the greater the degree of degeneracy.

For degenerate matter obeying Bose-Einstein statistics the expressions for p and C_v are given by equations (38) and (39) and hence substituting them in equation (42), we have (the exact expression)

$$\left(\frac{\partial T}{\partial V} \right)_{E_-} = - \frac{T}{(s+1)V} . \quad \cdots \quad (48)$$

Hence, in the non-relativistic case ($s = 3/2$),

$$\left(\frac{\partial T}{\partial V} \right)_{E_-} = - \frac{2}{5} \frac{T}{V},$$

and, in the relativistic case ($s = 3$),

$$\left(\frac{\partial T}{\partial V} \right)_{E_-} = - \frac{1}{4} \frac{T}{V} . \quad \cdots \quad (50)$$

Equations (43) and (48) show that for matter obeying Bose-Einstein statistics Joule effect always produces cooling.

As in the case of the Joule-Thomson effect the equation (43) for the non-degenerate case of Bose-Einstein statistics is only mildly convergent as $A_1 = \zeta(s) - 0$, and does not give sufficiently accurate values of $\left(\frac{\partial T}{\partial V} \right)$

as the gas approaches the state of degeneracy. We proceed as before to find out the nature of the curve showing the variation of $\left(\frac{\partial T}{\partial V}\right)\Big/\frac{T}{V}$ with A_1 at $A_1=\zeta(s)-0$ by evaluating $\frac{\partial T}{\partial V}\Big/\frac{T}{V}$ and its differential coefficient with respect to A_1 at the point $A_1=\zeta(s)-0$. We have from equation (14)

$$p=\frac{R}{V}\frac{T}{A_1}\ \Sigma\frac{A^n}{n^{s+1}}, \qquad \dots \quad (51)$$

and therefore

$$p_1=\frac{RT_0}{V}\frac{\zeta(s+1)}{\zeta(s)}. \qquad \dots \quad (52)$$

Substituting the values from (25) and (52) in (42) and simplifying, we obtain

$$\left(\frac{\partial T}{\partial V}\right)_1=-\frac{T_0}{V(s+1)}\left\{\frac{1-\dfrac{[\zeta(s)]^2}{\zeta(s+1)\zeta(s-1)}}{1-\dfrac{s}{s+1}\dfrac{[\zeta(s)]^2}{\zeta(s+1)\zeta(s-1)}}\right\}, \qquad \dots \quad (53)$$

which gives, for the non-relativistic case $(s=3/2)$,

$$\left(\frac{\partial T}{\partial V}\right)_1=-0{\cdot}4\,\frac{T_0}{V}, \qquad \dots \quad (54)$$

and, for the relativistic case $(s=3)$,

$$\left(\frac{\partial T}{\partial V}\right)_1=-0{\cdot}12\,\frac{T_0}{V}. \qquad \dots \quad (54a)$$

The slope of the curve at the limiting point is calculated in a similar way. We have

$$\frac{d}{dA_1}\left(\frac{\partial T}{\partial V}\right)_E=\frac{d}{dA_1}\left(\frac{p}{C_v}-\frac{T}{sV}\right).$$

Substituting the values of p and C_v from equations (51) and (24), we get

$$\frac{d}{dA_1}\left(\frac{\partial T}{\partial V}\Big/\frac{T}{V}\right)=\frac{1}{s}\frac{d}{dA_1}\left[\frac{\dfrac{1}{A_1}\Sigma\dfrac{A^n}{n^{s+1}}}{\left\{\dfrac{(s+1)}{A_1}\Sigma\dfrac{A^n}{n^{s+1}}-s\dfrac{\Sigma\dfrac{A^{n-1}}{n^s}}{\Sigma\dfrac{A^{n-1}}{n^{s-1}}}\right\}}-1\right]$$

$$=\frac{1}{s}\frac{d}{dA_1}\left[\frac{1}{(s+1)-sA_1^2\Big/\Sigma\dfrac{A^n}{n^{s+1}}\Sigma\dfrac{A^n}{n^{s-1}}}-1\right] \qquad \dots \quad (55)$$

which on differentiation and simplification using equation (20*a*) gives

$$\left[\frac{d}{dA_1}\left(\frac{\partial T}{\partial V}\Big/\frac{T}{V}\right)\right]_1 = -\frac{\dfrac{[\zeta(s)]^2\zeta(s+1)\zeta(s-2)}{[\zeta(s-1)]^3} - \dfrac{2\zeta(s)\zeta(s+1)}{\zeta(s-1)} + \dfrac{[\zeta(s)]^3}{[\zeta(s-1)]^2}}{\left\{(s+1)\zeta(s+1) - \dfrac{s[\zeta(s)]^2}{\zeta(s-1)}\right\}^2} \quad \ldots \text{(56)}$$

In the non-relativistic case, *i.e.*, $s=3/2$, this gives us

$$\left[\frac{d}{dA_1}\left(\frac{\partial T}{\partial V}\Big/\frac{T}{V}\right)\right]_1 = -0{\cdot}1295, \quad \ldots \text{(57)}$$

and in the relativistic case, *i.e.*, $s=3$,

$$\left[\frac{d}{dA_1}\left(\frac{\partial T}{\partial V}\Big/\frac{T}{V}\right)\right]_1 = - \;\cdot \quad \ldots \text{(58)}$$

The curves showing the variation of $\left(\dfrac{\partial T}{\partial V}\Big/\dfrac{T}{V}\right)$ with A_1 for a Bose-Einstein gas have been drawn in figure 2. The ordinate represents $\left(-\dfrac{\partial T}{\partial V}\Big/\dfrac{T}{V}\right)$ and the abscissa represents A_1. The curve NN is for the

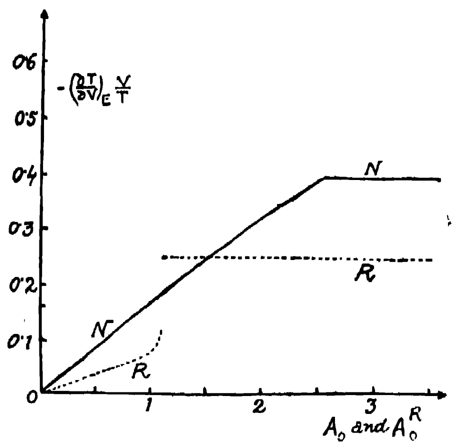

FIGURE 2

Joule effect for a Bose-Einstein gas. Curve NN is for the non-relativistic case and RR for the relativistic case.

non-relativistic case ($A_1=A_0$) and RR for the relativistic case ($A_1=A_0^r$). The discontinuity in the slope of the curves at $A_1=\zeta(s)$ has been determined from equation (57) and (58) which give the angles to be $7°\ 23'$ nearly in the non-relativistic case, and $90°$ in the relativistic case. As the ratio of the scales of the axes in the figure is 5 : 1, the angles correspond to about

33° for curve NN and 90° for curve RR. It will be noticed, as is readily shown from equations (48) and (53), that there is no discontinuity in the magnitude of the Joule effect in a Bose-Einstein gas as it passes from non-degeneracy to degeneracy in the non-relativistic case, *i.e.*, at $A_0 = \zeta\,(3/2)$. On the other hand there is a discontinuity in the relativistic case at $A_0^n = \zeta(3)$.

It is a pleasure to express my thanks to Dr. D. S. Kothari for his interest and guidance during my work.

REFERENCES

[1] D. S. Kothari, *Proc. Nat. Inst Sci. (India)*. **4**, 69 (1938).

[2] B. N. Srivastava, ,, ,, ,, ,, **4**, 75 (1938)

[3] D. V. Gogate, *Phil. Mag.*, **26**, 694 (1938) ; *Phil. Mag.*, **26**, 166 (1938).

DYNAMICS OF THE PIANOFORTE STRING AND THE HAMMER

PART IV (STUDY OF DURATION OF IMPACT)

By MOHINIMOHAN GHOSH
Burdwan Raj College, Bengal

(*Received for publication, January 25, 1940*)

ABSTRACT. The complete dynamics of the finite Pianoforte string and the hammer of any kind has been worked out in Parts I, II and III. In this part only expressions for the the duration of contact when the hammer strikes at different points of a finite string have been worked out. The comparison of the theoretical values, with those obtained—experimentally by different authors, is made graphically, and remarkable agreement is found in each case. It is found from the theory, that the duration of contact changes discontinuously with distance and for the higher values of the 'mass-ratio' the curve shifts towards the greater values of the 'duration' as was found experimentally by George, Kar-Ghosh and others. The comparison of the theoretical values with those obtained experimentally by M. Ghosh and Banerjee-Ganguli is made graphically and it is found that the agreement is remarkable, even when a massive hammer is used, *i.e.*, for a large 'mass-ratio' where Das and other theories fail completely. The variation of the duration of contact with different values of the elastic constant of the hammer, for a given striking distance, as is obtained from the theory, is also compared graphically with that obtained experimentally. There is very good agreement in this case.

INTRODUCTION

The dynamics of the Pianoforte string and the hammer has been developed completely[1] in Parts I, II and III. The theory has been tested in different ways. The pressure-time curve, for hard and elastic hammers, has been drawn for different cases. It is found that, in case of the hard hammer, the pressure changes periodically in a discontinuous manner. As the hard hammer is replaced by an elastic hammer, the discontinuous periodic rises of pressure lose their sharp angularities and humps become less and less pronounced. Similar behaviour of pressure-time curve for different values of the elastic constant was observed recently by Davy [2] and his co-workers. The fact that the shorter segment of the string sets in vibration as soon as the hammer comes in contact with the string was observed previously. No fruitful explanation of the phenomenon was, however, known. The present theory explains the same fully, as is evident from the time-displacement curve given in one of the previous papers. [3] The duration of impact of the hammer has also been previously calculated for

a few cases. In this paper an elaborate and systematic study of the duration of contact for hard as well as elastic hammer will be made, and the calculated values will be compared with those obtained experimentally.

The symbols to be used in the present paper have got the same meaning as in *Parts I, II and III.*

The expression for the pressure exerted by the hammer as derived previously is a function of time. And, as already pointed out, the duration of contact, Φ, *is the lowest positive root* obtained by solving $P_n(t)=0$.

HARD HAMMER

(*i*) *When the hammer strikes very near the end*, so that $\frac{a}{c}$ is very small, the pressure exerted by the hammer is given by [*vide* eq. (9), Part 1]

$$P=mv_0\frac{\mu^2+\nu^2}{\nu}e^{-\mu t}\sin\left(\nu t-\tan^{-1}\frac{2\mu\nu}{\mu^2-\nu^2}\right).$$

and the duration of impact is given by

$$\Phi=\frac{1}{\nu}\tan^{-1}\frac{2\mu\nu}{\mu^2-\nu^2},$$

where

$$\mu=\frac{M_1}{m_0\theta_1},\qquad \nu=\frac{1}{\theta}\sqrt{\frac{4M_1}{m_0}-\frac{M_1^2}{m_0^2}}.$$

The general expression of the pressure exerted by the hammer during contact is [*vide* eq. (56), Part III]

$$-P=\frac{2T}{c}\Big[f'_1(t)+\sum_1^n f'_{n+1}(t-n\theta_1)+\sum_1^n f'_{n+1}(t-n\theta_2)+2\{f_3'-f_2'\}(t-\Theta)$$

$$+\sum_1^n\{(n+2)f'_{n+3}-2(n+1)f'_{n+2}+nf'_{n+1}\}\{(t-\Theta-n\theta_1)+(t-\Theta-n\theta_2)\}$$

$$+2\{3f_5'-6f_4'+4f_3'-f_2'\}(t-2\Theta)\Big] \qquad \ldots \quad (56)$$

where $f'_n(t)=$

$$A^n v_0\Bigg[e^{-qt}.\sum_{r=1}^n(-)^{n+r-2}.\frac{\Gamma(n+r-1)}{\Gamma(n)\Gamma(r)}\beta^{r-1}\Big\{q^{n-1}.\frac{t^{n-r}}{(n-r)!}-{}^{n-1}C_1.q^{n-2}.\frac{t^{n-r-2}}{(n-r-2)!}$$

$$+{}^{n-1}C_2.q^{n-3}\frac{t^{n-r-3}}{(n-r-3)!}-+\Big\}+(-)^{2n-1}e^{-pt}\sum_{r=1}^n\frac{\Gamma(n+r-1)}{\Gamma(n)\Gamma(r)}.\beta^{r-1}.$$

$$\Big\{p^{n-1}.\frac{t^{n-r}}{(n-r)!}-{}^{n-1}C_1.p^{n-2}.\frac{t^{n-r-2}}{(n-r-2)!}+{}^{n-1}C_2.p^{n-3}.\frac{t^{n-r-3}}{(n-r-3)!}-+\Big\}\Bigg] \qquad \ldots \quad (56a)$$

when $q \neq p$ and $\beta = \frac{1}{p-q}$, $A = \beta(q+p)$; so

and $\quad 2\beta p = (A+1)$, $2\beta q = (A-1)$

and $$f'_n(t) = 2^n v_0 e^{-qt} \left\{ \frac{(qt)^n}{n!} - {}^{n-1}C_1 \frac{(qt)^{n+1}}{(n+1)!} + - + (-)^{n-1} \frac{(qt)^{2n-1}}{(2n-1)!} \right\} \quad \ldots \quad (56b)$$

when $\quad q = p$.

For hard hammer we put $E \to \infty$ in eq. (56a). From the above pressure equation, we are able to calculate the value of the duration of contact, for the particular case we require.

(*ii*) *When the striking distance a is finite and the other segment of the string b is large enough* compared to a so that no wave after suffering reflection from the end $x = l$, arrives at the hammer before the pressure terminates. The expressions for the pressure at different intervals are [*vide* eq. (13), Part I or eqs. (56) and (56a) for $b \backsim l \backsim \infty$ and $E \to \infty$]

$$P_1 = \frac{2T}{c} f'_1(t) = 2pv_0ce^{-qt}$$

$$P_2 = \frac{2T}{c} \left\{ f'_1(t) - f_2'(t_1) \right\} = P_1 + 2pv_0ce^{-qt}(1 - qt_1)$$

$$\ldots \qquad \ldots \qquad \ldots \qquad \ldots$$

$$P_{n+1} = P_n + \frac{2T}{c} f'_{n+1}(t_n)$$

$$= P_n + 2pv_0ce^{-qt_n} \left\{ 1 - {}^nC_1 . qt_n + {}^nC_2 \frac{q^2t_n^2}{2!} - + (-)^n \, {}^nC_n \frac{q^nt_n^n}{n!} \right\}. \quad \ldots \quad (69)$$

We find, from above, that $P_1 = 0$ has no finite root except at $t = \infty$ so that impact must not terminate during the first interval, $\theta_1 > t > 0$.

If the pressure terminates during the second interval, we get by solving $P_2 = 0$

$$\frac{\Phi}{\theta_1} = 1 + \frac{m}{4M_1} \left\{ 1 + e^{-\frac{4M_1}{m}} \right\} \quad \ldots \quad (70)$$

provided the maximum *mass-ratio* (*i.e.*, for $\Phi = 2\theta_1$) is given by

$$1 - \frac{m}{4M_1} \left\{ 1 + e^{-\frac{4M_1}{m}} \right\} = 0 \quad \ldots \quad (70.1)$$

which has a root $\frac{m}{M_1} = 3{\cdot}15$.

Thus the pressure terminates during $2\theta_1 > t > \theta_1$ provided $\frac{m}{M_1} \ngtr 3{\cdot}15$, *i.e.*, $a \nless 0{\cdot}32 \frac{m}{\rho}$.

If the pressure terminates during $3\theta_1 > t > 2\theta_1$ we get from the equation $P_3 = 0$

$$\left(\frac{\Phi}{\theta_1} - 2\right)^2 - \gamma_{2\cdot 1}\left(\frac{\Phi}{\theta_1} - 2\right) + \gamma_{2\cdot 2} = 0, \qquad \ldots \quad (71)$$

where
$$\gamma_{2\cdot 1} = \frac{m}{2M_1}\left(2 + e^{-\frac{4M_1}{m}}\right), \qquad \ldots \quad (71.1)$$

$$\gamma_{2\cdot 2} = \frac{m^2}{8M_1^2}\left[1 + e^{-\frac{4M_1}{m}}\left(1 - \frac{4M_1}{m}\right) + e^{-\frac{8M_1}{m}}\right], \qquad \ldots \quad (71.2)$$

provided the maximum *mass-ratio* (*i.e.*, $\Phi = 3\theta_1$) is given by

$$1 - \gamma_{2\cdot 1} + \gamma_{2\cdot 2} = 0. \qquad \ldots \quad (71.3)$$

Duration of contact is obtained by solving eq. (71).

The equation (71.3) has root $\frac{m}{M_1} = 6{\cdot}1$ approximately, so that the impact terminates during this interval provided $\frac{m}{M_1} \ngtr 6{\cdot}1$, *i.e.*, $a \nless 0{\cdot}16 \frac{m}{\rho}$.

If the pressure terminates during $4\theta_1 > t > 3\theta_1$ we get from the eqation $P_4 = 0$

$$\left(\frac{\Phi}{\theta_1} - 3\right)^3 - \gamma_{3\cdot 1}\left(\frac{\Phi}{\theta_1} - 3\right)^2 + \gamma_{3\cdot 2}\left(\frac{\Phi}{\theta_1} - 3\right) - \gamma_{3\cdot 3} = 0, \qquad \ldots \quad (72)$$

where
$$\gamma_{3\cdot 1} = \frac{3m}{4M_1}\left(3 + e^{-\frac{4M_1}{m}}\right), \qquad \ldots \quad (72.1)$$

$$\gamma_{3\cdot 2} = \frac{3}{8}\frac{m^2}{M_1^2}\cdot\left[e^{-\frac{8M_1}{m}} + e^{-\frac{4M_1}{m}}\left(2 - \frac{4M_1}{m}\right) + 3\right] \qquad \ldots \quad (72.2)$$

$$\gamma_{3\cdot 3} = \frac{3m^3}{32M_1^3}\left[e^{-\frac{12M_1}{m}} + e^{-\frac{8M_1}{m}}\left(1 - \frac{8M_1}{m}\right) + e^{-\frac{4M_1}{m}}\left(1 - \frac{8M_1}{m} + \frac{8M_1^2}{m^2}\right) + 1\right], \qquad \ldots \quad (72.3)$$

provided the maximum *mass-ratio* is given by, as is obtained by putting $\Phi = 4\theta_1$ in eq (72),

$$1 - \gamma_{3\cdot 1} + \gamma_{3\cdot 2} - \gamma_{3\cdot 3} = 0. \qquad \ldots \quad (72.4)$$

Duration of impact is obtained by solving eq. (72). The eq. (72·4) has root $m/M_1 = 10{\cdot}0$ approximately; so the impact terminates during this interval provided $\frac{m}{M_1} \ngtr 10$, *i.e.*, $a \nless 0{\cdot}1 \frac{m}{\rho}$.

In this way we can find out the expression for the duration of contact, when the impact terminates during any interval.

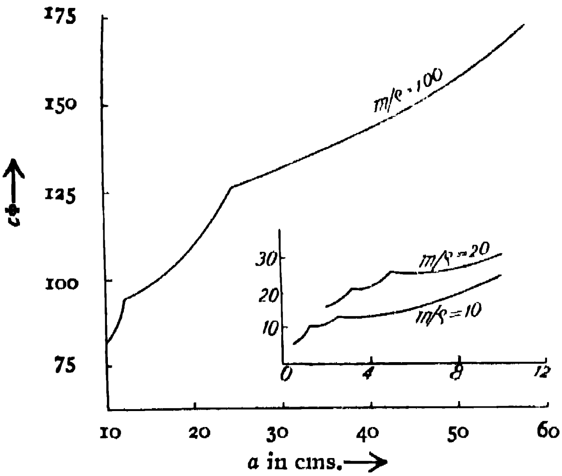

[FIGURE 1

Figure 1 shows the variation of the duration of contact with striking distance for different values of $\frac{m}{\rho}$ as predicted by the theory. We find that the duration of contact changes discontinuously with distance, and for higher values of $\frac{m}{\rho}$, the curve shifts towards the greater value of the duration of contact. The same was found experimentally by George[6], Kar-Ghosh[8], Banerjee-Ganguli[5] and others.

(*iii*) *The hammer strikes at the mid-point* $l=2a$. Equating $P_1=0$ as given by eq. (17.1), Part I, we find that the positive root other than zero is $t=\infty$, so the pressure in any case will not terminate during the first interval $\theta_1>t>0$.

If the pressure terminates during the interval $2\theta_1>t>\theta_1$, we get from $P_2=0$ as given by eq. (17.2).

$$\frac{\Phi}{\Theta}=1+\frac{m}{8M}\left(2+e^{-\frac{2M}{m}}\right). \qquad \cdots \quad (73)$$

This is valid, so long as the maximum *mass-ratio* $\frac{m}{M}$ does not exceed 1·7, which is obtained as the root of the equation

$$\frac{m}{4M}\left(2+e^{-\frac{2M}{m}}\right)=1. \qquad \cdots \quad (73.1)$$

When the pressure terminates during $3\theta_1 > t > 2\theta_1$ we get from $P_3 = 0$ [*vide* eq. (17.3)]

$$(\Phi-\Theta)^2 - \overset{*}{\gamma}_{2\cdot1}\frac{\Theta}{2}(\Phi-\Theta) + \overset{*}{\gamma}_{2\cdot2}\frac{\Theta^2}{4} = 0, \qquad \dots \quad (74)$$

where

$$\overset{*}{\gamma}_{2\cdot1} = \frac{m}{2M}\left(3 + e^{-\frac{2M}{m}}\right), \qquad \dots \quad (74.1)$$

$$\overset{*}{\gamma}_{2\cdot2} = \frac{m^2}{4M^2}\left[1 + \tfrac{1}{2}e^{-\frac{4M}{m}} + e^{-\frac{2M}{m}}\left(1 - \frac{2M}{m}\right)\right], \qquad \dots \quad (74.2)$$

provided the maximum *mass-ratio* $\frac{m}{M}$ is given by the equation,

$$1 - \overset{*}{\gamma}_{2\cdot1} + \overset{*}{\gamma}_{2\cdot2} = 0 \qquad \dots \quad (74.3)$$

which has a root 4.1 approximately; so the impact terminates during $3\theta_1 > t > 2\theta_1$ when $\frac{m}{M}$ lies between 1.7 and 4.1.

When the pressure terminates during $4\theta_1 > t > 3\theta_1$ we get from $P_4 = 0$ [*vide* eq. (17.4)]

$$\left(\Phi - \frac{3\Theta}{2}\right)^3 - \overset{*}{\gamma}_{3\cdot1}\frac{\Theta}{2}\left(\Phi - \frac{3\Theta}{2}\right)^2 + \overset{*}{\gamma}_{3\cdot2}\frac{\Theta^2}{4}\left(\Phi - \frac{3\Theta}{2}\right) - \overset{*}{\gamma}_{3\cdot3}\frac{\Theta^3}{8} = 0, \qquad (75)$$

where

$$\overset{*}{\gamma}_{3\cdot1} = \frac{3m}{4M}\left(4 + e^{-\frac{2M}{m}}\right), \qquad \dots \quad (75.1)$$

$$\overset{*}{\gamma}_{3\cdot2} = \frac{3m^2}{8M^2}\left[5 + e^{-\frac{2M}{m}}\left(3 - \frac{4M}{m}\right) + 2e^{-\frac{4M}{m}}\right], \qquad \dots \quad (75.2)$$

$$\overset{*}{\gamma}_{3\cdot3} = \frac{3m^3}{16M^3}\left[1 + e^{-\frac{2M}{m}}\left(1 - \frac{6M}{m} + \frac{4M^2}{m^2}\right)\right.$$

$$\left. + e^{-\frac{4M}{m}}\left(1 - \frac{4M}{m}\right) + \tfrac{1}{3}e^{-\frac{6M}{m}}\right], \qquad \dots \quad (75.3)$$

provided the maximum *mass-ratio* is given by the equation

$$1 - \overset{*}{\gamma}_{3\cdot1} + \overset{*}{\gamma}_{3\cdot2} - \overset{*}{\gamma}_{3\cdot3} = 0 \qquad \dots \quad (75.4)$$

which has a root $\frac{m}{M} = 7{\cdot}3$ approximately. Thus the pressure terminates during this interval, so long as $\frac{m}{M} \not< 4{\cdot}10$ and $\not> 7{\cdot}30$.

During the interval $5\theta_1 > t > 4\theta_1$ by putting $P_5 = 0$ [*vide* eq. (17.5)], the duration of contact Φ is obtained as the root of the equation

$$(\Phi-2\Theta)^4 - \overset{*}{\gamma}_{4\cdot1}\frac{\Theta}{2}(\Phi-2\Theta)^3 + \overset{*}{\gamma}_{4\cdot2}\frac{\Theta^2}{4}(\Phi-2\Theta)^2$$

$$-\overset{*}{\gamma}_{4\cdot3}\frac{\Theta^3}{8}(\Phi-2\Theta) + \overset{*}{\gamma}_{4\cdot4}\frac{\Theta^4}{16} = 0 \quad \ldots \quad (76)$$

where,

$$\overset{*}{\gamma}_{4\cdot1} = \frac{m}{M}\left(5 + e^{-\frac{2M}{m}}\right), \quad \ldots \quad (76.1)$$

$$\overset{*}{\gamma}_{4\cdot2} = \frac{3m^2}{4M^2}\left[9 + e^{-\frac{4M}{m}} + 4e^{-\frac{2M}{m}}\cdot\left(1 - \frac{2M}{m}\right)\right], \quad \ldots \quad (76.2)$$

$$\overset{*}{\gamma}_{4\cdot3} = \frac{3m^3}{8M^3}\left[7 + e^{-\frac{6M}{m}} + e^{-\frac{4M}{m}}\cdot\left(3 - \frac{8M}{m}\right)\right.$$

$$\left. + e^{-\frac{2M}{m}}\cdot\left(5 - \frac{16M}{m} + \frac{8M^2}{m^2}\right)\right], \quad \ldots \quad 76.3)$$

$$\overset{*}{\gamma}_{4\cdot4} = \frac{3m^4}{8M^4}\left[1 + e^{-\frac{8M}{m}} + e^{-\frac{6M}{m}}\left(1 - \frac{6M}{m}\right)\right.$$

$$\left. + e^{-\frac{4M}{m}}\cdot\left(1 - \frac{12M}{m} + \frac{16M^2}{m^2}\right) + e^{-\frac{2M}{m}}\left(1 - \frac{10M}{m} + \frac{16M^2}{m^2} - \frac{16M^3}{m^3}\right)\right], \quad (76.4)$$

provided the maximum mass-ratio is given by

$$1 - \overset{*}{\gamma}_{4\cdot1} + \overset{*}{\gamma}_{4\cdot2} = \overset{*}{\gamma}_{4\cdot3} + \overset{*}{\gamma}_{4\cdot4} = 0, \quad \ldots \quad (76\cdot5)$$

which has a root $\frac{m}{M} = 10{\cdot}4$ approximately. The pressure terminates during this interval if $\frac{m}{M}$ lies between 7·3 and 10·4.

In this way we can find out the duration of contact for any interval higher than $5\theta_1 > t > 4\theta$.

(iv) The hammer strikes at a point, little away from the mid-point, of the string, i.e., b is slightly greater than a.

If the pressure terminates during $\theta_2 > t > \theta_1$, we get the corresponding expression for the duration of contact by solving eq. $P_2 = 0$ [*vide* eq. (60), Part III]

$$\frac{\Phi}{\Theta} = \frac{a}{l}\left[1 + \frac{ml}{4Ma}\left(1 + e^{-\frac{4Ma}{ml}}\right)\right], \qquad \ldots (77).$$

provided the maximum mass-ratio which is obtained by putting $\Phi = \frac{2b}{c}$ is given by the equation

$$\frac{m}{4M}\left(1 + e^{-\frac{4Ma}{ml}}\right) = \left(1 - \frac{2a}{l}\right). \qquad \ldots (77.1)$$

Here we find that the maximum mass-ratio depends on $\frac{l}{a}$. The equation (77.1) is solved for different values of $\frac{b}{a}$ in order to get the maximum limit of the mass-ratio for the given interval (*vide* table 1).

TABLE I

l/a	Maximum m/M
2.2	0.36
2.4	0.65
2.6	0.79
2.8	0.93
3	1.04

If the pressure terminates during $2\theta_1 > t > \theta_2$ we get–from eq. $P_2 = 0$ [*vide* eq. (60), Part III]

$$\frac{\Phi}{\Theta} = \frac{1}{1 + e^{\frac{4M(b-a)}{ml}}}\left[\frac{a}{l} + \frac{m}{8M}\left(2 + e^{-\frac{4Ma}{ml}}\right)\right]$$

$$+ \frac{1}{1 + e^{-\frac{4M(b-a)}{ml}}}\left[\frac{b}{l} + \frac{m}{8M}\left(2 + e^{-\frac{4Mb}{ml}}\right)\right], \qquad \ldots (78)$$

provided the maximum *mass-ratio* which is obtained by putting $\Phi = 2\theta_1$ is given by

$$\frac{m}{4M}\,\frac{1}{\left\{e^{-\frac{4Ma}{ml}}+e^{-\frac{4M}{m}\left(1-\frac{a}{l}\right)}\right\}}\left[1+e^{-\frac{4Ma}{ml}}\left(1+\frac{4Ma}{ml}\right)\right.$$

$$\left.+e^{-\frac{4M}{m}\left(1-\frac{a}{l}\right)}\left(1+\frac{4Mb}{ml}\right)\right]=\frac{2a}{l}. \quad \ldots \quad (78.1)$$

When $a=b$, *i.e.*, at mid-point, the eq. (78) is evidently the same as eq (73).

(*v*) *Hammar strikes at* $\frac{l}{3}$ *from one end, i.e.,* $l=3a$, $b=2a$. If the pressure terminates during $2\theta_1>t>\theta_1$ we have from eq. $P_2=0$ [*vide* eq. (60), Part III]

$$\frac{\Phi}{\Theta}=\frac{1}{3}+\frac{m}{4M}\left(1+e^{-\frac{4M}{3m}}\right) \quad \ldots \quad (79)$$

provided the maximum *mass-ratio* $\frac{m}{M}$ is 1·04, as is given by the equation,

$$\frac{4M}{m}=\left(1+e^{-\frac{4M}{3m}}\right). \quad \ldots \quad (79.1)$$

If the impact terminates during $\Theta>t>2\theta_1$ we get from $P_4=0$, for $\theta_2=2\theta_1$ [*vide* eq. (60), Part III]

$$\left(\frac{\Phi}{\theta_1}-2\right)^2-\bar{\gamma}_{2\cdot1}\left(\frac{\Phi}{\theta_1}-2\right)+\bar{\gamma}_{2\cdot2}=0, \quad \ldots \quad (80)$$

where, $$\bar{\gamma}_{2\cdot1}=\frac{3m}{2M}\left\{3+e^{-\frac{4M}{3m}}\right\},$$

$$\bar{\gamma}_{2\cdot2}=\frac{9}{8}\frac{m^2}{M^2}\left\{e^{-\frac{8M}{3m}}+e^{-\frac{4M}{3m}}\left(1-\frac{4M}{3m}\right)+2\right\}, \quad \ldots \quad (80.1)$$

provided the maximum *mass-ratio* $\frac{m}{M}$ is given by (as $\Theta=3\theta_1$)

$$1-\bar{\gamma}_{2\cdot1}+\bar{\gamma}_{2\cdot2}=0, \quad \ldots \quad (80.2)$$

which has a root 1.76 approximately.

The comparison of the experimental values of the variation of the duration of contact with striking distance in the case of hard hammer, as given by M. Ghosh (fig. 2) and Banerjee-Ganguli (fig. 3), is made with those given by the present theory.

The duration of contact for hard hammer (*vide* Fig. 2) of mass 21·2 gm was observed for different striking distances, at a regular interval of 10 cms. from one end of the string of length 600 cms., and of linear density 0·05 gm./cm., stretched under tension 38·5 kilograms weight. With the above data as given by M. Ghosh, the duration of contact, which is the lowest positive root of the pressure equation, is calculated theoretically. These roots are obtained by solving the pressure equations numerically. They are also checked by the graphical method.

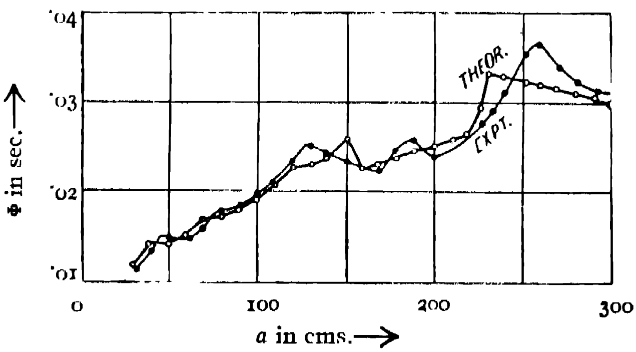

FIGURE 2

There are some striking distances at which double or triple contacts are observed. But these higher contacts, other than the first, are different from what is given by the dynamics of the struck string. These higher contacts may *slightly* modify the vibration-form of the string after impact. During impact, the hammer at first moves forward, then momentarily comes to rest, and afterwards starts moving backward, when after some time, it is separated from the string. Now, a reflected wave from either end while travelling along the string will pass through the point which was in contact with the hammer. If this reflected wave, at the instant of crossing the point of contacts, produces a displacement just equal to or greater than instantaneous separation-distance between the string and retarding hammer, then there is every possibility of fresh contact. The duration of such a contact is evidently much smaller than the first. As the velocity of wave propagation along the string is completely independent of the velocity of the hammer, so the phenomenon of multiple contact is influenced by the hammer velocity. Similar remark was also made by W. H. George. The experimental study of the same is in progress and will be published in due course.

The value of the duration of contact, when the hammer strikes the mid-point of the string, is calculated with the help of the eq. (73), as m/M is found to be less than 1·7. The values of the duration of contact, for the striking length 290 cms. down to 230 cms. are calculated with the help of eq. (78.1). Here the waves from the remoter end overtakes the hammer before it leaves the string.

Eq. (70) is used for the striking length 220 cms. down to 160 cms. as m/M is found to be less than 3·15. In these cases pressure terminates during the second interval before any wave from the remoter end overtakes the hammer. Eq. (61) is used for the striking length 150 cms. down to 90 cms. as $m/M_1 < 6{\cdot}1$. Here pressure is found to terminate during the third interval. Eq. (72) is used for the striking length 80 cms. down to 50 cms. as m/M_1 is found to be less than 10. Here the pressure is found to terminate during the fourth interval. For smaller striking lengths calculations are made graphically, where it is found that the pressure terminates during the fifth epoch.

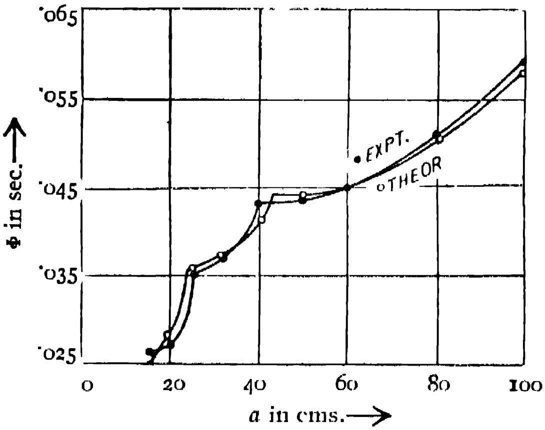

FIGURE 3

In figure 3 the values of the duration of contact when a hard hammer of mass 45 gms. striking at different points on the string of length 240 cms. and of mass 16·4 gms. stretched under a tension of 10·90 kilograms weight, are obtained by solving the pressure equations graphically. As for a massive hammer, that is, for a large mass-ratio, which is the case here, the pressure terminates after a large number of reflection of waves from the nearer end of the string, the algebraic method becomes too lengthy and so it is not followed here.

It is found that, when the hammer strikes at a distance 100 cms. from one of the ends, the pressure terminates before the fourth reflection from the shorter end, and the third reflection from the remoter end overtakes the hammer. Again when the striking distance is 80 cms., the pressure terminates before the fifth reflection from the shorter end, and the third reflection from the remoter end overtakes the hammer. In the same way, for the striking lengths, 60 cms., 50 cms., 40 cms., 30 cms., and 25 cms., the pressure terminates before the fifth, sixth, seventh, eighth, and tenth reflections from the shorter end respectively, and the second reflection from the remoter end in each case overtakes the hammer. For the striking distance 20 and 15 cms., it is found that the pressure terminates before ninth and tenth reflections from the nearer end and any reflection from the remoter end overtake the hammer. It is found from figures (2) and (3) that the agreement between the theory and experiment is remarkable.

In the case of the elastic hammer we have got very complicated forms of the pressure function. So in very rare cases the duration of impact can be algebraically solved.

When the hammer strikes very near the end, so that $\frac{a}{c}$ is very small, the displacement of the struck-point is given by [*vide* eq. (23), Part II]

$$y_a = \frac{Ev_0c}{T}\left[A^2e^{\alpha t} + \frac{A}{\nu}e^{\mu t}\sin(\nu t - \epsilon)\right]$$

where

$$A = \frac{1}{\sqrt{(\alpha-\mu)^2+\nu^2}}\,; \qquad \alpha = \frac{E}{2m}\cdot\frac{1}{\mu}+\frac{c}{a}\,;$$

$$\mu = -\frac{T}{2m_1c}\,; \qquad \nu = \sqrt{-\frac{2\mu c}{a} - \mu^2}\,;$$

$$m_1 = m_0 + \frac{Tm}{Ea}\,; \qquad m_0 = m + \frac{a\rho}{3}\,; \qquad \tan\epsilon = \frac{\nu}{\mu - a},$$

and the corresponding pressure is given by [*vide* eq. (26.2), Part II],

$$\begin{aligned}
-P = Eu &= \left\{\frac{T}{c}D + \frac{T}{a}\right\}y_a,\\
&= -m_1[2\mu D - (\mu^2+\nu^2)]y_a\\
&= m_1v_0c\frac{AE}{\nu T}\Big[A\nu(\mu^2+\nu^2-2\mu\alpha)e^{\alpha t} - (\mu^2+\nu^2)e^{\mu t}\\
&\qquad \sin\left(\nu t - \epsilon + \tan^{-1}\frac{2\mu\nu}{\mu^2-\nu^2}\right)\Big] \qquad \dots \quad (27)
\end{aligned}$$

and in the usual way the approximate value of the duration of contact is obtained, as given by

$$\Phi = \frac{1}{\nu}\left\{\tan^{-1}\frac{\nu}{\mu-a} - \tan^{-1}\frac{2\mu\nu}{\mu^2-\nu^2}\right\}. \qquad \dots \quad (81)$$

The expression representing the pressure functions in other cases of the elastic hammer have got three different forms depending upon the values of the elastic constant, *i.e.*, according as $\frac{E}{T} >=< \frac{16\rho}{m}$. Here graphical method may be helpfully adopted except when $\frac{E}{T} = \frac{16\rho}{m}$, where well-known Horner's method or Newton's method may also be followed for numerical solution. In every case, it is evident from the pressure equations that the pressure must not terminate during the first interval, except when $\frac{E}{T} < \frac{16\rho}{m}$. Here pressure exerted by the hammer is given by [*vide* eq. (40.1), Part II]

$$P_1 = 4\rho v_0 c \frac{\mu_1}{\nu_1} e^{-\mu_1 t} \sin \nu_1 t$$

where

$$\mu_T = \frac{Ec}{2T}\,; \qquad \nu_1 = \tfrac{1}{2}\sqrt{\frac{4E}{m} - \left(\frac{Ec}{2T}\right)^2}$$

and the duration of contact is given by

$$\Phi = \frac{2\pi}{\sqrt{\dfrac{4E}{m} - \left(\dfrac{Ec}{2T}\right)^2}}\,. \qquad \ldots \quad (8a)$$

The *elastic constant E* of the hammer, which is included in the pressure function *is distinctly different from Young's Modulus* but it depends upon the same, and also upon the size and the shape of the hammer, and upon the length of contact. It is the force in dyne acting upon the length of contact for a short time to produce unit compression. The magnitude of such a force, when acting for a long time, measured in an ordinary statical method, is much less than the dynamical value, but these two sets of values may be interrelated.

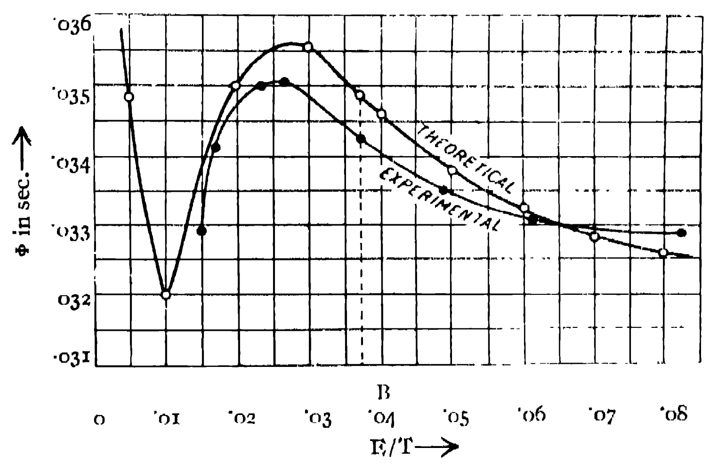

The dynamical value of $\frac{E}{T}$ is ·03 when the corresponding statical is 100/T.

FIGURE 4

In order to test the theory of the elastic hammer the duration of contact of elastic hammer for different values of the elastic constant E and for a given mass 21·2 gms. striking at the mid-point of a string of length 600 cms. of linear density 0·05 gm./cm. stretched under tension 38·5 kilograms weight is calculated. The experimental values giving the variation of the duration of contact with the variation of the elastic

constant of the hammer when strikes at mid-point of the string are taken from a paper of M. Ghosh.[4] The values of the elastic constants given in the paper are statical values, and are different from the dynamical values required by our formula. So the statical values are reduced to dynamical values by selection, and both are represented graphically in fig. 4. Here we find that pressure terminates during the second epoch. Φ corresponding to the point B in fig. 4, is calculated by the help of the pressure equation $P_2=0$ [*vide* eq. (47.2)], when $\frac{E}{T}=\frac{16\rho}{m}$ all the points on the right of B are calculated graphically by the help of $P_2=0$ [*vide* eq. (47.2)], when $\frac{E}{T}>\frac{16\rho}{m}$ and all the points on the left of B are calculated by the help of $P_2=0$ when $\frac{E}{T}<\frac{16\rho}{m}$. The agreement between the theory and the experiment is good.

My best thanks are due to Prof. K. C. Kar, D.Sc., of Presidency College, Calcutta, who has taken interest in this work.

PHYSICAL LABORATORY,
BURDWAN RAJ COLLEGE, BURDWAN.

REFERENCES

[1] Ghosh, M., *Ind. Jour. Phy.* **12**, 320 (1938) Part I; **12**, 439 (1938), Part II; **13**, 277 (1939), Part III.

[2] Davy, N., Littlewood, J. H. and McCaig, M., *Phil. Mag.*, **27**, 133 (1939).

[3] Kar, K. C., and Ghosh, M., *Zeit. f. Phys.*, **66**, 414 (1930).

[4] Ghosh, M., *Ind. Jour. Phy.*, **7**, 365 (1932).

[5] Banerjee, D., and Ganguli, R., *Phil. Mag.*, **7**, 346 (1929).

[6] George, G. H., *Proc. Roy. Soc.*, A **108**, 284 (1925).

DYNAMICS OF THE PIANOFORTE STRING AND THE HAMMER

PART V (SOME SPECIAL THEORIES)

By MOHINIMOHAN GHOSH
Burdwan Raj College, Bengal

(*Received for publication, February 20, 1940*)

ABSTRACT. The general theory of the finite Pianoforte string struck by an elastic hammer has been already developed in different papers. In this paper, the approximate conditions, necessary to reduce the general theory to obtain special theories given by different workers previously, are discussed. Kaufmann has considered two cases in which the hard hammer strikes (*i*) very near the end of the string, and (*ii*) at the mid-point of the string. The case of the hard hammer is obtained by considering in general theory the elastic constant of the hammer as large as infinite. All the expressions necessary for case (*i*) are obtained by considering the longer segment as large as infinite, and case (*ii*) is obtained by making two segments of the string equal. The expressions obtained by Helmholtz are obtained by considering the tension of the string large enough compared to the elastic constant of the hammer. The expressions obtained by Bhargava-Ghosh are obtained by the same approximation in the case of a semi-infinite string. The expressions as given by Das's theory are obtained by considering the longer segment to be as large as infinity, and that of Delemer is obtained by putting infinite for the elastic constant of the hammer, and, the hammer is considered to be a massive one. In order to explain the effect of the velocity of impact on duration of contact, the impact is considered in the light of Hertz's theory. A good agreement between the theory and the experiment is obtained. In this case the pressure exerted by the hammer on the string becomes appreciable after a certain instant when it comes in contact and leaves the string long after the pressure falls to a very small value. Similar was the assumption made by Lamb in his theory.

INTRODUCTION

The dynamics of the pianoforte string and a hammer has been completely developed in different papers.[1] The theory has been tested by the experimental datas supplied by different authors. In this paper it will be shown that the older theories which fail to explain fully the different experimental facts will come out as special cases of the present general theory. The approximations necessary for simplification of the general theory to the respective special theories will show their range of applicability.

The symbols used in this paper are same as before.[1]

The expressions for the displacement of the struck-point, the pressure exerted and the corresponding duration of contact for an elastic hammer striking very

near the end of a string are obtained in Part II [*vide* eq. (20)] and Part IV [*vide* eq. (27)].

$$y_a = \frac{Ev_0c}{T}\left[A^2e^{\alpha t} + \frac{A}{\nu}e^{\mu t}\sin(\nu t - \epsilon)\right] \qquad \ldots (23)$$

$$-P = \frac{Am_1Ev_0c}{T\nu}\left[\nu A(\mu^2+\nu^2-2\mu\alpha)e^{\alpha t}\right.$$

$$\left. -(\mu^2+\nu^2)e^{\mu t}\sin\left(\nu t - \epsilon + \tan^{-1}\frac{2\mu\nu}{\mu^2-\nu^2}\right)\right]$$

$$\Phi = \frac{1}{\nu}\left[\tan^{-1}\frac{\nu}{\mu-\alpha} - \tan^{-1}\frac{2\mu\nu}{\mu^2-\nu^2}\right] \qquad \ldots (17)$$

where,
$$A = \frac{1}{\sqrt{(\alpha-\mu)^2+\nu^2}}; \qquad \alpha = \frac{E}{2m}\cdot\frac{1}{\mu} + \frac{c}{\alpha}; \qquad \mu = -\frac{T}{2m_1c};$$

$$\nu = \sqrt{-\frac{2\mu c}{a} - \mu^2}; \quad m_1 = m_0 + \frac{Tm}{Ea}; \quad m_0 = m + \frac{\rho a}{3};$$

$$\epsilon = \tan^{-1}\frac{\nu}{\mu - \alpha}.$$

The eq. (23) can easily be reduced to what is obtained by Bhargava-Ghosh[2] by making α infinite, *i.e.*, when magnitude of T is infinitely large compared to the magnitude of E. This makes the pressure of impact, at $t=0$ finite, which however cannot be true for elastic hammer. This assumption, which is necessary for the above reduction, is equivalent to, neglecting the term of third differential D^3y_a in the equation of motion of the struck-point, [*vide* eq. (24), Part II], which however was neglected by the authors in building up their theory cited above. They have further *assumed* that the shorter segment vibrates like a *rigid rod* during impact.

Das[3] has also got an expression similar to *eq*. (23), on Kaufmann's assumption for the 'mass correction', *i.e.*, the shorter segment behaves like a *rigid rod* during impact. But the present theory is free from any such assumption. It has been already pointed out (*vide* page 440, Part II), previously, that Das's deduction is also not free from criticism.

For a hard hammer $E \to \infty$. This reduces

$$\alpha \to \infty; \quad EA \to 1; \quad \epsilon \to 0;$$

$$m_1 \to m_0; \quad \mu \to -\frac{T}{2m_0c}; \quad \nu \to \sqrt{\frac{T}{m_0a} - \frac{T^2}{4m_0^2c^2}}.$$

As for the hard hammer $E=\infty$, the expressions for y_a, P and the duration of contact Φ becomes identical with those obtained by Kaufmann [*vide* eq. (7) and (9), and eq. (67), Part IV].

The general expression for the displacement of the struck point as obtained in Part III, eq. (52) is

$$
\begin{aligned}
y_a = f_1(t) &+ \sum_1^n [f_{n+1}(t-n\theta_1) - f_n(t-n\theta_1)] \\
&+ \sum_1^n [f_{n+1} - f_n](t-n\theta_2) \\
&+ 2[f_3 - 2f_2 + f_1](t-\Theta) \\
&+ \sum_1^n [(n+2)f_{n+3} - (3n+4)f_{n+2} + (3n+2)f_{n+1} - nf_n](t-\Theta-n\theta_1) \\
&+ \sum_1^n [(n+2)f_{n+3} - (3n+4)f_{n+2} + (3n+2)f_{n+1} - nf_n](t-\Theta-n\theta_2) \\
&+ 2[3f_5 - 9f_4 + 10f_3 - 5f_2 + f_1](t-2\Theta), \qquad \ldots \quad (52)
\end{aligned}
$$

and the corresponding values of the pressure exerted by the hammer is [*vide* eq. (56), Part III]

$$
\begin{aligned}
-P = \frac{2T}{c}\Big[f'_1(t) &+ \sum_1^n f'_{n+1}(t-n\theta_1) + \sum_1^n f'_{n+1}(t-n\theta_2) \\
&+ 2\{f'_3 - f'_2\}(t-\Theta) \\
&+ \sum_1^n \{(n+2)f'_{n+3} - 2(n+1)f'_{n+2} + nf'_{n+1}\}(t-\Theta-n\theta_1) \\
&+ \sum_1^n \{(n+2)f'_{n+3} - 2(n+1)f'_{n+2} + nf'_{n+1}\}(t-\Theta-n\theta_2) \\
&+ 2\{3f'_5 - 6f'_4 + 4f'_3 - f'_2\}(t-2\Theta)\Big], \qquad \ldots \quad (56)
\end{aligned}
$$

where each functions which represents disturbances produced during impact can be expressed in three different forms depending upon the nature of the values of q and p,

$$[q,\ p] = \frac{Ec}{4T} \mp \frac{1}{2}\sqrt{\left(\frac{Ec}{2T}\right)^2 - \frac{4E}{m}},$$

that is, according as

$$\left(\frac{Ec}{2T}\right)^2 > = < \frac{4E}{m}.$$

(*i*) For $\left(\frac{Ec}{2T}\right)^2 > \frac{4E}{m}$ we get [*vide* eq. (30), Part II]

$$f_1(t) = Av_0\left[\frac{1}{q}(1-e^{-qt}) - \frac{1}{p}(1-e^{-pt})\right], \qquad \ldots \quad (30)$$

$$f_2(t_1)=A^2 v_0\left[\frac{e^{-qt_1}}{q}(1-A+qt_1)+\frac{e^{-pt_1}}{p}(1+A+pt_1)\right], \quad \ldots \quad (30.1)$$

$$f_3(t_2)=A^3 v_0\left[\frac{e^{-qt_2}}{q}\left\{\tfrac{3}{2}(A-A^2)+\tfrac{1}{2}(3A-1)qt_2-\frac{q^2t_2^2}{2!}\right\}\right.$$
$$\left.+\frac{e^{-pt_2}}{p}\left\{\tfrac{3}{2}(A+A^2)+\tfrac{1}{2}(3A+1)pt_2+\frac{p^2t_2^2}{2!}\right\}\right], \ldots \quad (30.2)$$

etc., where $A=\dfrac{q+p}{q-p}$.

(ii) For $\left(\dfrac{Ec}{2T}\right)^2=\dfrac{4E}{m}$;

$$f_1(t)=\frac{2v_0}{q}\left[1-e^{-qt}(1+qt)\right], \quad \ldots \quad (36.1)$$

$$f_2(t_1)=\frac{4v_0}{q}e^{-qt_1}\frac{(qt_1)^3}{3!}, \quad \ldots \quad (36.2)$$

$$f_3(t_2)=\frac{8v_0}{q}e^{-qt_2}\left\{\frac{(qt_2)^4}{4!}-\frac{(qt_2)^5}{5!}\right\}, \quad \ldots \quad (36.3)$$

etc.

(iii) And for $\left(\dfrac{Ec}{2T}\right)^2<\dfrac{4E}{m}$

$$f_1(t)=\frac{2\mu}{\nu}.v_0\left[\frac{\nu}{\mu^2+\nu^2}-\frac{1}{\sqrt{\mu^2+\nu^2}}e^{-\mu t}\sin\left(\nu t-\tan^{-1}\frac{\nu}{\mu}\right)\right], \quad \ldots \quad (39.1)$$

$$f_2(t_1)=\frac{2\mu^2}{\nu^3}.v_0 e^{-\mu t_1}\left[\sin \nu t_1-\nu t_1\cos \nu t_1\right], \quad \ldots \quad (39.2)$$

$$f_3(t_2)=\frac{\mu^3}{\nu^5}.v_0 e^{-\mu t_2}\left[\sqrt{(\mu^2+\nu^2)}\left\{\nu^2t_2^2\sin\left(\nu t_2-\tan^{-1}\frac{\nu}{\mu}\right)\right.\right.$$
$$\left.\left.+\nu t_2\cos\left(\nu t_2-\tan^{-1}\frac{\nu}{\mu}\right)\right\}+\mu\{2\nu t_2\cos\nu t_2-3\sin\nu t_2\}\right], \quad \ldots \quad (39.3)$$

etc.,

where $\mu=\dfrac{Ec}{4T}$; $\nu=\dfrac{1}{2}\sqrt{\dfrac{4E}{m}-\left(\dfrac{Ec}{2T}\right)^2}$.

Das [3] considered the case of a semi-infinite string and he admitted that the method adopted by him failed to consider the case of a finite string. Further,

even for a semi-infinite string he was not able to consider the case when $\left(\frac{Ec}{2T}\right)^2 = \frac{4E}{m}$ as in the present theory.

For semi-infinite string $b \rightarrow \infty$ $l \rightarrow \infty$ and every function in eq. (52) and (56) whose argument contains $\theta_2\left(=\frac{2b}{c}\right)$, or $\Theta\left(=\frac{2l}{c}=\frac{2a}{c}+\frac{2b}{c}\right)$ must vanish, as these functions will not appear before the time $t=\frac{2b}{c}$, *i.e.*, if the hammer is assumed to leave the string before $t=\frac{2b}{c}$. This however is not the case for a massive hammer. Thus for a semi-infinite string

$$y_n = f_1(t) + \sum_1^n \left[f_{n+1}(t-n\theta_1) - f_n(t-n\theta_1)\right],$$

and

$$-P = f'_1(t) + \sum_1^n f'_{n+1}(t-n\theta_1). \quad \ldots \quad (83)$$

These are exactly the expressions obtained by Das.[3]

In the case of the soft hammer when $\left(\frac{Ec}{2T}\right)^2 < \frac{4E}{m}$ we have, by the help of eqs. (30), (39.1) and (56),

$$-P = \frac{4pv_0c\mu}{\nu} e^{-\mu t} \sin \nu t \text{ during } 0 < t < \frac{2a}{c}, \quad \ldots \quad (84)$$

where μ and ν are given by eq. (38). When the hammer is very soft and light $\frac{Ec}{2T} \rightarrow 0$ so $\mu \rightarrow 0$ and $\nu \rightarrow \frac{E}{m}$ the eq. (84) reduces to

$$-P = \frac{Ev_0}{c} \sin \nu_0 t \text{ where } \nu_0 = \sqrt{\frac{E}{m}}. \quad (85)$$

This is the form of the pressure function which Helmholtz[4] *assumed* in solving the problem of the Pianoforte string. In this connection *he remarked that the magnitude of* ν_0 *increases as the elastic power of the hammer increases and the weight decreases.* This, however, is evident from the above deduction.

In the case of the hard hammer, *i e.*, when $E \rightarrow \infty$ $q \rightarrow \frac{2pc}{m}$ and $p \rightarrow \infty$, we have for the interval $0 < t < \frac{2a}{c}$, from eqs. (30), (52), and (56),

$$P_1 = 2pv_0 c e^{-\frac{2p}{m}ct} \quad \ldots \quad (86)$$

$$y_a = \frac{mv_0c}{2T}\left(1-e^{-\frac{2\rho}{m}ct}\right) \qquad \dots \quad (86{\cdot}1)$$

$$y_1 = \frac{mv_0c}{2T}\left\{1-e^{-\frac{2\rho}{m}(ct+x-a)}\right\} \qquad \dots \quad (86.2)$$

$$y_2 = \frac{mv_0c}{2T}\left\{1-e^{\frac{2\rho}{m}(ct-x+a)}\right\} \qquad \dots \quad (86.3)$$

as $c^2\rho = T$.

We shall get all the expressions obtained by Delemer[5] *from the above eqs.* (86), *when the hammer is considered to be a massive one* so that $\frac{\rho}{m} \to 0$. By retaining the first two terms of the expansion $e^{-\frac{2\rho}{m}ct}$ in the above eqs. (86), we get

$$P_1 = 2\rho v_0 c \qquad \text{(a constant)}, \qquad \dots \quad (87)$$

$$y_a = \frac{P_1}{2T}ct, \qquad \dots \quad (87.1)$$

$$y_1 = \frac{P_1}{2T}(ct+x-a), \qquad \dots \quad (87.2)$$

$$y_2 = \frac{P_1}{2T}(ct-x+a). \qquad \dots \quad (87.3)$$

These equations are *same as given by Delemer who assumed in his theory that the pressure exerted by the hammer during impact is constant.* This, however, is the case of a massive hammer.

When a hard hammer $(E=\infty)$ strikes at the mid-point of a string $(a=b)$ and $(l=2a)$ such that the pressure terminates during the second epoch, *i.e.*, $n=1$, we get, by putting $\theta_1=\theta_2$ in eqs. (32) and (56),

$$y_a = f_1(t) + 2[f_2(t+\theta_1) - f_1(t-\theta_1)]$$

$$= \frac{mv_0c}{2T}\left[\left(1-e^{-\frac{2\rho}{m}ct}\right) + 2\left\{1-e^{-\frac{2\rho}{m}(ct-2a)}\left\{1+\frac{2\rho}{m}(ct-2a)\right\}\right\}\right], \qquad \dots \quad (88)$$

and

$$P = \frac{2T}{c}[f'_1(t) + 2f'_2(t-\theta_1) - 2f'_1(t-\theta_1)]$$

$$= 2\rho v_0 c\left[e^{-\frac{2\rho}{m}ct} + 2e^{-\frac{2\rho}{m}(ct-2a)}\left\{1-\frac{2\rho}{m}(ct-2a)\right\}\right]. \qquad \dots \quad (89)$$

These are identical with those obtained by Kaufmann.[4]

It may be pointed out here that the theory given by Das does not take into account the reflection from the remoter end of the string. Das considered that the effect produced by the hammer when it strikes a finite string at a point dividing it into two unequal segments, was equal to the sum of two partial effects produced by the hammer, on two semi-infinite strings by striking at finite distances, which were equal to two segments respectively. This idea of Das leads to results different from[8] that of the Kaufmann for two equal segments, *i.e.*, when the hammer strikes at the mid-point. The difference arises after the time equal to the period of the vibration of the string measured from the beginning of the impact. This is due to the fact that Das has completely *ignored the effect of successive reflections of the waves from one end which has already suffered reflection from the opposite end.* It should, however, be noted that the present theory leads to the result identical with those of Kaufmann for all time.

The variation of the duration of contact with striking velocity in the case of the felt hammer was noticed by Weak[8] and Kaufmann and afterwards systematically studied by M. Ghosh.[9] In order to explain the above phenomenon we consider the period of impact to be divided into three *distinct* periods as Andrews[10] did in solving the collision problem of soft and elastic balls. It is assumed that in the first period the pressure exerted by the hammer-felt obeys Hertz's law and the string is not appreciably disturbed. After the compression has reached a certain value developing a finite pressure P_0, Hertz's law ceases to hold, and the string begins to be displaced. During this second period, the pressure exerted obeys Hooke's law, and the motion is given by the eqs. (19) and (19.1) and the corresponding dynamical behaviour is studied[1] previously. After the second period which may be called the 'Hooke's period' the extra compression, and so the corresponding pressure developed, is completely released, and the third period begins. As in this period Hertz's law is valid, it may be called the third 'Hertz-period.' It is assumed that the first and the third Hertz's periods have the same duration τ (say). Therefore the total duration of contact must be $\Phi_0+2\tau$ where Φ_0 is the duration of the second Hooke's period as calculated from our general theory in part IV, depending upon the *mass-ratios*, the striking length, and the elastic constant of the hammer, etc. Now the magnitude of τ is to be calculated.

The equation of motion of the hammer during the first or third 'Hertz-period' is

$$m\ddot{z}=m\ddot{y}_a+m\ddot{u}=-\epsilon u^{\frac{3}{2}}, \qquad \dots \quad (90)$$

where ϵ is a constant and $z=y_a+u$.

In passing we may remark E, that the elasticity of the hammer, which is

taken to remain constant during the second 'Hooke's period,' is proportional to $u^{\frac{1}{2}}$ in 'Hertz-period' [compare eq. (19) and eq. (90)].

As the string is not appreciably disturbed in a 'Hertz-period,' we assume $y_a=0$ approximately, so the eq. (90) becomes

$$\ddot{u}+\frac{\epsilon}{m}u^{\frac{3}{2}}=0.$$

On integrating the eq. (91), and evaluating the constant from the condition that at $t=0$, $\dot{u}=v_0$ and supposing that the limiting values of u and $\dot{u}$ at the end of first 'Hertz-period' are u_0 and v respectively, we have

$$u_0=\left(\frac{v_0^2-v^2}{n}\right)^{\frac{2}{5}}, \qquad \dots \quad (92)$$

where

$$n=\frac{4\epsilon}{5m}.$$

From eq. (92) we have for the time τ taken, to produce the compression u_0,

$$\tau=\frac{1}{v_0}\int_0^{u_0}\frac{du}{\sqrt{\left(1-\frac{n}{v_0^2}u^{\frac{5}{2}}\right)}}=\frac{1}{n^{\frac{2}{5}}v_0^{\frac{1}{5}}}\int_0^{x_0}\frac{dx}{\sqrt{(1-x^{\frac{5}{2}})}} \qquad \dots \quad (93)$$

where

$$x_0=n^{\frac{2}{5}}.\frac{u_0}{v_0^{\frac{4}{5}}}. \qquad \dots \quad (93.1)$$

After integrating term by term, we get

$$\tau=\frac{u_0}{v_0}\left[1+\frac{nu_0^{\frac{5}{2}}}{7v_0^2}+\frac{n^2u_0^5}{16v_0^4}+\frac{5n^3u_0^{\frac{15}{2}}}{136v_0^6}+\frac{35}{704}\frac{n^4u_0^{10}}{v_0^8}++\right]. \qquad \dots \quad (94)$$

As the total duration of contact Φ is given by

$$\Phi=\Phi_0+2\tau, \qquad \dots \quad (95)$$

so

$$\Phi-\Phi_0=\frac{2u_0}{v_0}\left[1+\frac{nu_0^{\frac{5}{2}}}{7v_0^2}++\right], \qquad \dots \quad (96)$$

where Φ_0 is calculated in the usual way from the pressure function, as given in part IV. As pointed out before, the algebraic solution of the pressure function for any value of E is rather difficult, so to verify the effect of the velocity of impact on the duration of contact we calculate Φ_0 taking $E=\infty$, *i.e.*, for a hard hammer. This value of Φ_0 will not introduce any serious error in showing the variation with velocity.

The data supplied by M. Ghosh[9] in this connection are used here to test the above theory giving the variation of Φ with velocity of impact.

The hammer of mass 21·2 gm. strikes at the mid-point of the string of length 600 cms. of line density 0·05 gm./cm. stretched under tension 38·5 kgms.wt.

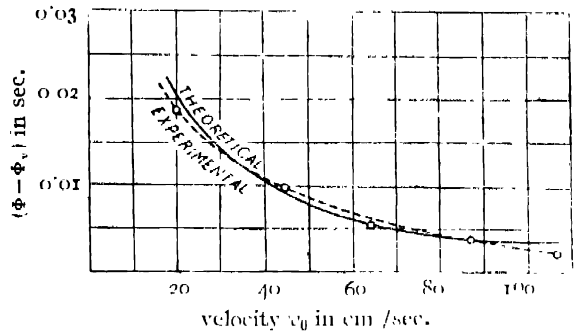

Figure 1.

The theoretical value of Φ_0 calculated from eq. (73) part IV is $2·09 \times 10^{-2}$ second, whereas the observed value is 3.086×10^{-2} seconds. The variation of $\Phi - \Phi_0$ with v_0 is calculated from eq. (96), taking only the first approximation and $u_0 = 0·2$ cm. Both experimental and theoretical variations are shown graphically. It is evident from the figure that the theory put forward agrees fairly well with the experiment.

It may be remarked here that the existence of the small pressure during Hertz-periods at the beginning and at the end of the impact which is the basis of the above calculation naturally reminds one of *Lamb's assumption* that "*the pressure exerted by the hammer on the string becomes appreciable after a certain instant when it comes in contact and leaves the string long after the pressure falls to a very small value.*"

My best thanks are due to Prof. K. C. Kar, D.Sc., of Presidency College, Calcutta, for the interest he took in the work.

DEPARTMENT OF PHYSICS,
BURDWAN RAJ COLLEGE,
BURDWAN.

REFERENCES

1 Ghosh, M., *Ind. Jour. Phys.*, **12**, 317, (1938) Part I; **12**, 431, (1938) Part; II **12**, 277, (1939) Part III ; **14**, 475 (1940) Part IV.

2 Bhargava, S., and Ghosh, R. N., *Phil. Mag.*, **47**, 1141 (1924) ; **49**, 121 (1925) ; Ghosh, R. N., **9**, 1174 (1930).

3 Das, P., *Proc. Phys. Soc.*, **40**, 29, (1927) ; *Proc. Ind. Assn.* **9**, 297 (1926) ; **70**, 75 (1926).

4 Kaufmann, W., *Ann. d. Phys. u. Chem* , **54**, 675 (1895).

5 Helmholtz, Sensation of Tone, translated by Ellis, 3rd edition, pages 380-384.

6 Delemer, J., *Ann. Sci. de Bruxell*, **30**, 299 (1905-1906).

7 Kar, K. C., and Ghosh, M., *Phil. Mag.*, **9**, 316 (1930).

8 Weak, C. K., *Ammeric. J. Science*, **32**, 366 (1884).

9 Ghosh, M., *Ind. J. Phys.*, **7**, 365 (1932).

10 Andrews, J. P., *Phil. Mag.*, **8**, 781 (1929); **9**, 593 (1930); Approved D.Sc. Thesis of the London University.

11 Lamb, H., *Dynamical theory of Sound.*

BOOK REVIEW

"BROADCASTING IN INDIA"

(A REVIEW OF THE REPORT* SPECIALLY OF CHAPTERS II AND

It is for the first time since April, 1930, when the control of Calcutta and Bombay radio stations passed over to the Government of India that an official report on the working of the Indian Broadcasting Administration up to 31st March, 1939, has been released to the public. During the next three years (1930-33), the Broadcasting in India made little progress and on one occasion it narrowly escaped being shut down. In January, 1934, the Government of India granted 2½ lakhs of rupees for a third medium-wave station at Delhi. The next year, a special fund of Rs. 20 lakhs was allotted and Mr. Fielden of the B.B.C. assumed charge as the first Controller of Broadcasting. In 1936, a further grant of Rs. 20 lakhs was added making a total of Rs. 40 lakhs; and Mr. Kirke of the B.B.C. arrived in India to suggest a scheme of expansion of broadcasting in this country.

KIRKE'S SCHEME AND AFTER

Kirke recommended the installation of seven medium-wave stations at various centres in addition to those existing at Delhi, Calcutta and Bombay and one short-wave station at Delhi for news transmission. He also proposed the purchase of the existing medium-wave station at Peshawar. Regarding the aerial power of medium-wave stations, he suggested 100 KW for one station, 5 KW for five stations and 2 KW for two stations. This scheme together with improvements on existing Calcutta and Bombay stations was estimated to cost Rs. 40·19 lakhs and the annual recurrent expenditure to Rs. 26 lakhs for the completed scheme.

In absence of data on reception conditions in India at different times of the year, an estimation of the areas which would be adequately served by his scheme could not be made, but it was predicted by him that the scheme would give 'A' service area with signal strength of 10 milli-volts per metre to about 14 million persons and 'B' service area with signal strength of 3 milli-volts per metre to

* Report on the Progress of Broadcasting in India, published by the Manager of Publications, Delhi, 1940.

35 million persons. It would be noted here that Kirke's forecast was subsequently found to be adequate for winter months only but not in summer months due to severe atmospheric disturbances prevailing in India.

Kirke wisely stressed in his report the necessity of establishing a Research Department and suggested taking up the work relating to (*a*) field-strength measurements, (*b*) transmission tests, (*c*) study of atmospheric disturbances, (*d*) recording of programmes and (*e*) development of radio links for relaying as well as advising the Engineering Department on the purchase of new radio and audio equipments.

He also dwelt in his report on the question of appointment of a suitable Chief Engineer to supervise technical and research departments and to build up a satisfactory organization As he did not seem to find in India any person (European or Indian) suitable for this appointment, he considered it desirable to bring a fully qualified man from England

Kirke's recommendations were based upon a compromise between providing service to urban areas from which large license revenues might be expected and providing such service to rural areas which might be partly maintained by revenues derived from urban areas.

After the return of Mr. Kirke to England, one of the B.B.C. engineers Mr. Goyder was appointed as the Chief Engineer in August, 1936. Mr. Goyder did not fully agree with Mr. Kirke's scheme. Considering the limited funds available to the Administration and the vastness of area to be served, he put forward a scheme of providing a basic second-grade short-wave service to the whole of the Indian continent and of supplementing the same by first-grade medium-wave service as funds become available. Kirke's scheme was modified as stated below. In addition to the existing medium-wave transmitters at Delhi, Calcutta, Bombay and Peshwar, installation of four 10-KW short-wave transmitters at each of the centres—Delhi, Calcutta, Bombay and Madras, one 5-KW short-wave news transmitter at Delhi, four 5-KW medium-wave transmitters at each of the centres—Lahore, Lucknow, Dacca and Trichinopoly and one 0·25-KW medium-wave transmitter at Madras were decided upon. The four 10-KW short-wave transmitters were regarded as almost covering the whole of India and providing a second-grade service not unsatisfactory to the average listener both by day and night. Goyder's scheme was accepted in preference to that of Kirke.

ENGINEERING AND TECHNICAL ACTIVITIES OF THE A. I. R.

The Engineering and Technical activities of the Department designated as the All India Radio (or A.I.R.) since June, 1936, have been presented in nine sections covering about 45 pages. They give an insight into the various classes of work which has been carried out during 1936-39 by the three departments of the Engineering Branch, namely, Research, Installation and Maintenance.

The results of field-strength measurements of the medium-wave stations at Lahore (5 KW), Lucknow (5 KW) and Delhi (20 KW) have been given. Direct ray measurements relating to Lahore have given average ground conductivity to be $1{\cdot}5 \times 10^{-13}$ e.m.u. and field strength varying between 30 and 59 mv/m over Lahore and between 7 and 8 mv/m over neighbouring district of Amritsar. Measurements relating to Lucknow have given average ground conductivity to be $1{\cdot}75 \times 10^{-13}$ e.m.u. and field strength varying between 28 and 58 mv/m over Lucknow and between 3·5 and 6·5 mv/m over Cawnpore. Measurements relating to Delhi have given average ground conductivity which varies from $1{\cdot}0 \times 10^{-13}$ to $1{\cdot}5 \times 10^{-13}$ e.m.u.'s. For a 5-KW station with normal ground conductivity prevailing in Northern India and assuming 20 *db* signal/noise ratio on 30% modulated signal, it will not be possible to maintain for 50% of time a range more than 50 miles and for 95% of time a range more than 11 miles. For 20-KW station, the range is about 70 miles for 50% of time and about 20 miles for 93% of time.

The measurements of indirect ray field strength of Indian medium-wave stations at Delhi during darkness hours are not without interest. In order to permit measurements on different stations to be compared, the measured figures have all been reduced to the equivalent field strength for one KW radiated. The figure shows the inverse-distance curve as well as the C.C.I.R. curve for a broadcasting station with 1 KW radiated. The field strengths of Lahore, Lucknow and Bombay stations approach the C.C.I.R. curve whereas those of Calcutta and Peshawar fall short of this.

It has been mentioned that the short-wave service in India is different from the short-wave services radiated from the European countries. Here in India the purpose of the service is to serve the area in which the station is located and hence the wave-lengths must be so chosen that they do not give skip distance around the station. Further to provide a short-wave service without skip distance over relatively short distances, the transmitting aerial must radiate energy at all vertical angles. An account of the experiments with half-wave horizontal dipole aerials placed at quarter wave-length and at half a wave-length above the electrical earth with reference to field strengths at nearer and farther points has been given.

A full section on the short-wave service is no doubt appropriate in the report of an administration which has adopted the basic scheme of providing second-grade short-wave service to India but it seems to be lacking in several essentials. The language and the method of presentation leave much to be desired. The interesting results arrived at from experiments on half-wave horizontal dipoles placed half a wave-length and quarter wave-length above the earth could have been presented in a much better way by enclosing some (quasi-maximum) field-strength—distance curves (up to 500 miles or more). Some results of 'fading studies' would also have been valuable.

A short account of the measurement of atmospheric disturbances is given. After discussing the two types of atmospherics—'long distance' and 'local,' the method of measurement has been described. Results of measurement for July, August and September, 1937, are given in the form of curves showing the signal field strength required in $\mu V/m$ with 30% modulated carrier to give 20 *db* signal/atmospheric ratio at various hours of the day on wave-lengths from 50 to 400 metres.

A description of the transmitting equipment and the associated aerial system of the short-wave and medium-wave transmitters installed by A.I.R. has been given in some details. The outstanding technical features have been brought out clearly and a number of figures has been enclosed to show schematic arrangement of connection, harmonic percentage and frequency response characteristics. An account has been presented in an interesting way of the Todapur receiving centre, which not only consists of aerial systems and equipments for diversity reception for rebroadcast purposes but serves also as the central observation station for periodical checking of wave-length, field strength and quality of transmission of A.I.R. stations. The figure which shows automatic gain control voltage variations with one, two and three receivers (of the diversity equipment) interlocked is interesting.

The studio design practice of the A.I.R. has been discussed at some length. After stressing on the need for a proper studio from listener's point of view, the three special requirements of studios, namely, (*a*) silence, (*b*) ventilation and (*c*) acoustics are discussed in details. The question of acoustic treatment then receives careful attention. Result of research leads to use of a 'vegetable fibre material' for sound absorption. With this material, instead of obtaining desired equal absorption over the audio-frequency range required, the absorption is high at higher frequencies and low at lower frequencies. To improve on this, the lower half of the total treated wall area has been proposed to be supported on battens in such a manner that energy on lower frequencies is absorbed. A number of reverberation time—frequency characteristics are given.

The village receiver problem has received due attention of the Research Department which has made experimental models based on their experiences of various difficulties. A tentative specification has been drawn up and circulated to the suppliers.

RESEARCH DEPARTMENT

In accordance with the recommendation of Mr. Kirke, a research department was created in April, 1937, with a research engineer and a technical staff of a few workers. Measurements of field strengths and atmospheric disturbances, experiments on diversity reception and acoustic treatment of studios and development of village receivers no doubt go to the credit of this new department. However, one cannot help remarking at this stage that both quality and quantity of the research

work leave much to be desired. A few cases of signal strength survey or a few sets of measurements on the strength of atmospherics during a period of two to three months can hardly be classed as research work.

The Research Department should be organised in a better way and strengthened for carrying on efficiently research and development works which are of immediate or future importance to the engineering side of broadcasting. The work and organization of the research department should be entrusted to a right sort of technical person having long research and development experience and capable of guiding research. A glance at the Appendix VII shows that the salary paid to the person entrusted with charge of the research department (*i.e.*, the Research Engineer) is a mere pittance in comparison to those of the other " senior headquarters officers " of the Administration. It may be difficult to attract the right sort of person for this purpose on this meagre salary. Similarly, the research staff—engineers and assistants—should have better salaries than those on maintenance and installation sides to attract first-grade men.

The head of the research department should be assisted by at least seven assistant research engineers and some twenty-five or more research assistants. The work of the research department could be carried out more or less under five main *divisions* as elsewhere :—(1) Signal strengths and Ionospheric measurements; (2) Atmospherics and Electrical Disturbances; (3) Aerials, feeders and diversity reception ; (4) Studio acoustics, sound-recording and audio-frequency work ; and (5) Equipments and Developments. For some of the work of this Department like ionospheric measurements, atmospheric measurements, etc., it would be desirable to open a few 'Observation Centres' in different parts of the country in addition to those located at the Headquarters and to obtain records of observation over sufficiently long periods. Finally, the publication of the results of investigations in suitable technical journals should form a part of research engineer's work.

CONCLUSION

In concluding the review, we will mention that no small credit is due to the chief executives connected with the Indian broadcasting service in view of the extent of the problem and the nature of difficulties to be surmounted. It is a tribute to their great enthusiasm and tenacity of purpose.

The report is profusely illustrated and contains numerous table, charts, graphs and diagrams supplying useful data. It is to be hoped that the next report will be published early.